



Technical Background and Conceptual Design Report 2007

Acknowledgements

Thanks to all the authors for their submissions.
Cover Page by Ampersand Design, Ardington, Oxfordshire

This report is available on the HiPER website – www.hiper-laser.org

List of Authors

Dunne, M.¹ ; Alexander, N.² ; Amiranoff, F.³ ; Aguer, P.⁴ ; Atzeni, S.⁵ ; Azechi, H.⁶ ; Bagnoud, V.⁷ ; Balcou, P.⁸ ;
Badziak, J.⁹ ; Batani, D.¹⁰ ; Bellei, C.^{5,11} ; Besnard, D.¹² ; Bingham, R.¹ ; Breil, J.⁸ ; Borghesi, M.¹³ ; Borneis, S.⁷ ;
Caruso, A.¹⁴ ; Chanteloup, J.C.³ ; Clarke, R.J.¹ ; Collier, J.L.¹ ; Davies, J.R.¹⁵ ; Dufour, J-P.¹⁶ ; Estrailier, P.¹² ;
Evans, R.G.^{1,11} ; Fajardo, M.¹⁵ ; Fedosejevs, R.¹⁷ ; Figueria, G.¹⁵ ; Fils, J.⁷ ; Feugeas, J.L.⁸ ; Galimberti, M.¹ ;
Gauthier, J-C.⁸ ; Giuliotti, A.¹⁸ ; Gizzi, L.A.¹⁸ ; Goodin, D.² ; Gregori, G.¹ ; Gus'kov, S.¹⁹ ; Hallo, L.⁸ ;
Hernandez-Gomez, C.¹ ; Hoffman, D.⁷ ; Honrubia, J.²⁰ ; Jacquemot, S.³ ; Key, M.²¹ ; Kilkenny, J.² ;
Kingham, R.¹¹ ; Koenig, M.³ ; Kovacs, F.¹² ; Krushelnic, K.¹¹ ; Labaune, C.¹⁶ ; Lancaster, K.¹ ; Leblanc, C.³ ;
Maire, P.H.⁸ ; Marklund, M.³⁴ ; Martin, W.¹ ; McEvoy, A.¹ ; McKenna, P.²² ; Mendonça, J.T.¹⁵ ;
Meyer-ter-Vehn, J.²³ ; Mima, K.⁶ ; Mourou, G.²⁴ ; Moustazis, S.²⁵ ; Najmudin, Z.¹¹ ; Nickles, P.²⁶ ; Neely, D.¹ ;
Norreys, P.²⁰ ; Olazabal, M.⁸ ; Offenberger, A.¹⁷ ; Papadogianis, N.²⁷ ; Perin, J-P.¹² ; Perlado, J.M.²⁰ ; Ramirez, J.²⁰ ;
Ramis, R.²⁰ ; Rhee, Y.²⁸ ; Ribeyre, X.⁸ ; Robinson, A.¹ ; Rohlena, K.²⁹ ; Rose, S.J.¹¹ ; Roth, M.³⁰ ; Rouyer, C.¹² ;
Rulliere, C.¹² ; Rus, B.²⁹ ; Sandner, W.²⁶ ; Schiavi, A.⁵ ; Schurtz, G.⁸ ; Sergeev, A.³¹ ; Sherlock, M.¹ ; Silva, L.¹⁵ ;
Smith, R.A.¹¹ ; Sorasio, G.¹⁵ ; Strangio, C.¹⁴ ; Takabe, H.⁶ ; Tatarakis, M.⁶ ; Tikhonchuk, V.²⁷ ; Tolley, M.¹ ;
Vaselli, M.¹⁸ ; Velarde, P.²⁰ ; Winstone, T.¹ ; Witte, K.⁷ ; Wolowski, J.⁹ ; Woolsey, N.³² ; Wyborn, B.¹ ;
Zepf, M.¹³ ; Zhang, J.³³

¹ Central Laser Facility, Science and Technology Facilities Council, Rutherford Appleton Laboratory, UK

² General Atomics Inc., San Diego, CA, USA

³ Laboratoire pour l'Utilisation des Lasers Intenses - Ecole Polytechnique, Paris, France

⁴ Conseil Régional d'Aquitaine, France

⁵ Dipartimento di Energetica, Università di Roma *La Sapienza* and Consorzio Nazionale Interuniversitario per le Scienze Fisiche della Materia, Italy

⁶ Institute of Laser Engineering, Osaka, Japan

⁷ Gesellschaft für Schwerionenforschung mbH, Darmstadt, Germany

⁸ Centre Lasers Intenses et Applications, Université Bordeaux 1, France

⁹ Institute of Plasma Physics and Laser Microfusion, Euratom Association, Warsaw, Poland

¹⁰ Di Milano Bicocca and Consorzio Nazionale Interuniversitario per le Scienze Fisiche della Materia, Italy

¹¹ The Blackett Laboratory, Imperial College, London, UK

¹² Commissariat à l'Energie Atomique, France

¹³ Queen's University of Belfast, Northern Ireland

¹⁴ Ente per le Nuove tecnologie, l'Energia e l'Ambiente, Italy

¹⁵ Instituto Superior Técnico, Lisbon, Portugal ¹⁶ Institute Lasers et Plasmas, Bordeaux, France

¹⁷ University of Alberta, Canada

¹⁸ Intense Laser Irradiation Laboratory, IPCF, Consiglio Nazionale delle Ricerche, Italy

¹⁹ Lebedev Physical Institute, Russian Academy of Sciences, Russia

²⁰ Universidad Politecnica de Madrid, Spain

²¹ Lawrence Livermore National Laboratory, USA

²² University of Strathclyde, Glasgow, UK

²³ Max-Planck-Institut für Quantenoptik, Garching, Germany

²⁴ Laboratoire d'Optique Appliquée, ENSTA - Ecole Polytechnique, France

²⁵ Technical University of Crete, Greece

²⁶ Forschungsverbund Berlin e.V., Germany

²⁷ Technological Educational Institute of Crete, Greece

²⁸ Laboratory for Quantum Optics, Korea Atomic Energy Research Institute, South Korea

²⁹ Academy of Sciences of Czech Republic, PALS, Czech Republic

³⁰ Technische Universität Darmstadt, Germany

³¹ Institute of Applied Physics, RAS, Russia

³² University of York, UK

³³ Laboratory of Optical Physics, Institute of Physics, Chinese Academy of Sciences, China

³⁴ Umeå University, Sweden

1 Foreword

This document provides technical details of the High Power laser Energy Research facility, HiPER.

The content is the result of a 2-year design study by over 50 senior scientists from 12 of the 15 nations now associated with HiPER. The design is now sufficiently mature that a formal proposal has been made to the European Commission to prepare the case for construction as part of the European strategic facility roadmap process (ESFRI) and Framework Programme 7.

HiPER is a multi-national laser facility designed to allow Europe to take a leading position in the pursuit of Inertial Fusion Energy, whilst offering an internationally unique capability for science in extreme conditions. It will open up entirely new areas of research, providing access to physics regimes which cannot be explored on any other science facility. It has been formally endorsed by 7 European nations at the governmental or national funding agency level, 2 regional governments, over 20 scientific institutions and has direct involvement from industry.

Inertial Fusion Energy (IFE) lies at the heart of the design of HiPER. Fusion is the holy grail of energy sources – combining abundant fuel with no greenhouse gas emissions, minimal waste products, and a scale that can meet mankind's long-term energy demands. Fusion combines hydrogen isotopes to create helium gas and a neutron which is captured to provide heat for a steam turbine. The IFE solution for fusion is a proven scientific concept. A laboratory demonstration of net energy production using lasers for IFE is now only 3 to 5 years away, marking the culmination of 40 years research. This will attract significant public and political attention, and so the HiPER project has been developed to provide a clear path forwards, based on a strong science mission.

The project already stretches beyond the EU, involving coordination with work in Japan, China, South Korea, Canada, Russia and the USA.

HiPER represents science with a strong societal goal.



Professor Mike Dunne, Coordinator of the HiPER project
June 2007

Contents

1	Foreword.....	3
2	Introduction to HiPER	7
2.1	Background.....	7
2.2	The Science mission of HiPER.....	9
3	Background on fusion and the role of IFE.....	10
3.1	Introduction.....	10
3.2	Significance of fusion energy	12
3.3	Confinement schemes - detail.....	13
4	Fusion Science Case and Design	20
4.1	Introduction.....	21
4.2	Basic driver requirements.....	22
4.3	Gain curves	25
4.4	Target design.....	29
4.5	Hydrodynamics of conically-guided implosions.....	34
4.6	Ignition laser pulse interaction and hot electron generation	37
4.7	Hot-electron transport and energy deposition	39
4.8	Laser-generated proton beams as alternative ignitors.....	50
4.9	Conclusions	51
5	Fundamental Science on HiPER.....	57
5.1	High Energy Density Physics	58
5.2	Atomic Opacity.....	59
5.3	Photoionised plasmas.....	60
5.4	Warm Dense Matter.....	60
5.5	New Diagnostic Techniques	61
5.6	Materials science.....	62
5.7	Laboratory astrophysics	63
5.8	Relativistic astrophysics with relativistic beams.....	65
5.9	Basic laser-plasma interaction studies	66
5.10	Nuclear Physics.....	67
5.11	Plasma accelerators.....	69
5.12	Fundamental Physics with Strong Fields.....	71
6	Large scale strategic facility development.....	79
6.1	Existing academic systems in the EU	79
6.2	Ignition scale laser facilities.....	80
6.3	International, Fast Ignition physics facilities.....	80
7	Role and development of the smaller scale European facilities.....	83
7.1	Introduction.....	83
7.2	Nature of the facility coordination needed for HiPER.....	83
7.3	Resources	84
7.4	Distributed science and diagnostic capabilities: a common approach between SSF labs	85
7.5	Specific actions and tasks	86
8	Experimental validation of the fusion programme	88
8.1	Introduction.....	88
8.2	Absorption and energy transfer to the fast electron beam.....	88
8.3	Divergence and collimation – novel techniques (shaped targets, etc.).....	89
8.4	Phase control.....	91
8.5	Hydrodynamics and mixing and tamping of the Au cone material.....	91
8.6	Fast electron transport in dense deuterium plasmas.....	93
8.7	Transition from the Ohmic to drag-heating regimes.....	93
8.8	Collective Stopping.....	94
8.9	Whole beam self-focusing.....	95

8.10	Colour and Z scaling.....	96
8.11	Proton / ion driven FI scaling experiments.....	97
8.12	Two stream instability – ion heating.....	97
8.13	Hole boring.....	98
8.14	Alternative geometries.....	99
9	Baseline Facility Design.....	101
9.1	Laser Design Philosophy.....	101
9.2	Compression beamlines.....	101
9.3	Energy perspective.....	102
9.4	Beam propagation perspective.....	105
9.5	Deformable mirror location.....	105
9.6	Front-end design.....	106
9.7	Amplifier design.....	107
9.8	Transport.....	109
9.9	Final Optics Assembly.....	109
9.10	Ignition Beamlines.....	110
9.11	HiPER Interaction areas.....	113
9.12	Interaction area requirements.....	113
9.13	HiPER Operational systems.....	114
9.14	HiPER Ancillary Systems:.....	116
9.15	Key HiPER Diagnostics.....	117
9.16	Conclusions for the facility design.....	122
10	Laser Development Options.....	124
10.1	Ignition Beam Compression Options.....	124
10.2	Coherently Locking the Ignition Beam sub apertures.....	125
10.3	Second Harmonic Ignition Beam Options.....	127
10.4	OPCPA Options.....	127
10.5	Diode Pumped Solid State Laser (DPSSL) Options.....	130
11	Target Manufacturing Capability and Delivery.....	131
11.1	Scope.....	131
11.2	Work package objectives.....	131
11.3	Technical background.....	131
11.4	Specifically identified challenges – risk identification.....	132
11.5	IFE target baseline design specification.....	133
11.6	Existing target fabrication capabilities relevant to HiPER.....	134
11.7	The role of European civilian institutions.....	135
11.8	The role of the CEA laboratories.....	136
11.9	The role of GA and LLNL.....	137
12	Fusion Reactor Design and Technology.....	138
12.1	Introduction.....	138
12.2	Examples of Fusion Technology Experiments.....	138
12.3	Chamber Gas Dynamics.....	140
12.4	Liquid Interactions.....	141
12.5	High-repetition rate chamber.....	143
12.6	Fast Ignition reactor conceptual design.....	144
13	Industrial engagement and component sourcing.....	147
13.1	Introduction.....	147
13.2	Optics.....	147
13.3	Components not developed for the NIF and LMJ systems.....	148
13.4	Technical Industrial Engagement.....	150
13.5	Conclusion.....	151
14	The HiPER Building.....	153

14.1	Introduction.....	153
14.2	Technical requirement for HiPER buildings.....	157
14.3	Laser Building.....	157
14.4	Target Area Building	157
14.5	Additional Buildings.....	158
14.6	Siting Issues	158
15	Operational Analysis.....	159
16	Participants and Support	161
16.1	Formal Participants of the HiPER project.....	161
16.2	International Partnerships	165
16.3	Other Partners	166
16.4	Forward plan	167

Appendices:

A1:	Fusion reactor designs.....	168
A2:	Cryogenic target capability	238
A3:	High repetition rate (diode pumped solid state) lasers.....	255
A4:	Submission to the European Community for “Preparatory Phase Project” funding.....	276

2 Introduction to HiPER

2.1 Background

This is an exciting time for plasma physics and its application to fusion energy production. We are entering a period of huge investment in facilities that should demonstrate the scientific basis for this much heralded source of energy. Recently the international community took the decision to fund the ITER project to the tune of around 10 billion Euros. It is expected that in the early 2020s this device will use magnetic fields to confine a large, low-density plasma in quasi-steady state such that it releases more energy than it consumes. Alongside this, France and the USA are constructing multi-billion-Euro laser facilities to achieve net fusion energy production for the first time in the laboratory. Producing in excess of 10 times more energy than the lasers deliver, this will provide the scientific foundations for a pulsed fusion energy source.

This approach, known as Inertial Fusion Energy (IFE), has been studied for over 40 years as an attractive long-term energy solution, and as a means for creating the most extreme conditions achievable anywhere on Earth. The physics underlying inertial fusion is already proven. This is the approach adopted by Nature – inertial fusion powers the stars. Far more importantly, the process of net energy production from inertial fusion has already been demonstrated on Earth in an offshoot of the US defence mission in the 1980s. Demonstration of net energy production using a laser is now anticipated in 2010 on the National Ignition Facility: just 3 years away. This world-altering event will require a clear response to the public – it is essential therefore that our scientific community clearly understands the future path to an energy programme following this event. The field is still in the Research and Development phase, requiring international cooperation over the next decade centred on a next generation laser facility to allow academic and commercial exploitation into the energy and basic science sectors. Europe is ideally placed to lead the world in this journey, but requires a focused programme to ensure timely progress.

The High Power laser Energy Research facility, HiPER, meets this need by opening up a credible route to inertial fusion energy for commercial purposes whilst offering an internationally unique capability in the science of extreme conditions.

Such a move has been made feasible by recent evidence supporting a revolutionary approach to laser-driven fusion, in which an order-of-magnitude reduction in the scale of the drive laser seems achievable. Optimisation of this so-called “fast ignition” approach will be a principal goal of HiPER. This will pave the way for the development of an integrated reactor programme.

Whilst the energy mission addresses one of the highest societal priorities, the scientific requirement for HiPER is overwhelming. Analysis during the 2-year design study clearly indicated that “fast ignition” was the prime technical solution that could provide an optimum balance of scientific excellence and long-term energy options. HiPER meets the clear demand from the international science community to deliver a step-change in laser capabilities to open up entirely new research programmes in areas as diverse as laboratory astrophysics, extreme material science, turbulence, and fundamental atomic, nuclear and plasma physics.

Because the scale of HiPER is significantly greater than existing academic lasers, an intermediate scale facility (PETAL, in the Région Aquitaine, France) has already been commissioned. PETAL has been accepted as an integral part of the strategic path to HiPER. This is a major commitment, providing an essential stepping stone both in terms of the science and the technology for HiPER and the international user base.

No comparable laser system is underway anywhere in the world – HiPER will be a highly effective international attractor to Europe. There are significant industrial opportunities for Europe as part of the HiPER project – in the design and build phase, the operational phase, and from the ensuing technical spin-out opportunities. Furthermore, the long-term industrial impact associated with laser fusion is huge in scope.

A representative timeline for HiPER is shown in Figure 2.1. A 2-year design phase has just been completed. A 3-year preparatory construction phase is now planned to establish a consortium of nations, funding agencies, scientific institutions and industry to construct and operate the facility. The timing reflects the expected progress on existing facilities: achievement of fusion ignition on NIF (and subsequently Laser Mégajoule), and the establishment of the route to “fast ignition” using the FIREX-I (Japan), OMEGA-EP (USA) and PETAL (France) lasers.

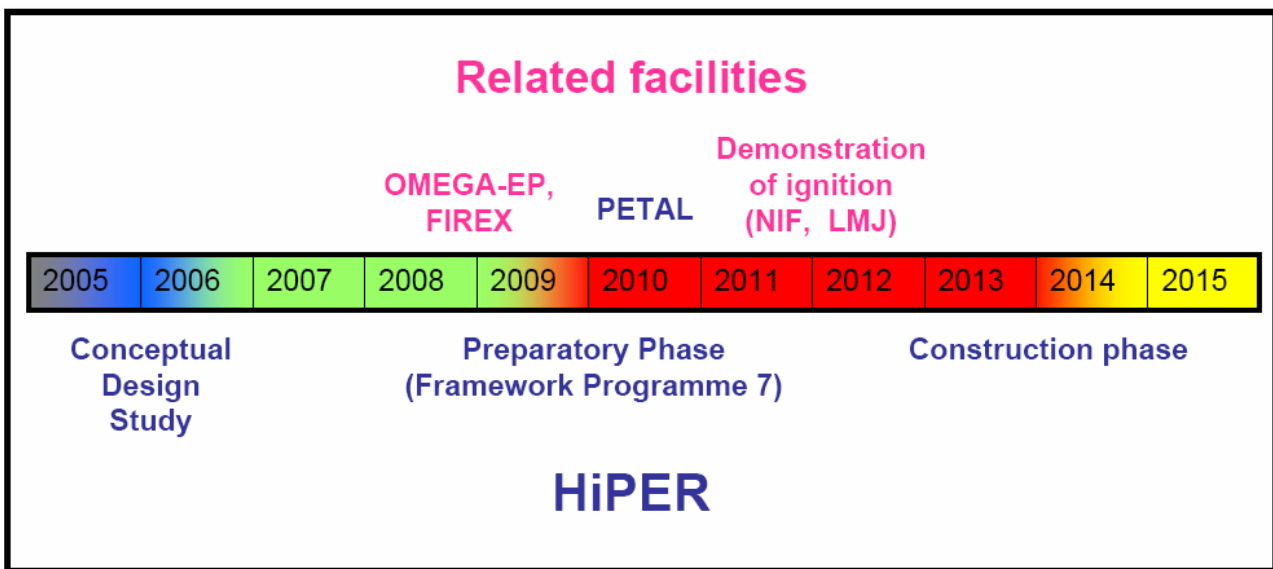


Fig 2.1 – HiPER milestones against the backdrop of international developments

In summary, HiPER represents a unique opportunity for Europe to take a leading role in the field of extreme science and ensure it targets the key challenge facing mankind – long term clean energy.

2.2 The Science mission of HiPER

Key to the needs of the large international user community is the provision of a flexible, responsive facility able to address a broad array of science programmes. The laser community has long experience of adapting its facilities for new users and new research areas. Lessons from facility operators and scientific users were pulled together in the conceptual design of HiPER to obtain a balance between the fusion energy mission and the wider science remit. The science programmes were selected for their compelling nature in terms of delivering an extreme science capability to Europe. The HiPER facility specification was then developed to provide an internationally leading capability in these areas.

The scope included:

- *Opacity and photoionization physics* - to address many outstanding fundamental atomic physics questions, along with their application to (for example) solar modelling.
- *Warm Dense Matter studies* – addressing the principal outstanding regime of material science in which there is no accepted theory (for which HiPER will offer exceptional probing and diagnostic capability).
- *Laboratory Astrophysics* – consistent with the fusion and high energy-density potential of HiPER, there is a wealth of astrophysical phenomena whose models could be tested in the laboratory, including supernovae evolution, proto-stellar jets, planetary nebulae, interacting binary systems, cosmic ray seeding and acceleration, and gamma-ray bursters.
- *Extreme Matter studies* – What are the fundamental properties of matter in extreme states? This includes studies in Gigagauss magnetic fields (otherwise only found in highly compact stellar objects, and in which the magnetic field dominates the electric field in determining sub-atomic motion), in Gigabar pressure regimes, in radiatively dominated systems, in burning plasmas, etc.
- *Turbulence* – how do compressible, nonlinear flows transition to turbulence and subsequently evolve? This is one of the few remaining fundamental uncertainties in classical physics.
- *Laser-plasma interaction physics* – including the question of how waves and matter interact under highly nonlinear conditions
- *Nuclear physics* under transient, excited state conditions – to study the effect of dense plasmas on nuclear cross sections, the behaviour of isomeric states via pump-probe studies of dressed states, and the creation of high density electron-positron pair plasmas and the evolution of the ensuing pair-fireball.
- *Production and interaction of relativistic particle beams* – for example, whether macroscopic amounts of relativistic matter can be created (then studied and utilised)
- *Fundamental physics at the strong field limit*

It is clear that HiPER will open up entirely new areas of research, providing access to physics regimes which cannot be explored on any other science facility. Full details of the science case are provided in the following chapters

3 Background on fusion and the role of IFE

3.1 Introduction

Research into controlled fusion as an energy source has spanned more than five decades and has involved the global scientific community. It represents one of the most important scientific challenges of the 21st century.

Fusion is the combination of two atomic nuclei to form a single heavier element. When two light elements are combined it turns out that their combined mass is less than that of the products. The “missing mass” is converted into energy following Einstein’s famous equation, $E=mc^2$. The amount of energy released can be very large, so that only tiny amounts of matter are needed to fuel a power station.

This is the opposite process to fission, where heavy elements (such as Uranium) are split apart to yield daughter nuclei (again with less mass than their parent nucleus). The difference between fusion and fission is essentially two-fold:

- Fission is relatively simple to harness, whereas fusion has proven very difficult
- Fission requires large assemblies of highly radioactive material, creating by-products with very long half-lives, whereas fusion uses only small amounts of fuel with by-products that can be simply managed.

Controlled fusion schemes typically involve two light nuclei, deuterium and tritium, which are isotopes of hydrogen. If the nuclei obtain enough energy to overcome their mutual (“Coulombic”) repulsion, they can undergo the fusion reaction shown in figure 3.1:

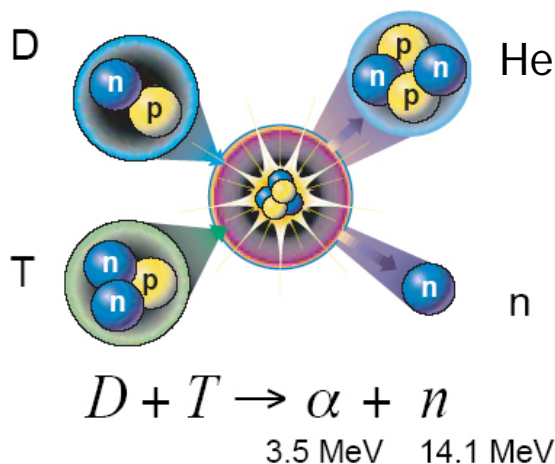
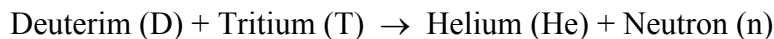


Fig 3.1 The principal fusion reaction

The by-products are thus Helium (also known as an alpha-particle) and a neutron. The helium is used to deposit energy into the rest of the fusion fuel to create a self-sustaining reaction. This means that only a relatively small amount of energy is needed to start the process, so that the reaction is highly efficient. The neutron escapes from the fuel, carrying a large amount of kinetic energy. If the fuel is surrounded by a blanket of material thick enough to stop the neutron then this kinetic energy will be converted into thermal energy. The blanket heats up, and this heat can be used to drive a conventional steam turbine.

The problem is that the fuel must be heated to temperatures of ~100 Million degrees Kelvin for this fusion reaction to occur. It must simultaneously be held at a sufficient density for a sufficient time to allow the process to run for long enough to produce a net amount of energy out.

At these temperatures matter enters the plasma state. Confining plasmas at 100 million degrees K provides the biggest challenge to controlling fusion. Under such conditions the plasma must be isolated away from vessel walls and prevented from expanding into the surroundings, thus quenching the fusion reactions. Many schemes have been proposed over the decades. They fall into two broad categories: Magnetic Fusion Energy (MFE) and Inertial Fusion Energy (IFE).

The leading approach to MFE utilises a torus shaped reactor called a ‘tokamak’ to produce and confine plasma using electric and magnetic fields. The torus is filled with gaseous DT fuel and is initially heated using ohmic currents, radio-frequency waves, and/or injected particle beams. The plasma is confined using toroidal and poloidal magnetic fields. The goal is to heat the plasma to the point where self heating due to DT fusion reactions allows the reaction to become self-sustaining. This point is known as “ignition” and represents one of the key goals of the ITER project. The intention is to produce energy from fusion reactions for about 8 minutes at the >100 MW level.

IFE takes the opposite approach. Rather than heating low density gases for relatively long periods, the idea is to produce very high densities for very short periods of time. It is therefore a “pulsed” approach, conceptually similar to the repeated cycles of chemical combustion in the engine of a car. The densities required are high: typically 20 times the density of lead, but the timescales are short: measured in picoseconds (10^{-12} s).

To do this, an energetic beam is used to symmetrically irradiate a small DT fuel capsule. The beam can be either a laser, x-rays, or an ion beam. The outer surface of the capsule heats up and expands outwards. Following Newton’s laws, the rest of the capsule undergoes an equal and opposite reaction: it implodes. Very high densities can be achieved by imploding the capsule into very small volumes.

IFE then takes one of two routes. It either uses a ‘diesel engine’ approach, whereby the capsule is imploded until it attains a sufficiently high density (and temperature) that its centre undergoes fusion. This approach is called “*central ignition*”. Or it uses a ‘petrol engine’ approach, whereby the capsule is partially imploded and then ignited by a spark plug (typically a high power laser). This is called “*fast ignition*”.

A key technology down-selection for HiPER will be driven by the repetition rate requirements of the driving laser. Two options currently exist – based on conventional technology or diode-pumped solid state lasers. A detailed cost-benefit analysis will be performed in the preparatory phase project.

Further details of these schemes are presented in section 3.3 and references therein.

3.2 Significance of fusion energy

Fusion energy is a uniquely attractive, environmentally clean power source. Using sea water as its principal source of fuel, there are no greenhouse gas emissions, nor any long-lived radioactive waste products. The benefits of fusion energy cannot be overstated in the current global setting where climate change, pollution, energy security and the ever increasing demand for consumption represent a principal challenge facing mankind [3.1].

Fusion is not a short term fix, nor will it address the immediate requirement to manage carbon emissions. It is a long-term, sustainable solution that will take a concentrated research and development effort across a range of options to realise its potential.

Fusion is an attractive energy source for a number of reasons:

- 1) **Low environmental impact** - The fusion process does not produce carbon dioxide and will therefore not contribute further to levels of CO₂ in the atmosphere. It does not produce long lived radioactive waste (as in fission power stations) and the associated problems/costs with storage of such material.
- 2) **Abundant fuel** – Deuterium, one of the isotopes involved in the fusion reaction is found in seawater in large quantities. A single cubic kilometre of seawater contains enough Deuterium to supply an amount of energy equal to the entire world's oil reserves. As such, fusion is able to meet our long-term requirements for power consumption. Tritium can be directly generated at the reactor site by utilising a Lithium blanket around the vessel[†]. This same blanket is used to extract the heat for the power plant.
- 3) **Energy Security** - fusion is an intrinsically secure source of energy for almost all nations, since the fuel is extracted from seawater and the reaction cycle at the power plant.
- 4) **Fusion is safe** – There is very little fuel present at any given time, therefore not enough fuel for runaway reactions. Melt-down or catastrophic release following an accident is therefore impossible. In the event of an accident the plasma will simply cool – the reactions cease immediately and so the process is intrinsically self limiting.
- 5) **Generation of Hydrogen** – In the future hydrogen is expected to play a significant role in energy generation for local or mobile requirements. The heat from a fusion reactor vessel can be used to generate large quantities of hydrogen for commercial and industrial applications.

Inertial fusion offers the further potential for more advanced fuels (with little or no tritium), and can also make use of liquid walls to contain the reactions, greatly easing two key technological problems. It could also allow more efficient burn (hence greater economy) and the extraction of electricity directly from the plasma products.

The technical problems associated with converting the scientific proof of principle of fusion into a commercial power plant should not be underestimated. As such, the approach is in the research and development phase, requiring international cooperation over the next decade to determine the best technical solutions. HiPER is designed to meet this requirement.

[†] Tritium (³H) is created by capturing the fast neutrons produced in the fusion reaction, for example in the ⁶Li(n,³H)⁴He reaction. Because the neutron capture process is not 100% efficient there is a need to multiply the neutron population prior to capture. This is done by introducing elements such as lead into the blanket, which can generate additional neutrons via (n,2n) reactions.

3.3 Confinement schemes - detail

3.3.1 Magnetic Fusion Energy (MFE)

MFE so far has been the most widely researched and well funded method of plasma confinement. Much progress has been made, for example using the JET (Joint European Torus) machine [3.2], in the UK. This device is currently the world's largest tokamak fusion research facility. This report will not focus on this confinement scheme but it is briefly discussed for completeness.

Ignition and gain

Ignition for MFE occurs when the energy derived from thermonuclear fusion products is greater than the energy required to heat the fuel to fusion temperatures in one confinement time. If the reactor operates in steady state, then once ignition has been reached the plasma can sustain itself indefinitely. The condition for breakeven ($Q=1$) is stated by the Lawson criterion [3.3]. For MFE this depends upon the number of particles, n , and the length of time for which they can be confined, τ , and so can be expressed as $n\tau > 1 \times 10^{20} \text{ m}^{-3}\text{s}$. Fusion devices currently operate their fields in a pulsed mode, where one pulse will typically last ~60 seconds. In the future superconducting coils will be used for steady state operation.

Progress

The JET [3.2] facility has operated over the last 20 years and represents a significant step towards demonstrating the feasibility of MFE as a power source. The facility has partners from 22 different countries in Europe and is currently run on behalf of them by the UKAEA [3.4]. JET has achieved three major milestones 1) 22 MJ of fusion in one pulse 2) 16.1 MW of peak fusion power 3) $Q=0.65$. Recently, JET has been used to investigate parameters for the International Thermonuclear Experimental Reactor (ITER) [3.5] such as plasma shaping and divertors for removing impurities in the system.

The ITER project is a massive global undertaking by Europe, Japan, China, India, Russia, South Korea, and the USA to build a next step reactor to demonstrate the feasibility of MFE as a future energy source. This reactor is designed to produce 500 MW of peak fusion power and this will result in a net gain of $Q=10$. The project will also develop technology needed make MFE work in a power plant scenario. ITER will be built in Cadarache, France with the first plasma expected by 2016 and ignition by ~2022.

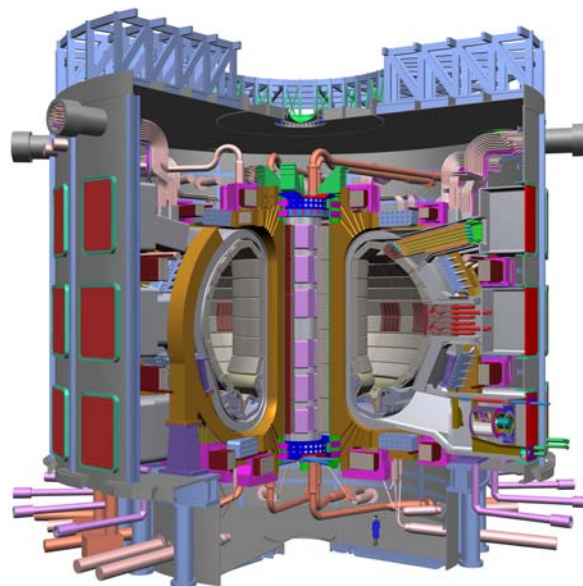


Fig 3.2 – Cutaway diagram of the ITER facility

3.3.2 Inertial Fusion Energy

The concept of Inertial Confinement Fusion (ICF) was developed independently in the USA and Russia. John Nuckolls published a seminal paper in 1972 [3.6].

An energetic beam is used to symmetrically irradiate a small DT fuel capsule. The beam can be either a laser, x-rays, or an ion beam. The outer surface of the capsule heats up and expands outwards. Following Newton's laws, the rest of the capsule undergoes an equal and opposite reaction: it implodes. Very high densities can be achieved by imploding the capsule into very small volumes.

Net energy production from inertial fusion has already been demonstrated on Earth in an offshoot of the US defence mission in the 1980s. Demonstration of net energy production using a laser is now anticipated in 2010 on the National Ignition Facility: just 3 years away. The process is represented schematically in figure 3.3.

There are two main irradiation schemes for IFE: indirect (x-ray) drive and direct (laser) drive. The physical principal behind indirect drive is to mount the DT fuel capsule inside a hollow high-Z cylinder called a hohlraum. Nanosecond duration lasers are used to irradiate the inner hohlraum walls to produce a relatively uniform thermal x-ray source (with a temperature of ~ 3 million degrees). The x-rays irradiate the capsule inside the hohlraum causing it to implode and finally to reach ignition due to shock heating. With this x-ray scheme there is some overlap with the physics of nuclear weapons. However, most of the physics associated with inertial fusion was declassified in 1995 [3.7], such that development for peaceful, energy applications is now possible.

Direct drive uses the lasers themselves to irradiate the capsule and thus to implode and ignite the fuel. This "all-optical" approach breaks the principle link to weapons science and is intrinsically more efficient. As such it has long been the focus for energy studies, with notable efforts in Japan, Europe and the USA.

Ignition and gain

The concept of ignition for IFE is slightly different to that described for MFE. Ignition occurs when the deposition of the helium nucleus in the fuel is enough to produce a self sustaining burn wave that propagates into the surrounding fuel. In an energy production scenario this would operate in a pulsed mode.

In IFE an equivalent criterion exists that determines the requirements for 'break even'. In this case $Q=1$ will be achieved when $\rho R > 3\text{gcm}^{-2}$, where ρ is the fuel density and R is the radius of the fuel.

Ignition and gain can be achieved when the energy balance equation is satisfied [3.7],

$$P_w + P_\alpha - P_e - P_b > 0$$

where P_w is work done on the fuel to compress it, P_α is thermonuclear heating rate per unit volume, P_e is loss per unit volume due to electron conduction, and P_b is the loss per unit volume due to bremsstrahlung emission.

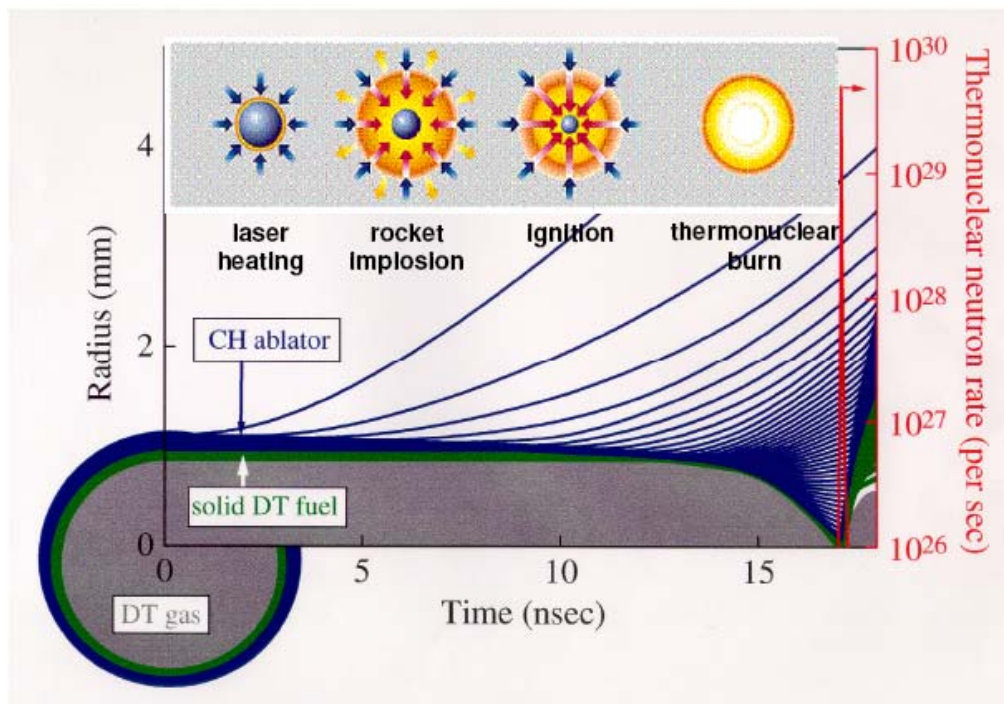


Fig 3.3 Generic implosion for a central ignition target [courtesy LLNL]

Important physical parameters

When a laser of intensity greater than 10^{14} Wcm⁻² interacts with the capsule, the laser energy is absorbed at the critical surface in the coronal underdense (less than critical density) plasma. This energy is then conducted to the higher density plasma which heats and expands (“ablates”) causing the rest of the fuel to converge to high density (ideally ~ 1000 g/cc). The position of absorption is determined by the laser wavelength, λ . Shorter wavelengths are absorbed closer to the ablation surface and hence will produce more efficient implosions.

For conventional “central ignition” IFE, shocks launched by the lasers converge on the centre of the fuel capsule to heat the material to fusion temperatures. In order for this to work the symmetry requirements of the beams are very high – both in terms of energy balance ($< 3\%$) and temporal synchronisation (< 10 ps). Capsule surface roughness must be < 1 μ m on the inside surface, and at the nm level on the outer. If these parameters are not achieved then instabilities such as Rayleigh-Taylor growth (RT) can be seeded (i.e. rippling of the capsule surface and mixing of hot and cold fuel). This limits the peak implosion velocity, and can quench ignition and burn. The ablation velocity can partially stabilise RT growth [3.8] and so this parameter must be optimised. However, in order to exert as much pressure as possible without a high change in entropy, Δs (which would limit compressibility), the laser pulse must be shaped to launch a series of shocks increasing in size [3.7].

This conflict between achieving high density and ‘hot spot’ formation means that the energy required to drive these capsules with conventional ICF is at the megajoule scale. Lasers of this size are now under construction (figure 3.4):

- National Ignition Facility, NIF, in the USA. 192 beams delivering 1.8 MJ at 351nm.
- Laser Mégajoule, LMJ, in France. 240 beams delivering in excess of 2 MJ at 351nm.

These are being designed to achieve “central ignition” with an energy gain of $Q \sim 10$ -30.



Fig 3.4 The National Ignition Facility

Fast ignition

Because of such stringent energy and symmetry requirements for conventional IFE (“central ignition”) a new scheme was proposed in 1994 [3.9]. Termed “Fast Ignition” (FI), the compression and heating phases are separated. This is shown schematically in figure 3.5.

In the compression phase the density requirements are significantly less than conventionally (typically $300\text{-}400\text{ g/cm}^3$ rather than 1000 g/cm^3) and there is no longer a need to ensure high symmetry of compression and shock convergence. This greatly eases the demands on the uniformity of both the laser and target. The driver energy can be as low as $200\text{-}300\text{kJ}$. As laser energy translates relatively directly to cost, this could substantially reduce the capital cost of an IFE plant.

In the heating phase, a high power laser is used to produce an intense beam of electrons or protons. This particle beam must deposit sufficient energy in the imploded fuel to induce ignition and thus a propagating burn wave. The physics associated with the generation, transport and energy deposition of this particle beam are not well understood and represent the principal challenge facing Fast Ignition.

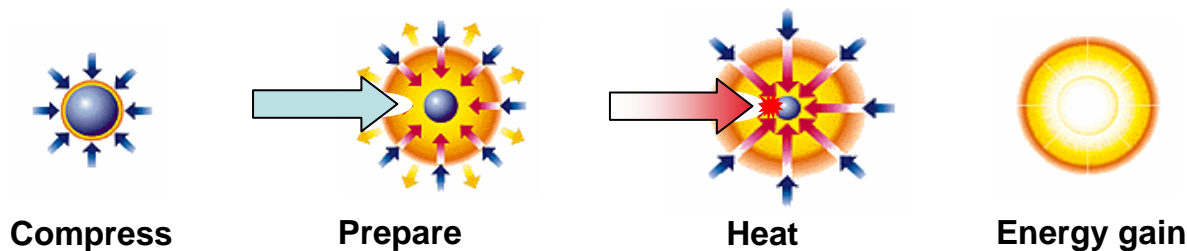


Fig 3.5 Stages of a Fast Ignition fusion implosion

Major laser facilities around the world are currently being upgraded to investigate the physics associated with Fast Ignition. The results from these studies will be used to optimise the design of HiPER. The three largest facilities are:

- FIREX [3.10] in Japan is an upgrade of the current GEKKO XII system at the University of Osaka, Japan. The phase 1 upgrade facility will consist of the construction of an ultra intense laser capable of delivering 10kJ in 10ps in conjunction with the compression beams which will deliver 10kJ of green light in 2ns. This should be completed for full operation in 2008. The phase 2 upgrade, if approved, will deliver 50kJ in 10ps for the heating laser and 50kJ of UV light in 3ns for the compression system. This is expected to demonstrate ignition after 2012.
- The OMEGA facility in the USA is adding a petawatt class laser (2.6 kJ, 1ps) to the existing 40 kJ compression system. Called OMEGA-EP [3.11], this system is expected to be operational in 2007.
- The PETAL laser facility in Bordeaux will couple a high energy petwatt laser (3.5 kJ in a few ps) with the existing LIL laser (60 kJ in 8 beams) and will come into operation in the period 2008-2010.

Recent research into Fast Ignition has centred on a target design in which the fuel is compressed around a gold cone (to keep a channel free from plasma and thus ease the particle beam transport phase) [3.12]. At stagnation an ultra intense laser is fired into the tip of the gold cone, producing copious amounts of hot electrons. These hot electrons need to have a mean energy that will allow them to stop and deposit energy in the dense fuel, raising it to fusion temperatures. A typical FI capsule geometry is pictured in figure 3.6.

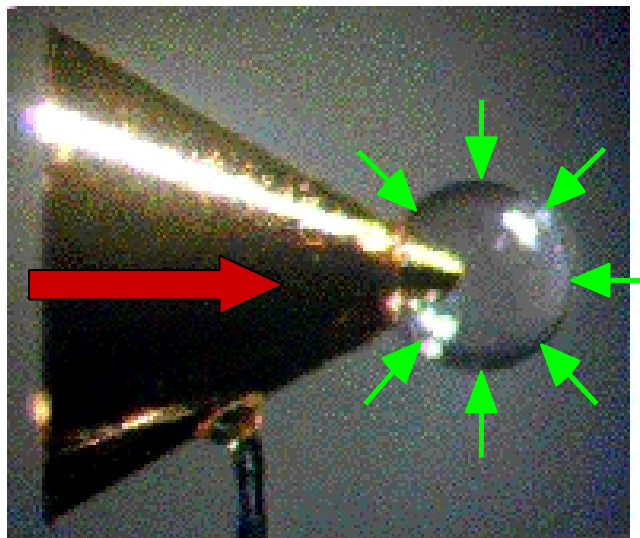


Fig 3.6 – Typical fast ignition capsule. Green arrows indicate compression beams and red arrow indicates heating beam.

In Fast Ignition the fuel assembly is relatively isochoric, with more mass assembled to a lower peak density [3.9], rather than isobaric in the case of central ignition. Greater fuel mass means greater fuel content and thus greater energy output. This translates into a higher gain (= energy out / energy in) for a given laser energy, with a threshold far smaller than conventional (central) ignition. This is shown in figure 3.7, which provides a generic prediction for the performance of Fast Ignition, if successful.

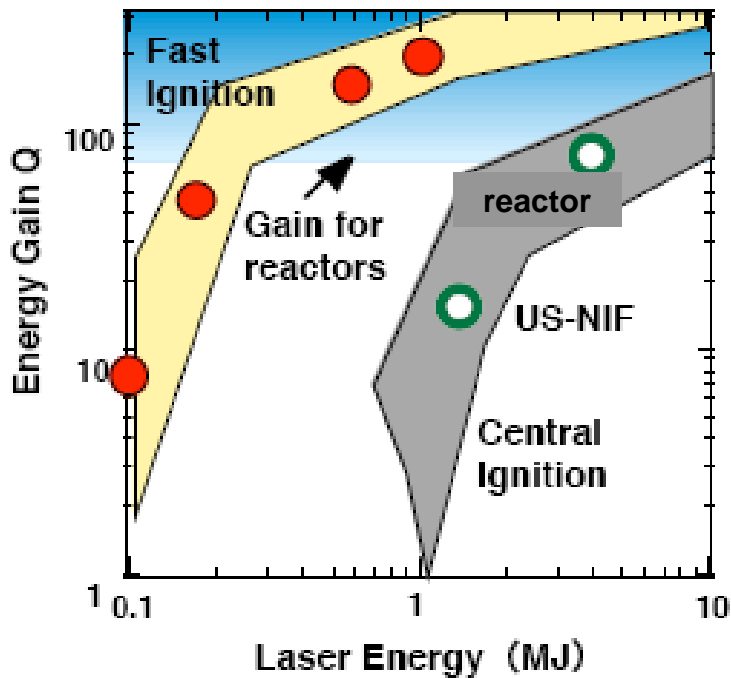


Fig 3.7 Energy gain as a function of laser size for “central ignition” and “fast ignition”.

Isochoric compression also has the advantage that the capsule implosion is less susceptible to hydrodynamic instabilities. The ratio of capsule radius to shell thickness is smaller. This parameter, known as the In-Flight Aspect Ratio, IFAR plays a role in the stabilisation of the implosion to RT instability and a smaller IFAR means a more stable implosion.

Experiments on this Fast Ignition scheme have now been underway for over 5 years, with very encouraging results. The first integrated fast ignition experiments with full compression and heating beam geometry were performed as part of a UK-Japanese collaboration using the GEKKO XII facility at Osaka University in Japan [3.12].

These experiments demonstrated the principle of the geometry and also showed that as the heater beam laser power increased from no laser to 0.5 PW the neutron yield obtained from D-D fusion reactions in the fuel increased from 10^4 to 10^7 . This showed that the injected electrons were contributing to the heating of the compressed fuel. However, MeV energy electrons would not classically be stopped in the density of fuel that was achieved in this experiment (~ 50 - 100 g/cc). This suggests that an anomalous stopping mechanism may have been responsible for the energy deposition and heating via the electrons. Electron energy transport and heating in ultra intense laser interactions with solid matter is now a wide and critical field of study to de-risk the concept of fast ignition.

In summary, Inertial Fusion Energy offers an attractive complementary solution to our long-term power production requirements. The physics of IFE is well understood, with net energy production due to be demonstrated using a conventional laser system in ~ 2010 on the National Ignition Facility in the USA. The path from there to a commercial power plant is still uncertain, with a large number of scientific and technological challenges. An advanced form of IFE known as “fast ignition” offers a particularly attractive solution, combining low capital facility cost with high efficiency and high energy output. HiPER is designed to explore the science of this approach and thus enable a future path to IFE power.

References

- [3.1] http://ipcc-wg1.ucar.edu/wg1/docs/WG1AR4_SPM_Approved_05Feb.pdf
- [3.2] J. Ongena, *Physica Scripta*, **T123**, 14 (2006)
- [3.3] J. D. Lawson, *Proceedings of the physical society B*, **70**, 6 (1957)
- [3.4] <http://www.ukaea.org.uk/>
- [3.5] ITER Technology special issue, *Fusion engineering and Design*, **55** (2001)
- [3.6] J. Nuckolls *et al*, *Nature*, **239**, 139 (1972)
- [3.7] J. Lindl, *Physics of Plasmas*, **2**, 3933 (1995)
- [3.8] H. Takabe *et al*, *Physics of Fluids*, **28**, 3676 (1985)
- [3.9] M. Tabak *et al*, *Physics of Plasmas*, **5**, 1626 (1994)
- [3.10] H. Azechi *et al*, *Plasma physics and controlled fusion*, **48**, B267 (2006)
- [3.11] J. H. Kelly *et al*, *Journal de Physique IV*, **133**, 75 (2006)
- [3.12] R. Kodama *et al*, *Nature*, **412**, 798 (2001), R. Kodama *et al*, *Nature*, **418**, 933 (2002)

4. The Fusion Science Case & Design

Preamble

HiPER will deliver a 3ω ($\lambda = 0.35 \mu\text{m}$), multi-beam, multi-ns-pulse of about 250 kJ and a 2ω beam of 70 kJ in about 15 ps. In this chapter we present studies on fast-ignitor targets driven by laser pulses with the HiPER parameters. First, we discuss general ignition and compression requirements, and present gain curves, based on an integrated model including ablative drive, compression, ignition and burn, and taking the coupling efficiency η_{ig} of the igniting beam as a parameter. It turns out that ignition and moderate gain can be achieved, provided that adiabat shaping is used in the compression and the efficiency η_{ig} exceeds 20%. Gains up to 100 could be obtained. According to present understanding, a 2ω ignition beam is required to make the hot-electron range comparable to the desired size of the hot spot. We then present a reference target and corresponding laser pulse family. Its design is based on 1D fluid simulation of compression, and 2D fluid and hybrid simulations of fast electron transport, ignition and burn. We have also performed preliminary analyses of the sensitivity to compression pulse shape, as well as to hot-electron source location, hot electron range and beam divergence. Models and perturbation codes have been used to study the Rayleigh-Taylor instability. Crucial issues for the design that have so far not been studied in detail include high-convergence cone-guided implosions, and the generation of the hot electron beam and its transport in low-to-moderate density plasmas. Here, we briefly review theoretical and computational studies, as well as experimental data, on such key issues. In addition, we report our recent preliminary work on the hydrodynamics of cone-guided targets and on laser-plasma interaction at ultra-high intensity.

4.1 Introduction

In this Chapter we study the case for fast ignition at total laser energy of 200 – 400 kJ, with less than 100 kJ for the igniting beams (the parameters envisaged for the HiPER facility [4.1]), and produce a preliminary target design and a set of laser beam specifications.

We recall that fast ignition [4.2, 4.3, 4.4] is an approach to Inertial Confinement Fusion (ICF) [4.5, 4.6] in which the ignition spark is created in a precompressed fuel by an ultraintense driver. It offers potential advantages [4.2, 4.4] (lower ignition threshold, higher energy gain, reduced sensitivity to Rayleigh-Taylor instability) over standard central ignition [4.5, 4.7]. On the other hand, it requires efficient coupling of an ultraintense beam to the compressed fuel; here, if the plasma density is 300 g/cm^3 , the beam has to deliver [4.8] 15–20 kJ in 20 ps into a volume with typical dimensions of about $20 \text{ }\mu\text{m}$.

In the standard Fast Ignition (FI) scheme [4.2] the hot spot is created by fast electrons generated by an ultraintense laser pulse. Crucial issues for the scheme are the efficient generation of a collimated beam of fast electrons and their transport from the critical density layer to the compressed fuel. Recent experiments [4.9, 4.10] indicate that the desired laser-fuel coupling might be achieved by using of conically guided laser beams. There, a hollow cone of high-Z material, inserted into an otherwise standard spherical target, provides an open path for the intense ignitor beam, which thus produces the hot electrons close to the compressed fuel. A coupling efficiency of about 25% was inferred in the aforementioned experiments [4.9, 4.10], in which the energy of the intense pulse was of a few hundred joules.

Overviews of fast ignition research have been published recently [4.11, 4.12]. A comprehensive review of status and perspectives of the scheme is provided by a series of technical papers [4.13].

The experiments to be performed within the next few years at OMEGA-EP [4.14] (Laboratory for Laser Energetics, University of Rochester) and at FIREX [4.15] (Institute of Laser Engineering, Osaka University) will test the fast ignition scheme at laser energy of 2.5 –10 kJ, thus providing much needed information on several key issues. Further data will be provided by experiments on PETAL [4.16], which is part of the HiPER project. In this report, we address the design of targets for a next step, namely, the demonstration of ignition. We pursue the same conically-guided concept, with direct-drive laser compression and laser-generated hot-electron driven ignition.

We start (Sec. 4.2) by briefly reviewing the ignition conditions and discussing how the ignition beam parameters depend on fuel density, laser-to-fuel coupling efficiency (η_{ig}), laser wavelength and hot electron penetration depth¹. Using scaling laws for fuel density and confinement parameter [4.18], we then estimate the compression laser energy. In Sec. 4.3 we use an integrated gain model to generate gain curves and analyze their sensitivity to various parameters. In particular, we show how ignition thresholds and gain critically depend on the control of instabilities during compression and on the efficiency η_{ig} . Following this preliminary analysis, we have designed a reference target, compressed by a 132 kJ laser pulse (with wavelength $\lambda = 0.35 \text{ }\mu\text{m}$). The design is based on one-dimensional (1D) simulations (complemented by instability analysis) of the implosion and compression of a spherical target, and on two-dimensional (2D) model simulations of the stages of ignition and burn. The latter assume that a beam of fast particles with given properties impinges onto the compressed fuel. Targets scaled from the reference one at smaller and larger energy have also been designed. First studies of the sensitivity of the design to parameter changes have also been carried out. It turns out that if a 100 kJ ignition laser beam can be adequately focused and coupled to the fuel with efficiency $\eta_{\text{ig}} \simeq 25\%$, targets compressed by 100–300 kJ pulses achieve energy gain in the range 50-100.²

The analysis and the results presented in Secs. 4.2–4.4 refer to a generic spherical target. Some

¹Secs. 4.2–4.4 summarize results presented in Ref. [4.17]

²Analogous conclusions have been reached in a recent study by the LLE team of Betti and coworkers [4.19].

specific features of the actual HiPER targets are discussed in Sec. 4.5–4.7. In particular Sec. 4.5 discusses the hydrodynamics of conically guided implosions. Interaction of the ultra-intense ignition beam and hot electron generation is discussed in Sec. 4.6, while hot electron transport in the dense fuel and stopping in the hot spot is dealt with in Sec. 4.7. An alternative option of fast ignition by laser accelerated protons is discussed in Sec. 4.8.

4.2 Basic driver requirements

4.2.1 Fast ignition: ignition laser and fuel compression requirements

General beam requirements for fast ignition were determined by a large series of two-dimensional (2D) numerical hydrodynamics simulations, where the ignition energy is injected in the form of fast particles impinging onto a sphere of precompressed DT, at uniform density ρ . Optimal values of the pulse energy E_{ig} and intensity I_{ig} to be delivered to the fuel can be parametrized as a function of the density as [4.8, 4.20]

$$E_{\text{ig}} = E_{\text{opt}} = 18 \left(\frac{\rho}{300 \text{ g/cm}^3} \right)^{-1.85} \text{ kJ}, \quad (4.1)$$

$$I_{\text{ig}} = I_{\text{opt}} = 6.8 \times 10^{19} \left(\frac{\rho}{300 \text{ g/cm}^3} \right)^{0.95} \text{ W/cm}^2. \quad (4.2)$$

Corresponding optimal pulse duration and focal spot size are

$$t_p = t_{\text{opt}} = 21 \left(\frac{\rho}{300 \text{ g/cm}^3} \right)^{-0.85} \text{ ps}; \quad r_b = r_{\text{opt}} \simeq 20 \left(\frac{\rho}{300 \text{ g/cm}^3} \right)^{-0.97} \mu\text{m}. \quad (4.3)$$

These results are obtained for parallel cylindrical beams of radius r_b (with box profiles in radius and time), of unspecified particles with preassigned penetration depth \mathcal{R} , uniform stopping power, and straight path. Replacing the box profiles with more realistic Gaussian profiles leads to energy requirements larger by about 30%. On the other hand, by exploiting hydrodynamics effects associated to beam stopping, it is also possible to achieve ignition with energy smaller (up to about 40%, according to some simulations) than the value of Eq. (4.1) [4.21, 4.22, 4.23]. We therefore continue to use Eq. (4.1) as a reference optimal ignition energy.

Equations (4.1)–(4.3) apply to particle penetration depth $0.3 \leq \mathcal{R} \leq \mathcal{R}_0 = 1.2 \text{ g/cm}^2$. For longer penetration depth the required energy and intensity increase approximately linearly with \mathcal{R} . Larger focal spots require larger energy, although they allow for smaller intensity. Eqs. (4.1) and (4.2) can indeed be extended to account also for non-optimal range and focal spot (and still optimal pulse duration), by writing [4.12, 4.24]

$$E_{\text{ig}} \geq E_{\text{opt}}(\rho) \times \max\left(1, \frac{\mathcal{R}}{\mathcal{R}_0}\right) \times \begin{cases} \max\left(1, \frac{r_b}{r_{\text{opt}}}\right), & r_b \leq 2.5 r_{\text{opt}} \\ 2.5 \left(\frac{r_b}{2.5 r_{\text{opt}}}\right)^2, & r_b \geq 2.5 r_{\text{opt}} \end{cases} \quad (4.4)$$

and

$$I_{\text{ig}} \geq I_{\text{opt}}(\rho) \times \max\left(1, \frac{\mathcal{R}}{\mathcal{R}_0}\right) \times \begin{cases} \min\left(1, \frac{r_{\text{opt}}}{r_b}\right); & r_b \leq 2.5 r_{\text{opt}} \\ 0.4. & r_b \geq 2.5 r_{\text{opt}}. \end{cases} \quad (4.5)$$

The above equations concern the energy actually delivered to the hot spot. The driver (laser in our case) energy will be larger than the energy delivered to the hot spot by a factor $(1/\eta_{\text{ig}})$,

with η_{ig} the coupling efficiency of the ultra-intense igniting beam. The driver intensity will be $I \simeq I_{\text{ig}}(r_{\text{b}}/r_{\text{f}})^2/\eta_{\text{ig}}$, where r_{f} is the focal spot radius. Taking the same radius r_{b} for both laser spot size and particle beam radius in the compressed fuel, the laser beam energy and intensity required for ignition will be, respectively,

$$E_{\text{ig}}^{\text{laser}} = E_{\text{ig}}/\eta_{\text{ig}}; \quad I_{\text{ig}}^{\text{laser}} = I_{\text{ig}}/\eta_{\text{ig}}. \quad (4.6)$$

Let us consider ignition by laser-produced hot electrons. For hot electron range, we use the standard parametrisation [4.12]

$$\mathcal{R} = 0.55 f_{\mathcal{R}} \frac{\lambda_{\text{ig}}}{1.06 \mu\text{m}} \left(\frac{I_{\text{ig}}^{\text{laser}}}{10^{19} \text{W/cm}^2} \right)^{\frac{1}{2}} \text{ g/cm}^2. \quad (4.7)$$

where $f_{\mathcal{R}}$ is a parameter of order unity (see below), $I_{\text{ig}}^{\text{laser}}$ is the incident laser intensity and λ_{ig} is the laser wavelength. Equation (4.7) is obtained by writing the hot electron range as

$$\mathcal{R} = 0.6 f_{\mathcal{R}} T_{\text{hot}} \text{ g/cm}^2, \quad (4.8)$$

and approximating the hot electron temperature T_{hot} as (see Ref. [4.25] and the discussion in Sec. 4.6)

$$T_{\text{hot}} = \left[\frac{I_{\text{ig}}^{\text{laser}}}{1.2 \times 10^{19} \text{W cm}^2} \left(\frac{\lambda_{\text{ig}}}{1.06 \mu\text{m}} \right)^2 \right]^{\frac{1}{2}} \text{ MeV}, \quad (4.9)$$

where $I_{\text{ig}}^{\text{laser}}$ is the incident laser intensity and λ_{ig} is the laser wavelength. The scaling laws provided by Eqs. (4.8)–(4.9), as well the parameter $f_{\mathcal{R}}$ will be discussed in Sec. 4.7.2.

The coupling efficiency η_{ig} depends on ultraintense laser absorption, hot electron generation and transport to the dense fuel. These complex processes are not yet fully understood (see, e.g., Ref. [4.26], and Secs. 4.6 and 4.7 below). In our models, we take the coupling efficiency η_{ig} , as a free parameter. As a reference value, we shall use $\eta_{\text{ig}} = 0.25$, as inferred from the quoted experiments on fast heating of compressed cone-guided targets [4.9, 4.10].

The previous equations show that the range of the hot electrons entering Eq. (4.4) cannot be taken as an independent variable. Indeed, it depends on the laser intensity $I_{\text{ig}}^{\text{laser}}$ [Eq. (4.6)], which, in turn, has to satisfy the ignition condition Eq. (4.5). General expressions for the laser ignition energy, obtained from Eqs. (4.4)–(4.7), are given in Ref. [4.17]. Here it suffices to give the expression applying to densities and focal spots of planned ignition experiments:

$$E_{\text{ig}}^{\text{laser}} \geq 93 \left(\frac{\rho}{300 \text{ g/cm}^3} \right)^{-0.9} \left[\frac{f_{\mathcal{R}} \lambda_{\text{ig}}}{0.5 \mu\text{m}} \frac{0.25}{\eta_{\text{ig}}} \right]^2 \text{ kJ}. \quad (4.10)$$

Laser energy thresholds for fast ignition versus fuel density are plotted in Fig. 4.1, for $\eta_{\text{ig}} = 0.25$ and different values of $f_{\mathcal{R}} \lambda_{\text{ig}}$. The thresholds given by Eq. (4.10) are shown by thick lines. The spot radius is limited to $r_{\text{b}} \geq r_{\text{min}} = 20 \mu\text{m}$ in Fig. 4.1a), and to $10 \mu\text{m}$ in Fig. 4.1b). We see that ignition with less than 100 kJ and focal spot $r_{\text{b}} \geq 20 \mu\text{m}$ (consistent with present experiments) requires $f_{\mathcal{R}} \lambda_{\text{ig}} \leq 0.5 \mu\text{m}$, i.e either range shortening and/or laser wavelength of $\frac{1}{2} \mu\text{m}$ or shorter. The fuel density should exceed 300 g/cm^3 . In the following, we shall take $f_{\mathcal{R}} \lambda_{\text{ig}} = 0.4 \mu\text{m}$ as a reference value. Finally, notice that when Eq. (4.10) applies, then $E_{\text{ig}}^{\text{laser}}$ is independent of r_{b} (for $r_{\text{b}} \leq 2.5 r_{\text{opt}}$). This may relax focussing requirements [4.12].

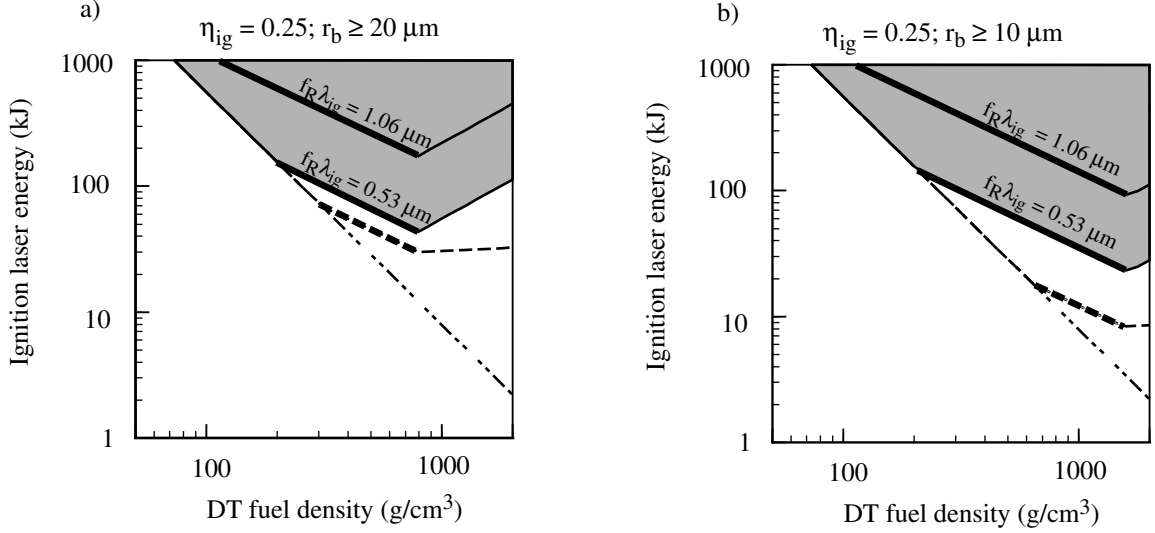


Figure 4.1: Laser ignition energy for hot-electron driven fast ignition versus density of the precompressed fuel, for different values of the parameter $f_{\mathcal{R}}\lambda_{ig}$ (see labels on the solid curves), and two different values of the minimum spot radius, (a) $r_b \geq 20 \mu\text{m}$; and (b) $r_b \geq 10 \mu\text{m}$. In both cases, the dashed curve assumes range independent of intensity and anyhow shorter than 1.2 g/cm^2 ; the dot-dashed line is the ignition scaling law that assumes optimal particle range and optimal beam radius. Both figures refer to intense beam coupling efficiency $\eta_{ig} = 0.25$. (Adapted from Ref. [4.17].)

4.2.2 Burn propagation, confinement parameter & compression laser energy

High gain also requires burn propagation from the hot spot to the whole compressed fuel. According to simulations [4.21, 4.27, 4.24], this can be achieved if the fuel confinement parameter (areal density) $\langle \rho R \rangle = \int \rho dR$ exceeds $1\text{--}1.5 \text{ g/cm}^2$.

The confinement parameter achieved by a target implosion depends on target design and laser pulse characteristics. For laser direct-drive and optimized targets with initial aspect ratio in the range 2–6, according to Betti and Zhou [4.18] we can write

$$\langle \rho R \rangle_{\text{max}} = \frac{1.46}{\alpha_{if}^{0.55}} \left(\frac{0.35 \mu\text{m}}{\lambda_c} \right)^{1/4} \left(\frac{E_c^{\text{laser}}}{100 \text{ kJ}} \eta_a \right)^{0.33} \left(\frac{u_{\text{imp}}}{3 \times 10^7 \text{ cm/s}} \right)^{0.06} \text{ g/cm}^2 \quad (4.11)$$

where u_{imp} is the implosion velocity, α_{if} is the isentrope parameter³ at the shell inner surface at the end of the acceleration stage, E_c^{laser} is the energy of the compression laser pulse, and η_a is the absorption efficiency. From Eq. (4.11) we find that adequate areal density can be achieved by an implosion driven by 100–150 kJ of laser light, if the fuel isentrope parameter is $\alpha_{if} \leq 1$.

We then address the requirements set by the high fuel density needed for efficient ignition. Again according to Ref. [4.18], the peak density achieved as the implosion stagnates is well fitted by

$$\rho_{\text{max}} = \frac{788}{\alpha_{if}} \left(\frac{I_0}{10^{15} \text{ W/cm}^2} \frac{0.35 \mu\text{m}}{\lambda_c} \right)^{0.13} \left(\frac{u_{\text{imp}}}{3 \times 10^7 \text{ cm/s}} \right)^{0.96} \text{ g/cm}^3, \quad (4.12)$$

³The isentrope parameter is defined as ratio of the actual matter pressure to pressure of degenerate matter at the same density; for equimolar DT, $\alpha = P(\text{Mbar})/2.1\rho^{5/3}$, with ρ in units of g/cm^3 .

where I_0 is the compression laser intensity (measured at the initial shell outer radius). Assuming that the average density of the igniting fuel is $\rho = 0.6\rho_{\max}$ we then find that density $\rho = 300\text{--}350\text{ g/cm}^2$ is obtained for u_{imp} in the range $2.1\text{--}2.4 \times 10^7\text{ cm/s}$, if $\alpha_{\text{if}} = 1$, and the intensity is limited to $I_0 \leq 3 \times 10^{14}\text{ W/cm}^2$. It is worth observing that this is considerably smaller than that required for central ignition of a small capsule $[(3.5\text{--}4) \times 10^7\text{ cm/s}]$, and thus makes the imploding capsule more robust with respect to Rayleigh-Taylor instability (RTI). Betti and Zhou [4.18] have designed targets with even smaller implosion velocity, which is feasible due to the choice of a smaller isentrope ($\alpha_{\text{if}} = 0.7$) and higher intensity ($I_0 = 10^{15}\text{ W/cm}^2$). A better appraisal of design options and constraints will follow from the model discussed in the next section.

4.3 Gain curves

In this section, we analyze design options in parameter space, using gain curves $G = G(E_{\text{tot}})$ generated by a simple integrated gain model. In the following $G = E_{\text{fus}}/E_{\text{tot}}$ is the target energy gain, E_{fus} is the energy released by fusion reactions, and $E_{\text{tot}} = E_{\text{c}}^{\text{laser}} + E_{\text{ig}}^{\text{laser}}$ is the total laser energy.

4.3.1 Constrained gain model

The gain model we use, detailed in Ref. [4.17], is based on that developed by Tabak and Callahan [4.28, 4.12] and is similar to that of Ref. [4.19]. We refer to single-shell all-DT targets imploded by direct laser irradiation, and take into account laser driven ablation and pressure generation, rocket-like implosion, pressure and density multiplication at stagnation [4.18], and then fast ignition, burn and depletion of the compressed fuel. For ignition we use the results of Sec. 4.2.1, applied to a fuel assembly with density $\rho = 0.6\rho_{\max}$, with ρ_{\max} given by Eq. (4.12). For the burn fraction we take

$$\Phi = \frac{\langle \rho R \rangle}{\langle \rho R \rangle + H_{\text{B}}} \times \min \left[1, \left(\frac{\langle \rho R \rangle}{1.5\text{ g/cm}^2} \right)^2 \right], \quad (4.13)$$

with $\langle \rho R \rangle$ given by Eq. (4.11), and $H_{\text{B}} = 7\text{ g/cm}^2$. Above the threshold $\langle \rho R \rangle = 1.5\text{ g/cm}^2$, this is just the standard expression for burn efficiency in inertial confinement fusion.

The model gives a unique value of the gain for each set of values of total laser energy E_{tot} , compression laser intensity I , shell in-flight-aspect-ratio A_{if} (discussed below), for given values of the wavelengths λ_{c} of the compression laser and λ_{ig} of the ignition laser, and of the additional free parameters, namely the in-flight-shell isentrope α_{if} , the absorption efficiency of the compression laser λ_{c} , and the range multiplier $f_{\mathcal{R}}$. In the following, we shall use the model to generate gain curves $G = G(E_{\text{tot}})$, by taking the maximum gain at a given E_{tot} , for appropriately constrained values of I , A_{if} , of the free parameters of the model, and of the RTI growth factor Γ_{\max} .

This latter factor is introduced to take into account in a simple way the limitations set by the Rayleigh-Taylor instability (RTI)⁴ at the ablation front, which threatens shell integrity during the implosion. Indeed, growth of RTI perturbations must be kept below some maximum level. We enforce this in our gain curves, by requiring that the maximum exponential RTI growth factor $\Gamma_{\max} \leq 6$, where $\Gamma_{\max} = \max_l [\int \gamma_l(t) dt]$, and γ_l is the linear growth rate of spherical mode l . According to our model,

$$\Gamma_{\max} = \frac{\alpha_{\text{T}}^2 A_{\text{if}}}{3\beta_{\text{T}}(1-x)r_{\alpha}}, \quad (4.14)$$

where x is the payload mass fraction (imploding mass to shell mass at the onset of the laser main pulse), α_{T} and β_{T} are the so-called Takabe coefficients [4.29], for which we take the values [4.30]

⁴see, e.g., refs. [4.5] and [4.6], and the extensive literature quoted therein.

$\alpha_T = 0.95$ and $\beta_T = 2.7$, and $r_\alpha(x)$ is a parameter taking the shape of the entropy profile into account. For shells driven by standard shaped pulses generating a uniform entropy profile in the shell, $r_\alpha = 1$. In such a case, the in-flight-aspect-ratio A_{if} of direct-drive shells with $x \simeq 0.6$ must be limited to about 22, which does not allow to achieve the needed implosion velocity.⁵

This occurs because a low isentrope is required in order to achieve the desired fuel compression keeping the drive energy reasonable, but low entropy of the materials to be ablated also means low ablation velocity, and hence modest RTI growth reduction by ablation. RTI growth can instead be reduced, without degrading compression substantially, by using adiabat shaping techniques [4.31, 4.32, 4.12], which produce low entropy in the payload and much higher entropy in the ablator. In our design (see Sec. 4.4) we implement adiabat shaping by the type-2 relaxation method proposed in Ref. [4.32]. The effect of this entropy-shaped profile on RTI growth is taken into account by the factor $r_\alpha(x)$. For our designs, $r_\alpha \simeq 1.7$ for $x = 0.4$ and $r_\alpha \simeq 2$ for $x = 0.6$. We can then allow for values of A_{if} as large as 45.

4.3.2 Reference gain curve & sensitivity to parameters

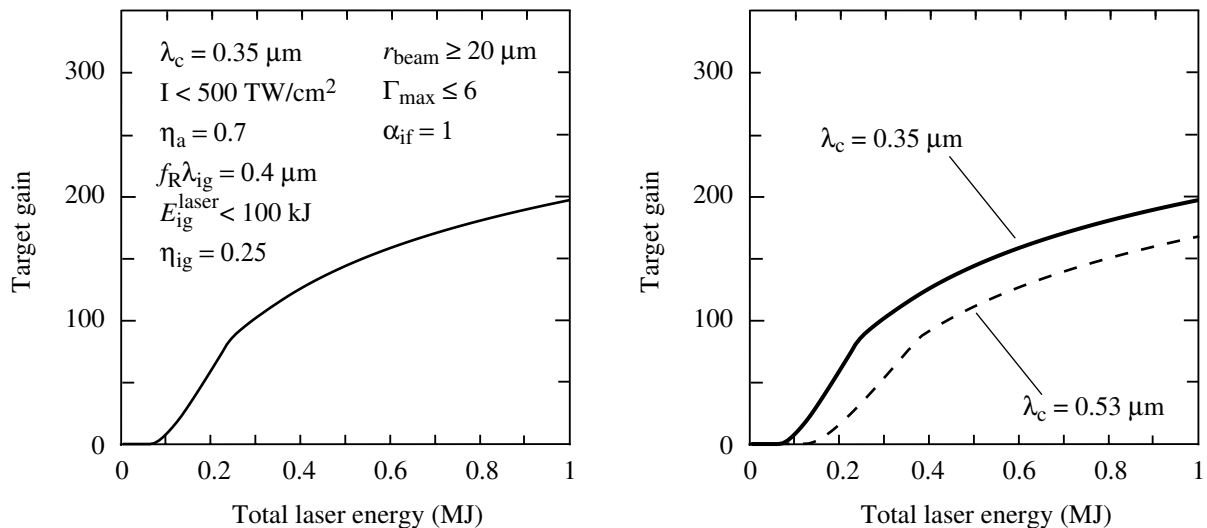


Figure 4.2: Reference gain curve (solid) and values of the relevant parameters; right hand side frame: the same reference curve and (dashed) a curve for $\lambda_c = 0.53 \mu\text{m}$ and the same limitation to $I_c^{\text{laser}} \lambda_c^2$ as in the reference case. In this case ignition cannot be achieved with $E_{\text{ig}}^{\text{laser}} \leq 100 \text{ kJ}$; the curve is for $E_{\text{ig}}^{\text{laser}} = 150 \text{ kJ}$.

The model above has been used to generate gain curves and study their sensitivity to parameters. In our analysis we take focal spot size $r_b \geq 20 \mu\text{m}$. With one exception, we take compression laser wavelength $\lambda_c = 0.35 \mu\text{m}$. A reference gain curve, shown in Fig. 4.2, has been obtained by setting $f_{\mathcal{R}} \lambda_{\text{ig}} = 0.4 \mu\text{m}$, $\eta_a = 0.7$, $\eta_{\text{ig}} = 0.25$, $\alpha_{\text{if}} = 1$ (with adiabat shaping), and limiting the intensity

⁵For the sake of comparison with other designs, it is worth mentioning the relation between A_{if} and the commonly used *IFAR*, defined as the ratio of the shell radius to the shell thickness, when the shell radius is (3/4) of the initial inner radius, and the shell thickness is the distance between densities that are $1/e$ times the peak density. We approximately have $(IFAR) \simeq A_{if}/[1.2(1-x_{\text{av}})r_\Delta]$. Here the coefficient 1.2 is the so-called ice-block factor [4.5, 4.12] accounting for the non-uniform profile of an equilibrium, flat-adiabat, accelerating layer, the factor $(1-x_{\text{av}})$ accounts for ablation up to the time $t = t_{\text{av}}$ when *IFAR* is measured, and r_Δ for the increase in thickness due to adiabat shaping. For the reference design discussed later, we get $(IFAR) \simeq 0.75A_{if}$, in agreement with simulations.

Table 4.1: Values of the model parameters used to generate the gain curves of Fig. 4.2 and Fig. 4.3

curve label	η_a	α_{if}	shaping	$(E_{ig}^{laser})_{max}$ (MJ)	η_{ig}	$f_{\mathcal{R}}\lambda_{ig}$ (μm)
a)	0.7	1	yes	0.1	0.25	0.4
b)	0.7	1	yes	0.5	0.25	0.4
c)	0.85	0.7	yes	0.1	0.33	0.4
d)	0.7	1	no	0.1	0.25	0.4
e)	0.7	1	no	0.5	0.25	0.4
f)	0.7	1	yes	0.1	0.25	1
g)	0.7	1	yes	0.5	0.25	1
h)	0.7	1	yes	0.5	0.15	0.4
i)	0.7	1.5	yes	0.5	0.25	0.4

to $I < 5 \times 10^{14} \text{W/cm}^2$, the RTI growth factor to $\Gamma_{max} < 6$, and the ignition laser pulse energy to $E_{ig}^{laser} < (E_{ig}^{laser})_{max} = 100 \text{ kJ}$. (In fact, $E_{ig}^{laser} \simeq 100 \text{ kJ}$ along all the curve, but at the lowest total energies.) We see that the threshold for gain is about 100 kJ of total laser energy, while $G = 50$ is achieved at $E_{tot} \simeq 200 \text{ kJ}$ and $G = 100$ at $E_{tot} = 320 \text{ kJ}$.

The use of a longer laser wavelength, namely $\lambda_c = 0.53 \mu\text{m}$, requires an ultraintense pulse of about 150 kJ (well above HiPER specifications), and raises the total energy for ignition to about 200 kJ. Moreover this choice lowers the gain substantially at energy of a few hundred kJ (see the dashed curve in the right hand side frame of Figure 4.2). We therefore tentatively discard the 2ω option for HiPER.

In Fig. 4.3 we show how the gain curves change when different values are assumed for some of the above parameters (see Table 4.1). Here curve a) is the reference curve discussed above. Curve b) shows that allowing for larger ignition laser does not affect the low energy portion of the gain curve, but leads to higher gain at large driver energy: $G = 255$ at $E_{tot} = 1 \text{ MJ}$. Curve c) shows that for optimistic assumptions on absorption efficiency ($\eta_a = 0.85$), intense beam coupling efficiency ($\eta_{ig} = 0.33$), and adiabat ($\alpha_{if} = 0.7$), the ignition threshold becomes as small as 50 kJ and gain $G = 100$ is obtained at $E_{tot} = 100 \text{ kJ}$. We instead see [curve e)] that replacing the adiabat-shaped implosion with a flat-adiabat one the ignition threshold raises to $E_{tot} \simeq 250 \text{ kJ}$. Curve g) shows that the choice of $f_{\mathcal{R}}\lambda_{ig} = 1 \mu\text{m}$, i.e. of longer ignition laser wavelength λ_{ig} and/or larger range multiplier $f_{\mathcal{R}}$ leads to a dramatic increase of the ignition threshold. Notice that in both cases the ignition laser energy is well above 100 kJ. No gain can be achieved, instead, with $E_{ig}^{laser} < 100 \text{ kJ}$ [see curves d) and f)]. Finally, curve h) shows the effect of lowering the coupling efficiency to $\eta_{ig} = 0.15$, and curve i) that of increasing the adiabat to $\alpha_{if} = 1.5$. In both cases we allow for ignition laser energy up to 0.5 MJ.

4.3.3 Design space analysis at total energy of 250 kJ

The above gain curves indicate that significant gain can be achieved at total laser energy of 200–250 kJ, if a few key parameters take the assumed reference values. This suggest a more detailed analysis of the design space at total driver energy of 250 kJ. In Figure 4.4a) we show iso-gain contours in the intensity vs in-flight-aspect-ratio (I, A_{if}) plane. In the same plane we also show contours of the RTI growth factor Γ_{max} . We see that maximum gain is achieved at an intensity of about 10^{14} W/cm^2 . However, the gain depends weakly on I . Increasing I allows to operate at lower A_{if} and lower Γ_{max} , although at the expense of increased risk of undesired negative effects

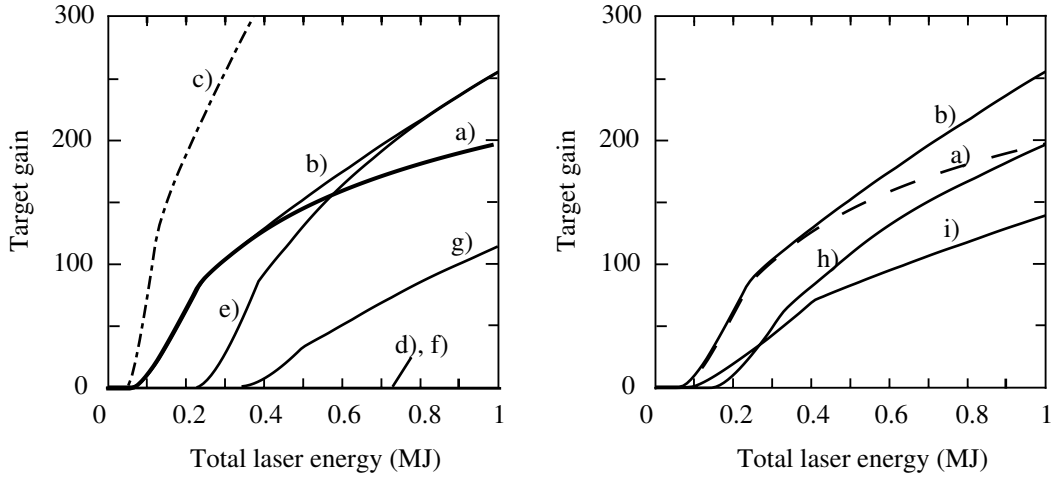


Figure 4.3: Gain curves obtained from the gain model, with values of the parameters as listed in Table. 4.1. b) as the reference curve but allowing for a larger ignition energy, $E_{\text{ig}}^{\text{laser}} < (E_{\text{ig}}^{\text{laser}})_{\text{max}} = 0.5$ MJ; c) with optimistic assumptions on $\eta_a = 0.85$, $\eta_{\text{ig}} = 0.33$, and $\alpha_{\text{if}} = 0.7$; curve e) refers to a flat-adiabat target; curve g) to the case with $f_{\mathcal{R}}\lambda_{\text{ig}} = 1 \mu\text{m}$; curve h) refers to smaller $\eta_{\text{ig}} = 0.15$; curve i) to larger adiabat, $\alpha = 1.5$. (Adapted from Ref. [4.17].)

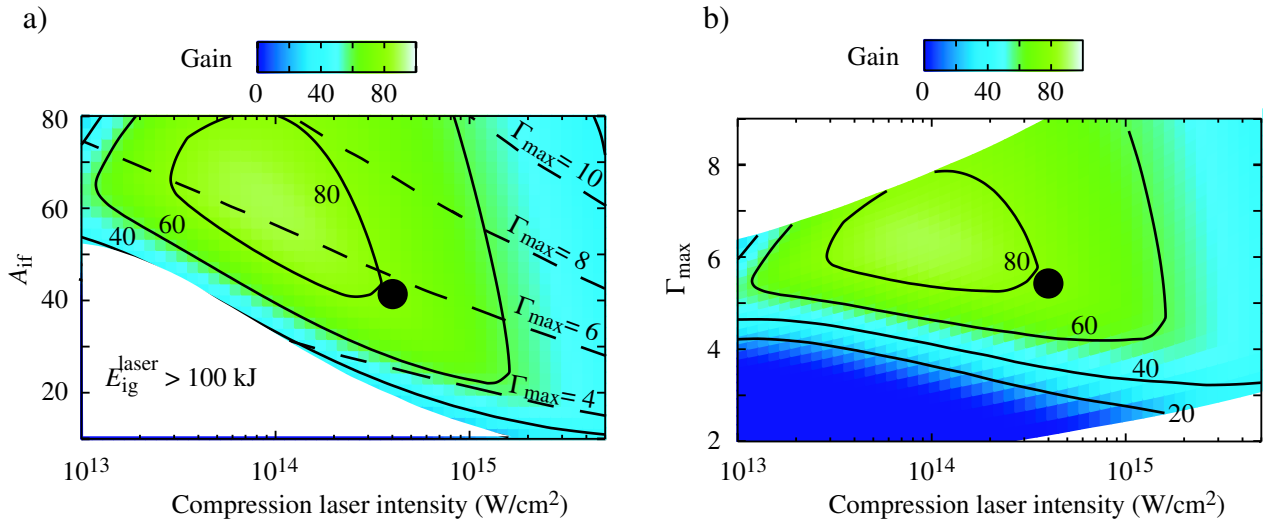


Figure 4.4: Iso-gain contours for 250 kJ total driver energy a) in the intensity vs A_{if} plane; b) in the plane intensity vs maximum RTI exponential growth factor Γ_{m} . Values of the parameters are $\lambda_c = 0.35 \mu\text{m}$; $\eta_a = 0.7$; $f_{\mathcal{R}}\lambda_{\text{ig}} = 0.4 \mu\text{m}$; $\eta_{\text{ig}} = 0.25$; $\alpha_{\text{if}} = 1$ (with adiabat shaping). In a) the dashed curves indicate the values of the Γ_{m} , and the white area on the lower left hand side corresponds to targets requiring $E_{\text{ig}}^{\text{L}} > 100$ kJ. The reference design point is indicated by the filled circle, and corresponds to the maximum gain which can be achieved with $\Gamma_{\text{max}} < 6$ and $A_{\text{if}} < 45$. (Adapted from Ref. [4.17].)

due to laser-plasma parametric instabilities. Figure 4.4b) shows similar gain curves in the intensity vs maximum RTI growth factor plane. We see that large gain can be achieved for a wide range of compression laser intensities, while limiting the growth of RTI.

According to the above results we choose laser intensity in the range $(3-5) \times 10^{14} \text{W/cm}^2$ and design the laser pulse in order to achieve entropy shaping with the goal of keeping $\alpha_{\text{if}} \simeq 1$ at the inner surface of the imploding shell. The black circles in Figs. 4.4a) and b) indicate the selected operating point in the relevant spaces.

4.4 Target design

We have designed a family of targets driven by compression pulses in the range 90–260 kJ, with the reference case driven by 132 kJ. We consider compression laser wavelength of $0.35 \mu\text{m}$ and assume tangential focusing with $f/18$ lenses, and parabolic intensity distribution within each beam. In order to limit dangerous effects of plasma and hydro-instabilities we allow for a peak intensity of $5 \times 10^{14} \text{W/cm}^2$ and for maximum RTI growth factor $\Gamma_{\text{max}} < 6$, respectively.

Target design has been based on 1D simulations of target implosions, and on 2D simulations of ignition and burn, assuming an initially symmetric fuel configuration and ignition by an external beam. Important symmetry issues related to cone-guide, as well as issues concerning electron beam generation and transport are not considered here. Some of them are discussed in later sections.

The design has been performed by using the Rome’s group codes IMPLO [4.33] and DUED [4.34], but several aspects have been subsequently analysed with Madrid’s codes (SARA [4.35] and a 2D hybrid code [4.36]), and by the CELIA’s code CHIC [4.37]. The three groups independently confirm most of the results. In a presently preliminary analysis, the CELIA group obtains the same fuel density as obtained by IMPLO, but somewhat lower confinement parameter. This may be due either to different assumptions concerning beam geometry, or different physical models for radiation. However, the reference performance is recovered by increasing the laser energy, still remaining in the foreseen HiPER operating window.

The IMPLO physical model includes two-temperature (2T) Lagrangian hydrodynamics, with flux-limited conductivities, real matter equation-of-state, and 2D laser-beam ray-tracing, accounting for plasma refraction and inverse bremsstrahlung absorption. Very simple models for radiation transport have been used. Most of the simulations just include bremsstrahlung losses from the corona and from the hot spot. We have also performed simulations with a three-temperature (3T) model in which radiation is transported via single group flux-limited diffusion. Comparing simulations with the two models (as well as CHIC and SARA simulations with multi-group diffusion models), we observe negligible differences in the ablation and implosion stages. The 3T simulations lead to slightly lower peak density and about 20% lower maximum confinement parameter of the compressed fuel. This is due to reabsorption of the bremsstrahlung emitted by the hot spot at the shell inner surface, just about the time of shell stagnation. However, the effect is probably overestimated by the 3T model which underestimates the mean free path of the energetic photons coming from the hot spot, thus concentrating energy deposition in a thin layer surrounding the hot spot.

Ignition and burn stages have then been studied with DUED 2D simulations taking as initial conditions the compressed spherically symmetric configuration computed by the previous 1D simulations. The fuel is then irradiated by a cylindrical beam (with box profiles in space and time) of particles with assigned penetration depth and constant stopping power. In the version used in this study, DUED includes 3T hydrodynamics, flux limited conductivities, real matter equation of state, deuterium-tritium fusion reactions, fuel depletion, alpha-particle single-group time-dependent diffusion, as well as the above model for the heating by the external particle beam. The code uses a Lagrangian mesh, with discrete, conservative automatic rezoning. Additional ignition simulation

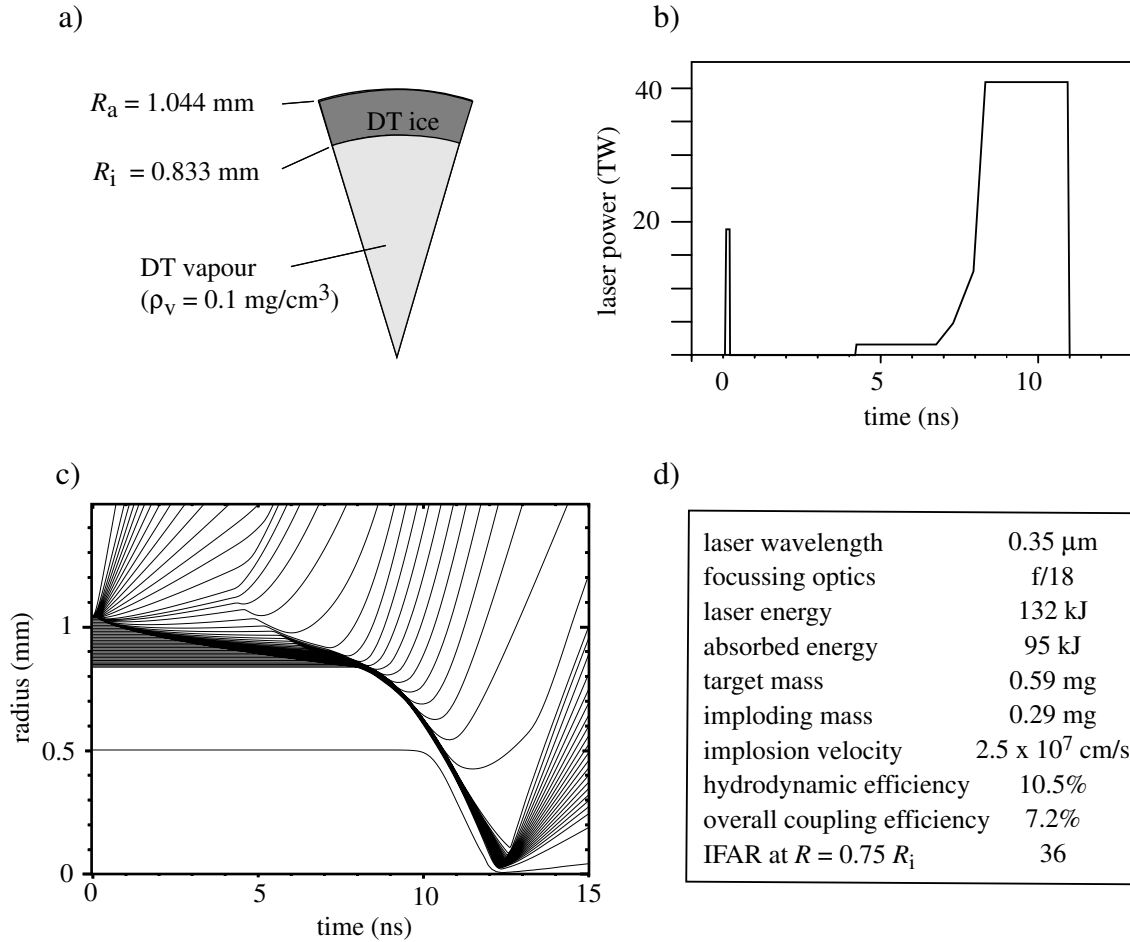


Figure 4.5: Reference target, imploded by a 132 kJ laser pulse: a) target sketch, b) laser pulse (notice the adiabat-shaping prepulse), c) Radius vs time flow chart (for the sake of clarity, only a small number selected lagrangian trajectories are shown); d) drive parameters and main implosion results. (Adapted from Ref. [4.17].)

have been performed with the hybrid code [4.36], studying ignition triggered by a more realistic Maxwellian electron beam originating at some distance from the compressed fuel. Results of this study are reported in Sec. 4.7.3

4.4.1 Reference design

We consider a very simple, all-DT target concept. A more realistic design will probably include some degree of high-Z dopant in order to avoid radiative preheating of the fuel and employ a DT-filled, very low-density plastic foam as an ablator.

Our reference design is shown in Fig. 4.5. The all-DT capsule has a mass of 0.59 mg, 50% of which is ablated. The laser pulse [see Fig. 4.5b)], with total energy of 132 kJ, consists of an intense picket, with power of 19 TW and FWHM of 125 ps, followed, after about 4 ns, by the compression pulse. The first picket serves to shape the adiabat by using type-2 relaxation [4.32]; when the main pulse peaks, the adiabat has a minimum value of about 0.8 at the inner surface and is about 8 at the ablation front. At this time about 20% of the mass has already been ablated. The transit of the final shock raises the in-flight-adiabat at the inner surface to about 1.

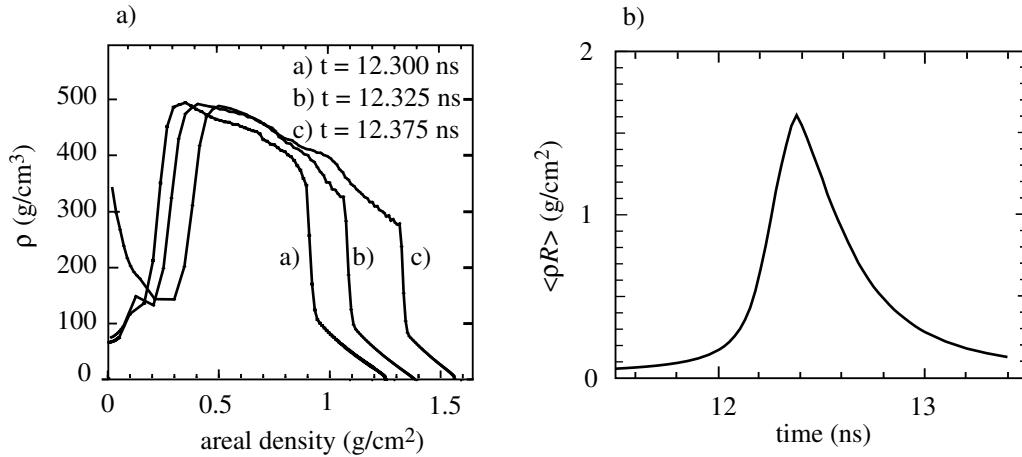


Figure 4.6: For the same target as in Fig. 4.5, fuel density vs areal density $\int \rho dR$ at times about compression maximum, and b) time evolution of the confinement parameter $\langle \rho R \rangle$. (Adapted from Ref. [4.17].)

Implosion and compression

The implosion radius-vs-time flow chart and some of the main parameters and implosion results are shown in Figs. 4.5c) and d), respectively. The density peaks to about 500 g/cm³ (see Fig. 4.6a) at time $t = 12.3$ ns and is larger than 300 g/cm³ over a large portion of the target. Notice, however, that an outer portion of the fuel (with areal density of about 0.2 g/cm²) has not been reached yet by the reflected shock and stays at much lower density. Here the igniting particles will deposit rather ineffectively part of their energy. Figure 4.6b) shows that the areal density peaks at 1.58 g/cm² at time $t = 12.375$ ns, and stays above 1.2 g/cm² during an interval of about 200 ps.

RTI growth at the ablation front

We have analyzed RTI growth by computing the growth factor $\Gamma(l)$, using the values of acceleration, radius, ablation rate and peak density from 1D simulations. The resulting growth factors are plotted in Fig. 4.7 for the reference target as well as for a scaled target driven by a 262 kJ beam (see below). In the figure we also show Γ_l for the same targets driven by pulses generating flat adiabat profiles (and resulting in the same values of final density, implosion velocity and confinement parameter). We see that adiabat shaping almost halves RTI growth. The fastest growing modes have $l \simeq 200$ and maximum growth factor $\Gamma_{\max} \simeq 5$. These results have been recently been confirmed by an analysis performed by the CELIA group using the PERLE perturbation code [4.38]. (Actually, PERLE predicts slightly lower growth rates.)

Scaled targets

The reference target and pulse can be scaled in size and energy in a straightforward manner. We simply keep fixed the laser intensity and the shell initial aspect ratio, and scale mass and energy as R^3 , and times as R . Taking the previous target, with mass $M_0 = 0.59$ mg as reference, we designed a *small* target with mass $(2/3)M_0$ and a *large* target with mass $2M_0$. After scaling, the pulse has been optimized by small changes to the initial picket. The main target parameters are summarized in Table 4.2. Simulations show that all targets achieve nearly the same density, in agreement with Eq. (4.12), while the areal density scales in good agreement with Eq. (4.11).

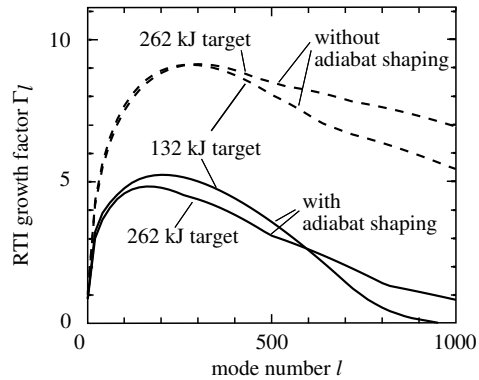


Figure 4.7: RTI exponential growth factors Γ_l for the target of Fig. 4.5, and for a larger scaled target, with and without adiabat shaping. (From Ref. [4.17].)

Table 4.2: Main parameters of the three targets studied in this report.

	<i>small</i>	reference	<i>large</i>
outer radius (mm)	0.912	1.044	1.316
inner radius (mm)	0.728	0.833	1.050
total mass (mg)	0.39	0.587	1.17
E_c^{laser} (kJ)	89	132	263
max $\langle \rho R \rangle$ (g/cm ²)	1.33	1.58	1.99
max fusion yield (MJ)	6.5	13	38
max $\langle \rho R \rangle$ (g/cm ²) (3T model)	1.06	1.28	1.62

Ignition and burn

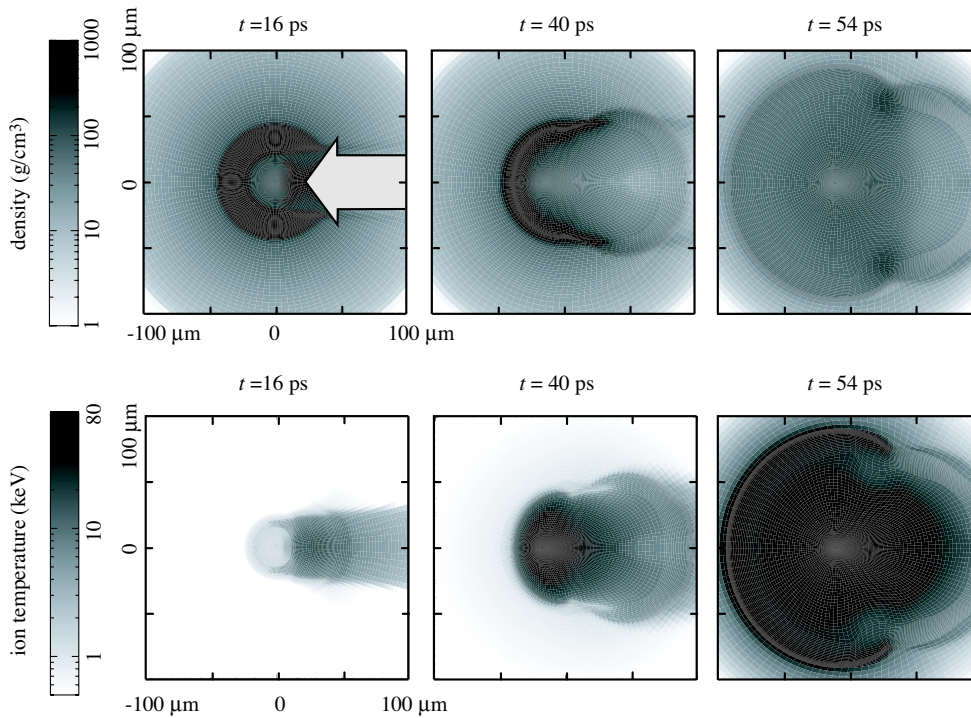


Figure 4.8: 2D simulation of the beam-driven fast-ignition and subsequent burn of the target illustrated in Fig. 4.5. The frames show density and temperature maps at selected times. The origin of time here corresponds to time $t = 12.35$ ns in the 1D simulation. Beam parameters are given in the main text. The arrow in the top left frame indicates the incoming particle beam. (From Ref. [4.17].)

An example of a 2D simulation of the ignition of the reference target is shown in Fig. 4.8. The 1D, 2T IMPLO results at time $t = 12.35$ ns have been taken as initial conditions. A 16-ps long, $20 \mu\text{m}$ in radius, pulse of particles with assigned penetration depth \mathcal{R} impinges on the fuel. In this case, $\mathcal{R} = 1.2 \text{ g/cm}^2$, the beam intensity is 10^{20} W/cm^2 , and the total particle beam energy is 20 kJ. Assuming coupling efficiency $\eta_{\text{ig}} = 0.25$, the laser intensity is $4 \times 10^{20} \text{ W/cm}^2$ and the assumed range is consistent with Eq. (4.7) with $f_R \lambda_{\text{ig}} \simeq 0.4 \mu\text{m}$. The corresponding ignition laser energy is 80 kJ. According to the 2D simulation, the target releases 13 MJ of fusion energy, which, assuming again $\eta_{\text{ig}} = 0.25$, results in gain $G \simeq 60$. Similar results (with gain in the range $G = 52$ – 57) are obtained with intensity reduced to $7.5 \times 10^{19} \text{ W/cm}^2$, somewhat longer pulse and/or larger focal spot, and total beam energy of 18–20.5 kJ. In these cases, $f_R \lambda_{\text{ig}} \simeq 0.5 \mu\text{m}$.

When the initial condition is taken from the 1D, 3T IMPLO simulation (giving smaller confinement) the fusion yield is estimated to decrease to about 10 MJ, and the gain to 40. Detailed computations are in progress.

4.4.2 Gain scaling & preliminary sensitivity analysis

Gain scaling vs total laser energy

We have performed a series of runs for each of the three targets studied in the previous section. When beam parameters and beam synchronization are optimized, the targets compressed by 92,

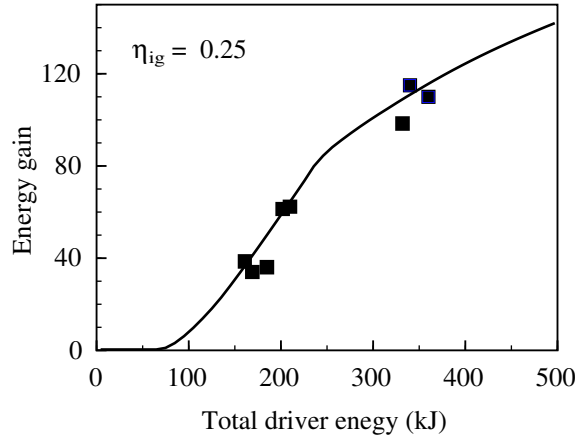


Figure 4.9: Gain vs total laser energy. Points: Data from 2D simulations (such as that of Fig. 4.8), assuming coupling efficiency of the fast ignition beam $\eta_{ig} = 0.25$. Curve: reference gain curve, as in Fig. 4.2. (From Ref. [4.17].)

132, and 270 kJ pulses, release about 6, 13 and 38 MJ of fusion energy, respectively. In all cases the energy of the igniting particle beam is 18–20 kJ and the fast particle penetration depth is 0.9 or 1.2 g/cm². Assuming again $\eta_{ig} = 0.25$, the target gains are about 40, 60, and 110 respectively. As shown in Fig. 4.9, these results are in good agreement with the reference gain curve shown in Fig. 4.2 and discussed in Sec. 4.4.

Sensitivity to electron range, timing, pulse shaping

We have also analyzed the sensitivity of our results to compression pulse timing, to a few beam parameters of the ignition beam, and to relative timing of the two pulses.

Analysis with CHIC shows that 10% variation of foot power implies 10% variation of peak density and areal density. The density appears to be more sensitive to variations than the areal density. The required shock timing accuracy is estimated to be about ± 200 ps.

We have then analyzed how fusion performance depends on particle penetration depth and igniting beam energy. As shown in Fig. 4.10a), we find that for each value of the penetration depth there is a sharp ignition threshold. Such a threshold depends on \mathcal{R} , with optimal $\mathcal{R} \simeq 1.2$ g/cm³ for the reference target. This is clearly seen in Fig. 4.10b), where the ignition energy is plotted as a function of \mathcal{R} for the three considered targets.

Finally, concerning the synchronization of the ignition pulse with the compression pulse, we find that the ignition pulse must be fired within a 75–100 ps window, centered about 30–50 ps before the time of peak $\langle \rho R \rangle$. The window widens somewhat with increasing beam energy (see Fig. 4.11).

4.5 Hydrodynamics of conically-guided implosions

Our design has been based on 1D spherically symmetric simulations of fuel implosions. However, the most promising approach to fast ignition relies on cone-guided implosions. Detailed studies of radiation driven NIF-size or reactor-size targets by US groups indicate that the presence of the cone does not influence very much the achievable peak compression and fuel confinement [4.39]. By proper cone and target design cone guided shells can even achieve higher ρR than equivalent spherical shells. Simulations of present, lower energy experiments, as well as of planned FIREX-I

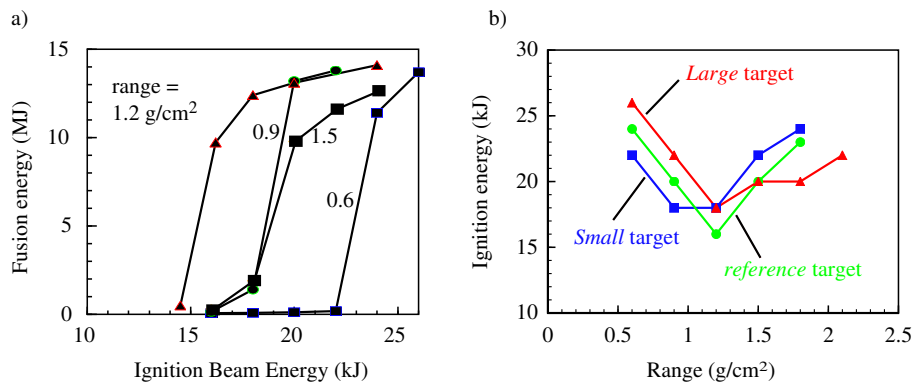


Figure 4.10: a) Fusion energy vs energy delivered by the igniting beam, for the reference target and different values of the penetration depth of the igniting particles; b) Ignition energy vs range for the three targets considered in the present study. (From Ref. [4.17].)

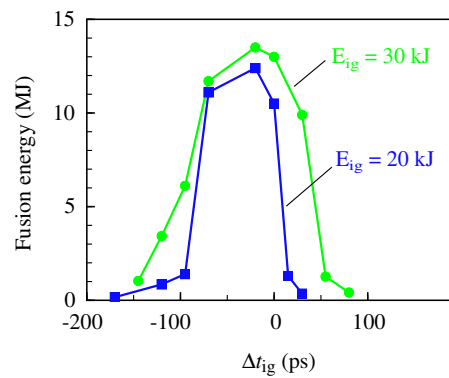


Figure 4.11: For the reference target, fusion energy vs timing of the ignitor beam. Here, $\Delta t_{ig} = t_{igp} - t_{\rho R}$, where t_{igp} is the time at which the ignition pulse is fired and $t_{\rho R}$ is the time at which the areal density is a maximum. (From Ref. [4.17].)

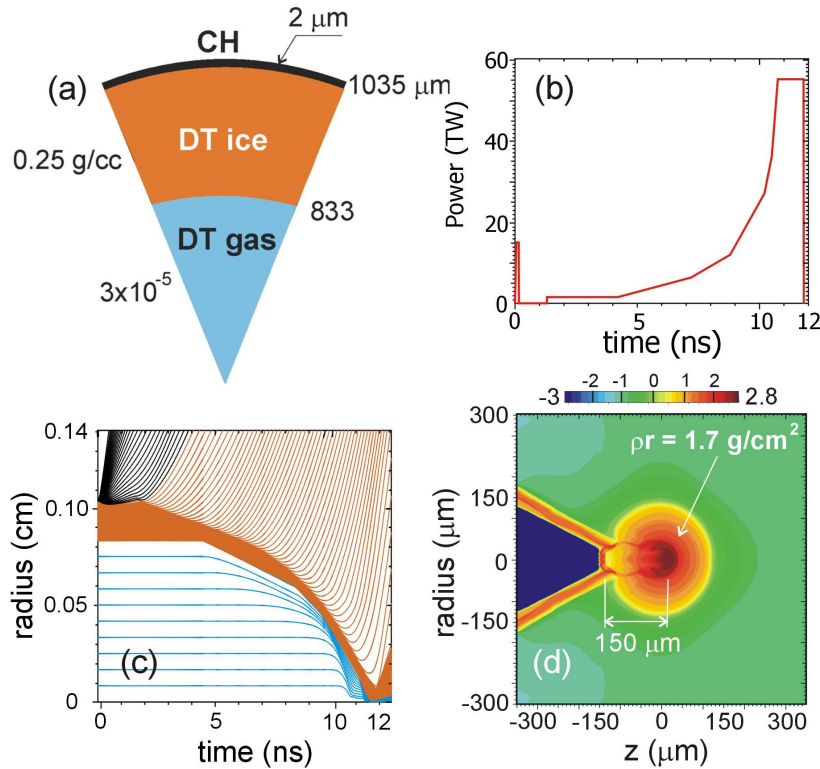


Figure 4.12: Simplified simulation of a conically-guided fuel capsule. (a) Capsule configuration, (b) laser pulse, (c) flow diagram of the 1D capsule evolution, and (d) density isocontours of the compressed target at the time of peak ρR in units of $\log_{10}[\rho/(\text{g}/\text{cm}^3)]$. The cone material is gold with a thickness such that the shock wave produced at the outer surface does not breakout before the target ignition takes place. The cone half-angle is 30° .

targets, however, show a number of features which deserve attention. (For a review, see, Ref. [4.39]). In particular, radiation from the shell may heat the inner portion of the gold, that expand and either contaminate the fuel or hinder its compression. Also, it must be proved that the fuel can slide on the gold surface without being contaminated. Finally, no study has so far been performed taking into account a realistic 3D irradiation geometry.

At the moment, detailed calculations of cone targets are beyond the current capabilities of the open-source radiation-hydrodynamics codes existing in Europe. However, we have already performed a simplified study combining 1D and 2D hydrodynamics calculations. We start with the simulation of 1D target implosion and when the shell is approaching the target centre, the 1D profiles are remapped onto a 2D Eulerian mesh and the calculations are continued including the presence of the cone. Calculations have been performed with the 1D/2D radiation hydrodynamics code SARA [4.35] including laser absorption by inverse bremsstrahlung, SESAME equations of state [4.40], flux-limited thermal conduction, and (for the moment) neglecting radiative transfer.

The simulation refers to a target [see Fig. 4.12(a)] similar to the reference one discussed in Sec. 4.4. The target is illuminated by the laser pulse shown in Fig. 4.12(b). The pulse energy is 135 kJ, the implosion velocity reaches 2.4×10^7 cm/s at the time of peak implosion kinetic energy, the in-flight entropy parameter $\alpha_{\text{if}} \approx 1$, the maximum density of the 1D compression $550 \text{ g}/\text{cm}^3$ and the peak $\rho R = 1.5 \text{ g}/\text{cm}^2$.

The 1D profiles are mapped onto a 2D r-z cylindrical mesh including the gold cone at 10.7 ns

when the outer radius of the shell is around $300 \mu\text{m}$ (see Fig. 4.12(c)). From that time, the 2D code computes the target compression until 11.8 ns, when the peak ρR occurs. The configuration of the imploded core at that time is shown in Fig. 4.12(d). It is in agreement with the experimental results of cone target implosion [4.41, 4.42] and also with recent calculations [4.43].

It is worthwhile to note that the shell accumulates in a nearly spherical blob, pushing the DT gas initially located at the capsule centre towards the sides of the cone. As a consequence, the fuel reaches higher compressions with cone than without cone. This configuration is obtained when the implosion velocity has a polar asymmetry along the shell, i.e. the implosion velocity is maximum in front of the cone tip and minimum at the cone surface. Otherwise, the imploded core would have an U-shaped configuration with the initial low density gas confined inside the U. This configuration would have a substantially lower ρR in the fast electron propagation direction than the blob configuration shown in Fig. 4.18(d). Here, we have used a 10% amplitude P_1 asymmetry⁶ of the implosion velocity to obtain a peak $\rho R = 1.7 \text{ g/cm}^2$.

4.6 Ignition laser pulse interaction and hot-electron generation

When intense laser light interacts with plasma there are many mechanisms that result in the acceleration of electrons to energies well above the mean thermal energy. In conventional ICF, whether direct or indirect drive, these fast electrons set an upper limit on the usable laser intensity. In Fast Ignition these superthermal electrons become a useful energy source and their unique properties of high energy and high current density make possible the heating of the fusion core within its inertial disassembly time.

The main parameter characterising ultraintense laser interaction is the dimensionless vector potential $a_0 = e\mathcal{E}/m_e c\omega$ ⁷ which can also be written as

$$a_0^2 = \frac{I[\lambda(\mu\text{m})]^2}{1.37 \times 10^{18} \text{ W/cm}^2} \quad (4.15)$$

At laser intensities above those corresponding to $a_0 = 1$, i.e. $I[\lambda(\mu\text{m})]^2 > 1.37 \times 10^{18} \text{ W/cm}^2$ the electron oscillations are relativistic and the electron orbits are strongly distorted by the $\mathbf{v} \times \mathbf{B}$ force. The orbits are not closed and tend to drift in the direction of the laser propagation. The drift is opposed by the quasi-static charge separation of electrons and ions but the smallness of the laser focal spot size means that the motion is not easily computed except by fully self consistent plasma simulations. The acceleration mechanism is sometimes described as $\mathbf{v} \times \mathbf{B}$ acceleration, as *vacuum acceleration* or as *direct laser acceleration*, in practice all three processes occur in the steep density gradients and strongly non-uniform laser foci. In all cases the effect is to accelerate the electrons to an energy of about the ponderomotive potential of the laser

$$\Phi_{\text{pond}} = [(1 + a_0^2)^{1/2} - 1]mc^2. \quad (4.16)$$

The energy is ill defined because of the complexity of the electron orbits and the many ways in which the electrons can leave the focus and be returned by the quasi-static electric and magnetic fields. Experimentally [4.44, 4.45] and in computer simulations [4.25, 4.46] the electron energy spectrum resembles a relativistic Maxwellian distribution with average energy (temperature) Φ_{pond} . If we assume $T \simeq \Phi_{\text{pond}}$, and linearize Eq. (4.16) around $I[\lambda(\mu\text{m})]^2 = 1.35 \times 10^{19} \text{ W/cm}^2$ we get

$$T_{\text{hot}} = 1.3 \left[\frac{I_{\text{ig}}^{\text{laser}}}{1.2 \times 10^{19} \text{ W/cm}^2} \left(\frac{\lambda_{\text{ig}}}{1.06 \mu\text{m}} \right)^2 \right]^{\frac{1}{2}} \text{ MeV}, \quad (4.17)$$

⁶With P_1 the Legendre polynomial of order 1.

⁷Here e is the electron charge, \mathcal{E} is the electric field, m_e is the electron mass, c is the velocity of light, and ω is the laser angular frequency.

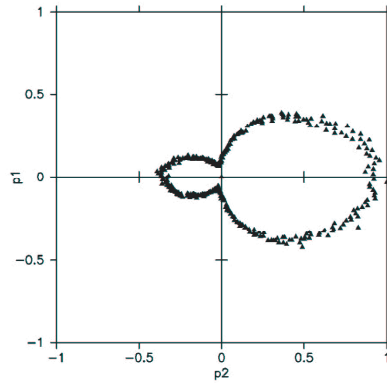


Figure 4.13: Angular distribution of energetic electrons generated at $a_0 = 5$ on a target with density $100 n_c$ and $1 \mu\text{m}$ front surface density gradient using the Osiris computer model.

close to the approximation used in Secs. 4.2 and 4.3. This scaling of electron energy with $I\lambda^2$ is borne out by a range of experiments spanning the sub-relativistic and relativistic ranges up to irradiances around 10^{21} W/cm^2 . Current experiments with intense short laser pulses are almost entirely with laser wavelengths in the range $0.8 \mu\text{m} - 1.06 \mu\text{m}$. Wide experience at lower intensities and our theoretical understanding of the acceleration mechanisms lead us to have very strong confidence in the $I\lambda^2$ scaling throughout the parameter range of interest for Fast Ignition.⁸

Computer modelling with detailed particle in cell (PIC) methods gives results in agreement with the experiments and shows that detailed aspects of the electron distribution are dependent on the shape of the electron density profile with which the laser interacts. Long density gradients give rise to more absorption and somewhat broader angular distributions than with the short scale length plasmas as would arise with very short laser pulses and low levels of pre-pulse. An example of an angular distribution at $I\lambda^2 = 3 \times 10^{19} \text{ W/cm}^2$ with rather steep density gradients calculated with the Osiris PIC model is shown in Fig. 4.13 (taken from Ref. [4.46]).

Concerning the efficiency of hot electron generation, experimental data summarized in Fig. 4.14 indicate that the high efficiency required for Fast Ignition is indeed achieved at high laser intensity.

In the Fast Ignition scenario many parameters of the laser generated electron beam are constrained. The electron range and spot size are dictated by the required ignition of hot spot, and the duration must be less than the hydrodynamic disassembly time of the fuel. Simultaneously the beam must supply enough energy to heat the fuel to ignition temperature. These requirements appear to be met by a CPA laser of 70 kJ supplying 30 kJ of hot electron energy in 15 psec with a value of $I\lambda^2 \approx (3-7) \times 10^{19} \text{ W/cm}^2$. This requires a laser operating wavelength in the range $0.3 - 0.5 \mu\text{m}$.

The scale of laser needed to define this operating point more precisely is beyond the present capabilities of the European laser laboratories. Some new results will be available from OMEGA-EP in the USA in 2009 and from Firex II in Japan somewhat later, the HiPER study period will concentrate on reducing the uncertainties concerning the operating point of the ignition laser through coordinated experimental and theoretical work.

⁸More uncertain, however, are both the $I\lambda^2$ exponent $\frac{1}{2}$ in Eq. (4.17), and the front factor, which depends on plasma density profile, pulse length, etc.

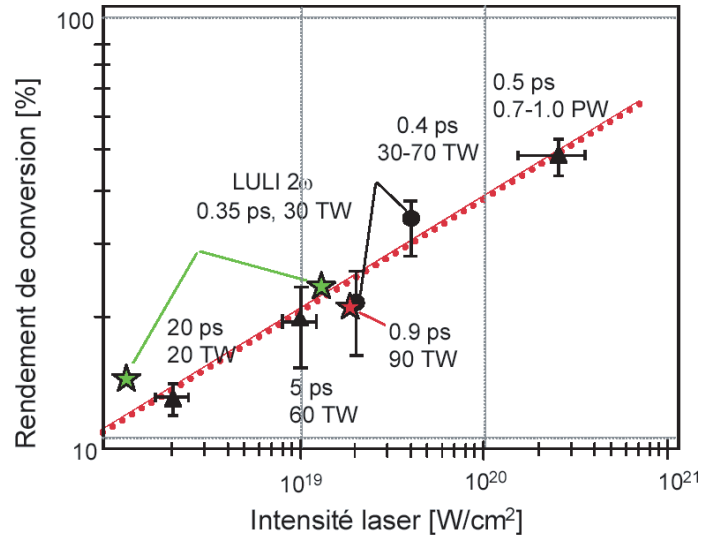


Figure 4.14: Efficiency of hot electron production vs laser intensity. (After Ref. [4.47]; data from Refs. [4.44, 4.48, 4.49, 4.50].)

4.7 Hot-electron transport and energy deposition

4.7.1 Transport

A laser with an irradiance of 10^{20} W/cm², generating electrons with an average energy around 3 MeV produces an electron beam with a current density of 10^{13} A/cm² and a total current of 200 MA in a 30 μ m spot. These parameters are extreme by any standards and are well beyond the experience of other laboratory experiments. The current hugely exceeds the Alfvén current for the propagation of an un-neutralised electron beam and the required return current is a large perturbation on the background plasma at solid densities.

In these circumstances the propagation of the beam electrons becomes a self-consistent problem in plasma physics with the electric and magnetic fields induced by the beam electrons playing a major role in their transport [4.51, 4.52]. Simple models exist which are low frequency approximations in that they neglect the displacement current in the solution of Maxwell's equations. These models are very good approximations in the case of electron transport in the high density core of an ICF target but are less valid in the interpretation of present day experiments at solid densities. Very importantly these models show that the self-generated magnetic fields act to focus the laser generated electrons and improve the geometric coupling from the laser interaction region to the fusion core. Figure 4.15 shows the change in beam behaviour from filamentation to self-focussing [4.53] as the background plasma density is increased as predicted by the implicit PIC model LSP [4.54]. The computer model agrees well with an analytic estimate of this self focussing threshold [4.55].

Given that a large part of our understanding proceeds by the comparison of theory and experiment on existing facilities there is a substantial effort in improving our modelling capability for present experiments, including as many real world effects as possible, such as the full Maxwell equations and the effect of collisions. In the full Maxwell equations the combination of the forward electron beam and its return current is unstable to a current filamentation frequently described as a Weibel instability [4.56, 4.57, 4.58]. Without the displacement current only the resistive form of the mode is present [4.52, 4.59] with a rather slower growth rate. Some collisionless simulations

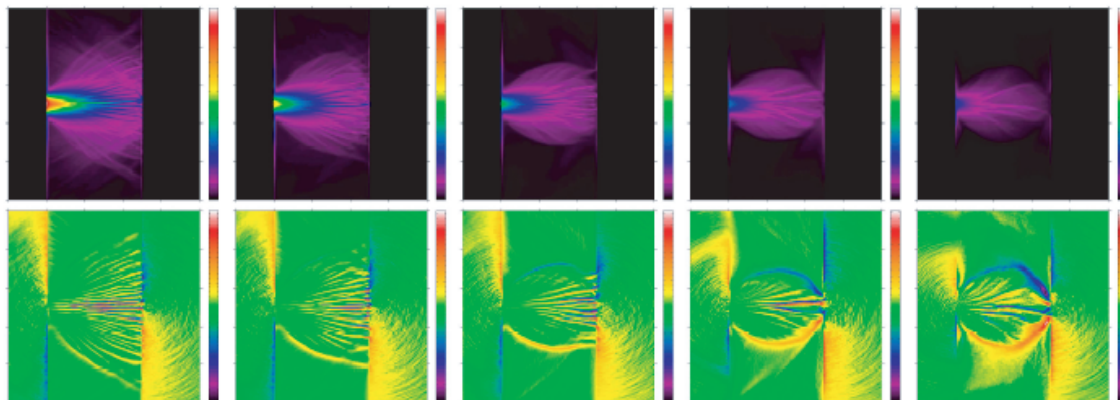


Figure 4.15: The change in electron transport as the target density increase from (left) 0.25 g/cm^3 to (right) 4.0 g/cm^3 . The upper image is the target temperature and the lower the self-generated magnetic field.

show an enormous enhancement of the energy loss from the beam electrons during the growth of the filamentation [4.60] as energy is transferred to the magnetic field and to transverse electron motion. Modelling the whole electron transport problem requires large computer resources due to the range of time and length scales that must be considered [4.53], from the electron range (around $100 \mu\text{m}$) to the background electron skin depth ($0.01 \mu\text{m}$) or even the background electron Debye length ($0.001 \mu\text{m}$ or less).

Experimental investigations of electron beam transport with existing lasers [4.61, 4.62, 4.63, 4.64] are made difficult by uncertainties in front surface conditions due to laser pre-pulse effects and the inevitability of measuring source distribution and transport properties together rather than independently. Diagnostics such as $K\text{-}\alpha$ emission are often influenced by the reflection (refluxing) of electrons in the front and rear surface Debye sheaths and imaging of X-ray emission from heated material is difficult with a spatial resolution high enough to resolve the likely Weibel modes. For the purpose of Fast Ignition it is important to understand the behaviour of low Z target materials (i.e. for DT $Z = 1$) which may allow instabilities that would be collisionally suppressed in higher Z targets due to growth of the electron beam emittance. Our present experiments in low Z plasmas are limited to CH plastic material which frequently confuses the interpretation of experiments since it is initially electrically insulating. Experiments in pre-heated CH or in Be metal would be very valuable given that cryogenic D_2 experiments are very expensive and difficult.

Although there remain significant uncertainties in the details of fast electron transport it has been possible to obtain good agreement between models and experiments of bulk material heating. Figure 4.16 shows the agreement between measured target temperature and computer modelling for a thin layer of Aluminium embedded in a CH substrate taken from reference [4.64]. It is important to build confidence in our understanding of the transport and stopping mechanisms with new, careful experiments and associated developments in modelling and computational capability.

In the context of HiPER it is very important to stress that the fusion pellet provides an environment which is much easier to understand than the current experiments since in the highly compressed core the beam electrons are a much smaller fraction of the background density and the problem is more nearly perturbative. The main issues for HiPER will be in understanding the electron beam propagation close to its source where it will be a large fraction of the background density.

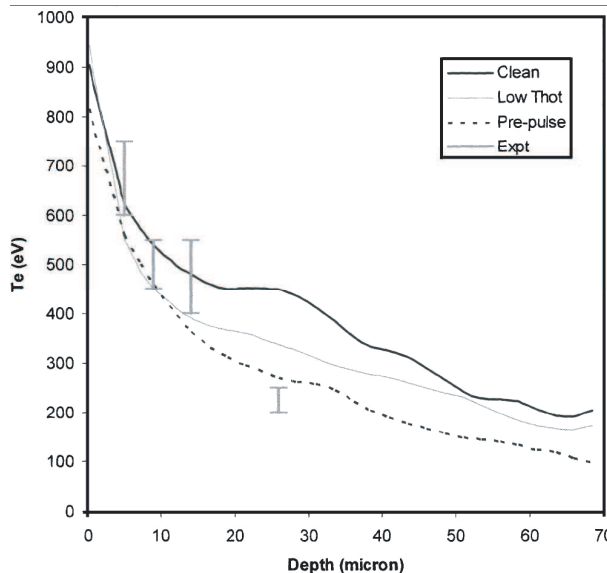


Figure 4.16: Agreement of computer model including laser pre-pulse with measured temperature of layers of Aluminium buried at various depths in CH substrate

4.7.2 Energy deposition by laser-accelerated electron beams

In this subsection we deal with electron beam energy deposition to the compressed fuel. In particular, we discuss the coupling efficiency η_{ig} of the laser ignition beam and the factor $f_{\mathcal{R}}$, that have taken as free parameters in the model of Sec. 4.3. In the next subsection we will present numerical simulation of electron beam driven fast ignition of a precompressed DT assembly.

Concerning the efficiency η_{ig} , we can factorize it as

$$\eta_{\text{ig}} = (\eta_d \eta_\theta \eta_E \eta_M) \eta_{\text{las-he}} = \eta_{\text{eb}} \eta_{\text{las-he}}, \quad (4.18)$$

where $\eta_{\text{las-he}}$ is the efficiency of production of hot electrons directed towards the core (see Sec. 4.6), η_d accounts for energy deposition outside the hotspot and the non-uniform deposition along it under the assumption of an initially parallel beam, η_θ accounts for deposition outside the hotspot arising from the beam initial divergence, η_E and η_M account for energy loss arising, respectively, from the electric and magnetic fields outside the core. We now first review stopping power expressions, and then discuss these efficiency factors.

Stopping power. Energy deposition by a *fast* electron is described by [4.65]

$$\frac{dE}{ds} = \frac{dp}{dt} = -\frac{4\pi n_e e^4}{m_e v^2} \left(\ln \frac{1.241 \gamma m_e v^2}{\sqrt{\gamma + 1} \hbar \omega_p} + \frac{0.409}{\gamma^2} - \frac{0.818}{\gamma} \right) \equiv \frac{D}{v^2}, \quad (4.19)$$

where p , E , v and γ are the momentum, energy, speed and Lorentz factor of the fast electron, respectively, s is the distance along its path and n_e and ω_p are the electron density and plasma frequency of the medium it is travelling in.⁹

⁹This expression is calculated using the Møller formula to describe energy exchanges from E_{cut} to $E/2$, which is the maximum energy exchange since we are interested in the fast electron, and formulas for the perturbation of the medium (excitation of oscillations and polarization) by a charged particle moving at a constant velocity to describe

If we assume that D in Eq. (4.19) is constant¹⁰ then we can obtain simple, but still accurate solutions for the stopping distance and time:

$$s_{\text{stop}} = \frac{E_0^2}{1.96E_0 + 1} \frac{1.56}{1 - 0.048 \ln \rho} \text{ g/cm}^2 \quad (4.20)$$

$$t_{\text{stop}} = \frac{m_e c^3}{D} \left(\frac{p_0}{m_e c} - \arctan \frac{p_0}{m_e c} \right), \quad (4.21)$$

where the subscript 0 indicates initial values, E_0 is the electron energy in MeV, ρ is the DT plasma density in units of g/cm^3 . We see that the scaling of Eq. (4.20) with electron energy differs from that of Eq. (4.7) by a factor of $1 - 1/\gamma_0$. At a density of 300 g/cm^3 , a linear approximation to Eq. (4.20), centred about $E_0 = 1 \text{ MeV}$, is given by Eq. (4.7), with

$$f_{\mathcal{R}} = 1.2 \frac{1}{0.66 + 0.34E_0^{-1}}. \quad (4.22)$$

Computations by other authors lead to the same dependence of the stopping length on the energy, but to somewhat smaller front factor; e.g., Li and Petrasso's results [4.66] agree at 1 MeV with Eq. (4.7) with $f_{\mathcal{R}} = 1$, when dragging and blooming are neglected.

The stopping times [Eq. (4.21)] for 1 MeV electrons at the above density are a fraction of a ps, so energy deposition in the core will be effectively instantaneous.

Angular scattering: dragging and blooming. Equation (4.19) gives the energy deposition along an electron's path, but this will not correspond to the energy deposition along a beam of electrons because angular scattering causes the paths to wind up in a random fashion. The mean squared angular deflection per second of a fast electron due to collisions with atoms or ions is given approximately by [4.67]:

$$\frac{d\langle\theta^2\rangle}{dt} = \frac{8\pi Z n_e e^4}{p^2 v} \left[\ln \left(16.4 \frac{\lambda_s}{\lambda_{\text{dB}}} \right) - 0.419 \frac{v^2}{c^2} \right], \quad (4.23)$$

where λ_{dB} is the de Broglie wavelength of the fast electron (h/p) and λ_s is the screening length of the atoms or ions. In a plasma this is the Debye length. An example of axial and radial energy deposition profiles for an MeV electron in 300 g/cm^3 DT, calculated with a Monte-Carlo code using Eqs. (4.19) and (4.23), is given in Fig. 4.17. It shows that 95% of the electron energy is deposited in an effective penetration depth $\mathcal{R} \simeq 0.85s_{\text{stop}}$. This leads to an analogous reduction of the factor $f_{\mathcal{R}}$.

Qualitatively similar results are shown in Fig. 4.18a), presenting results of a simulation with a hybrid code [4.36], solving the relativistic Fokker-Planck equation with standard Coulomb cross sections by the Monte Carlo method [4.68]. The figure shows the deposition pattern of a 2.2 MeV electron beam impinging perpendicularly on a DT slab. The beam is collimated a half of the electron range, being subject to scattering and beam *blooming* in the second half. This simulation agrees quantitatively with the results reported in Ref. [4.66].

Stopping of beam with Maxwellian energy distribution. Actual beams are characterised by an energy distribution $f(E)$. Electrons with different energy have different range. Accurate

energy exchanges below E_{cut} . The arbitrary cut-off cancels out, giving some confidence that this approach is accurate, despite its failure to describe intermediate energy exchanges. The difference between media lies in the definition of fast. For a plasma it is sufficient for the electron to have a speed a few times the thermal velocity, or the Fermi velocity in a degenerate plasma, for Eq. (4.19) to be a good approximation. Bremsstrahlung has been neglected, which is a reasonable approximation for electron energies less than 100 MeV in hydrogen.

¹⁰To this purpose we approximate the term in parentheses in Eq. (4.19) with $\ln(m_e c^2 / \hbar \omega_p)$

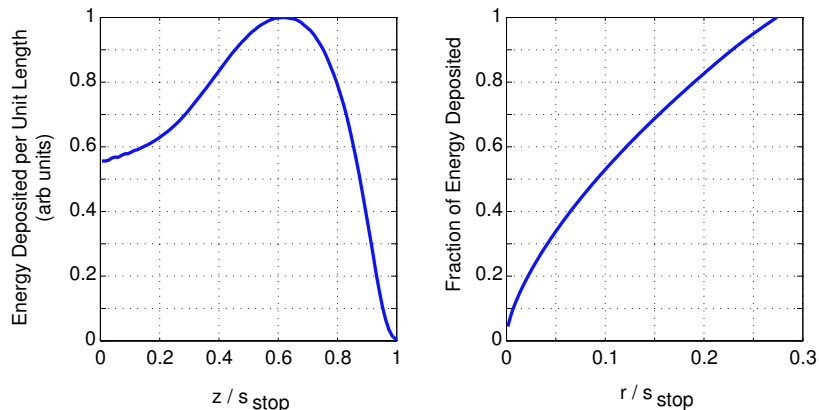


Figure 4.17: Average energy deposition profiles for an MeV electron in 300 g/cm^3 DT. The z -axis is aligned along the initial direction of motion. Distances are given as fractions of the electron’s stopping distance to give results that are practically independent of the electron energy and DT density.

computations of the energy deposition can only be performed by simulations. However, useful qualitative results can be obtained by using relatively simple models. For instance, in the case of a 3D Maxwellian distribution in the strongly relativistic limit (with mean energy of $3k_B T$), one finds that energy deposition along the beam initial direction z is roughly described by a decreasing exponential [actually, a polynomial times $\exp(-E_{\min}(z)/k_B T)$, with $E_{\min}(z)$ the minimum electron energy required to travel a distance z].

The heating efficiency η_d of such a beam, i.e. the fraction of the electron beam energy actually used to heat a cylinder of dense DT with depth \mathcal{R}_0 up to the ignition temperature, has then been computed, leading to the result shown in Fig. 4.19. There, we show estimates of the efficiency as a function of the ratio $\langle E \rangle / E_{\min}(\mathcal{R}_0)$ between the beam average energy and the minimum electron energy required to travel the distance \mathcal{R}_0 . The figure shows an estimated (conservative) efficiency, computed assuming by requiring the energy deposition to exceed the optimum value of $E_{\text{ig}}/\mathcal{R}_0$ over the length of the hotspot \mathcal{R}_0 . Since this maybe an underestimate, we also consider an upper bound to the efficiency by requiring the total energy deposited in the hotspot to be E_{ig} . For comparison, we also show a curve assuming uniform heating. The upper bound on the efficiency is only significantly higher for low mean energies. The conservative estimate gives a maximum efficiency at a mean energy of $\langle E \rangle \approx 1.32 E_{\min}(\mathcal{R}_0)$. This can be interpreted as giving a lower effective range than predicted by the mean energy, lowering $f_{\mathcal{R}}$. For our reference values $\rho = 300 \text{ g/cm}^3$ and $\mathcal{R}_0 = 1.2 \text{ gcm}^2$ the maximum efficiency is approximately 0.5 at a mean energy of 1.9 MeV, and we could increase this to 3 MeV and still obtain an efficiency of approximately 0.4.

Diverging beams. So far we have assumed that the electrons are initially moving parallel to one another, but laser accelerated electron beams typically diverge. To estimate the decrease in efficiency that this will lead to let us assume that the electrons are being emitted uniformly within a cone of half angle θ_c from a region with the same radius r_b as the region we wish to heat and at a distance S from the core. If we ignore the energy deposited over the distance S , then assuming uniformly heated volumes we obtain

$$\frac{1}{\eta_\theta} \sim 1 + \frac{2\mathcal{R}_0^2 + 6R_0 S + 6S^2}{3r_b^2} (1 - \cos \theta_c). \quad (4.24)$$

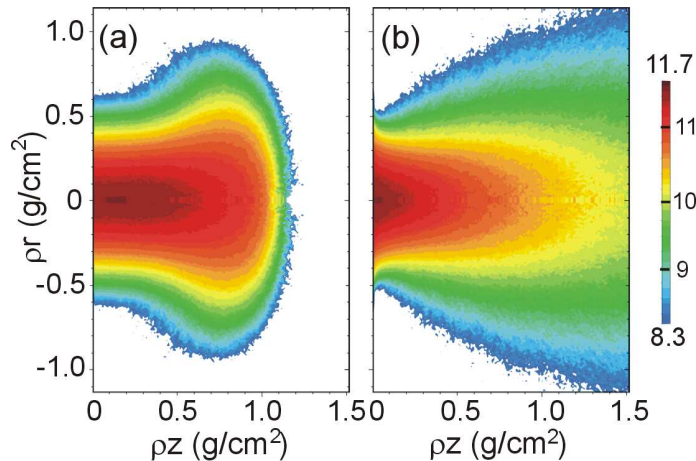


Figure 4.18: Energy deposition isocontours of (a) 2.2 MeV electrons impinging perpendicularly on a DT slab at 300 g/cm^3 , and (b) electrons with the spectral distribution explained in the text, with a mean energy $\langle E \rangle = 2.2\text{ MeV}$ and a divergence half-angle of 22° (FWHM). Energy deposition is plotted in logarithmic scale with arbitrary units.

Experiments with various solid targets indicate half angles in the heating pattern of $15\text{--}20^\circ$ for values of $I\lambda^2$ between $10^{19}\text{--}10^{20}\text{ W cm}^{-2}\ \mu\text{m}^2$ [4.46], higher values of $I\lambda^2$ giving higher cone angles. If we take $\theta_c = 20^\circ$, $\mathcal{R}_0/r_b = 2$ and $\mathcal{S} = 0$ we obtain $\eta_\theta = 0.86$, but if $\mathcal{S} = r_b$ this falls to 0.66, and it will fall rapidly as this distance increases.

The effect discussed above is clearly seen in Fig. 4.18b) showing an example of energy deposition by a beam with super-gaussian shape in radius with $\text{FWHM} = 20\ \mu\text{m}$, divergence half-angle $\theta_c = 22^\circ$ (FWHM) and 1D relativistic maxwellian distribution with $\langle E \rangle = 2.2\text{ MeV}$. This figure is the result of a simulation with the hybrid code described in Ref. [4.36]. Notice the apparent range *lengthening* due to beam energy spectrum and the subsequent delocalization of the fast electron energy deposition. [This effect depends to a large extent on the energy distribution, being maximum for a 1D Maxwellian distribution and substantially smaller for a 3D Maxwellian with the same mean energy $\langle E \rangle$. For instance, the fractions of the beam energy deposited outside the simulation box in the case of Fig. 4.18b) are 23% and 7.5% for 1D and 3D distributions, respectively.]

Ohmic heating. Energy deposition can also occur due to the electric field generated by the beam. Detailed estimates of Ohmic heating show that it will be negligible in the core [4.69], while it could lead to energy loss in the cone tip or corona before the electrons enter the core. We can represent this by an efficiency η_E . Extensive hybrid code modelling of laser-solid interactions, where the densities involved are similar to those where the field generation will be important, leads us to believe that $\eta_E > 0.7$ could reasonably be expected. This energy loss will also lower the mean energy of the electrons entering the core by a factor of approximately η_E [4.70, 4.71], giving $f_{\mathcal{R}} \propto \eta_E$.

Role of self-generated magnetic fields. The self-generated magnetic field can focus the beam [4.72], reduce the penetration depth by winding up the electron trajectories and turn electrons back to the source [4.73]. Magnetic inhibition could be particularly detrimental, if the electrons are generated at a distance from the core that exceeds the beam radius, since it would reduce the total energy of electrons reaching core *and* increase their mean energy, as only electrons below the mean energy are turned back. Expressing this in terms of an ignition efficiency η_M , we could expect an increase in the mean energy of order $1/\eta_M$, giving $f_{\mathcal{R}} \propto 1/\eta_M$. Extensive hybrid code

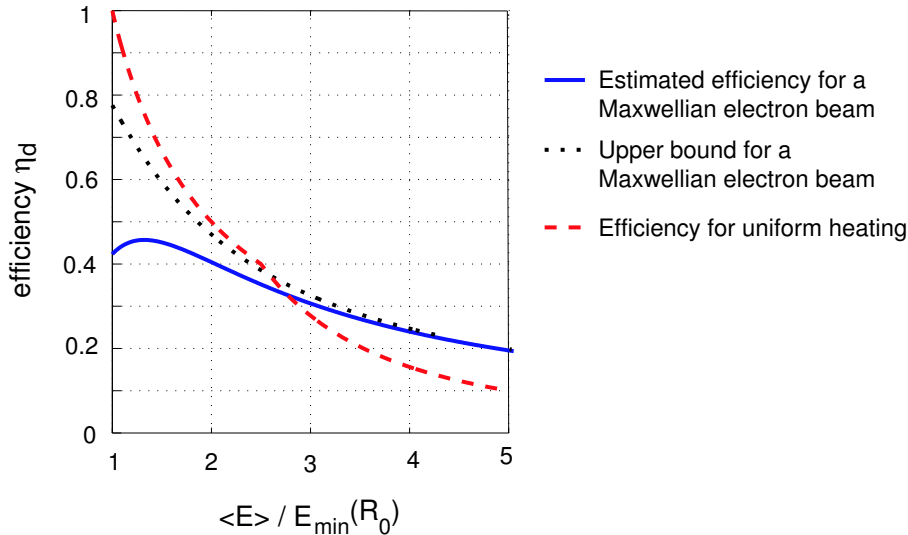


Figure 4.19: Deposition efficiency for a beam with Maxwellian energy distribution and zero divergence as a function of the ratio of its mean energy $\langle E \rangle$ to the minimum kinetic energy required to travel a distance \mathcal{R}_0 .

modelling of laser-solid interactions has shown that even when magnetic inhibition is significant $\eta_M \simeq 0.8$. The reason for this is that as lower energy electrons are turned back the forward current is reduced, an additional return current is provided and the momentum of the electrons in the forward current is increased. The effect of the magnetic field on electron propagation can be gauged by the dimensionless parameter eA/p , where A is the magnetic vector potential. A value greater than $\langle \sin^2 \theta_c \rangle$ shows that magnetic focusing will occur and a value greater than 1–2 shows that magnetic inhibition will occur. The region of interest is the corona and the cone tip, where Ohmic heating is likely to dominate. In Ref. [4.74] we showed that in these circumstances the maximum value of A is given by

$$\frac{eA}{p} \sim \frac{2.5}{\gamma\beta} \left(\frac{Z \ln \Lambda}{10} \right)^{1/2} [T_0(\text{keV})]^{-1/4} \left(\frac{n_e}{2.4 \times 10^{23} \text{ cm}^{-3}} \right)^{1/2} \left(\frac{t}{10 \text{ ps}} \right)^{1/2}, \quad (4.25)$$

where T_0 is the initial temperature. This shows that magnetic focusing should occur early on in the pulse, which would significantly increase the value of η_θ given by Eq. (4.24), but it also shows that magnetic inhibition should occur. In the cone tip this could be avoided by making it thinner than the radius of the beam, or by using a material with a lower density than gold. The electron density of solids scales roughly as Z , giving $A \propto Z$, indicating that there should be a considerable advantage in making the cone tip out of a lower Z material, such as plastic or Beryllium.

Concluding remarks. In conclusion, we have discussed the factors that determine the efficiency η_{ig} [Eq. (4.6)] and the range factor $f_{\mathcal{R}}$ [Eq. (4.8)], which gives the effective range as a function of mean energy, for an electron beam with a Maxwellian energy distribution and a given cone angle. The limiting efficiency factors are η_d and $\eta_{\text{las-he}}$, while it should be possible to maintain the others close to 1, if the fast electrons are generated sufficiently close to the core. Concerning the range factor, we have shown that, when stopping, dragging and blooming, deposition by a Maxwellian distribution, are considered, $f_{\mathcal{R}} \simeq 1$. Electric and magnetic field effects can also affect the range. In addition, one has to account for possible variations in the mean energy of the laser accelerated electron beam from the ponderomotive potential [Eq. (4.9)]. With further, better controlled and

better diagnosed experiments, combined with improved modelling, the factors $\eta_{\text{las-he}}$ and $f_{\mathcal{R}}$ should be accurately determined during the HiPER preparatory phase. In particular, experiments on PETAL [4.16] could provide key information under HiPER-relevant conditions.

4.7.3 Hybrid simulations of electron transport in the compressed fuel and ignition

The gain curves, target design and the parametric study presented in Secs. 4.3–4.4 were based on simplified assumptions concerning electron transport. Here we present a study taking into account the spectral distribution and angular divergence of the fast electron beam as well as the Coulomb and collective interactions with the imploded DT. We also study how the efficiency of hot spot generation is affected by the position of the electron source.

Some of our results are rather general, other specifically apply to fast electrons generated close to the plasma core, at the cone tip of a cone guided target. In an igniting target, a multi-PW electron beam will carry a current of the order of 1 GA, almost 10^4 times larger than the Alfvén current, which has to be transported over a distance of the order of 100 - 150 μm between cone tip and dense core through a high-gradient plasma profile.

Here, we use an integrated 2D code in cylindrical $r - z$ geometry [4.36] to study ignition of the imploded fuel taking into account the beam transport from the cone tip to the dense fuel. It employs the hybrid model proposed by Bell [4.51] and further developed by Davies [4.71] and Gremillet *et al.* [4.52]. This is adequate for describing self-magnetized transport in high-density fuel, where kinetic energy transfers and most of the beam-plasma instabilities are suppressed by collisions [4.75]. The beam deposits energy into plasma electrons in two ways: by direct Coulomb deposition and via return current ohmic heating with power density ηj_r^2 , where j_r is the return current and η is the plasma resistivity, assumed classical Spitzer. Our model also includes thermal electron conduction, fusion reactions, alpha particle energy deposition [4.76] and hydrodynamics, and a tabulated equation of state.

The imploded fuel configuration used here is shown in Fig. 4.20. It is similar to that obtained in the study of cone target compression presented in Section 5 and consists of 0.18 mg DT fuel compressed into a spherical blob of 400 g/cm^3 peak density with a supergaussian distribution of 82 μm diameter (FWHM) sited on a density pedestal of 1.5 g/cm^3 (the *halo*). We have taken the distance d from the cone tip to the blob centre as a parameter, ranging from 75 to 150 μm . For simplicity, a uniform initial DT temperature of 300 eV has been assumed, which sets the initial resistivity to a level of $3 \times 10^{-8} \Omega\text{m}$.

A beam of fast electrons is injected from the left at $z = 0$. We imagine that it emerges from the tip of a cone at this position. The injected beam has Gaussian profiles in space and time with spot radius of 20 μm , peak power from 2.6 to 4 PW and duration from 12 to 20 ps. We have assumed a 1D relativistic Maxwellian energy distribution for fast electrons with temperatures given by the ponderomotive scaling formula [Eq. (4.16)], using the local laser intensity, also assumed Gaussian in radius and time. The peak laser intensity varies from 1.9 to $2.3 \times 10^{20} \text{ W/cm}^2$; the laser wavelength is 0.53 μm . The corresponding electron mean energies range from 2 to 2.2 MeV within FWHM and from 1.5 to 1.6 MeV averaged over the whole beam cross section.¹¹ We have artificially varied the laser-to-electron conversion efficiency $\eta_{\text{las-he}}$ from 42% to 50%, depending on the pulse energy. The parameters described above can be combined to give fast electron pulse energies from 24 to 58 kJ. An initial beam divergence half-angle (FWHM) $\theta_c = 22^\circ$ has been taken from the experiments reported by Kodama *et al.* [9, 10]. However, we have also considered cases

¹¹According to our previous results [4.77], electron kinetic energies about 2 MeV maximize the beam coupling with the dense core. The same electron energies have been considered in the recent study by Betti *et al.* [4.19].

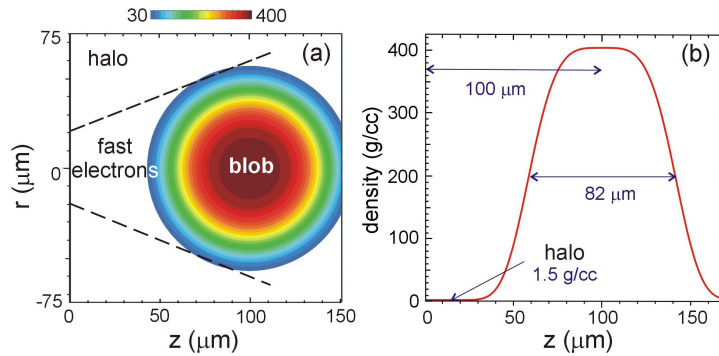


Figure 4.20: Central cut through imploded target configuration: (a) density isocontours in g/cm^3 and (b) density profile at $r = 0$.

with $\theta_c = 30^\circ$, consistent with the ponderomotive acceleration formula $(\tan^{-1}[2/(\gamma - 1)]^{1/2})$, and $\theta_c = 40^\circ$ to study the sensitivity of the ignition energy on beam divergence.

Fast electron energy deposition

Beam interaction with the halo. In the lower density region, return currents heat plasma electrons up to temperatures $T_e \approx 10$ keV much higher than the ion temperature, in a few picoseconds. Here, field generation is suppressed due to low resistivity, and magnetic fields saturate at relatively low levels of (≤ 100 T). Therefore, beam electrons propagate in that region with approximately the initial divergence angle. At higher densities ($\rho > 20 \text{ g/cm}^3$), electron temperatures are lower, resistivities higher and efficient energy transfer from electrons to ions takes place, so that $T_i \approx T_e$. Higher resistivities lead to enhanced field generation and beam collimation by the azimuthal magnetic field B_θ (≤ 0.9 kT) [4.77]. The fast electron energy deposition obtained with the present model with and without taking into account the self-generated fields are compared in Fig. 4.21. It is seen that the beam collimation increases the peak energy density deposited by a factor of 2. Beam collimation is also predicted by the analytical model by Bell and Kingham [4.55] for the beam parameters used here, even for $\theta_c = 40^\circ$.

The filamentation of the B_θ field recently observed in 3D simulations [4.77] is also seen in the present 2D simulations for distances d from the cone tip to the blob greater than $125 \mu\text{m}$. The filamentation takes place at the beginning of the density ramp, where resistivities are higher than in the low density halo and the plasma density is not high enough to dump collective modes. The current density oscillations lead to the fragmented energy deposition shown in Fig. 4.21(c).

Beam interaction with the dense core At high densities, DT heating is almost exclusively due to Coulomb deposition of fast electrons. Despite ohmic heating by return currents plays only a minor role for the overall energy balance [as can be seen by comparing Figs. 4.21c) and d)], self-generated fields contribute to the core heating indirectly via beam collimation.

The density and ion temperature distributions just after the end of the pulse are shown in Figs. 4.22 a) and b). Notice that both distributions have a pattern consistent with fragmented energy deposition. The peak ion temperature exceeds 10 keV. We emphasize that fragmented energy deposition does not appear for shorter distances.

The electron beam coupling efficiency η_{eb} , defined here as the energy fraction of the electron pulse deposited at densities higher than 200 g/cm^3 , is plotted in Fig. 4.23 (left frame) as a function of the distance d , for different values of the initial divergence half-angle θ_c . Taking into account

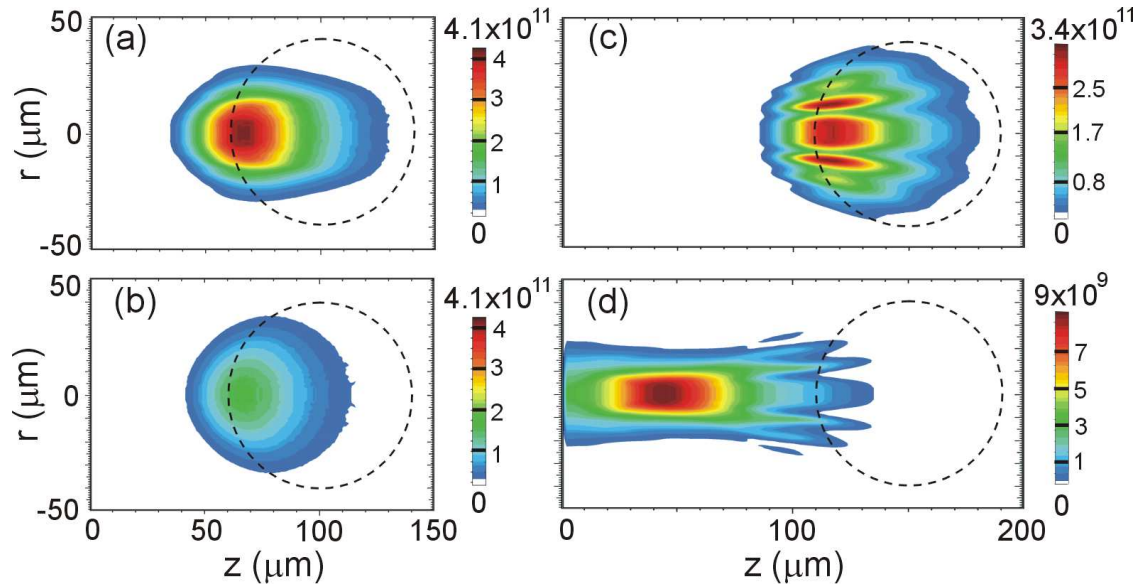


Figure 4.21: Energy density in (J/cm^3) deposited by fast electron beams, with initial divergence half-angle of 22° , for the target configuration shown in Fig. 4.20, and two different values of the distance between the cone tip and the blob: $100 \mu\text{m}$ (left frames) and $150 \mu\text{m}$ (right frames). Upper row [(a) and (c)]: Coulomb energy deposition in full simulation with self-generated fields. (b) Coulomb energy deposition in simulations with self-generated field artificially suppressed; (d) Ohmic heating in full simulation. Dashed circles show the initial position of the $200 \text{ g}/\text{cm}^3$ density contours.

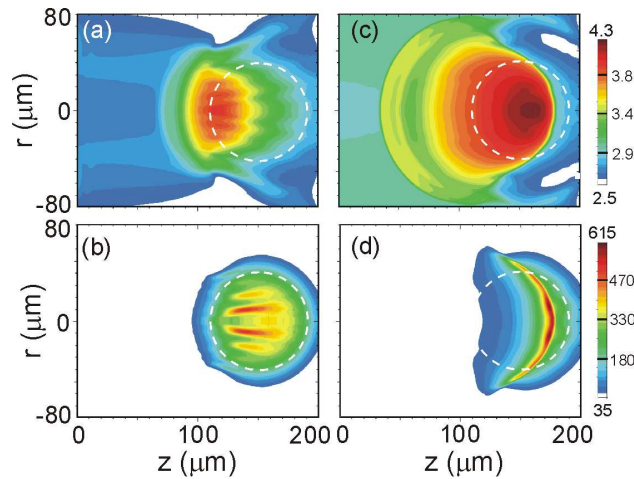


Figure 4.22: Ion temperature and plasma density isocontours for the same case as in Fig. 4.21c) and d): (a) and (b) at the end of the fast electron pulse (18 ps), and (c) and (d) at 45 ps, when ignition is propagating. Temperatures are given in units of $\log_{10}(T_i/\text{eV})$ in (a) and (c), and densities in g/cm^3 in (b) and (d). Dashed circles indicate the initial position of the $200 \text{ g}/\text{cm}^3$ density contour.

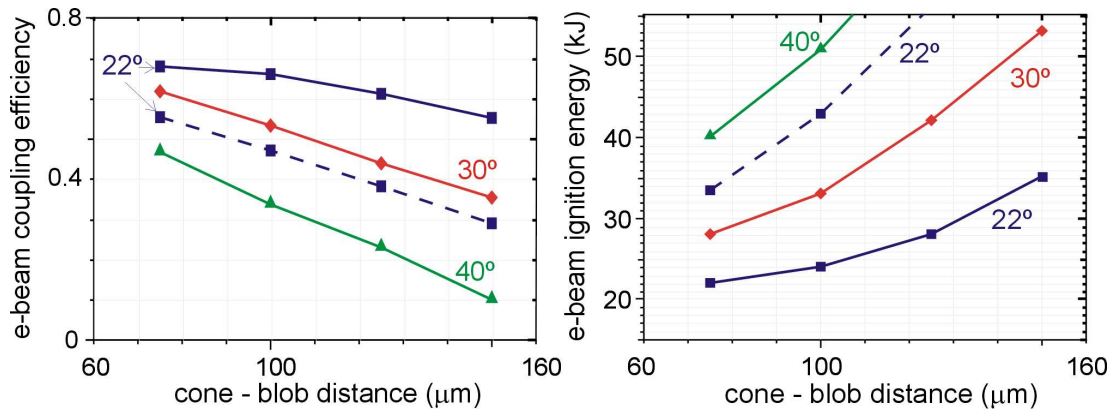


Figure 4.23: Dependence of electron beam coupling efficiency (left) and electron beam energy required for ignition (right) as a function of the cone-blob distance, for different values of the initial divergence half-angle of the fast electrons. The dashed lines refer to the case with self-generated fields artificially suppressed.

that the actual coupling efficiency is the product $\eta_{ig} = \eta_{eb}\eta_{las-he}$ (with η_{las-he} the laser-to-fast electron conversion efficiency, which can be estimated as 40%), the efficiency $\eta_{ig} \geq 25\%$ assumed in the reference design requires imploded configurations with $d < 130 \mu\text{m}$ if $\theta_c = 22^\circ$, or $d < 80 \mu\text{m}$ if $\theta_c = 30^\circ$. The important role played by beam collimation is also apparent from the figure.

DT fuel ignition

The density and ion temperature maps of an igniting target at selected times are shown in Fig. 4.22, referring to the case $d = 150 \mu\text{m}$. The oscillations produced in those profiles by the fragmented energy deposition shown in Figs. 4.22a) and b) are swept out by the ignition wave, which has an almost spherical shape, as seen from Figs. 4.22c) and d).

We have performed series of simulations to obtain the ignition energy as a function of the cone-blob distance d and the initial divergence half-angle θ_c . Results are plotted in Fig. 4.23 (right hand side). The need for making these two parameters as small as possible is apparent. The imploded target configuration of Fig. 4.20 heated by electron beams with $\theta_c = 22^\circ$ will ignite with energies between 24 and 35 kJ, depending on the distance d . For $\theta_c = 30^\circ$ the electron beam ignition energy increases to 28–57 kJ.

In conclusion, our study shows that the currents required for fast ignition can be transported through the steep gradients of the plasma corona toward the high-density fuel core and can ignite it with beam energies of 20 – 30 kJ. Collective effects play a major role for core heating improving the coupling efficiency substantially, in an indirect way, by means of beam collimation taking place in the density ramp. These conclusions rely on the hybrid PIC modelling used in our study and therefore on the distribution function assumed for electron injection. In this context, a good characterisation of the fast electron source, i.e. spectrum, angular divergence and laser-to-electron conversion efficiency, is of paramount importance. On the other hand, the integrated simulations shown above evidence a large dependence of the ignition energy on the distance between the cone tip and the dense blob. According to those simulations, ignition with the 70 kJ short-pulse laser proposed for HiPER could be obtained for assemblies with $d \leq 130 \mu\text{m}$, provided hot electrons are generated with efficiency of about 40% and beam divergences $\theta_c = 22^\circ$, similar to those measured in the ILE cone-target experiments [4.9, 4.10]. The distance d has to be reduced to $75 \mu\text{m}$ if $\theta_c = 30^\circ$.

4.8 Laser-generated proton beams as alternative ignitors

Laser-driven proton fast ignition (PFI) has been proposed [4.78] as an alternative approach to fast ignition (For a review see Ref. [4.79].) It would exploit high efficiency of the particle beam energy deposition in a compressed DT fuel, as well as good control of the beam production and transport. On the other hand, a critical point is the proton beam production efficiency that is lower than that of the electron beam production. The parameters of the proton beam required for ignition were determined [4.80, 4.81] (with some simplifying assumption on the proton beam and the fuel) using the 2D radiation-hydrodynamic code DUED. For a DT fuel density of $300 - 400 \text{ g/cm}^3$ and the proton beam radius $20 \text{ }\mu\text{m}$ they are roughly as follows: beam energy (deposited in the fuel) of $10 - 20 \text{ kJ}$, beam intensity of 10^{20} W/cm^2 , proton pulse duration of $10 - 20 \text{ ps}$, mean proton energy of about 5 MeV . In particular, this means that the number of protons heating the fuel should be at least 2×10^{16} and the proton density in the beam should be about $4 \times 10^{22} \text{ cm}^{-3}$. If the proton beam has a Maxwellian distribution the proton source must be placed at a distance of less than 1 mm from the compressed fuel to avoid power spread due to velocity dispersion.

At present, two laser methods of proton beam generation seem to have potential to meet the PFI requirements: Target Normal Sheath Acceleration (TNSA) (e.g. [4.82, 4.83, 4.84, 4.85] and Skin-Layer Ponderomotive Acceleration (SLPA) (e.g. [4.86, 4.87]). In TNSA, protons are accelerated at the rear surface of the foil target by a virtual cathode (Debye sheath) created by hot electrons produced by a laser at the target front and penetrating through the target. In SLPA, the ponderomotive pressure of a laser pulse at the target front drives a dense neutralized proton bunch (plasma block) of proton density $n_i > n_{ec}$ (with n_{ec} the plasma critical density). At relativistic laser intensities, MeV proton bunches of proton densities $> 10^{22} \text{ cm}^{-3}$ can be produced with this method [4.88, 4.89, 4.90]. PFI concepts using either TNSA beams [4.78, 4.91] or SLPA beams [4.87, 4.92] have been proposed. For both cases a guiding cone which protects the proton source foil against shocks and x-rays generated in the fuel are considered to be used. In the case of PFI using TNSA beams, strong focusing of the proton beam, ensuring an increase of the proton density by more than 1000 times is necessary to reach the density required for ignition. Moreover, since protons are extracted only from a very thin ($< 0.1 \text{ }\mu\text{m}$) layer at the rear target surface, to reach the required number of protons ($> 2 \times 10^{16}$) the area of the proton source has to be relatively large (with diameter d_s of a few mm) and the distance, d_{sf} between the proton source and the fuel has to be relatively long $d_{sf} \simeq d_s$. As a consequence, a proton beam of narrow energy spectrum is necessary to prevent excessive elongation of the proton pulse due to proton velocity dispersion. Highly efficient generation of such a proton beam and strong focusing of the beam without significant energy loss seem to be the most challenging tasks for PFI with TNSA beams.

In the case of PFI with SLPA beams only a slight focusing of proton beam using a shaped target or employing several overlapped beams generated from planar targets is sufficient to reach required densities of protons heating the fuel (as proton densities at the source are high). Moreover, for sufficiently long (ps) driving pulses protons can be generated from a fairly thick (several μm) solid-density layer. It means that the proton source area can be relatively small (d_s of a few hundred μm) and the proton source-fuel distance can be small as well. As a result, the proton velocity dispersion does not cause non-acceptable elongation of the proton pulse when using non-monoenergetic beam. However, the energetic efficiency of the SLPA beam production at input parameters relevant to PFI is still an undetermined value and needs detailed studies and careful optimization of the laser-target system. The PETAL facility [4.16] first, and later the HiPER laser facility, could allow experimental studies of this approach to fast ignition at energy level exceeding that of any existing facility, and possibly approaching conditions relevant to inertial fusion energy.

4.9 Conclusions

In this Chapter of the HiPER Technical Design Report we have documented target studies for fast ignition demonstration at total laser energy below 400 kJ, with less than 100 kJ for the ultraintense ignitor beam. These studies have led to a preliminary target design and to a set of specifications for the laser beams.

It turns out that ignition and significant energy gain can be achieved with a HiPER-class facility, provided certain conditions are met. First, the power of compression beams should be accurately time-tailored in order to shape the entropy profile inside the imploding shell, allowing for efficient fuel compression, while at the same time limiting the growth of the Rayleigh-Taylor instability. This is technically demanding, but otherwise tested and well understood. The crucial issue, instead, seems to be the coupling efficiency of the ultraintense beam to the compressed fuel, which must exceed 20%. This implies good conversion of the laser energy into forward directed hot electrons with penetration depth matching the optimal size of the hot spot required to trigger ignition. According to present understanding, such conditions could be met by laser pulses with intensities somewhat in excess of 10^{20} W/cm², and 2ω or 3ω frequency (lower frequencies resulting in the generation of too much energetic electrons).

Our design has been performed with the best codes at disposal of the collaborating groups of Rome, Madrid, Bordeaux, Rutherford & London, and Lisbon. We are confident about our modeling of compression (and more generally, of hydrodynamics and energetics), of stability, and of heating and burn. On the other hand, we have not yet addressed a few crucial issues self-consistently. These concern, in particular, the implosion of a cone-guided target, driven by a realistic laser beam pattern, and ultraintense laser interaction, hot electron generation and transport in a low density plasma. We are currently planning the upgrade of our codes. In the meantime, we are using information from theory, model simulations, and experiments. The latter have been performed at intensities comparable to those required for fast ignition, but at much lower total energy. We have therefore to rely on considerable extrapolations. We believe that the experiments to be performed in the next few years at the laser facilities Omega-EP, FIREX, and PETAL, supplemented by a well coordinated computational effort, will greatly contribute to addressing these topics, reducing the uncertainties concerning the operating point of the ignition laser.

Bibliography

- [4.1] M. Dunne, *Nature Physics* **2**, 2 (2006).
- [4.2] M. Tabak, J. Hammer, M. E. Glinsky, W. L. Kruer, S. C. Wilks, J. Woodworth, E. M. Campbell, M. D. Perry and R. J. Mason, *Phys. Plasmas* **1**, 1626 (1994).
- [4.3] N. G. Basov, S. Yu. Gus'kov, L. P. Feokistov, *J. Sov. Laser Research* **13**, 399 (1992).
- [4.4] A. Caruso, in *Proceedings of the IAEA Technical Committee Meeting on Drivers for Inertial Confinement Fusion*, Paris, France, Nov. 14–18, 1994, ISBN-2-7272-0178-8, edited by J. Coutant (Commissariat à l'Énergie Atomique, Limeil, 1995), p. 325.
- [4.5] J. Lindl, *Inertial Confinement Fusion* (Springer, New York, 1998); also: *Phys. Plasmas* **2**, 3933 (1995).
- [4.6] S. Atzeni and J. Meyer-ter-Vehn, *The Physics of Inertial Fusion* (Oxford University Press, Oxford, 2004).
- [4.7] J. H. Nuckolls, L. Wood, A. Thiessen, and G. B. Zimmermann, *Nature (London)* **239**, 172 (1972).
- [4.8] S. Atzeni, *Phys. Plasmas* **6**, 3316 (1999).
- [4.9] R. Kodama, P. A. Norreys, K. Mima, A. E. Dangor, R. G. Evans, H. Fujita, Y. Kitagawa, K. Krushelnick, T. Miyakoshi, N. Miyanaga, T. Norimatsu, S. J. Rose, T. Shozaki, K. Shigemori, A. Sunahara, M. Tampo, K. A. Tanaka, Y. Toyama, T. Yamanaka, and M. Zepf, *Nature (London)* **412**, 798 (2001).
- [4.10] R. Kodama, H. Shiraga, K. Shigemori, Y. Toyama, S. Fujioka, H. Azechi, H. Fujita, H. Habara, T. Hall, Y. Izawa, T. Jitsuno, Y. Kitagawa, K. M. Krushelnick, K. L. Lancaster, K. Mima, K. Nagai, M. Nakai, H. Nishimura, T. Norimatsu, P. A. Norreys, S. Sakabe, K. A. Tanaka, A. Youssef, M. Zepf, and T. Yamanaka, *Nature (London)* **418**, 933 (2002).
- [4.11] M. Tabak, D. S. Clark, S. P. Hatchett, M. H. Key, B. F. Lasinski, R. A. Snavely, S. C. Wilks, R. P. J. Town, R. Stephens, E. M. Campbell, R. Kodama, K. Mima, K. A. Tanaka, S. Atzeni, and R. Freeman, *Phys. Plasmas* **12**, 57305 (2005).
- [4.12] M. Tabak, D. Hinkel, S. Atzeni, E. M. Campbell, and K. Tanaka, *Fusion Sci. Technol.* **49**, 254 (2006).
- [4.13] E. M. Campbell, R. R. Freeman, and K. A. Tanaka (Guest Editors), Special Issue on Fast Ignition, *Fusion Sci. Technol.* **49**, N. 3, (2006).
- [4.14] J. A. Delettrez, J. Myatt, P. B. Radha, C. Stoeckl, S. Skupsky, and D. D. Meyerhofer, *Plasma Phys. Contr. Fusion* **47**, B791 (2005).

- [4.15] N. Miyanaga, H. Azechi, K. A. Tanaka, T. Kanabe, T. Jitsuno, Y. Fujimoto, R. Kodama, H. Shiraga, K. Kondo, K. Tsubakimoto, Y. Kitagawa, H. Fujita, S. Sakabe, H. Yoshida, K. Mima, T. Yamanaka, and Y. Yzawa, in *Inertial Fusion Sciences and Applications 2003*, edited by B. Hammel, D. D. Meyerhofer, J. Meyer-ter-Vehn, and H. Azechi (American Nuclear Society, Lagrange Park, Illinois, 2004), p. 507.
- [4.16] N. Blanchot, E. Bignon, H. Coïc, A. Cotel, E. Couturier, G. Deschaseaux, N. Forget, E. Freysz, E. Hugonnot, C. Le Blanc, N. Loustalet, J. Luce, G. Marre, A. Migus, S. Montant, S. Mousset, S. Noailles, J. Nauport, C. Rouyer, C. Rullière, C. Sauteret, L. Videau and P. Vivini, "Multi - Petawatt High Energy Laser Project on the LIL Facility in Aquitaine", in *Topical Problems of Non-linear Wave Physics*, A. Sergeev, ed., Proc. SPIE **5975**, 30 (2005); also: N. Blanchot, G. Marre, J. Nauport, E. Sib, C. Rouyer, S. Montant, A. Cotel, C. Le Blanc, and C. Sauteret, *Appl. Opt.* **45**, 6013 (2006)
- [4.17] S. Atzeni, A. Schiavi and C. Bellei, *Phys. Plasmas* **14**, (2007) 052702.
- [4.18] R. Betti and C. Zhou, *Phys. Plasmas* **12**, 110702 (2005).
- [4.19] R. Betti, A. A. Solodov, J. A. Delettrez and C. Zhou, *Phys. Plasmas* **13**, 100703 (2006).
- [4.20] S. Atzeni, in *Inertial Fusion Sciences and Applications 99*, ed. by C. Labaune *et al.*, (Elsevier, Paris, 2000), p. 415.
- [4.21] S. Hatchett, M. Tabak, R. Turner, and R. Stephens 2001, in *Proceedings, 28th European Conference on Controlled Fusion and Plasma Physics and 5th Workshop of Fast Ignition of Fusion Targets, Funchal, 2001*, edited by C. Silva, C. Varandas and D. Campbell (European Physical Society, Mulhouse, 2001), *Europhys. Conf. Abstracts* **25A** paper W.18, p. 33 (workshop section).
- [4.22] M. Herrmann, S. Hatchett, and M. Tabak, *Bull. Am. Phys. Soc.* **46**, 106 (2001).
- [4.23] M. Temporal, *Phys. Plasmas* **13**, 122704 (2006).
- [4.24] S. Atzeni and M. Tabak, *Plasma Phys. Controll. Fusion* **47**, B769 (2005).
- [4.25] S. C. Wilks, W. L. Kruer, M. Tabak, and A. B. Langdon, *Phys. Rev. Lett.* **69**, 1383 (1993)
- [4.26] R. R. Freeman, D. Batani, S. Baton, M. Key, and R. Stephens, *Fusion Sci. Technol.* **49**, 297 (2006).
- [4.27] S. Slutz, and M. C. Herrmann, *Phys. Plasmas*, **10**, 234 (2003).
- [4.28] M. Tabak and D. Callahan, *Nucl. Instr. Meth. A* **554**, 48 (2005).
- [4.29] H. Takabe, K. Mima, L. Montierth, and R. L. Morse, *Phys. Fluids* **28**, 3676 (1985).
- [4.30] R. Betti, V. N. Goncharov, R. L. McCrory, and C. P. Vernon, *Phys. Plasmas* **5**, 1446 (1998).
- [4.31] S. E. Bodner, D. G. Colombant, A. J. Schmitt, and M. Klapisch, *Phys. Plasmas* **7**, 2298 (2000).
- [4.32] K. Anderson and R. Betti, *Phys. Plasmas* **11**, 5 (2004).
- [4.33] S. Atzeni, *Plasma Phys. Controll. Fusion* **29**, 1535 (1987).

- [4.34] S. Atzeni, A. Schiavi, F. Califano, *et al.*, Comput. Phys. Commun. **169**, 153 (2005), and refs. therein. Information on the DUED nuclear package is given in S. Atzeni and M. L. Ciampi, Nucl. Fusion **37**, 1665 (1997). The general scheme of the DUED code was described in S. Atzeni, Comput. Phys. Commun. **43**, 107 (1986); the rezoning algorithm is presented in S. Atzeni and A. Guerrieri, in *Proceedings of the 13th Int. Conf. on Numerical Methods in Fluid Dynamics*, Lecture Notes in Physics Vol. 414, edited by M. Napolitano and E. Sabetta (Springer-Verlag, Berlin, 1993), p. 376; for details on the mesh generation scheme: S. Atzeni and A. Guerrieri, Laser Part. Beams **9**, 443 (1991).
- [4.35] J.J. Honrubia, J. Quant. Spectrosc. Radiat. Transf. **49**, 491 (1993).
- [4.36] J.J. Honrubia, *et al.*, Phys. Plasmas **12**, 052708 (2005); J.J. Honrubia *et al.*, Las. Part. Beams **24**, 207 (2006); Las. Part. Beams **22**, 129 (2004).
- [4.37] R. Abgral, J. Breil, P.-H. Marie and J. Ovadia, A cell-centered Lagrangian scheme for two-dimensional compressible flow problems, SIAM J. Sci. Comp., in press.
- [4.38] M. Olazabal *et al.*, submitted to Phys. Plasmas (2007).
- [4.39] S. P. Hatchett, D. Clark, M. Tabak, R. E. Turner, C. Stoeckl, R. B. Stephens, H. Shiraga, and K. Tanaka, Fusion Sci. Technol. **49**, 327 (2006).
- [4.40] D.P Lyon and J.D. Johnson (Eds.), The LANL equation of state database, LA-UR-92-3407, Los Alamos, NM (1992).
- [4.41] R. B. Stephens, S. P. Hatchett, R. E. Turner, K. A. Tanaka, and R. Kodama, Phys. Rev. Lett. **91**, 185001 (2003).
- [4.42] R. B. Stephens, S. P. Hatchett, M. Tabak, C. Stoeckl, H. Shiraga, S. Fujioka, M. Bonino, A. Nikroo, R. Petrasso, T. C. Sangster, J. Smith, and K. Tanaka, Phys. Plasmas **12**, 056312 (2005).
- [4.43] H. Nagatomo *et al.*, Phys. Plasmas **14**, 056303 (2007).
- [4.44] K Yasuike, M H Key, S P Hatchett et al Rev Sci Instrum 72, 1236 (2001)
- [4.45] Y. T. Li, J. Zhang, et al Phys Rev E 69, 036405 (2004)
- [4.46] J S Green, V Ovchinnikov, R G Evans et al submitted to Phys Rev Lett (2007)
- [4.47] S. Baton, L'Allumeur Rapide, Lecture delivered at l'Ecole de Physique, Les Houches, 11–23 Sept. 2005; see: www.ilp.u-bordeaux1.fr/fr/formations/leshouches.html
- [4.48] F. N. Beg *et al.*, Phys. Plasmas **2**, 447 (1997).
- [4.49] K. B. Wharton *et al.*, Phys. Rev. Lett. **81**, 822 (1998).
- [4.50] F. Pisani, A. Bernardinello, D. Batani, A. Antonicci, E. Martinolli, M. Koenig, L. Gremillet, F. Amiranoff, S. Baton, J. Davies, T. Hall, D. Scott, P. Norreys, A. Djaoui, C. Rousseaux, P. Fews, H. Bandulet, and H. Pepin, Phys. Rev. E **62**, R5927 (2000).
- [4.51] A. R. Bell, J. R. Davies, S. Guerin and H. Ruhl Plasma Phys. Controlled Fusion **39**, 653 (1997)
- [4.52] L. Gremillet, G. Bonnaud, F. Amiranoff Phys. Plasmas **9**, 941 (2002)

- [4.53] R. G. Evans High Energy Density Physics **2**, 35 (2006)
- [4.54] D. R. Welch, D. V. Rose, B. V. Oliver, R. E. Clark Nucl. Instrum. Methods. Phys. Res. A **464**, 134 (2001)
- [4.55] A. R. Bell and R. J. Kingham Phys. Rev. Lett **91**, 035003 (2003)
- [4.56] F. Califano, F. Pegoraro, S. V. Bulanov Phys. Rev. E **56** 963 (1997)
- [4.57] L. O. Silva, R. A. Fonseca, J. W. Tonge, W. B. Mori, J. M. Dawson Phys. Plasmas **9**, 2458 (2002)
- [4.58] A. Bret, L. Gremillet and J. C. Bellido Phys. Plasmas **14**, 032103 (2007)
- [4.59] R. W. Short, J. Myatt Paper F01 35th Anomalous Absorption Conference, Fajardo, Puerto Rico June 26 2005
- [4.60] M. Honda and J. Meyer-ter-Vehn Phys. Plasmas **7**, 1302 (2000)
- [4.61] M. H. Key, M. D. Cable et al Phys. Plasmas **5**, 1966 (1998)
- [4.62] P. A. Norreys, M. Santala et al Phys. Plasmas **6**, 2150 (1999)
- [4.63] J. A. Koch, M. H. Key et al Phys. Rev. E **65**, 016410 (2001)
- [4.64] R. G. Evans, E. L. Clark et al Appl. Phys. Lett. **86**, 191505 (2005)
- [4.65] International Committee on Radiation Units Report No. 37 (I.C.R.U., 1984).
- [4.66] C. K. Li and R. D. Petrasso, Phys. Plasmas **13**, 056314 (2006).
- [4.67] C. J. Joachain, *Quantum Collision Theory*, 3rd ed. (North-Holland, Amsterdam, 1987).
- [4.68] J. Sempau *et al.*, Nucl. Instr. Methods in Phys. Res. B **207**, 107 (2003).
- [4.69] J. R. Davies, Phys. Rev. E **68**, 056404 (2003).
- [4.70] B. R. Wienke, Jn. Comput. Phys. **51**, 208 (1983).
- [4.71] J. R. Davies, Phys. Rev. E **65**, 026407 (2002).
- [4.72] W. H. Bennett, Phys. Rev. **45**, 890 (1934), and **98**, 1584 (1955).
- [4.73] H. Alfvén, Phys. Rev. **55**, 425 (1939).
- [4.74] J. R. Davies, J. S. Green and P. A. Norreys, Plasma Phys. Control. Fusion **48**, 1181 (2006).
- [4.75] A.J. Kemp, Y. Sentoku, V. Sotnikov and S.C. Wilks, Phys. Rev. Lett. **97**, 235001 (2006).
- [4.76] J.J. Honrubia and J.M. Aragoes, Nucl. Sci. Eng. **93**, 386 (1986).
- [4.77] J.J. Honrubia and J. Meyer-ter-Vehn, Nucl. Fusion **46**, L25 (2006).
- [4.78] M. Roth, T. E. Cowan, M. H. Key, S. P. Hatchett, C. Brown, W. Fountain, J. Johnson, D. M. Pennington, R. A. Snavely, S. C. Wilks, K. Yasuike, H. Ruhl, F. Pegoraro, S. V. Bulanov, E. M. Campbell, M. D. Perry, and H. Powell, Phys. Rev. Lett. **86**, 436 (2001).
- [4.79] M. H. Key, R. R. Freeman, S. P. Hatchett, A. J. MacKinnon, P. K. Patel, R. A. Snavely, and R. B. Stephens, Fusion Sci Technol. **49**, 440 (2006).

- [4.80] S. Atzeni, M. Temporal, J. Honrubia, Nucl. Fusion **42**, L1 (2002).
- [4.81] Temporal *et al.*, Phys. Plasmas **9**, 3098 (2002).
- [4.82] S.P. Hatchett *et al.*, Phys. Plasmas **7**, 2076 (2000).
- [4.83] S.C. Wilks *et al.*, Phys. Plasmas **8**, 542 (2001).
- [4.84] M. Zepf *et al.*, Physical Review Letters **90** 064801 (2003).
- [4.85] T.E. Cowan *et al.*, Phys Rev. Lett. **92**, 204801 (2004).
- [4.86] J. Badziak *et al.*, Plasma Phys. Control. Fusion **46**, B541 (2004).
- [4.87] J. Badziak *et al.*, Laser Part. Beams **23**, 401 (2005).
- [4.88] A. Macchi *et al.*, Phys Rev. Lett. **94**, 165003 (2005).
- [4.89] J. Badziak *et al.*, Appl. Phys. Lett. **89**, 061504 (2006).
- [4.90] D. Klimo and J. Limpouch, Laser Part. Beams **24**, 107 (2006).
- [4.91] M. Key *et al.*, Proc. IFSA 2005, J. Phys. IV France **133**, 371 (2006).
- [4.92] J. Badziak and J. Wolowski, IAMPI 2006 conf., Szeged, 1-5 October 2006, paper Mo1.

5 Fundamental Science on HiPER

The HiPER laser facility will be a uniquely valuable tool for scientific discovery. The long pulse beams (~200 kJ) combined with ultra-high intensity beams (~70 kJ) will allow the study of new branches of physics. The high energy long pulse beams allow the creation of uniform samples of material at high energy density which are important in many extreme astrophysical, geophysical and fundamental physics scenarios. The ultra-high intensity beams allow access to conditions dominated by relativistic effects such as relativistic plasmas, electron-positron plasmas, particle acceleration and QED effects. Furthermore, the unique combination of long and short pulses, high power and high intensity permits the access, in a single facility with unprecedented detail, to advanced diagnostics of material properties under high energy-density conditions. Similarly, new physical regimes combining material energy density, photon energy density and electric and magnetic energy density can be accessed which otherwise are only achievable in astrophysical objects.

HiPER will be unique as a civilian laser facility which is of sufficient size to create significant fusion gain while operating in an environment which places high importance on basic scientific understanding. HiPER will provide a second, fully equipped target area, independent of the fusion facility which will be subject to only minimal amounts of activation from neutrons and high energy charged particles and will be able to maintain a high throughput of laser shots to accumulate significant and comprehensive data sets.

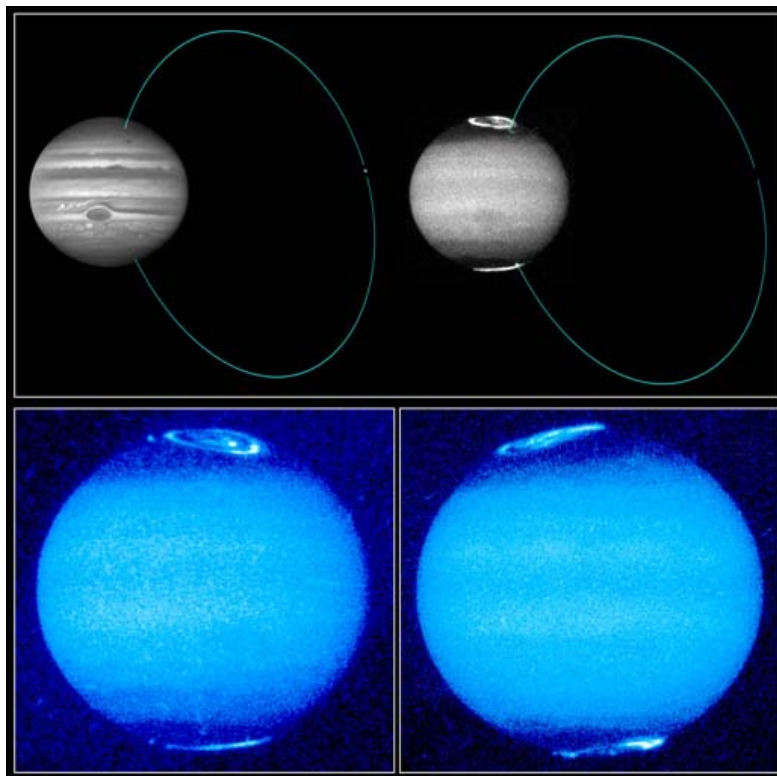
Whilst a number of the topics discussed below will be studied to varying degrees on other laser systems, HiPER will provide a uniquely attractive contribution to these fields:

- It will access a very wide range of target conditions by virtue of its combination of long and short pulse beams.
 - An initially solid target can be isochorically heated by the short pulse beams; or a target can be compressed by shock waves driven by the long pulse beams and then isochorically heated; or a target can be heated by radiative coupling and then allowed to expand before being heated by the short pulse laser; or a target can be imploded to very high density as in the design of fusion targets. Finally, use can be made of the output of the fusion target to access entirely new regimes.
- It will provide unique diagnostic opportunities through its short pulse high intensity beams
 - For example, x-ray Thomson scattering at very high energy; proton radiography to track the motion of buried tracer layers in thick targets; proton probing of electric and magnetic field contours; continuum absorption spectroscopy from subsidiary hohlraums; electron diffraction using the output of short-pulse plasma accelerators, etc etc
- It will provide a volume of scientific data that will be unmatched on other large scale laser facilities, via the separate provision of dedicated fusion and basic science target areas
- It will offer access to the science of extreme conditions to European scientists, who otherwise would only have marginal access to defence lasers [Dunne (2005)]

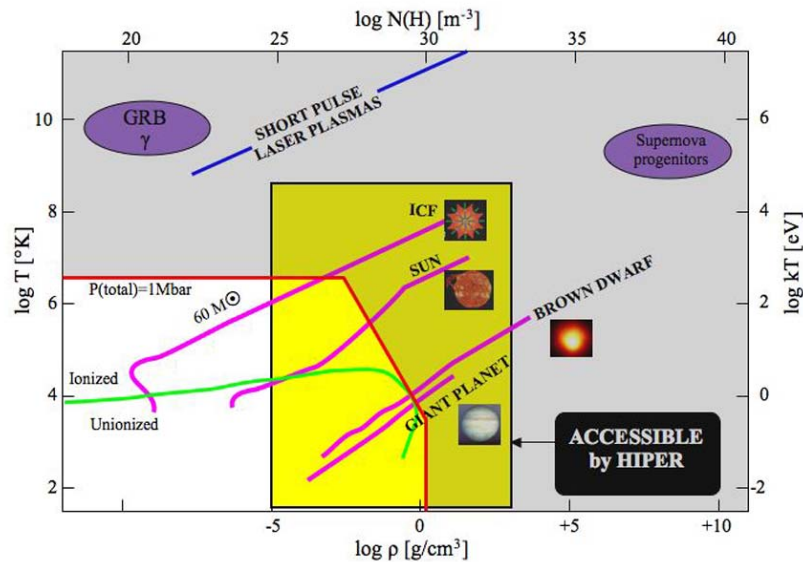
5.1 High Energy Density Physics

High Energy Density Physics (HEDP) has been identified by the US National Academy of Sciences [Connecting Quarks with the Cosmos BPA 2003] as one of the most important and timely areas of science for investigation over the next decade because of its application in fundamental physics and in astrophysics. HEDP encompasses the study of material properties at densities from normal solid densities up to a hundred times solid and temperatures up to around one million Kelvin. Such material occurs in fusion plasmas, in stellar interiors and (at the lower temperature range) in planetary cores. HEDP also encompasses material in astrophysical plasmas although some of the more extreme degenerate plasmas remain as yet inaccessible to laboratory tools.

Many of the structure and transport properties of HEDP materials are required to be measured with some precision, say 1% and with typical experimental resolutions of around 10 micron this means that sample sizes of 1mm cube and upwards are needed. With energy densities of $5 \times 10^{12} \text{ J m}^{-3}$ this gives an energy in the sample of 5kJ and since typical hydrodynamic efficiencies of converting laser energy to sample energy are less than 10% the required laser energy is of order 100kJ and upwards. HiPER fully meets this requirement and, as we will describe below, adds the critical diagnostic opportunities afforded by the ultra-intense beams. It is insufficient to simply create the HEDP conditions – a robust, quantitative diagnostic suite is required to interrogate the dynamic processes in order to adequately test competing predictions.



Magnetic fields around the gas giant planets depend on the conductivity of the core material. Postulated metallic phases of hydrogen at high pressure are within the range of investigation with HiPER.



Density temperature diagram of hydrogen

5.2 Atomic Opacity

The emission and absorption of (typically X-ray) photons is often the dominant process of energy transport in astrophysical plasmas. For an ion with more than a few electrons and particularly in the case of partly filled atomic shells the quantum mechanical calculations of atomic cross-sections and rates are difficult (often intractable with realistic computations) and so require confirmation by experiment. In dense plasmas the transfer of energy by radiation is sensitive to the distortion and broadening of atomic energy levels by collisions and the shifting of ionisation limits by the proximity of other ions (pressure ionisation, Chiu and Ng 1999). Competing theories can produce Rosseland mean opacities differing by 50%, which directly affects calculations of energy flow in radiative objects (Popovics et al 2000, Perry et al 1991). Validation of the range of applicability of these theories is thus of great value.

For some years uncertainties over the opacity of material in the solar interior contributed to uncertainty over the apparent deficit of solar neutrinos. Substantial work on the opacity of iron and neighbouring elements has resolved this (Bahcall and Pinsonneault 2004) to the extent that nuclear rather than atomic physics is now the dominant source of error in the solar neutrino problem. Likewise helio-seismology (Lindsay and Braun 2000) has required accurate temperature-density profiles for the sun and driven programmes for the calculation and measurement of solar opacity. The ability to progress from helio-seismology to stellar seismology in the detection of low- l -modes in stellar spectra now means that opacities are required over a wider range of densities and temperatures than in the purely solar observations. Radiation transport in accretion disks, in the atmospheres of collapsed objects and in the dynamic atmospheres of Cepheid variables and novae continue to drive the requirements for good opacity data.

On HiPER the substantial long pulse and short-pulse laser energy enables a broad range of target conditions to be created, as described above.

Very importantly HiPER allows the creation of target samples which are large enough and of long enough duration to be in Local Thermodynamic Equilibrium (LTE) and can in the other extreme produce unprecedented dynamic rates of change which create such extreme states of material as 'hollow atoms' (Evans et al 2005) where (for example) the two 1S electrons can be preferentially removed with the outer shell electrons remaining in place.

5.3 Photoionised plasmas

Photo-ionisation dominated plasmas are rare in the laboratory but occur frequently in astrophysical plasmas. The ionised nebulae around hot stars with a large fraction of their radiation in the EUV are dominated by photo-ionisation and more extreme and perhaps more important examples are around the nuclei of highly active galaxies such as Seyfert galaxies and in QSOs. The dominance of radiative processes means that the ionisation balance at a given temperature is quite different to a collisionally dominated plasma and uncertainties in photo-ionisation cross sections are reflected in temperature uncertainties as deduced from X-ray spectra.

Recreating these conditions in the laboratory is difficult but possible with large lasers such as HiPER. Photoionised plasmas are frequently described by the photoionisation parameter $\xi = 16\pi^2 J/n_e$ (where J is the radiation intensity and n_e is the electron density) measuring the relative importance of photo-induced processes to collisional processes. Large values of ξ can be created at low densities but then large volumes of plasma are required to guarantee conditions of LTE. Inevitably large values of ξ require large inputs of energy into the plasma. Typically targets use doped low-density foams inside hohlraums to allow measurement of the distribution of ionisation in photoionised plasmas with very high photoionisation parameter ($\xi > 100 \text{ erg cm s}^{-1}$). HiPER will achieve these extreme conditions because it will reach hohlraum radiation temperatures of at least 250eV, allowing the attainment of ξ values approaching those in a QSO (quasi-stellar-object). This is to be compared to the most extreme conditions achieved so far in the laboratory where the Z-machine at Sandia National Laboratory in the USA (Foord et al 2004, Rose et al, 2004) achieved a plasma with a photoionisation parameter $\xi \sim 20 \text{ erg cm s}^{-1}$.

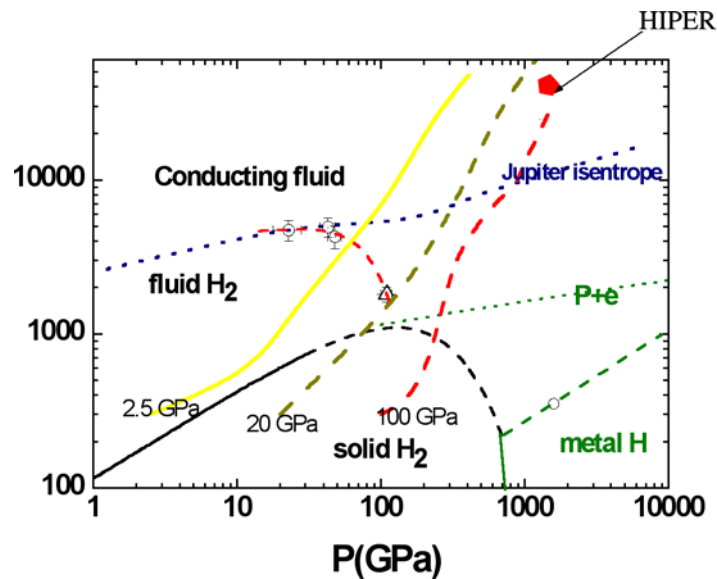
Driving photoionised plasma experiments with the output from an ignition capsule on HiPER will allow even more extreme conditions to be achieved. The radiation field generated would be higher than could be achieved using a laser-heated hohlraum and calculations suggest that a photoionisation parameter $\xi \sim 1000 \text{ erg cm s}^{-1}$ would be possible which is as high as is believed to exist anywhere in the Universe.

5.4 Warm Dense Matter

Warm Dense Matter (WDM) is an important part of the HEDP parameter space, ranging in density from normal solids to around 10 x compression and in temperature from 0.1 eV to perhaps 100 eV. This state of matter is at the frontier between condensed matter physics and plasma physics where the electrostatic energy of the electrons and ions is comparable to their kinetic energy and the material is somewhat ordered. There are no applicable perturbative methods and over part of the phase space degeneracy effects add a quantum dimension to the otherwise classical problem. One of the main purposes for the study of WDM is the direct relevance for the understanding of earth and planetary interiors (Guillot 1999). Internal structure models are very sensitive to Equation of State (Saumon Chabrier and Wagner 1995) and phase transitions while the variation of transport properties across phase changes is important to dynamo models. HiPER will make a unique contribution to WDM research since it will be able to provide more laser shots, covering a wider range of material conditions and providing superior diagnostics to other large laser systems.

Most of the needed measurements lie on the so-called planetary isentropes, the planets having been generated by very slow accretion and quasi adiabatic compression. Therefore there is a need to develop new experimental methods to reach such conditions. They will be based on the use of high power lasers coupled to another technique, changing initial conditions (such as diamond anvil cells compression or proton beam isochoric heating) to access P-T conditions unreachable by any one of these techniques alone. In the case of hydrogen (the EOS of warm dense hydrogen models giant

planets and brown dwarfs) this will produce data on a strongly correlated degenerate plasma, that would certainly be a reference in quantum many-body physics. According to present status of preliminary experiments, we shall expect to reach initial pressure in the sample around 30-50 GPa which is 10 times above what is currently tested. Such high initial pressures conditions will provide data up to a few thousands of GPa along the Jupiter isentrope (see figure).



Phase diagram of hydrogen. The star corresponds to the maximum pressure reached along the Jupiter isentrope.

5.5 New Diagnostic Techniques

The knowledge of Equation Of State (EOS) and related parameters of dense matter has been the target of a large effort, in particular in the development of relevant diagnostics to perform high precision measurements. Shock-wave-EOS experiments require that two parameters, usually the shock and fluid velocities, be measured to infer the thermodynamic properties of the material. Moreover, these existing measurements cannot lead to a good precision on an important physical quantity as density. Therefore the development of direct probing techniques to obtain information on other shock parameters, such as density, would allow precise absolute EOS determinations and would represent a real breakthrough in the field. The development of ultra high intensity beams allows for probing of dense materials ($\rho > 1 \text{ g/cm}^3$) with X-ray and proton sources than cannot be produced by standard long pulses beams ($E > 10 \text{ keV}$). Moreover proton or ion beams source can also provide a good way to investigate WDM, for instance by tracking the position of thin tracer layers, while having high spatial and time resolution.

X-ray scattering is the most exciting and important development in dense plasma diagnostics for some decades. The method is possible only because ultra-high power lasers can be used to produce high brightness, narrow linewidth X-ray sources which are of high enough photon energy to penetrate significant amounts of dense plasma. Thomson scattering (Glenzer et al 1999, Gregori et al 2003) can measure both electron and ion temperatures, electron density and also the average degree of ionisation $\langle Z \rangle$.

As the photons produced by the resonant line of a secondary plasma are Compton scattered through the high density sample, they are also dispersed in energy by the Doppler effect. This technique thus allows the direct measurement of the electron velocity distribution function in a high density medium. Clearly, this method is directly scalable to measurements of temperature in matter at extreme densities and pressure, as the one achieved during the compression phase in an implosion

capsule. In this respect, the development of efficient multi-keV X-ray sources is a necessary step as a penetrating radiation probe is required for scattering off the imploding core. Indeed, this will also require multi-kJ picosecond laser pulses as the ones proposed in the HiPER project. At the same time, as the core compresses, matter undergoes a transition from an ideal state to a Fermi degenerate system. Such systems are usually very hard to model and measure with conventional optical diagnostics. On the other hand, since X-ray scattering directly probes the electron distribution function, the interpretation of the data is considerably simplified.

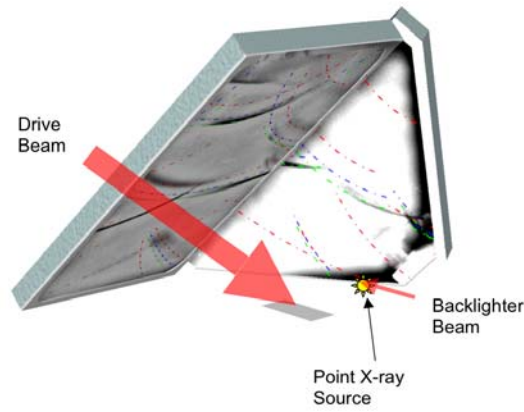
X-ray Thomson scattering is a key diagnostic method for both the fusion and non-fusion experiments on HiPER. The method will provide EoS and transport related measurements in WDM which are not easily measured by any other methods. In the ICF implosion dynamics Thomson scattering will be an important diagnostic of shock timing and compression, which is of vital importance for the success of the inertial confinement fusion mission.

5.6 Materials science

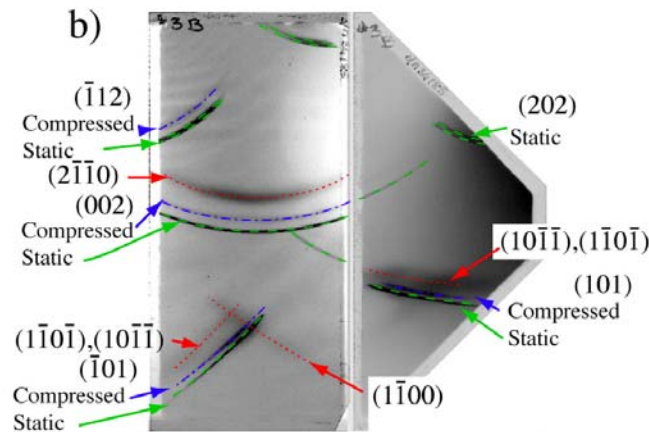
Over the past few years materials science has rapidly become a burgeoning area of study with high-power-lasers. There are two main reasons for this. Firstly, high energy lasers, such as the proposed HiPER system, afford the opportunity to create states of matter which are still in the solid phase, but otherwise completely unobtainable. Secondly, such off-Hugoniot states (and indeed those on the Hugoniot) can be interrogated directly by short burst of X-radiation that can be synchronously generated with separate laser beams, allowing the structure of the material to be directly interrogated by X-ray diffraction and/or EXAFS techniques. For example, recent work has shown that the K-shell X-rays produced from laser-produced plasmas can be used to directly observe the motion of atoms during shock-induced phase transitions (Kalantar et al, 2005; Yaakobi et al, 2005; Hawreliak et al, 2006; Kadau et al, 2007).

The energy capacity of HiPER, combined with laser pulse shaping in long pulse mode will mean that it will be capable of compressing materials quasi-isentropically. In this mode of compression it is proposed that a ramped pressure wave, several nanoseconds in duration, is launched into the material of interest. Before the ramp has had time to steepen into a shock, the material is compressed along the isentrope, rather than the Hugoniot (strictly speaking it is a quasi-isentrope, with differing strength properties than true isentropic compression). Sophisticated target designs with layers of differing impedance can also keep the compression of a specific layer close to isentrope. The main point here is that for solid materials it is predicted that a machine such as HiPER should be able to compress crystals to pressures of order 10-15Mbar, whilst still keeping them in the solid phase. It should be noted that along the Hugoniot, a typical crystal melts about 2Mbar, so the very high shock pressures produced in the past (tens, or even hundreds of MBar) have all produced matter in the liquid or plasma, rather than solid state.

Static methods of compressing crystals using diamond-anvil cells are limited by the strength of diamonds to 3.5Mbar. Therefore high-power lasers offer a method of producing matter, under conditions that in many cases is of interest from a planetary science point of view that cannot be produced by any other methods. As we have noted above, with lower energy lasers it has already been shown that the crystallographic phase of matter under compression can be directly interrogated on sub-nanosecond timescales with laser-plasma produced X-rays: The figures below show the type of experimental set up we envisage, along with data showing the shock-induced phase transition in iron (see Kalantar et al, 2005, and Hawreliak et al, 2006).



Schematic diagram for the experimental set up to perform x-ray diffraction on sub-nanosecond timescales from laser-shock-compressed targets. One set of laser beams, focussed to a tight spot, produces a hot plasma which is a copious source of K-shell x-radiation. These quasi-monochromatic x-rays diffract from a driven crystal, and are recorded on a wide angle detector as shown.



Raw diffraction image from a laser shocked crystal showing diffraction from pristine bcc iron, elastically compressed bcc iron, and iron that has changed into the hcp phase (with a reduction in volume of order 15-18%) due to laser-shock compression. The diffraction image was taken with a nanosecond burst of K-shell x-rays emitted by a laser-produced plasma. See references Kalantar et al, 2005, and Hawreliak et al, 2006 for further details.

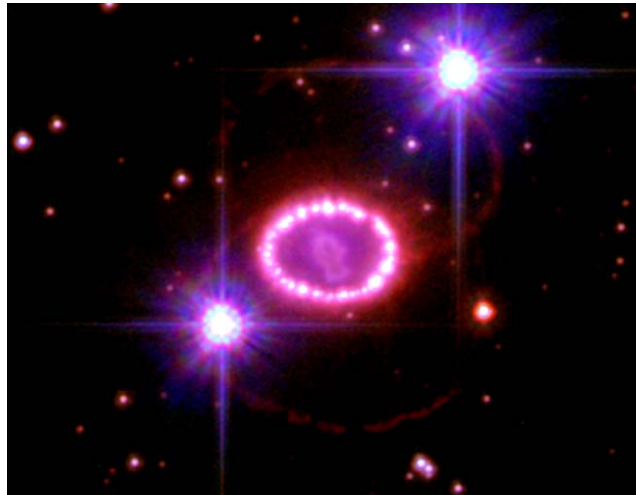
5.7 Laboratory astrophysics

For many years laboratory astrophysics concentrated on the interpretation of astrophysical spectra in terms of the atomic transitions and rates. This played an important role in the determination of temperatures and densities in astronomical objects. More recently it has been possible to create laboratory plasmas which are in many ways scaled analogues of their astrophysical counterparts. Ryutov (1999, 2006) showed that with suitable Euler scalings of density, velocity, space and time it is possible to bridge the many orders of magnitude between laboratory and astrophysical plasmas.

The physics of plasmas plays a vital role in many astrophysical phenomena and the incorporation of these fundamental concepts in the interpretation of observations cannot be underestimated, and in many cases is essential for a proper explanation. Many astrophysical systems are complex and non-linear. The multi-scale nature of much of this physics remains beyond numerical simulation, so a direct experimental approach is particularly helpful. Furthermore, astrophysics relies on remote sensing, whereas experiment allows repeated *in situ* probing and the freedom to alter input conditions. In addition, experiments can test or validate sophisticated multi-dimensional

computer models in relevant physical regimes.

Fortunately, the required high energy density in the laboratory plasmas means that laser produced plasmas are often a suitable analogue system and laboratory experiments have sought to model a variety of astrophysical situations such as supernova expansion, collisionless and radiative shock waves and the instabilities of jets flowing into the interstellar medium. Even when the laboratory system fails to fully scale to its astrophysical counterpart there is an important opportunity to exercise the astrophysical computer models (and their users!) in an environment where systematic changes to the experiment and the model are possible.



Supernova SN1987A showing the instability of the radiative shock wave passing through the circumstellar medium around the star. (Image from NASA / ESA Hubble telescope)

HiPER offers the opportunity to extend many of the existing experiments to regimes which are better analogues of the astronomical source by providing longer temporal and spatial scales as well as far greater flexibility in the introduction of dissipative terms (radiation, magnetic fields, etc). The combination of energetic long and short duration laser beams enables the creation of plasmas to simulate the ejection of winds and jets from highly evolved stars into the interstellar medium, the formation of collisionless shocks and many other high energy density systems. Future possible experiments included studies of cosmic ray seeding and acceleration, mechanisms for gamma ray bursters, and also fundamental studies of exotic astronomical processes such as electron-positron plasmas and photon bubbles. With regard to the underlying physical processes, HiPER will enable the study of colliding plasma systems, highly nonlinear hydrodynamic instabilities and the transition to turbulence under high Mach number conditions, the behaviour of photon-dominated plasmas and macroscopic relativistic plasmas.

Some examples of scaled experiments include:

- Protostellar jets expanding into the interstellar medium can be scaled with HiPER to more realistic conditions where the plasma and MHD properties separate from the purely fluid instabilities in the present experiments (Rosen et al 2005). HiPER can produce hotter plasmas with large embedded magnetic fields generated from the thermo-magnetic source. Larger scale jets produced by a laser the size of HiPER have a larger ‘inertial range’ between the scale length of viscous effects and the size of the jet. Dimotakis (2000) suggests this is a pre-requisite to trigger turbulent mixing.
- Collisionless shock experiments (Woolsey et al 2001) can be performed where the overall size of the laboratory system is large enough to contain the ion Larmor radius and thus

model the effect of magnetised ions for the first time.

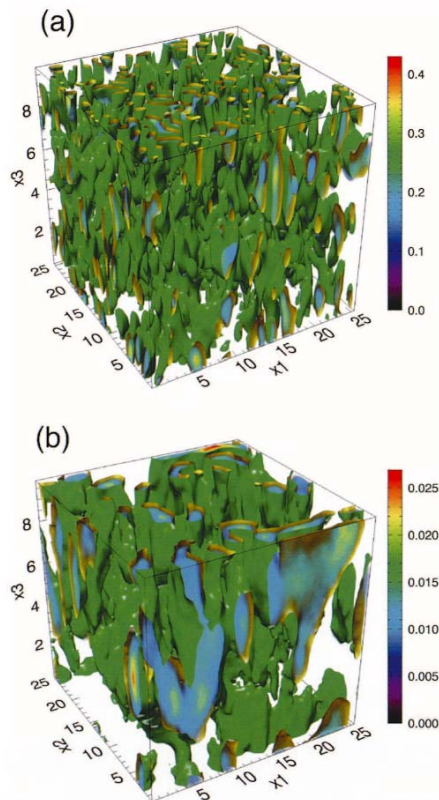
- Radiative shock experiments (Keiter et al 2002) can be performed at higher source temperature where the structure of the radiative precursor is better separated from the main shock front. Experiments on larger systems will give high resolution measurements of the unstable growth of the Vishniac instability (Vishniac 1983, Ryu and Vishniac 1991, Leygnac et al 2006).
- The potential to generate enormous magnetic fields (in excess of a GigaGauss) over long length scales can lead to conditions otherwise only found on the surfaces of white dwarf and neutron stars. This allows the study of atomic systems in which the magnetic rather than the electric field dominates, motion of charged particles and characteristics of collective plasma processes influenced by the ultra intense magnetic fields.
- The short pulse ultra-high intensity beams of HiPER open up totally new areas of astrophysical application such as the ability to generate large volumes of electron positron plasma, and a laboratory analogue of the exotic photon bubble instability (Klein and Arons 1991, Arons 1992) that is predicted to occur (and may have been observed by Jernigan et al 2000) in accretion powered pulsars. Intense photon bubbles are thought to be present in the low altitude atmosphere above the surface of neutron stars. The laboratory experiment requires radiation temperatures of the order of 100eV-1000eV at densities of about $10^{-3} \text{ g cm}^{-3}$ and magnetic fields $> 0.1 \text{ GGauss}$ such that the radiation pressure exceeds the thermal pressure. This requires high laser energy (to create a macroscopic plasma) and simultaneously high intensity ($\sim 10^{22} \text{ W/cm}^2$). HiPER would provide this capability.

The goal of laboratory astro-plasma experiments remains the exploration of combinations of fundamental physical processes in a controlled environment. This field provides a common frontier for both the experimentalist and the theoretician interested in laboratory and astrophysical plasma research.

5.8 Relativistic astrophysics with relativistic beams

The possibility of producing intense relativistic beams (see below) opens the way to the exploration of relativistic astrophysical scenarios, such as gamma ray bursters or pulsars. This experimental approach to relativistic astrophysics has to rely on the possibility to easily access relativistic beams. In different relativistic astrophysical scenarios plasma physics aspects are thought to play an important role; controlled experiments are being designed to provide answers to some of the outstanding problems in this field.

The radiation from pulsars, gamma ray bursts and blazar jets is associated with relativistic electron beams. Experiments using relativistic beams in laboratory plasmas may be able to shed light on the key radiation processes. Moreover, in gamma ray bursts, electron-positron-proton streaming instabilities are unstable to the Weibel instability (Gruzinov and Waxman, 1999; Medvedev and Loeb, 1999). This generates B fields, which in turn lead to the synchrotron radiation features observed in these most extreme explosions of the Universe. Experiments with relativistic streams can not only complement recent findings of numerical experiments (Silva et, 2003), but also to provide information about the magnetic fields generated by these streams as relativistic shocks form, and their long time evolution, but also about the mechanisms for particle acceleration through collective plasma mechanisms (e.g. plasma wakefield acceleration) and radiation generation in the tangled magnetic field structure.



Structure of the magnetic field in the early stages of the collision of two relativistic plasma streams ($e-e^+$) for two different times (a) linear stage of the Weibel instability, (b) saturation stage of the instability). For details, see Silva et al, 2003.

Similar scenarios are also common in blazar jets, where the radiation is generated by e-beams moving into high B field regions resulting in maser emission. Similarly with pulsars, where e-beams are thought to be unstable to streaming instabilities. The production of gamma rays and positrons can also be studied using relativistic e-beams or colliding plasma configurations, as well as the creation of laboratory neutron star atmospheres (with ultra intense B-fields) and photon bubbles.

The possibility to examine the formation of collisionless shocks is also of paramount importance. The generated relativistic streams of particles in HiPER can lead to the onset of nonlinear structures that will evolve to high Mach number collisionless shocks. Collisionless shocks are pervasive in astrophysics, and the possibility to examine in detail how particles are accelerated in these structures can provide answers to how particles/cosmic rays are accelerated in the Universe.

Furthermore, the possibility to heat small targets to relativistic temperatures, combined with the presence of long scale length plasmas, also opens the possibility to study the interaction of intense x-rays radiated from these sources with plasmas, and to observe parametric instabilities, and particle acceleration driven the broadband photon beams, in conditions similar to those present in many astrophysical scenarios (C. Thompson et al, 1994).

5.9 Basic laser-plasma interaction studies

The conditions available in HiPER open the possibility not only to perform experiments in fundamentally new regimes but also to explore more standard regimes with very fine detail and/or novel configurations. This is of significant relevance in laser-plasma interaction studies dominated by nonlinearities and parametric instabilities, which are relevant/dominant in many applications.

The propagation of pulses (both nanosecond and picosecond) of peak powers expected for HiPER in a dilute medium (gas) involves strong nonlinear effects, no matter whether the pulse is focused and how tight is the focusing. Indeed, most of the instabilities related to the propagation depend on power rather than on intensity. A detailed study of the propagation of the HiPER pulses in gas along tens of meters path would be of particular interest. The characterization of large plasmas produced by optical gas breakdown may have considerable interest in related fields, such as next-generation particle accelerators (for example, as are being planned on the Extreme Light Infrastructure facility). Long-scale thermal and ponderomotive self-focusing and filamentation can be studied in conditions of well-defined momentum ($\Delta k \ll k_0$) and large size plasmas.

At higher intensity, laser-matter interactions will induce relativistic self-focusing. This effect is countered by the defocusing effect of photo-ionisation. When these effects balance each other, the laser light can be self-guided. The self-focusing and self-guiding phenomena as well as other collective phenomena in laser plasma (e.g. Raman and Brillouin instabilities) can be studied in a preformed plasma produced by a pre-pulse preceding the high intensity main pulse, or using a low-contrast laser pulse.

Furthermore, the high level of power of HiPER can not only lead to record intensities, but also to have high (but not extreme) intensities on solid samples of relatively large surface area. Many basic physical phenomena involving momentum transfer to the sample from the laser pulse, both directly via radiation pressure and indirectly via ablation and fast particle backward ejection have been investigated for more than 20 years, but most of the measurements are extrapolations from data obtained in conditions far from the 1-D geometry. In such conditions the contribution of transverse effects was important and difficult to evaluate. Similar uncertainties were left also from the study of energy deposition and laser-plasma instabilities, due to the spread of the k -vectors consequent to the tight focusing required at that time to reach high intensities. The possibility to perform experiments in long-scale length plasmas opens the opportunity to study and to understand in detail these scenarios and these instabilities under idealised conditions.

5.10 Nuclear Physics

HiPER offers a combination of plasma conditions and extreme fields which bring new opportunities in the study of nuclear physics. Extreme plasma density, high particle fluxes and ultra-intense electric fields all bring new features to laboratory based experiments.

5.10.1 Nuclear reactions under extreme conditions

The high energy density conditions made possible by the high energy beams of HiPER will enable nuclear reactions to be studied under conditions of high density and temperature. Nuclear reaction cross sections can be studied in hot plasma, where the presence of ions and clouds of electrons produces screening effects. HiPER will facilitate experiments to benchmark theoretical estimates of screening effects on nuclear reaction rates. It will enable the study of the effects of screening on thermonuclear reactions, important for nuclear burn and for modelling the processes at the centre of stellar environments.

HiPER will produce exceptionally high neutron fluxes both from the burning fusion core (10^{19} neutrons in 10^{-10} sec and from direct fusion in the laser electric field (see below, 10^{11} neutrons in 10^{-13} sec from a 10×10 micron source). These neutron fluxes are large enough to measure the neutron capture in short lived isotopes in the astrophysically important r-process reactions (Terasawa 2001,

Qian 2005) and also the very rare double neutron capture events. The second (non-activated) target chamber in HiPER means that many shots can be accumulated to measure small cross sections.

Bursts of 10^{19} neutrons will be produced in the nuclear burn. These short pulses of neutrons can be used for neutron scattering research, radioisotope production, fundamental physics research, radiography and activation analysis (Ledingham et al., 2003).

5.10.2 Direct nuclear excitation using laser radiation

The peak powers available from the HiPER beams reconfigured for OPCPA will exceed 150 PW and powers extending up to 1 EW are envisaged. This will lead to focused laser intensities exceeding 5×10^{24} W/cm² and possibly up to 5×10^{26} W/cm². The corresponding electric fields at the focus of laser pulses at these intensities exceed 10^{17} V/m and 10^{19} V/m respectively, which can directly induce keV to 100 keV shifts in nuclear levels. HiPER will thus, for the first time, enable experiments on direct nuclear excitation by laser radiation. In addition, the ability to produce synchronised high energy particle and radiation beams from laser-plasma interactions can provide a probe of these ‘dressed’ nuclear states, enabling pump-probe experiments to be performed on the nucleus. Furthermore, laser-plasma acceleration schemes could be used to produce beams of excited nuclei for fundamental nuclear physics experimentation.

5.10.3 Nuclear and particle radiation source

Beams of GeV protons and several hundred MeV gamma rays, produced with the high power HiPER beams can be used to produce pions. At rest pions have a lifetime of 20ns. However the possibility exists to use a laser plasma accelerator (over picoseconds timescale) to accelerate pions to increase their energy and lifetime (R. Davidson et al, 2003). In turn high energy pions decay to produce a source of muons and neutrinos. Thus HiPER can be used to drive a high energy particle source.

The development of HiPER will also enable the study of electron-positron plasmas in the laboratory. At laser intensities about 2×10^{18} W/cm² the electron quiver energy in the laser field exceeds the electron rest energy and superthermal electrons are produced. These relativistic electrons can produce electron-positron pairs via the Bethe-Heitler and trident processes when interacting with high-Z ions.

Experiments performed using a petawatt laser at the Lawrence Livermore National Laboratory have demonstrated electron-positron pair production (T. E. Cowan *et al.*, 2000). Simulations with particle-in-cell codes have shown that in principle pair densities as high as 10^{-3} of the background electron density is possible when focusing petawatt class lasers of sufficient duration onto a gold target (Liang, Wilks, and Tabak, 1998). The HiPER 70 kJ laser of 10 ps pulse duration illuminating a single gold target would in principle produce copious numbers of electron positron pairs, which when the laser radiation is turned off, will expand much quicker than heavier ions, creating a pair fireball.

5.10.4 Nuclear Fusion in the Laser Electric Field

Deuterons and Tritons oscillate in the electric field of the laser with different velocities due to their different charge to mass ratios. At 10^{23} - 10^{24} Wcm⁻² the differential velocity is close to the peak of the D-T fusion reaction cross section and fusion will occur due to the laser quiver velocity. Above 2×10^{23} Wcm⁻² the relativistically corrected critical density exceeds 1 gm cm^{-3} so the laser light will directly penetrate solid material and self-focussing will help to extend interactions beyond the Rayleigh length. The expected neutron yield from D-T is in the range 10^9 - 10^{11} neutrons

depending on the efficacy of self-focussing. The neutron pulse duration is the same as the laser pulse length.

At and above 10^{24} Wcm⁻² the D-³He and p-¹¹B fusion reactions have significantly large cross sections. D-D and T-T reactions are not excited since there is no difference in quiver velocity.

In the setting of a high repetition rate, high energy beam for HiPER this offers the opportunity for a variety of material studies under the action of high flux repetitively pulsed neutron irradiation as would occur in a fusion reactor scenario.

5.11 Plasma accelerators

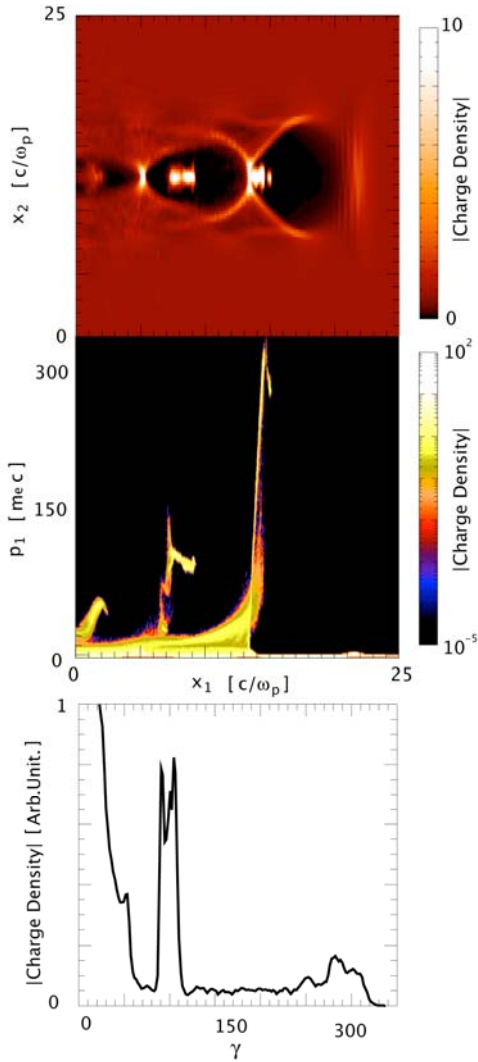
An emerging application of intense lasers is plasma-based accelerators, either of electrons or of ions. The acceleration mechanisms are significantly different in both cases but in all cases the plasma acts as a transformer of the transverse fields of the laser into the ultra high longitudinal fields capable of accelerating particles to high energies in very short distances. The combination of high energy with ultra high intensity in HiPER provides exciting opportunities and establishes the conditions to probe and to explore future plasma-based accelerators with lasers.

5.11.1 Laser-plasma electron accelerators

Recent experimental results with short laser pulses have demonstrated the generation of monoenergetic electron bunches (energy spread < 10%) in the 100s of MeV to GeV energy range (Mangles et al, 2004; Geddes et al, 2004; Faure et al, 2004; Leemans et al, 2006). These electron bunches show sub-nC total charge and, by themselves, represent already an outstanding tool for science, with many different applications. These results have been obtained with laser pulses with intensities close to 10^{19} W/cm², pulse durations ranging from 80 fs to 30 fs, with a normalized vector potential $a_0 \sim 1-3$ range, operating close to the bubble, or blow-out, regime (Pukhov and Meyer-ter-Vehn, 2002).

Theoretical estimates and numerical simulations indicate that 100GeV electron beams can be produced with longer pulses (~ 100 fs), and higher energies per pulse (~ 1 kJ) if the experiments are set-up to occur in the blow-out regime (W. Lu et al, 2006). HiPER provides the opportunity to use either the ignitor beam or future upgrades to high intensity to achieve 100GeV electron beams.

It is clear that higher energy beams with sub-nC total charge will require laser pulses with higher energy. Furthermore, the matching conditions for the blow-out regime will require smaller densities, and thus longer pulses in order to maintain the efficiency of conversion to monoenergetic beams high. The availability within HiPER of different options in terms of pulse length/energy will provide a unique opportunity to best determine the conditions to operate in the blow-out regime, and thus to produce stable mono-energetic multi-GeV beams.



Typical scenario associated with the blow-out regime, depicting the typical features of electron acceleration in this regime, obtained from a numerical simulation (from top to bottom: electron density, p_1x_1 phase space and energy distribution of the electrons)



Laser drive electron accelerators can achieve energies equivalent to the SLAC linear accelerator in just a few metres length

5.11.2 Laser-plasma proton accelerators

Ion acceleration with lasers has also shown significant progress in recent years. The most explored mechanism leading to relativistic ion acceleration is associated with the space charge field generated in the back surface of solid targets (Borghesi et al, 2006; Fuchs et al, 2006). This electric field arises from the fast electrons, pushed by the radiation pressure of the laser, leaving the target. The ion beam acceleration is highly efficient, and the ion energy per nucleon is proportional to the laser pulse energy. The strongly nonlinear physical processes, leading to generation of relativistic electrons, fast electron transport and fast ions, need to be investigated experimentally at extreme laser pulse parameters.

HiPER will provide not only the ability to operate at ultra energies and ultra high intensities but also to provide very wide focal spots, and thus proton beams. Laser-induced production of protons at very high intensities has tremendous promise because the proton beam becomes highly directional with increasing laser intensity. More sophisticated configurations, such as multilayer targets and alser pulse shaping also make it possible to generate protons having energy spread of ~5% (Borghesi et al, 2006; Schwoerer et al, 2006, Robinson et al 2007).

Fast ions (mainly fast protons) provide a wealth of application (fast ignition, plasma accelerators, medicine, nuclear physics, physics of elementary particles) (Borghesi et al, 2006; Badziak et al, 2006). Furthermore, at higher laser intensities the direct ion probing techniques of dense matter (plasmas) are become an important diagnostic technique, allowing for proton radiography of imploding thermonuclear targets (Borghesi et al, 2006). The development of direct ion probing techniques to obtain information on shock parameters, such as density, would allow precise absolute EOS determinations and would represent a real breakthrough in the field. The proton or ion beams source can provide a good way to investigate WDM while simultaneously providing high spatial and temporal resolutions.

5.12 Fundamental Physics with Strong Fields

As well as the applications of the ~70kJ ~ps ignitor laser pulse, HiPER offers the longer-term potential to be reconfigured in an OPCPA amplification mode. This could generate 10 kJ in 10 fsec, providing a power of 1 Exawatt. Focused to a spot of 1 micron the irradiance would be 10^{26} Wcm^{-2}

The decision on whether to progress to such a new configuration would be determined by the results from other laser facilities (particularly the proposed ELI facility). A reconfigured HiPER would open the potential for extremely high-end fundamental physics studies. It would not be well suited for operation as a user-applications based facility: that should be left to dedicated facilities such as ELI.

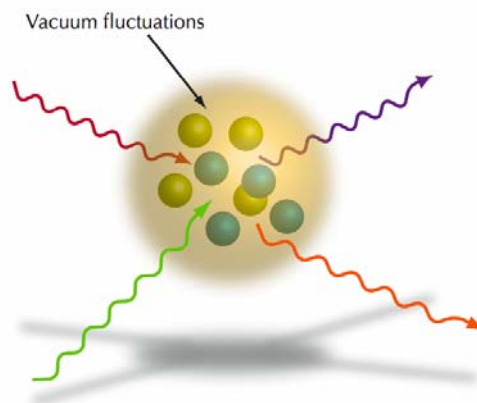
Based on these prospects, the HiPER facility would open up possibilities to do new and exciting experiments concerning fundamental physics, in particular issues related to the quantum vacuum (Buchanan, 2006). Established topics, such as the Lamb shift, could be probed with unsurpassed accuracy in new environments. Some issues related to theoretically well-known subjects, such as photon splitting (frequency down conversion in an external field) and pair production (creation of electron-positron or other matter-antimatter pairs from the vacuum), could be investigated using the high photon flux provided by HiPER. Corrections to e.g. Landau quantization of the electron due to quantum vacuum effects could be found experimentally, something of importance for the physics of strongly magnetized objects, such as magnetars.

Collective photon effects, such as four-wave mixing, will be possible to produce new photons from the quantum vacuum, and the structure of these photons would shed light on QED and the possible corrections to standard quantum field theoretical particle models. The Unruh effect, of major importance for our understanding of the link between quantum field theory and spacetime structure, could be experimentally analyzed, giving important insight on strong field gravity outside black hole horizons. The large number of photons is also likely to give a means for investigating *dynamical* quantum vacuum effects, such as laser pulse compression in external fields, a field never before examined experimentally (Marklund and Shukla, 2006; Salamin et al, 2006; Mourou, Tajima and Bulanov, 2006).

5.12.1 QED Physics

There are a number of effects that arise from the vacuum polarisation due to virtual lepton pairs, the $e^+ e^-$ pairs being the lightest and therefore the first to appear.

Photon-photon scattering in vacuum (see Fig. V.1) arises due to the interaction described in lowest order by the well known 'box diagram'. Two wave interactions are forbidden by energy-momentum conservation, three wave interactions must be co-linear and are difficult to detect and four wave mixing is the obvious effect to pursue (Lundström et al, 2006; Lundin et al, 2006; Moulin and Bernard, 1999; Bernard et al, 2000). Four wave mixing should be observed before HiPER is built (see Fig. V.2) but the lowest order QED contributions to four wave mixing are well studied and contribute to the Lamb shift and the anomalous electron and muon magnetic moments where they are measured very precisely. HiPER offers the opportunity to study four wave mixing beyond lowest order where the Fermion propagators have to be evaluated in the strong field of the laser (essentially as Volkov states and there are higher order QED and even QCD corrections to the vacuum polarisation (Bern et al, 2001).



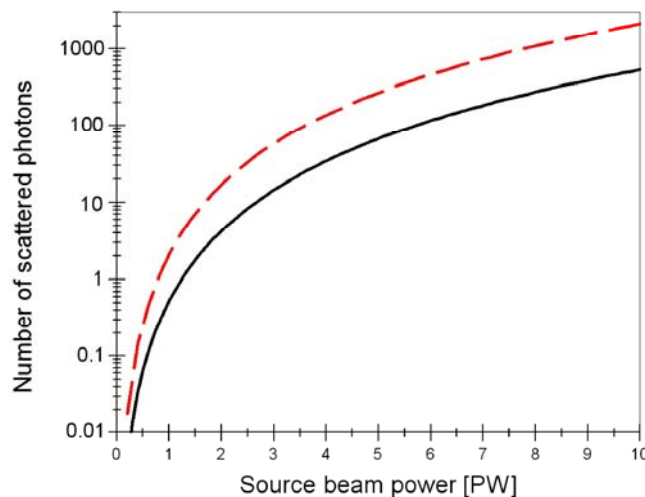
The conceptual interpretation of elastic photon-photon scattering, where two incoming photons interact via vacuum fluctuations to produce two photons with, in general, different frequency and propagation directions.

HiPER also offers the opportunity to combine the ultra-intense light source with high energy electron beams created by laser acceleration in low density plasmas and therefore intrinsically synchronised with the laser pulse.

Our best estimate of the electron energy that can be achieved in an accelerator pumped by the fast ignition beam of HiPER is around 100 GeV. The electron energy E scales with the laser energy J as

$E \sim J^{2/3}$ so splitting the laser into two beams to pump opposed accelerators does not give a dramatic loss in energy

With its associated electron accelerator, HiPER becomes a flexible tool to study a variety of photon scattering and pair creation processes. At an electron energy of 100 GeV the Lorentz factor is 2×10^5 and the laser photons are upshifted by a factor of $4\gamma^2$ to 160 GeV. The gamma ray photons are also polarised so there is a powerful opportunity to build a gamma gamma collider with photon energies up to 160 GeV. It has been argued that the smallness of the photon-photon cross section is potential window into new physics such as the existence of extra dimensions (Cheung 2000, Davoudiasl 1999, Arkani-Hamed et al 1998, Anoniadis 1998).



The estimated number of photons, due to four-wave mixing in the polarized vacuum, as a function of laser beam power (Lunström et al, 2006; Lundin et al, 2006). The dashed curve is for three independent source beams, while the solid curve assumes beam splitting. We see that a statistically significant number of photons can be achieved with a facility like HiPER.

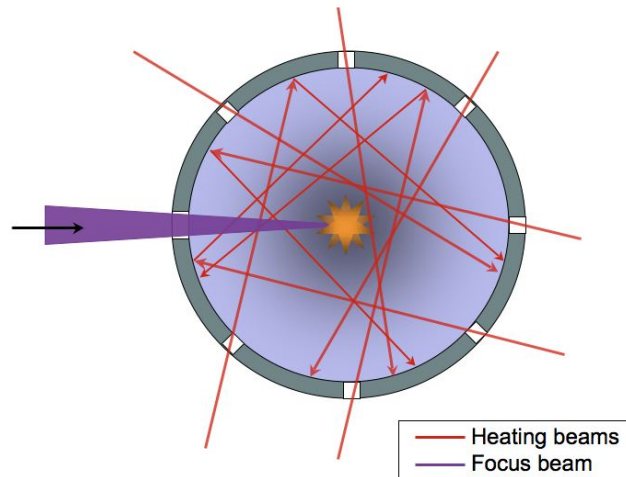
With much lower energy gamma photons, around 1 MeV, the Breit-Wigner process of $\gamma + \gamma \rightarrow e^+ + e^-$ (Burke et al, 1997) can be systematically studied as a function of the gamma energy and polarisation. One of the photons can be a laser photon (since there always exists an inertial frame in which the photon energies are equal) and then the non-linear corrections to the Breit-Wigner process and its multi-photon analogue, $\gamma + n\gamma' \rightarrow e^+ + e^-$ (Bula et al, 1996) can also be investigated.

HiPER can also extend the QED pair creation studies to μ and π particles and in principle can produce baryon pairs through QCD processes.

5.12.2 Collective and dynamical QED processes

While the above processes are dependent on the collective nature of intense laser pulses, the properties of the systems involved is largely kinematic. However, a completely new possibility of doing *dynamical* collective vacuum physics opens up with a system such as HiPER, quite distinct from the experiments done in a particle physics community. In particular, creating an intense photon gas using microcavities and an array of intense laser sources and letting this gas interact with a main laser pulse from HiPER (see Fig. V.3), one might be able to mimic photon propagation in the very early Universe (Marklund, Brodin and Stenflo, 2003). One can show that the collective interaction between intense photons in vacuum will generate pulse collapse scenarios in two and three dimensions. In such a pulse collapse, the intensity of the pulse theoretically grows unbounded

in a finite time. It is however clear that higher order QED vacuum effects will come into play, and maybe also pair creation, at which the pulse collapse will be halted. These higher order effects are currently not well investigated, and the possibility of doing experiments on such systems would provide valuable information for further theoretical and numerical studies. A further interesting opportunity is the formation of intense filaments of pulses in the quantum vacuum. Thus, one might dynamically probe the quantum vacuum using HiPER in the same way as one has probed nonlinear optical systems over forty years with intense lasers. Although the above is speculative (not on the theoretical level however), for weakly nonlinear systems, dynamical vacuum birefringence in photon gases could also be investigated using similar setups (Marklund and Shukla, 2006).



Schematic of the principle behind creating an intense photon gas using microcavities and a multiple-beam setup in conjunction with a main pulse. Vacuum birefringence effects of a photons gas could be probed.

5.12.3 Electron Positron Micro Collider

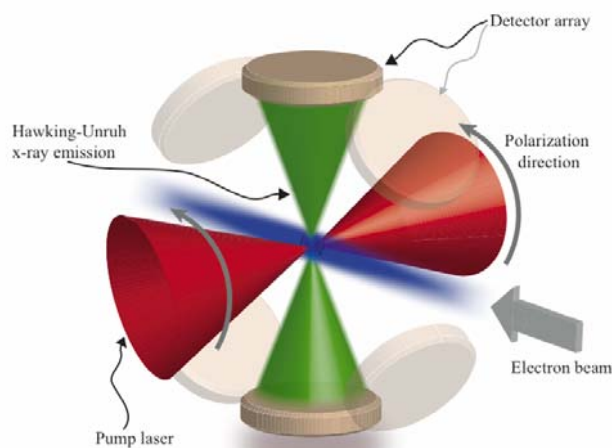
In any process that produces electron-positron pairs such as the well-known trident process in the Coulomb field of high Z nuclei (Liang, Wilks and Tabak, 1998), the electron and positron will be born at essentially the same location and will oscillate in anti-phase in the laser field (Blaschke et al, 2006). With the superimposed oscillation and drift at large values of $a_0 = eE/m\omega$ the particles will not return to their birthplace but will accurately re-collide (Henrich, Hatsagortsyan and Keitel 2004) since the drift is proportional to e^2 . Essentially all pairs will collide giving a huge increase in luminosity compared with a conventional electron-positron collider. At 10^{26} Wcm^{-2} the collision energy will be around 5GeV and the pairs will be spin-correlated.

5.12.4 Approaching the Schwinger Limit

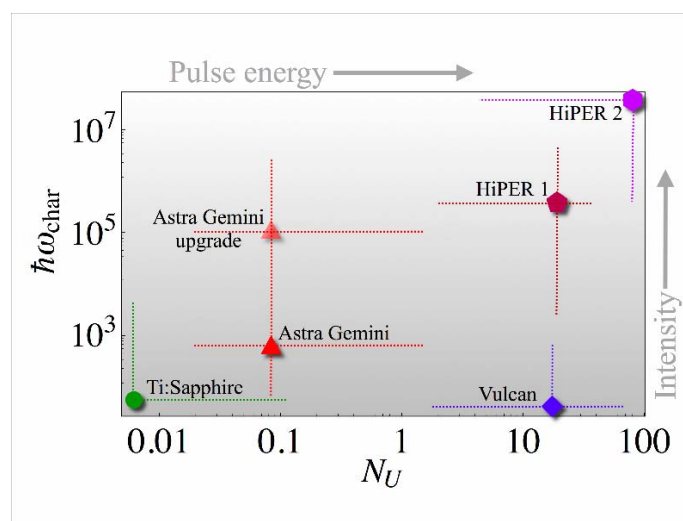
Schwinger (1951) showed that at electric fields corresponding to $E\lambda_C \sim mc^2$ where λ_C is the Compton wavelength, the vacuum will spontaneously create electron- positron pairs as the virtual pairs from vacuum polarisation can acquire enough energy from the field to move on to the mass shell and become real. In an oscillating field the Schwinger mechanism requires that $\mathbf{E} \cdot \mathbf{B}$ and $E^2 - B^2$ should both be non-zero and so it does not apply to a single plane wave (Marklund and Shukla, 2006). Strongly converging or colliding beam geometry is required and at the intensities available to HiPER the $e^+ e^-$ production rate should be detectable. Deviations from the expected rates would again be a likely indicator of new physics since the laser excitation of the vacuum is essentially adiabatic and the QED processes can be calculated very precisely.

5.12.5 Unruh Radiation

Unruh radiation (Unruh 1976) is the analogue of Hawking radiation from black holes when the gravitational field of the black hole is replaced by an accelerating frame of reference. An observer in the accelerating frame should observe a black body radiation field with temperature $kT_U = \hbar a / 2\pi c$. For an electron accelerating in a laser field the Unruh temperature becomes large ($kT_U \sim mc^2$) (Chen and Tajima, 1999) coincidentally when the electric field is of order the Schwinger field. Chen and Tajima (1999) have suggested that Unruh radiation is detectable at much lower irradiances, around 10^{24}Wcm^{-2} , since the Unruh radiation has a different polar pattern compared with the orbital (Larmor) radiation of the electrons. HiPER can move well in to the realms of intense Unruh radiation since a high energy electron interacting with the laser field 'sees' an intensity higher by a factor of γ . 1GeV electrons (from an associated accelerator) interacting with the HiPER beam at 10^{25}Wcm^{-2} will see an intensity of 10^{31}Wcm^{-2} , and will be very strongly scattered from the MeV radiation field associated with the Unruh temperature. A specific setup making use of combined multiple-beam laser system and an electron beam would constitute a feasible setup for Unruh radiation detection, taking into account spectral properties of the emissions (see Fig. V.4). In Fig. V.5 we also see that the HiPER facility would improve the chances of detection immensely compared to current systems.



The setup for the detection of Hawking-Unruh radiation (green) due to the interaction between two laser beams (red) and an electron beam (blue). The Unruh emission is in the soft x-ray regime.



The calculated characteristic photon energy in units of eV as a function of the number of photons due to Unruh emission. We see that as the pulse energy and intensity increases, the possibility of detecting of this effect would be significantly improved

References for section 5

- I Anoniadis et al, Phys Lett B, 436, 257 (1998)
- N Arkani-Hamed, S Dimopoulos and G Dvali, Phys Lett B, 429, 263 (1998)
- J Arons Ap J 388, 561 (1992)
- J. Badziak et al., Laser Part. Beams, **23**, 401 (2005).
- J N Bahcall et al Phys Rev Lett 78, 2, 171 (1997)
- Z. Bern et al, SLAC Report SLAC-PUB-8974 (2001)
- D. Bernard et al., Eur. Phys. J. D 10, 141 (2000)
- D. B. Blaschke et al., Phys. Rev. Lett. 96, 140402 (2006).
- M. Borghesi et al., Fusion Sci. Technol. **49**, 412 (2006)
- M. Buchanan, Nature Physics 2, 721 (2006)
- C. Bula et al., Phys. Rev. Lett. 76, 3116 (1996)
- D.L. Burke et al., Phys. Rev. Lett. 79, 1626 (1997)
- P. Chen and T. Tajima, Phys. Rev. Lett. 83, 256 (1999)
- C Chenais-Popovics et al Ap J Suppl 127, 275 (2000)
- K. Cheung, Phys Rev D 61, 015005 (2000)
- G Chiu and A Ng Phys Rev E 59, 1, 1024 (1999)
- T. E. Cowan et al., Nucl. Inst. Meth. A455, 130 (2000)
- Connecting Quarks to the Cosmos. Eleven Science Questions for the new Century,
Board on Physics and Astronomy, National Academies Press 2003
- R. Davidson ed., Frontiers in High Energy Density Physics,
National Research Council, The National Academies Press (2003).
- H Davoudiasl, Phys Rev D 60, 084022 (1999)
- P E Dimotakis J Fluid Mech 409, 69 (2000)
- M Dunne, Nature Physics 2, 2 (2006)
- R G Evans et al, Appl Phys Letts., 86, 191505 (2005).
- J. Faure et al, Nature 431, 541 (2004)
- M E Foord et al, Phys Rev Lett, 93, 055002 (2004)
- J. Fuchs et al., Nature Phys. **2**, 48 (2006)
- C. Geddes et al, Nature 431, 538 (2004)
- S H Glenzer et al Phys Rev Lett 82, 1, 97 (1999)
- G Gregori et al J Phys A Math Gen 36, 5971 (2003)
- A. Gruzinov and E. Waxman, Astrophysical Journal 511, 852 (1999)
- T Guillot Science 286, 72 (1999)
- J. Hawreliak et al, Phys. Rev. B 74, 184107 (2006)
- G Jernigan et al Ap J 530, 875 (2000)
- K. Kadau et al Phys. Rev. Lett. 98, 135701 (2007).
- D. H. Kalantar et al, Phys. Rev. Lett. 95, 075502 (2005)

- P A Keiter et al Phys Rev Lett 89, 16, 165003 (2002)
- R I Klein and J Arons ‘Stellar Atmospheres: Beyond Classical Models’ ed L Crivillari
Boston: Kluwer (1991)
- K. Ledingham et al., Science 300, 1107 (2003)
- W. Leemans et al, Nature Physics 2, 696 (2006)
- S Leygnac et al Physics of Plasmas 13, 113301 (2006)
- E. P. Liang, S. C. Wilks, and M. Tabak, Phys. Rev. Lett. 81, 4887 (1998)
- C Lindsey and D C Braun Solar Physics 192, 261 (2000)
- W. Lu et al, arXiv:physics/0612227
- J. Lundin et al., Phys. Rev. A 74, 043821 (2006)
- E. Lundström et al., Phys. Rev. Lett. 96, 083602 (2006).
- S. P. D. Mangles et al, Nature 431, 535 (2004)
- M. Marklund and P. K. Shukla, Rev. Mod. Phys. 78, 591 (2006)
- M. Marklund, G. Brodin, and L. Stenflo, Phys. Rev. Lett. 91, 163601 (2003)
- M. Medvedev and A. Loeb, Astrophysical Journal 526, 697 (1999)
- R. N. Mohapatra and S. Nasri, Phys. Rev. Lett. 98, 050402 (2007)
- F. Moulin and D. Bernard, Opt. Comm. 164, 137 (1999)
- G. A. Mourou, T. Tajima, and S. V. Bulanov, Rev. Mod. Phys. 78, 309 (2006)
- T S Perry et al Phys Rev Lett 67, 27, 3784 (1991)
- A. Pukhov and J. Meyer-ter-Vehn, Appl. Phys. B 74, 355 (2002)
- Y -Z Qian Nuclear Physics A 752, 550c (2005)
- R. Rabadan, A. Ringwald, and K. Sigurdson, Phys. Rev. Lett. 96, 110407 (2006)
- B. Remington et al, Science 284, 1488 (1999)
- B. Remington et al, Rev. Modern Phys.78, 755 (2006)
- A P L Robinson et al Plasma Phys Controlled Fusion 49, 373 (2007)
- S J Rose, Contemporary Physics, 45, 109 (2004).
- S J Rose et al, J Phys B: Atom Molec Opt Phys, 37, L337 (2004).
- P A Rosen et al Astrophysics and Space Science 298, 121 (2005)
- D Ryutov et al Ap J 518, 821 (1999)
- D Ryutov and B A Remington Plasma Phys Controlled Fusion 48, L23 (2006)
- Y. I. Salamin et al, Phys. Rep. 427, 41 (2006).
- D Saumon, G Chabrier and H M Van Horn Ap J Suppl 99, 713 (1995)
- J. Schwinger, Phys Rev 82, 664, (1951)
- H. Schwoerer et al., Nature **439**, 445 (2006).
- L. O. Silva et al, Astrophysical Journal 596, L121 (2003)
- M Terasawa et al Ap J 562, 470 (2001)
- C. Thompson et al., Astrophysical Journal 422, 304 (1994)
- W. Unruh, Phys Rev D 14, 870 (1976)

E T Vishniac ApJ 274, 152 (1983)

D Ryu and E T Vishniac Ap J 368, 411 (1991)

N C Woolsey et al Phys Plasma 8, 2439 (2001)

B. Yaakobi et al, Phys. Rev. Lett. 95, 075501 (2005)

E. Zavattini et al., Phys. Rev. Lett. 96, 110406 (2006)

6 Large scale strategic facility development

The step-change in scale from existing academic laser systems to HiPER means that considerable development is needed in the scientific underpinning, in the technology maturity, and in the approach of the community to its research programmes. As a result of the work performed in the 2-year design phase, there is now an outstanding level of coordination, communication and common purpose in the large scale laser community within Europe.

6.1 Existing academic systems in the EU

At present, there are three laser systems within the EU capable of delivering in excess of a kilojoule of energy. These are:

- Vulcan, at the Central Laser Facility (UK)
- LULI-2000, at the Ecole Polytechnique (France)
- PALS, at the Institute of Physics (Czech Republic)

Great use will be made of these facilities as part of the preparation for HiPER, as detailed in the experimental validation programme (see section 8). This will be coupled to fundamental physics analyses and the development of diagnostics and experimental and theoretical techniques at the substantial number of smaller scale facilities (see section 7).



Photos of the Vulcan (left), LULI (middle) and PALS (right) laser facilities.

Vulcan, operated by the STFC Central Laser Facility, is at the time of writing the world's most powerful, most intense laser system, delivering in excess of 1 Petawatt onto a focal spot to create an irradiance of 10^{21} W/cm². It also provides a short pulse beam of energy >100 J coupled to a 6-beam long pulse capability. Dedicated access to these facilities has been made available to the HiPER consortium, as part of a 4-way agreement between CLF, LULI, PALS and Laserlab-Europe.

The CNRS and CEA support the operation and development of the *Laboratoire pour l'Utilisation des Lasers Intenses* (LULI) in Paris where some of the most advanced facilities in the world for experimental laser-plasma physics exist. Access to these facilities and the expertise contained therein will also be crucial for risk reduction in the HiPER mission.

It has been agreed between the three French agencies (CEA, CNRS, Region Aquitaine) that all HiPER related activity will be co-ordinated and managed by the *Institut Lasers et Plasmas (ILP)* in Bordeaux. ILP is the coordinating Institute in France for research in lasers and plasmas. It officially represents the associated laboratories working on these subjects from CNRS, CEA, University Bordeaux1 and Ecole Polytechnique.

The *Ministry of Education, Youth and Sports* (MSMT), as a funding agency, are formal partners to the HiPER preparatory phase project. Execution of the Czech participation will be through the *Academy of Sciences of the Czech Republic* (CAS). The CAS operates and develops the *Prague Asterix Laser System* (PALS), which is one of the leading experimental facilities in Europe for laser plasma interactions. Access to this system will be made available for HiPER related work, as discussed above.

Further detail on these systems can be found at:

- Vulcan: <http://www.clf.rl.ac.uk/Facilities/vulcan/index.htm>
- LULI-2000: <http://www.luli.polytechnique.fr/>
- PALS: <http://www.pals.cas.cz/pals/index.html>

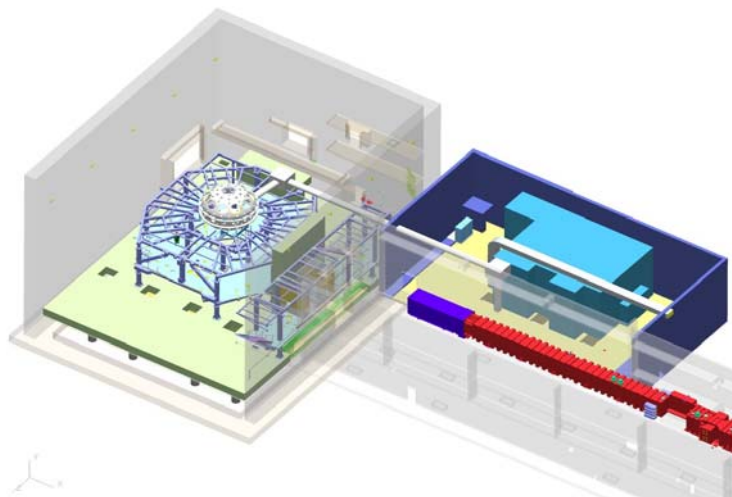
6.2 Ignition scale laser facilities

As described throughout this document, extensive use will also be made of experience from the ignition-class laser systems, NIF and LMJ, with regard to technology options, operational experience, scientific results, and large project issues. These facilities are described in more detail in section 14.

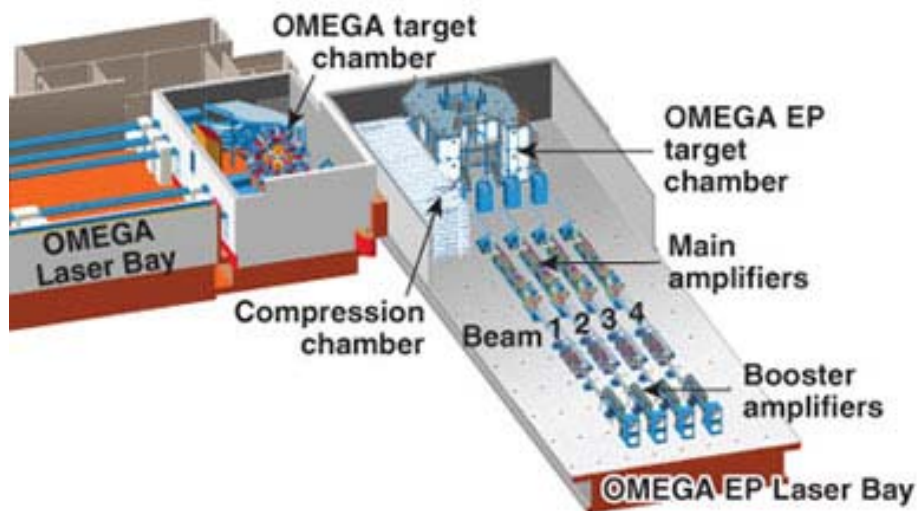
6.3 International, Fast Ignition physics facilities

Coupled to these academic and ignition laser systems, it will be essential over the coming period to make optimum use of the emerging suite of intermediate scale laser systems (at the tens of kilojoule energy level). This is required both to define the most promising route to Fast Ignition, and to ensure that Europe is sufficiently experienced to make good use of HiPER. There are three principal intermediate scale facilities emerging with which the HiPER project will be seeking collaborative experiments:

- OMEGA-EP: At the Laboratory for Laser Energetics, University of Rochester, New York, USA. See: <http://omegaep.ile.rochester.edu/>
- FIREX-I: At the Institute for Laser Engineering, Osaka University, Japan. See: <http://www.ile.osaka-u.ac.jp/>
- PETAL: At the Centre d'études scientifiques et techniques d'Aquitaine (CESTA), Bordeaux, France. See: <http://petal.aquitaine.fr/>



The PETAL laser facility, in CESTA, France, will couple a new 3.5 kJ short pulse laser system to the existing 60 kJ LIL laser system.



*The
EP laser*

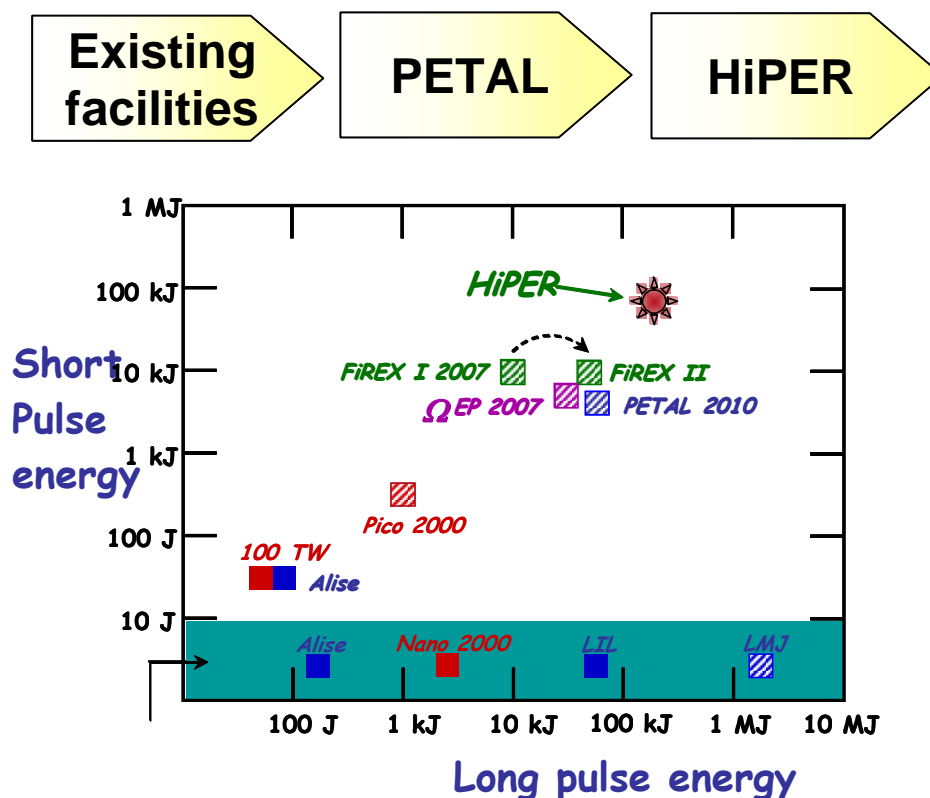
will couple two new short pulse beams, 2.6 kJ apiece, with two additional long pulse beams into the existing OMEGA 60-beam 50 kJ implosion facility. This will provide an ideal configuration for studying the physics underpinning Fast Ignition. The facility will progressively come online from 2007-2009.



The FIREX project in Japan will couple a new 10 kJ short pulse (4-beamlet) laser system called LFEX with the existing 12-beam, 10 kJ GEKKO-XII implosion facility. This has been specifically designed to study the physics of fast ignition. A key goal is to achieve sufficient coupling of electron energy into an imploded DT target to raise its temperature to 5 keV. This facility will progressively come online from 2007-2010. Successful achievement of its design goals is required to allow a positive decision on a major upgrade, FIREX-II, which would couple 50 kJ short pulse “ignitor” energy to a 50 kJ implosion system (in the existing laser building).

The CEA has developed near Bordeaux (CEA-CESTA) over the last decade or so the *Ligne d'Intégration Laser* (LIL) and the multi-billion Euro *Laser MégaJoule* (LMJ) systems that are central pillars of its national strategy to advance the Inertial Confinement Fusion concept. It therefore brings to the HiPER project unrivalled expertise within Europe. The HiPER strategy relies heavily on leveraging this expertise and the huge defence programme investment it represents into the civilian arena for the pursuit of fusion energy through the HiPER mission. The CEA's technical and political involvement is substantial and they are formally prepared to make available to HiPER people, information, technology, costs etc that will be crucial to developing HiPER. The CEA also provides an important portal to French industry that has developed most of the technology for LMJ.

Moreover, the local regional funding agency, the *Conseil Régional d'Aquitaine* (CRA) in conjunction with the French government, has recently invested more than 40 M€ in the PETAL enhancement to the LIL system to explore the fast ignition approach to Fusion Energy. CRA as a funding agency is also a formal partner in the HiPER project. Construction of the PETAL facility in the Région Aquitaine represents a very major step towards the realisation of HiPER. It provides a local "stepping stone" that will ensure the project partners are able to tackle the myriad of scientific, technological, operational and organisational issues associated with large scale laser science. Preparation of the HiPER proposal has led to its formal joining together with PETAL under a common strategic plan. The agreed approach is to evolve from existing facilities, to PETAL, to HiPER, with all three tiers playing a major role during the operational phase of HiPER.



In recognising the importance of the PETAL system to the HiPER mission, the CEA and CRA have agreed to the reconfiguration of PETAL system as per the needs of the HiPER project. An international panel of experts has thus recently been appointed to advise on the exact nature of this development.

7 Role and development of the smaller scale European facilities

7.1 Introduction

This section describes the coordination platform for the development of smaller scale facilities (SSF) already operating in the area of intense and ultraintense laser interactions **with active programmes in Inertial Confinement Fusion and Fast Ignitor related studies**. This platform will enable SSF to provide access for dedicated experiments that do not necessarily require beam time at large scale facilities (e.g. CLF, LULI). Within this initiative, SSFs will also serve as attraction points for young researchers to be hired within other EU programmes (MC, COST, etc). This approach will contribute to establish the “people” issue as a critical one and will contribute to the growth of the community in view of the large number of scientists with expertise in Inertial Fusion Energy required for the HiPER project. Smaller Scale facilities identified for participation to this task will provide **support to the HiPER scientific programme** on the basis of their specific expertise and existing undertaking. To this purpose, smaller scale facilities **will be encouraged and supported** to further expand their research capabilities in their primary area of expertise.

It is well established in the scientific community that HiPER is fundamentally a European science R&D facility that will allow, for the first time, a coordinated effort towards Inertial Fusion Energy (IFE). It is also clear that the complexity and the scale of the undertaking are unique and calls for an unprecedented coordination of existing laser facilities, laboratories and groups actively engaged in IFE or related fields. In view of this approach and following the recommendations of the European Strategy Forum on research Infrastructures (ESFRI), the HiPER community has, since its first general meetings, shared the need of a significant growth of the scientific community to both :

- a) consolidate a medium-term programmatic activity on Inertial Fusion Energy and
- b) establish a coordination activity among existing Laboratories, *and Laser Facilities* targeted to address weak/risky issues of the inertial approach to fusion energy.

In this section we identify the role and need for a high priority participation of SSFs to the HiPER project. Specific actions have been identified to address items a) and b) above.

7.2 Nature of the facility coordination needed for HiPER

As discussed in previous sections, HiPER’s approach to IFE is based upon the so-called Fast Ignitor approach. The demonstration of fast ignition, along with the repetition rate issue, are the key milestones that will change the character of IFE from applied research to a viable future alternative route to an efficient energy source. In view of the programmatic character of HiPER, participating scientists will need to carry out a whole range of systematic studies aimed at advancing the understanding of critical physics issues of FI. This type of *systematic* research, when compared to topical/frontier research where emphasis is given to new interaction regimes and novel physical mechanisms, is often regarded as somewhat “less attractive” for individuals and research groups continuously facing competitive access to gain funding and use of facilities where impact and novelty play a key role in selection criteria. In this scenario, SSF participating to HiPER will provide dedicated access to lasers and target areas complementary to large scale facility. Attracting financial support for the instrumental and human resources needed to provide access is the objective of sub-task 6a1 “Integration and Framework Coordination” within of WP6 “Technical risk management”.

Remarkably, it was a common view among HiPER meeting participants that, once established as a long term EU initiative and integrated in national research programmes, HiPER will attract significant local funding and will also enable HiPER-related activity in new and existing EU programmes (LASERLAB, MC training Sites, Relevant COST actions etc.) dedicated to *systematic*

studies in a similar fashion as other large international collaborations (e.g. ITER). Also covered within HiPER WP6 is the participation to IFE programmes in US and Japan, as well as in other countries where rapidly growing IFE activity exists, which is regarded a necessary step to develop needed expertise presently not available in EU.

7.3 Resources

A preliminary survey was carried out during the initial stages of the HiPER project to encourage active involvement in the project of the IFE scientific community and related topics. In a later stage, each group running a SSF that had expressed interest in the HiPER infrastructure was asked to fill a standard form to identify their possible participation in terms of existing expertise, institutional medium term work programme, possible research field of involvement and contribution and type of support required to accommodate HiPER tasks. Thanks to this initiative, it was possible to identify a range of topics for which experimental and/or theory resources may be made available to address risky project issues identified in the other topics and subtopics. A summary of this list is provided below, with a short identifier including Institution, Contact person and Main Topic. The complete identification document for each group is provided in a separate attached document.

Institute for Optics and Quantum Electronics, Jena Germany Eckhart Foerster; Laser development, X-ray Source for time resolved X-ray diffraction

Laboratory for Attosecond and High-Field Physics, Max-Planck-Institut für Quantenoptik, Garching, Germany, Contact person Dr. Stefan Karsch - Ultra-Short laser development (OPCPA&Ti-Sapphire), Attosecond science, LPI, Particle acceleration and radiation sources

Gesellschaft für Schwerionenforschung, Darmstadt, Germany, Contact person Markus Roth - Es.: Laser development, LPI, X-ray Source, Fusion Related, Ion stopping

Physique at Haute Intensité, CEA-Saclay (FRANCE), Contact person Dr. Philippe Martin - Laser diagnostics development, High Intensities High Order Harmonic sources, Fast Particle generation and diagnostics, Plasma diagnostic on sub-picosecond time scales.

Intense Laser Irradiation Laboratory, CNR, Area della Ricerca del CNR – Pisa, Italy, Contact person A.Giulietti; - LPI, optical scattering, X-ray time-res. Spectroscopy, K-alpha imaging and spectroscopy - Charged particle acceleration in plasmas; particle beam diagnostics.

Laboratory for Intense Lasers, Center for Plasma Physics, Instituto Superior Técnico, Portugal, Contact person Luís Silva, Gonçalo Figueira (Head) - Laser-plasma interaction and high power laser development (CPA Ti:sapphire-Nd:glass, OPCA, diode-pumped ytterbium media)

Laboratorio Laser di Potenza, Milano Dipartimento di Fisica “G.Occhialini”, Università di Milano Bicocca, Milan, Italy, Contact person Prof. Dimitri Batani - Laser development, X-ray Source, Fast Ignition related studied, Shock Wave and Hydrodynamics related studies.

Institute of Plasma Physics and Laser Microfusion (IPPLM), Warsaw, Poland, Contact persons: J. Badziak and J. Wolowski - Study of physics of laser-matter interaction at medium and high intensities, Study of phenomena related to ICF proton fast ignition - numerical modelling and small-scale experiments.

CELIA, University Bordeaux 1, Jean-Claude Gauthier - Laser development, harmonics, X-ray Source, Fusion Related, Attosecond pulses, Laser ablation and micromachining

Max-Born-Institute, Berlin, Peter V. Nickles - LPI (ion and electron acceleration), , Proton Radiography, X-Ray Laser etc., Ti:Sa Laser Development, X-ray Source; Ti:Sa Laser Development; X-ray Source.

Centre for Plasma Physics, Marco Borghesi, Queen's University of Belfast (QUB), Belfast, UK, Laser-plasma interaction; (particle acceleration, x-ray sources, x-ray scattering); Laser development.

TOPS lab, University of Strathclyde (TOPS), Paul Mc Kenna, Glasgow, Scotland; Laser-plasma accelerators (electrons and ions); wakefield acceleration and application to free electron lasers; Raman processes; terahertz generation Laser-based nuclear physics diagnostic development

Laboratory of Optoelectronics, Lasers & Plasma Technology, Department of Electronics/ Technological Educational Institute of Crete (T.E.I. of Crete), Contact person: Assoc. Prof. Michael Tatarakis, , Laser-plasma interactions, Plasma diagnostics, Point intense X-ray sources, Pulsed power plasma generators (X-pinch, Z-pinch), X-ray backlighting, CW laser development, Coherent X-ray sources, Attosecond pulses research*, Secondary sources from laser matter interactions, Theoretical back up scientific team, Electronic Design & Automation

PALS, Institute of Physics, Prague, Bedrich Rus - Development and applications of X-ray lasers, XUV and X-ray diagnostics, keV X-ray spectroscopy, ion spectroscopy

7.4 Distributed science and diagnostic capabilities: a common approach between SSF labs

A rich background of expertise in experimental and theoretical investigation in laser-plasma physics in the IFE relevant regime exists in the above cited labs which is the result of dedicated activity enabled by a broad set of laser laboratories and university departments that are partially interconnected via a range of research programmes EU-wide. This knowledge enables scientists to continuously advance knowledge using diagnostic techniques that are crucial in the understanding of some basic issues in IFE.

Diagnostic issues are extensively discussed in other sections of this report. Here we recall two examples of diagnostic techniques, namely K-alpha imaging and optical probing, with the purpose of discussing the potential benefit that a coordinated approach may have on the community.

It is well known that K-alpha imaging is a key technique in the study of propagation of fast electrons in matter, a fundamental issue in the Fast Ignitor approach to IFE. In fact, the most effective way to unfold the dynamics of electron propagation is through detection of k-alpha radiation emitted as a consequence of electron impact in the target substrate. This is presently approached by using layered targets and by detecting k-alpha emission from each layer. Imaging of such emission allows the history of propagation of electrons to be recovered. This technique benefits from the use of fine X-ray optical systems, based upon diffracting crystals, to achieve spectrally resolved imaging. Examples of SSF where this expertise is well established are QUB, IOQ, and CNR. More recently, the availability of very low noise CCD detectors allows direct imaging with spectral discrimination of photons at the 50 eV level. Dramatic development of this technique has taken place, for example, at LOA, IOQ, CNR. Further, these studies are integrated with the implementation of novel techniques for the simultaneous characterization of spectral and angular properties of fast electrons, a key step in the understanding of electron propagation dynamics, as demonstrated in collaborative research under the LASERLAB framework between CEA-SACLAY, CNR and LULI. Further growth of expertise in advanced X-ray imaging techniques in Europe may arise from collaborations between above cited existing European

frameworks (LASERLAB) and leading detector manufacturing companies (e.g. ANDOR). (*see for example M. Galimberti et al., Rev. Sci. Instrum. 76, 053303 (2005); L. A. Gizzi et al., Phys. Plasmas 10, 4601 (2003); F. Y. Khattak et al., Phys. Rev. E 74, 027401 (2006); L. Labate et al., Appl. Phys A, in press (2006); M. Manclossi et al., Phys. Rev. Lett. 96, 125002 (2006); Ch. Reich et al., Phys. Rev. E 68, 056408 (2003); D. Riley et al., Phys. Rev. E 71, 016406 (2005); M. S. Wei et al. Phys. Rev. E 70, 056412 (2004)*)

HiPER will provide the ideal framework in which an integrated diagnostic system dedicated to fast electron propagation can be successfully developed through the combined effort of European groups working in this field. An integrated diagnostic system of this kind is expected to provide unambiguous information on the dynamics of propagation of fast electrons in plasmas that will dramatically improve the understanding of FI physics in dedicated experiments at Large Scale Facilities. A non-exhaustive list of SSF that already participating include CNR, IOQ, QUB, U.BICOCCA and RAL, where, remarkably, dedicated access for FI related experiments is already being granted within the HiPER science programme in addition to standard access frameworks.

Optical probing is another example of a robust and unique diagnostic technique for a) characterization of underdense, coronal plasmas and b) study of propagation of intense pulses in plasmas. It also plays a crucial role in detecting beam degradation processes (filamentation, self-focusing, break-up etc ..) in ICF related experiments. Recently, the use of an ultra-short optical pulse as a probe pulse can provide information on propagation and interaction of intense pulses in plasmas with unprecedented temporal and spatial resolution, provided issues like probe transit time and other transient phenomena are unfolded. Moreover, the implementation of probing techniques based upon the use of high order harmonics provides now a significant opportunity of probing higher densities with very high temporal resolution. The understanding of laser-target interaction in the FI-like regime will require a reliable understanding of laser-plasma coupling conditions, starting from propagation in the underdense plasma blow-off originated by pulse pedestal/prepulse. This will be crucial to control energy and quality of the fast electron beam produced during the interaction. All these diagnostic techniques are being developed in SSF including TEI, QUB, CNR and CEA-Saclay. Coordination that will come from HiPER will promote joint work for the design of robust integrated diagnostics for advances optical probing that will be established at the non-implosion target areas planned for fusion and non-fusion science at HiPER. (*F. N. Beg et al., Phys. Plasmas 4, 447 (1997); M. Borghesi et al., Phys. Rev. E 54, 6769 (1996); S. Dobosz et al., Phys. Rev. Lett. 95, 025001 (2005); D. Giulietti et al., Phys. Plasmas 9, 3655 (2002); L.A. Gizzi et al., Phys. Rev. E (2006); L.A. Gizzi et al. Phys. Rev. E, 49, 5628 (1994); P. Squillaciotti et al., Phys. Plasmas 11 226 (2004)*)

7.5 Specific actions and tasks

A number of specific actions have been identified to address development of SSF and their integration in the HiPER infrastructure. These actions will involve directly and indirectly a significant number of participating institution and reflect the actual workpackage structure. In fact, workpackages from 3 through 6 will enable execution of those tasks the will address SSF integration. A list of identified tasks and their “host” WPis outlined below.

Task a) Integration and Framework coordination; Expertise “procurement” at a laboratory level; HP lasers, HE astrophysics; magnetic fusion, neutron facilities, HEP/accelerators; (links with **all** WPs from 3 through 6).

Task b) Smaller Scale Facility Capability development: SSF Networking; Identify existing HiPER-relevant capabilities not supported otherwise; Diagnostic standardization; Target

Area and targetry development; (link with WP6) - Systematic studies for code benchmarking; (link with WP4)

Task c) Design of experiments at *Large Scale facilities for FI relevant studies: link with large scale facilities (RAL, LULI, PETAL, PHELIX)*; Access to non-EU facilities. *Connect to science case to back-up key experiments*; Large Scale Facility Upgrade: PETAL; Ensure synchronization between experimental configuration and model requirements. This task generates conditions for ensuring flow of information between different tasks to update information needed for detailed design (*link with WP6 and 4*).

Task d) Interlacing with existing programmes and networking activities – LASERLAB, Marie-Curie training sites, relevant COST actions; - Establish links with access programmes for non-competitive (programmatic) experimental programme; - Distribute information of existing funding opportunities for mobility (short term visits); - Stimulate programmatic activity via targeted workshops and meetings. (links with **all WPs**);

8 Experimental validation of the fusion programme

8.1 Introduction.

The fast ignition concept was first proposed in 1994 [8.1] and received immediate and widespread interest around the world for three reasons. First, more fusion fuel can be compressed to high density for reduced drive energy compared with the conventional central spark ignition concept for inertial fusion, leading to higher fusion energy gain. Second, the drive symmetry requirements can be significantly relaxed because the in-flight aspect ratio of these implosions is significantly larger, thus reducing the growth of the Rayleigh-Taylor hydrodynamic instability. Third, the enormous energy densities of the PetaWatt laser pulse needed to heat the hot spot to ignition temperatures were (and are) of great interest to the fundamental physics of laser-matter interactions and many spin-offs of the research could (and have been) envisaged. To date, thirteen years after the concept was first published, no show stoppers have yet been identified, despite the extremely close experimental and theoretical scrutiny that the concept has undergone. Recent reviews of this scrutiny that includes a full discussion of the concept, associated experiments, theory and computational modelling have been published by Campbell *et al.* [8.2].

This is not to say that there all questions have been fully answered. In this paper, 14 areas of concern for HiPER have been identified. They are listed in order of priority for experimental validation over the next three years of the detailed design phase of the project. We do not expect that answers to all outstanding questions can be addressed fully in this time period, since they will require many PW laser shots to answer in a fully satisfactory manner and there are a limited of shots available across the European laser facilities, but significant progress is likely to be made on many of them. We remain optimistic that these areas of concern can be addressed and that fast ignition will remain a strong candidate for the realisation of inertial fusion energy.

8.2 Absorption and energy transfer to the fast electron beam.

The efficiency with which laser energy is absorbed by (initially) solid targets has long been one of the most fundamental aims of theoretical laser-plasma physics. The calculation of this parameter is of vital importance to any inertial confinement scheme dependent on laser pulses. This is particularly true for the fast ignition approach because this scheme utilises both low and high laser intensities. The absorption efficiency effectively determines the viability of the entire scheme. From an experimental point of view, the knowledge gained to date is very positive. It is now possible, with some reasonable degree of certainty, to say what the absorption efficiency is likely to be for a given experimental set-up, i.e. given parameters such as the type of target, intensity of the laser beam and its associated contrast ratio.

In terms of the energy conversion efficiency from the laser beam to the inwardly directed fast electron beam, Wharton *et al.* measured the absolute K_{α} x-ray signal that indicated a conversion efficiency of between 20 % – 30 %. [8.3] Kodama *et al.* obtained conversion efficiency with or without a large scale-length preformed plasma of 20 % - 25 % and 40 %, respectively [8.4]. Similarly Norreys *et al.* inferred a conversion efficiency of 20 % - 30 % from bremsstrahlung radiation in solid targets [8.5]. These measurements were performed with intensities on target between 10^{18} Wcm⁻² and 3×10^{19} Wcm⁻². Measurements up to 2.5×10^{20} Wcm⁻² have been obtained at LLNL (with a 0.5 ps 1 PW laser) and show conversion efficiencies up to 40% with irradiation at ω (1 micron laser wavelength).

A somewhat different result is that reported by Theobald *et al.* By absolute K_α measurements which indicated a conversion efficiency at 10% at $4 \times 10^{20} \text{ Wcm}^{-2}$ on target, by comparison with a computational model that includes refluxing and confinement of the fast electrons within the target [8.6]. This conversion efficiency estimate is somewhat lower than the other measurements, but some caution is needed in interpreting these results, since the conversion efficiency in the modelling is very dependent on the shape of the initial electron distribution used. Clearly at very high intensities more experimental results are needed, but conversion efficiencies still seem to remain quite high.

Another important point is the scaling of conversion efficiency with laser wavelength, a parameter which may need to be changed in order to optimize the average energy of the fast electron beam. Several measurements have been performed with Ti:S lasers, showing high efficiencies again. Irradiation of targets with $2\omega_0$ of Nd:glass laser light, we recall the measurement of Pisani *et al.* in the range $2 \times 10^{18} \text{ Wcm}^{-2}$ to $2 \times 10^{19} \text{ Wcm}^{-2}$, which shows conversion efficiencies perfectly comparable with those obtained at ω_0 [8.7].

Probably the most outstanding issue, however, remains a systematic study of the conversion efficiency as a function of the scale-length of the plasma, which the laser creates and continually interacts with. Low density foams have been shown to increase the absorption (inferred from an increase in the X-ray yield) [8.8], but these structures are difficult to model (and thus optimise) computationally. More controlled structured targets are needed for comparison with theory. In addition, the ~ 10 ps pulse durations needed for fast ignition provide a new challenge in maintaining high absorption efficiency over the entire pulse length, since hole boring and/or profile steepening will both occur [8.9]. Very recent results also suggest that very high efficiencies are possible, which can only spell good news for fast ignition.

The theoretical understanding of absorption still poses many outstanding questions. In the early days, theories could be developed based on some expansion parameter (usually the strength of the oscillation) and a given density profile (usually constant or step-like). With the advent of higher-powered lasers, such expansion parameters are difficult to construct, the density profile becomes strongly inhomogeneous and the absorption becomes interlinked with transport processes [8.10]. Furthermore, real experimental situations are likely to involve many processes simultaneously and fully temporally and spatially resolved simulations have yet to be carried out. In particular, our currently available models only tend to be applicable to a given intensity, temperature and scale-length [8.11]. It must be stressed that finding a satisfactory description of the entire process, from low-intensity ablation due to the pre-pulse to high intensity hole-boring within a single model is still outside of our capabilities, even in one dimension.

8.3 Divergence and collimation – novel techniques (shaped targets, etc.).

The fast electron beam divergence is the second vital ingredient to the success of the fast ignition approach. While recent experiments have revealed a large divergence pattern, very promising ideas have been proposed to control this effect and should, if the theory is correct, provide a route to narrower beams with a more suitable divergence angle requirement for fast ignition.

Computational modelling using the two dimensional hydrodynamics code LASNEX of cone-shell implosions have been performed [8.12]. Those simulations showed that if the fast electron beam has too large a beam divergence (i.e. $\geq 50^\circ$) then, for realistic core-cone wall interface distances ($\sim 180 \mu\text{m}$ in those calculations), the PW laser energy requirements approach 150 kJ, which is too far from practical implementation, even on the National Ignition Facility. While there is obviously scope for optimising the core-cone end-wall distance by suitable target design, the simulations confirm that beam divergence plays a crucial factor in the viability of fast ignition.

For example, the pioneering cone-guided experiments at Osaka University by Kodama *et al.* [8.13,8.14] have been successfully modelling using both the LSP [8.15] and ANTHEM [8.16] codes. These models both used an electron beam divergence of 27° and a PW laser to fast electron beam energy conversion efficiency of 20 %. While differing in the details, the fact that both computational models reproduce the experimental observations of the ion temperature is very encouraging.

The divergence of the fast electron beam has been studied by imaging the optical transition radiation and the X-ray K_α emission from laser irradiated metallic targets. The measurements have provided a divergence angle of 34° [8.17] and 40° [8.18] respectively for intensities on target between 10^{19} Wcm^{-2} and $5 \times 10^{19} \text{ Wcm}^{-2}$. Recent shadowgram and X-ray K_α emission measurements have indicated a larger (64°) beam divergence angle for intensities of $5 \times 10^{20} \text{ Wcm}^{-2}$ on target, albeit with laser pulses of 0.5 ps duration [8.19]. A new study (conducted in Nov/Dec 2006 on the Vulcan PW laser facility) has confirmed a divergence angle of $35 (+/-13)^\circ$ for pulses of direct fast ignition relevance to fast ignition (5 ps) at intensities on target of $3 \times 10^{19} \text{ Wcm}^{-2}$.

If the results giving a large beam divergence at very high intensities are confirmed, then we may need to limit the maximum irradiance on target to something of the order of $5 \times 10^{19} \text{ Wcm}^{-2}$, unless new techniques are employed to control the beam divergence. This must be seen as a very high priority for the risk reduction investigation over the next three years.

One possible approach was proposed by Campbell *et al.* [8.20]. This uses radial layered targets or vacuum gaps to generate a negative radial gradient in the plasma density. By doing so, strong confining radial electric fields are generated in the radially graded foil. The idea has been tested in implicit hybrid-PIC modelling using the LSP code and has been found to very effective in collimating the fast electron beam. The idea has a great deal of merit, as recent cone-wire targets have shown that the fast electrons are confined to the wire by a combination of radial electric field and azimuthal magnetic fields [8.21]. It therefore appears that vacuum gaps may well provide the confining radial electric field, as expected. A fast ignition relevant concept experiment is shown in Figure 8.1.

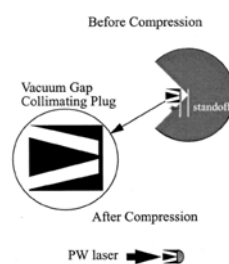


Figure 8.1. Schematic of a vacuum gap concept to collimate the fast electron beam in a cone geometry. From Fig. 5 of Campbell *et al.* [8.20].

One possible problem with this approach is the possibility of the collimating effect being destroyed by plasma filling of the vacuum gap. Experimental and theoretical studies needed to be done to examine this. If this is unavoidable then other solutions need to be examined. Current theoretical studies in the Plasma Physics group in the CLF are based around controlling the self-generated magnetic field by laser pulse shaping. On the same line, recent experiments performed at CLF in a different context (that of optimization of laser-produced proton sources) have nevertheless shown that by controlling the spatial shape of the laser pedestal it is possible to steer and control proton

emission, a result which implies the capability of controlling electric and magnetic fields inside the targets.

The ideas are complementary and would suit experimental campaigns using the Vulcan and LULI PW laser facilities. Both approaches can then be pursued and assessed independently. If successful, this work should be applied to higher energy lasers (OMEGA EP, FIREX and PETAL) for further validation with higher temperature plasmas.

Also, in general, we must still perform experiments, which are addressed to elucidate the origin of the divergence of the fast electron beam, and the possible ways, if any, of controlling it. One interpretation seems to relate the divergence to a Weibel-like instability in the region where the laser is absorbed and the fast electron beam created. However it should also be related to the different absorption mechanisms, the plasma scale length in front of the target, etc.

8.4 Phase control.

The PW beam-line for HiPER will, by necessity of the high energy requirement, be composed of multiple beam-lets, each amplified in its own laser chain. The combination of these beam-lets into a single beam poses questions concerning the overall phase control requirement. The particular issues include the effects on the electron temperature (generated in the laser-plasma interaction) of intensity “hot spots” in the focal plane due to coherence effects, as well as the absorption efficiency and the fast electron beam divergence pattern.

In some ways, this question is similar to the optimisation of the shape of the inner wall of the cone targets [8.22]. In this case, those parts of the intensity profile that lie far outside the focal spot are reflected by a plasma mirror (generated on the inner surface of the cone) to the cone tip. If one thinks of this process in terms of ray-tracing, those rays on the outer portion of the spatial intensity profile will have a different path length compared with those within the focal spot after reflection from the plasma mirror. The intensity profile at the cone tip will then consist of a speckle pattern with superimposed intensity spikes due to the coherent constructive interference.

Experiments need to be performed that examine these issues in a controlled manner to compare with theory and thus assist the design of the facility. We envisage experiments where either random or distributed phase plates are inserted into the high intensity beam. These are used to generate a focal spot of a known diameter comprising beam-lets of either random or known phase. This will “mock up” the full HiPER beam. The effects on the electron temperature, efficiency and divergence can then be determined in an open geometry with plane targets and compared with cone attached targets. The results can then be used as a benchmark for experiments designed on PETAL, whose phased array high energy PW beam is under construction and due for experiments in 2008-2010.

8.5 Hydrodynamics and mixing and tamping of the Au cone material.

A potentially serious impediment to the success of DT filled cone-shell implosions is the ablation of the Au material from the cone walls. This ablation is caused by hard X-rays (generated in the coronal laser-plasma interaction during the acceleration phase of the implosion) that manage to penetrate through accelerating ablator/fuel to the cone wall. If a sufficient amount of high Z material is ablated and swept up into the core at stagnation, then bremsstrahlung losses could exceed those of alpha-particle deposition and quench the thermonuclear burn wave [8.23].

Radiographic and areal density measurements of fast ignition relevant implosions have been performed using the GEKKO XII laser facility in Japan [13] and the OMEGA laser facility in the United States [8.24, 8.25]. The experiments have shown :

1. Cone guided compression works – good agreement with hollow plastic shell implosions has been shown with two-dimensional radiation hydrodynamic computer simulations. Compressed densities of $50 - 100 \text{ gm}^{-3}$ have been achieved. Although further experiments may be needed to show that very high degree of compression are indeed achievable, these are very encouraging results indeed.
2. Adiabatic pulse shaping works – thick, $40 \text{ }\mu\text{m}$ plastic shells filled with D_2 or DHe mixtures were imploded on a low-adiabat ($\alpha \sim 1.3$) and with a low-implosion velocity to generate massive cores of compressed plasma with high areal densities optimal for fast ignition. The same implosions with empty plastic shells are expected to reach 1.3 gm^{-2} across the core, which is enough to stop fast electrons with energies up to 4.5 MeV , typical of fast ignition scenarios.
3. X-ray and/or electron preheat causes some gold material across the cone – core gap and that this process is more pronounced for indirect drive. This effect is not expected to scale with IFE implosions (due to the increased thickness of the ablator / DT fuel providing a better attenuation length).
4. Misalignment of the cone axis or drive symmetry imbalance degrades the compressed density and can lead to turbulent mixing into the cone-core gap.

Two possibilities have been suggested to mitigate the ablation of the gold material – either tamping the cone with a thin plastic (CH) layer [26] or to use an intrinsic DT ice layer that forms on the cone wall as the tamp material [27]. In addition, at early times in the acceleration the Kelvin Helmholtz instability could be generated at the interface of the gold cone and the ablator/fuel capsule. Additional material tamping may need to be added closer to the initial shell diameter position to mitigate this effect.

We envisage experiments that use a shaped laser pulse (similar to that needed for the HiPER baseline target design) to irradiate a plastic foil to simulate the X-ray and hot electron production in the laser-plasma interaction. The ablation of material from a gold foil placed at different distances from the primary foil, with the ablated material being diagnosed using a monochromatic backlighting source. The opacity of the ablated gold plasma to the backlighting source can then be used to infer the dynamics and suitability of tamping by different thickness plastic and Be-coatings.

We also envisage similar experiments (e.g. V-groove type open geometries) to test whether Kelvin Helmholtz instability is important in the early stages of the implosion. In the context of hydrodynamical experiment for fast ignition, a first experiment has recently been performed using the Alisé laser of CEA in Bordeaux, in which the sliding of a laser-accelerated target attached on a support has been studied in order to mimic the sliding of the pellet shell along the cone surface. Although very preliminary, this experiment gives the idea of what can be done using already existing European laser installations. Relevant experiments in this field are probably limited only by our ability to imaging them. More experiments could also be performed during the next preparatory phase for HiPER on non-European facilities in the U.S. and in Japan in collaboration with researchers from those countries.

8.6 Fast electron transport in dense deuterium plasmas.

Most studies of laser-solid interactions to date have been performed with medium – high Z metallic targets. They have shown the divergent fast electron beams discussed in section 3. These irradiated materials have a resistivity that rises between 1 eV and 10 eV, plateaus between 10 eV and 100 eV and then falls thereafter [8.28]. Even in the high temperatures above 100 eV, their resistivity is at least an order of magnitude higher than that of the compressed deuterium-tritium fuel in the HiPER base line design. Consequently, fast electron energy transport in compressed deuterium or deuterium-tritium mixtures is likely to be very different to those in current day laser-solid experiments.

This is illustrated by a number of transport experiments in lower Z plastic targets. In the initial plasma production phase in low temperature plasmas, the transport is complicated by ionisation induced instabilities [8.29]. In higher temperature plasmas, experiments have shown a transition from a uniform beam pattern with a 20° divergence angle to one with an annular beam structure [30]. This indicates the beam propagation inside the target is hollow at intensities on target of $3 \times 10^{19} \text{ Wcm}^{-2}$. Norreys *et al.* concluded that this effect was most likely to due to a fall in resistivity (η) with target heating. The electric field set up to draw the return current is given by Ohm's law $E = \eta j$ (where j is the current). Ohmic heating is given by ηj^2 , so if the resistivity falls faster than linearly with temperature then the electric field will change from increasing with current density to decreasing with current density (once the temperature has risen significantly). This causes the magnetic field to fall and to change sign, leading to hollowing of the beam instead of focusing of it.

In addition to beam hollowing, other effects become important, particularly when the beam density approaches that of the background plasma. Filamentation of the fast electron beam can occur when there is a change in background density and this has been confirmed experimentally [8.31]. Filamentation of the fast electron beam has also been observed in a number of other experiments [8.32], although the real origin of such filamentation really still remain an open question, partially because of the inability of the computational models that are currently available to fully simulate the experimental conditions. Filamentation has been shown to be important in the beam transport between the gold end wall and the fuel plasma in the cone-core gap of the 3D simulations of Honrubia of the HiPER baseline target design. Such simulations also showed how, in those conditions, most of the fast electron beam is prevented to cross the density gap at the cone-wall plasma interface, and therefore cannot reach the compressed core. This happens both because of the (filamented) self induced magnetic field at the interface, and because of the charge separation at the gap.

Experiments to explore the transport physics between the cone-core gap are essential in the risk reduction period. Such experiments require a cylindrical implosion of a deuterium filled capsule and different cone-diagnostic foil distances. A concerted design effort is needed to match the density and temperature conditions of the cone-core gap in the baseline design with those generated in the compressed plasma of the cylindrical implosion. It will make it possible to benchmark hybrid-PIC modelling.

8.7 Transition from the Ohmic to drag-heating regimes.

In the HiPER facility, the required high-intensity laser energy greatly exceeds the energy available on current laser systems around the world. It is therefore important that to test the understanding of the basic physics of laser-plasma interactions at higher energies before the high-powered laser required by the HiPER project are built.

From a theoretical standpoint, one expects a significant rise in background electron temperature with the move from the currently available lower energy regime into the required higher energy regime. Theoretical modelling and experimental results indicate we are increasingly able to understand the basic physics at lower energies. There the resistivity of the background plasma plays a strong role in determining how the background responds to the fast electron currents because the electric (and hence by induction magnetic) fields produced are heavily dependent on the interplay between background electron motion and the fast electron current. We are able to estimate the background electron temperature and the role of the fields in solid targets [8.36-39], though the modelling is hampered somewhat by the need to include solid-state physics at low temperatures. Experiments have also been performed by propagating the fast electron beam in foam targets [8.40,41]. Here higher background temperatures are expected because of the lower density of the material and indeed in this regime it was found that fast electron penetration showed a scaling in agreement with Spitzer's law for plasma resistivity, thus overcoming the need for including solid state description of resistivity. Such result may give some indication towards scaling to higher material temperatures.

At higher energies, the models predict background plasma temperatures become so high that the electron transport enters a different regime, in which resistivity can no longer lead to significant slowing of the fast electrons [8.42]. It must be stressed that one-dimensional Vlasov-Fokker-Planck simulations now underway indicate that the propagation of the fast electron current is not hindered in this regime, but this study needs to be extended to higher dimensions in this design phase, since beam-plasma instabilities may give rise to anomalous resistivity when the background density approaches the fast electron beam density [8.43]. Equally, it will be important to experimentally determine how the fast electron motion is affected by electromagnetic fields and indeed the interplay between the fields and the beam to complement the numerical modelling.

It is interesting to note that this expected change in propagation distance means that the gold end wall can be thicker than that needed to prevent shock breakout. In the Osaka experiments that thickness was 5 μm in total. This relaxation is fortunate because the total number of electrons in the HiPER ignition beam will exceed the available number in this thickness of gold (assuming a 40 μm focal spot) and the electron beam must be drawn from the return current largely supplied from this plasma. Experiments are needed to confirm the optimisation of the end wall thickness in the baseline design.

8.8 Collective Stopping

Collisional effects are thought to play a secondary role in determining the penetration range and the energy deposition of fast electron with respect to electromagnetic (collective) effects. Nevertheless, they are generally not negligible and should be carefully considered. Until now there is no experimental measurements supporting the theoretical models for stopping power of fast electrons nor in the compressed fuel (very dense and hot mixture of DT) nor for warm dense matter states.

A series of experiments devoted to measuring the stopping power of warm strongly compressed matter (e.g. by using laser-driven shocks) becomes now possible in European laser facilities which couple long (ns) and short laser beams respectively for compression (shock generation) and for the generation of the fast electron beam or proton beams. Such measurements should indeed be done both in the framework of electron-driven fast ignition and for the proton-driven fast ignition approach. The main difference consists in the fact that trajectory of (massive) protons can be assumed to be straight, as opposed to those of (light) electrons which suffer from straggling effect. Such experiments should be performed during the HiPER preparatory phase, in order to validate existing models.

An aspect of particular concern is the correlation effects on the stopping power, i.e. the fact that in a very dense beam the particles interact with each other. Until now there have been a few theoretical works which show that indeed correlation effects may be relevant but they do not allow any definite conclusion. Also there are no experimental measurements to support such models and this needs to be corrected in the detailed design phase.

Most of the work concerns correlation effects in the stopping power of fast ions (and hence protons). Lontano et al. [8.44] studied the stopping power of an ensemble of a large number of fast heavy ions moving in a plasma with a distribution function which has a small spread both in space and in velocity (therefore a much simpler case as compared to the wide energy spectrum of laser-generated protons). Following this work, there was a proposal of for an experimental investigation [8.45] that, until now, has not been performed.

Concerning collective electron stopping effects, Deutsch et al. have studied the problem of collisional stopping power in the framework of EXISTING models for stopping power in dense plasmas [8.46]. The interaction of relativistic electrons produced by ultra-fast lasers in a strongly pre-compressed thermonuclear fuel was analytically modelled. Energy loss to target electrons was treated through binary collisions and Langmuir wave excitation. The authors discuss the possibility of correlation effects playing some role, without really addressing the subject.

Following this work, in 1999 Deutsch and Fromy published a paper specifically devoted to correlation effects [8.47]. They investigated the stopping of intense and relativistic electron beams (REB) from short-pulse lasers interacting with a pre-compressed deuterium-tritium fuel. They used the Bohr–Fermi formalism with a large impact parameter. Dynamical intrabeam correlation was treated through long-range collision with target electrons. In some cases, this was shown to be quantitatively significant and affecting the overall REB penetration in the DT fuel leading to shorter stopping ranges (although the authors conclude that this yields an easier access to fuel ignition through hot spot production, in reality the effect may either be positive or negative depending on the specific parameters).

Finally, in 2001, Mima and Lontano also addressed the problem of correlation effects in fast electron stopping power [8.48] using a simple model which neglects straggling and relativistic effects. It is clear that the theoretical studies presented in the literature do not allow any conclusions to be drawn, not only on the relevance of correlation effects, but also on whether play an important role or not.

It must also be stressed that, apart from the occurrence of straggling, another main difference between a relativistic fast electron beam and a beam of energetic protons arises from the fact that the divergence, the energy spread (and the mutual Coulomb repulsion) of the particles introduces a finite decorrelation time, thereby limiting the importance of correlation effects in the stopping power. However such decorrelation is much less important for electrons because, due to the relativistic time effect, the real interaction time for electrons will be expanded with respect to (non-relativistic) ion beams. Therefore correlation effects may be much more important for electrons. However they might be fairly important for protons too due to the very high brightness (large number, short duration, laminar flow) of laser-generated proton beams.

8.9 Whole beam self-focusing.

Whole beam self focusing of the incident high-intensity laser beam has been studied at Osaka University in experiments using a 50 TW laser pulse interacting with a 100 μm scale-length preformed plasma [8.4]. Three separate propagation modes were identified: (a) filamentation that occurred when the laser pulse was focused onto the original target surface position (b) whole beam

self focusing that occurred when the focus was placed at the critical surface and (c) stimulated Raman forward scatter that occurred when the laser pulse was focused into the coronal plasma.

The interesting feature of the whole beam self-focusing channel mode is that it forms a natural “cone” shape in the preformed plasma, as illustrated in Figure 8.2. One potential difficulty is that the leading edge of the laser pulse itself self-focuses to a much higher $I\lambda^2$, thereby generating electrons with a larger kinetic energy than required for fast ignition. On the other hand, preliminary evidence from Osaka University is that electron spectrum (measured at the chamber wall) does not change when this process occurs – suggesting that the laser pulse interacts primarily with the channel walls [8.49].

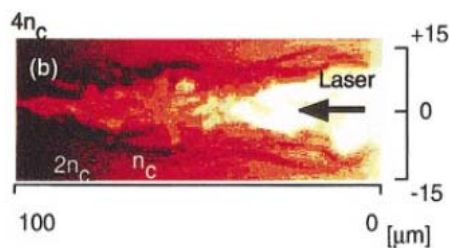


Figure 8.2. Ion density map at 1.1 ps after the start of the laser pulse from a 2D PIC simulation, indicating whole beam self-focusing into overdense regions close to the target surface. From reference [8.4].

The experiments need to compare energy transport results obtained for solid density targets with those generated through the whole beam self-focusing effect with the preformed plasma. These experiments can be performed on Vulcan, LULI 2000 and PETAL. They will be the first investigation of fast ignition relevant conditions for this process, i.e. the correct $I\lambda^2$ and pulse duration. The experiments will allow the characterisation of both the properties of the electron beam (whether self-focusing of the laser pulse allows the intensity to become too high) as well as its subsequent propagation in the solid density plasma (i.e. conversion efficiency and collimation). It will also help determine if cavitation of the channel becomes important (since ion motion can occur on this timescale) and whether beam pointing via the hosing instability becomes an issue.

8.10 Colour and Z scaling.

The colour of the PW heating pulse for HiPER is a real constraint on the final design of the laser system. Estimates from the ponderomotive scaling of the laser pulse indicate that the laser pulse may have to be frequency converted to second harmonic in order to reduce the kinetic energy of the fast electrons so as to be within the stopping range of the dense DT fuel in the hot spot [8.9] (although it is clear that the modelling did not take into account the whole complexity of fast electron transport and may therefore be not quantitatively correct).

However, recent particle-in-cell simulations have indicated that the fast electron energy in multiple ps-duration laser pulses can be lower than the ponderomotive potential energy of the laser pulse by a significant fraction [8.50]. This is caused by the acceleration of the electron bunch occurring in a time-dependent manner – hole-boring in preformed plasma with initial large density scalelength occurs very quickly such that after a short period of time (half a picosecond) the scalelength is less than the wavelength of the laser pulse. The acceleration distance is reduced by the relativistic increase in the electron mass. The kinetic energy that the electrons acquire is then reduced by a

factor $(\gamma n_c / n_s)^{1/2}$, where $\gamma = (1 + a^2/2)^{1/2}$, a is the normalised vector potential, n_c is the critical density and n_s is the density in the skin depth.

The effect may be good news for fast ignition – the PW laser pulse interacts with the Au end wall. Detailed studies of energy transport in high Z materials with 5-ps duration PW laser pulses are needed to confirm this new prediction. Again the effect of prepulse and plasma scalelength in front of the Au foil is an issue which needs to be addressed.

8.11 Proton / ion driven FI scaling experiments.

The production of collimated multi-MeV proton and ion beams from solid targets irradiated by ultraintense lasers has continued to attract considerable interest since the pioneering work done on both the VULCAN and the Nova PW laser facilities. The possibility of using such a proton beam as a ignitor beam (i.e. Proton Fast Ignition (PFI)) was first suggested by Roth *et al.* [8.51], and the same authors have also published a more extensive article on this matter [8.52].

There are a number of issues which affect the feasibility of PFI. Firstly, and foremost, there is the matter of energetics. The most detailed theoretical study of the heating of the compressed fuel by a proton beam was done by Temporal *et al.* [8.53]. Their reference case suggested that a minimum of 26 kJ of proton energy was required for ignition. The highest conversion efficiency observed experimentally is 12% [8.54]. On this basis around 200 kJ of short-pulse laser energy is required. This estimate makes it unlikely that PFI ignition experiments are possible on HIPER with a specification of 70 kJ of short-pulse laser energy.

However it is not inconceivable that the ignition energy could be revised downward, and that the conversion efficiency might be revised upward. In the study of Temporal *et al.*, it was noted that if the proton energy spectrum could be controlled then the proton energy required for ignition could be reduced to 10 kJ. Considerable progress has been made in the field of spectral control [8.55,56], and improving conversion efficiency [8.57]. Given the rapid progress being made in the field of ultra-intense laser-plasma interactions, the factor of two improvements required to change the prospects of PFI on HIPER are very much possible.

Other issues include the focussing of the proton beam, and the survival of the proton source during fuel compression. A great deal of experimental and theoretical work has been done on the focussing of the proton beam, and it seems quite likely that it will be possible to focus down to spot sizes of 10 μ m (currently 50 μ m has been demonstrated experimentally). Simulations have also shown that a protective shield can be used to keep the source foil intact despite the intense flux of x-ray radiation that is produced during fuel compression.

In summary, current estimates suggest that PFI ignition experiments on HIPER are unlikely with 70-100 kJ of short-pulse laser energy. However, this estimate could change completely over the next few years. Conversion efficiency and ignition energy requirements need to be studied more extensively. Even if PFI is eventually regarded as not being a primary objective of HIPER, it should still be recognized that HIPER could be invaluable to PFI research.

8.12 Two stream instability – ion heating.

High ion temperatures (that exceed the background electron temperatures) have been observed in PW laser-solid interaction with deuterated plastic targets, as observed by neutron spectroscopy [8.58]. The heated layer were confined to a small region close to the front of the target and this was confirmed by placing thin layers of ordinary plastic of increasing thickness over the target and observing a reduction in both neutron yield and signal width (which are both related to the ion

temperature). While the amount of energy transferred to the ion population was small (~1%) it does suggest the development of a new plasma instability that cascades the laser energy to the ion population without significantly heating the background plasma. Further measurements since then have confirmed that this process is highly non-linear and the experiments were just on the intensity threshold for the observation of this effect.

It has been proposed that the preferential heating of the ions observed in the original experiment is caused by two coupled instabilities, as described by Mendonça et al. [8.59]. First, the two-stream instability occurs between the electrons accelerated into the target by the fast electrons induced by the laser-plasma interaction and the electron return current provided by the background electrons in the target. This drives up large amplitude electrostatic waves that themselves become modulationally unstable, decaying resonantly into ion-acoustic waves. These ion acoustic waves are heavily damped, leading to ion heating without significant electron heating (because the electrons support high frequency plasma oscillations that are not significantly affected by collisions). The measurements have been reproduced using hybrid-PIC simulations, but some caution is needed in interpreting these results due to numerical heating effects in the code.

The experiments do suggest an alternative approach to hot spark formation in fast ignition where one relies on this instability to heat the core rather than collisions. This might be achieved by using a higher intensity picosecond laser pulse, providing that this is compatible with the growth rate of the coupled instability in the deuterium-tritium fuel.

Indeed, Mendonça et al. have proposed this mechanism as an explanation for the coupling to the ion population in the Osaka University cone-shell implosion experiments [8.59]. They suggest that this mechanism is responsible for the heating on the edge of the compressed core in those experiments, where the lower plasma density matched the growth rate of the instability. Since it is of the utmost importance to identify the underlying plasma physics processes responsible for ion heating in these implosions, additional shots need to be undertaken on Vulcan PW (where the neutron spectrometer is located) in the detailed design phase to further elucidate the physics of this mechanism. If successful, they should inform experiments on higher energy PW facilities (e.g. PETAL) as a precursor to HiPER experiments. Their aim needs to be to confirm whether the HiPER PW beamlines should have the capability of higher intensity (i.e. shorter ps) pulse durations to target for hot spark formation.

8.13 Hole boring.

Much of this risk reduction exercise has concentrated on energy transport experiments relevant to cone-shell implosions, as these targets appear to circumvent many of the plasma physics problems associated with hole-boring in a long underdense coronal plasma (as suggested in the original fast ignition paper). These problems appear formidable – both the fire-hose and filamentation instabilities have been observed with electron beam propagation in plasmas whose background density is comparable to the beam density [8.60].

Nevertheless, one should not rule out this possibility, particularly given the knowledge base of assembling high quality DT ice layers in full spherically symmetric capsules. Experiments can be envisaged on Vulcan, LULI and PETAL to test the integrated approach. It should be noted that the OMEGA laser facility in the United States plan to use a combination of high intensity laser pulses for their integrated fast ignition experimental campaign to study this effect. If this approach is found to be practical on the OMEGA facility, then the HiPER facility design should have the capability of combining a spherical symmetry irradiation with the delivery of 100 ps / 10 ps hole boring / ignition pulses to target.

8.14 Alternative geometries

The first cone-guided compression experiment for fast ignition was conducted by a UK-Japan team on the Vulcan laser facility in 1999 [8.61]. In that experiment a plastic foil, containing a deuterated plastic signature layer, was driven down the inside of the cone by the nanosecond duration laser pulse. At stagnation, the short pulse was fired into the apex of the cone and an increased neutron signal was observed for the first time. That particular closed geometry was chosen by the team because the Vulcan laser was not able to deliver sufficient energy to target to generate compressed densities above a few gcm^{-3} .

Since then, extensive numerical design work has been carried out at Sandia National Laboratory on hemispherical target designs using a gold glide plane. A summary of that work is given by Slutz et al. [8.62]. The experimental work started with the Z machine and were indirectly driven by X-rays generated in a wire array Z-pinch. The Z machine stores 11.5 MJ of electric energy in its capacitor banks and was able to generate more than 2 MJ of soft X-rays. The capsule implosions were backlit using 6.7 keV iron backlighting target foil. Remarkably good agreement between a series of radiographs of the implosions and synthetic images generated from the radiation hydrodynamics code. The simulations have indicated that compressed densities of 130 gcm^{-3} and areal densities of 0.84 gcm^{-2} can be achieved. The simulations confirm that a wide parameter space is available to optimise the compressed density in hemispherical and “ice-cream” cone-guided compression geometries.

One notices immediately that the LIL-PETAL laser facility has a 4-beam cluster available for hydrodynamics experiments with a total drive energy of 40 kJ of UV light. That is equivalent to the full specification of HiPER over the full 2π . This provides a unique facility to test the hydrodynamics of the HiPER baseline implosions and allows the interesting possibility to be asked as to whether the HiPER facility could or should be reconfigured at a later stage into a single sided cluster arrangement to drive implosions equivalent to 3 MJ of direct drive energy. That is a truly exciting possibility.

References for Chapter 8:

- [1] M.Tabak et al., *Phys. Plasmas* **1**, 1626 (1994).
- [2] E.M.Campbell et al., *Fusion Sci. Tech.* **49**, 249 (2006).
- [3] K.B.Warton, et al., *Phys. Rev. Lett.* **81**, 822 (1998).
- [4] R.Kodama et al., *Phys. Plasmas* **8**, 2268–2274 (2001).
- [5] P.A. Norreys et al., *Phys. Plasmas* **6**, 2150 (1999).
- [6] W.Theobald et al., *Phys. Plasmas* **13**, 043102 (2006).
- [7] F.Pisani et al., *Phys. Rev. E*, **62**, R5927 (2000).
- [8] K.A.Tanaka et al., *Phys. Rev. Lett.* **96**, 255006 (2006).
- [9] S.C.Wilks et al., *Phys. Rev. Lett.* **69**, 1383 (1992).
- [10] H. Ruhl et al., *Phys. Rev. Lett.* **82**, 2095 (1999).
- [11] K. Eidmann et al., *Phys. Rev. E* **62**, 1203 (2000).
- [12] S. P. Hatchett, *6th Fast Ignitor Workshop*, Florida (2002).
- [13] R.Kodama et al., *Nature* **412**(6849), 798 (2001).
- [14] R.Kodama et al., *Nature* **418**(6901), 933 (2002).
- [15] R.B. Campbell et al., *Phys. Rev. Lett.* **94**, 055001 (2005).
- [16] R.J. Mason, *Phys. Rev. Lett.* **96**, 035001 (2006).
- [17] J.J.Santos et al., *Phys. Rev. Lett.* **89**, 025001 (2002).
- [18] R.B. Stephens et al., *Phys. Rev. E* **69**, 066414 (2004).
- [19] K.L. Lancaster et al., *Phys. Rev. Lett.* **98**, 125002 (2007).
- [20] R.B. Campbell et al. *Phys. Plasmas* **10**, 4169 (2003).
- [21] R. Kodama et al., *Nature* **432**(7020) 1005 (2004).

- [22] M. Nakatsutsumi et al., *Phys. Plasmas* (in press).
- [23] A. Caruso et al., *J. Expt. Theor. Phys.* **97**, 948 (2003).
- [24] R.B. Stephens et al., *Phys. Plasmas*. **12**, 05312 (2005).
- [25] C.D. Zhou et al., *Phys. Rev. Lett.* **98**, 025004 (2007).
- [26] T. Johzaki et al., 9th Fast Ignition Workshop, Boston (2006).
- [27] J. Pasley et al., 9th Fast Ignition Workshop, Boston (2006).
- [28] R.R. Freeman et al., *Fusion Sci. Tech.* **49**, 297 (2006).
- [29] M. Manclossi et al., *Phys. Rev. Lett.* **96**, 125002 (2006).
- [30] P.A. Norreys et al., *Plasma Phys. Control. Fusion* **48**, L11 (2006).
- [31] M.S. Wei et al., *Phys. Rev. E* **70** 056412 (2004).
- [32] D. Batani, et al., *Phys. Rev. Lett.*, **94**, 055004 (2005).
- [33] M. Tatarakis et al., *Phys. Rev. Lett.*, **81**, 999 (1998).
- [34] R.B. Stephens, et al., *Phys. Review E*, **69** 066414 (2004).
- [35] S.P. Hatchett *private communication* (2005).
- [36] J.R. Davies et al., *Phys. Rev. E* **59** 6032 (1999).
- [37] A.R. Bell et al., *Plasma Phys. Control. Fusion* **48**, R37 (2006).
- [38] E. Martinolli, et al., *Phys. Rev. E*, **70**, 055402(R) (2004).
- [39] E. Martinolli, et al., *Phys. Rev. E*, **73**, 046402 (2006).
- [40] D. Batani, et al., *Phys. Rev. E*, **65**, 066409 (2002).
- [41] J.R. Davies, *Phys. Rev. E*, **68**, 056404 (2003).
- [42] M.E. Glinsky *Phys. Plasmas* **2**, 2796 (1995).
- [43] Y. Sentoku, *Phys. Rev. Lett.* **90**, 155001 (2003).
- [44] M. Lontano and F. Raimondi *Phys. Rev. E* **51**, 6211 (1995).
- [45] D'Avanzo et al, *Nuovo Cimento*, 19 D, p.685 (1997).
- [46] C. Deutsch, et al., *Phys. Rev. Lett.* **77**, 2483 (1996).
- [47] C. Deutsch and P. Fromy *Phys. Plasmas* **6**, 3597 (1999).
- [48] K. Mima and M. Lontano (*private communication* (2001)).
- [49] K.A. Tanaka (*private communication* (2006)).
- [50] Y. Sentoku, 9th Fast Ignitor Workshop, Boston (2006).
- [51] M. Roth et al., *Phys. Rev. Lett.*, **86**, 436 (2001).
- [52] M. Roth et al., *Plasma Phys. Control. Fusion*, **47**, B841 (2005).
- [53] M. Temporal et al., *Phys. Plasmas*, **9**, 3098 (2002).
- [54] R. Snavely et al., *Phys. Rev. Lett.*, **85**, 002945 (2000).
- [55] M. Hegelich et al., *Nature*, **439**, 441 (2006).
- [56] H. Schworer et al., *Nature*, **439**, 445 (2006).
- [57] Ping *et al.*, *Bulletin of the American Physical Society* (2006)
- [58] P.A. Norreys et al., *Plasma Phys. Control. Fusion* **47**, L49 (2005).
- [59] J.T. Mendonca et al., *Phys. Rev. Lett.* **94**, 245002 (2005).
- [60] M. Tatarakis et al., *Phys. Rev. Lett.* **90** 175001 (2003).
- [61] P.A. Norreys et al., *Phys. Plasmas* **7**, 3721 (2000).
- [62] S.A. Slutz et al., *Fusion Sci. Tech.* **49**, 374 (2006).

9 Baseline Facility Design

9.1 Laser Design Philosophy

There are two principal technology options for HiPER:

- Evolution of NIF / Laser Mégajoule (LMJ) technology. This would provide “single shot” operation every ~ hour at low technical risk.
- Implementation of high repetition rate technology (~1 shot per second) based on diode-pumped solid-state lasers (DPSSL). This would require significant technical development, which is explored in the next section.

Down selection will be made during the course of the 3-year preparatory phase project, based on a detailed cost/benefit analysis, discussions with allied efforts in Japan and the USA, and strategic assessment of the balance of the basic science and fusion application missions of HiPER.

This section will consider the NIF/LMJ technology option.

9.2 Compression beamlines

The theoretical plasma physics work supporting the HiPER project has determined that the requirements shown in table 1 are needed to obtain Inertial confinement fusion with a gain of order 50 using the fast ignition technique.

<i>Energy</i>	Specification (compressor beams) 200 kJ
<i>Wavelength</i>	2 ω baseline, 3 ω option
<i>Pulse length</i>	5ns
<i>Pulse shape</i>	Yes (adiabatic shock plus ramp plus final, <200ps resolution)
<i>Focusing geometry</i>	Spherically symmetric with missing cone ≤ 40 deg
<i>Minimum number of beams</i>	42 (set in part by single beam performance)
<i>Focal spot size</i>	1.5 to 2 mm on target

Table 1. Facility specification for the compression beams.

The primary laser science and technology challenges to realizing a high-energy, high-power laser include: producing high energy pulses with sufficient control over the pulse bandwidth; spectral phase and wavefront quality to allow compression; and focusing it to meet the requirements discussed above [9.1]. NIF and LMJ facilities are both being completed and their baselines have been demonstrated on the Beamlet single laser line, the LIL and the upcoming NIF beam lines [9.2, 9.3].

The latest generation of high-energy lasers uses square beams with multipass geometries that allow higher-density packaging and efficient extraction of stored energy. The laser medium is Nd-doped phosphate glass since it is available in large quantities with clear apertures up to 40 x 40 cm². Typical bandwidth of 17 nm (FWHM) allow compressing pulse down to 1 ps pulse width.

All solid-state laser designs are based on the following block diagram whatever the number and size of the beams :

- Front-end,
- main amplifier section,
- transport,
- final optics assembly (frequency conversion, and focusing to target chamber centre).



Figure 9.1 : main sub-systems as a block diagram

HIPER must take advantages of ten years of both NIF and LMJ design and engineering studies :

- beam shape is a square from the front-end output to the final assembly,
- beams are put together as bundles of 4 beams (from amplifier main section to the target), bundles of 8 beams inside the main amplifiers,
- components of the same type are assembled in Line Replaceable Units allowing easy and quick repair, maintenance and operation,
- focal spot is “conditioned” with wavefront correction in the main amplifier section and a continuous phase plate somewhere in the Final Optics Assembly,
- laser design includes smoothing by spectral dispersion.

In order to design the whole laser baseline, two points of view will be discussed:

- Energy perspective
- Beam propagation perspective

The high intensity regime will lead to non linear effects that will introduce distortions in the spatial, temporal and spectral profiles of the beams. Limits will be set to avoid too high a non linear effect, allowing laser operation in a “safe” regime. The redline performance is limited by :

- $\Delta B < 2$ in the main laser,
- $I < 2.5 \text{ GW/cm}^2$ & $\Delta t < 2 \text{ ns}$ (Raman in air),
- $I \times L < 25 \text{ GW/cm}$ in the 3ω section

The laser damage threshold of optical components is of primary concern, because damage occurs and grows as a function of laser fluence. On most optical components, it is assumed :

- a $t^{0.5}$ law for damage fluence scaling with pulse. Most of the time, damage fluence is given at 3 ns pulse width.
- threshold fluence at which damage is growing shot after shot (4 to 5 J/cm² at 3ω).

9.3 Energy perspective

In order to meet the energy requirements above it is necessary to assess the number of beams and the size of these beams. This can be determined by the following calculation. The calculation is split in 3 phases :

1. The amplification volume depends on 4 parameters

- the energetic conversion efficiency at 3ω , $\eta_{3\omega}$: the transmission of the transport & FOA sections, T_{FOA} ; the extraction efficiency of the amplifiers, η_{ext} ; the stored energy density of the amplifier, ρ_{sto} .

➤
$$V = \frac{E_{3\omega}}{\eta_{3\omega} T_{FOA} \eta_{ext} \rho} \quad \text{and} \quad S = \eta_{mod} \frac{E_{\omega}}{F_{dam}}$$

2. The amplification surface S depends on 2 parameters :

- the modulation depth in the near field after amplification, η_{mod} the maximum available fluence (damage threshold at 1ω), F_{dam}

3. The laser surface D^2 depends on two parameters :

- the small signal gain, g_0
- the reflection coefficient at which gain is depleted by ASE, R

$$D = -\frac{\ln(R)}{g_0} \frac{1}{n\sqrt{n^2+1}} \quad \text{and} \quad N = \frac{S}{D^2}$$

Combining the equations from 1, 2 and 3 above, it is possible to get the number of laser slabs N_p that depends on 2 parameters : the laser slab thickness, e ; the refraction coefficient of the amplifying medium, n ; the number of passes inside the gain medium.

The general formulae is as follows :

$$N = \frac{\eta_{mod} \frac{E_{3\omega}}{\eta_{\beta\omega} T_{FOA} F_{dam}}}{D^2}$$

With « standard » data, $\eta_{3\omega} = 0.5$, $T_{FOA} = 0.8$, $\eta_{mod} = 1.5$, $F_{dam} = 20 \text{ J/cm}^2$, $R = 0.0045$, $g_0 = 0.05 \text{ cm}^{-1}$, $n = 1.5$, one gets : $E_{3\omega} = 300 \text{ kJ} \Rightarrow S = 5.625 \cdot 10^4 \text{ cm}^2$, then with $D = 40 \text{ cm}$, $N = 35.1$.

At this point, it is possible to calculate the number of beams as a function of the most important or critical parameters : $\eta_{3\omega}$, η_{mod} and F_{dam} .

The high intensity regime will lead to non linear effects that will introduce distortions in the spatial, temporal and spectral profiles of the beams. Redlines have been set to avoid excessive non linear effects and so to allow the laser to operate in a “safe” regime. The redline performance is limited by:

- $\Delta B < 2$ in the main laser $\Rightarrow 1.5 < \eta_{3\omega} < 2$
- at the same time if the pulse width is 5 ns, then the average intensity at the output of the main amplifier section will be : $2 \text{ GW/cm}^2 < I < 2.7 \text{ GW/cm}^2$ and peak intensity cannot exceed 4 GW/cm^2 because $I_{peak} = F_{dam} / \tau_{pulse}$.
- in that intensity range, frequency conversion crystals have a typical 1 cm thickness that allow clear apertures up to $40 \times 40 \text{ cm}^2$ and conversion efficiency up to 70 % (energetic) per crystal (that is $\eta_{3\omega} = \eta_{2\omega} \times \eta_{2+1\omega} = (0.7)^2 = 0.5$ because the third harmonic generation process is second harmonic generation plus frequency mixing)
- 37 cm beams are the maximum that can be sustained on KDP crystal when the Raman effect is taken into account [9.4]

	$E_{3\omega/2\omega}$ (kJ)	η_{mod}	$\eta_{3\omega}$	T_{FOA}	F_{dam}	D (cm)	N	$E_{1\omega}$ (kJ)/beam
<i>HIPER</i> $_{3\omega}$	270	1.5	0.5	0.8	20	37	37	18.25
	270	2	0.5	0.8	20	37	49.3	13.7
	270	2	0.5	0.8	15	37	65.7	10.3
<i>HIPER</i> $_{2\omega}$	270	1.5	0.7	0.8	20	37	26.4	18.25
	270	2	0.7	0.8	20	37	35.2	13.7
	270	2	0.7	0.8	15	37	47	10.3

Table 9.2 : variation of the number of beams when modulation depth and damage fluence vary at the output of the 1ω section; top 3ω option and bottom 2ω option; in each option, high drive regime at the top, low drive regime at the bottom.

If it is assumed that beams are put together in clusters of 8 beams then 48 beams has been deduced to be a good compromise allowing both low drive regime at 2ω and medium drive regime at 3ω . LIL experiments have shown that the medium drive regime was in the range :

- 100 mJ / 3 to 5 ns per beam at the frond-end output
- 15 kJ / 3 to 5 ns per beam at the output of the main amplifier section
- $\eta_{\text{mod}} = 2$ in the near field at the output of the main amplifier section

It is quite easy to calculate the output energy from an amplifier with a modified Frantz-Nodvik type equation when both the number of slabs and the number of passes are to be optimised. In the case of the LIL experiment :

- gain coefficient per slab = $g_{ol} \approx 0.245$ ($G = \text{Exp}[g_{ol}] \approx 1.28$)
- including optical losses (lenses coating, spatial filtering, mirrors ...) gives an effective gain coefficient per slab $g_{ol} \approx 0.225$ ($G = \text{Exp}[g_{ol}] \approx 1.25$)
- when input energy is set to 100 mJ, output fluence exceeds saturation fluence in the very last slabs

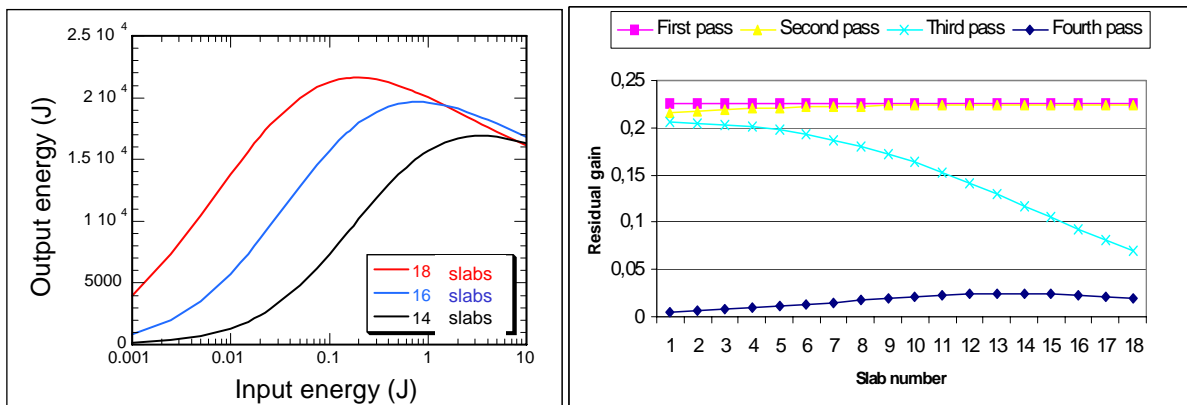


Figure 9.2 : on the left, 1ω output energy as a function of input energy for 3 different amplifiers with 14, 16 and 18 slabs; on the right residual gain in the main amplifier section (18 slabs) after 1, 2, 3 & 4 passes. At the end of the 3rd pass, residual gain decreases rapidly and after the 4th pass residual gain is quite low in all slabs because all the energy has been extracted.

9.4 Beam propagation perspective

The basic principles of beam propagation are :

- multipass beam propagation through amplifiers
- image relay planes from the front-end output (near field) to the frequency conversion crystals (near field)
- spatial filtering in pinholes (far field)
- wavefront correction with a deformable mirror

The simplest way to mix all these requirements are as follows :

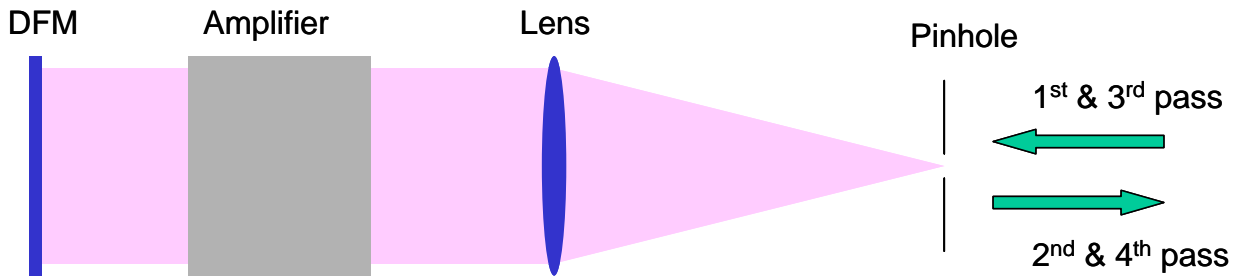


Figure 9.3 : principle of associating spatial filtering in the far field with a multipass amplification geometry and wavefront correction in the near field.

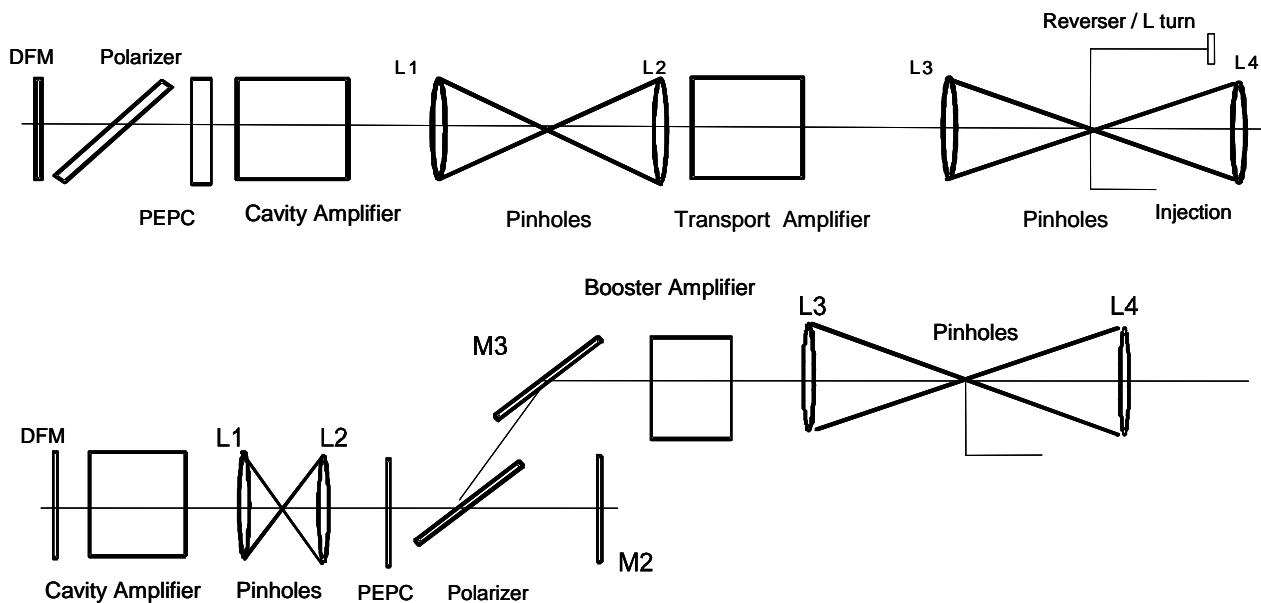


Figure 9.4: Different multipass geometries with two amplifiers. Top is the LIL/LMJ design (4 passes in the two amplifiers). Bottom is NIF design (2 passes in the booster amplifier and 4 passes in the cavity amplifier).

9.5 Deformable mirror location

Such high energies in the 1ω main amplifier section could only be obtained with a tight control of the beam alignment and with an efficient wavefront correction [9.5]. Indeed, the more pumped slabs used in a beamline the stronger the aberrations. For example, with 15 pumped slabs, the peak-to-valley wavefront distortion is about 5 to 6λ . With such aberrations and without any correction, the beam hits the final spatial transport filter pinhole producing a high risk situation for the facility safety and a poor quality beam. To avoid this kind of disagreement, a pre-correction is applied to

the deformable mirror (DFM) before the shot to compensate for Prompt Pumped Induced Aberration (PPIA), resulting in a good quality spot size for the final pinhole crossing [9.6].

It is possible to estimate the wavefront aberration with a simple approach. If : Ab = aberration ; INJ = injection; $AMPLI$ = amplifier ; DT = reverser (“demi-tour”), then the total aberration at the spatial filter (FST) location is :

$$\begin{aligned} \text{FST1} &= Ab_{INJ} \\ \text{FST2} &= Ab_{INJ} + 2 Ab_{AMPLI} \\ \text{FST3} &= Ab_{INJ} + 2 Ab_{AMPLI} + 2 Ab_{DT} \\ \text{FST4} &= Ab_{INJ} + 4 Ab_{AMPLI} + 2 Ab_{DT} \end{aligned}$$

Setting the correction :

$$(Ab_{INJ} + 4 Ab_{AMPLI} + 2 Ab_{DT})/2 \text{ to the DFM,}$$

you will get :

$$\begin{aligned} \text{FST1} &= Ab_{INJ} \\ \text{FST2} &= \frac{1}{2} Ab_{INJ} - Ab_{DT} \\ \text{FST3} &= \frac{1}{2} Ab_{INJ} + Ab_{DT} \\ \text{FST4} &= 0. \end{aligned}$$

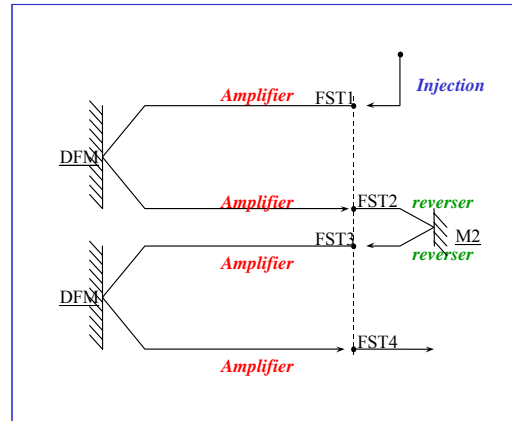


Figure 9.5_: wavefront correction when the deformable mirror is located in the middle of the main amplifier.

The wavefront correction set to the DFM shows that DFM location is best in the middle of the amplifier : total budget is 4 at the input or the output, 2 in the reverser and 1 in the middle of the amplifier.

9.6 Front-end design

NIF and LMJ are highly parallel systems of flashlamp-pumped neodymium-doped phosphate glass lasers. All these lasers are driven by the injection laser system consisting of a single master oscillator, pulse shaping systems that produce nanojoule level pulses with arbitrary waveform generation (AWG) capability, and preamplifier modules (PAM) that condition and further amplify the pulses to the Joule level prior to injection into the main laser system.

The front-end set-up is shown figure 9.6. The laser starts at the fibre oscillator. It is a single longitudinal mode CW oscillator the wavelength of which is locked to 1053 ± 5 pm. A first phase modulator at 2 GHz is used to create 0.1 nm bandwidth to avoid non linear Brillouin effect in large fused silica components.

A second phase modulator is used for smoothing by spectral dispersion, the typical bandwidth is 0.5 nm. Then the line is split in 48 beam lines in 3 steps (figure 9.6).

Given all the losses introduced by the optical components (amplitude and phase modulators, insulators, couplers, etc.), on the order of 80 dB, fiber-based amplifiers are required with a total gain of around 100 dB. This requirement results in the use of three Yb³⁺-doped fiber-based amplifiers with single-pass gains on the order of 30 dB [9.7].

The output power of the oscillator should be in the range 5 to 10 mW, giving an output power at the end of the fiber-based amplifiers of 200 to 400 mW per beam and the Pre Amplifier Module (PAM) must be able to raise the energy from the nJ level to a typical 100 – 200 mJ in two steps :

- a regenerative amplifier able to deliver 10 to 20 mJ
- a power amplifier

The Average Waveform Generator (AWG) is able to shape the pulse (for example 1 point every 100 ps for a maximum 15 or 20 ns pulse width). In figure 6 one Average Waveform Generator “feeds” a bundle of 4 beams, but it is possible to have one AWG per beam allowing many interesting combinations between the foot pulse and the main pulse instead of having the same shaped pulse on all the beams. The PAM also contains the spatial square shape design for the beam.

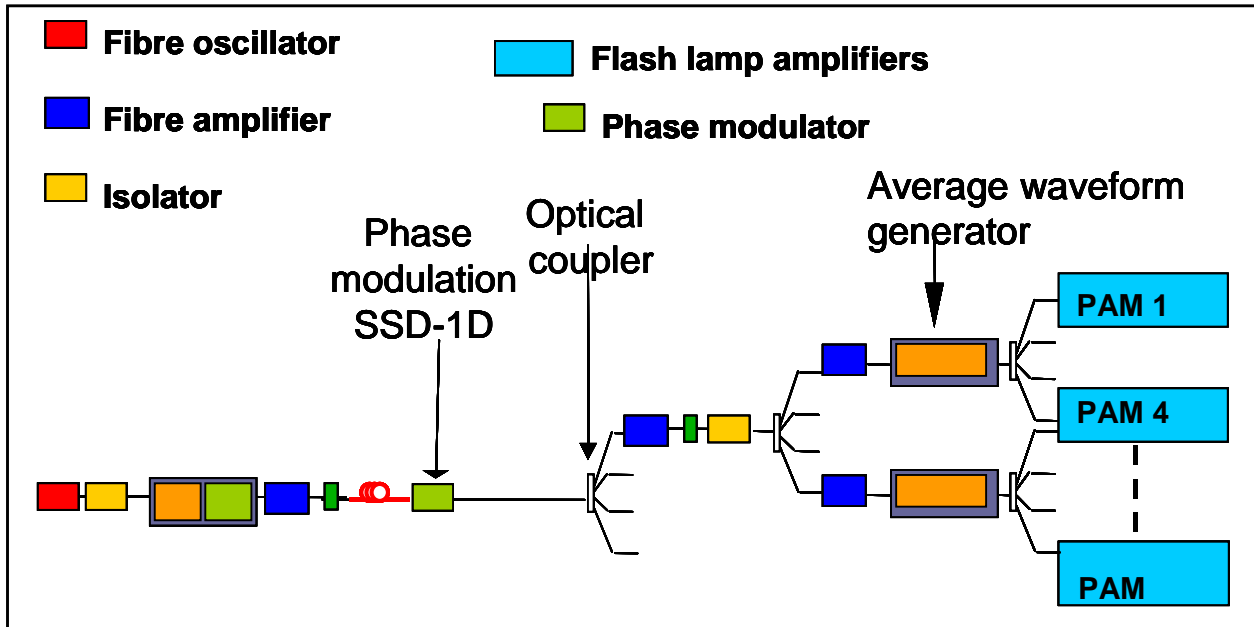


Figure 9.6 : front-end lay-out. One single oscillator is split in 48 beam lines in 3 steps.

9.7 Amplifier design

The LIL-LMJ amplification scheme consists of 2 amplifiers in a 4 pass design. The output from the front-end is a square beam approximately 4 cm wide. Each amplifier has 9 laser slabs. Laser slabs are made of Schott LG-770 or Hoya LHG-8 phosphate glass doped with Neodymium.

At the injection, the beam goes through the first Transport Spatial Filter and travels through both amplifiers up to the deformable mirror at a constant width (37 cm). Then back to the second Transport Spatial Filter where it makes an L-turn through the reverser whose magnification is 1/5. After one more round trip through the main amplifier section, the beam will leave through the fourth Transport Spatial Filter and go to the transport mirrors to reach the target bay. This concept has been validated during LIL commissioning and it has been shown that the average gain per slab was equal to 1.23 when flash lamps were driven at 0.2 explosion fraction. See figure 9.7.

Both amplifiers are based on 9 units of 4x2 arrays. Each amplifier looks like a huge metallic box that is hung from the main frame. The whole space underneath this main frame is used by special cart vehicles that can place or remove the Line Replaceable Units (LRU) during maintenance operations. An amplifier will be filled with lamp cassettes and laser slab cassettes. There are two types of lamp cassettes : side cassette with 6 lamps and central cassette with 8 lamps. The total number of lamp cassettes per amplifier is $3 \times 9 = 27$ lamp cassettes and $2 \times 9 = 18$ laser slab cassettes. All laser slabs are at Brewster incidence and the beam polarization is P type (horizontal plane).

In the NIF design, there is only one amplifier inside the regenerative cavity (leading to a four pass design) and the booster amplifier design is only two passes. In the LIL/LMJ design, both amplifiers are used in the four pass design: after the second pass through both amplifier, it is necessary to reflect the laser beam back down the beamline to achieve the third and fourth pass. See figure 9.4 for details.

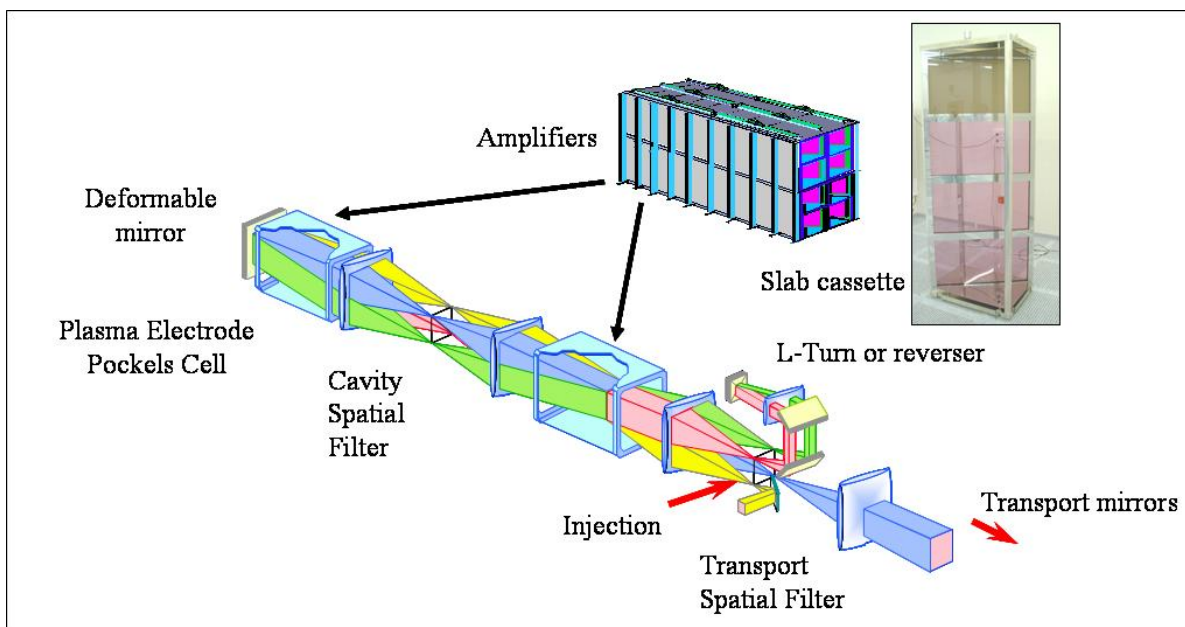
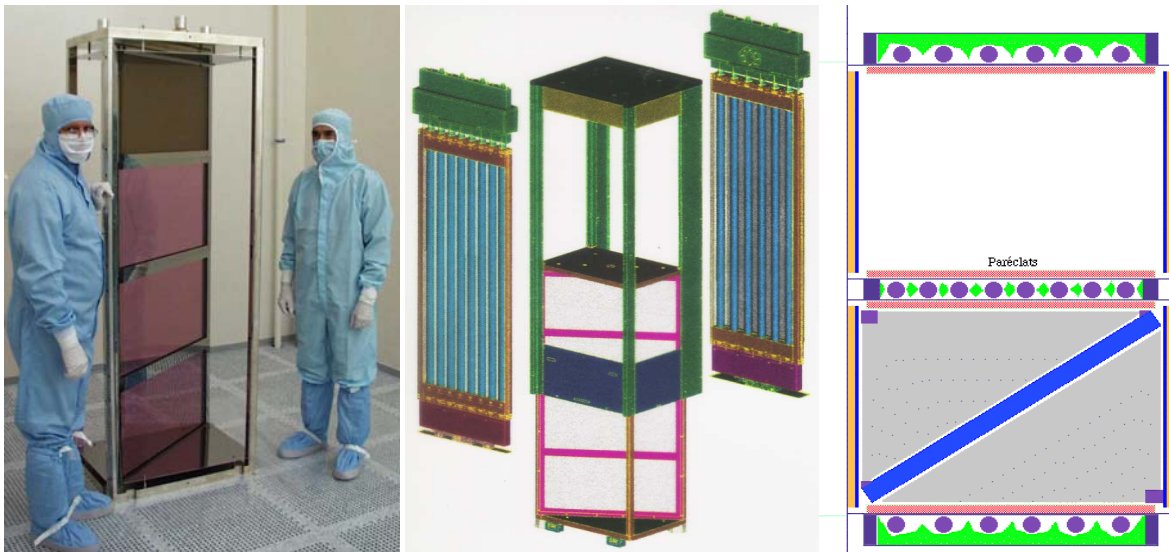


Figure 9.7 : at the top are pictures of the slab cassette (left), slab cassette with two lamp cassettes (centre) and a top view of a slab mounted (right) . At the bottom is a single beam line showing the multipass amplification scheme.

The L-turn concept is based on a reduced collimated beam and requires a single lens and a plane mirror. This single lens is associated with the first lens of the transport spatial filter section to form a telescope whose magnification is $1/5$. The plane mirror (called M2) is located at the image plane of the deformable mirror (back mirror called M1). There are two more mirrors in the L-Turn to reduce the size of this section (so far the L-Turn looks like a Z). Because of the $1/5$ magnification, the beam inside the L-Turn is an 8 cm square beam. To avoid any back reflections from spatial filter lenses, an active switch is located between the deformable mirror and the first lens of the Cavity Spatial Filter. A Plasma Electrode Pockels Cell (PEPC) associated with a large polarizer will provide a typical 10^4 extinction ratio on both polarizations during each round-trip [9.8]. A polarizer

the incidence plane of which is vertical will prevent the Main Amplifier Section from lasing when the PEPC voltage is off. During the four pass round trip, the PEPC voltage is set to V_{π} . This device has been validated on LIL. A large-aperture Plasma Electrode Pockels Cell acts as an optical switch to thwart parasitic oscillations and possible back reflections from the MAS.

9.8 Transport

The geometry itself depends on the shape of the building whether it is a U shape (NIF, LLE) or an H shape (LMJ). Both geometries require 5 to 6 transport mirror per beam.

Careful attention should be taken to the length of the transport section because of longitudinal stimulated Raman scattering in air (SRS) [9.9, 9.10]. Raman scattering increases quickly to a significant loss of energy (Stokes energy to pump energy ratio in %) when :

- Intensity at 1ω is greater than 2.5 GW/cm^2 ,
- Pulse width is greater than 2 ns (stationary case),
- Propagation length is greater than 35 m,
- Modulation depth = peak intensity / average intensity is greater than 2

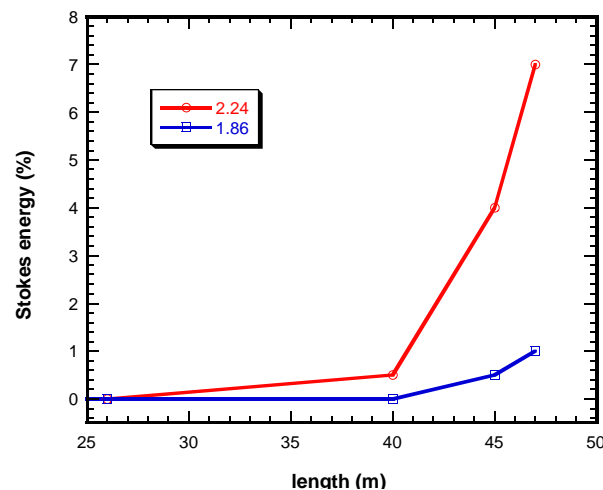


Figure 9.8 : Stokes energy as a function of length as calculated with Miro [9.9, 9.11] with LIL data at 3.3 GW/cm^2 peak intensity at 1ω for a 5 ns shaped pulse (modulation depth = 2.24 at the main amplifier output) and with expected LMJ data (modulation depth = 1.86 at the main amplifier output).

Because NIF transport length is greater than 55 m, beam tubes filled with Argon are being used to avoid any drawback with longitudinal SRS. LMJ transport length will be split in two parts : depending on beam path, the maximum length shall not exceed 37 m under air and approximately 10 m in beam tube filled with Argon.

9.9 Final Optics Assembly

For the Final Optics Assembly (FOA), a number of different functions need to be taken into account [9.12] :

- frequency conversion
 - KDP and or KDDP crystals for Second and Third Harmonic Generation (respectively SHG and THG). The frequency converters uses a Type I-Type II third

harmonic generation scheme, consisting of a 14-mm-thick KDP doubler crystal and a 10-mm-thick DKDP tripler crystal. Frequency conversion efficiency is managed per beam through the detuning angle of both doubler and tripler KDP crystals

- beam conditioning
 - continuous phase plate [9.13, 9.14] devoted to beam smoothing/shaping and the debris shield plate. Current phase plates used for LIL activation are designed to obtain a 850 μm diameter circular focal spot at the target chamber centre [9.2, 9.15]
- focusing beams to the target chamber centre
 - lens, parabolic mirror or focusing grating
- overlapping focal spots inside bundle
 - wedge lens, prism, off axis parabola, focusing grating
- colours or harmonics separation
 - dichroic mirror, grating, prism

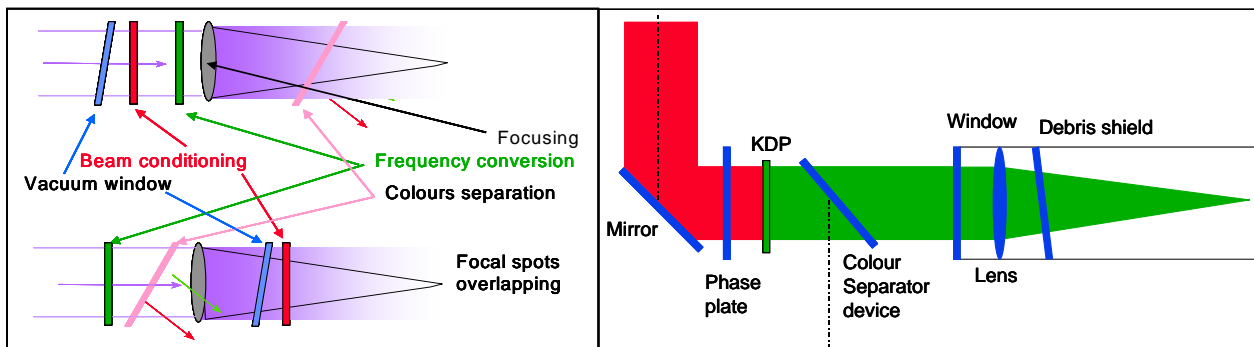


Figure 9.9 : left are basic principles of the final optics assembly : top is NIF like, bottom is LIL like. Right is an example of a 2ω configuration that can be switched to 3ω when adding a KDP for THG and replacing the Colour Separator Device.

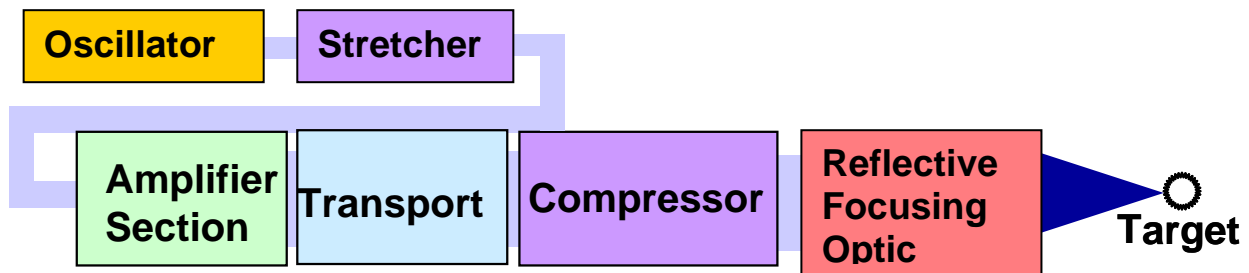
9.10 Ignition Beamlines

The plasma physics gives a required specification as shown below:

	<i>Specification</i>
<i>Energy</i>	80 kJ
<i>Wavelength</i>	1ω baseline, 2ω option
<i>Pulse length</i>	10 ps
<i>Cone angle</i>	<40 degree full angle
<i>Focal spot size</i>	40 microns FWHM (phasing tbd)
<i>Synchronisation with heating beams</i>	<50 ps
<i>Pulse contrast</i>	10^{-7}

Table 9.3. Facility specification for the ignitor beam.

Basing the Ignition beamlines on the PETAL (Petawatt Aquitaine Laser) design, the 80 kJ can be reached using 24 beam lines, each elementary beam delivering 3.35 kJ of compressed energy. This output energy allows to use a front-end identical to the PETAL front-end. The main amplifier system will be classical LIL/LMJ architecture with 16 slabs. Concerning the longitudinal chromatism, it would be certainly corrected not for temporal considerations (1.5 ps compared to the 10 ps pulse duration specification) but for spatial considerations on the focal spot.



The specification for the pulse duration is within the range of the Omega EP laser at the University of Rochester having a tunable pulselength from 1 ps to 100 ps. The 10 ps pulse is a chirped pulse, with a direct correspondence between time and spectrum profiles. The contrast ratio of 10^{-7} required a stretcher system with a spectral bandwidth of more than 16 nm to avoid repulses on the profile due to the energy on the spectral clip. This value is higher than the PETAL specification due to the highest pulse duration.

Concerning the synchronisation, the solution used on the LIL facility reaches the specification. This solution uses a master timing generator at 155.52 MHz and several splitters allowing the distributions of different signals throughout the LIL facility. With the actual technologies, a synchronisation of ± 50 ps has been demonstrated.

The phasing between the 24 beams will be very difficult to measure and so to control. This is addressed further in the next chapter. However without phasing and by considering a perfect pointing between beams, the total envelope of the focal spot can be in the $40 \mu\text{m}$ specified with speckles inside like in case of focusing with phase plate [9.10]. Then the pointing of the ignitor beam will depend on the pointing between different quads. The 24 beams are grouped in 6 quads mounted on 3 chains. The pointing specification of $50 \mu\text{m}$ is within the pointing specification for the PETAL system.

Classically, the frequency conversion at 2ω is implemented after the compression stage. This

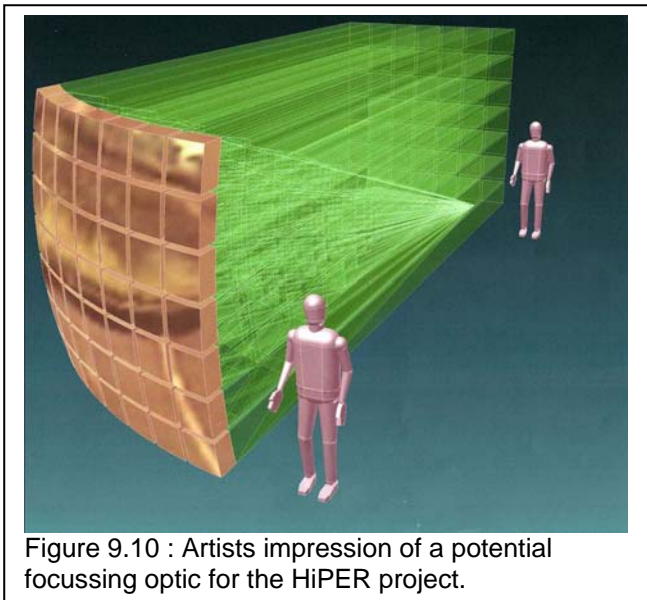


Figure 9.10 : Artists impression of a potential focussing optic for the HiPER project.

configuration allows flexibility of the facility to change the between the fundamental operating wavelength and the frequency doubled wavelength. So for the HiPER design, the frequency conversion is assumed to be after the compression stage. Again, this is addressed further in the next chapter. The pulse duration before conversion has to be increased from 10 ps to 15 ps to obtain 10 ps after conversion. The thickness of the KDP type I required is around 5 to 10 mm. The crystal has to be not too thin for fabrication considerations and not too thick for spectral bandwidth considerations. In this condition, assuming a 50% efficiency, the energy on target is 40 kJ. Taking into account the grating damage threshold evolution versus time ($\tau^{0.3}$) [9.16], the compressed

energy can be increased by a factor 2 between PETAL and HiPER to compensate the 2ω conversion losses. This increase requires more energy in the front-end and will generate more non-linear effects in the main amplifier system. However for a 10 ps pulse, these non linear effects have less impact. These two points have to be studied to confirm the final performances on target. More, damage threshold studies have to be done to confirm the performances of the mirrors and parabola for such high fluences.

Due to the short pulselength after compression the final focusing optic has to be reflective. Also the focusing arrangement would be unique due to the need for a 40 deg cone angle. It is anticipated to take advantage of developments in the Astronomical community in producing segmented primary mirrors for large aperture telescopes such as the Gran Telescopio Canarias (GTC) and the Keck Telescopes. This could yield a hybrid focusing system for the expected 24 beams.

9.11 HiPER Interaction areas

This section outlines the experimental and operational requirements for the HiPER Target Areas. This will form the basis for the detailed design and layout of the interaction chambers, target areas and support facilities and has been compiled through discussion with the user community and existing large facility staff. To enable the HiPER facility to deliver its objectives it is envisaged that up to four interaction areas will be required.

9.12 Interaction area requirements

A summary of the HiPER interaction facility requirements is given in the table below. These requirements were drawn up through discussion with scientists and engineers, looking forward on a 10-15 year timescale and looking at the scientific and operational resources necessary to deliver the project objectives. These requirements encompass initial commissioning and optimisation experiments, as well as full fusion yield experiments, materials and debris testing and scientific discovery experiments.

	Priority	CPA beam energy requirements	Long pulse energy requirements	Interaction geometry
Fusion area	1	Full	Full	Spherical
Fundamental science	1	50 kJ	Full	Cluster
Fusion materials and technology	2	1kJ @ 1 Hz	-----	Cylindrical
Diagnostics and calibration	3	10kJ	10kJ	Rectangular

Summary of HiPER interaction chamber requirements

The size of the fusion chamber, coupled to the expected facility activation from high-energy particles means that accessing the experiments on a regular basis will not be practical. As a stand-alone chamber this would significantly reduce the scientific flexibility and the ability to perform testing, diagnostic changes, replacement of parts etc. As a result, the fundamental science, fusion materials testing and diagnostics facilities have been designed to enable pre-tests of equipment and diagnostics as well as to perform key areas of research without the drawbacks of access problems to the main fusion area. A brief overview of each area is provided below:

Fusion Area: The Primary chamber for integrated fast ignition and high-yield fusion experiments with PW and kJ beamlines.

The area will operate with a spherical configuration to produce uniform irradiation, using all the implosion beams. A short pulse, high intensity beam in the form of a large cluster will be used for fast ignition studies. By reconfiguring the cluster geometry of the short pulse, it will also be possible to provide the capability for backlighting of implosions.

The area will initially operate with DD reactions, but once DT reaction studies begin, contamination will limit access to the chamber, requiring tritium clean-up procedures.

Fundamental Science Area: A 50 kJ cluster configuration for High Energy Density (HED) and high-fields physics experiments, with provision for a short pulse, high intensity beamline for use as a backlighter.

This facility will enable a broad base of science programmes (see section 5), and will also permit the study of the underlying physics of the fusion implosion without requiring the full capability of the fusion target area. It will operate in a mode where short term access will be available, unlike the main fusion chamber once DT reaction physics begins. This area enables a flexible research program for optimising and developing the implosion studies simultaneously to the main fusion program. Cluster geometry will achieve multi-GBars pressure drives to simulate compressed states of matter found in both ICF and laboratory astrophysics experiments. A two cluster configuration (in opposing geometry) will be required to create HED conditions with the flexibility of shaped drive experiments to explore the complex interplay between radiation and hydrodynamic transport in astrophysical objects.

Fusion Materials and Technology Facility: A high average power (1 kJ 10 Hz, or 10 kJ, 1 Hz) facility specifically for testing materials and damage issues relevant to fusion experiments.

This facility will enable the study of materials under the extreme conditions of the facility, such as structural changes, activation and radiation damage from high-energy particle bombardment, relevant for the long-term fusion program. See Section 12 and Appendix 1 for background information.

Diagnostics and Calibration facility: Coupled to the high average power beamline, as above. A specific facility designed for diagnostic commissioning and development. Mainly devoted to the preparation of large diagnostics, target injectors and manipulator systems. This facility will be used for pre-testing of all diagnostics moving into the main fusion and science facilities.

One option for this beamline is to build it remotely from the main HiPER facility, perhaps coupled to an ancillary source (e.g. an accelerator) to enable a broad science mission based on this beamline, whilst still meeting the diagnostic development requirements of HiPER.

9.13 HiPER Operational systems

Target transfer and loading capability: Cryogenic target handling capability will be required for the Fusion and fundamental science interaction areas. This will be based on the technology used for LMJ but modified to operate along a vertical axis. Specifically, the target positioner will be mounted on a port at the top of the chamber and the shroud retractor mounted on an opposing port in the base of the chamber. The system is being designed by CEA and is detailed in section 11 and Appendix 2.

Non cryogenic targets for all interaction areas will have dedicated target insertion and manipulation devices based around a load lock system. For the case of multiple targets standardised containers holding multiple target arrays will be attached to the interaction chamber via the load lock.

Radiation load-lock (as appropriate for each facility), transport systems and chamber loading will be handled separately for cryo and non cryo-targets, utilising robotic systems and fully automated transport mechanisms.

Diagnostic handling and installation hardware: The fusion facility will operate in a long term fixed mode, hence diagnostics installation will be through access periods after activation decay has

taken place. The science, fusion materials research and diagnostics facilities will all have the provision for “fast access” in order to change diagnostics when beginning new research programs.

Blast shield handling facility: Blast shields for all areas will require careful handling, cleaning and optical inspection facilities, requiring cleanroom conditions and incorporating interferometric and microscopic inspection facilities. Blast shields will be required for at least the fusion and science experimental areas, requiring storage of stocks and processing of removed shields for contamination control.

Blast shield automated installation robot: Automated insertion systems for the replacement of blast shields is required to counter the restrictions on post shot access due to facility activation. Local replacement units, facilitated by a larger scale radiation load-lock system are considered. Blast shield lifetime data will be known from NIF and LMJ operational experience.

Short pulse beamline parabola & debris protection: Current designs around optical re-imaging through secondary optics are being followed to reduce damage effects on the parabola. Blast shield systems similar in design to the long pulse beamlines are also considered, using the characterization facilities to ensure both reliable and high optical quality of blast shields. Compatibility with standard blast shield installation is required to be maintained.

Standardisation of interface and control system: All areas will operate with compatible control systems to ensure all areas can operate effectively with the overall control system. Standardisation of interfaces for all systems, including both target area facilities and diagnostics is required to ensure backup systems are available. Test facilities will be provided for software/hardware interface testing off-line, ready for staging in the diagnostics and calibration facility. Optical communication systems are to be employed to minimise EMP and radiation effects.

Triggers: Highly synchronised cascaded trigger systems will be employed for accurate triggering of both equipment and diagnostic probes. Optical trigger systems will be used in order to reduce EMP effects on control and diagnostic systems.



Integrated master control room in operation at the National Ignition Facility.

9.14 HiPER Ancillary Systems:

Control facilities: The fusion and fundamental science areas will operate from a central control space, operating with dedicated diagnostics stations for each experimental area. Materials testing and diagnostics areas will be operated from a separate control space. A master control room will supervise all shot operations and route beam delivery to the appropriate target areas. This master control room will have access to all power conditioning, diagnostics acquisition and triggering systems. It is envisioned that a control room of this type will be comparable to the one already in place for other fusion-class scale laser systems. A picture of the control room at the National Ignition Facility is shown in the above figure.

Facility Conditions: The facilities will all operate with appropriate cleanroom conditions, with both temperature and humidity stabilisation. Structural controls to limit vibration will also be employed, separating the facility structure from the beamline structures.

Vacuum and Tritium recovery system: Operational methods from NIF, LMJ and Omega will be put into practice, following appropriate safety legislation and protective systems. Links with Tokamak MFE systems and pulsed neutron sources operating with tritium recovery systems will be established, and best practise will be incorporated. The fusion facility is not expected to have personnel access on a regular basis and will operate under full vacuum as far as possible. Safety interlock systems will be incorporated on all facilities and dry air let-up where nitrogen systems will restrict entry times.

Data manipulation: Central storage and data access will be required throughout the facility, utilising new e-science protocols for data manipulation and analysis. A central portal for all remote data access will be provided. Communication systems will employ fibre-optic techniques for EMP suppression.

Shielding: Personnel protection shielding is addressed in another section. Shielding for high-sensitivity detectors will be required, requiring the use of localised protective systems to eliminate specific gamma, electron, neutron and EMP interference with diagnostics and control equipment. Radiological handling facilities: Robotic systems for the safe extraction of active components is required, along with air-lock systems for extraction from the chambers without breaking vacuum. This process will speed up access possibilities into the main chambers whilst protecting workers from active components. Radiation lock-load systems may be required, with appropriate transport systems for extraction from the experimental areas.

Radiological storage areas: Storage of activated materials from neutron, gamma and proton activation (as well as active debris coating) will be required, both for diagnostics purposes as well as for personnel safety. Storage facilities will also use standard analysis systems to monitor the extracted materials during their decay. Storage facilities will be located locally to the areas to minimise exposure probabilities.

Diagnostic storage: The fusion and fundamental science areas will operate with an array of permanent diagnostics, however the other areas will make use of a selection of diagnostics that can be tailored to the exact measurements being performed. Diagnostics not in use, as well as operational spares for Fusion and science diagnostics will be stores locally.

9.15 Key HiPER Diagnostics

Diagnostics will be essential to understand all the phases of a HiPER driven advanced fast ignition interaction, namely implosion and mixing, Fast Ignition beam generation and propagation and energy deposition and burn. The diagnostics and techniques can be divided into three categories:-

PROBING

- X-ray & 4ω Thomson scatter, X-ray diffraction, VISAR, white light reflectivity advanced optical, XRL / HHG probing, interferometry, shock transit, electron deposition/scattering, time-resolved proton imaging, Raman, Absorption spectroscopy

PARTICLE EMISSION

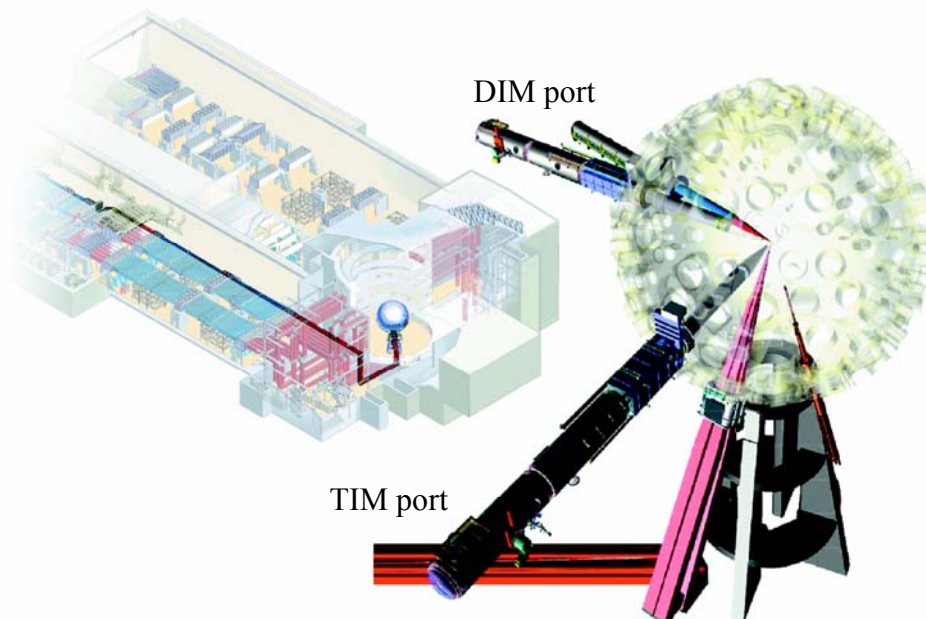
- electron spectral & angular distribution, ion emission and imaging, neutron spectroscopy - neutron imaging, nuclear activation, debris capture,

PHOTON EMISSION

- high energy x-ray imaging & emission spectroscopy, penumbral imaging, k-alpha imaging (conventional & single photon techniques), nuclear diagnostics, ultra fast x-ray streak camera, detector developments, XUV pyrometry, very low-T pyrometry,

This section summarises the current state of the art for diagnostics in these categories and the route to delivering the necessary hardware to ensure that the HiPER facility achieves its objectives.

All movable diagnostics will be inserted via a Diagnostic Injection Manipulator (DIM) analogous to the one already implemented at the NIF and LMJ. The Fusion and fundamental science areas will have approximately 20 DIM ports available for diagnostics and flexible configurations. The other two areas require approximately 5 DIM systems for diagnostics testing purposes. It is expected that any DIM port can be reconfigured as target injection manipulator (TIM) as required by the particular experimental configuration. An example of DIM plus TIM setup for the National Ignition Facility is shown in the figure below. In addition to movable diagnostics, a set of fixed diagnostics will be available for HiPER. These detectors will include alignment cameras, time-of-flight diagnostics for neutrons and x-ray/gamma rays, and static x-ray imagers (e.g., pinhole cameras).



Example of diagnostics injection (DIM) and target handling (TIM) at the NIF.

	CPA beam energy requirements	Long pulse energy requirements	Target areas	Diagnostics ports
Alignment cameras	N/A	N/A	all	Fixed (on 3 different ports)
Laser backscatter	1 beam	Full, with full aperture access on 1 beam	Fusion Science Mat.	Fixed (1 port)
Gated x-ray imager	1 beam	Full	Fusion Science	1 DIM
Proton probing	2 beams	Full	Fusion Science	2 DIM's
X-ray radiography	2 beams	Full	Fusion Science	1 DIM
X-ray imaging	1 beam	Full	Fusion Science Mat.	1 DIM (plus fixed x-ray pinhole cameras)
X-ray scattering/diffraction	2 beams	Full	Fusion Science	2 DIM's
Advanced optical probing	1 beam & low energy probe	Full	Science	1 DIM
Nuclear and gamma ray detectors	1 beam	Full, 10kJ	Fusion Science Mat.	Fixed (1 or more ports)
Neutron time-of-flight Detectors	1 beam	Full, 10kJ	Fusion Science Mat.	Fixed (1 or more ports)
Electron detectors (spectrometer, FFLEX)	1 beam	Full, 10kJ	Fusion Science Mat.	Fixed (1 port)
Ultrafast time-resolved x-ray emission (Streak and framing cameras)	1 beam	Full, 10kJ	Fusion Science Mat.	1 DIM

Summary of HiPER diagnostics preparation requirements.

These diagnostics are under continuous development through existing research programs to improve resolution and temporal capabilities as well as dynamic range. Probing systems are under development to probe even higher density matter through many of the various techniques described below. These key areas of diagnostics developments are taking place through collaborations between many of the large research groups throughout the EU, as well as in partnership with international groups.

Probing

Proton probing [9.17]

Density detection via proton imaging will be essential for dynamical probing of shocked and compressed material, e.g. in integrated fast ignition (FI) experiments. This is a complementary approach to hard x-ray radiography for the characterisation of the presence of non-uniformities during the early stages of the implosion of a capsule. The diagnosis of compressed cores is more challenging due to resolution degradation caused by multiple scattering. Probing through densities of FI/ICF interest requires proton energies in excess of 100 MeV, above current capabilities, but well within sight of current developments. Such energies will also allow density diagnosis of planar shocks in solid targets of moderate thickness.

A related area of application is the investigation of proton stopping in plasmas, via the observation of spectral modification of the transmitted beam, also of crucial importance for applications such as proton FI.

Field detection via the diagnosis of proton deflection is probably the most important application of proton probing.

X-Ray Radiography [9.18]

This is one of the primary diagnostics techniques for implosion symmetry and density measurements under both ICF and HED conditions. It requires multi-kJ short-pulse backlighter beams to produce high energy x-rays to radiograph the relevant dense plasma states. This technique also links to the k-alpha imaging discussed later in this section.

X-ray scattering [9.19] and Diffraction [9.20]

X-ray scattering is an accurate diagnostics of electron temperature and electron density in laser plasmas. As the photons produced by the resonant line of a secondary plasma are Thomson/Compton scattered through the high density sample, they are also dispersed in energy by the Doppler effect. The technique allows the direct measurement of the electron velocity distribution function in a high density medium. This method is directly scalable to measurements of temperature in matter at extreme densities and pressure, such as those achieved in the implosion. The development of efficient multi-keV x-ray sources is a necessary step as a penetrating radiation probe is required for scattering off the imploding core. This requires multi-kJ picosecond laser pulses. As the core compresses, matter undergoes a transition to a Fermi degenerate system. Since x-ray scattering directly probes the electron distribution function, the interpretation of the data is simplified. We envision x-ray scattering as a core diagnostics for implosion dynamics as well as shock timing and compression, which is of direct relevance for the success of inertial confinement fusion. X-ray diffraction is complementary to x-ray scattering as it allows to resolve changes in the structural properties of dense plasmas. In these experiments, the elastically (Bragg) scattered x-rays will be observed over a range of angles to deduce changes in the separation and internal arrangements of the ions.

Advanced Optical Probing [9.21]

Optical probing is a robust and unique diagnostic technique for the characterization of underdense plasmas and the study of propagation of intense pulses in plasmas. Primary techniques for the extraction of plasma density and gradient profiles will be shadowgraphy and interferometry. The use of an ultra-short optical pulse as a probe pulse can provide information with unprecedented temporal and spatial resolution.

The implementation of probing techniques based on high order harmonics provides a significant opportunity of probing higher densities with unprecedented temporal resolution.

Particle Emission

Nuclear diagnostics [9.22]

Nuclear activation provides a primary diagnostic of fast particles and radiation with energy sensitivity in the range of interest for HiPER. This type of nuclear diagnostic is completely insensitive to particles of low energy; selection of specific reactions removes potential ambiguity in particle identification; and there is considerable flexibility in the size and shape of the activation sample.

Nuclear diagnostics can be used to measure energy and angular distributions and total yield, and can be applied to measure many of the properties of inertial fusion and fast ignition processes, including nuclear yield, electron and ion temperatures and potentially implosion/burn history. Diagnosis of the dense core of an ignited pellet is possible due to the highly penetrating nature of neutrons, gamma rays and high energy protons produced. Nuclear diagnostics can be used to directly measure fusion reaction products, making it particularly valuable at determining the overall effectiveness of a target design and enables tuning of experimental parameters related to the fusion plasma conditions. Nuclear diagnostics can also play an important role in many of the non-fusion based science programmes on HiPER, for example charged particle acceleration.

A set of core nuclear activation diagnostics based on known techniques, already successfully used on existing large lasers, will be designed for specific routine deployment on HiPER. This involves the choice of appropriate samples and activation reactions with well-known cross sections which can be used to accurately obtain spectral, spatial and yield measurements of neutrons, ions and gamma radiation over a wide dynamic range. Absolute yields of reaction products can be determined using these techniques. Typically the activated sample is removed from the target area and the radioactivity is measured off-line using gamma-ray spectroscopy techniques. Significant developmental work would be required to enable “in-situ” detection techniques in noisy plasma environments using radiation hardened detectors.

Radiochemistry diagnosis of neutron activated ablation material (or radiochemical tracers) should also be employed and collection and analysis of activated gases and debris will also be a useful diagnostic technique.

The second approach involves the design of a number of innovative nuclear diagnostic techniques to measure specific parameters of the fusion and fast ignition processes, and to address specific requirements for the science programme. Examples may include the development of gamma detection systems for fusion reaction history measurements, application of nuclear diagnostics of charged particles to enable the measurement of yield from neutronless reactions (such as D-3He) and techniques for combined imaging and spectral measurements of fast neutrons. Both the fusion and the non-fusion science programmes on HiPER will also drive the development of nuclear

diagnostic capability to higher energy and density systems. Higher nuclear yields are expected and it should be possible to observe lower cross section and higher threshold energy reactions.

Electron diagnostics [9.23]

In Fast Ignition, the required electron beam is characterized by a small divergence, high flux and an average energy of multi MeV. The electron diagnostic necessary for this purpose will be able to give information about spectrum with angular distribution principally in the region of electron energy up to some tens of MeV. The capability to detect the presence of high energy electrons will be useful. It is also necessary that this detector be able to work with a total electron energy of several Kilo-joules, without damaging. A simple magnetically based dispersive instrument will be adequate for characterizing any electrons escaping the interaction region. To characterize electrons within the interaction will require combining a number of techniques including k-alpha imaging, excitation spectroscopy and tracer layer techniques to fully characterize the transport of electrons. This will require ongoing development and testing in conditions to ensure that the final diagnostic is able to work properly in the field of ICF.

Neutron time-of-flight spectrometer [9.24]

For Inertial fusion, plasma collective motion effects affect the energy of emitted neutrons by a significant Doppler shift. The measurement of neutron spectrum allows studies of ion velocity distribution. A multi-channel neutron time-of-flight spectrometer (N_TOF_S) will be designed and developed in order to measure fuel ion temperatures and secondary neutron spectra results from interactions and surrounding materials.

The proposed work will be based on simulation and preliminary experimental tests for the development of a new neutron time-of-flight spectrometer optimised for high fluxes. This will include numerical methods to simulate resulting neutron emission spectra from the perturbed velocity distributions as predictions and comparison with experimental measurements performed using actual laser facilities. Detection of neutrons requires scattering resulting from organic scintillators, in which recoil protons can be produced and detected providing sufficient information for measurement of the neutron spectrum. For the N_TOF_S design phase neutron transport calculations were used to quantify the relative importance of different parameters such as thickness, response function, dimension and shape of the scintillators. Moreover, Monte-Carlo calculations, in the design phase, are necessary in order to avoid effects such as neutron multiple scattering in the scintillators themselves as well as from surrounding material and protection walls. To perform accurate neutron spectroscopy of the fusion plasma, neutrons will be selected by a collimator, which will create a beam of neutrons and define the spectrometer's line-of-sight. The multi-channel N_TOF_S will be composed by a series of detectors consisting of individual, commercially manufactured, PMT- scintillator units in a predefined 3-dimensional arrangement at a relatively large distance (higher than 20 meters) from the interaction chamber. The design and development phase required laboratory tests of the individual scintillation detectors of the multi-channel N_TOF_S including development of software for control and electronics to acquire data.

Photon Emission

Ultra fast streak camera [9.25]

The understanding of the time evolution of short-pulse laser-plasmas encompasses the possibility of directly measuring the local electron and charge particles transport on time scale comparable with the laser pulse length. On the other hand, the current streak camera technology is only able to achieve time resolution in the order of 1 ps with very modest dynamic range. New streak camera technologies have been recently proposed and their implementation into the HiPER project may be relevant. These will allow sub-picosecond time resolution at high sensitivity and dynamic range.

The possibility of time resolved measurements will indeed permit a more direct validation of predictive capabilities of currently available and newly proposed simulation tools.

Crystal Spectroscopy [9.26]

The propagation of fast electrons is a fundamental issue in fast ignition. The most effective way to unfold the dynamics of electron propagation is the detection and imaging of x-ray emission from inner shell transition that are stimulated by the passage of the high energy electrons. Inner shell detection systems will be primarily based around spherically bent crystals as well as high reflectivity mosaic crystals, both imaging and spectrally resolving plasma emission from target and tracer layers on a range of detectors from Image Plates or CCD's to single photon techniques and gated imaging. There is a growing expertise in Europe aimed at developing advanced imaging techniques in this field through collaborations between within existing European frameworks (LASERLAB) and collaboration with leading detector manufacturing companies.

9.16 Conclusions for the facility design

The laser specification laid down by the plasma physics community for the HiPER laser system to achieve an inertial confinement fusion gain of the order of 50-100 can be brought about by adapting much of the laser technology developed throughout the world over the last 10 years. There is a clear low-risk solution which would meet the baseline requirements.

Exploration of more advanced laser options, offering significantly enhanced capability will be considered in the next section.

The HiPER experimental areas have been designed to provide an operational balance that allows a simultaneous fusion programme and a robust basic science programme. This requires two main target areas as part of the baseline design. Analysis of the long-term fusion materials and technology issues would benefit from an additional dedicated area, as would the diagnostic development. The cost-benefit analysis for these latter two areas will be performed over the next period.

A comprehensive suite of diagnostics will be required for HiPER. These will require a focused programme of development on the various European and international laser facilities over the next decade.

The design and scientific mission of HiPER will be unique, but much can be learned from the experience in existing and emerging systems, particularly OMEGA, NIF (USA), FIREX (Japan), LMJ (France) and the network of smaller scale facilities across Europe.

References for Chapter 9:

- [1] J. Zuegel, S. Borneis, C. Barty, B. Le Garrec, C. Danson, N. Miyanaga, P. Rambo, C. Leblanc, T. Kessler, A. Schmid, L. Waxer, J. Kelly, B. Kruschwitz, R. Jungquist, E. Moses, J. Britten, I. Jovanovic, J. Dawson, B. Blanchot : "Laser challenges for fast ignition", Fusion Science and Technology, 49, April 2006, pp 453-482
- [2] J.M. Di-Nicola et al. "The LIL facility quadruplet commissioning", IFSA 2005, Biarritz, 4-9/9/05, J. Phys. IV France 133 (2006) 595-600
- [3] C. Haynam et al. « The national ignition facility performance status », IFSA 2005, Biarritz, 4-9/9/05, J. Phys. IV France 133 (2006) 575-585
- [4] C. Barker and R. Sacks, SPIE 2633 (1995) 501-505

- [5] Adaptool, RTD project of the 5th Framework Plan HPRI-CT-1999-50012 (<http://improving-ari-fp5.jrc.it/access>)
- [6] H. Ward et al. « Computation of thermally distorted wavefronts in high power lasers : comparison with LIL experiments », IFSA 2005, Biarritz, 4-9/9/05, J. Phys. IV France 133 (2006) 687-689
- [7] A. Jolly et al., « Front-end sources of the LIL-LMJ fusion lasers : progress report and prospects », Opt. Eng. 42(5) 1427-1438 (May 2003)[8] J. Gardelle et al., « A New Regime of Plasma-Electrode-Pockels Cell Operation for the Laser MegaJoule Project », p.510, IFSA01, Elsevier.
- [9] E. Bordenave and T. Chies : “ Numerical simulations of SRS in LIL transport section with Miro propagation code and comparison with ENOLT diagnostic results”, IFSA 2005, Biarritz, 4-9/9/05, J. Phys. IV France 133 (2006) 661-663
- [10] G. Herring et al. Opt. Letters 11 (1986) 348
- [11] O. Morice et al., “Laser Pulse Propagation Calculations using Miró software”, p.717, IFSA99, Elsevier. & O. Morice : “Miró : complete modelling and software for pulse amplification in high power laser systems”, Optical Engineering, 42, n°6,1530, (2003).
- [12] A. Boscheron et al., « Final Optic Assembly Design for the Laser MegaJoule », p.536, IFSA01, Elsevier & A. Boscheron et al., “Laser Diagnostic Setup for The LIL Start-up and Qualification”, p.863, IFSA01, Elsevier.
- [13] J. Néauport et al., « Large Continuous Phase Plate Design, Manufacturing and Control », p.514, IFSA01, Elsevier.
- [14] L. Videau et al., “Which smooting technique for the LMJ project”, p.660, IFSA99, Elsevier.
- [15] B. Le Garrec et al. “Métrologie des faisceaux et de la tache focale de la LIL” , UVX2006, Colleville/mer, 6-9/6/06, J. Phys. IV France 138 (2006) 297-307
- [16] I. Jovanic, C. G. Brown, B. C. Stuart, W. A. Molander, N. D. Nielsen, B. F. Wattellier, J. A. Britten, D. M. Pennington, C. P. Barty, “Precision damage tests of multilayer dielectric grating for high energy PW lasers”, Laser induced damage in optical materials, Proc. SPIE vol 5647, 34-39 (2004).
- [17] M. Borghesi *et al.*, Phys. Plasmas 9, 2214 (2002); C.K. Li *et al.*, Phys. Rev. Lett. 97, 135003 (2006); C.K. Li *et al.*, Rev. Sci. Instrum. 77, 10E725 (2006)
- [18] H.-S. Park *et al.*, Rev. Sci. Instr. 75, 4048 (2004)
- [19] D. Riley *et al.*, Phys. Rev. Lett. 84, 1704 (2000); S.H. Glenzer *et al.*, Phys. Rev. Lett. 90, 175002 (2003)
- [20] D.H. Kalantar *et al.*, Phys. Rev. Lett. 95, 075502 (2005)
- [21] A. Rundquist *et al.*, Science 280, 1412 (1998)
- [22] TJ Murphy, *et al.*, Rev. Sci. Instr. 72 , 773-779 (2001)
- [23] Glinec *et al.*, Rev. Sci. Instrum. 77, 103301 (2006)
- [24] T. J. Murphy, *et al.*, Rev. Sci. Instr. 72, 850-853 (2001)
- [25] P. Janimaagi, Proc. SPIE 5194, 171 (2003)
- [26] P.K. Patel *et al.*, Plasma Phys. Controlled Fusion 47, B833 (2005); G. Gregori *et al.*, Contrib. Plasma Phys. 45, 284 (2005)

10 Laser Development Options

10.1 Ignition Beam Compression Options

The HiPER Ignition Beam delivered from the main laser amplifier system will necessarily comprise of up to 24 sub apertures. Temporal compression of these beams in a compact and flexible geometry will be an important consideration. Conventionally, as exemplified by the Nova or Vulcan PW lasers, compression has been achieved with two gratings in a vacuum chamber approximately 12 meters in length. HiPER will require even longer stretched pulse durations in order to efficiently extract the energy stored in the amplifier system. Scaling this approach will therefore not be possible as such an approach would require grating separations of approximately 30 meters and a vacuum chamber that would be very difficult to accommodate in a multi beam target area. Current work on existing systems around the world has led recently to the development of new, compact, high-dispersion compressor designs [1]. Recently a novel mixed-grating, compact compressor design was proposed by LLNL that uses Multi-layer Di-electric (MLD) gratings and produces three times the dispersion of the Nova PW compressor while occupying a length of less than 5 meters (see figure 10.1). Compactness is achieved by using two sets of different groove density gratings for the compressor. The first set uses gratings with 1750 l/mm and produces a spatially chirped output and half of the compression. The second set has a slightly higher dispersion per meter of separation, accomplishes the remaining pulse compression and removes the spatial beam chirp. Since the grating sets have different separations, it is possible to produce an output beam that is parallel to the input beam but offset by a fixed amount. This allows the gratings to be placed in close proximity to one another and greatly reduces the overall footprint of the compressor arrangement. An evolution of such an approach would be required for HiEPR, optimally configured as per the requirements and constraints of the overall design.

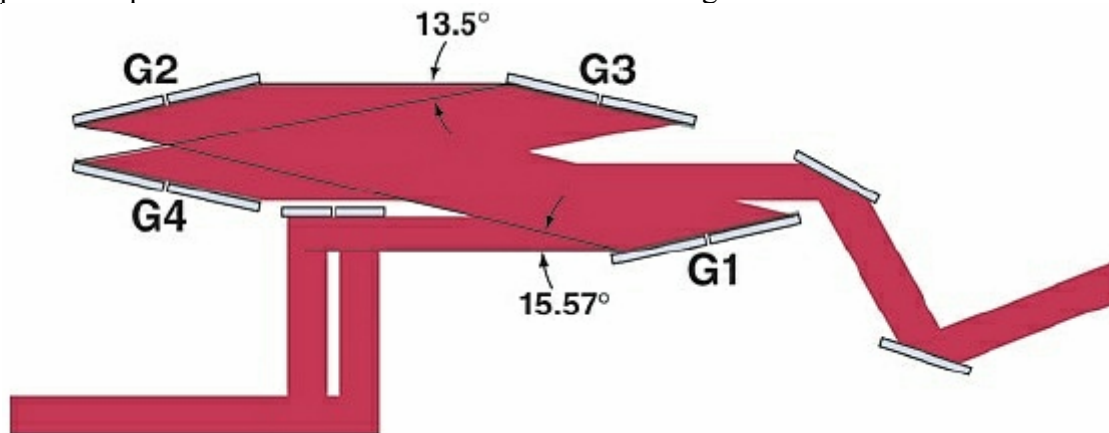


Figure 10.1 Compact mixed grating pulse compressor

To meet the requirements of fast ignition, HiPER will need to generate pulses of $\sim 70\text{kJ}$ in $\sim 10\text{ ps}$. This represents a major technological challenge for the final grating of the pulse compressor and any optics experiencing the high peak power of the compressed pulse. Scaling of gold coated gratings, which have a short-pulse laser damage threshold of $0.25 - 0.3\text{ J/cm}^2$ on the grating surface, is impractical because even 30kJ would require a 12 m^2 aperture which is well beyond the state of the art. The most promising grating technology to withstand the compressed pulse energy for fast ignition lasers is a holographically formed grating fabricated on a multi-layer dielectric (MLD) coating to form a highly efficient reflection grating[2]. Laboratories around the world have combined together to increase the damage thresholds of these gratings with remarkable success. The highest reported damage thresholds at 10 ps pulse length are already around 2.7 J/cm^2 on the grating surface - nearly ten times higher than that of gold coated gratings. The world largest MLD gratings are currently $80 \times 40 \times 10\text{ cm}$ in size and are manufactured at LLNL (figure. 10.21). The limitation with this aperture size arises from the scale of the optics required to produce the holographic Interference pattern (see figure 10.2b). Recently, an alternative approach to the

manufacture of large aperture MLD gratings that uses a scanning technique to holographically write the grating pattern has been developed in the USA by the Plymouth Grating Laboratory (PGL). This technique sees a interference pattern generated in a small 1mm diameter beam. The MLD substrate is then scanned in a raster pattern fashion in this writing beam, with sophisticated control loops ensuring high fidelity and stability of the writing. In principle, this technique is easily scaleable to large aperture and already large (91cm x 50cm) gratings have been manufactured using this technique for the FIREX system at the Institute of Laser Engineering (ILE), Osaka Japan

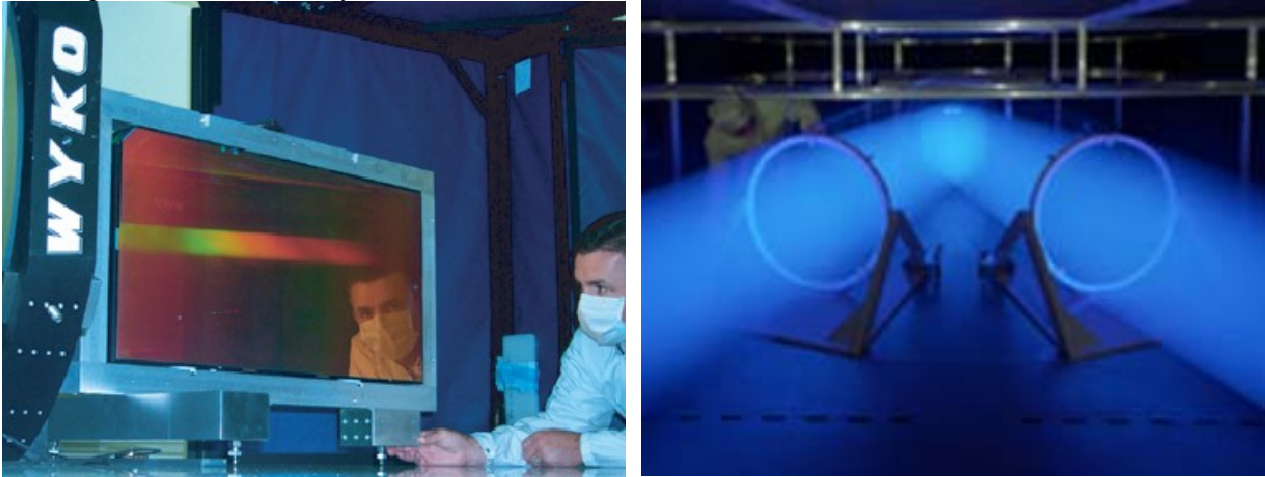


Figure 10.2: (a) (left) The world's first 80 cm scale, optical quality MLD grating fabricated at LLNL and (b) (right) The 1m diameter holographic writing facility used to make it

Filling the full aperture of a 91 x 50 cm grating having a LDT of 2.7 J/cm^2 would yield a maximum energy of 7 kJ at 10 ps, with a safety factor of 1.8 below the damage threshold. Further scaling the available aperture is clearly an area of development that HiPER would need to explore further to ensure the largest possible single grating surfaces are available

10.2 Coherently Locking the Ignition Beam sub apertures

The ignition beam necessarily is generated in a number of sub apertures. Irrespective of the number and maximum size of these sub apertures (gratings) used to form the ignition beam, the question of whether they can interact with the target in an independent manner arises. This is one of the crucial questions that will be addressed in the next few years as part of the experimental programme. It is however, quite possible and even likely, that to ensure efficient coupling of the ignition beam to electrons it will be necessary to have some degree of spatial and temporal coherence between the sub apertures that form the ignition beam. Techniques will therefore need to be developed to enable this. In recent years there has been much work in the related area of grating tiling. Grating tiling is the idea of coherently coupling multiple gratings together such that they appear to function as a single large grating [3]. For each of the gratings within the compressor, $N \times M$ sub-aperture gratings can be adjacently mounted to form a larger tiled grating [4]. When aligned they will act as a monolithic optical element. For example, the four-grating compressor shown in Fig. 10.3 is being developed for OMEGA-EP with each tiled grating containing three sub-aperture gratings. Simplistically, the aperture and therefore the maximum energy capacity, of a tiled-grating compressor (TGC) is increased by a factor of $N \times M$ over that of compressors limited to a single grating aperture.

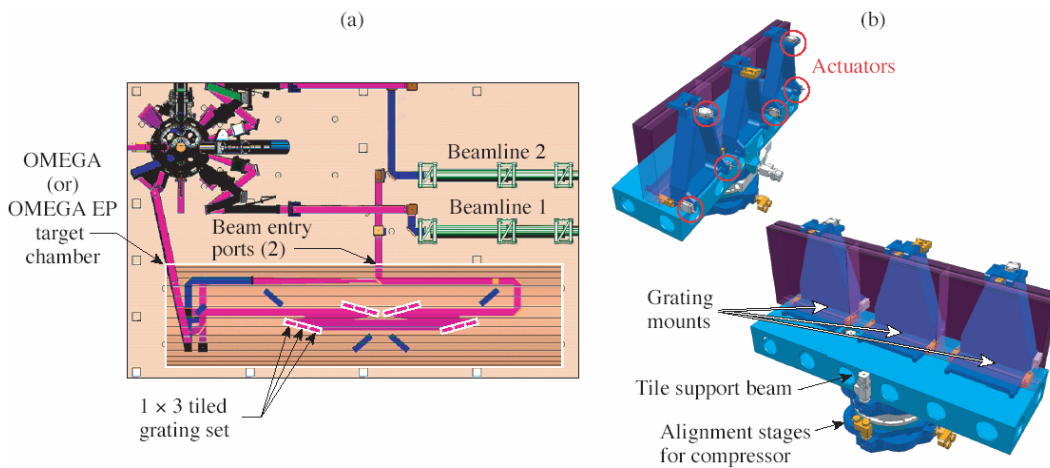


Figure 10.3: OMEGA-EP compressor design with four tiled-grating assemblies (TGA's) composed of three gratings in each TGA. (a) Individual mounts in the TGA coherently align the grating tiles, while alignment stages control the entire assembly, (b) Assembly drawings of the grating mounts

Accurate control of the position and orientation of the grooves of each grating presents a significantly greater challenge than that associated with mirror arrays. Generally, there are six degrees of freedom between any two gratings that affect the optical performance of a tiled-grating system; however, a reduction of degrees of freedom to three adjustments per tile can be realized through pairing of compensating parameters. LLE Rochester has developed a far-field-based approach that makes grating tiling practical [5]. A precise grating tiling was successfully demonstrated by LLE by compressing a Fourier transform-limited, 650-fs, CPA laser pulse using one set of tiled gratings.

HiPER will need to significantly build on this approach as the number of sub-apertures is significantly higher and determine the most appropriate techniques to coherently spatially and temporally lock these together. Although this appears to be a daunting task it is similar challenge to the well established scheme deployed by the astronomy community to construct very large telescopes using an array of mirrors [6]. For example, the Gran Telescopio Canarias (GTC) is nearing completion in La Palma, Canary Isles. It is the most advanced segmented mirror telescope project in the world. It has a 10.4m primary mirror telescope working in the near infrared region of the spectrum (2.2-4.8 μm). The primary mirror is constructed from 36 mirror segments which are regular hexagons of side size 936 mm (figure 10.4). These are mounted on an active frame having sensors accurate to 'within nanometers'. With a primary focal length of 16.5 m this gives the GTC primary optic an f-number of 1.6, which is far faster than expected f-number requirements for the IFE laser. The scale of it however is comparable to the likely requirements for HiPER and the technological solutions will therefore be applicable.

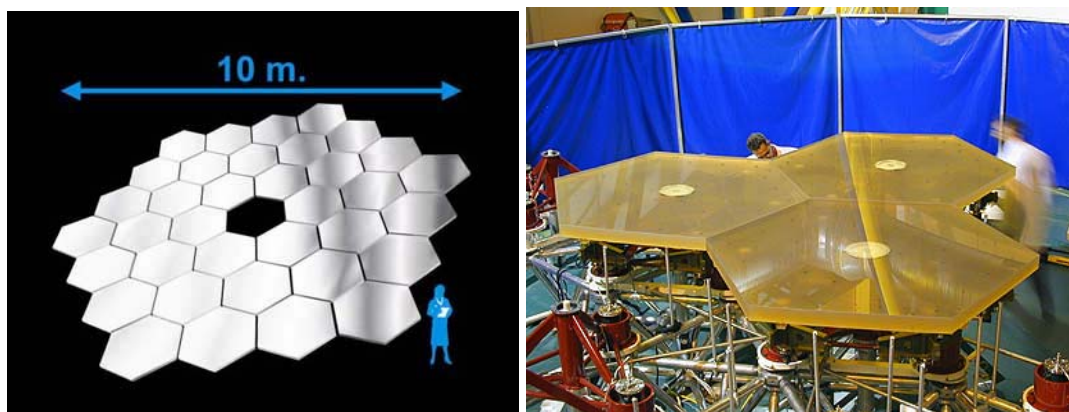


Figure 10.4 GTC primary mirror layout, and completed GTC mirror segments

10.3 Second Harmonic Ignition Beam Options

The possible requirement to operate the ignitor beam at its 2nd harmonic will provide a considerable challenge. Usually, the provision of harmonics is straightforward through frequency doubling and tripling crystals placed at the end of the laser chain, as is the case for example, in the compression beams of HiPER. Converting the ignition beam to its harmonics however presents a considerable challenge given the very short pulse duration of ~10 ps. Ideally, one would follow the same approach as for the compression beams but the demanding requirement for mm thin, large aperture crystals to do so is a substantial technical challenge that would need to be addressed. A second option could be to convert the beam to its second harmonic before compression and thus whilst it is still “long”. Whilst this enables existing crystal technology to be used, it introduces the requirement to use compression gratings that will now operate at this harmonic wavelength. To date, these do not exist in an efficient and high damage threshold form. However, with the advent of dielectric gratings, it could be possible to design and manufacture a grating that could be made to operate at 2ω or 3ω . It is clear therefore that development work will be required to determine the most appropriate route if indeed the requirement to operate the ignition beam at its second harmonic materialises.

10.4 OPCPA Options

In designing a large scale science facility it is particularly important to pay attention to potential future developments to ensure that an internationally competitive capability can be maintained throughout the life of the facility. There exists an exciting potential upgrade path for HiPER which would provide access to extreme pulse powers and intensities. The possibility exists for single pulse powers well in excess of 1 Exawatt (EW, 10^{18} W) by combining multiple long pulse beam lines into a single ultra-short pulse. This would be achieved through the implementation of a revolutionary technique on the system known as *Optical Parametric Chirped Pulse Amplification* (OPCPA) [7,8].

Pulse powers at the EW level are some three orders of magnitude greater than the highest laser power produced to date, and would be two orders of magnitude in excess of any other planned laser system. These unprecedented powers, when focussed, would generate sufficiently high optical intensities to open up completely new and unexplored areas of fundamental physics [9].

The OPCPA technique (see Figure 10.5) takes advantage of one or more high energy beam lines operating in a long pulse mode (kilojoules in nanoseconds in either the 2nd or 3rd harmonic) to “pump” an *optical parametric amplifier* (OPA). The OPA is a non-linear optical crystal of the same type used for frequency doubling and tripling described earlier. Synchronously with this pump, a low energy, chirped, broadband “seed” pulse of comparable duration is also injected into the OPA and the crystal conditions arranged such that parametric gain occurs. This process can be repeated in a serial manner with multiple OPA’s and multiple pump beams. Consequently energy is transferred from the pump system to the seed pulse thereby producing a very high energy, ultra-broad band output pulse that can be compressed in the conventional manner. In this way it is possible to harness the very high energies produced by the narrowband Nd:glass system in a broadband, extremely short duration pulse, typically tens of femtoseconds.

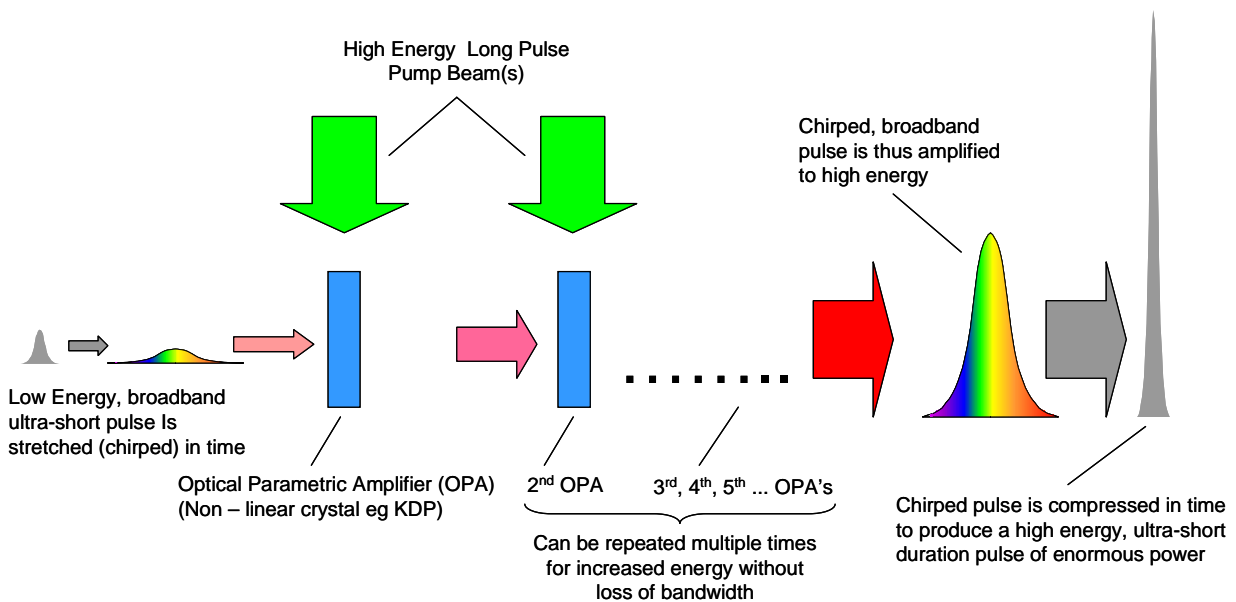


Figure 10.5: Schematic of an OPCPA scheme. Narrowband high energy pump beams are used to amplify a low energy broad band seed beam in a series of non-linear crystals. In this way it is possible to produce an output pulse that has both high energy and short duration i.e. very large power

The OPCPA process has a number of highly desirable properties that include:

- Very large, directional gains using very little material
- Extremely broadband amplification bandwidth
- High efficiency
- Excellent spatial and temporal beam quality
- Scalability
- Variability of pump & seed wavelengths through choice of crystals and geometry

The only crystal material however that is available at large aperture is KDP and its deuterated isomorph (KD*P). However, it transpires that these particular crystals, which are also used for the frequency doubling and tripling process for the long pulse beams are also extremely well suited as parametric amplifiers in an OPCPA scheme pumped by the harmonics of an Nd:glass system. A number of theoretical [10] and experimental studies [11] of this technique have been conducted over recent years, principally using the VULCAN laser at RAL. These studies have concentrated on demonstrating the potential of the technique at increasingly large apertures and power and have been very successful. For example, the most recent experiments [12] conducted at RAL have seen the production of a 35J, 85 fs pulse (equivalent to 0.4 PW) using just a 10 cm diameter beam. Clearly with the energy available on the HiPER system the scope for access to far greater powers and intensities is obvious and it is worth highlighting this potential through two example scenarios.

Example Scenarios

Two scenarios can be contemplated that essentially define the maximum power than can be reasonably expected under two different sets of assumptions. They are:

Scenario 1 – 150 Petawatt (150×10^{15} W) - *A relatively low cost, low risk scenario where no fundamental technology development is required and advantage is taken of technology which has already been demonstrated to date.*

The largest multi-layer dielectric (MLD) gratings (for operation at 1.053 μm) that have been manufactured to date are by the Lawrence Livermore National Laboratory (LLNL) and have dimensions of 40 x 80 cm, with a nominal damage threshold of 0.5 Jcm^{-2} at a pulse length of 30 fs. Assuming a 2 x 2 tiled array is constructed and operated at 80% of this value, the maximum energy that can be handled is 5.12 kJ. If a KDP OPA is utilised then the gain bandwidth limit of this system (figure 10.6), including the known bandwidth of the dielectric gratings, will support a 30 fs pulse duration or a pulse power exceeding 150 PW. If focussed with a 1.6 m diameter F#1 parabola to 1.5 times the diffraction limit,

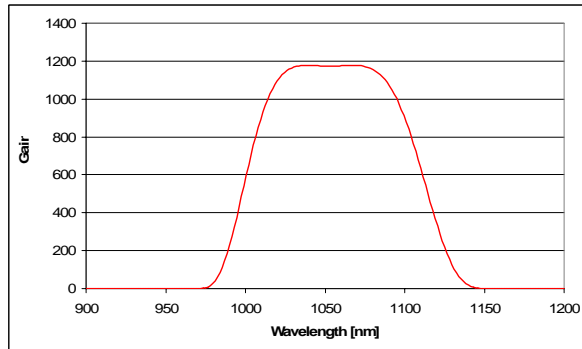


Figure 10.6: Calculated gain bandwidth for KDP with a pump beam wavelength of 526 nm for gains of approximately 1000

intensities of $5 \times 10^{24} \text{ Wcm}^{-2}$ can be anticipated. This would require about 7% of the long pulse capability to drive four sequential KDP parametric amplifiers to produce the pulse energy.

Scenario 2 – 2.5 Exawatt (EW, $2.5 \times 10^{18} \text{ W}$) - *A higher cost, higher risk scenario that assumes a development programme aligned to this system is initiated that produces some modest advance in technology, principally concerning diffraction gratings*

The manufacturing method used to fabricate the MLD gratings at LLNL is essentially limited today by their requirements for NIF and therefore this sets the size of the fabrication technology used in the processing. However, as indicated earlier new techniques are now becoming available that could see this restriction being removed. One can therefore reasonably assume a modest scaling of the grating aperture to 1.0 m x 1.0 m and once again the gratings tiled in a 2 x 2 array. In terms of damage threshold, the performance of gratings in the time range relevant for fast ignition (10-20 ps) has improved significantly (factor of 8) in recent years with little effort being expended in the ultra-short pulse window of 10-100 fs. This has, of course, been driven by the requirements of NIF and OMEGA-EP. One can reasonably assume that given the resources of a similarly focussed programme, the technology associated with MLD gratings might be sufficiently developed in the ultra-short pulse region such that a factor of 2 increase in damage threshold could be realised.

These two developments, which we do not believe are unreasonable to contemplate over ten year timescale would increase the energy handling capacity to some 40 kJ in a beam of 2 m x 2 m.

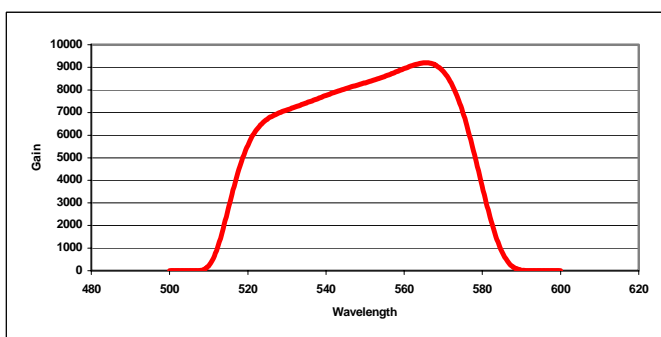


Figure 10.7: Calculated gain bandwidth for KDP with a pump beam wavelength of 351 nm. Gains are approximately those that would be required to reach 40 kJ

Nd:glass system and seeded at 540 nm could support a 15 fs pulse duration.

Finally, current MLD technology is designed to operate at 1053 nm, again in response to the requirements of the current fast ignition Nd:glass systems. However, because the grating technology is di-electric based one could also consider that it would be possible to design and manufacture gratings to operate at an arbitrary wavelength in much the same way one can with dielectric mirrors today. In turn, this would enable even broader amplification bandwidth schemes to be contemplated in the OPA. For example (Figure 10.7), a KDP amplifier pumped by the 3rd harmonic of the

Assuming such development, one could anticipate a pulse power of some 2.5 EW and intensities greater $5 \times 10^{26} \text{ Wcm}^{-2}$ using a 3 m diameter F#1 parabola. This would require about 70% of the HiPER long pulse capability configured to pump a sequence of KDP crystal arrays.

It clearly important therefore that in considering options for the HiPER system, an OPCPA configuration is explored in greater detail.

10.5 Diode Pumped Solid State Laser (DPSSL) Options

One of the key questions that the HiPER preparatory phase study will address is to what extent the role of Diode Pumped Solid State Lasers (DPSSL) should play. Clearly, in advancing the argument for IFE through HiPER, it is necessary to address the key questions that relate to future drivers that could enable IFE to be produced at a repetition rate suitable for commercial exploitation. The natural question arises therefore of whether existing DPSSL technology is or will be in the medium sufficiently mature and robust that it could allow the whole of the HiPER system to be rep rated. If not, what needs to be addressed and what contribution could it make to HiPER. HiPER, as part of its preparatory phase, will need to explore the variety of DPSSL options available to it. As a baseline, a detailed examination of the technological, strategic and financial issues related to producing a 10kJ beamline for HiPER is presented in Appendix 3.

References for Chapter 10

- [1] C.P.J. Barty et al., Nucl. Fusion 44 S266 (2004).
- [2] See: [i] L. Li and J. Hirsh, “All-dielectric, high-efficiency reflection gratings made with multilayer thin-film coatings”, Optics Letters, June 1, (1995); [ii] B. W. Shore, M. D. Perry, J. A. Britten, R. D. Boyd, M. D. Feit, H. T. Nguyen, R. Chow, G. E. Loomis, and L. Li, “Design of High-Efficiency Dielectric Reflection Gratings,” J. Opt. Soc. Am. A 14, 1124, (1997); [iii] K. Hehl, et.al., “High-efficiency dielectric reflection gratings: design, fabrication, and analysis”, Applied Optics, October 20, 1999; [iv] J.A. Britten, W.A. Molander, A.M. Komashko and C.P.J. Barty, Proc. SPIE V5273, 1, (2004).
- [3] T. J. Kessler et al., “Demonstration of Coherent Addition of Multiple Gratings for High-Energy Chirped-Pulse-Amplified Lasers,” Opt. Lett., 29, 635, (2004)
- [4] T. Zhang, M. Yonemora, and Y. Katp, Opt. Comm., 145, 367 (1998)
- [5] T. J. Kessler et al., US patent application 20040227956, November 18, (2004)
- [6] G. Chanan, et.al., Appl. Opt., 37, 140, (1998)
- [7] A Dubietis *et al*, Optics Communications, **88** (1992) 437
- [8] I Ross *et al*, Optics Communications, **144** (1997) 125
- [9] For a review see T Tajima & G Mourou, Physical Review Special Topics – Accelerators & Beams, **5** (2002) 031301
- [10] I Ross *et al*, Journal of the Optical Societ of America, **19** (2002) 2945
- [11] I Ross *et al*, Applied Optics, **39** (2000) 2422; J Collier *et al*, Applied Optics, **38** (1999) 7846
- [12] J Collier *et al*, International Conference on Ultra Intense Lasers, Lake Tahoe, Oct 2004: O Chekhlov *et al*, Optics Letters, **31** (24), (2006) 3665

11 Target Manufacturing Capability and Delivery

11.1 Scope

Target manufacturing and delivery for HiPER is discussed in two main themes: 1) technical issues relating to production and 2) associated issues, such as infrastructure and target design specification. Aspects of commercialisation are also considered.

This work has been compiled through coordination of European academic groups, the CEA groups in France associated with Laser Megajoule, and the private sector (General Atomic Inc.) in the US.

It should be noted that the baseline target design is only at the conceptual stage whose details have not yet been fully established. This is because the design will be informed by the upcoming experimental programmes on European, US and Japanese facilities.

The above themes can be addressed by establishing a sufficiently broad target fabrication capability including particularly close and efficient integration with the physics, modelling and experimental work streams during the period of this project. Furthermore work on new materials to produce high efficiency targets will be similarly embedded and integrated within the target fabrication activity.

11.2 Work package objectives

The task ahead has been broken down into the following areas:

- 1) Generate design specifications for HiPER targets (IFE and complex experimental targets). Specifically for IFE targets to examine high gain solutions, including the use of new materials.
- 2) Assess technical feasibility of producing all target types, prioritised through analysis of the risks to timely delivery.
- 3) Identify risks for target production and propose methods of risk reduction.
- 4) Assess European capability to fabricate the majority of targets for all HiPER programmes, specifically identifying infrastructure which needs to be put in place, including timescales.
- 5) Propose structure for target fabrication activity that is maximally integrated with all relevant work packages to ensure rapid response to evolutions in design (modelling) and experimental programmes.

11.3 Technical background

The HiPER programmes will require a wide range of solid targets for “high energy density” physics studies. Such targets can be classified into three (overlapping) types: a) high gain for IFE science, b) high gain for IFE scale-up to a commercial reactor programme, and c) science programmes.

In general type a) targets will almost certainly have a thin-walled microballoon component with an internal layer of solid deuterium or deuterium/tritium ice. For some targets the layer may be carried on a foam. It is anticipated that significant improvements in yield can be achieved by advances in foam materials and technology. Also many of the type a) targets will have a cone inserted through the side of the microballoon. Initial experiments, for example in electron or proton transport, will not require the ice layer, however, cryogenic targets will need to be fielded as the experimental campaigns progress.

Targets of type b) will have the same general features as type a) but the emphasis will be towards demonstrating high number scale-up capabilities, simplifying the physics design and relaxing the specifications whilst maintaining robust performance.

Targets of type c) will encompass a wide range of morphologies and materials including multi-component targets and multi-element target clusters. Also a range of type c) targets will be used to experimentally establish parameters required for (iteratively) designing target types a) and b). In addition, theoretical and experimental analysis of target debris, shrapnel and radiation production will be integrated into the target design and fabrication activities.

Because IFE targets are central to the HiPER project and since they are the most technically challenging to make they will be discussed in more detail here.

11.4 Specifically identified challenges – risk identification

Extensive discussions have been held to identify specific issues (across all target types) where there is uncertainty or risk at a level which needs to be specifically addressed. The results are summarised in the following table:

1	Cryogenic capability
1.1	Cryogenic layering of non-spherical target (solid ice and foam)
1.2	Tritium Handling
1.3	Capsule/cone joint at cryogenic temperatures
1.4	Cryogenic target (transport and) insertion
2	New/novel materials
3	Capsule and cone production
4	Metrology
5	High number scale-up
6	Modelling of materials and processes to inform fabrication
7	Target design/positioning to reduce debris
8	Range of targets for science programmes

Established (but challenging) technology

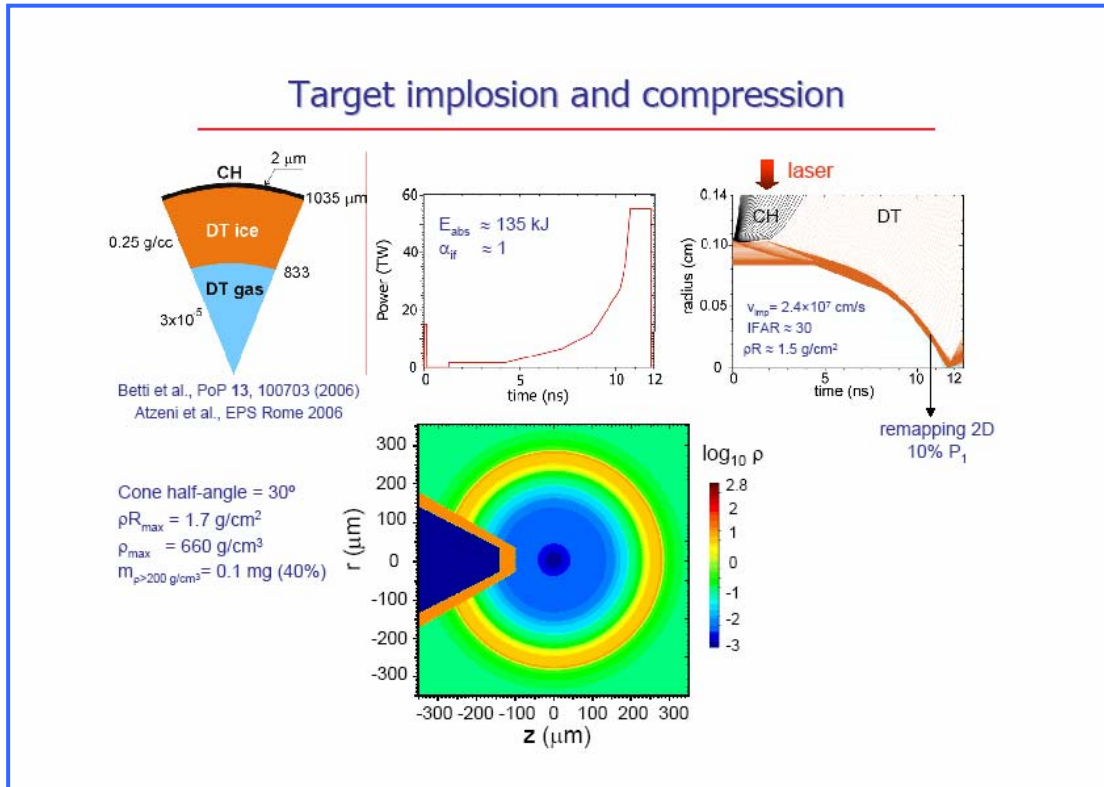
Shading key

Technology requiring significant innovation for HiPER

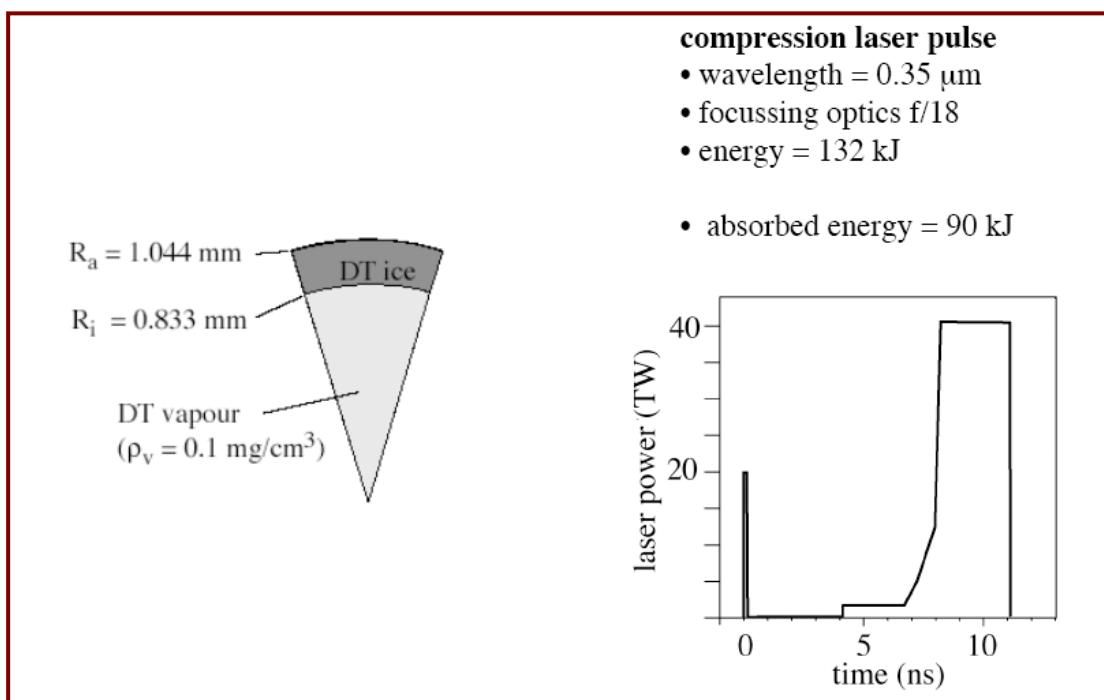
11.5 IFE target baseline design specification

At this stage in the HiPER project a detailed design specification for fusion target(s) has not been finalised and indeed the design will be iteratively refined as the experimental programmes progress. However, two proposals for conceptual baseline designs are explored here to illuminate discussion of target fabrication issues. These are shown schematically below:

Baseline IFE Target #1



Baseline IFE Target #2



11.6 Existing target fabrication capabilities relevant to HiPER

The current capabilities for target fabrication that have been considered for HiPER fall into three communities:

- Academic European laboratories and universities.
Currently within the EU there are a number of centres of expertise in microtarget fabrication. The centres are distributed throughout the EU and are currently not well co-ordinated since historically there has been no need. In 2006 RAL co-ordinated two target fabrication workshops:
 - An EU Target Fabrication workshop with Laserlab (Framework 6) funding. The meeting was attended by 15 delegates from 12 institutions across 8 countries. The workshop assessed current EU target fabrication facilities and capabilities and proposed collaboration mechanisms which are currently being introduced.
 - A HiPER Target Fabrication workshop which was attended by 16 delegates from 12 institutions and 9 countries. Discussion mainly focussed on identifying specific technical challenges for HiPER targetry (reported above) and how to address those challenges, both technically and in terms of developing sufficient infrastructure within the EU.
- CEA France.
As part of the Laser Megajoule (LMJ) programme there are two main centres of expertise:
 - Specifically for cryogenic capability the Low Temperature Laboratory of CEA/Grenoble (SBT) has, since 1994, been in charge of the conceptual design and prototype production of cryogenics for LMJ.
 - The Valduc laboratory which has a comprehensive capability for fusion target manufacture
- US infrastructure: General Atomics Inc. and Lawrence Livermore National Laboratory
 - The Chemistry and Materials Science Directorate of Lawrence Livermore National Laboratory, through the NanoScience Laboratory, has an established (experimental and multi-scale modelling) programme in the development of new materials that should significantly increase the efficiency of high energy density targets and lead to increased yield in IFE targets.
 - GA (General Atomics Inc.) is a US-based commercial company which produces a large variety of microtargets and components for high power laser experiments. The company has access to a wide range of techniques and expertise including close integration in cryogenic target delivery programmes. GA also has experience in examining feasibility and commercial issues associated with the scale-up of fusion target production for a power production programme.

Although European researchers have significant strength in the physics research related to fast ignition, the capability in Europe for the *production* of complex targets is scarce and/or limited to defence laboratories. A key task for the preparatory phase must therefore be to establish a credible route to securing an effective capability in a timely fashion.

Some technologies developed at LMJ and NIF could clearly be directly extended to HiPER and the future IFE power production programmes. Collaboration with experienced groups will significantly decrease the risks for HiPER as well as reduce the length of many R&D programmes.

To enable the required level of target fabrication for HiPER it is essential to increase collaboration across EU within civilian programmes to develop core capabilities and to collaborate with facilities and companies that have relevant experience during this preparatory phase.

HiPER target fabrication will deal with a range of significant technical challenges. Target fabrication also occupies a place within HiPER from which, when optimised, significant utility can be achieved by providing target delivery in a highly time responsive mode to design modifications and on-going experimental feedback.

11.7 The role of European civilian institutions

The academic institutions will bring a fresh perspective that should offer an excellent opportunity to look for novel targetry solutions both in terms of operational organisation and technical challenges. All targetry issues for HiPER can be analysed from a fresh perspective and look to propose innovative and cost-saving solutions. A principal goal for HiPER is to establish a route for commercial IFE and so such an approach could yield considerable IP and financial gain.

Lead tasks for the academic European institutions:

Task Description	Deliverables
Lead, specify and co-ordinate HiPER target fabrication activities.	Progress according to delivery plan.
Analysis of European infrastructure requirements to enable all necessary aspects of HiPER IFE target fabrication.	Report specifying actions required to install all necessary infrastructure including timescales.
Analysis of fabrication capabilities which will be required for HiPER science programmes targets.	Report describing current capabilities and identifying required additional capabilities.
Examine new materials, especially for improving yield of IFE targets.	Report on production, characterisation and suitability of new materials.
Study foam layering of shells.	Report on production, characterisation and suitability of layered foams.
Detail tritium handling procedures.	Document summarizing tritium handling procedures.
Computational modelling of cone-shell target layering including target and thermal (shroud) environment. Modelling of structural integrity.	Summary of results of thermal and structural modelling.

11.8 The role of the CEA laboratories

CEA has extensive experience in producing cryogenic targets which are similar in design to HiPER cryogenic targets. The experience includes the full range of devices required for placing a cryogenic target in an interaction chamber, such as target positioner, layering shroud, shroud remover, cryostats and ancillary equipment.

The main responsibility for CEA will be to propose designs for fielding HiPER cryogenic targets by modifying and extending established technologies.

Task Description	Deliverable
<p>Design a system to field HiPER cryogenic targets based on modifying existing technology for both fill tube and permeation.</p> <p>Cryogenic infrastructure: design of cryostats, DT fill apparatus, target positioner, thermal shroud and shroud remover; mK control of target fill and layering.</p> <p>Specify permeation facility and technologies for transport of cryogenic targets.</p>	<p>Produce report covering all aspects of cryogenic target production for HiPER including infrastructure.</p>
<p>Produce cost estimates for HiPER single shot cryogenic capability.</p>	<p>Breakdown of costings for delivering single shot cryogenic capability.</p>

Cross-cutting themes:

- Link to chamber design workpackage (vacuum must be less than 10^{-6} mb to avoid condensation on outside of shroud).
- Link to tritium handling subtask
- Integrate all packages with modelling, materials science and physics groups.

11.9 The role of GA and LLNL

The collaboration which already exists between UPM (Spain) and LLNL in the development of new materials for increasing the efficiency of high energy density targets will be extended for application to HiPER IFE targets.

Task Description	Deliverables
Propose plausible methods for mass-production of cone-shell targets including mass-production of; capsules and foam shells, capsule hole cutting, assembly and layering. Perform laboratory-scale demonstration of key techniques.	Report covering suggested methods for mass-production. Report on scaled demonstration of mass-production techniques including confidence analysis for full scale up.
Analyse high repetition rate injection and tracking techniques including target placement accuracy.	Report on injection and tracking techniques including assessment of accuracy acceptability and repercussions for HiPER design.
Cost analysis for continuous high repetition rate (cryogenic) IFE target production and insertion including; optimised solution(s) and infrastructure (such as a target manufacturing plant).	Report detailing cost analysis for high repetition rates.
Examine new materials, especially for improving yield of IFE targets.	Couple to European institution work

12 Fusion Reactor Design and Technology

12.1 Introduction

An essential aspect of the HiPER project will be to ensure adequate progress in the development of the engineering and material technology required for a subsequent IFE power production programme. This will require close coordination with the international community, as well as with the MFE and advanced fission communities, given the scale of the tasks.

A list of potential experiments in the HiPER facility concerning the assessment of Fusion Technology (relevant for future DEMO IFE reactors) is presented on the basis of a review of previous work on Inertial Fusion Reactors (Fast Ignition / KOYO-F, and central ignition).

A detailed overview of prior work on IFE reactor designs is provided in APPENDIX 1, as are the references and acknowledgements for contributions to this section.

A number of conceptual reactor designs have been developed over the past 20 years. In some cases small experiments have been performed to investigate aspects of the basic physics that support the proposed technologies. In this section we highlight the work performed (mainly in Japan) on a fast ignition variant of a commercial IFE reactor, called KOYO-F. An important aspect of the HiPER project will be to catalyse a renewed, coordinated international effort in the reactor design and technology areas. The facility itself needs to be able to address key issues associated with the emerging design requirements. Analysis of the relevance of these experiments and consequent simulation will be a key task in this Preparatory Phase.

HiPER will provide essential data for IFE in areas of Fusion Technology (in addition to targets or lasers themselves), such as:

- Target chamber phenomena and materials response to target emissions (x-ray, ions, neutrons)
- Prototypical IFE fusion power technologies in the chamber area
- Performance testing of IFE target fabrication and injection methods.

HiPER can thus play a critical role in providing the basis for design of the follow-on “demonstrator reactor” in these areas.

12.2 Examples of Fusion Technology Experiments

Using a well established radiation output from a HiPER fusion target, beneficial knowledge of future technologies could be obtained. For example: nuclear heating, transport and activation, tritium management, IFE materials science, and safety/environmental issues. This would provide early experience in prototypical IFE fusion power technologies. The main impact to consider is their contribution to the total HiPER shot envelope and allowed chamber activation, along with all other user-group shots.

Preliminary proposals include:

- Experimental investigation of the relation between capsule performance and injection acceleration methods
- Time-resolved measurements of radiation-driven shock velocities, multiple shocks (etc) in high gain materials.

- Precision x-ray vaporization experiment
- First-wall material response experiment
- Chamber gas-dynamic and wall-stress experiment
- Many different material source and debris/shrapnel calibration experiments
- Integral activation measurements in IFE neutron spectrum
- Measurement of attenuated neutron streaming up beam ports (with plugs)
- Studies in pulsed-neutron activation analysis
- Irradiation effects on optical fibres
- Benchmarking multi-scale modelling calculations of neutron damage of low-activation materials
- Radiation damage of optical and structural components in HiPER itself or for DEMO IFE facilities
- Debris damage to first wall materials
- Thermo-mechanical damage of optical and structural components
- Tritium removal from molten salt in small testing close samples in some adequate position
- Mini-blanket benchmark experiments
- Feasibility of neutron-multiplying target chamber walls for ICF reactors
- Benchmarking neutron activations of out-of-chamber components and penetration shields for IFE reactors
- Radiation damage limit of new materials for shielding IFE reactors
- Induced radioactivity and biological dose measurements
- Nuclear heating measurements
- Sensitivity of capsule performance to fabrication quality (of course this aspect is general in HiPER but we include here because it is certainly a key aspect for future IFE commercial technology)
- Sensitivity of capsule performance to beam pointing accuracy (of course this aspect is general in HiPER but we include here because it is certainly a key aspect for future IFE commercial technology)
- Target injection (different methods)
- Neutronics experiments under prototypical conditions to IFE are a key issue with two principal objectives: (a) To provide a sufficient experimental database to permit approval and licensing of an IFE device, (b) Verification of the predictive capabilities of various computational codes and associated materials databases in assessing the nuclear performance of various reactor components. This will allow a quantification of the design margins and safety factors to be implemented in future IFE blanket and shield design (system-dependent).

It is noted that a number of the above issues are common to the MFE programme (i.e. associated with the ITER facility). The detailed issues are different – for example, the neutrons generated in the plasma of MFE devices and incident to the first wall / blanket / shield have different angular/energy distributions than those generated in IFE devices and hence different design margins are anticipated. As such, the proposed experiments can be broadly classified as (a) experiments that

validate generic nuclear response and (b) bulk and penetration shielding experiments. Coordination and direct combination with the work associated with MFE is a key objective of this task.

An economics study associated with many of the above issues (as with bulk target manufacture) is also required.

12.3 Chamber Gas Dynamics

For the option of solid first walls with some gas protection (see appendix for details), the goal will be to determine efficacy of chamber gas fill to mitigate debris and soft-x-ray ablation, and its compatibility with laser beam propagation and with cryogenic targets.

IFE benefit: Improves viability of IFE reactors concepts.

Impact on HiPER: Compatibility with cryogenic targets, diagnostics, laser propagation.

The issues to be addressed here can be performed on any suitably configured ignition facility. The discussion below is taken from discussions associated with potential experiments on NIF. There will be specific issues associated with the direct (laser) drive and fast ignition options for HiPER which will need dedicated assessment to suitably inform the design of a future IFE plant. Laser driven fast ignition targets will have different debris production, different x-ray, ion and neutron spectra and fluence, and different sensitivities to their environment.

The measurement of the time at which the chamber conditions recover after a shot to allow injection of the next target and the entrance of the driver beams for the next shot is a key factor in determining an IFE chamber "clearing time. Some of the phenomena important to the clearing time can be studied in the HiPER chamber with an initial gas fill low enough to allow beam propagation without having to provide large pumping (we assume it is not important to pump the gas down to a high vacuum).

The magnitude of (and inhomogeneities in) the gas number density can adversely affect the propagation of the driver beams, especially if the beams enter the chamber prior to the time density inhomogeneities can smooth out. The clearing time of an IFE chamber is important because it establishes the maximum repetition rate of the chamber, which can limit the economical advantages of IFE. It is also important to determine the stress history on the first wall and its higher-order moments. The maximum stress is affected by the number of times that shock waves reverberate between the first wall and the centre of the chamber, and especially by the 3-D aspects of the stress. Both of these effects are dependent on chamber geometry (especially symmetry). The (3-D) higher-order moments of the stress can be critical to the design of the chamber, and are difficult to calculate. The gas-dynamics experiments are thus important in determining the design of the first wall for IFE, especially if smaller chambers will be considered, for their thicknesses are dominated by stress considerations and not by buckling.

Protection of the final optics from soft x rays, plasma debris, and small projectiles is critical for affordable operation of the any laser based IFE facility. However, there has been only limited research both theoretically and experimentally to assess the real impact of these hazardous target emissions. Certainly the experience to be gained from Ignition Facilities such as NIF and LMJ will be critical.

Preliminary proposals for experiments in this area include the investigation of different target chamber gas fills, and the analysis of target-generated fireballs and laser induced breakdown with dense fill gases. For example:

- **Chamber dynamics and clearing time.**

Measure the time history of conditions relating to the gas dynamics and fireball behaviour inside the target chamber for various gas-fill pressures, including the reverberations of accompanying shock waves and the establishment of the late-time thermalized pressure $P(t)$. This objective will determine many aspects important to the clearing, or recovery time in an IFE chamber. This objective will also determine the pressure above which fireballs are evident, and the effective opacities of the gas at relevant fireball conditions.

- **Final optics and wall erosion.**

Assess the erosion hazard to first-wall, final optic materials from target x rays, plasma debris, and particulates as a function of fill gas pressure. This objective requires varying the fill pressure and noting the differences in the erosion rates for various wall and optical materials placed inside the chamber. It requires deployment of diagnostics to measure the prompt momentum transfer (ablation impulse) to the first wall and to the final-optics surfaces. It is also desirable to measure the history of the average wall stress, and to correlate the average stress with the calculated stress history inferred from the measured ablation impulse and the measured $P(t)$ from the above experiment. It is also desirable to measure the nonuniformity of peak wall stress as a function of wall position, and thereby assess the importance of higher-order moments in the peak wall stress history arising from the 3D nature of the chamber wall (e.g., the chamber ports).

- **Driver beam transport.**

Help assess the optimum gas-fill pressure for laser beams, and measure the decay of ionization in ambient gas versus time, important to the study of ion beam transport in various pressure regimes. This objective requires diagnostic deployment to determine the loss of laser irradiation because of SRS, and to analyze the transient temperature, pressure, and density conditions measured above at times many-tens of milliseconds after a shot. For ion beams, this objective does not require the use of such beams; instead, it requires the assessment of the impact of the dynamical conditions inside the chamber on the transport (propagation, neutralization, etc.) of the ions as inferred through additional analyses.

- **Impact on cryogenic targets.**

Measure the impact (especially thermal load and condensation) of a gas fill on a cryogenic target. This objective requires (1) measurement of the buildup of sublimed Ar on the target materials, (2) assessment of the impact of this buildup on the energy-delivering capability of the driver beams, and (3) determination of the added thermal load on the cryogenic cooling systems.

12.4 Liquid Interactions

The goal here is to provide data on disruption of both liquid jets and liquid film layers by neutrons and X-rays for protected-wall IFE concepts such as HYLIFE-II (see Appendix).

IFE-benefit: Extends IFE fusion chamber lifetimes with renewable liquid-protected walls.

Impact on HiPER: Liquid debris ejected into chamber, impact on cleanup system.

Specific Preliminary Proposals include:

- Stability of liquid metal curtains due to shock-wave interaction (splashing)
- Response of first-wall tubes due to target blast
- Condensation effects

- Ablation, gas dynamics, and condensation experiments for IFE
- Isochoric (neutron) heating effects
- Blast effects on film protectant thickness and stability
- Film/substrate interactions due to blast impulse
- Damage rates at dry spots on film protected surfaces

In some of the presently proposed concepts for IFE reactors a protective liquid metal film such as liquid lead is renewed between shots by seeping through a porous structural wall in front of a solid breeding blanket. In others, a liquid lead eutectic or molten-salt coolant is channelled through porous tubes or loose-weave cloth-like channels, with the outer surfaces maintaining a protective liquid film layer. In HYLIFE-II, neutronicly thick jets of molten-salt “FLiBe” are used to protect structural walls from neutrons as well as target x-rays and debris. Some issues common to all of these concepts are the effects of isochoric (constant volume) neutron heating generating transient internal pressures whose subsequent relaxation can cause rapid expansion motion, the effect of surface shocks on the liquids due to soft x-ray ablation and debris, the generation of momentum due to the above effects propelling liquid droplets and jets, the effects of recondensation of vapour back onto the remaining liquid, and the recovery times to re-establish the desired liquid flows after disruptions from each shot (different in each case). Data from these experiments are generally used to benchmark various computer models of these interactions important to future IFE power plant designs. The objective of the Liquid Interactions Experiment is to provide a common experimental test envelope, common diagnostic set, and liquid containment/clean-up for all those experiments with liquid interactions so that the HiPER impacts in the chamber are considered within this one common envelope. The required doses of x-rays and/or neutrons could be varied as required for each test either by adjusting the distance between the target and the sample at fixed yield (e.g., at 20 MJ baseline yield, by varying the distance to target from 0.2 m, to 1 meter, or by varying the target yield.

The major HiPER impact issue with all such experiments is associated with the management of significant quantities of liquids and their condensable vapours which may be released into the chamber. Of particular concern is both the potential condensation of liquids on the final optics and diagnostic windows, compounded by the neutron activation of such materials. The selection of liquids used in experiments to simulate liquid interactions expected in an IFE environment should be first tested for compatibility with the cleanup system. Nonetheless, the less liquids and condensable vapours released, the faster the cleanup will be. Thus, the experimental envelope need to be designed to intend to minimize the release of such condensable and liquids by several methods: 1) Use of a frost-coated window for experiments on the effects of isochoric neutron heating only, providing enough volume within the enclosure to completely and safely contain the liquids vapour pressures generated within the enclosure. 2) Use of fast-closing shutter, which can trap most of the slower moving liquid splash, for experiments that need shots with an initially open aperture for combined x-ray, debris and neutron doses. 3) Use of an internal baffle and cold-trap to rapidly decrease condensable vapour pressures inside the enclosure, mitigating the expulsion of liquids and vapour out the entrance aperture. 4) Combined use of the common liquid experiment enclosure with some proposed cryogenic *mini-chamber* so that exhaust from the common liquid experiment enclosure can be cold trapped within the *mini-chamber*.

12.5 High-repetition rate chamber

The goal of this series of experiments is to provide relevant simulations of protected-wall IFE chamber clearing for single shot and multishot bursts. This would be performed by inserting an overcoated mini-chamber scaled in size to about 100 J/cm^2 wall fluence. The concept of a “Mini-Chamber” is an old idea given in the references of Tobin and Logan where a review of potential experiments for NIF relevant for IFE is done and essentially used here in many aspects due to the close involvement of one of the HiPER partners (UPM) in this study. Another chamber for multishots as programmed in HiPER would perform similar goals including this original minichamber inside.

IFE benefit: Determine gas-dynamic constraints on maximum IFE chamber pulse-rate.

Non-IFE benefit: May allow higher-yield shots with reduced debris-loading on optics.

Impact on HiPER: -about 1 m diameter internal chamber; stagger-firing of laser sections for hi-rep.

The goal of this experiment is to provide a relevant simulation of protected-wall IFE chamber clearing with single shot and multi-shot bursts using $\sim 1 \text{ m}$ diameter, vented minichambers surrounding targets inserted inside the HiPER target chambers. The minichambers would be supported independent of the target positioner on a rigid vertical column, entering the chambers through the bottom 2 m port in the existing NIF design. The size of a reusable minichamber would be scaled down to increase the mini-chamber wall energy deposition due to debris, soft x-rays, and neutrons from the typical level of 1 J/cm^2 at the HiPER target chamber wall at 5 meters radius (as with NIF), to a higher $\sim 100 \text{ J/cm}^2$ wall fluence more representative of protected-wall IFE fusion chambers.

To simulate chamber clearing and vacuum recovery from vaporization of renewable solid and liquid materials protecting walls in IFE concepts, mini-chamber structural walls would be coated with sacrificial coatings or films of materials such as frost or vaporizable solids chosen to simulate transient conditions relevant to IFE. Different mini-chambers can be designed for different targets, including single-shot experiments with high-yield ignition targets, as well as smaller chambers for short 5 Hz bursts of injected foil or disk laser non-ignition targets designed to simulate clearing in a high-pulse rate IFE chamber. The multi-shot experiments would require the capability to stagger-fire different sections of the laser system at 200 ms intervals (or make direct use of the high repetition rate HiPER option, if selected). HiPER would thus be a first step in encountering high-rep-rate challenges of IFE. The mini-chamber experiments complement small-sample wall material experiments by addressing integral chamber dynamic responses at both an IFE-relevant energy fluence and in an IFE-relevant enclosed geometry, which includes important effects of venting and condensation back onto the walls. The single-shot experiments would determine most of the gas-phase dynamics needed to determine basic chamber clearing rates and momentum transfer to structures and liquids, while the multi-shot experiments would include wall ablation changes due to the redeposition of hot condensates from recent previous pulses.

Specific Preliminary Proposals include:

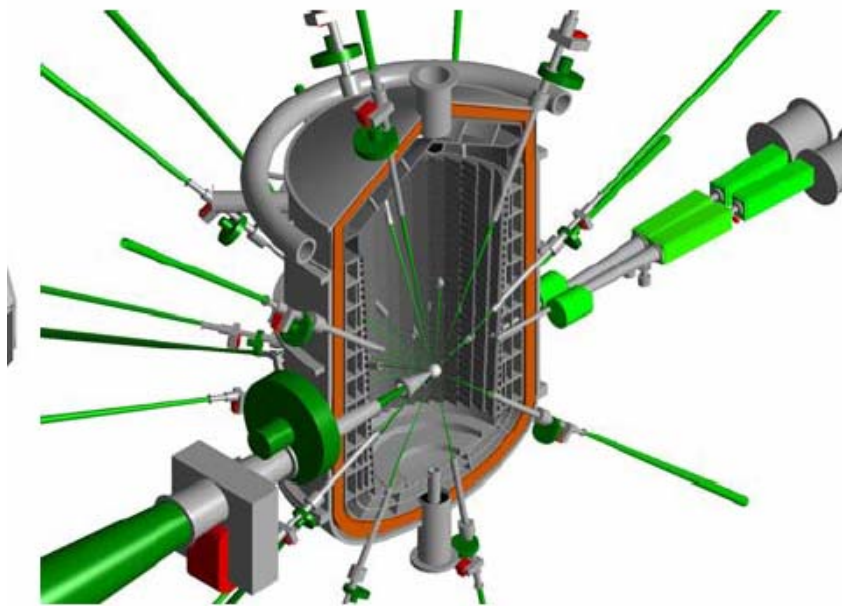
- Study effects of post-ignition chamber conditions on injected targets
- First-wall condensation experiment
- High-rep-rate target chamber dynamics experiment/frosted minichamber for debris-trapping
- Performance evaluation of the cavity during self-clearing
- Evacuation of noncondensibles from cavity
- Chamber conditions after a shot

12.6 Fast Ignition reactor conceptual design

The KOYO-F conceptual reactor proposed by the Institute of Laser Engineering (ILE) of the University of Osaka is based on a laser with 32 beams for compression and one heating beam (Norimatsu et al.). This is presented here to illustrate a potential extension of the Fast Ignition approach to the reactor scale. Many technology issues need to be addressed during the next phase of IFE development. This will require close international coordination.

	Compression laser	Heating laser
Wave length	3ω	1ω
Energy/pulse	1.1 MJ	100 kJ
Pulth width	TBD	30 ps
Pulse shape	Foot pulse + Main pulse	Flat top (2 ps reise time)
Beam number	32	1 bundle
F number	depends on plant design	$F/10 \sim 20$
Uniformity	1 % (foot pulse)	-----
Spot size	Controlled focusing pattern	$\leq 50 \mu\text{m}$
Rep-rate	16 Hz	16 Hz

Typical requirements for a Fast Ignition reactor

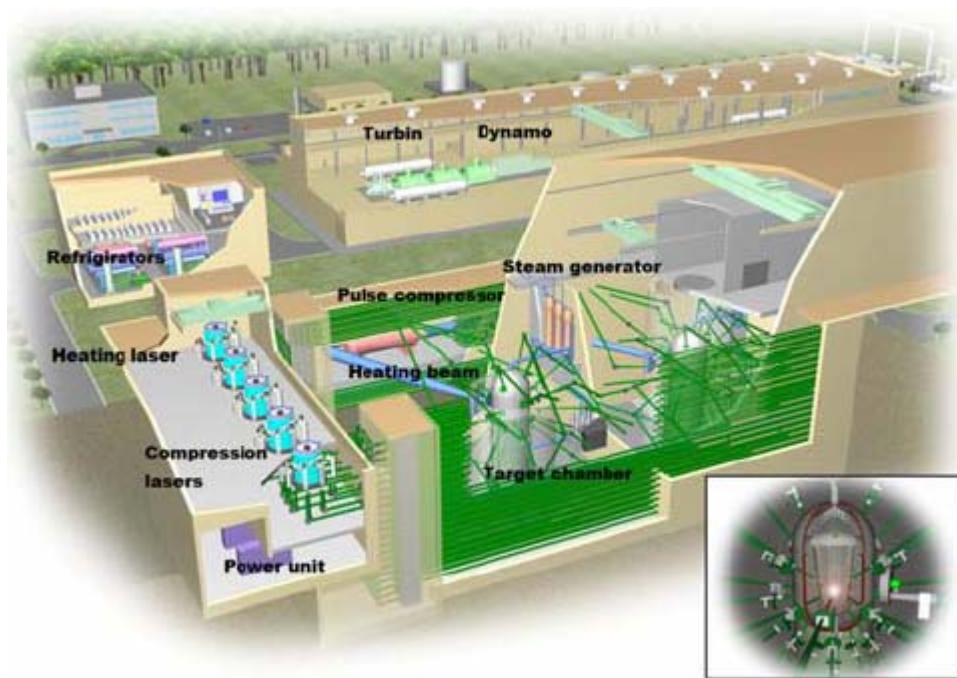


Cross-sectional view of the KOYO-F fast ignition reactor (Norimatsu et al.)

The reactor proposes a Cascade surface flow with mixing channel in order to protect the wall, using SiC panels coated with wetable metal in such a way that tilted first panels make no stagnation point of ablated vapor. In order to have a synchronized system it is proposed to use compact rotary shutters with 3 synchronized disks. The surface flow is mixed with inner cold flow step by step to reduce the surface temperature.

Net output	1200 Mwe (300MWe x 4)
Laser Energy	1.1 MJ
Target gain	165
Fusion output per pulse	200 MJ
Pulse rep-rate in reactor	4 Hz
Blanket energy multiplication	1.2
Thermal output per reactor	916 MWth
Total output at plant	3664 MWth (916 MWth x 4)
Thermal to electricity efficiency	41.5 % (LiPb temperature 500C)
Total electric output of plant	1519 MWe
Laser efficiency	11.4 % (Compression), 4.2%(heating), Total 8%(including cooling power)
Rep-rate of laser	16 Hz
Recirculating power for laser	240 MWe (1.2 MJ x 16 Hz / 0.08) (Yb-YAG laser operating at 150 - 220K)
Total plant efficiency	1200 MWe (1519 MWe- 240 Mwe-79MWe Aux.)

Basic specification for KOYO-F



Bird's eye view of the KOYO-F reactor design (Norimatsu et al)

Some conclusions from the ARIES integrated IFE reactor studies (Najmabadi et al.) that are very significant for assessing the HiPER studies in Fusion Technology were:

- The detailed characterization of the target yield and spectrum has a major impact on the chamber
- It is better to use a thin armor instead of a monolithic first wall for dry-wall concepts;
- In this case of dry-wall concepts with direct-drive targets, the most stringent constraint is imposed by target survival during the injection process
- For relatively low yield targets (250 MJ), an operational window with no buffer gas may exist.
- For dry-wall concepts with indirect-drive targets, a high buffer gas pressure would be necessary that may preclude propagation of the laser driver and require assisted pinch transport for the heavy ion driver;
- Generation and transport of aerosols in the chamber is the key feasibility issue for wetted-wall concepts.

13 Industrial engagement and component sourcing

13.1 Introduction

As discussed in Section 5, there are two principal options for HiPER. For one it is proposed to use, wherever possible, similar technology to the two large lasers currently under construction: the National Ignition Facility, NIF in the USA [10.1], and Laser Megajoule, LMJ in France [10.2]. As such the project will be making much use of the optical fabrication techniques and equipment already put in place by these facilities. This represents leverage from two multi-billion Euro scale development programmes and so offers a relatively low risk option for HiPER.

There are still areas in this design which will require significant industrial engagement over the course of the preparatory phase project to ensure a viable production route exists. Also, there is healthy competition in many areas of technology (as well as for the overall project management and civil construction aspects). Likely partners will be explored over this next phase.

In this section we highlight some of the key supply issues where specialist industry is required.

13.2 Optics

The prospect of a very large scale laser system within Europe is an excellent opportunity to engage, support and develop the technical industrial community.

The licenses for many of the processes developed for the NIF and LMJ lasers are owned by the DoE and/or CEA including that for the 46 x 81 x 4.1 cm Nd:glass laser discs. In informal discussions during the 2-year design phase, both parties expressed a willingness to permit the processes to be used by the HiPER project in conjunction with the relevant manufacturers. Using the NIF/LMJ designs reduces the risk of finding and facilitating suppliers in a lot of the key optics and associated assemblies. There are however a relatively small number of key optics which should be reviewed.



Figure 13.1 : Nd:doped phosphate laser glass coming off the production line of the continuous melt process developed for the NIF and LMJ laser systems.

With an initial estimated requirement of 1300 laser discs the most obvious issue for HiPER is the availability of sufficient laser glass since the continuous melt production lines [10.3] for NIF and LMJ will have been shut for several years before construction could begin. The HiPER project will need to explore options including mothballing; starting up production again with the two previous glass suppliers Hoya [10.4] and Schott [10.5]; and seeking other potential sources such as Shanghai Institute of fine Opto-Mechanics (SIOM) [10.6] in China, or options in Russia.

The HiPER project is likely to have a frequency conversion and focusing system based on the successfully commissioned LMJ prototype LIL [10.7]. It comprises a 1ω grating, two Potassium Di-Hydrogen Phosphate (KDP) crystals for second and third harmonic (3ω)

generation, and a 3ω focusing grating. These optics specifically developed for LIL/LMJ are currently only manufactured by Jobin Yvon [10.8]. Alternative sources could be LLNL [10.9], Plymouth Grating Laboratory [10.10], Carl Zeiss [10.11] or General Atomics [10.12].

Harmonic conversion crystals and Pockels cell crystals do not appear to be critical items at this time as current designs perform reliably on NIF and LMJ. Large aperture Plasma Electrode Pockels Cells (PEPC) [10.13] required for the switching and the isolation from back reflections of the main amplifier are used in NIF, LIL as well as in Omega-EP [10.14] at the University of Rochester. The performance of these is thoroughly characterised. Large aperture Faraday isolators are proposed and being evaluated for the FIREX [10.15] laser system at the ILE in Japan (1.25 meter clear aperture) and might be another route to provide fail-safe protection from target retro-reflections for HiPER.

The final wavelength of the laser will be ultimately determined by the specific requirements of the plasma physics of the fusion interaction. The issues of the final wavelength for the compression pulse will be determined by the absorption properties of the target balloon. This is determined by the product of intensity and the square of the wavelength, $I\lambda^2$, which should be minimized. This suggests the use of the third harmonic of this type of laser ($\lambda=351\text{nm}$). However, third harmonic brings with it a significant decrease in the laser damage threshold of all subsequent optics and so work will be performed to assess the viability of operating at the second harmonic.

13.3 Components not developed for the NIF and LMJ systems

Although for the baseline design the HiPER system will be similar to the NIF and LMJ lasers for over 90% of the components, the remaining 10% hold the greatest challenge. Even so it should be possible to draw upon the experiences of other sectors of the European scientific spectrum to reduce the risk to the project.

Ignitor beam focusing: A single optic for the focusing of 24 off 400 mm by 400 mm beams is impractical due to cost, delivery timescales, and damage issues. Developments over the last few years in the large telescope community have seen extremely large telescopes (> 10 m diameter) constructed from multiple segments. These include KECK and Gran Telescopio Canarias (GTC) telescopes [10.16, 10.17]. The HiPER project has already engaged SAGEM SA [10.18] who is the manufacturer of the primary reflector for the GTC. The GTC has an f/1 primary mirror with a segment to segment alignment accuracy of +/- 5nm [10.19]. This technology will need to be fully harnessed to handle the high energy side of laser work to fulfil the requirements of the HiPER project, not an issue relevant to the telescope community.

Alternative options also exist (for example OptIC-Technium in the UK), coupled to the growth of the optical telescope community's demands. To ensure close collaboration in this area, a Memorandum of Understanding (MoU) has been signed between HiPER and the European-Extremely Large Telescope (E-ELT) project (along with the ELI laser project).

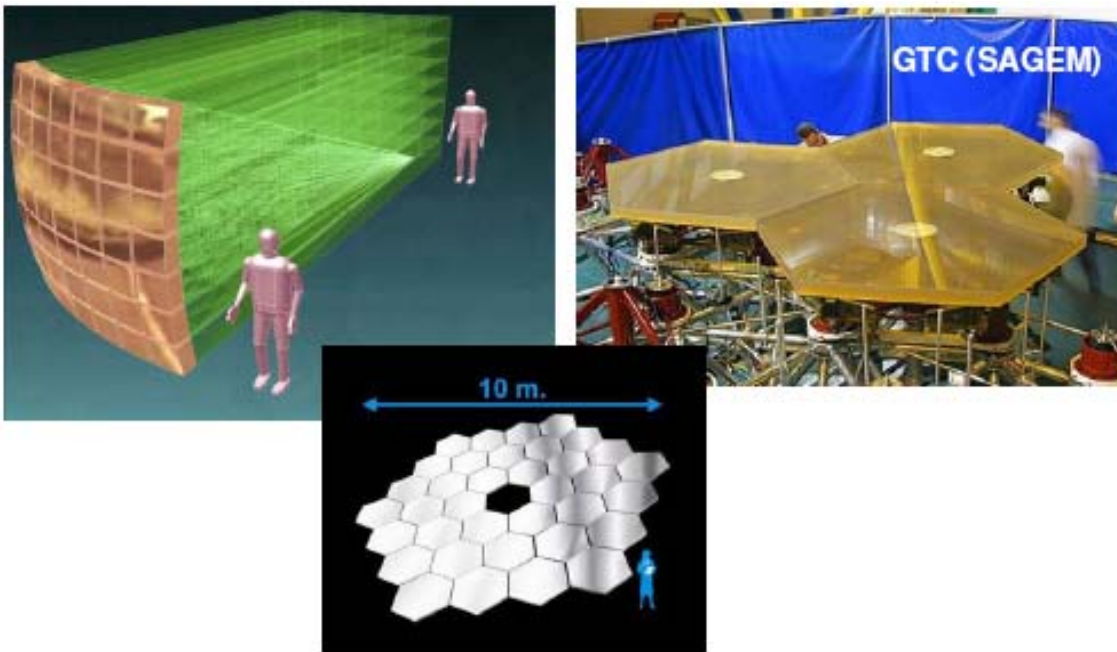


Figure 13.2: a) schematic of the multi-segment focusing optic for HiPER. b) Mirror segments undergoing final polishing at SAGEM REOSC for the GTC telescope. c) Overall size of the primary mirror on the GTC Telescope made up of 36 segments.

Ignitor beam frequency conversion: Requirements for the optimum wavelength of the short-pulse ignition beam are less well defined at present and will be determined by the experimental campaigns in the forthcoming months. The most promising option seems to be the second harmonic wavelength, 527 nm. The issue then arises as to which wavelength the pulse compression occurs at i.e. will HiPER frequency convert prior to compression or compress the pulse prior to frequency conversion. The first option would require significant effort to develop gratings with sufficiently high laser damage threshold at 527 nm. The second option would use previously developed pulse compression grating technology but would require only few mm thick Potassium Di-hydrogen Phosphate (KDP) frequency doubling crystals having sufficiently good transmitted wavefront quality. With the very high intensities involved in the short pulse these KDP crystals would be highly likely to damage and would also produce significant beam break up, affecting the quality of the focal spot achieved.

Dielectric gratings of sufficient size have been extremely difficult to obtain in previous years but the investment in large aperture lasers, specifically FIREX and OMEGA EP has resulted in a considerably increased capability. There are potentially three major suppliers of gratings with the capability to supply gratings of the appropriate specifications for HiPER: LLNL, Plymouth Grating Laboratories, and Jobin-Yvon. Progress in the past few years in production of gratings for the Omega EP laser at the University of Rochester and the FIREX laser at the University of Osaka has resulted in increased confidence that these components will not be a major source of concern in the timeframe of HiPER construction.

13.4 Technical Industrial Engagement

The HiPER project has engaged with suppliers in wider industrial fields linked to the project including suppliers of high power diode stacks, manufacturers of optical production equipment, high voltage equipment suppliers for capacitor banks, solid state laser manufacturers, Pockels cell driver unit manufacturers and flashlamp suppliers. A summary of current contacts for technical components is provided in the table below. Other links (e.g. to project management, civil design and construction, etc) are not reproduced here.

<i>Industrial partner</i>	<i>Previous expertise</i>	<i>Potential supplier of:</i>
<i>AMTRON GmbH</i>	<i>LULI and Max Born Institute</i>	<i>Control and supply systems of high power laser diodes</i>
<i>Société Européenne de Systèmes Optiques (SESO)</i>	<i>Partnered with CEA on LMJ. Worked with LLNL. LULI, Osaka, RAL</i>	<i>High damage threshold optics, Direct off-axis manufacturing of mirrors, Serial production of large optics (lenses or plates);</i>
<i>DILAS</i>	<i>12 years experience in High Power Diode lasers</i>	<i>High Power Diode lasers – selecting, qualifying, testing</i>
<i>Hamamatsu Photonics KK</i>	<i>All major laser labs</i>	<i>Precision electronic and opto-electronic devices</i>
<i>Gooch and Housego PLC</i>	<i>Suppliers to NIF and LMJ</i>	<i>KDP and Quartz waveplates. General optics coated to withstand high laser fluences</i>
<i>CVI Technical Optics Ltd</i>	<i>All major laser labs</i>	<i>Fully customised complex optical components. Design and supply opto mechanical sub assemblies</i>
<i>Heraeus Noblelight Ltd</i>	<i>30 years experience in arc and flash lamp manufacture</i>	<i>Flash lamps</i>
<i>Kentech Instruments Ltd</i>	<i>All major laser labs</i>	<i>Pockel cell drivers. X-ray streak cameras, waveform generators for laser pulse shaping</i>
<i>Cleveland Crystals Inc</i>	<i>Supplier to NIF and LMF, LIL projects</i>	<i>KDP and KD*P crystals. Plasma electrode pockel cell crystals</i>
<i>Corning Inc</i>	<i>Involved in PHELIX, LMJ, LIL, NIF</i>	<i>Synthetic Fused Silica blankets</i>
<i>Glassman Europe Limited</i>	<i>All major laser labs</i>	<i>High voltage DC power supplies, HV dividers for accurate measurement</i>
<i>Saint-Gobain Ceramics</i>	<i>LMJ, LULI, GSI</i>	<i>Flash lamps</i>
<i>Plymouth Grating Laboratory</i>	<i>ILE, LLE</i>	<i>Gratings and Diffractive Optics</i>
<i>SAGEM - REOSC</i>	<i>LMJ</i>	<i>Refining the specification of optical components (mirrors, parabola, lenses</i>
<i>HOYA</i>	<i>LMJ, NIF</i>	<i>Laser glass</i>

<i>Horiba Jobin Yvon</i>	<i>All major laser labs</i>	<i>Large aperture dielectric gratings</i>
<i>Tinsley</i>	<i>25 years experience and supplier to NIF, Omega, LMJ</i>	<i>Optical finishing processes</i>
<i>Thales</i>	<i>All major laser labs</i>	<i>Solid state lasers, power and nanosecond pump lasers</i>
<i>JENOPTIK Laser</i>	<i>IST, MPQ, Jena</i>	<i>Diode laser pump modules and pump optics. Optics for beam line configurations</i>
<i>OpTIC</i>	<i>Telescope Industry</i>	<i>Optronics technologies, capability in large optical surfaces and laser equipment</i>

Table 13.1: List of technical companies approached in support of the HiPER project.

13.5 Conclusion

The HiPER project can reduce the risk associated with designing a laser system from the ground up by basing the system design on the NIF and LMJ designs. By engaging supply companies at an early stage issues associated with NIF and LMJ standard optics can be readily resolved. It is essential the HiPER project adapts as much as it can from other branches of science for the Ignition beamlines.

The prior 2-year design phase has already established key industrial contacts in the technical and project delivery areas. This preparatory phase will see the formalisation of these links to ensure low-risk passage to the subsequent construction phase.

References for chapter 13

- [1] The National Ignition Facility: enabling fusion ignition for the 21st century, George H. Miller et al 2004 Nucl. Fusion 44 S228-S238
- [2] The Laser Mégajoule (LMJ) Project dedicated to inertial confinement fusion: Development and construction status, Noël Fleurot, Claude Cavailler and J.L. Bourgade Fusion Engineering and Design, Volume 74, Issues 1-4, November 2005, Pages 147-154, Proceedings of the 23rd Symposium of Fusion Technology - SOFT 23
- [3] Laser Challenges for Fast Ignition, FUSION SCIENCE AND TECHNOLOGY. Volume 49 · Number 3 · April 2006 · Pages 453-482. J. D. Zuegel, S. Borneis, C. Barty, B. Legarrec, C. Danson, N. Miyanaga, P. K. Rambo, C. Leblanc, T. J. Kessler, A. W. Schmid, L. J. Waxer, J. H. Kelly, B. Kruschwitz, R. Jungquist, E. Moses, J. Britten, I. Jovanovic, J. Dawson, N. Blanchot
- [4] Hoya Corporation USA, 3400, Edison Way, Fremont, CA 94538-6190, USA
- [5] Schott Glass Technologies Inc, 400 York Avenue, Duryea, PA 18642, USA
- [6] Shanghai Institute of Optics and Fine Mechanics (SIOM), Chinese Academy of Sciences, PO Box 800-211, Shanghai 201800, P.R.China
- [7] Ligne d'Integration Laser (LIL), <http://www-lmj.cea.fr/html/rubrique231.html>
- [8] HORIBA Jobin Yvon SAS, 16-18 rue du Canal, 91165 Longjumeau Cedex, France
- [9] Lawrence Livermore National Laboratory, PO Box 808, Livermore, CA 94550, USA

- [10] Plymouth Grating Laboratory, 70 Industrial Park Road, Plymouth, MA 02360, USA
- [11] Carl Zeiss GmbH, Goeschwitzer Str. 51 – 52, 7740 Jena, Germany
- [12] General Atomics, 10240 Flanders Court, San Diego, CA92121, USA
- [13] 2X1 prototype plasma-electrode Pockels cell (PEPC) for the National Ignition Facility, Rhodes, Mark A.; Fochs, Scott N.; Alger, Terry W. Proc. SPIE Vol. 3047, p. 203-206, Solid State Lasers for Application to Inertial Confinement Fusion: Second Annual International Conference
- [14] Status of the OMEGA EP High-Energy Petawatt Laser Facility, Stoeckl, C. et al, American Physical Society, 48th Annual Meeting of the Division of Plasma Physics, October 30-November 3, 2006, abstract #NO3.001
- [15] 10-kJ PW laser for the FIREX-I program, Miyanaga, N. et al, Journal de Physique IV (Proceedings), Volume 133, Issue 1, June 2006, pp.81-87
- [16] The design of the Keck Observatory and Telescope, Keck Observatory Report no.90, 1990
- [17] Gran Telescopio CANARIAS, Conceptual Design, GTC project document GEN/STMA/0012-L, 1997
- [18] SAGEM SA, REOSC Department, Avenue de la Tour Maury, 91280 Saint Pierre du Perray, France
- [19] Gran Telescopio CANARIAS: current status of its optical design and opto-mechanical support system, GTC project document PUB/OPTI/0013-L

14 The HiPER Building

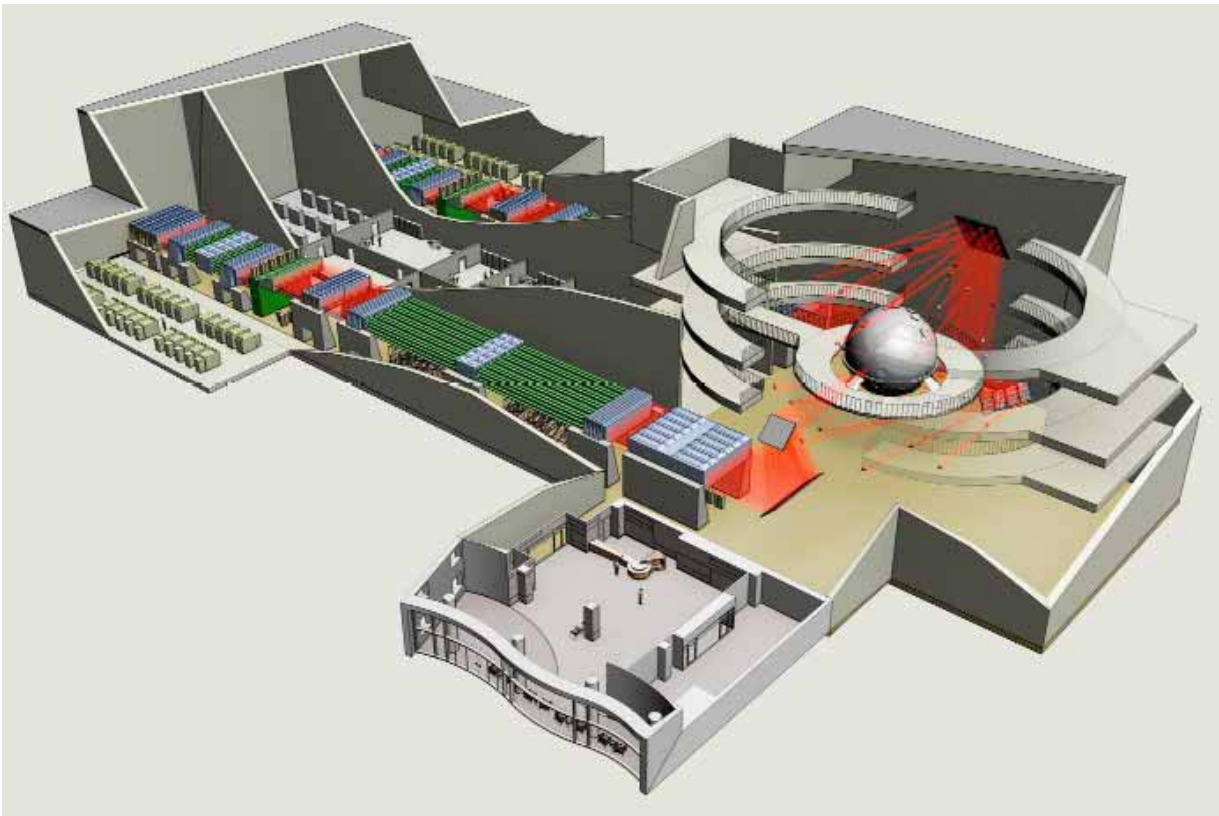


Figure 14.1 Aerial Schematic of HiPER

14.1 Introduction

A conceptual design of the HiPER building has been produced during the 2-year design phase. The detailed layout and design of the buildings and utilities await ratification of the final specification (due in this preparatory phase). This section lays out the current conceptual design.

This baseline is site non-specific. It assumes that there are no HiPER related scientific or support buildings readily available, but that any chosen site will have a general level of local facilities that the HiPER project will not have to provide i.e. roads, services, security, restaurant, engineering, hostels etc. Of course if other buildings on the finally chosen site can be used or adapted for HiPER specific activities then this would reduce the scope of what is finally built by the HiPER project.

There are two comparable large laser systems being constructed worldwide, NIF in the USA and LMJ in France. This HiPER initial baseline design has been based on information and experience gathered on these facilities.

	NIF	LMJ	HiPER
Beams	192	240	60
Laser Bays	2	4	2
Target Areas	1	1	At least 2
Length	600ft (183m)	300m	~200m
Width	400ft (122m)	100m	~75m
Height	85ft (26m)	35m	~30m
Optics Assembly Building	25,000-square-ft		
Estimated Cost	\$260 million	€300 million	~€150 million
Temperature Stability	one-half degree Fahrenheit (0.3°C)	21 ⁰ C ±0.3	21 ⁰ C ±0.3
Target Chamber diameter	33ft (10m)	10m	10m
Radiation shielding	6ft (1.8m) concrete walls	1m concrete walls at 33m ø and 2m at 50m ø.	~ 3m concrete walls

Table 14.1 Comparison of main features between NIF, LMJ and HiPER

	HiPER
Stability	1µm
Laser Floor Slab	~0.5-1m thick
Cleanliness–laser room	ISO 8 (Class 100,000)
Cleanliness-switchyard	ISO 7 (Class 10,000)
Capacitor Bank	~5MW, 100MJ
Target Area	~40m diameter

Table 14.2 Additional parameters for HiPER Buildings



Figure 14.2 Aerial view of NIF

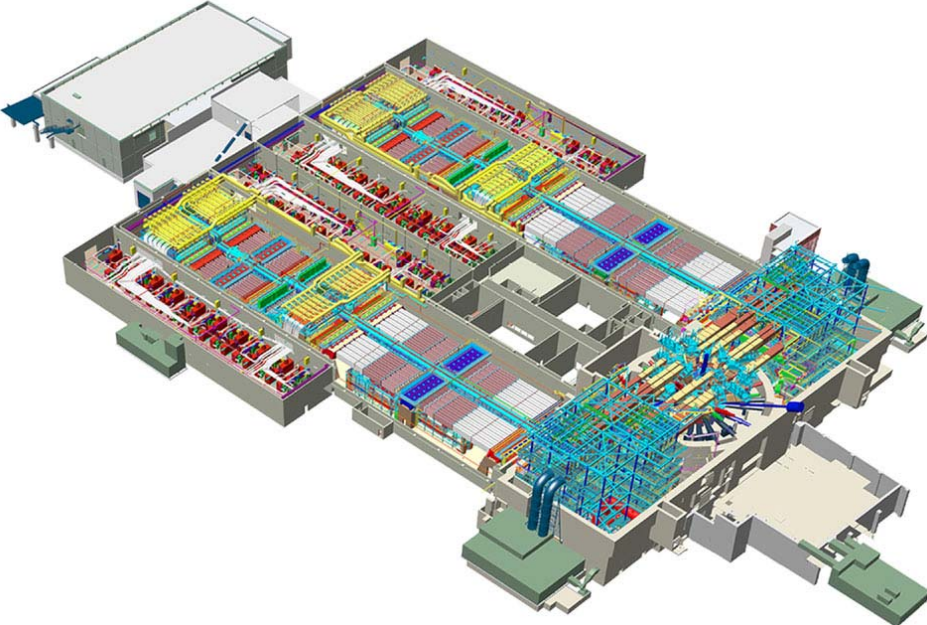


Figure 14.3 Aerial Schematic of NIF

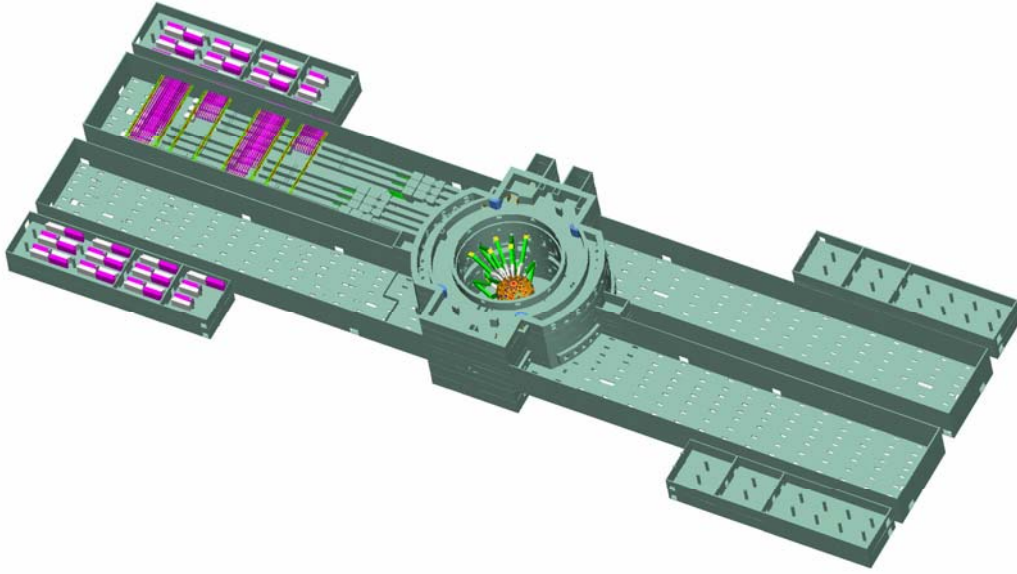


Figure 14.4 Aerial Schematic of LMJ



Figure 14.5 Aerial schematic of LMJ building

14.2 Technical requirement for HiPER buildings

14.3 Laser Building

The laser building has been designed to consist of 2 laser bays with central front end and control rooms between them and outer capacitor bank rooms. Each bay will require a large (~10T) crane plus floor space for laser equipment removal and replacement. The demanding requirements of the HiPER laser and target systems lead to unusual features in their buildings. The lasers must be pointed very precisely. This pointing precision contributes to a number of unusual requirements relating to stability and vibration for the Laser Building. For stability, the laser system should probably be supported on concrete pedestals that are mounted on thick (~.5 - 1m) single-pour concrete slabs which are decoupled from the walls and foundations of the building. The laser building needs to be temperature-controlled to maintain laser positioning. This in turn requires a high number (~15) of full air changes per hour and sophisticated air-handling systems that have very low vibration. This will probably be high level air input through the ceiling (~50% of area) with air return through the floor into plenums below the floor.

14.4 Target Area Building

The baseline design for HiPER is to accommodate up to four target areas:

- Main Fusion Energy area (all beams). Priority 1.
- A Fundamental Science area (all short pulse beams plus a long pulse cluster). Priority 1.
- High Rep Rate area for fusion technology development. Priority 2.
- High Rep Rate area for diagnostics testing. Priority 3.

This multiple target area requirement will add significant complexity in the laser switchyard although of course there are considerably less beams than for NIF / LMJ.

For the baseline (NIF/LMJ-technology) design of HiPER (see section 9), there are several options for the single beam, high repetition rate (DPSSL) areas (i.e. for the diagnostics and fusion technology applications). It is conceivable that one or both of these capabilities are accommodated in a staged fashion, perhaps even at a remote site to maximise scientific advantage (e.g. coupled to an accelerator source).

The Target Area Building will contain the high steel structures switchyard that hold the large turning mirrors to direct the laser beams toward the target. Because the Fundamental Science Target Area in particular will require considerable flexibility of beam delivery this complexity will need to be built into the switchyard. These switchyard structures must be very stable and resistant to vibration and will probably have at least five floors for access to the chamber, input optics, target inserters, diagnostics etc. Consequently, the steel structures will be robust, and anchored into the building, resulting in a very stiff structure. At the centre of the main Fusion Target Area Building will be a large diameter (~10m) target chamber. For stability reasons, the target chamber support pedestal will be an integral part of the Target Area Building concrete structure. This concrete structure includes thick (~3m) walls surrounding the chamber for radiation protection with compensating shielding doors or labyrinths where entry is required.

14.5 Additional Buildings

Additional building and facilities will be needed, for example:

- A separate Utilities Building will isolate the precisely pointed lasers from the vibrations and thermal impact caused by utilities that the facility will need such as power, cooling and hot water, air conditioning, de-ionised water, He, N₂, Vacuum, Ar and compressed air;
- An Optics Assembly Building with a large receiving area and connected clean rooms will be needed to receive optics and laser components, test them, store them and consequently assemble the components in rooms with stringent cleanliness controls and
- Local Offices, Flashlamp and Amplifier Test, Data Analysis, Computer, General lifting and moving equipment, Fork Lift Trucks etc, R&D Labs, Laser and Target Diagnostics Labs, Materials and Damage Testing facility, Radiological handling & storage areas, Target Fabrication, Target Assembly/Characterisation Lab, Cryo Lab, On or off site DT filling Lab and Storage Areas.

14.6 Siting Issues

As mentioned above, this baseline is site non-specific. When choosing the final location for HiPER a number of issues will need investigating for example: current infrastructure, availability of existing buildings for HiPER use, geotechnical stability, of ground, other local sources of vibration. Local planning permissions etc., nuclear safety and any other local rules will need to be addressed as will the decision for the location of DT facilities.

15 Operational Analysis

The primary task in the design of a large facility such as HiPER is the necessity to precisely define the needs and objectives required for the investment. This must include the performance of the facility in order to reach the required science goals, but also the available budget for the construction and the operational phase (without forgetting decommissioning), the operational organisation, the machine survey and maintenance and the available manpower.

The final system will be a trade off of all above parameters, analysed using a detailed performance-cost model. This need to be built with independent parameters defining the life cycle of the facility. In addition a complete risk analysis is necessary to reach a realistic picture: scientific, technical, industrial, manpower (skills), organization and political, etc.

Many of the fundamentals of this approach are common to all large facilities, and indeed in the case of HiPER, much overlap can be expected with the detailed analysis performed for other large laser facilities.

The life cycle profile describes the following parameters for each type of activity to be performed:

- the occurrence
- the period when it occurs
- the duration
- the associated system configuration
- the goal of the system for this activity

From the above description, one can extrapolate:

- the parameters to manage the availability and maintainability
- the parameters to manage the operation cost

The life cycle profile is derived from:

- the users needs
- the operational constraints

The operational analysis of a large laser facility requires the following parameters to be defined:

- the diagnostics configurations (type, number and position)
- the target types (cryogenic, radioactive, etc)
- the laser parameters: number/campaign, the ratio of successful shots required, the laser performance (energy, intensity, symmetry, smoothing, number of beams ...)
- degraded modes

Practically for a facility like HiPER, specific characteristics should be taken into account. These could include:

- The goal : to achieve inertial fusion with fast ignition and a laser driver (this includes cryogenic targets and laser specifications)
- The operating consequences : radioactivity in experimental areas which lead to radioprotection and safety procedures which may forbid access
- The physics goal requires specific energy and power levels from the laser system. This induces a design trade off to determine the intensity per beam (for both compression and ignition beams). The optics damage phenomena which is proportional to intensity, will lead to optics maintenance criteria impacting on operational cost and availability of the machine.

- Number of calibration shots needed
- The shot cycle duration
- The number of shifts/day
- The activities which cannot be done simultaneously

Once the life cycle profile is determined with some assumptions for the operational parameters, one can define the system availability, from which is allocated the equipment availabilities. This impacts the equipment design and the integrated logistic support (ILS) from which equipment reliability and maintenance tasks can be described.

The following iterative model can be set up.

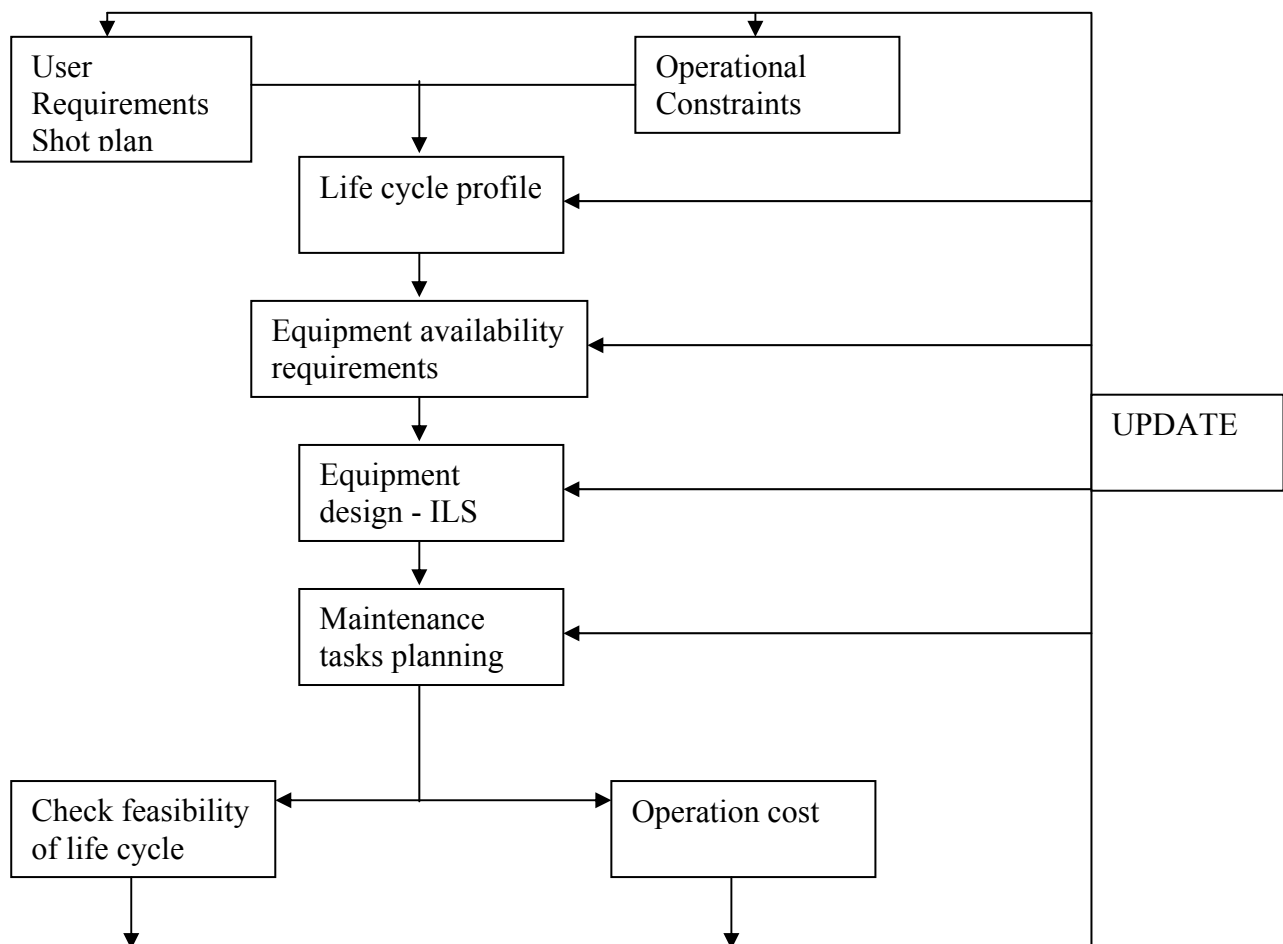


Figure 15.1 Operational analysis model

During the preparatory phase it will be necessary to develop and adapt the model to optimise the technical design, the performance, operation and management of the HiPER facility. It will be possible to derive the method from existing facilities and in particular drawing from the experience within CEA.

16 Participants and Support

HiPER is an international project that benefits from the involvement, either formally or informally, of partners drawn from Europe, Asia and North America.

16.1 Formal Participants of the HiPER project



Figure 16.1 Map of Europe indicating the countries where institutions have signed up as formal participants of the HiPER project. Note that USA is involved through the formal participation of General Atomics (GA)

Of the formal participants approximately half are engaged at the funding agency or ministerial level and almost all of the partners are providing significant levels of co-funding to advance the HiPER mission. The HiPER partnership strikes a healthy balance between the political engagement necessary to move key decisions forwards and academic engagement to principally address risk issues. Other European and International partners are involved due to their specific expertise in key areas. Great care has been taken during the 2-year design phase to select a balanced team capable of taking on the challenge of the preparatory phase project. Details of the formal participants are presented below

European Commission - The European Commission is formally the contracting body for the HiPER Preparatory Phase Project. However, the preparatory phase process is very much one of building partnerships and thus the existing relationship between the HiPER consortium and the EC is much more one of parity and proactive engagement, rather than a traditional one of customer-supplier. In the preparation of the HiPER proposal this positive and active engagement from the

Directorate General for Research Infrastructures, as a partner, has been very welcome and we fully expect this to continue during the preparatory phase. The EC brings considerable political and strategic advice which the HiPER mission will benefit greatly from. It also provides the basis for engagement with other European agencies, for example, the European Investment Bank (EIB) which will be vital for the financial engineering aspects of HiPER

United Kingdom – the project benefits from the formal involvement of the Science and Technology Facilities Council (STFC). This funding agency has the main responsibility within the UK for all strategic investments in major scientific infrastructures. It operates and develops a wide range of large scale infrastructures that include the world renowned Rutherford Appleton Laboratory (RAL), which includes the UK's High Power Laser programme, the Central Laser Facility (CLF). Access to the CLF as part of the HiPER mission has been formally agreed by STFC. UK academia is also heavily involved in the HiPER project and this is also represented by the STFC involvement. The STFC has formally endorsed the project and has agreed to take the lead and co-ordinating role in the HiPER preparatory phase project. This level of engagement in the HiPER mission enables the STFC to credibly provide the strategic leadership that will be needed to advance the HiPER mission.

France – the engagement of France in the HiPER project is very substantial. Both of the major national funding agencies in France – the Commissariat à l'Énergie Atomique (CEA) and the Centre National de la Recherche Scientifique (CNRS) are formal participants of the project and are fully engaged at the highest levels of their respective organisations. Support for the HiPER mission in France has been formally secured at ministerial level. This level of political engagement of France in the HiPER mission has and will continue to be absolutely vital to its success.

The CEA has developed near Bordeaux (CEA-CESTA) over the last decade or so the Ligne d'Intégration Laser (LIL) and the multi-billion Euro Laser MégaJoule (LMJ) systems that are central pillars of its national strategy to advance the Inertial Confinement Fusion concept. It therefore brings to the HiPER project unrivalled expertise within Europe. The HiPER strategy relies very heavily on leveraging this expertise and the huge defence programme investment it represents into the civilian arena for the pursuit of fusion energy through the HiPER mission. The CEA's technical and political involvement is substantial and they are formally prepared to make available to HiPER people, information, technology, costs etc that will be crucial to developing HiPER. The CEA also provides an important portal to French industry that has developed most of the technology for LMJ.

Moreover, the local regional funding agency, the Conseil Régional d'Aquitaine (CRA) in conjunction with the French government, has recently invested more than 40 M€ in the PETAL enhancement to the LIL system to explore the fast ignition approach to Fusion Energy. CRA as a funding agency is also a formal partner in the HiPER project. Access to the PETAL system will be a key element of reducing risk within the HiPER project and crucially, in recognising the importance of the PETAL system to the HiPER mission, the CEA and CRA have agreed to the reconfiguration of PETAL system as per the needs of the HiPER project. An international panel of experts has thus recently been appointed to advise on the exact nature of this.

Furthermore, the CNRS and CEA support the operation and development of the Laboratoire pour l'Utilisation des Lasers Intenses (LULI) in Paris where some of the most advanced facilities in the world for experimental laser-plasma physics exist. Access to these facilities and the expertise contained therein will also be crucial for risk reduction in the HiPER mission. This access has now been formally agreed. Finally, both agencies support the Centre Lasers Intenses et Applications at the University of Bordeaux-I (CELIA) which hosts one of the worlds leading theoretical and computational plasma physics teams. This team has been placed at the disposal of the HiPER mission and will be important in developing target point designs for HiPER.

It has been agreed between these three agencies (CEA, CNRS, RA) that all HiPER related activity will be co-ordinated and managed by the Institut Lasers et Plasmas (ILP) in Bordeaux. ILP is the

coordinating Institute in France for research in lasers and plasmas. It officially represents the associated laboratories working on these subjects from CNRS, CEA, University Bordeaux1 and Ecole Polytechnique.

Italy – The HiPER preparatory phase project benefits from the formal support of the Italian Science Ministry, the Ministero dell' Università e della Ricerca (MUR). This enables two of the primary national scientific funding agencies of Italy, the Consiglio Nazionale delle Ricerche (CNR) and the Ente per le Nuove Tecnologie, l'Energia e l'Ambiente (ENEA) to be formal participants of the HiPER project. In particular, CNR supports the Intense Laser Irradiation Laboratory (ILIL-CNR) which is focused on fundamental aspects of high-intensity laser interactions with matter. Studies of direct relevance to inertial fusion are also performed at ILIL within a Ministry of University project (MIUR-FIRB-BLISS), coordinated by ILIL. ENEA hosts a laser laboratory which has pioneered the field since the mid 60's. Finally, the project benefits from the formal participation of the Universities of Rome "La Sapienza", Milan-Bicocca and Pisa through the Consorzio Interuniversitario per le Scienze Fisiche della Materia (CNISM). It brings considerable academic expertise in theoretical and experimental laser-plasma and inertial fusion physics, including the advanced models and codes used for defining the HiPER parameters. These collaborating university groups are partly funded by national competitive programmes (MIUR-PRIN) on intense laser interaction and also participate in the above quoted FIRB-BLISS project

Spain – Spain's formal participation in the HiPER project at funding agency level has been agreed through the support of the Ministerio de Educacion Y Ciencia (MEC), as well as at regional funding agency level through the formal support of the Direction General for Universities And Research, Comunidad Autonoma de Madrid (CAM). This national and local ministerial level involvement is to be formally delegated to the Universidad Politécnica de Madrid (UPM) which will represent the Spanish interest in HiPER as well as bringing to the project crucial skills and capabilities. This includes some of the most advanced computational modelling of ICF and fast ignition physics at the Grupo de Investigación en Fusión Inercial (GIFI) which has formed the basis of the preliminary specification of HiPER. Furthermore, key target design and fabrication issues, materials studies and understanding the physics of technology for inertial fusion energy which are vital to the HiPER mission are enabled through the expertise at the Instituto de Fusión Nuclear (DENIM). The UPM is also an access portal to one of the world's most powerful supercomputers, MARENOSTRUM in Barcelona as well as MARGARIT supercomputer in Madrid. Access to both systems will be made available to the HiPER project through the UPM

Czech Republic – The Ministry of Education, Youth and Sports (MSMT), as a funding agency, are formal partners to the HiPER preparatory phase project. Execution of the Czech participation will be through the Academy of Sciences of the Czech Republic (CAS). The CAS operates and develops the Prague Asterix Laser System (PALS) and is one of the leading experimental facilities in Europe for laser plasma interactions. Access to this system will be made available for HiPER related work and a formal agreement covering this is now in place.

Greece – The participation of Greece in HiPER has been secured at funding agency level through the formal involvement as partners of the General Secretariat for Research and Technology (GSRT). Furthermore, the HiPER project benefits from the participation of the Technological Educational Institute of Crete (TEI) and the Technical University of Crete (TUC) who bring valuable expertise in experimental plasma physics and diagnostics.

Portugal – The Portuguese Science Ministry, the Fundação para a Ciência e a Tecnologia (FCT) has formally agreed to its involvement at a funding agency level as a partner to the HiPER project. Furthermore, the Instituto Superior Técnico, Universidade Técnica de Lisboa (IST) will be a formal partner in HiPER thereby securing the involvement of some of the world's foremost computational plasma scientists.

Poland – Poland will participate in the HiPER project through the formal involvement of the Institute of Plasma Physics and Laser Micro-fusion (IPPLM) in Warsaw. The institute has many

years experience in laser plasma interactions and will concentrate on a variant of the fast ignition concept – proton fast ignition. Participation of the Polish Ministry of Science and Higher Education is currently being negotiated. Their future involvement could release additional national funds.

Germany – The involvement of Germany is through the participation of the Gesellschaft für Schwerionenforschung mbH (GSI) and the Technische Universität Darmstadt (TUD). GSI is a large organisation that is home to the PHELIX High Power Laser system. PHELIX is unique internationally in that it is coupled to a heavy ion accelerator and thus will offer major experimental opportunities both in fast ignition physics and other areas of Warm Dense Matter (WDM). This is complemented by the TUD who have significant expertise in WDM and target fabrication

Russia – Two institutes of the Russian Academy of Sciences are formal participants. These are the Institute of Applied Physics (IAP-RAS) in Nizhny Novgorod and the Quantum Radiophysics Division of the P.N. Lebedev Physical Institute (LPI) in Moscow. The involvement of these two partners brings access to the considerable resources of the RAS, and in particular advanced large aperture laser technology (IAP-RAS) and target design and fabrication (LPI)

United States of America – General Atomics Inc. (GA) is the world’s leading organisation for the manufacture of ICF targets. Their role in developing and producing the specialist cone targets required for the fast ignition approach to ICF will be absolutely vital to the credibility of the HiPER mission. There is no other organisation worldwide that has the necessary skills or technology to make such targets to the specifications required in the timescale needed. This is reflected in many ways in the close working relationship that exists between GA and the CEA in France. The involvement of GA in the HiPER project brings key advantages as it will both enable HiPER to benefit from the many years of investment this expertise represents and will, through closer working, stimulate the growth of a European capability in this crucial area.

16.2 International Partnerships

The following international partner countries are also involved in the HiPER project through the involvement of the listed institutes

Asia



Figure 16.2 Current Asian nations with institutions involved in HiPER

Korea – The Korean Atomic Energy Research Institute (KAERI) are supporting the HiPER mission and we fully expect a bi-lateral agreement between HiPER and KAERI once the HiPER project is launched. Collaborative access to their facilities and linking to their research programme has already been agreed. Korean Government funds to advance this collaboration are being sought.

China – Support for the HiPER project from China is strong. Formal agreements are planned once the project receives the go-ahead. A UK-China agreement has recently been signed which significantly aids this process and has already led to Chinese involvement in HiPER related science projects in the UK. As well as an obvious academic benefit, this will also open up alternative supply routes for key components, thereby reducing future risk. We have secured the formal engagement, at the highest levels, of the Chinese Academy of Sciences (CAS), Shanghai Jiaotong University (SJU), and the Shanghai Institute of Optics and Fine Mechanics (SIOM).

Japan – Academic collaborative links to Japan on laser fusion science are naturally very strong given the leading role that the Institute of Laser Engineering (ILE) at Osaka University has played in recent years. The ILE are very strong supporters of the HiPER mission and bi-lateral agreements are in place between the ILE and several of the European partners involved in HiPER. Continuation of this collaboration is already planned, which opens up access to the FIREX laser facility at the ILE for HiPER related work. The FIREX facility is a major laser infrastructure dedicated to the pursuit of the fast ignition approach to inertial fusion energy.

North America



Figure 16.3 Current North American nations with institutions involved in HiPER

Canada – Formal agreements are in place linking HiPER to the emerging fusion programme in the Alberta province of Canada. This is represented through the involvement of the University of Alberta (UofA) in the HiPER mission who are currently midway through a process of securing substantial funds for a Canadian Laser Fusion programme. Secondment of Canadian scientists to the HiPER partners in Europe is being planned as part of the early stages of this programme.

USA – It is expected that the strong link to the USA will see the secondment of EU personnel working on the HiPER project to the Lawrence Livermore National Laboratory (LLNL) as well as to GA (a formal partner) to facilitate critical technology transfer. Early engagement with the US Department of Energy, Office of Fusion Energy Science (DOE - OFES) has indicated a strong desire to align their science programme with HiPER as part of our long-term goal of a fully international roadmap.

16.3 Other Partners

Industrial Links – Working with industrial partners will be a central issue during this preparatory phase to ensure costs are well known and supply routes are available for the construction of HiPER. Already, there has been a significant engagement with many potential industrial stakeholders in HiPER and this will continue during the preparatory phase (see previous chapter on industrial engagement)

Other Preparatory Phase Projects – There is much to be gained during the preparatory phase through working with the other projects. This applies equally to technical and scientific issues, as well as those related to strategic, governance, financial engineering and legal aspects. Furthermore, there is the potential for both risk and cost sharing in places. We propose to work with other

projects and have already signed two Memoranda of Understanding (MoU) covering these issues with the Extreme Light Infrastructure (ELI) and the European Extremely Large Telescope (E-ELT). In a similar fashion we have signed an MoU with the Laserlab-Europe Integrated Infrastructure Initiative.

16.4 Forward plan

Critical to the success of this next preparatory phase will be to convert the significant support already obtained from these nations and organizations into commitment for the construction phase. This will require a robust cost-benefit analysis, clarity in the through-life funding mechanisms and sources, an agreed framework for the accountabilities and responsibilities that follow from funding, an achievable procurement strategy, an agreed site, and a detailed understanding of how HiPER will impact the existing science and energy communities and facilities. The project also needs to ensure coordination between the fundamental building blocks of a laser fusion energy programme (the laser source; the target supply; the reactor design; and the inherent plasma physics) and management of key risks in these areas that could threaten construction.

The project has addressed these critical areas in designing the management structure, work plan, deliverables and milestones for the forthcoming preparatory phase.

Appendix 1: Full-Scale Fusion Reactor Chambers (Background Material)

CONCEPTUAL REACTOR DESIGNS

HY-II.- HYLIFE-II design

HY-II.1.- Introduction

More than two decades ago, the researchers of Lawrence Livermore National Laboratory devised a reaction chamber with a thick liquid lithium array of jets that were injected between the explosions and the chamber walls. The liquid served to attenuate fast neutrons before they strike the chamber walls, lengthening the lifetime of components, and also served to breed tritium fuel. This design was called HYLIFE, which stands for high-yield lithium-injection fusion energy. The other meaning implied by the name HYLIFE is the long life of the reactor chamber and components.

In 1991 the original concept was redesigned, incorporating enhanced safety features and re-examining all the conceptual designs of the plant components. The new design, called HYLIFE-II, replaced the liquid lithium with the molten salt flibe (Li_2BeF_4), thus eliminating the fire hazards associated with the use of lithium. An additional advantage of using flibe is the remarkable low solubility of tritium in it. HYLIFE-II uses a 5 MJ heavy ion driver to illuminate indirect-drive targets producing 350 MJ yield. The gain (defined as the ration of fusion energy out of a target to driver energy onto the target) is reduced from 400 in the original design to the modest value of 70 in HYLIFE-II.

This means that in order to maintain the nominal production of electrical power, the repetition rate must be increased from 1.5 to 6 Hz. Figure HY-II.1 shows the HYLIFE-II power plant. A circular recirculating induction accelerator delivers energy to the indirect-drive targets, producing six microexplosions per second and producing 940 MW of electrical power.

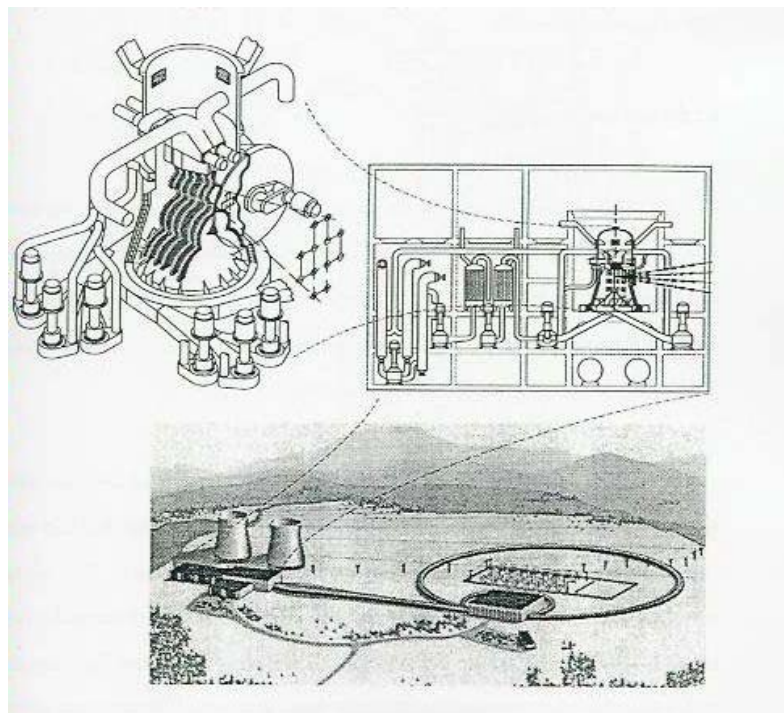


Figure HY-II.1. Conceptual design for the IFE power plant HYLIFE-II

HY-II.2.- Flibe flow circuits

The flibe shielding circuits inside the chamber include oscillating flow and steady flow (see Figure HY-II.2). The remaining inside circuit consists in spray nozzles. Flibe spray inside the vessel increases the liquid surface area to aid in vapour condensation after each shot. Two more flibe circuits are contained inside the blanket structure. They consist of a cooling circuit and a shielding circuit.

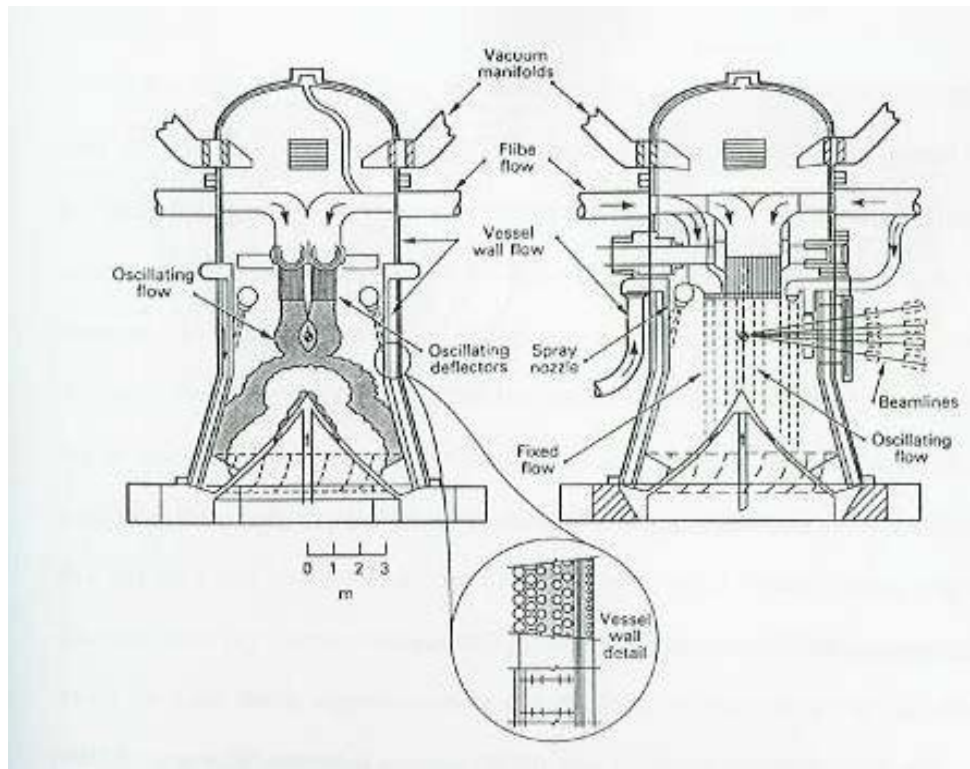


Figure HY-II.2. Reaction chamber in the conceptual design HYLIFE-II

The higher repetition rate requires careful attention to clearing of debris and liquid splash from the heavy-ion-beam paths between pulses. One way to achieve high pulse rate is to arrange for a short distance between the nozzles that inject the flibe and the microexplosion and to oscillate the jet nozzles horizontally as shown in Figure HY-II.3. As the pulse rate increases, the flow speed of the liquid out of the nozzles increases. This way, a pocket is formed in the flow where the target is injected and the microexplosion occurs. The inner pocket of flibe would flow at a rate of approximately 12 m/s.

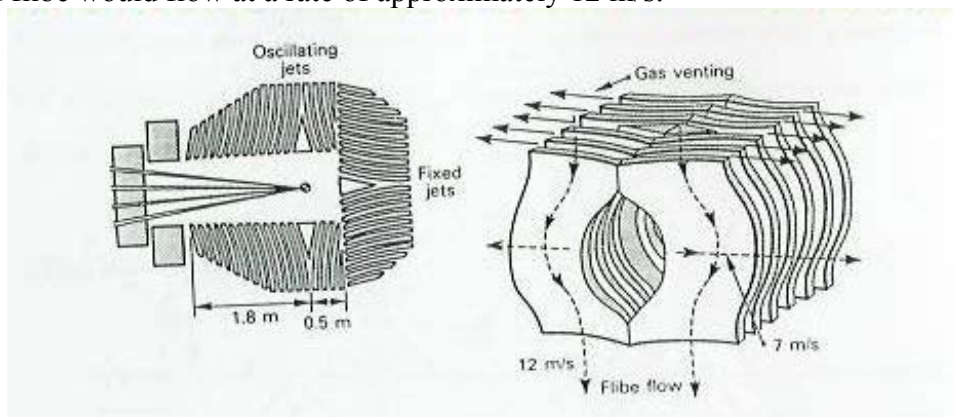


Figure HY-II.3. Fixed and oscillating flibe flow inside the HYLIFE-II chamber

Following the microexplosion, the resulting flibe splash must be cleared away enough to allow target injection and beam propagation for the next shot. It is the oscillating motion of the incoming liquid that sweeps away splashed liquid left over from the previous target ignition, and clears the region inside the pocket. The beam path outside the oscillating flow region will be cleared by the drag from the venting vapour formed in the previous microexplosion.

HY-II.3.- First structural wall and blanket configuration

The HYLIFE-II first structural wall (FSW) requires about 50 cm of flibe shielding in order to obtain a 30-year lifetime. The FSW/blanket structure is necessarily complex in order to satisfy several requirements such as serving as vacuum and tritium barrier and providing adequate heat transfer to the cooling system. In addition, it is subjected to severe cyclic pressure loads. The FSW/blanket structure consists of four distinct shells. Figure HY-II.2 also shows detail of the FSW and blanket assembly. Stainless steel type 304 (SS304) substitutes the stainless steel type 316 from the original design due to the identification of an incompatibility between flibe and the manganese in the original candidate for structural material.

The FSW is made from 10 cm diameter tubes with a 1.2 mm wall thickness. The tubes are separated by 2.5 cm spacer bars, which are 1.2 mm thick. An additional 50 cm of flibe provides shielding between the FSW and the second shell. Perforated rings are used to interconnect these two shells, providing the adequate hoop strength to the structure. The flibe between the FSW and second shell reduces the neutron heating and thermal stress in the second shell. Both the second and third shells are 2.5 cm thick and they are separated by a 2.5 cm gap. Flibe flowing in this annular space at 1 m/s velocity is used for cooling both shells. The region between the third and fourth shells is 10.2 cm thick and consists of a permeable insulation with a slowly flowing purge gas. The outer shell is a 1.6 mm thick container surrounding the entire FSW/blanket assembly. As for the outer shells, support rings are also used here to interconnect the structures and provide the needed strength.

HY-II.4.- Plant parameters

HYLIFE-II has a head recovery system with two main functions. The first one is to prevent splash and upward deflection of rapidly falling flibe streams. The second mission of this system is partial recovery of the dynamic head prior to the pump inlets. Through the appropriate use of vanes and diffusers, approximately 50% of the dynamic energy in the flibe would be recovered as it exits the chamber. Downwards moving liquid flibe would encounter the turning vanes where direction is changed to nearly horizontal. Liquid would then travel through the four diffusers on its way to the twelve bypass pumps.

Despite the particle recovery of the dynamic head, the flibe will still require a considerable amount of pumping power. From the total auxiliary power estimated to operate the HYLIFE-II reactor vessel, the main power requirement is for pumping the flibe. Also it has been calculated that the oscillating flow mechanism will need an 850 kW drive motor. Table HY-II.1 shows a summary of the plant parameters for the 1 GWe reference case and for an enhanced power case of 2 GWe. For accident analysis purposes the present work will focus on the 1 GWe case.

Table HY-II.1 Nominal plant parameters for HYLIFE-II: 1 GWe reference case and 2 GWe enhanced power case

	Reference Case: 1 GWe	Enhanced Case: 2 GWe
Driver energy (MJ)	5	6.7
Target gain	70	90
Yield (MJ)	350	600
Energy multiplication	1.18	1.18
Repetition rate (HZ)	6	7
Fusion power (MW)	2100	4220
Thermal power (MW)	2500	5000
Thermal efficiency (%)	43.0	43.0
Availability (%)	75.0	75.0
Gross electrical power (MW)	1075	2150
Recirculating power (MW)	135	216
Driver input power	85	134
Bypass pumping power ^a	32	46
Other pumping power ^b	18	36
Net electrical power (MWe)	940	1934

^aFlibe

^bIncludes pumping power in the heat transport system and steam generator

HY-II.5.- Plant component and layout

Figure HY-II.4 shows the plant layout up to the point where steam is generated for use in a conventional power plant. The flibe enters the steam generators at a temperature of 923 K (650°C) and leaves at 873 K (600°C). The most recent version of HYLIFE-II is based on an advanced supercritical steam cycle with improved efficiency of 43%. The efficiency of the

tritium removal system permits going from flibe to steam without an intermediate loop. The steam generators have double-walled tubes, which are chosen for increased reliability, minimizing water leakage into the radioactive flibe. The double-walled tubes also help decrease tritium migration into the steam; however, the greatest transport resistance is across the flibe film at the tube walls. A purge of helium flowing between the double-walled piping provides for the removal of the tritium that diffuses through the inner pipe wall.

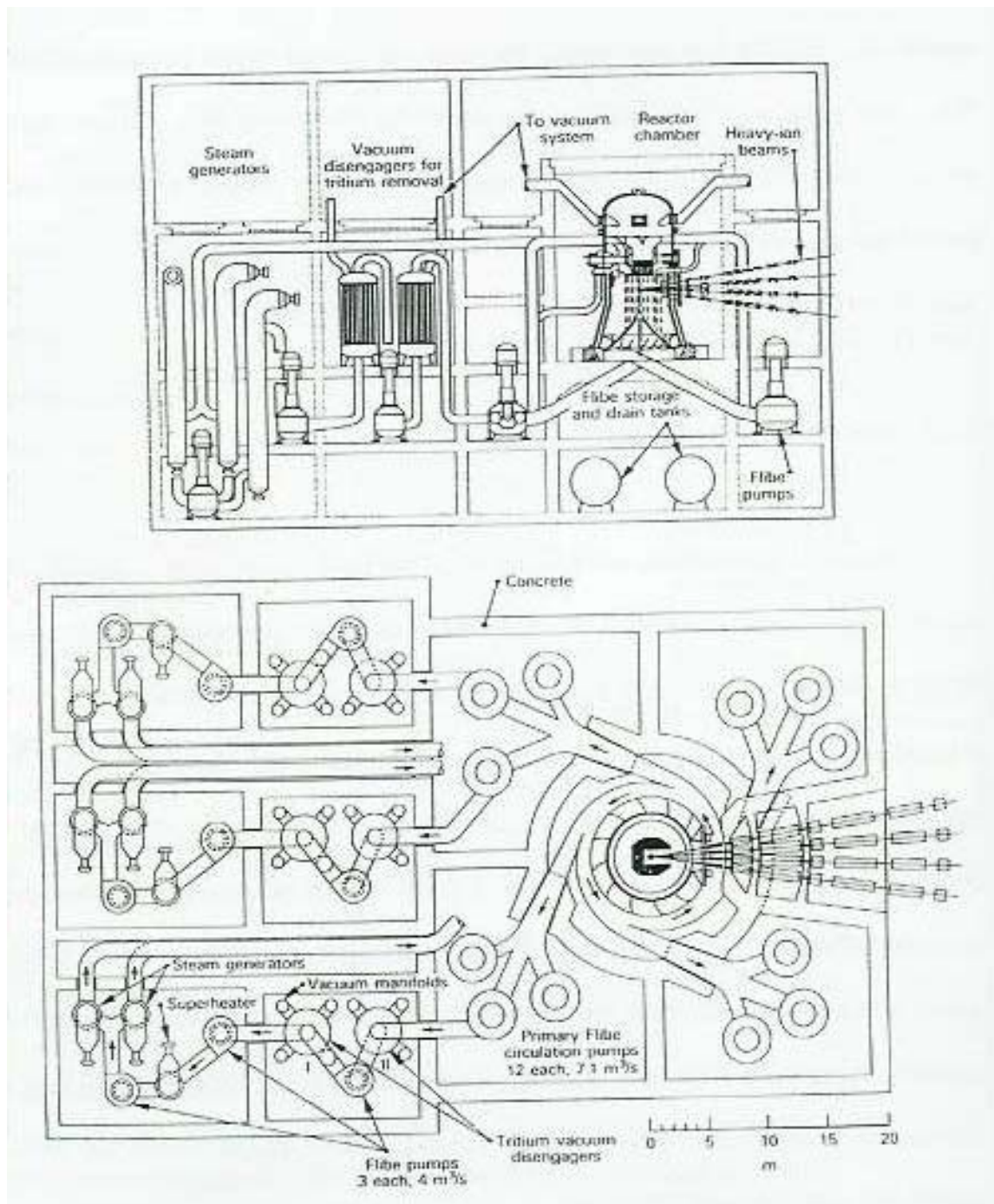


Figure HY-II.4. Elevation and plan views of the HYLIFE-II power plant layout

Practically all of the unburned tritium gas emitted by exploding targets will be removed by the vacuum pumps on the reactor chamber. In order to be conservative, it is assumed that almost none of the tritium produced in the flibe by neutron reactions with lithium will diffuse

out of the flibe while in the chamber. A vacuum disengager has been designed to remove the tritium from the molten salt coolant. The calculated tritium inventory in the 1240 m³ of flibe is as low as 0.5 g because of its low solubility in flibe. The disposition of two vacuum disengagers in series will reduce the tritium concentration in flibe by a factor of 10⁵.

It must be noticed that at this point there is not a definitive detailed design for some components of the power plant. Unlike other IFE designs, HYLIFE-II research has continued since the publication of the final report. For example, due to accelerator cost considerations, the original design including only 12 beams for target illumination has been modified, and the latest designs include a much larger number of beams, typically 160 to 192. The need to get to an agreement between accelerator designers, and still be able to guarantee a reasonable lifetime for the superconducting magnets using the appropriate shielding will be determinant to define a final self-consistent design for HYLIFE-II. Although the author has tried to include the most recent design information for this work, apologies are given in advance for any overlooked detail.

SOM.- SOMBRERO DESIGN

SOM.1.- Introduction

In 1990 the DOE Office of Fusion Energy commissioned the Sombrero IFE design study. A research team was assembled by W.J. Schafer Associates. This team consisted of Bechtel, General Atomics, Textron Defence Systems and the University of Wisconsin. The study began in late 1990, and it was about a year later, in early 1992, when the final report was published. The name of Sombrero comes from “solid moving breeder reactor”. Sombrero is a conceptual design study of a 1000 MWe KrF laser-driven IFE power plant utilizing direct drive targets in a near symmetric illumination configuration. The sixty beams of the KrF laser would deliver a total energy of 3.4 MJ to the target. The target yield would be 400 MJ for a gain of about 118. The required repetition rate would be 6.7 Hz.

The chamber is constructed of a low activation carbon/carbon (C/C) composite, and the blanket consists of a moving bed of solid Li₂O particles 300-500 μm in size flowing through the chamber by gravity. The particles are transported in a helium carrier gas at 0.2 MPa. This blanket configuration gives a breeding ratio of 1.25 and an energy multiplication factor of 1.08. The first wall is protected by 0.5 torr of xenon gas. Xenon is chemically inert and has a high x-ray absorption cross section. The xenon gas would absorb the energy from the target x-rays and debris and reradiate it to the first wall (FW) over a time scale long enough to prevent extreme temperatures that would damage the wall.

SOM.2.- First wall and blanket design

The Sombrero chamber is made of a 4d weave C/C composite and has a cylindrical central region with conical ends. The chamber configuration is shown in Figure SOM.1. At the midplane the chamber radius is 6.5 m, the cylindrical section is 5.2 m in height, and the angle between the side of one of the conical sections and the side of the cylinder is 135°. This means that the vertices of the cones would be 9.1 m away from the centre of the chamber. The chamber is divided in 12 independent vertical modules (i.e. every 30° in the horizontal plane) each with individual supply and return tubes connected to the common supply and return manifolds. The sixty beams penetrations are located in five cones above and below the

chamber midplane. The cones above the chamber midplane have polar angles of 25.8° , 45.6° , 60° , 72.5° , 84.3° , and the ones located below have the correspondent complementary angles. With this configuration beam ports do not face each other across from the target. This way if a beam does not hit the target, instead of propagating through another beam port, it will hit the FW.

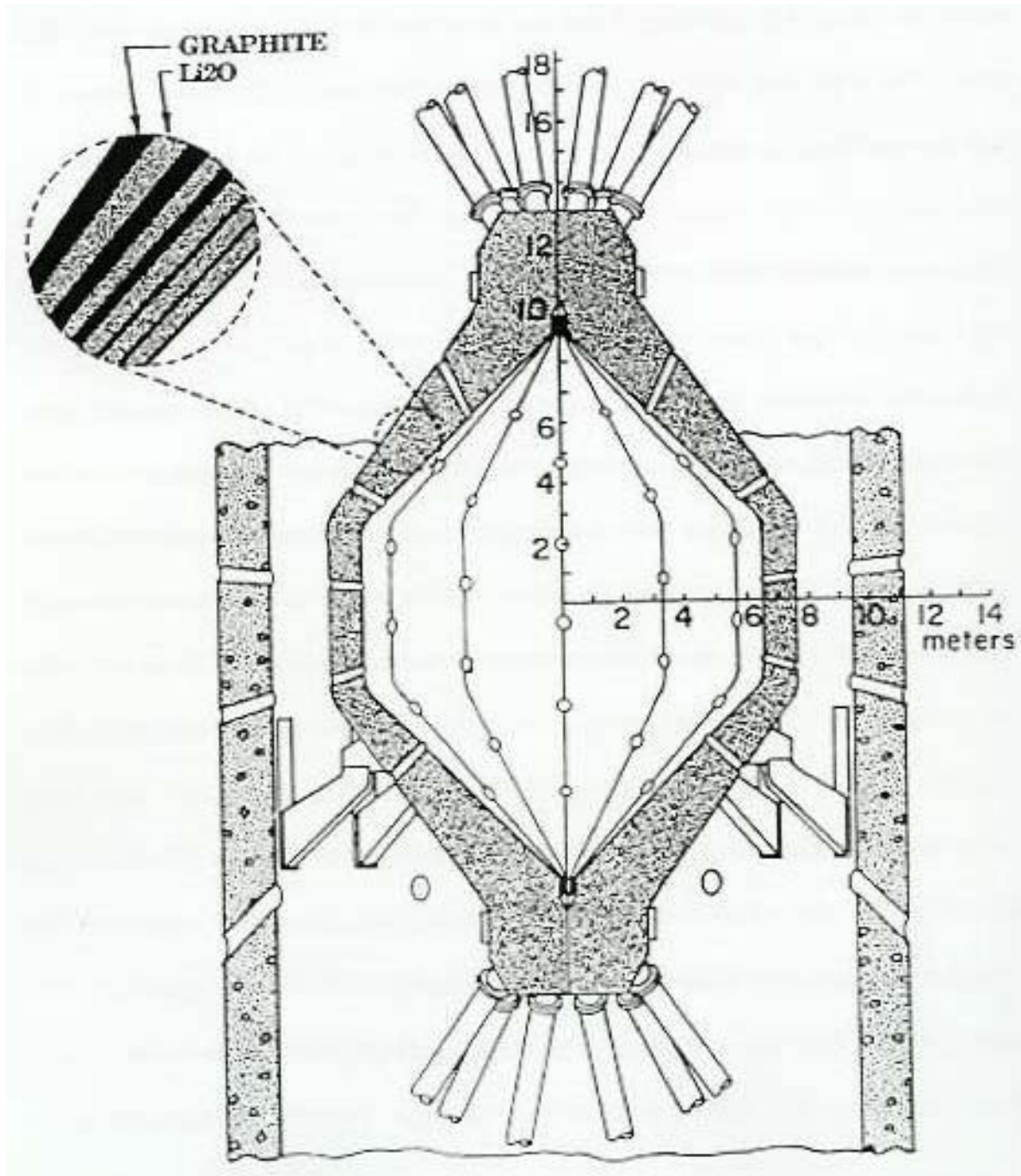


Figure SOM.1. Vertical section of the Sombrero chamber

Figure SOM.2 shows the radial build of the FW/blanket assembly at the midplane. The FW is 1 cm thick made of C/C composite. The blanket is divided in three regions with different composition. The innermost section is 19 cm thick and consists of 3% carbon composite and 97% Li_2O particles. The second and third zones are 40 cm thick each and have a 20% and 50% carbon fraction, respectively. The increasing carbon fraction serves as a neutron reflector

and enhances the energy absorption and tritium breeding within the blanket. The overall blanket/reflector thickness at the midplane is 1 m. The blanket assembly reaches a maximum thickness of 1.75 m at the top of the conical regions.

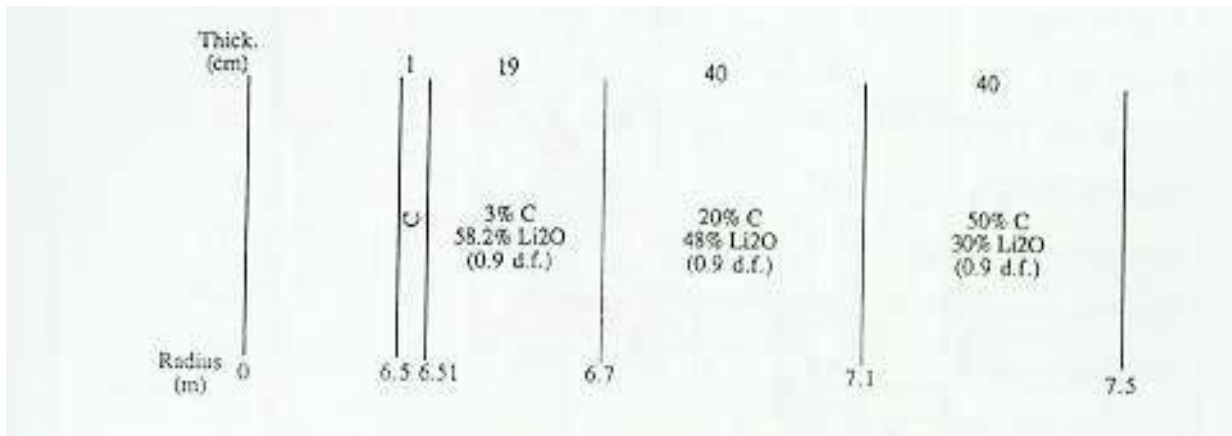


Figure SOM.2. Radial build of the Sombrero FW/blanket assembly at the midplane

Throughout the blanket, the Li_2O flow rate remains constant at 1.12 m/s. The theoretical density of Li_2O is 2.01 g/cm^3 , but it is assumed that the material is 90% density, and the moving bed has a 60% Li_2O fraction, giving the effective density a value of 1.08 g/cm^3 . The inlet temperature of the Li_2O into the chamber is 550°C . At the FW, the outlet temperature is 700°C , and 800°C at the back. The equilibrated outlet temperature from the chamber is 743°C .

SOM.3.- Plant parameters

Table SOM.1 shows the relevant parameters of the Sombrero design. We have added an extra-column showing the same parameters in the HYLIFE-II case, in order to enable comparison.

Table SOM.1 Plant parameters for the Sombrero and HYLIFE-II designs

Plant parameters	SOMBRERO	HYLIFE-II
Driver	KrF laser	Heavy-ion beams
Driver energy (MJ)	3.4	5
Driver efficiency (%)	7.5	35.0
Type of target	Direct drive	Indirect-drive
Target gain	118	70
Target yield (MJ)	400	350
Rep-rate (Hz)	6.7	6.0
Energy multiplication	1.08	1.18
Chamber material	C/C composites	SS304

Breeding material	Li ₂ O particles	Flibe
Breeding ratio	1.25	1.17
Fusion power (MW)	2677	2100
Thermal power (MW)	2891	2500
Cycle efficiency (%)	47	43
Gross electric power (MWe)	1359	1075
Driver power (MWe)	304	85
Auxiliary power (%)	55	50
Net electric power (%)	1000	940

SOM.4.- Plant components and layout

Figure SOM.3 shows the layout of the reactor building for the Sombrero design.

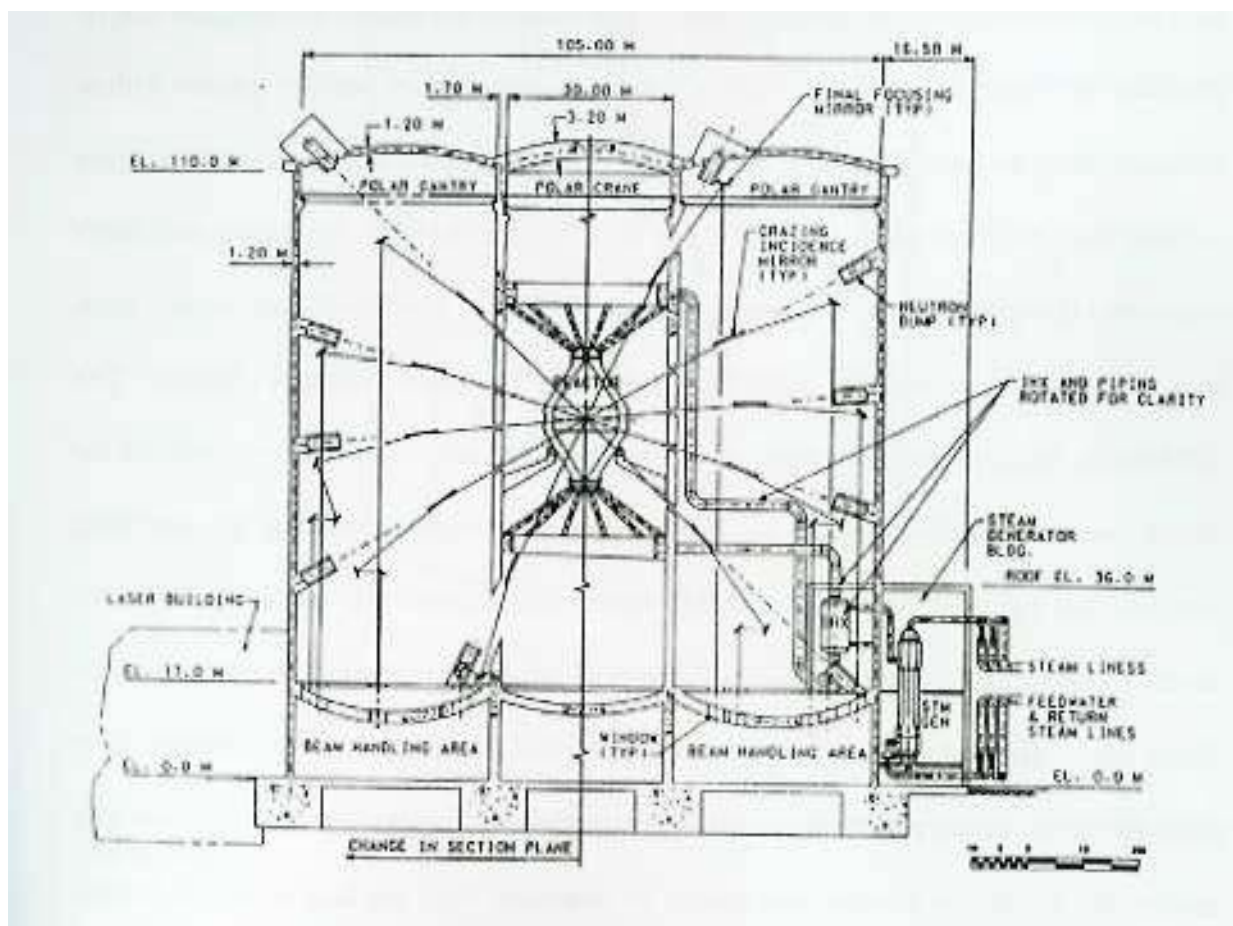


Figure SOM.3. Overall cross-section of the Sombrero reactor building

The target chamber is located in the middle of the building. At 1.7 m thick concrete shield with an inner radius of 10 m surrounds the chamber. The shield enables hands-on maintenance of the components that are located outside within only 24 hours after the reactor

shutdown. It also provides the necessary structural support for the chamber and serves as a central column support for the reactor building roof.

The laser beams penetrate the reactor building through the lower level, and are then reflected vertically through windows in the floor of the reactor building, as can be observed in Figure SOM.3. These windows serve as the primary barriers against tritium diffusion into the laser building. After being reflected upwards, the laser beams are incident onto the final focusing mirrors (FFMs). The FFMs focus the beams and direct them onto the grazing incidence metal mirrors (GIMMs), which will then deflect them into the chamber through the appropriate ports in the shield wall and chamber. The GIMMs are located at a 30 m radius from the target, and are in direct line-of-sight of the fusion neutrons leaking through the beam ports. It is expected that at the operating temperatures the lifetime of the GIMMs would be increased by self-annealing. The neutron traps located in the reactor building wall would be the next component in the direct line-in-sight of primary non-scattered neutrons. The FFMs are at a radius of 50 m from the centre of the target chamber. Given that these dielectric coated mirrors are very susceptible to neutron damage and cannot be annealed, they are located out of line-of-sight of primary neutrons. Figure SOM.4 shows an isomeric perspective of the optic elements configuration in the Sombrero reactor building.

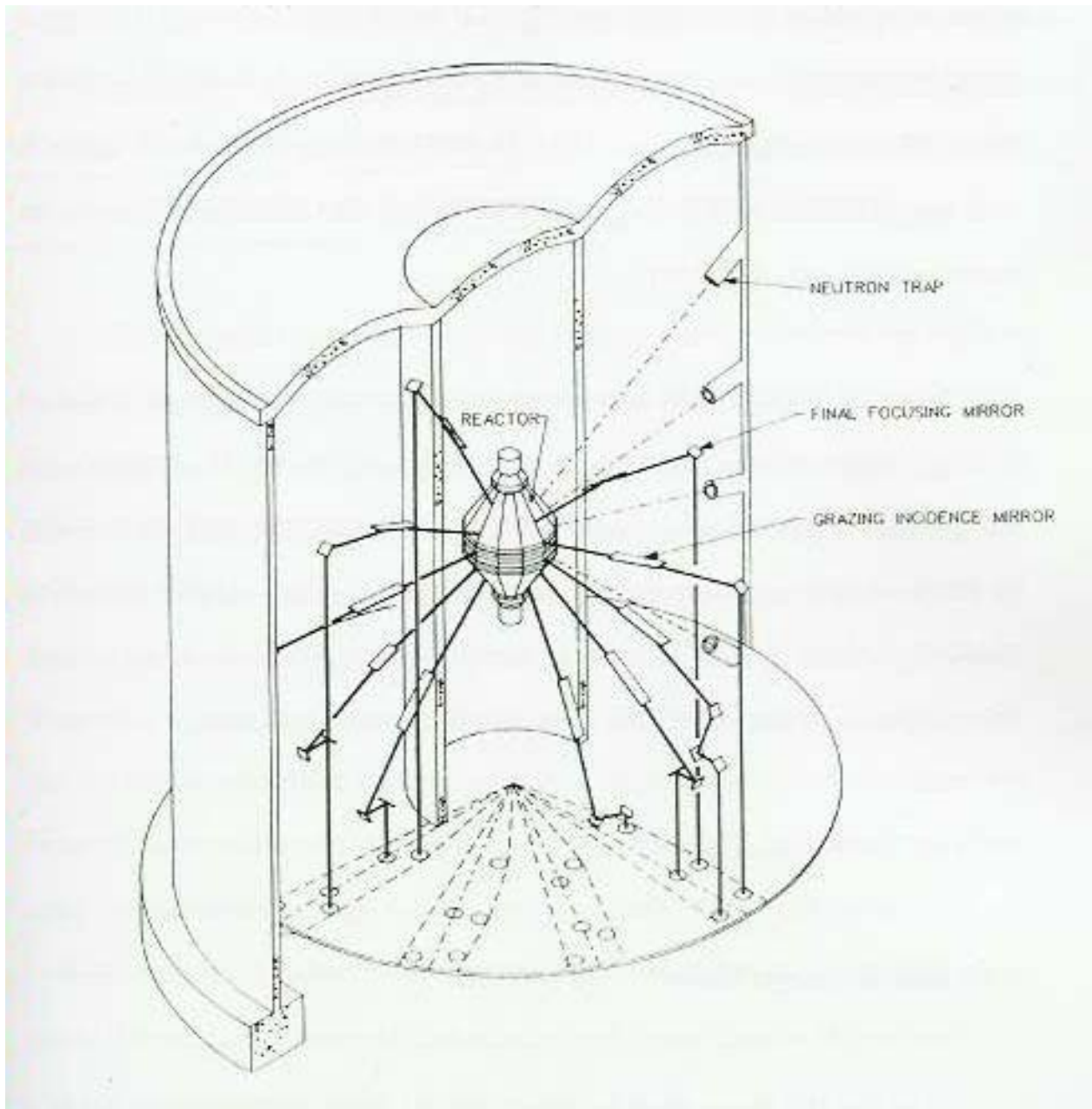


Figure SOM.4. Isomeric view of the optics configuration in the Sombrero reactor building

The Sombrero reactor building which houses the chamber and optics is approximately 110 m in diameter and 115 m in height. Since Sombrero would not use beam tubes for laser transport, the building itself serves as vacuum vessel. The reactor building is maintained at an atmosphere of 0.5 torr of xenon gas. A vacuum system is used to recover unburned tritium and target debris. The building concrete walls are 1.2 m thick and the neutron traps for leaking neutrons through the GIMMs are located on the reactor building walls.

Recently, a new version of the Sombrero design using a DPSSL (diode-pumped solid-state laser) instead of a KrF laser has been proposed. In this new version the open solid-angle fraction increases from 0.25% in the original design to the new value of 5%. We include in following sections a detailed neutronics analysis for both versions of Sombrero, in order to study the effect of the open solid-angle fraction on the radiation damage to the optic elements and the activation of the reactor components.

TARFAB.- TARGET FABRICATION FACILITY

TARFAB.1.- Reference target factory

The first IFE power plants to operate will use deuterium-tritium (DT) fuel (it is expected that second and third generation reactors will work with advanced fuels different than the DT cycle). Thus, every IFE power plant will require a target fabrication facility on-site. The target factory is a major source of tritium and, if for an indirect-drive power plant, also a source of activated target material. All of these materials may be subjected to potential accident release. The baseline design for a target production facility contains a DT handling and storage facility, a fuel container (capsule) production facility, a system for filling the capsules with DT fuel, a measurement system for quality assurance (QA) purposes, and a target storage and delivery section.

The steady-state tritium inventory, and thus, the quantity of tritium that might be mobilized during an accident, is a function of the target fabrication and fill technologies. For indirect-drive target designs, radioactive, recycled target high-Z materials will also be present in the target fabrication facility. In order to reduce the tritium and high-Z material inventories in the facility, it is important to minimize the production time per target and thus the inventory of targets being handled at any one time. It can be achieved by designing a compact production equipment and overall building area. Important safety features include segmenting the inventory into multiple parallel production lines, and including an expansion tank to limit releases. To further enhance the safety characteristics of the facility, the production stages and components are compartmentalized to reduce the consequences of a tritium leak in any one part of the system. A summary of the features of each type of target is included next.

TARFAB.2.- Indirect-drive targets

Indirect-drive targets require high-Z materials for the conversion of laser or ion energy into x-rays that ablate the outer shell of the capsule and cause the target implosion. Here we will consider a generic high-Z material for the reference indirect drive target for our safety analysis. Once the release fraction of such material under accident conditions is obtained, we will use this result to evaluate the consequences of using any of the typical materials proposed in the most recent reference designs.

We will focus in the most recent heavy-ion-driven, distributed-radiator designs developed by the target engineers at Lawrence Livermore National Laboratory.

The “full-size” target is driven by 5.9 MJ for a gain of 68, while the “close-coupled” target requires only 3.3MJ and has a gain of 133. A schematic of each design is showed in Figures TARFAB.1 and TARFAB.2.

Even though these designs use a beryllium shell and ablator, it is expected that IFE power plants will use plastic shells to enable diffusion fill of capsules. Whereas the tritium inventories in both types of capsule are around 2.4 mg, the volume of the close-coupled design is more than 2 times smaller than that of the full-size target (volumes are 1.6 m³ for the full-size design and only 0.7 for the close-coupled target).



Figure TARFAB.1. Schematic of the design of an indirect driven target type “full-size”



Figure TARFAB.2. Schematic of the design of an indirect driven target type “close-coupled”

TARFAB.3.- Direct-drive targets

The reference design that we will assume for the direct-drive target is based on the Sombrero power plant study. This capsule consists of a plastic shell ablator with an inner solid DT fuel layer. The ablator would be vaporized by the energy deposition and would be blown away from the fuel surface, pushing against the fuel and causing the implosion. The tritium inventory of this target would be 2.4 mg. It would be shot at 6.7 Hz with a yield of 400 MJ for a production of 1000 MW of net electric power. Figure TARFAB.3 shows the schematic a direct-drive capsule design.

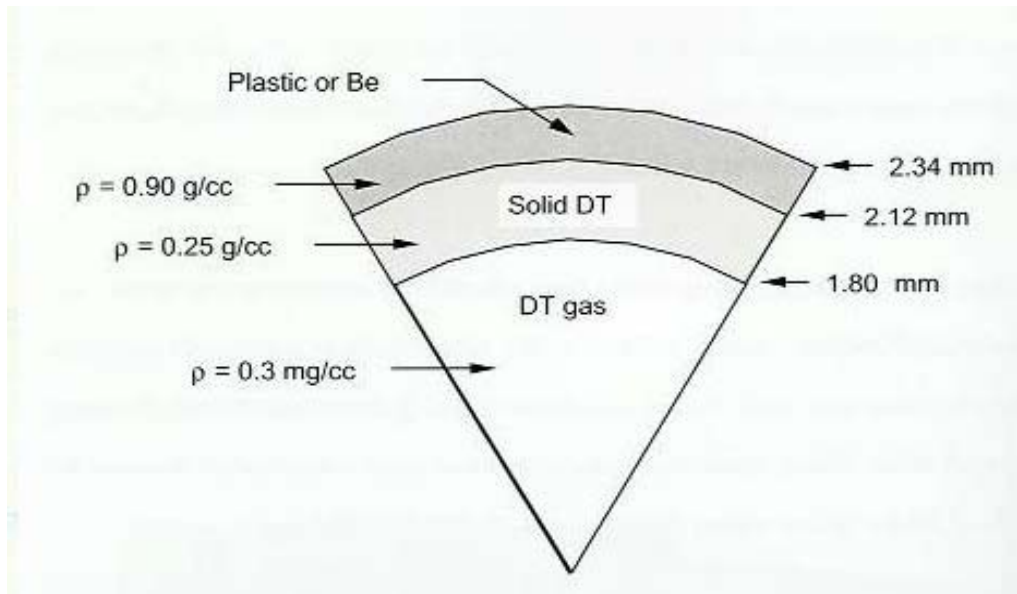


Figure TARFAB.3. Schematic of the reference capsule for direct drive

The different filling procedure and times for each type of target will be discussed in a following section in detail. However, it is worth pointing out that for the case of direct-drive targets, the fill time are significantly longer due to the relatively thin-walled capsules, which will not support as great pressure gradients as in the case of indirect-drive designs.

NEUHY-II.- NEUTRONICS ANALYSIS FOR HYLIFE-II

In order to calculate radioactivity releases and doses to the public under accident conditions, first we need to know the activation product source term. We have simulated neutron transport and activation of materials using the TART and ACAB codes respectively.

A 3-D model of HYLIFE-II was created for neutron transport calculations with the TART code. This model allowed us to obtain the neutron flux in 175 energy groups for the different zones of interest in the power plant. Figure NEUHY-II.1 shows a view the HYLIFE-II model where the different zones are represented with different colours. The model includes the 60 cm thick flibe inner pocket, the stainless steel type 304 (SS304) chamber/blanket structures with the additional flibe circuits between the first three shells, and a concrete shielding for magnets protection. The final magnets of the heavy-ion driver are included in this model for purposes of optimization of superconductor magnets lifetime calculations, which will not be discussed in the present work.

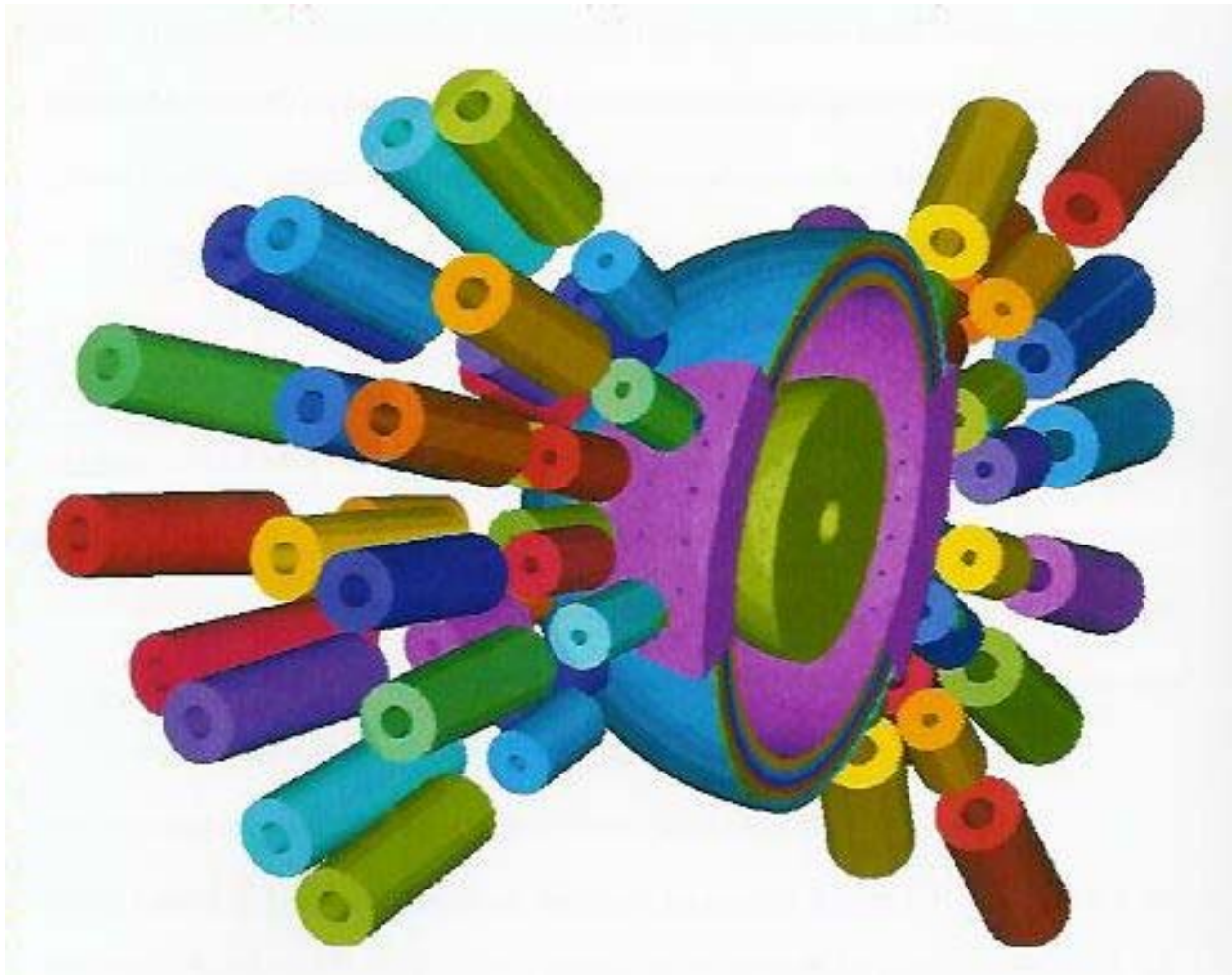


Figure NEUHY-II.1. TART model used for neutron transport calculations

The model also includes a 1 m thick confinement concrete building at 20 m distance from the target, which is not shown in the picture for clearness purposes.

With this model we obtained the energy-dependent neutron path-lengths in the flibe, SS304 and concrete structures, and TARTREAD code converted them into neutron fluxes to be used in the activation calculations. Activation of components and decay heat results were obtained from the ACAB activation code following 30 years of plant operation. For the present work, the pulsed nature of the irradiation is ignored and it is approximated with the “equivalent steady study” method. Table NEUHY-II.1 shows the most contributing nuclides to the activities of the different components at the beginning of the accident (shutdown).

Table NEUHY-II.1 Most contributing nuclides (>1%) and total activities of the different components

SS304		Flibe		Inner shielding		Confinement building	
Nuclide	(%)	Nuclide	(%)	Nuclide	(%)	Nuclide	(%)

FE 55	2.45E+01	N 16	5.87E+01	AL 28	3.38E+01	AL 28	3.28E+01
MN 56	1.70E+01	O 19	1.79E+01	NA 24	2.15E+01	NA 24	1.92E+01
CR 51	1.54E+01	F 18	1.23E+01	CA 45	9.79E+00	AR 37	1.58E+01
CO 58	7.87E+00	F 20	1.11E+01	MN 56	7.99E+00	CA 45	8.75E+00
CO 60	6.74E+00			AR 37	7.87E+00	MN 56	6.84E+00
MN 54	5.20E+00			K 42	4.78E+00	K 42	4.23E+00
CO 58M	4.50E+00			SI 31	4.53E+00	SI 31	4.07E+00
CO 60M	3.84E+00			FE 55	3.42E+00	FE 55	3.03E+00
FE 59	3.55E+00			N 16	1.95E+00		
V 52	2.18E+00			CA 49	1.09E+00		
AS 76	1.88E+00			SC 49	1.09E+00		
CO 57	1.72E+00						
Total Activity (Bq)	1.76E+17	Total Activity (Bq)	6.39E+18	Total Activity (Bq)	1.70E+16	Total Activity (Bq)	8.40E+11

It must be noticed that this part of the calculations (neutron transport and activation results) is common for the different heat transfer and thermal-hydraulics models have been developed for each particular scenario. We have focused on severe accident analysis in order to predict the consequences in the worst possible cases. Even though the probability of such severe accidents is very low during the plan lifetime, one needs to be conservative at this early stage of the development of the IFE designs so that lessons can be learned and intelligent decisions made.

NEUHY-II.1.- LOCA analysis results for HYLIFE-II

This present section describes the results on what has been considered to be one of the most severe possible accidents in the HYLIFE-II design. We assume a total loss of coolant accident (LOCA) where all the liquid flibe is lost at the beginning of the transient eliminating the possibility of removal of the radioactive decay heat of structures by the cooling system. A simultaneous break of all the beam tubes is also postulated, which provides a flow path from the target chamber to the confinement. In addition, 1 m² breaks in both the inner shielding wall and the confinement building wall are assumed. These breaks provide a pathway for release of radioactive material to the environment.

In order to perform an accident doses analysis, first we need to know the source term of radioactivity that is released to the environment. Once the activation of structures during the plant operation has been calculated, thermal transients and aerosol transport calculations have been performed. Given the activity release and the specific dose of each isotope, the accident dose may be calculated.

NEUHY-II.1.1.- Time-temperature history of reactor components

Prior to the calculation of radioactivity release fractions, one needs to know the time-temperature histories of the different reactor components during the accident. This is used to determine the activation products source term available for mobilization, which will later be used as input data for the MELCOR thermal-hydraulics calculations.

In this case the only energy source is the radioactive decay heat from the activated material in the reactor components. Once the accident begins, it is conceivable that fusion reactions could continue to occur for a short period of time. Several factors must be considered: accelerator operation, target injection, and beam propagation through a varying environment. If accelerator operation and target injection both continue, then beam propagation ultimately will determine when ignition is no longer possible. We have assumed a complete loss of coolant accident combined with multiple breaks in the beam tubes, shielding, and confinement building. These breaks will allow air to enter the beam tubes and chamber, and this air will result in the inability to propagate the heavy ion beams to the target.

Langdon discusses the pressure of gas that is allowable for successful beam propagation. For an unneutralized beam, a background pressure of more than 13 Pa (conservatively assuming lithium gas) guarantees that stripping and plasma instabilities will destroy the beam. For a fully neutralized beam, a pressure of about 2700 Pa will produce multiple scattering, which will destroy propagation. If we conservatively assume that the beams are fully neutralized, then fusion yield might continue until enough air enters the beam tube to raise the pressure to 2700 Pa.

To determine the time required to reach 2700 Pa within the beam tubes, a simple MELCOR calculation was performed. We see that 2700 Pa is reached within only 50 ms, and thus, a plant operating at 6.4 Hz will not be able to ignite the next target before beam propagation is halted due to air pressure.

Considering then that decay heat from activated materials is the only existing source available of heat, a CHEMCON calculation was developed using a simple 1-D cylindrical model. This model consists of four stainless steel shells that represent the tubes containing the flibe, first structural wall, blanket structure and vacuum vessel, an inner concrete shield and the confinement building wall. We have ignored the flibe inside the chamber and in the blanket circuits given that here we assume a total loss of coolant. Conduction, convection and radiation heat transfer was calculated between these structures. Figure NEUHY-II.2 shows a schematic of the CHEMCON model for HYLIFE-II.

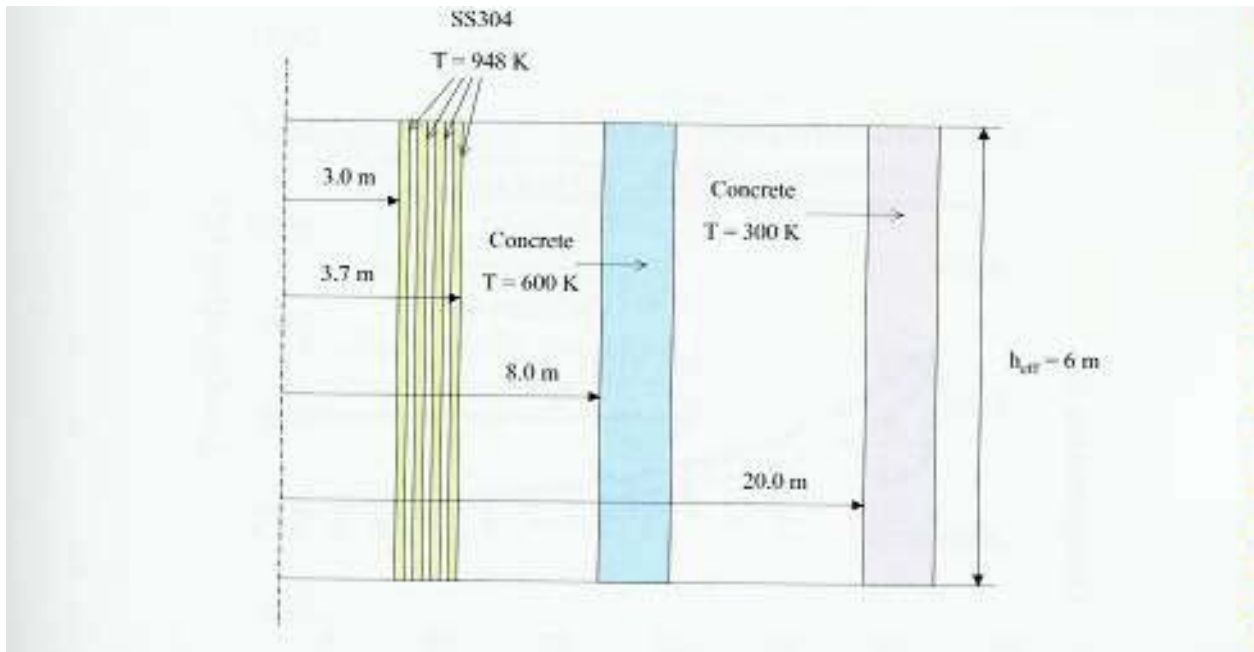


Figure NEUHY-II.2. Schematic of the CHEMCON model for the long-term thermal evolution in a LOCA accident in HYLIFE-II

The activation and decay heat results were obtained from the ACAB activation code following 30 years of plant operation and fluxes in structures were calculated with TART Monte Carlo neutron transport code. Figure NEUHY-II.3 shows the thermal transient in the different reactor components due to the decay heat from the activation products.

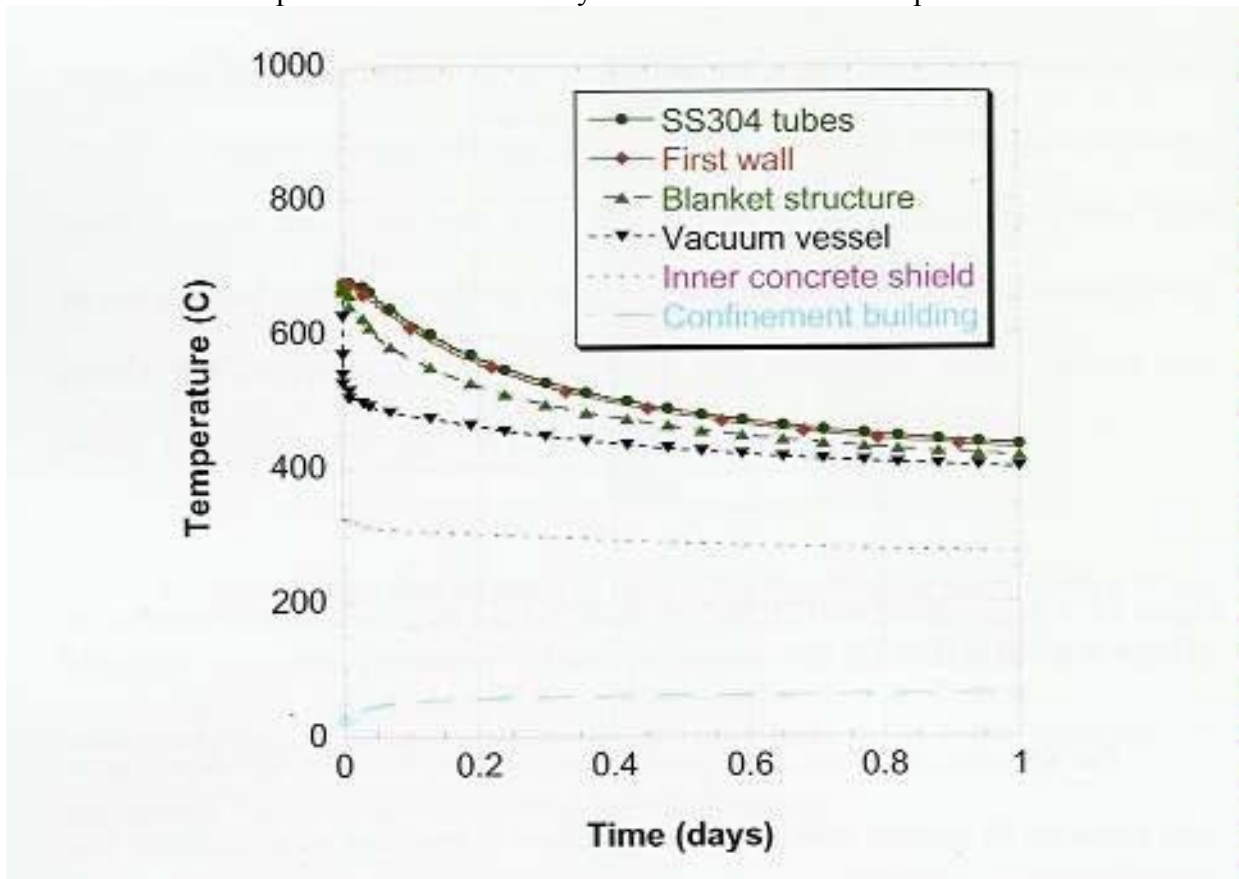


Figure NEUHY-II.3. Temperature evolution in the various reactor components during the first day following the LOCA in HYLIFE-II

The first wall temperature, initially being 675°C, displays a mild peak at 679°C at about 15 minutes, after which it gradually falls. This indicates that the radioactive afterheat is low enough to avoid melting of the stainless steel structure ($T_{\text{melt}} \sim 1400^{\circ}\text{C}$) or any over-stress damage. This result eliminates the possibility of volatilization of the stainless steel structures during the accident, which would result in a significant increase in the radioactive mobilized mass.

In order to protect the first structural wall from direct neutron fluxes, the updated HYLIFE-II design considers a flibe pocket 60 cm thick which is the value used in our final accident analysis. A parametric study was developed in order to evaluate the benefit of a thick liquid wall on the activation of the structures and accident temperatures. ACAB calculations were performed for different flibe pocket thickness and irradiation times of 3 and 30 years irradiation. Figure NEUHY-II.4 shows the maximum accident temperatures obtained with CHEMCON for the different cases.

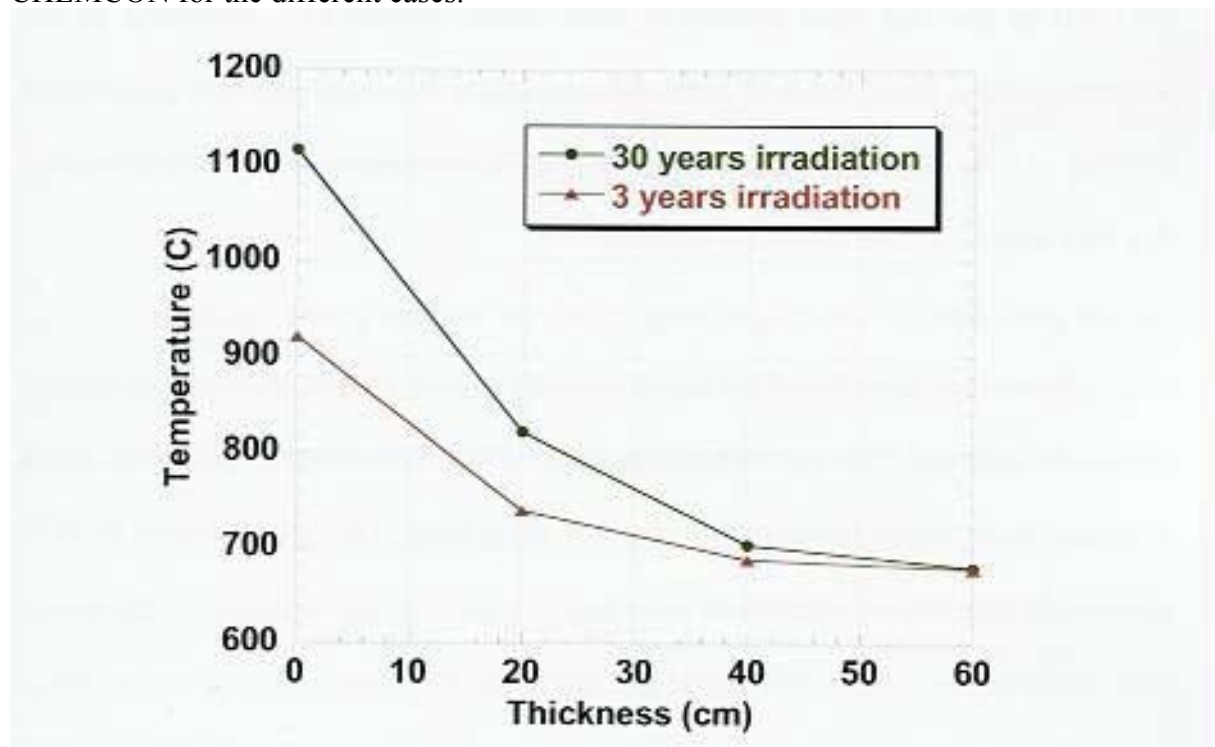


Figure NEUHY-II.4. Maximum accident temperatures reached at the first structural wall for different flibe pocket thickness

It can be observed that an unprotected wall would not reach the melting point either. This result is very important when accounting for the stainless steel mobilized masses. Figure NEUHY-II.4 also shows the benefit of introducing a thick liquid protection. For example, note that for thickness > 15 cm, a 30-yr protected wall is better than a 3-yr unprotected wall in terms of maximum accident temperature.

NEUHY-II.1.2.- Activation products source term

There are four main sources of radioactivity that must be considered in this accident scenario for HYLIFE-II. First, the x-rays from each target vaporize a maximum of 10 kg of flibe. Although we assume a total LOCA, our analysis conservatively includes this flibe aerosol with its activation products.

Second, it is estimated that approximately 140 g of tritium would be trapped within the chamber, blanket, and piping. We assume that entire tritium inventory is converted to the more radiotoxic HTO form. This yields a mass of HTO aerosol of 930 g, which we round up to 1 kg.

Third, we assume that the corrosion of type 304 stainless steel (SS304) by flibe within the chamber and blanket can be limited to $10\mu\text{m}/\text{y}$ via corrosion control methods. Additionally, we assume that the flibe clean-up system can maintain the mobilizable inventory of corrosion products to a $1\mu\text{m}/\text{y}$ supply. Given a total surface area of 1040 m^2 , we obtain a corrosion product inventory of 8.3 kg in the total flibe volume.

Finally, we use data from oxidation-driven mobilization experiments on PCA performed at the Idaho National Engineering and Environmental Laboratory (NEEL) to calculate an additional 0.5 kg of SS304 (we assume that SS304 mobilization will be the same as that from PCA) that is mobilized under exposure to steam at the accident temperatures previously calculated. Adding this 0.5 kg to the 8.3 kg of corrosion products, we have ~ 9 kg, which we round up to 10 kg of SS304. Considering that only about 5% of the flibe is present in the chamber at any given time, we end up getting 0.5 kg of SS304 as corrosion and oxidation products.

It is worth noting that we are being quite conservative in assuming that the corrosion products will be in an aerosol form and available for mobilization (one could make an argument that the corrosion products would leave with the flibe during the LOCA). Additionally, our assumption of steam oxidation driven mobilization is conservative –because the secondary system uses water, it is credible that some water could collect in low points of the plant, but the layout will be designed to avoid water anywhere near the flibe ducts. At temperatures of interest, oxidation-driven mobilization from PCA under exposure to air occurs at a rate that is about 900 times lower than that under exposure to steam. Additionally, interaction with steam would generate H_2 gas, which could conceivably lead to an explosion and be the cause of the large break in the containment building wall.

NEUHY-II.1.3.- Radioactivity releases and off-site doses

To estimate release fractions, a MELCOR model of HYLIFE-II was developed. This model consists of four stainless steel shells, which represent the SS304 tubes, first wall, blanket structure and vacuum vessel, a concrete inner shield and the containment building. The beam tubes were also modelled, considering an updated HYLIFE-II version that includes 96 beams per side. Beam tubes and volumes within the vacuum vessel are assumed to be at vacuum. The SS304 shells are initially at their operating temperature of 675°C .

The radioactive source term described in the previous section is used as input data for the masses of activated material that is available for mobilization during the transient.

We have considered a severe accident consisting of a total LOCA, with loss of all the liquid flibe, with simultaneous failure of the beam tubes, the concrete inner shielding and the

confinement. The total failure of the beam tubes (the area of the break is modelled as the calculated area of the total number of beams) means that the inner volumes are going to have a flow path towards the outer volumes, which are filled with air at atmospheric pressure. Both the inner shield and confinement walls are initially at an estimated temperature of 32 °C. Additionally, we assume a double failure of the inner shielding and concrete building (each of these breaks is 1 m² in area) that provides a pathway to the environment. This model is used by MELCOR to simulate the progression of the accident.

The MELCOR heat transfer package considers conduction, convection and radiation between the structures. The aerosol transport module treats SS304 and flibe aerosol nucleation and agglomeration, vapour condensation, gravity settling and gaseous/liquid transport. A new module introduced by INEEL allows simulation of HTO transport and condensation. Calculations of tritium migration from the stainless steel shells were also developed using TMAP (Tritium Migration Analysis Program) rather than assuming an instantaneous liberation from the structures. These calculations showed that at the operating temperature of 675°C, the tritium migration from the steel is fast enough (>90% in only 1.5 hour) that there is no difference when comparing with the results from the instantaneous migration assumption.

The transient is considered to be one month long. Table NEUHY-II.2 shows the fraction of the source term masses that are released to the environment during the accident, as well as the final doses. It can be noticed that from the initial 0.5 kg of SS304 that is mobilized, only 63 g are released to the environment. Approximately 1.1 kg (out of 10 kg) of flibe is released. Finally, due to partial condensation of the HTO on the colder walls of the building, we get a release fraction of 86% of the initial 1 kg mobilized. Once a detailed layout of the containment building is available, it may be possible to significantly reduce this release fraction.

Table NEUHY-II.2 Mobilized masses/activities, release fractions and off-sites doses for the different considered radioactivity source terms in case of a LOCA in HYLIFE-II

Radioactive source	Mobilized mass/ activity	Release fraction	Off-site dose
SS304 corrosion/oxidation	0.5 kg/1.31·10 ¹² Bq	13%	3.3 μSv/0.33 mrem
Vaporized flibe	10 kg/4,37·10 ¹⁴ Bq	11%	2.3 μSv/0.23 mrem
HTO trapped in steel	1 kg/4,99·10 ¹⁶ Bq	86%	4.6 mSv/460 mrem

With these data about the activity released in units of Bq, and the adequate dose conversion factors (DCF) in units of Sv/Bq, off-site doses can be obtained. Of the total inventory in the reactor at the moment of shutdown (just before the accident happening), all the radionuclides whose contribution to the radioactivity release was above 3.7 x 10⁷ Bq (1 mCi) were

considered for dose calculation purposes. The DCF library has been updated to include radionuclides that were missing from traditional (fission) libraries as some of these radionuclides may be important for fusion doses. Data on DCF were obtained using the MACCS2 code in order to calculate early doses (defined as the equivalent effective doses with 50 years commitment, resulting from the first 7 days of exposure during the plume passage). In addition to direct cloudshine and inhalation during plume passage, our doses also consider contributions from groundshine, and inhalation of resuspended material. Typical weather conditions and ground level release were assumed as recommended by the Fusion Safety Standards. These hypotheses correspond to the Case 1.

With these assumptions, the results from Table NEUHY-II.2 show that the dominant dose from the tritium in HTO form, which gives a total of 4.6 mSv (460 mrem). Both the SS304 and the flibe make small contributions to the total dose, being 3.3 μ Sv (0.33 mrem) and 2.3 μ Sv (0.23 mrem), respectively. If conservative weather conditions (Case 2) are assumed instead of typical, then the calculated doses would be about 10 times higher. On the other hand, assuming an elevated release in typical weather conditions (Case 3) would result in doses an order of magnitude lower than those calculated in the case of ground level release.

It should be pointed out that about 75% of the SS304 dose comes from ^{60}Co , and for the flibe, ^{18}F is the only contributor to the dose. From the total activity due to ^{18}F at the moment of the reactor shutdown (7.84×10^{17} Bq = 21 MCi), only 5.36×10^{13} Bq (1.45×10^3 Ci) are vaporized and available for mobilization during the accident. The final quantity of activity from the ^{18}F that is released to the environment is 5.63×10^{12} Bq (1.52×10^2 Ci).

The final result is that even with the various conservatisms introduced in the calculation, the off-site accident dose is under 5 mSv (0.5 rem). This is relevant result given that it is below the limit of 10 mSv (1 rem) given in the DOE Fusion Safety Standards, which means no sheltering and evacuation are needed. The results of this LOCA analysis were presented at the 13th International Symposium on Heavy Ion Inertial Fusion (San Diego, California, Mar. 2000), and accepted for publication in Nuclear Instruments and Methods in Physics Research A.

NEUHY-II.2.- LOFA analysis results for HYLIFE-II

In order to further advance a complete safety analysis for HYLIFE-II, a range of other accident scenarios must be considered. In the previous section we analysed a total LOCA where all the liquid flibe was lost at the beginning of the transient. Here we will focus on alternative accidents that involve the coolant. In this case the liquid flibe present in the chamber and blanket structures in the moment of the accident will be available for mobilization and release. Here we introduce a new version of the MELCO thermal-hydraulics code recently developed by the Idaho National Engineering and Environmental Laboratory (INEEL) that substitutes flibe for water as the working fluid.

The accident scenario considered here consists on a loss of flow accident (LOFA), with simultaneous failure of the blanket structure. During a LOFA, which could be initiated by failure of the pumping system, the flibe present inside the target chamber (the fraction vaporized during the last shot plus the flibe from the protective liquid wall) will be available for mobilization and release. Further, we estimate the flibe release fraction in the case that there was a failure in the blanket structure. In this case the entire flibe inventory present in

the first wall/blanket assembly in the moment of the accident would also be available for mobilization. In order to obtain a radioactivity fraction released to the environment, we postulate a break in the beam tubes outside of the reactor building. This constitutes the bypass needed to communicate the target chamber with the environment. With the results on the radioactivity release fractions, and the adequate dose conversion factors (DCF), the accident dose may be calculated.

NEUHY-II.2.1.- Time-temperature history of reactor components

During a thermal transient in the plant, the potential energy sources must be identified in order to determine the temperature excursions of the different components. In this case the only energy source is the radioactive decay heat from the activated material in the reactor structures. Once the accident begins it is conceivable that fusion reactions could continue to occur for a short period of time. As explained in the previous LOCA analysis, several factors must be considered: accelerator operation, target injection, and beam propagation through a varying environment. If accelerator operation and target injection both continue, then beam propagation will determine when ignition is no longer possible. We have assumed that the beam tubes failure occurs outside the confinement building, allowing the air to penetrate the chamber, and resulting in the inability to propagate the heavy ion beams to the target.

Considering then that the decay heat from activated materials is the only energy source during the transient, a CHEMCON calculation was developed using a simple HYLIFE-II 1-D cylindrical model. This model, shown in Figure NEUHY-II.5 consists of four stainless steel shells that represent the FSW/blanket structure. It also includes the flibe liquid wall inside the chamber and the two circuits trapped in the blanket during the LOFA, an inner concrete shield and the confinement building.

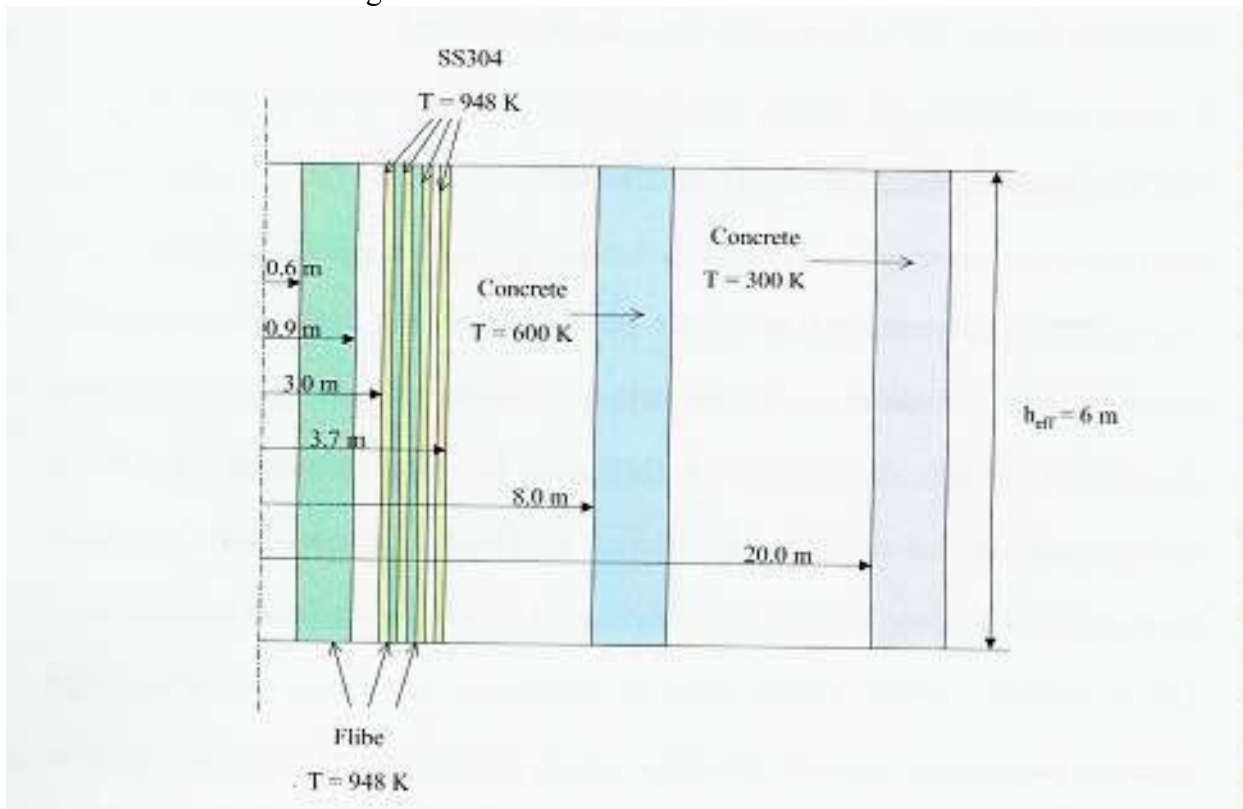


Figure NEUHY-II.5. Schematic of the CHEMCON model for the long-term thermal evolution in a LOFA in HYLIFE-II

Figure NEUHY-II.6 shows the time-temperature history of the different components during the LOFA transient. Due to the low radioactive afterheat, the first wall temperature, initially at 675°C, experiences an insignificant peak of tenths of a degree at about 10 hours, after which it gradually falls. This indicates that the stainless steel temperature will remain far below its melting point during the all transient ($T_{\text{melt}} = 1400^{\circ}\text{C}$). This result eliminates the possibility of volatilization of activated stainless steel or any over-stress damage during the accident.

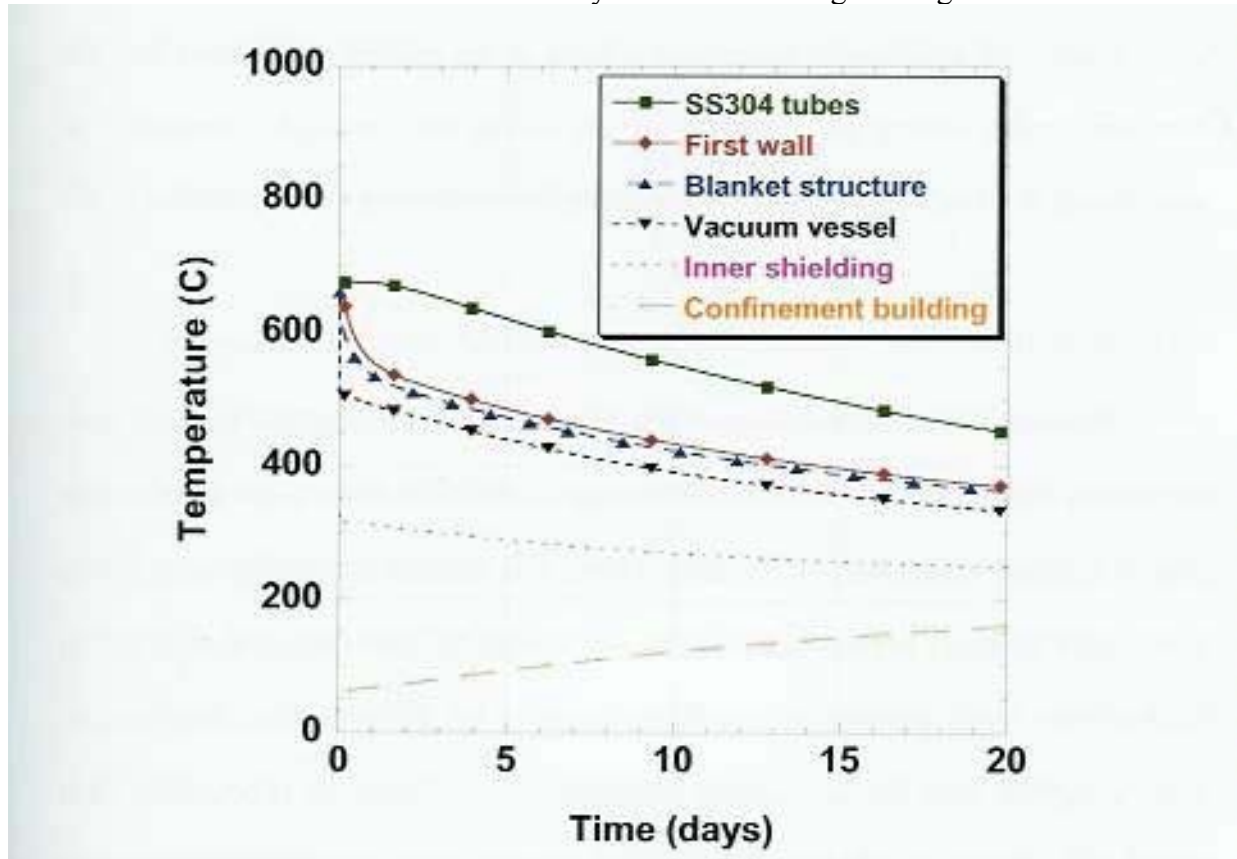


Figure NEUHY-II.6. Time-temperature history of the various reactor components due to the radioactive decay in a LOFA in HYLIFE-II

NEUHY-II.2.2.- Activation products source term

There are three main radioactivity sources to be considered in a LOFA scenario in HYLIFE-II. First is the flibe with its activation products. When we studied the total LOCA the only flibe mass to be considered were the 10 kg vaporized by the x-rays from the last ignited target. However, in this case and as a consequence of the loss of flow, the protective liquid wall in front of the FSW would also be standing as a pool inside the target chamber. If additionally we assume a break in the blanket piping, then the flibe from the blanket cooling and shielding circuits would leak inside the chamber. That would result in a total mass of about 140 tonnes of flibe available for mobilization in this case.

Second, as before, we assume that the corrosion of type 304 stainless steel (SS304) by flibe within the chamber and blanket can be limited to $1 \mu\text{m}/\text{y}$ via corrosion control methods. Additionally, we assume that the flibe clean-up system can maintain the mobilizable

inventory of corrosion products to a 1-y supply. Given a total surface area of 1040 m², we obtain a corrosion product inventory of 8.3 kg in the total flibe volume. Also, using data from oxidation-driven mobilization experiments on PCA performed at INEEL, we calculate an additional 0.5 kg of stainless steel that would be oxidized at the accident temperatures (we assume that SS304 mobilization will be the same as that from PCA). Adding up the corrosion and oxidation products, we obtain around 10 kg of SS304 in the total flibe volume. Considering that only 5% of the flibe inventory is present in the chamber at any given time, we obtain a total of 0.5 kg of SS304 mobilized during the transient.

Finally, it is estimated that approximately 140 g of tritium would be trapped within the chamber, blanket and piping. We conservatively assume that the entire tritium inventory is converted to the more radiotoxic HTO form, yielding a total mass of about 1 kg of HTO.

NEUHY-II.2.3.- Radioactivity releases and off-site doses

In order to estimate release fractions, a MELCOR model of HYLIFE-II was developed. This model consists of the FSW and blanket structures, beam tubes (considering an updated HYLIFE-II version which includes 96 beams per side), inner shield and confinement building. The heavy-ion beam tubes and the target chamber are assumed to be at vacuum. The radioactive source term described in the previous section is supposed to be available for mobilization during the transient. This version of the MELCOR code uses flibe as the operating fluid. MELCOR heat transfer package considers conduction, convection and radiation between the structures. The aerosol transport module treats the aerosol nucleation and agglomeration, vapour condensation, gravity settling and gaseous/liquid transport.

A. Flibe Release and Off-site Doses

We have performed a series of MELCOR calculations in order to characterize the behaviour of the flibe in accidental conditions not involving the total loss of the liquid coolant previously addressed. We assume a LOFA accident with failure in the blanket structure and a break in the beam tubes that would constitute a bypass between the target chamber and the environment. We have assumed different severities of the tubes breakage, ranging from the total failure of the 192 beam tubes to the case were a single tube breaks. The occurrence of blanket flibe leakage directly to the beam tubes was also studied. Given that a special region of shielding for the focusing magnets separates the beam tubes from the blanket, we discarded this possibility.

We have obtained the released mass in each scenario and then considered three sets of accident conditions for off-site dose calculations purposes. First set is called “typical case with ground release” and assumes average weather conditions (wind speed = 4 m/s, atmospheric stability class D), and radioactivity release at ground level.

Second, the “conservative case with ground release” (Case 2) considers conservative weather conditions (wind speed = 1 m/s, atmospheric stability class F) and ground level release.

Finally, the “typical case with elevated release” (Case 3), also considers average weather conditions but the release is produced through a smoke-stack 100 m above ground level.

Table NEUHY-II.3 shows the results for mass released and off-site doses in the different described scenarios.

Table NEUHY-II.3 Released flibe mass (kg) and off-site doses (mrem) in case of a LOFA in HYLIFE-II

Beam tubes failure fraction	Mass released	Dose Case 1	Dose Case 2	Dose Case 3
100%	5.54	1.24	16.6	0.23
50%	4.56	1.02	13.7	0.19
25%	2.63	0.59	7.89	0.11
1 beam tube	0.13	0.03	0.39	0.005

Given the low afterheat and the temperature decrease of structures during the transient, the liquid flibe is not going to suffer volatilization and will mostly remain in the form a pool in the chamber/blanket area. The 10 kg of vaporized flibe generated by the last target, will immediately be converted into fog at the beginning of the accident, and then transported from the chamber to the beam tubes, allowing some of this fog to deposit on structures before reaching the environment.

In the first three cases (100%, 50% and 25% of beam tubes failing), the mass released turns out to be larger than that obtained in the LOCA study, where we only accounted for the 10 kg of vapour and obtained a release fraction of 11%. This is because then, we considered that the beam tubes would fail inside the inner shield building, having the mobilized material to travel from here to the confinement building and next to the environment through the postulated breaks in the walls. This scenario allowed larger surface areas and longer travel time for the flibe to deposit before leaking through the breach in the confinement building wall.

Results show that even in the case of 100% beam tubes failure, the dose in the most pessimistic conditions is less than 17 mrem, demonstrating the inherent radiological safety of the HYLIFE-II design relative to the use of flibe. It must be noticed that the isotope ^{18}F contributes in a 99% to the final dose.

Other than activation concerns, flibe has some chemical and toxicity issues. First and foremost, the escaping beryllium compounds, notably BeF_2 , pose a health hazard. The recommended limit is $25 \mu\text{g}/\text{m}^3$ for peak exposure to beryllium and its compounds. If we assume a release of 1 kg of flibe (containing 340 g of BeF_2) that escaped to the environment under conservative weather conditions over a period of 1 hour, the concentration at a 1 km site boundary would only temporarily reach $3 \mu\text{g}/\text{m}^3$. However, the beryllium concentration

within the plant could require worker protection. Another concern relative to the use of flibe in HYLIFE-II is the potential of HF formation. When the lithium is fissioned by neutron interaction, it leaves a free fluorine atom to combine with available hydrogen. HF poses a corrosion threat and has its own health risks. One method that has been proposed to control flibe pH is the presence of beryllium flowing pebbles or fingers which would allow the HF or free fluoride ions to react back to VeF_2 .

B. SS304 release and Off-site Doses

With the previously described MELCOR model we also obtained the release fractions of SS304 corrosion and oxidation products in the various scenarios. An initial mass of 0.5 kg was used for the aerosol source term and the aerosol nucleation and agglomeration, gravity settling and transport during the accident were simulated. We also calculated the correspondent DCF for the different accident conditions and results are shown in Table NEUHY-II.4.

Table NEUHY-II.4 Released SS304 mass (kg) and off-site doses (mrem) in case of a LOFA in HYLIFE-II

Beam tubes failure fraction	Mass released	Dose Case 1	Dose Case 2	Dose Case 3
100%	0.27	1.40	20.9	0.13
50%	0.22	1.13	16.8	0.11
25%	0.12	0.64	9.60	0.06
1 beam tube	0.009	0.05	0.68	0.004

It can be observed that in the most pessimistic case (100% of the beam tubes fail and conservative weather conditions with ground release) the accident dose to the public would be less than 21 mrem. In this case about 75% of the total dose comes from the radioisotope ^{60}Co , being followed in importance by the isotopes ^{58}Co and ^{59}Fe . It must be pointed out that in the first three beam tubes failure cases, the radioactivity release results to be larger than that obtained in the LOCA analysis (only 0.07 kg of SS304 were released then). This is due to the effect of the smaller available surface for aerosol deposition and shorter travel time to the environment in this particular bypass scenario.

C. HTO Release and Off-site Doses

In order to simulate the HTO transport and condensation on structures we made use of a former version of the MELCOR code which uses water as the working fluid in stead of flibe (at this point no-multifluid version of the code is available yet). An instantaneous release of the tritium from the SS304 structures was assumed. Calculations of tritium migration from the stainless steel shells were also developed using TMAP (Tritium Migration Analysis Program). These calculations showed that at the operating temperature of 675°C, the tritium migration from the steel is fast enough (>90% in only 1.5 hour) that there is no difference when comparing with the results from the instantaneous migration assumption. Results show that in this case 100% of the tritium is released. The non-existence of a cold structure (like the confinement building wall in the case of LOCA analysis) where this tritium would condense and avoid being released, leads to the result of a 1 kg of HTO release to the environment.

The consequent off-site dose from the tritium in case of average weather conditions with ground level release would be 0.5 rem. The dose would result in only 47 mrem if the release occurred through an elevated stack. If pessimistic weather conditions were assumed instead, then the accident dose would be 6.4 rem. As occurred in the case of the LOCA accident, the tritium dominates the total result, being the contribution of the flibe and SS304 less than 1% of the final accident dose.

As a summary from the previous results we can say that even though the entire flibe inventory present in the chamber and blanket at the moment of the accident is available for mobilization, the release fraction is small enough to result in off-site doses lower than 20 mrem, demonstrating the inherent radiological safety of HYLIFE-II relative to the use of flibe. The final accident dose is clearly dominated by the 140 g of tritium trapped in the stainless steel structures and released during the accident.

For the most pessimistic scenario, where a failure of all of the beam tubes occurs, we obtain an accident dose of 0.5 rem. This dose considers average weather conditions (as recommended by DOE Fusion Safety Standards) and assumes ground level release. This result is below the 1 rem limit for public protection in case of accident, and means that an evacuation plan would not be needed in this case. The results of this analysis were presented at the 14th ANS Technology of Fusion Energy Meeting (Park city, Utah, Oct. 2000) and have been submitted for publication to the journal Fusion Technology.

SOMSAF.- SAFETY ANALYSIS RESULTS FOR SOMBRERO

Sombrero (solid moving breeder reactor) is a conceptual design of a 1000 MW_e laser-driven inertial fusion energy (IFE) power plant. Safety and environmental issues in the Sombrero IFE power plant design have been given a strong emphasis since the original report. The Sombrero concept uses a low activation material (C/C composite) in the chamber structures. The blanket consists of a moving bed of solid Li₂O particles flowing through the chamber, eliminating the risk of chemical reactions usually associated with the use of lithium. The chamber is surrounded by a 1.7 m thick shield wall at a radius of 10 m with an additional 1 m thick confinement building wall at a radius of 55 m.

However, recent work has pointed out some key issues involving safety that were not completely addressed at that time, and which need to be reviewed in order to maximize the Sombrero design attractiveness. Since the time of the original study, the nuclear community (fission and fusion) has reached a consensus and established more restrictive safety goals.

Also since that time, new experimental data has been published on tritium retention in carbon/carbon composites, revealing the need for an updated safety evaluation of the Sombrero design.

In the present work, we have adopted the principle of considering if not the worst, one of the worst possible accident scenarios. Here we assume a loss of flow accident (LOFA) with loss of circulation in the four loops of the primary coolant system. In addition, a 1m² break in the confinement building wall is assumed, leading to a loss of vacuum accident (LOVA) simultaneously with an air ingress event. Even though the probability of such a severe accident would be extremely low we must adopt a conservative methodology at this early stage, to later perform similar analysis considering more frequent and less severe accidents.

SOMSAF.1.- Neutronics analysis for Sombrero

In order to calculate off-site doses in a particular scenario, first we need to know the source term of radioactivity that is released to the environment. Neutron transport and activation, heat transfer, and thermal-hydraulics and aerosol transport calculations have been performed. Given the activity release and the specific dose of each isotope, the accident dose may be calculated.

In this section we present the results for the Sombrero neutron transport and activation analysis. Previous studies of the safety and environmental aspects of the Sombrero did not completely address the issues associated with the final focus system. While past work calculated neutron fluences for a grazing incidence metal mirror (GIMM) and a final focus mirror, scattering off of the final optical component was not included, and thus, fluences in the final focus mirror were significantly underestimated. In addition, past work did not consider neutron-induced gamma-rays. Also, power plant lifetime waste volumes may have been underestimated, as neutron activation of the neutron dumps and building structure were not addressed.

Here we use a 3-D Sombrero model for neutronics calculations, which includes the chamber/blanket structures, inner shielding and confinement buildings, and final optics system and neutron dumps. Not only did we perform neutronics analysis for the traditional KrF laser driven Sombrero design, but also we considered the effect of broadening the open solid angle fraction of the beam penetrations (from 0.25% to 5%) to allow for a diode pumped solid state laser (DPSSL).

In the following sections we present the results of a detailed neutronics analysis for Sombrero with the purpose of addressing oversights of previous studies and study the effect of 3-D modelling and the presence on the final optics in the model.

SOMSAF.1.1.- DPSSL versus KrF laser driven for Sombrero

A diode-pumped solid-state laser (DPSSL) appears to have attractive features that would be amenable to its use as a driver of an IFE power plant. Key outstanding issues are related to the cost of the diodes, degradation of final optics, cooling of optical components at a high repetition rate (~ 5 Hz), and adequate uniformity of the laser beams. One possible solution to obtaining the total uniformity that is needed is to increase the solid-angle fraction subtended by the laser beams (which of course decreases the solid-angle subtended by the first wall and blanket).

The Sombrero conceptual design, which originally used a KrF laser driven, has been modified in order to enable a DPSSL driver. To adapt the design to the new laser, the open solid-angle fraction for the beam ports has been increased from the value of 0.25% in the original design to 5%, while the number of beams (60) has been kept constant. Instead of using grazing-incidence metal mirrors (GIMMs), the modified design uses transmissive wedges for the final optical components. These components are needed to bend the beam so that the final focus mirrors, which are expected to be more sensitive to neutron damage, can be removed from direct line-of-sight of the fusion neutrons. The wedges sit 30 m from the target and the final focusing optics lie 50 m from the target. These distances are consistent with the previous Sombrero study. The rest of the reactor geometry used in this work has been kept the same as presented in the Sombrero final design report, except for the size of the optics and the neutron dumps, which has been increased to accommodate the larger open solid-angle fraction per beam. Figure SOMSAF.1 shows a vertical cross-section of a model of Sombrero design with these new characteristics.

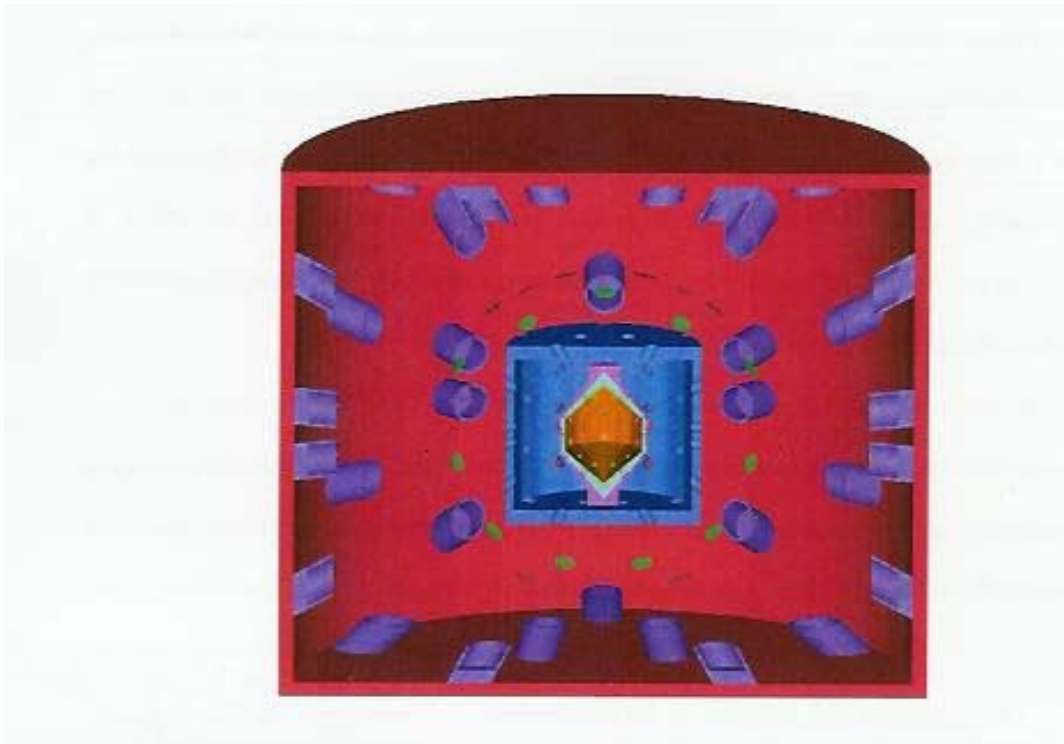


Figure SOMSAF.1. Vertical cross-section of the Sombrero power plant design

Neutron dumps are used to protect the final focusing mirrors from neutrons that could scatter off of the back wall. Since the neutron dumps are larger with the DPSSL design, the final focusing mirrors must be moved farther from the beam axis and the bending angle at the wedge must be increased as well. Table SOMSAF.1 shows some of these values for both of the Sombrero versions.

Table SOMSAF.1 Plant parameters for the KrF laser and DPSSL driven Sombrero concepts

Feature	Original (KrF) SOMBRERO	DPSSL- SOMBRERO
Total open solid-angle fraction	0.25%	5%

Number of beams	60	60
Open solid-angle fraction per beam	4.17E-05	8.33E-04
Half-angle of each beam	0.74 degrees	3.31 degrees
Penetration radius at the first wall	8.4 cm	37.6 cm
Line-of-sight radius at the final optical element	38.7 cm	173.4 cm
Line-of-sight radius at the neutron dump	64.6 cm	289.0 cm
Thickness of the wall of the neutron dump	50 cm	50 cm
Depth of the neutron dump	193.8 cm	500 cm
Required deflection angle to miss the neutron dump	4.85 degrees	18.9 degrees
Deflection angle of the final optical element	GIMM = 60.0 degrees	Wedge = 37.8 degrees

(Values calculated assuming circular penetrations)

In order to increase the deflection angle of the wedges, the thickness would also have to be increased. To avoid unreasonably thick wedges, the configuration of the final optical components has been modified to minimize the bending angle. One possible solution consists of splitting each beam in two so that two focusing mirrors are standing on either side of the neutron dump. The two final focusing mirror arrays send their respective beams to a single combined wedge array. An alternate method of reducing the bending angle would be the use of a rectangular or elongated configuration for the beams, as opposed to a square configuration. Such a configuration would require rectangular penetrations in the chamber and rectangular neutron dumps, but it would result in a considerable reduction of the bending angle. Figures SOMSAF.2, SOMSAF.3 and SOMSAF.4 show these configurations for one of the sixty penetrations. Figure SOMSAF.2 depicts a square array of beamlets (each of the sixty beams would actually consist of multiple “beamlets”). Figure SOMSAF.3 shows how the beams could come from two final focusing mirrors, and Figure SOMSAF.4 shows how the bending angle can be reduced through the use of a rectangular array of beamlets.

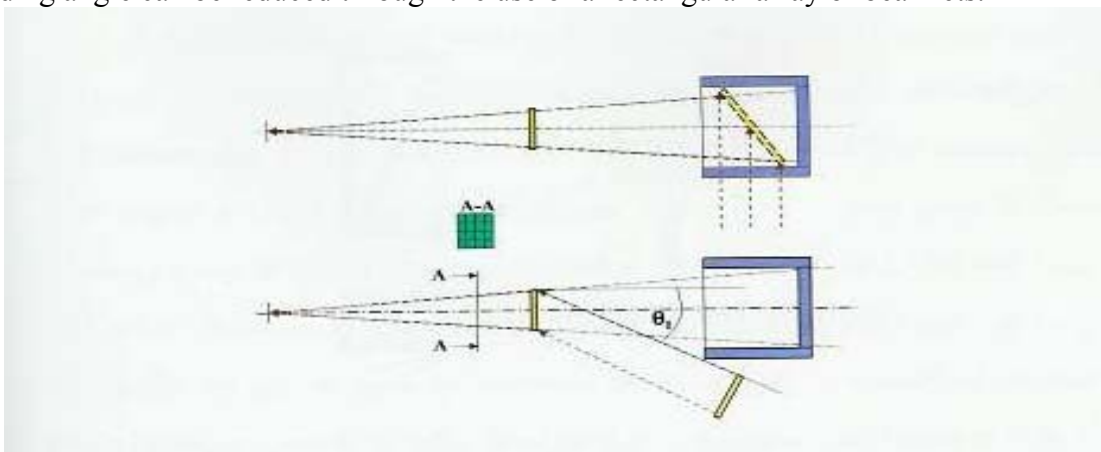


Figure SOMSAF.2. The baseline wedge/neutron dump design would use a square array of beamlets for each of the main beams. A wedge bending angle of 17.04° would be required

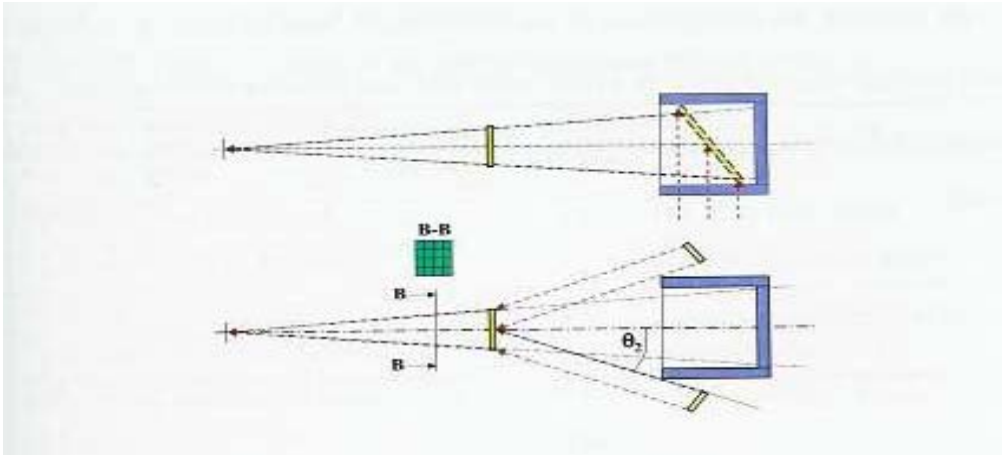


Figure SOMSAF.3. By switching to two final focusing mirrors, the wedge bending angle can be reduced to 11.53°

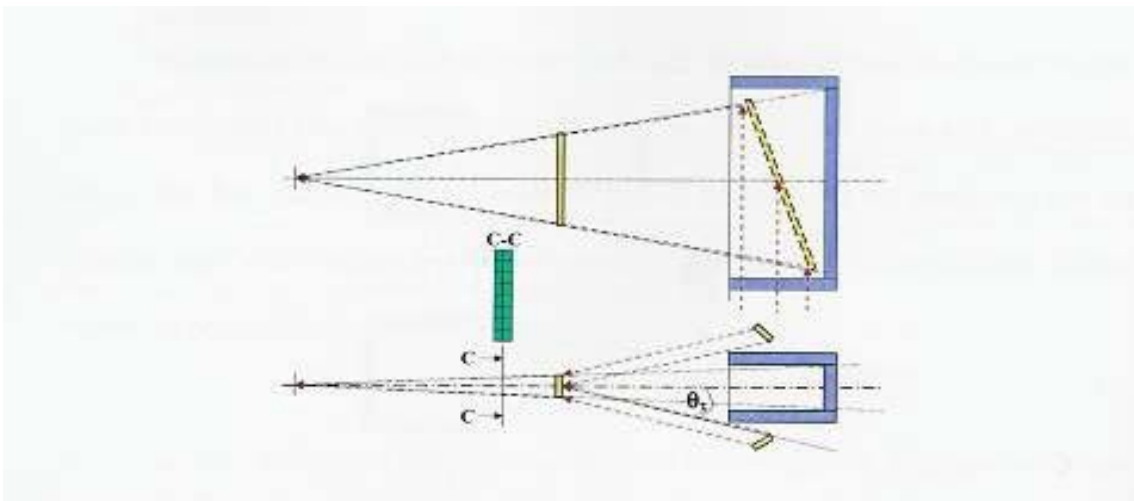


Figure SOMSAF.4. Using a rectangular array instead of a square one, the bending angle can be reduced to only 6.77°

By changing the configuration of the beamlets, the bending angle, θ , is reduced from the baseline value of 17.04° to 11.53° when two final focusing mirrors are used and then to only 6.77° with a rectangular array of beamlets. Assumptions made include the following:

- wedge is 30 m from the target
- neutron dump starts 45 m from the target, is 5 m deep, and has a wall thickness of 0.5 m
- final focusing element(s) stand just outside the neutron dump

SOMSAF.1.2.- Overview of previous work

In order to compare our results to previous studies, we have reviewed previous work that was completed for the Sombrero and SIRIUS-P IFE power plant designs. Both designs are for a 1000 MW_e KrF laser-driven IFE power plant utilizing direct drive targets in a near symmetric illumination configuration. In both cases, 60 beams providing a total of 3.4 MJ of energy are used at a repetition rate of 6.7 Hz and a target gain of 118. The main difference between the designs is the value of the open solid-angle fraction (0.25% for Sombrero and 0.4% for

SIRIUS-P) and the position of the optics (GIMM at 30 m and final focusing mirror at 50 m for Sombrero, and GIMM at 25 m and final focusing mirror at 45 m for SIRIUS-P). Table SOMSAF.2 shows the values of these and other geometric parameters for both cases.

Table SOMSAF.2 Plant parameters of the KrF Sombrero and SIRIUS-P designs

Original (KrF) SOMBRERO	SIRIUS-P
KrF laser driven	KrF laser driven
GIMM at 30 m from target	GIMM at 25 m from target
Final focus at 50 m from target	Final focus at 40 m from target
60 beams	60 beams
Solid-angle fraction = 0.25%	Solid-angle fraction = 0.4%
Penetrations modelled as cones with 0.74° half angle	Penetrations modelled as cones with 1° half angle
C/C first wall at 6.5 m from target	C/C first wall at 6.5 m from target
Inner concrete shield at 10 m from target	Inner concrete shield at 10 m from target
Outer shield at 50.5 m from target	Outer shield at 42 m from target

These two designs have been studied in order to validate our methodology, and calculations have been made in order to repeat the results that were presented for both of them. However, as today's codes and capabilities have been improved, some approximations have been found in those previous works.

It has been found that neutron-induced gamma-ray doses in the final optical or focusing components were not considered then. Recent work in support of the National Ignition Facility (NIF) indicates that gamma-ray doses can be of great importance when estimating the lifetime of optical components.

In the Sombrero work 1-D scaling was performed in order to achieve the fast neutron flux at the position of the final focusing mirror (reported to be 8.6×10^9 n/cm²s). Our calculations have shown this flux to be higher when performing 3-D calculations that consider the secondary neutrons scattered by the GIMM.

For the SIRIUS-P work 2-D and 3-D calculations were made. For the 2-D model the GIMM was not considered so, the scattering of the neutrons in this element was not taken into account. In the 3-D representation the GIMM was included in the model. A conical reflector was used at the boundary to obtain the results for the whole geometry. It has been found however, that a series of circular cones cannot fill an entire sphere or cylinder without overlap and/or holes. The magnitude of the bias introducing when using a conical reflector depends on factors such as smoothness of the flux, in space and direction.

Finally, in order to predict the expected lifetime for the optics, neutron and gamma fluence limits have yet to be determined. The Sombrero and SIRIUS-P studies estimate the optics lifetime assuming a range of neutron fluence limits. Using these "limits", the expected lifetime in full-power-years was calculated. A complete analysis would require more material data about the fast neutron and gamma-ray fluence limits.

SOMSAF.1.3.- Neutronics model of Sombrero

3-D neutronics calculations have been performed using the TART98 Monte Carlo neutron and photon transport code. The neutron spectra in regions of interest have been calculated in 175 energy groups.

Only one octant of the 4π total geometry was modelled with the associated first wall (FW), blanket, inner and outer shield, optics, and neutron dumps. Three reflecting planes located at the origin and perpendicular to x, y and z axes were used, and a point neutron source was used at the origin emitting neutrons isotropically with the Sombrero target energy spectrum. The 3-D model used for the neutronics calculations is shown in Figure SOMSAF.5.

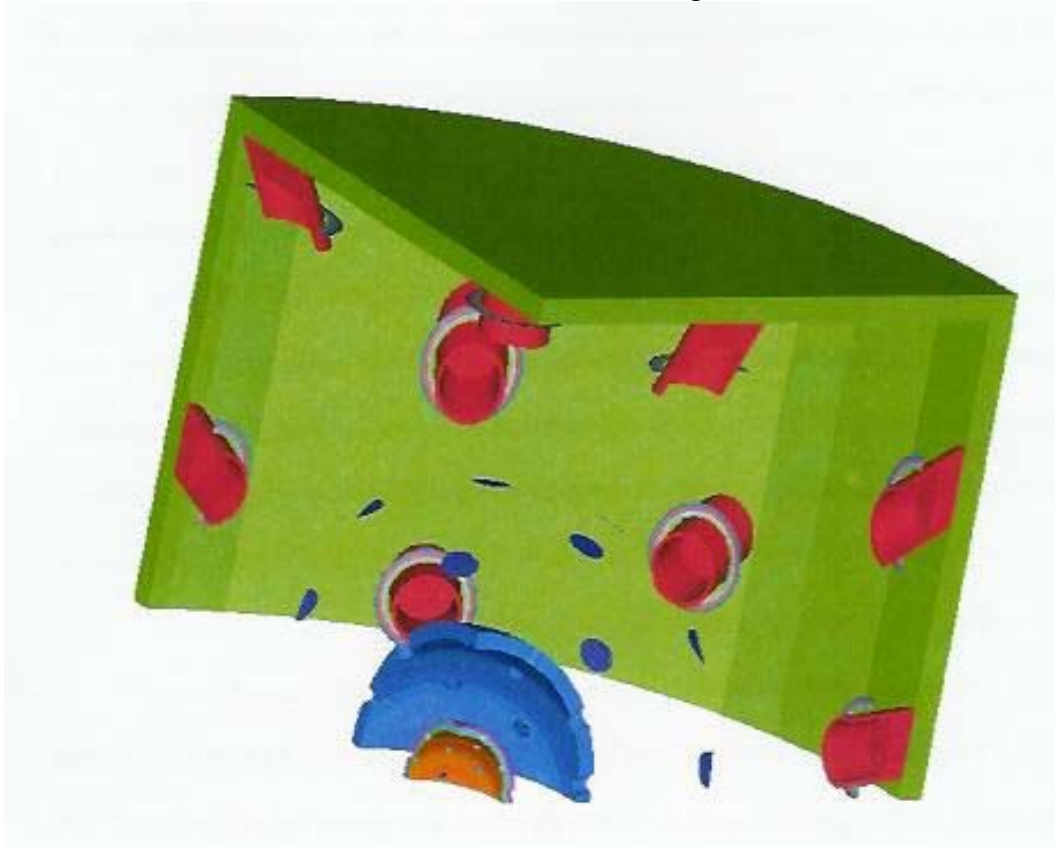


Figure SOMSAF.5. 3-D model of Sombrero used for neutronics calculations in the present work

The model includes the detailed radial build of the Sombrero design at the midplane for the blanket/reflector, which consists on a moving bed of solid Li_2O particles flowing through the chamber by gravity. The overall thickness is 1 m, with an inner radius of 650 cm. The FW consists of a 1 cm thick C/C composite zone and is followed by a 19 cm region in which the carbon fraction is 3%. The third and fourth zones are each 40 cm thick and have 20% and 50% fraction of carbon, respectively. Increasing the carbon fraction toward the back of the blanket provides a built in reflector, which gets cooled by the Li_2O breeding material. Of the total mass flow rate through the reactor, 57% goes through the FW channel, while remaining 43% goes to the rest of the channels. We assume that the Li_2O is 90% density, and the moving bed has a 60% of this material, giving the effective density of Li_2O a value of 1.08 g/cm^3 .

The 1.5 m thick inner shield and the cylindrical reactor confinement building are included in the model. The neutron dumps have been modelled with cylindrical geometry using a variety of aspect ratios (AR = depth divide by diameter) to analyse its influence on the dose at the final focusing optics. The inner shield is composed of 70 vol% boron-frits concrete and 20 vol% steel. The containment building and the neutron dumps are made of ordinary concrete (a homogeneous mixture of concrete with 0.14 wt% boric acid; the concrete is then mixed with 1 vol% (3.24 wt%) ASTM A-706 steel rebar).

The wedges are located at 30 m from the target and are made of pure fused silica. Calculations have also been performed for other locations of the wedges relative to the target, in order to perform a sensitivity analysis. A baseline wedge thickness of 1 cm was used, but other thickness values have been investigated as well. In order to approximate the location of the final focusing mirror, results have been obtained in different rings around the neutron dumps.

All the free space inside the reactor is filled with xenon gas at 0.5 torr in order to protect the first wall from target emissions.

Dose rate fluxes from gamma-rays and fast neutrons have been obtained at the optical elements. As said before, the results for the final focusing mirrors are reported in different cylindrical zones around the neutron dumps composed of xenon gas. The fast neutron fluxes have been calculated considering only that part of the spectrum with energy values over 100 keV.

Once neutron transport is complete, the TARTREAD code is used to interactively interpret the results and create an input file for the ACAB radionuclide generation/depletion code. The FENDL/A-2.0 activation cross-section library has been used.

Neutron activation calculations have been completed assuming 30 years of “full-power” continuous irradiation, using a fusion power of 2677 MW. For the present work the pulsed nature of the irradiation is ignored and it is approximated with the “equivalent steady state” (ESS) method. Activation results have been obtained for cooling times of up to 100 years.

ACAB output includes radionuclide inventories, biological hazard potentials, afterheat, contact dose rates, waste disposal ratings (WDR), and other activity related parameters that the user may request. The ACAB output gives results by radionuclide as well as totals for each index. We have reported the results of WDR and contact dose rates.

The waste-disposal rating is given by
$$WDR = \sum_i \frac{A_i / V}{SAL_i}$$

Where A_i is the activity of the i^{th} radionuclide, SAL_i is its specific activity limit given by Fetter, Cheng and Mann, and V is the component volume in m^3 . Summation over all radionuclides provides a single value. A WDR less than unity indicates that a component would qualify for disposal via shallow land burial. It must be noted that the WDR is only used in this work as an index to quantify relative hazards. It does not implicate that shallow land burial will be an available method for waste management nor that it will necessarily be the best choice for waste disposal.

The contact dose rates can be used to analyse occupational exposures for the various power plant components. They are given as a function of time after shutdown. Contact dose rates are calculated using a semi-infinite medium approximation, which assumes that the radionuclides are present at a constant concentration (calculated for the finite component). This approximation leads, in general, to a conservative estimation of the actual dose rates that would be present for a finite component.

SOMSAF.1.4 Neutronics analysis results

As first step to confirm the importance of modelling the final optic (wedge or GIMM), a calculation was made just taking into account the secondary neutron flux (not the direct line-of-sight neutrons, but the neutrons resulting from scattering) at the final focusing mirror position. The same case was run first with a 1 cm thick wedge at 30 m from the target position, and then without the wedge. No neutron dump was modelled in this case to avoid its contribution to scattered neutrons.

As is shown in Figure SOMSAF.6, the contribution of the neutrons that are scattering by the wedge needs to be considered as it represents more than a 60% of the total secondary neutron flux. Another important aspect for the neutronics understanding to be observed in the same figure is the fact that the flux curve remains relatively flat with the distance away from the beam axis. This implies that the wedges are a scattering source for more than one set of mirrors (i.e., wedges are cross-talking).

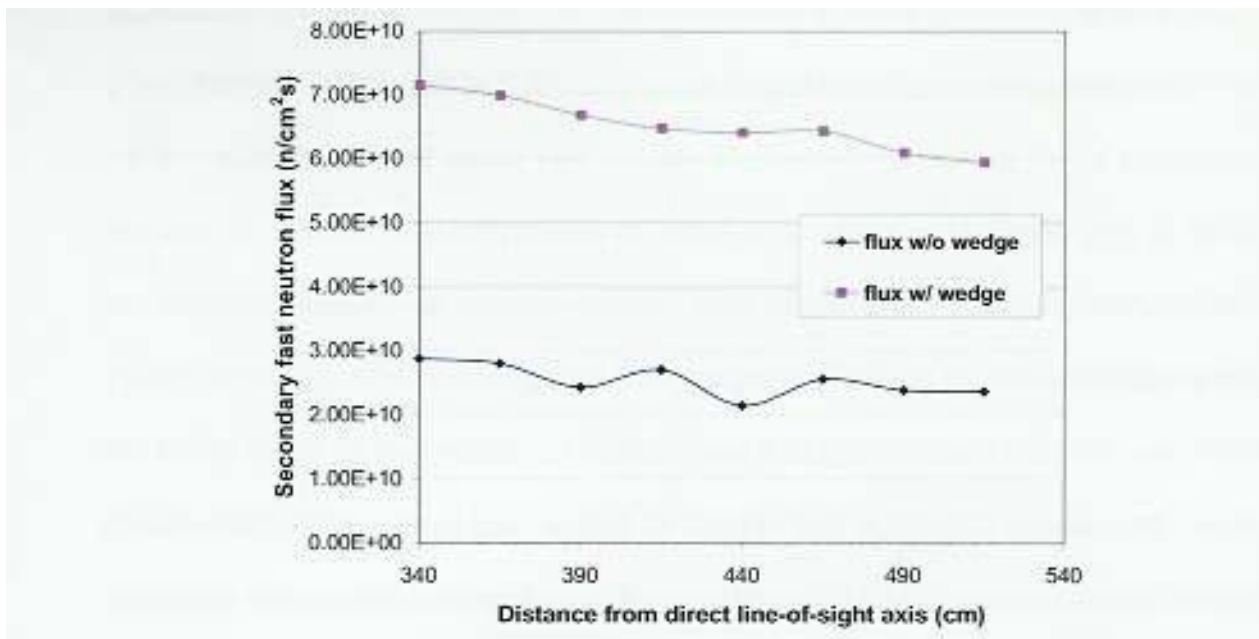


Figure SOMSAF.6. Comparison of the secondary neutron flux at the final focusing mirror position in the cases with and without wedges

Figure SOMSAF.7 shows the fast neutron fluxed at the final focusing mirror as a function of the distance from the beam axis for three different open solid-angle fractions.

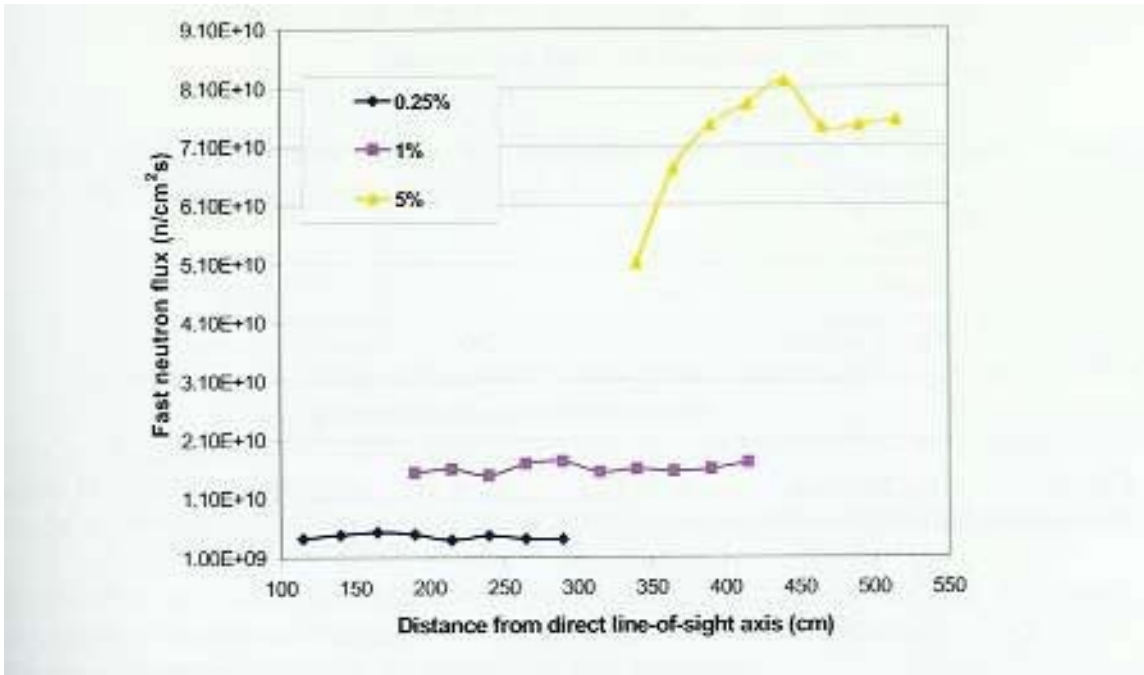


Figure SOMSAF.7. Fast neutron fluxes at final focusing mirror position in the cases of open solid angle fractions equal to 0.25, 1 and 5%

In all the three cases the aspect ratio of unity was used for the neutron dumps. Since neutrons scattering off of the wedges dominate, the fast neutron flux at the final focusing mirror scales approximately with the total open solid-angle.

Calculations have been made for different thickness of the wedges (1, 3 and 5 cm), and the results suggest that neutrons scattered off of the wedges dominate the fast neutron flux at the final focusing mirror position. This result is shown in Figure SOMSAF.8.

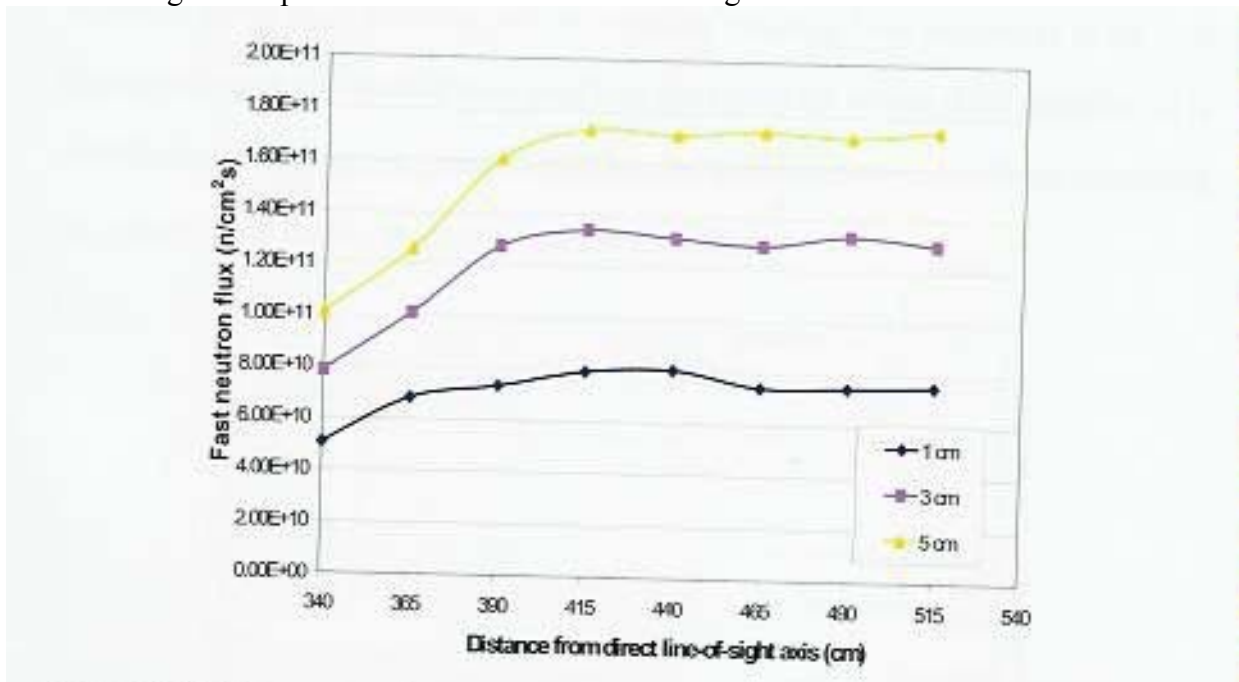


Figure SOMSAF.8. Fast neutron fluxes at final focusing mirror position in the cases of wedge thickness equal to 1, 3 and 5 cm

Different aspect ratios (AR = depth divided by diameter) have been considered for the neutron dumps. Results have been obtained for values of AR = 1, 2 and 3. Figure SOMSAF.9 shows the fast neutron fluxes at the final focusing mirror for the different aspect ratios of the dumps in the case of 5% total open solid-angle. Whereas larger aspect ratios are clearly beneficial, the sizes of the dumps with 5% open solid angle are probably excessive for AR > 1.

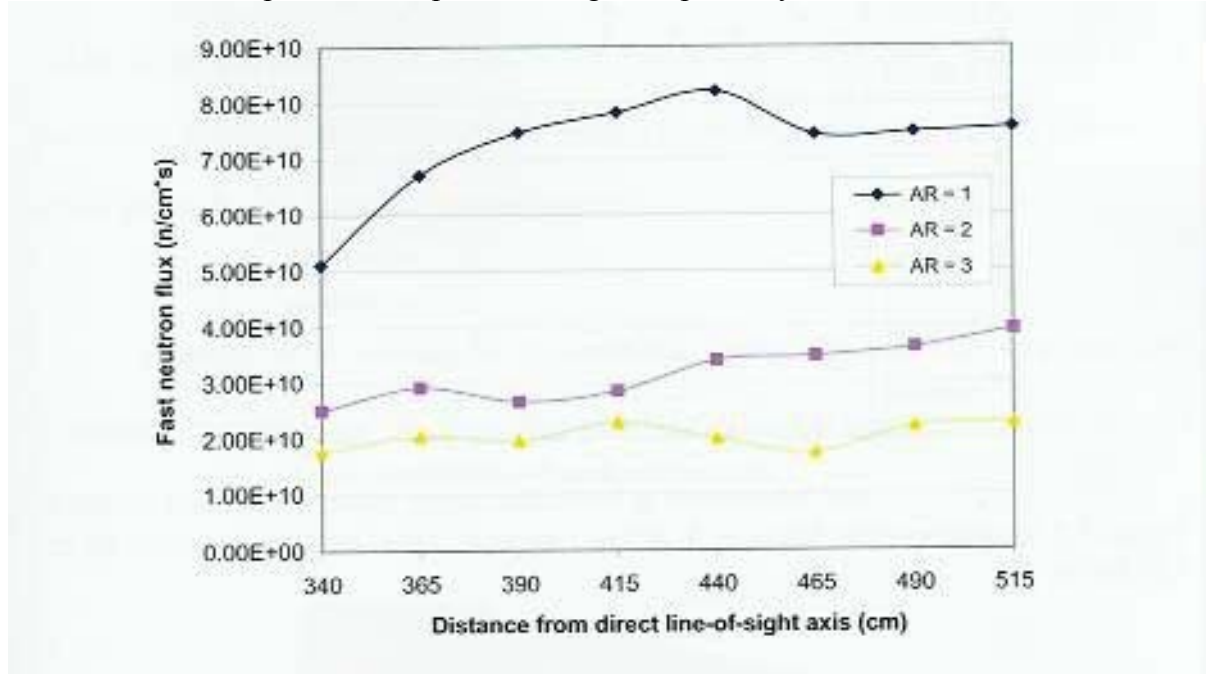


Figure SOMSAF.9. Fast neutron fluxes at final focusing mirror position in the cases of aspect ratio of the neutron dumps equal to 1, 2 and 3

In order to address the effect of having a greater number of beams for the same open solid-angle fraction, a case with 120 penetrations instead of 60 was performed. As can be observed in Figure SOMSAF.10 reducing the diameter of the wedges and penetrations did not show any major improvement in the flux levels at the final focusing optic, given that the different penetrations are interacting with each other.

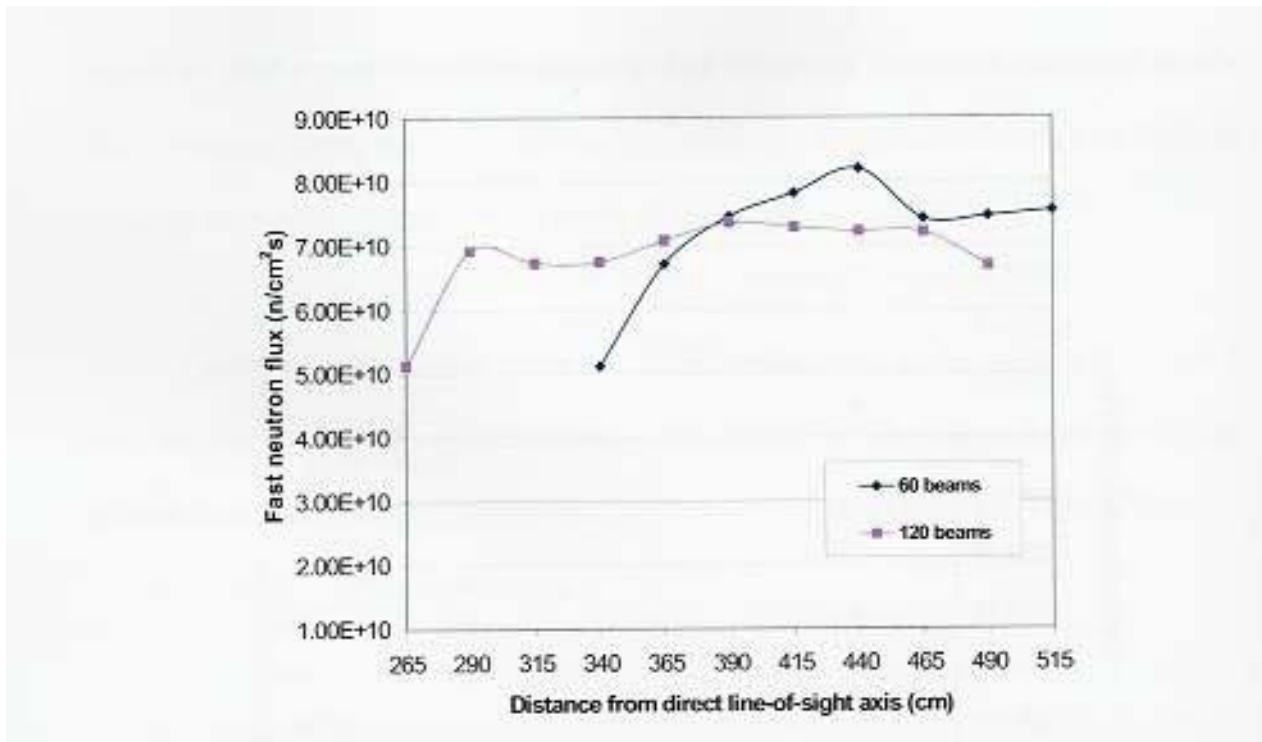


Figure SOMSAF.10. Fast neutron fluxes at final focusing mirror position in the cases of 60 and 120 beams

To study the impact of changing the stand-off distance of the wedges, a calculation was made with this distance being 20 m in stead of 30 m from the target. The results in the fast neutron flux at the final focusing mirror were rather insensitive to this parameter, but obviously the flux in the wedges would be greater. Figure SOMSAF.11 show this effect for the flux on the final focusing mirror.

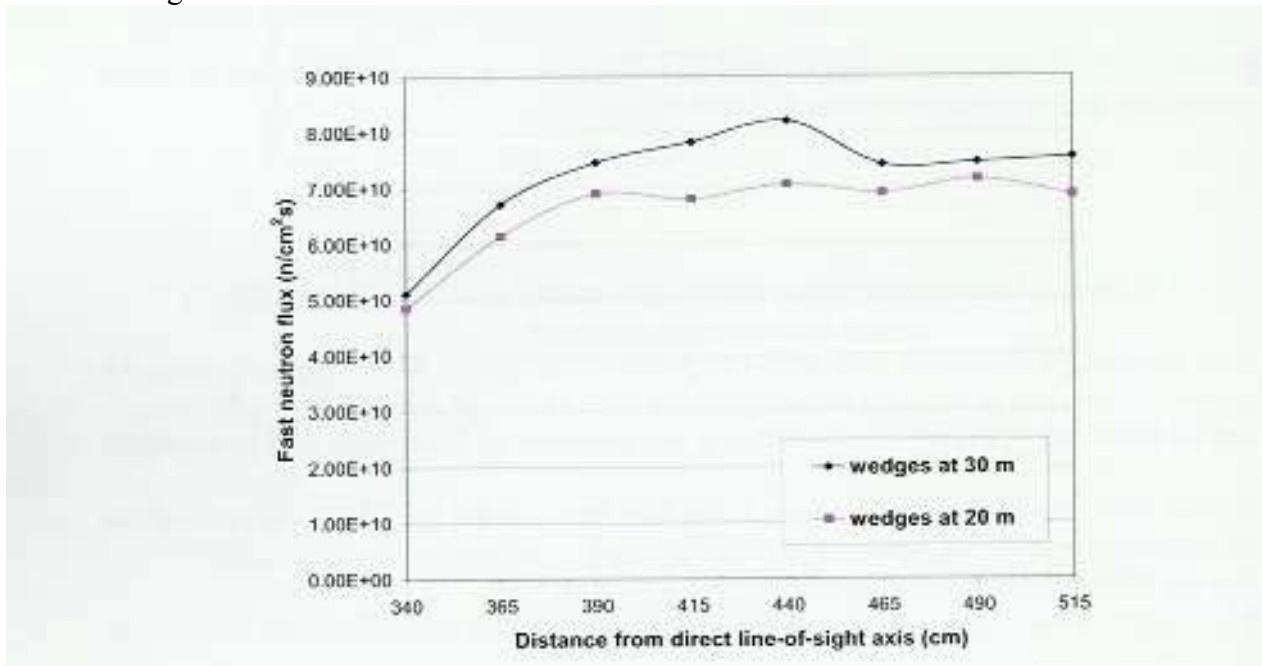


Figure SOMSAF.11. Fast neutron fluxes at final focusing mirror position in the cases that the wedge stand-off distance is 20 and 30 m from the target

A model with rectangular penetrations instead of circular ones was also developed, in order to explore the effect of having elongated beam penetrations in order to reduce the bending angle.

This model, which is shown in Figure SOMSAF.12, resulted in no significant effect on the neutron and gamma ray fluxes in the optics, but the benefit in allowing a smaller bending angle for the beam is still significant. In fact, even though we compared the results for the wedges being 1 cm thick, a smaller bending angle would require smaller wedge thickness.



Figure SOMSAF.12. 3D model of the DPSSI driven Sombrero version with rectangular penetrations

After completing the above sensitivity analyses for the various parameters, a set of final results has been obtained and is presented for a base case of 5% total open solid-angle fraction, 60 penetrations, aspect ratio of the neutron dumps equal to one, and wedges 1 cm thick standing at 30 m from the target. It must be noted that the design of the final optic wedges is not finalized, if thicker wedges are needed, the fluxes would be higher as shown in Figure SOMSAF.8. Some variations to the base case are also given (e.g., distance to final optic and open solid angle fraction). Figures SOMSAF.13 to SOMSAF.22 show the results of our analyses for the following parameters.

1. Fast neutron and gamma-ray fluxes at the wedges.
2. Neutron and gamma dose rates at the wedges.
3. Fast neutron and gamma-ray flux.
4. Neutron and gamma dose rates at the final focusing mirrors.
5. WDR for concrete (building and neutron dumps).
6. Contact dose rates for concrete.
7. Lifetime projections for the optics.
 - a) wedges
 - b) final focusing mirrors

Figures SOMSAF.13 and SOMSAF.14 show the neutron and gamma fluxes and neutron and gamma dose rates for the different stand-off distance of the wedges. The fast neutron fluxes for these optical elements are 90% from direct line-of-sight neutrons. The wedges would be

made of fused silica operated at high temperature (around 400°C) to promote self-annealing of the optic. Although neutrons are dominant, the gamma-ray contribution must be considered for a complete analysis of the optics lifetime.

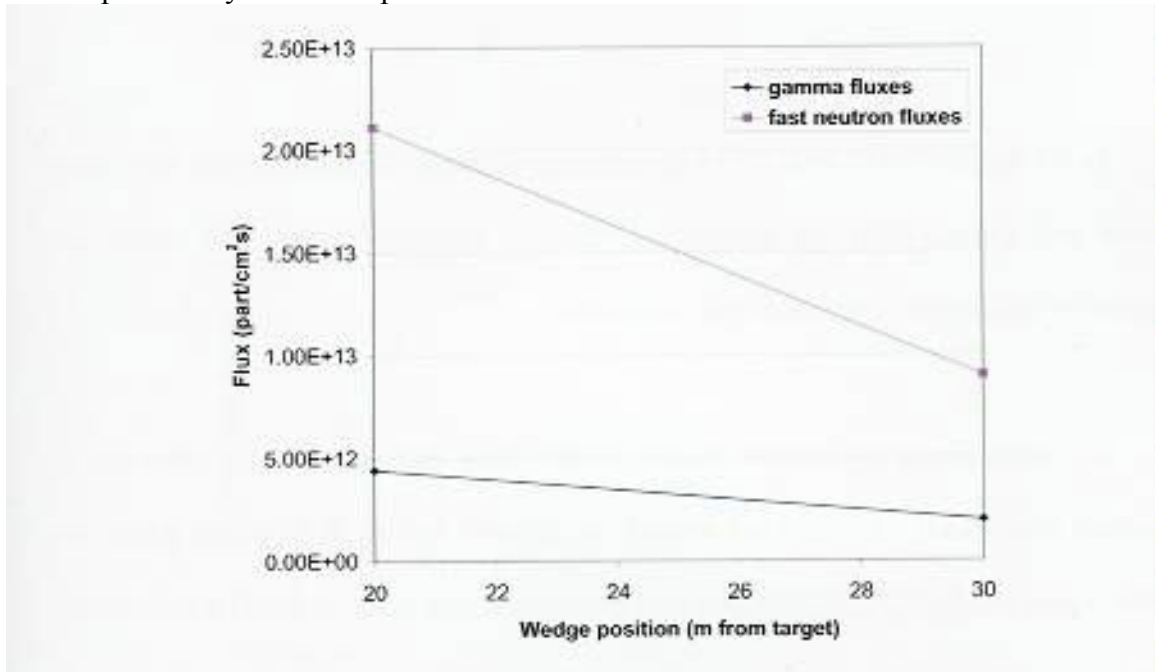


Figure SOMSAF.13. Gamma-ray fast neutron fluxes at the wedge as a function of its position (m from target)

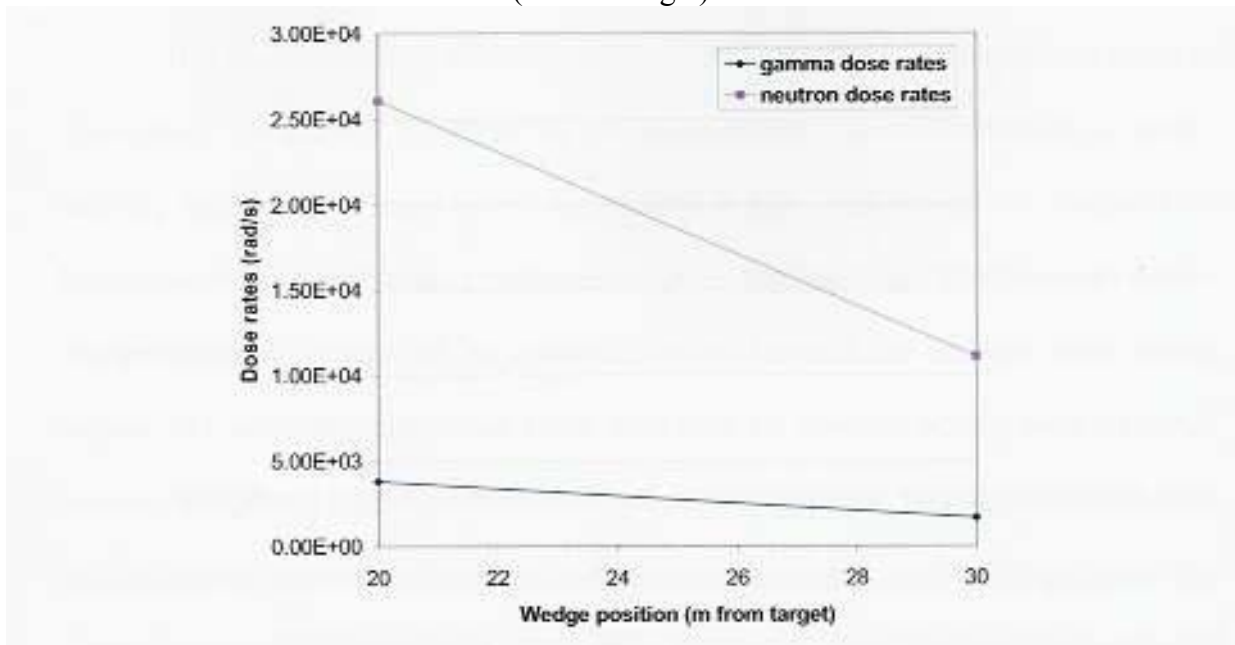


Figure SOMSAF.14. Gamma-ray and neutron dose rates at the wedge as a function of its position (m from target)

In the figures SOMSAF.15 and SOMSAF.16 the same parameters (fluxes and dose rates from neutrons and gamma-rays) are shown, for the final focusing mirror. The results are presented as a function of the total open solid-angle.

As noted in the description of our model, these results have been obtained in cylindrical rings made of xenon gas around the neutron dumps, in locations where the mirrors would reside. The radial position of these rings was taken to be 47.5 m from the target.

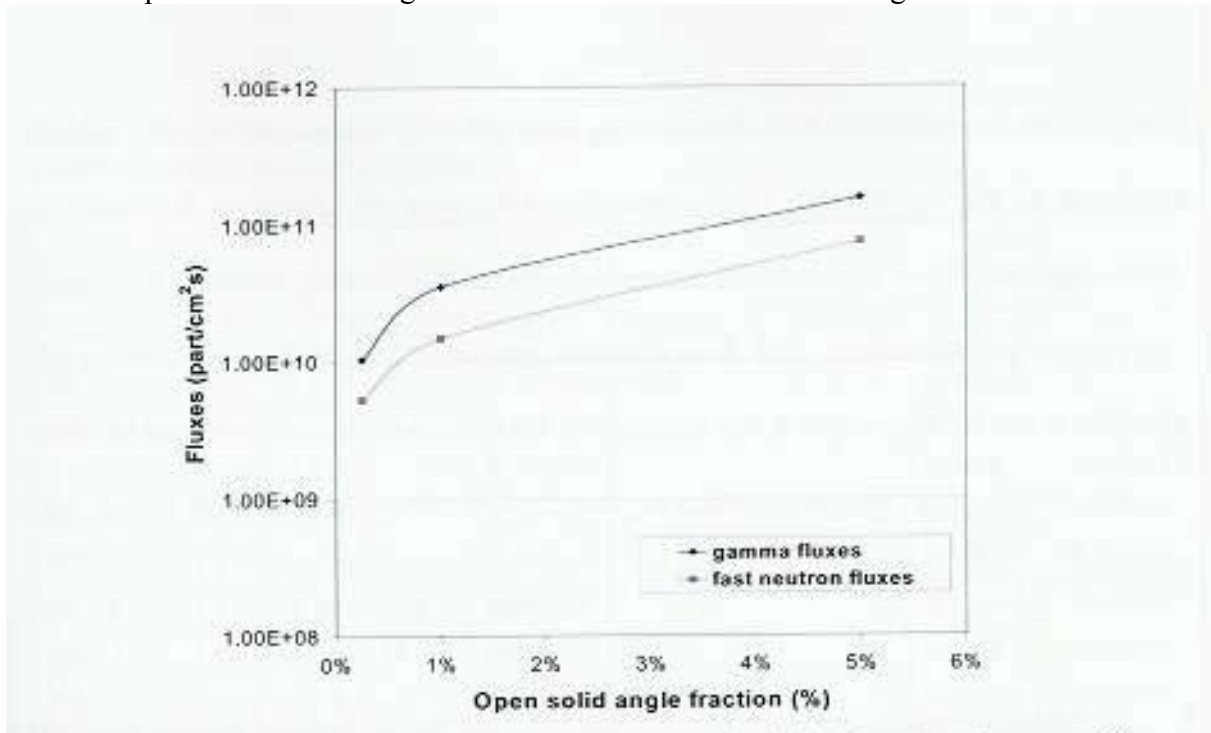


Figure SOMSAF.15. Gamma-ray and fast neutron fluxes at the final focusing mirror position as a function of the open solid angle fraction

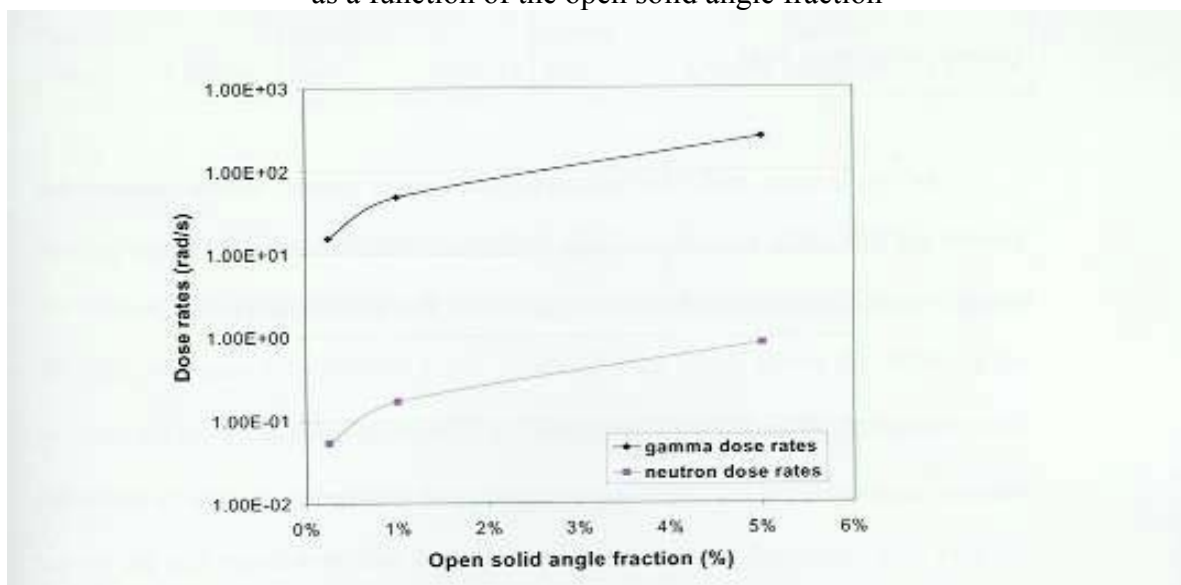


Figure SOMSAF.16. Gamma-ray and neutron dose rates at the final focusing mirror position as a function of the open solid angle fraction

It can be observed that the neutrons and gammas that scatter off the wedges dominate, so the contribution from neutrons and gammas that penetrate the dumps is relatively small. These figures show the consequences of increasing the open solid-angle fraction: the fluxes and dose rates increase proportionally to the open solid-angle fraction. It can be observed that the gamma flux and dose rate, so once more the importance of taking into consideration the gamma-rays is shown.

All the previous results have been obtained from the neutron and gamma transport calculations. Once neutron transport is complete, the TARTREAD code is used to interactively interpret the results and create an input file for the ACAB radionuclide generation/depletion code.

As we already said, the activation calculations results include radionuclide inventories, biological hazard potentials, afterheat, contact dose rates, waste disposal ratings (WDR), and other activity related parameters that the user may request.

Table SOMSAF.3 shows the most contributing nuclides to the activities of the different chamber components at the beginning of the accident (shutdown). It must be noted that we have only considered here those radionuclides with half-lives longer than one second and which contribute with more than 15 to the total activity in each component.

Table SOMSAF.3 Most contributing nuclides (>1%) and total activities of the different chamber components in Sombrero

CC/FW		C/C Blanket		Li ₂ O		Xe gas	
Nuclide	(%)	Nuclide	(%)	Nuclide	(%)	Nuclide	(%)
AL 28	3.72E+01	AL 28	3.43E+01	N 16	9.97E+01	XE131M	3.39E+01
AR 37	2.15E+01	AR 37	2.44E+01			XE133	2.06E+01
F 20	1.18E+01	F 20	9.67E+00			XE135	1.33E+01
NA 24	6.30E+00	NA 24	8.78E+00			XE129M	9.91E+00
PB207M	4.59E+00	NE 23	4.58E+00			XE133M	8.22E+00
NE 23	4.57E+00	PB207M	4.00E+00			XE135M	6.24E+00
MG 27	2.88E+00	MG 27	2.75E+00			XE127	2.98E+00
P 32	2.09E+00	P 32	2.30E+00			XE134M	2.52E+00
FE 55	1.92E+00	SI 31	2.07E+00				
MN 56	1.08E+00	V 52	1.36E+00				
AL 29	1.02E+00	FE 55	1.22E+00				
Total Activity (Bq)	6.14E+14	Total Activity (Bq)	1.36E+15	Total Activity (Bq)	5.79E+18	Total Activity (Bq)	1.41E+16

As the first wall and blanket easily meet waste disposal rating (WDR) criterion for shallow land burial (WDR < 1), only the results for the concrete of the building and the neutron dumps

are reported in this section. Figure SOMSAF.17 shows the WDR for the containment building and for the neutron dumps as a function of the open solid-angle fraction.

As would be expected due to their exposure to line-of-sight neutrons, the neutron dumps have a much higher WDR value than the building. WDR for the neutron dumps increases slowly with the open solid-angle. WDR for the building shell is proportional to the open solid-angle fraction, but is not significant as it is $\ll 1$. This makes the waste management rather insensitive to the open solid-angle fraction. It should be noted that the neutron dumps are unimportant from the waste volume perspective (they are around 0.1% of the building shell volume in the largest case), and thus, the total waste volume does not change as the open solid-angle fraction is increased.

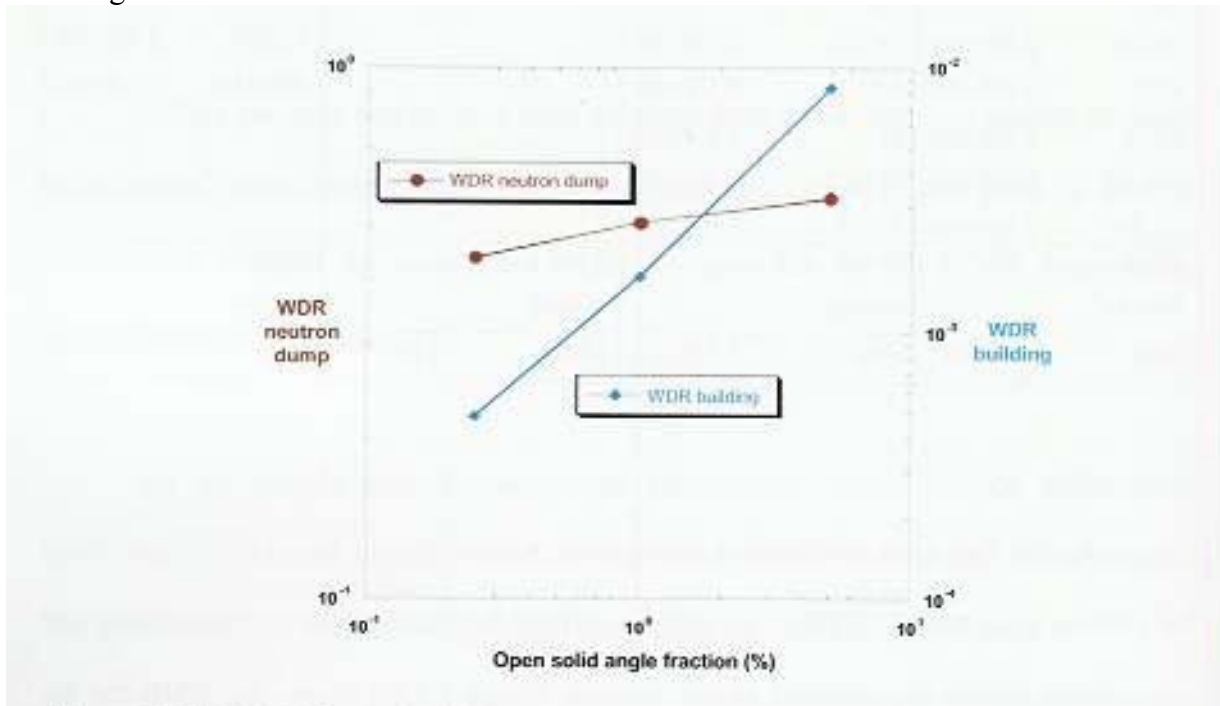


Figure SOMSAF.17. WDR for the building shell and the neutron dump as a function of the open solid angle fraction

The contact dose rates for the building and a single neutron dump are shown respectively in Figures SOMSAF.18 and SOMSAF.19 as a function of the cooling time after shutdown.

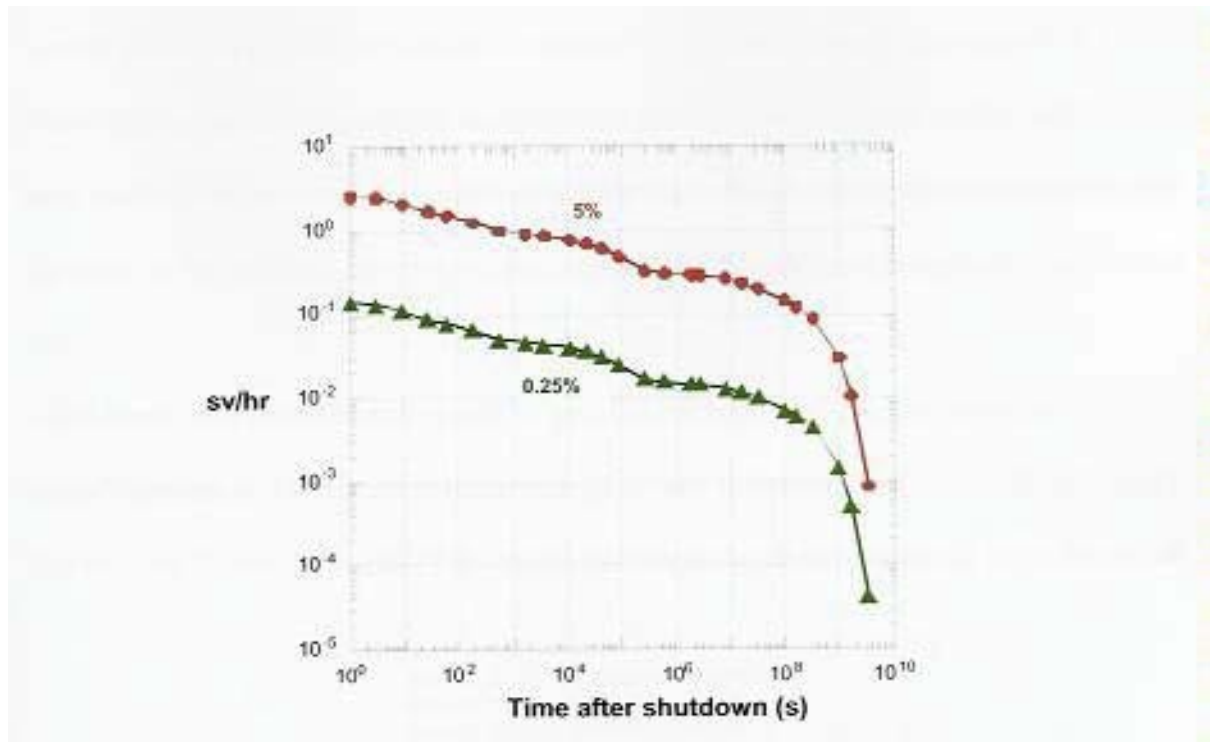


Figure SOMSAF.18. Contact dose rates for the building shell as a function of time after shutdown in the cases of open solid angle fraction equal to 0.25% and 5%

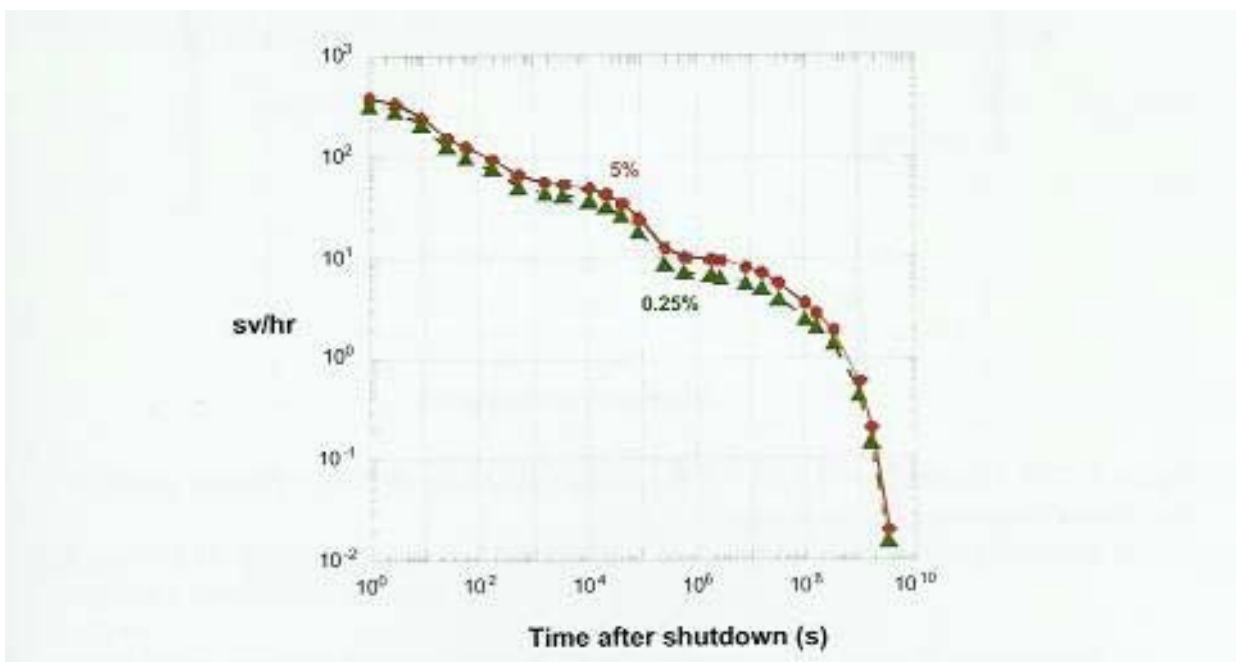


Figure SOMSAF.19. Contact dose rate for the neutron dump as a function of time after shutdown in the cases of open solid angle fraction equal to 0.25% and 5%

The results are given in Sv/h for two different solid-angle fractions: 0.2% and 5%. It can be observed that neutron dumps produce a significantly higher contact dose rate, which is independent of the solid-angle fraction.

Finally estimates of the expected lifetime of the optical elements have been made. Figure SOMSAF.20 shows the lifetime of the wedges as a function of the fast neutron fluence limit and of the distance from the wedge to the target.

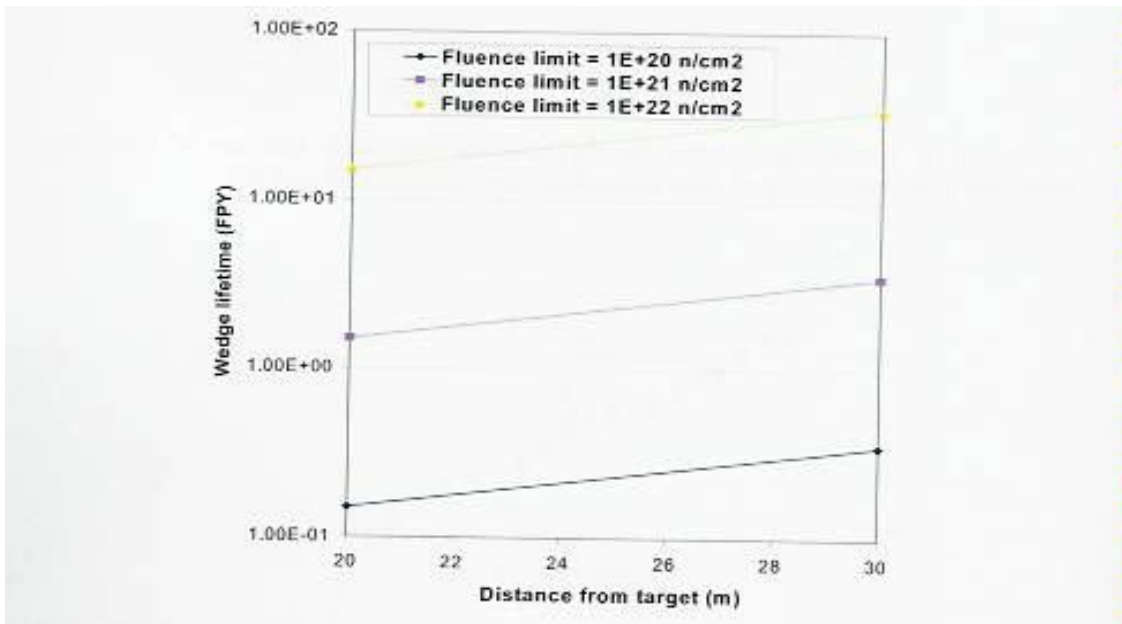


Figure SOMSAF.20. Lifetime prediction for the wedge assuming different fluence limits as a function of its position (m from target)

Assuming a fluence limit of 10^{21} n/cm², as done in the Sombrero report, the lifetime of the wedges standing at 20 m from the target is estimated to be 1.5 full-power years (FPY). If the distance is increased to 30 m the lifetime increases to 3.5 FPY. It is clear that the lifetime of the wedges is very sensitive to the neutron fluence limit and also to the damage recovery via self-annealing. Experimental data on radiation damage to the wedges are essential to allow for a more accurate prediction of their lifetime.

Results for the final focus mirrors are given in Figure SOMSAF.21 as a function of the fast neutron fluence limit and of the open solid-angle fraction.

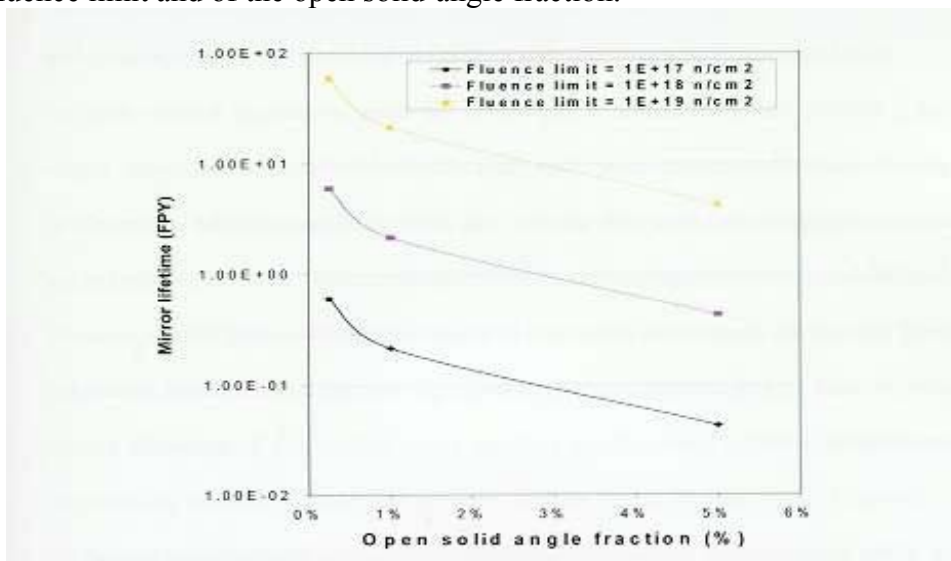


Figure SOMSAF.21. Lifetime prediction for the final focusing mirror assuming different fluence limits as a function of the open solid angle fraction

There is very little data on neutron damage to dielectric mirrors. If we make the conservative assumption that a multilayer mirror with no colour centre will have a fast neutron fluence limit of 10^{18} n/cm² the lifetime of the final focus mirrors for an open solid-angle fraction of 5% would be about 0.4 FPY. Again experimental data on the effect of radiation damage on the reflectivity of the dielectric coating of the final focus mirror are required.

SOMSAF.1.5.- Summary of neutronics analysis

In order to make the Sombrero design suitable for an inertial fusion power plant using a DPSSL driver instead of a KrF laser, the open solid-angle fraction must be increased to obtain suitable smoothing. The broadened beam lines require bigger penetrations through the first wall, blanket and inner shielding, and the radius of the optical elements used to focus and direct the beams must also be increased. Finally, the size of the neutron dumps, which are used to protect the final focusing mirrors, must be increased such that the footprint of the line-of-sight neutrons is contained within the neutron dump.

We have searched the possible solutions to reduce the bending angle needed for the final optic to redirect the beam from the final focus mirror (standing next to the neutron dump) towards the target. With this purpose, a rectangular-elongated configuration, which allows the beam to come from either side of the neutron dump, has been proposed.

An overview of previous neutronics analysis has been made, and problems with some assumptions have been identified and addressed. In order to perform an accurate calculation, a 3-D model of the Sombrero reactor has been developed, taking into consideration the first wall, blanket/reflector, inner shielding, wedges, final focusing mirrors, neutron dumps and containment building. 3-D neutronics calculations have been performed. Sensitivity analyses have been developed to quantify the effect of the various design parameters.

The importance of modelling the wedges in order to account for the scattering of neutrons has been demonstrated. The fast neutron flux at the focusing optic has been shown to be dominated by secondary neutrons scattered by the wedges and interaction between the different penetrations has been observed. It has been shown that the fast neutron flux on the focusing optic is proportional to the open solid-angle fraction, as well as the thickness of the wedges. As a result, a smaller value of the open solid-angle fraction will translate directly into a longer lifetime of the focusing optic. This reduction in the open solid-angle fraction can be achieved by increasing the bandwidth of the laser. It is also recommended that wedges be as thin as practical as this will also reduce the scattered radiation.

Using a greater number of beams for a constant open solid-angle fraction does not have a significant influence on the fluxes in the final focusing optic, but would definitely be desirable in order to reduce the thickness of the wedges. The same conclusion can be obtained from reducing the wedge stand-off (and consequently increasing its distance from the final focusing optic), which has resulted not to have a significant effect on the neutronics at the focusing optic.

It has been observed that contact doses rates and waste management are rather insensitive to the open solid-angle fraction. Neutron dumps dominate the contact doses and also the total WDR for the concrete, and show a slow increase with the open solid-angle fraction.

It should be noted that more experimental data are needed on radiation damage to optical materials. Without such data, component lifetimes cannot possibly be accurately projected. Lifetimes have been calculated assuming different neutron fluence limits for both the wedges and the final focusing mirrors. It has been shown that in order to determine the lifetimes of the final optics in laser driven inertial fusion reactors, 3-D analysis and detailed modelling is essential. The final results obtained on the fluxes and doses show the importance of considering not only the neutrons but also de gamma-rays in radiation damage analysis for the optics.

The results of this neutronics analysis generated a study on the radiation damage and waste management options for the Sombrero final focus system and neutron dumps. The results of this study were presented at the IFSA (First International Conference on Inertial Fusion Sciences and Applications), (Bordeaux, France, Sept. 1999), and published in the journal Fusion Sciences and Applications, and as internal report of the Lawrence Livermore National Laboratory.

SOMSAF.2.- LOFA analysis results for Sombrero

An important goal of the original study was the achievement of a safe and environmentally attractive reactor of relatively simple design. However, recent work has pointed out some key issues involving safety that were not completely addressed at that time, and which need to be reviewed in order to maximize the Sombrero design attractiveness.

Since the time of the original study, the nuclear community (fission and fusion) has reached a consensus and established more restrictive safety goals. Also since that time, new experimental data has been published on tritium retention in carbon/carbon composites, revealing the need for an updated safety evaluation of the Sombrero design.

In the present work, we have adopted the principle of considering the worst possible accident scenario. Here we assume a LOFA with loss of flow in the four circuits of the primary coolant loop. In addition, a 1 m² break in the confinement building wall is assumed, leading to a LOVA simultaneously with an air ingress event. Even though the probability of such a severe accident would be extremely low we must adopt a conservative methodology at his early stage, to later perform similar analysis considering more frequent and less severe accidents.

In order to perform this analysis we have adopted and adapted computer codes and methodologies traditionally used by the MFE community. The CHEMCON heat transfer code has been used to simulate the time-temperature evolution of the plant components during the transient. Some modifications have been introduced in the CHEMCON oxidation package for an enhanced tracking of the oxidation front. The temperature excursion of the different components is then used to determine the activation products source term available for mobilization, which will later be used as input data for the MELCOR thermal-hydraulics calculations.

SOMSAF.2.1.- Time-temperature history of reactor components

In order to calculate the temperature excursions of the different plant components one must account for the various energy sources existing during the transient. Three possible sources (fusion reactions, decay heat and oxidation heat) have been identified and will be discussed next.

Once the accident begins, it is conceivable that fusion reactions could continue to occur for a short period of time. During a LOFA accident about 0.44% of the graphite of the first wall is going to evaporate, increasing the carbon partial pressure of the reactor building by 1 torr and preventing the laser beam from propagating to the target. This way, no more fusion reactions would be possible and hence the reactor would be shutdown.

The radioactive decay heat from activated materials so as the oxidation heat from the exothermic combustion of carbon when in presence of air, will constitute the two only energy sources in the scenario. In order to calculate the long-term thermal evolution of the reaction components in the reactor we have developed a simple 1-D model of Sombrero. This model includes the detailed radial build of the Sombrero design at the midplane for the blanket/reflector, which consist on a moving bed of solid Li_2O particles flowing through the chamber by gravity. The overall thickness is 1 m, with an inner radius of 650 cm. The FW consists of a 1 cm thick C/C composite zone and is followed by a 19 cm in which the carbon fraction is 3%. The third and fourth zones are each 40 cm thick and have 20% and 50% fraction of carbon, respectively. Increasing the carbon fraction toward the back of the blanket provides a built in reflector, which gets cooled by the Li_2O breeding material. Of the total mass flow rate through the reactor, 57% goes through the FW channel, while remaining 43% goes to the rest of the channels. We assume that the Li_2O is 90% density, and the moving bed has a 60% of this material, giving the effective density of Li_2O a value of 1.08 g/cm^3 . A 1.7 m thick inner shield is also included in the model, which is showed in Figure SOMSAF.22.

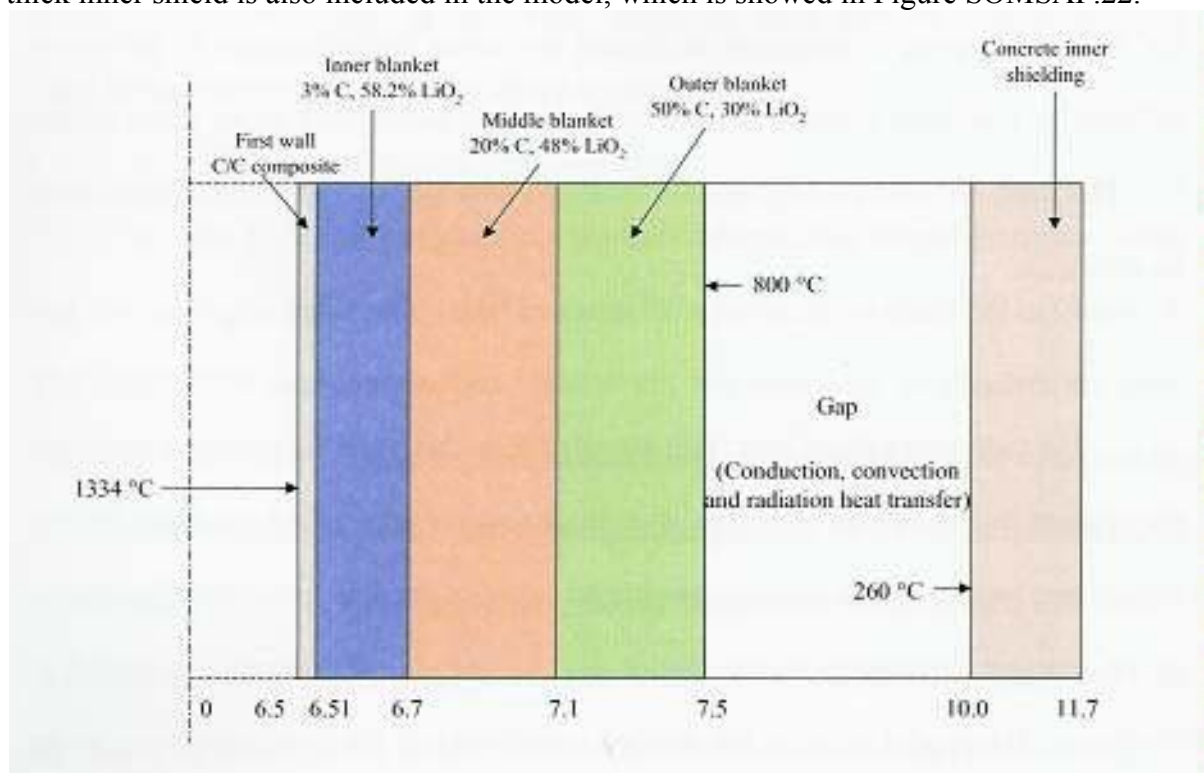


Figure SOMSAF.22. Schematic of the CHEMCON model for the long-term thermal evolution in a LOFA in Sombrero (distances given in m)

In first place we have studied the evolution of the radioactive afterheat during the accident ignoring the potential oxidation phenomena as a consequence of the air reaching the carbon structures. The results show that the decay heat is low enough to allow a rapid cooling of the first wall (FW) and blanket structures (the temperature of the FW drops below 1000°C in less

than a minute). Figure SOMSAF.23 shows the temperature evolution of the different components during the transient, due to the radioactive decay heat.

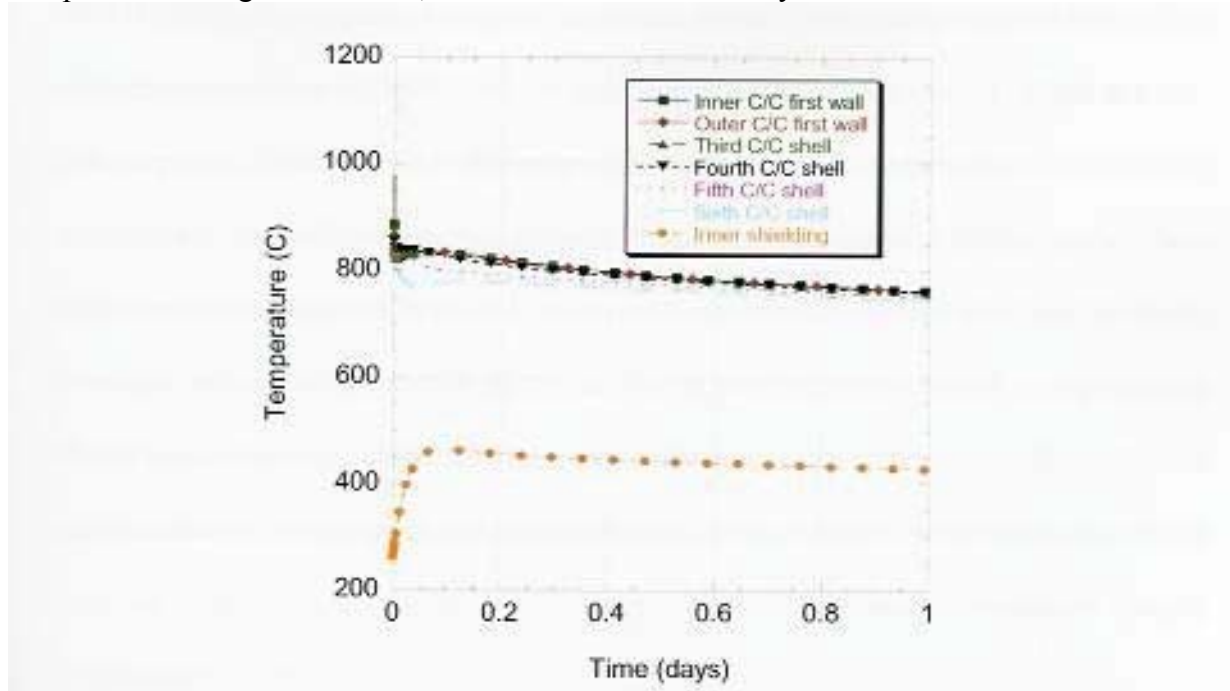


Figure SOMSAF.23. Time-temperature history of the various reactor components due to the radioactive decay heat during a LOFA in Sombrero

We assumed a LOFA with loss of flow in the four circuits of the primary coolant loop. In addition, a 1 m² break in the confinement building wall is assumed, leading to a LOVA simultaneously with an air ingress event. Once the accident begins, it is conceivable that the incoming air will start oxidizing the carbon structures, producing CO gas as a result of the reaction. In order to determine the importance of the oxidation of the carbon at those temperatures, we developed a detailed analysis of the air/carbon oxidation phenomena under these circumstances.

As a result of the oxidation front penetration, the Li₂O granules that no longer have structural support will drop from the chamber onto the floor of the inner shield. In order to address the oxidation of carbon structures we performed a series of CHEMCON and MELCOR calculations. It must be noticed that CHEMCON can only model the oxidation for components consisting of a single material. As our blanket is composed of both carbon and Li₂O, we made a two-step calculation to address the oxidation process. The first case only considers the carbon structures in the FW/blanket and the oxidation process of these components. As there is no Li₂O sitting next to the carbon (we suppose it has already dropped and is standing on the inner shield floor), we cannot account for the Li₂O heat capacity to remove part of the oxidation and decay heat from the carbon. Results are shown in Figure SOMSAF.24.

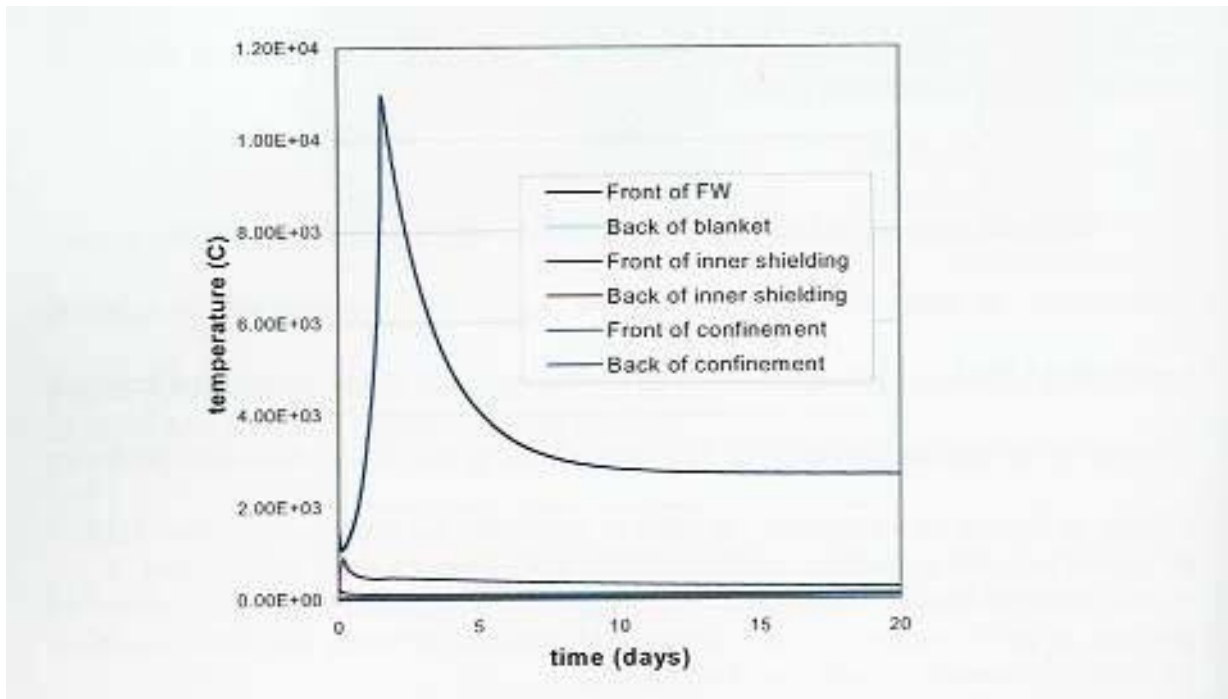


Figure SOMSAF.24. Temperature evolution of the different components in Sombrero during the oxidation carbon/air without Li_2O

The temperature in the first wall reaches a peak at around 11000°C . Temperatures start dropping after all the carbon has been oxidized, which happens within 1.5 days. This temperature increase is significantly overestimated (in the real situation part of the Li_2O granules would still reside inside the solid carbon structures that have not yet been attacked by the oxidation front and would then remove part of the oxidation and decay heat from the carbon due to its own heat capacity). The Li_2O granules, which are sitting on the inner shield floor, would also experience a temperature excursion due to radiation from the carbon and conduction and convection from the atmosphere. Given that the temperature at the inner shield surface reaches a peak of 900°C after ~ 4 hours, in this case we can predict that the Li_2O temperature will remain close to its ordinary working temperature.

A second calculation was performed in order to have an estimation of the highest temperature that the Li_2O granules still residing in the blanket structure could reach. We used the oxidation heat resulting from the previous run and together with the radioactive afterheat of the structures we modelled a time and space dependant heat source. This model assumes that all the Li_2O stands in the same position sitting next to the carbon structures during the whole transient. This is not a realistic model, but allows us to account for the maximum heating of the Li_2O as it receives the oxidation heat from the carbon. On the other hand we can predict that the temperature of the carbon in this case is going to be much lower than in the first case as we are accounting for the heat capacity of the Li_2O . The results of the calculation are shown in Figure SOMSAF.25.

It can be observed that initially the temperatures of the FW/blanket decrease due to convection and radiation to the outer surfaces, and then increase to reach a peak temperature around 1200°C one and a half days after the beginning of the accident. This value is under the first wall working temperature, which we assume to be 1485°C and is the initial FW temperature considered at the beginning of the accident. Note that this result is an upper limit

for the Li_2O temperature during the accident (the real case would be somewhere in between this one and the first case).

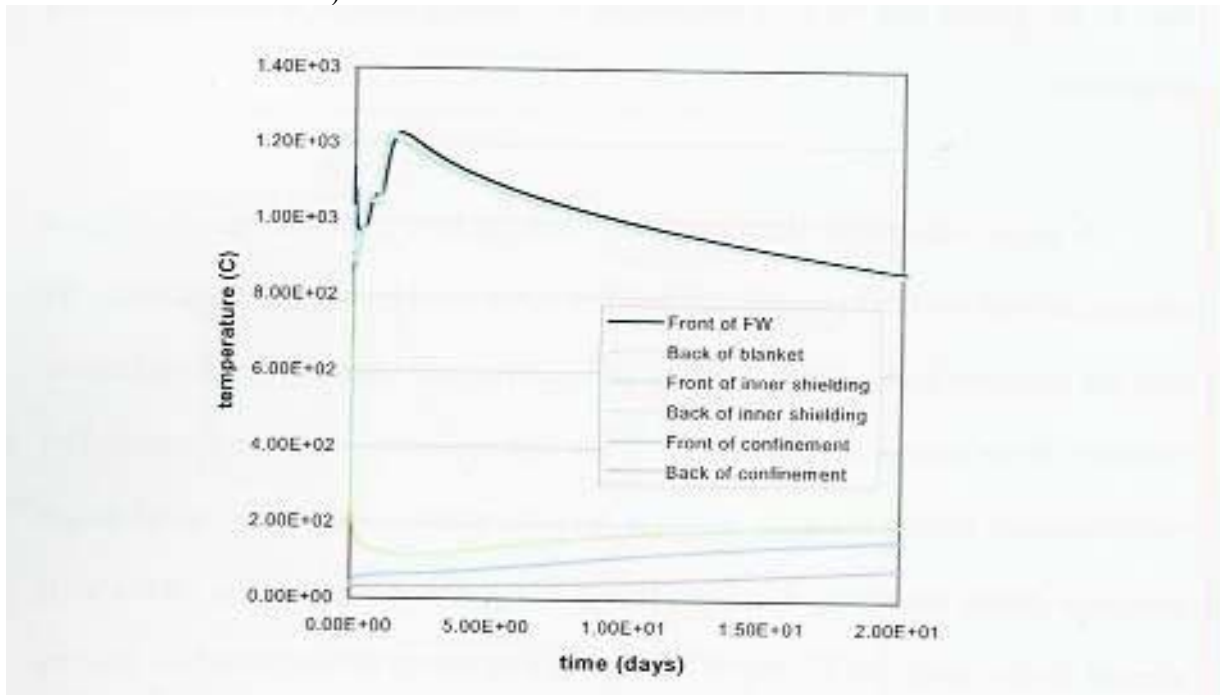


Figure SOMSAF.25. Temperature evolution of the different components in Sombbrero during the oxidation carbon/air with Li_2O

As a consequence of the above results, one can assume that the temperature of the Li_2O will remain close to its normal working temperature. It can be then argued that if mobilization of impurities would occur at this temperature, a simple thermal treatment could be used to purify the Li_2O before its use in the reactor. If, on the other hand, mobilization of impurities is not important at these temperatures, then the release fraction of this material can be easily calculated by modelling the aerosol transport, deposition and final release, as impurities would still be part of the solid Li_2O granules during the progression of the accident.

Also, a CHEMCON calculation was performed in order to address the oxidation of the 1 cm thick C/C first wall in a more realistic way (model including the Li_2O in the blanket and only considering the oxidation of the 100% C/C composite first wall). This can be achieved given the oxidation here is limited to a region made of a single material (FW only instead of FW plus blanket structures). With this calculation we obtained that the time that took for the FW to be completely oxidized was only 2.25 hours.

In order to perform a more realistic assessment of the oxidation process of the carbon structures and its consequences, some thermal-hydraulics phenomena should be considered. In the previous oxidation calculations, the oxygen mass that is available for oxidation is supposed to be unlimited. This means that the correlations that the code uses to obtain the oxidation rate should be scaled by the partial pressure of the oxygen in the real conditions, divide by the partial pressure of the oxygen in air at 1 atm. In order to obtain this partial pressure of the oxygen in the surroundings of the FW, two factors must be considered. First one should account for the travel time of the oxygen since the time that it penetrates the building through the break in the confinement until the moment that it reaches the carbon structures. Second, the oxygen must diffuse through a CO layer that is being generated by the oxidation.

An iterative process was needed to account for these effects. First, with the oxidation code CHEMCON we obtained an overestimated CO source due to no oxygen limitation. Then we used this source as an input for the thermal-hydraulics code MELCOR, to obtain an underestimated partial pressure of the oxygen in the proximities of the chamber. This time dependant partial pressure was used to scale the correlations for the oxidation rate, and a new CHEMCON case was run to obtain a new CO source, which would in this second iteration be underestimated due to the small amount of oxygen from the previous MELCOR run. After various iterations we reached a convergent solution, which showed that the FW would burn in about 7 hours. This means that oxidation would still be significant despite of the fact that the afterheat is low enough to allow rapid cooling of structures at the beginning of the transient. The MELCOR model used for these iterations basically consisted of four control volumes (chamber, boundary layer, inner shielding volume and confinement) and three heat structures, which represent the FW/blanket, the inner shield and the building wall. The break in the confinement was assumed to be 1 m² in area. Figures SOMSAF.26 and SOMSAF.27 show respectively the partial pressures of the oxygen and the CO in each of the control volumes during the accident.

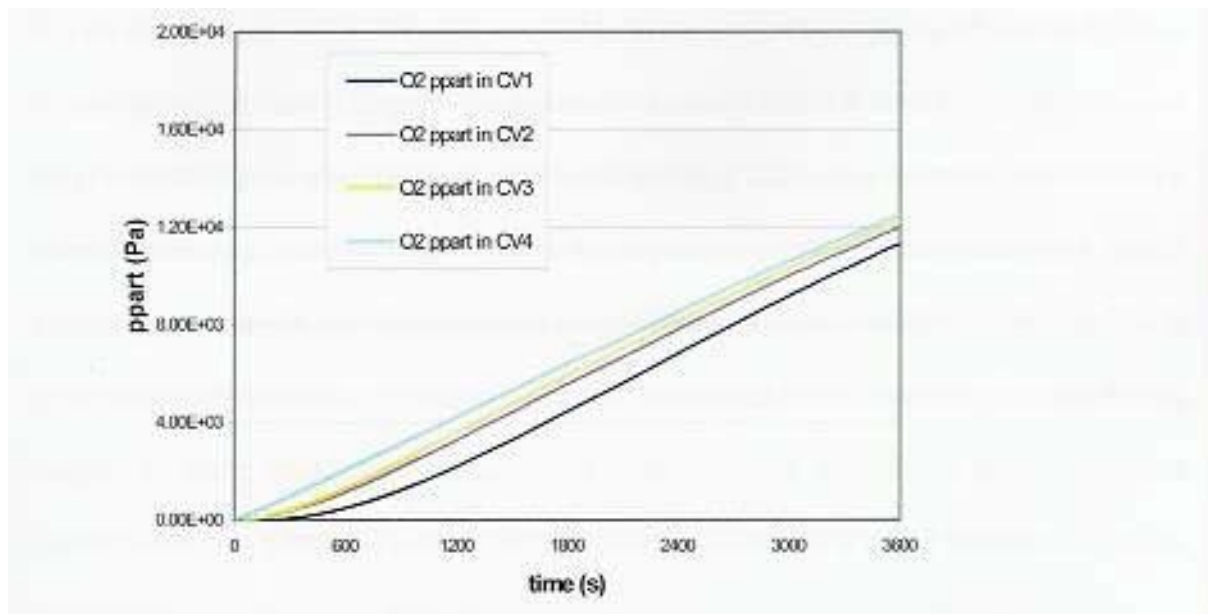


Figure SOMSAF.26. Oxygen partial pressure for the different control volumes of the MELCOR model for Sombrero during the first hour of the accident

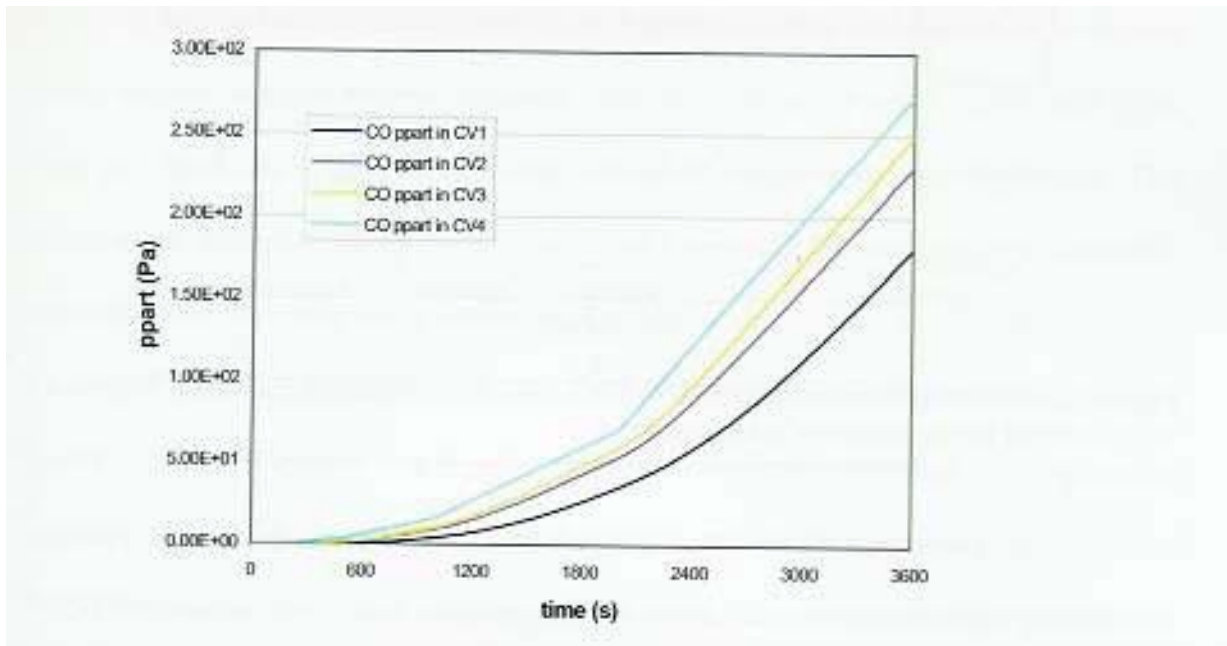


Figure SOMSAF.27. CO partial pressure for the different control volumes of the MELCOR model for Sombrero during the first hour of the accident

Finally, in order to make a parametric study on how the confinement wall break area influences the oxidation process we used the previous MELCOR model, with no CO source this time, and ran a series of cases where the area ranged from 3 m^2 to the area of a single beam penetrating the building, which is 0.07 m^2 . The results are plotted in Figure SOMSAF.28. In order to translate these partial pressures into oxidation rates, a similar iterative process as described above should be developed, feeding back the CO source and oxygen partial pressure from one code to another.

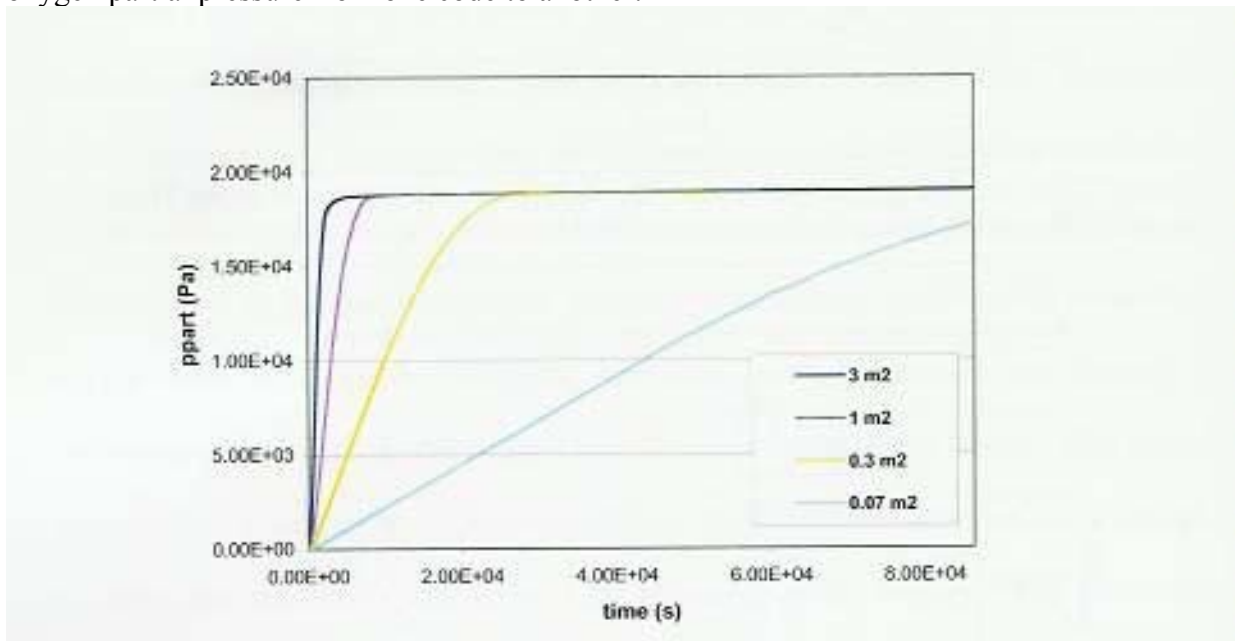


Figure SOMSAF.28. Oxygen partial pressure in CV2 (boundary layer) of the MELCOR model for Sombrero for the different break areas

As a consequence of the relevance of these results, the Idaho National Engineering and Environmental Laboratory is currently working in a new MELCOR version that includes an

oxidation package and couples the thermal-hydraulics phenomena with the oxidation calculations to automatize the iterative process presented here.

It must be noted that the correlations used by CHEMCON are based on experimental data of graphite oxidation with air dating more than 10 years ago. However, these results are meaningful given that the oxidation of the chamber structures would have a great impact on the radioactive mobilized fractions. All the carbon with its impurities and activation products would be mobilized in CO form, so as the tritium trapped in these structures. The activated Li₂O granules would also be available for mobilization, but given the size of the particles this would be a minor contribution to the final released radioactivity fraction.

In order to avoid the oxidation of the Sombrero carbon structures in an air ingress event, several solutions will be discussed next. First, a passive safety feature such as a inert gas filled tank with a rupture disk should be simple enough to implement. This would allow the gas to fill up the building when a certain differential pressure is reached, preventing the oxygen to reach the target chamber. Also, different oxidation experiments have been done with protective coatings on carbonaceous composite materials, such as Si-B-C coatings. Finally, alternative materials other than C/C composites should also be considered (some discussion has been already made about the usage of SiC in the blanket structures, keeping the high-conductivity C/C composite as first wall material).

SOMSAF.2.2.- Activation products source term

Assuming that the carbon structures of the FW/blanket assembly are going to suffer oxidation during the accident, there will be four main sources of radioactivity that must be considered in this scenario. First, all the carbon with its impurities and activation products will be mobilized in CO form. The CO gas will be transported inside the reactor and finally released through the breach in the building wall.

Second and as a consequence of the oxidation of the graphite, the tritium trapped in these structures will be released. In the original report it was estimated that only 10 grams of tritium would be retained in the graphite reactor structure. Recent data about tritium trapping in C/C composites has shown that this number was then underestimated. We have adopted the more realistic value of 11 kg of tritium for the total of FW/blanket graphite shells. This mass, together with the steady state inventory of the Li₂O (162 g), the helium carrier gas (5 g), the reactor Xe gas (4.6 g) and the target feed system (1 g) results in a total of 1172.6 g of tritium that will be mobilized during the transient. We conservatively assume that the tritium is released in the more radiotoxic form of HTO.

Third, we assume that fraction of the Li₂O inventory present in the chamber in the moment of the accident (1/3 of the total 2000 tonnes of Li₂O) will be also mobilized as a consequence of the combustion of its structural support. Given the size of the granules (300 to 500 μm in diameter) most of them will deposit on the reactor horizontal structures, resulting in a minor release fraction.

Finally, the Xe gas that fills the reactor will also be mobilized and finally released through the break in the confinement.

It must be noticed that if oxidation could be prevented, then only 172.6 g of tritium and the atmosphere of Xe gas would constitute the radioactive mobilized sources.

SOMSAF.2.3.- Radioactivity releases and off-site doses

In order to estimate release fractions, a MELCOR model of Sombrero was developed. This model includes the FW/blanket assembly, the inner shielding and the confinement building. The radioactive source term described in the previous section is used as input data for the MELCOR calculations. We have considered a severe accident consisting of a LOFA, with loss of flow in all of the four cooling loops, with simultaneous LOVA produced by failure of the confinement building and consequent air ingress. This model is used by the code to simulate the progression of the accident.

MELCOR heat transfer package considers conduction, convection and radiation between the structures. The aerosol transport module treats the aerosol nucleation and agglomeration, vapour condensation, gravity settling and gaseous/liquid transport. A new module introduced by INEEL allows simulation of HTO transport and condensation.

A. Results with graphite oxidation

Assuming that the graphite reactor structures suffer oxidation, we calculated the source term mobilization and release fractions to the environment, so as the final doses. We have considered three options for the chamber filling gas. In the first case we use Xe, including all its activation products. Second, we report results for the case that the iodine and cesium isotopes could be removed from the Xe gas by the chamber vacuum system. Finally, we show the results for the case where Kr is used instead. It can be noticed that the gaseous species (graphite in CO form and the chamber filling gas) result in a release fraction of 100%. Due to the size of the Li₂O granules, most of them will deposit on the reactor horizontal structures, resulting in a 1 kg release from the initial 667 tonnes mobilized. Because of the partial condensation of the HTO on the colder building walls, we get a release fraction of 19% from the initial 1.173 kg mobilized. With the data about the activity released and the adequate DCR, off-site doses can be obtained. The DCF library has been updated to include radionuclides maybe important for fusion. Early doses were calculated using typical weather conditions and ground level release as recommended by the Fusion Safety Standards.

Results in Table SOMSAF.4 show that the dominant dose comes from the Xe gas, giving a result of 4.69 rem. The graphite from the FW/blanket structures results in a dose of 0.17 rem, and the Li₂O makes a negligible contribution to the final dose. The design using Xe would lead to a final accident dose of 5.64 rem if the non-xenon activation products were included in the release. This value would be reduced to 1.19 rem assuming that the iodine and cesium isotopes can be separated by the chamber vacuum system. For a modified Sombrero using Kr instead of Xe, we calculate a total accident dose of 1.06 rem.

Table SOMSAF.4 Mobilized activities, release fractions and off-site doses, with graphite oxidation in case of a LOFA in Sombrero

Radioactive source	Mobilized activity (Bq)	Release fraction (%)	Off-site dose (rem)
C-FW	6.1E+14	100	0.05
C-blanket	1.4E+15	100	0.12
Li ₂ O	5.8E+18	1.5E-4	0.00

HTO	4.2E+17	19	0.78
Xe	1.4E+16	100	4.69
Xe*	1.4E+16	100	0.24
Kr	8.8E+15	100	0.11
Total w/Xe	6.2E+18		5.64
Total w/Xe*	6.2E+18		1.19
Total/w/Kr	6.2E+18		1.06

Xe* = Xe without iodine and cesium activation products

Given that our goal is an accident dose below the 1 rem limit given by the DOE Standards, other design modifications have been considered. Other than the activation products from the Xe gas in the chamber, the most contributing source to the final dose is the tritium. The quantity of tritium that condenses on the confinement building walls will depend on the time-temperature history of those structures.

In order to keep the temperature of the building inner surface as low as possible, a high conductivity material could be useful. The Sombrero report used concrete with 2.8% vol. mild steel as the building material. We have studied different alternatives, and here we propose two options. First, increasing the steel content to 5% would reduce the release fraction of the tritium to 145 and the dose to 0.59 rem. This would result in a final dose of 1 rem in the case of Xe with removal of iodine and cesium isotopes, and 0.87 rem in the case of Kr used as a chamber gas. Another alternative would be replacing the material with 97% concrete and 3% aluminium. This would also affect the thermal conductivity of the building and thus, the condensation of tritium on the walls. The tritium release fraction would be reduced to 11% and the off-site dose to 0.4 rem. This would result in a total accident dose of 0.81 rem in the case of Xe with the iodine and cesium isotopes being removed, and 0.68 rem if the chamber gas is Kr.

B. Results without graphite oxidation

Assuming that oxidation of graphite does not occur, the only radioactive source terms would be the 172,6 g of tritium trapped in other parts than the graphite chamber, and the reactor filling gas (Xe or Kr). The results in this case are shown in Table SOMSAF.5.

Table SOMSAF.5 Mobilized activities, release fractions and off-site doses, without graphite oxidation in case of a LOFA in Sombrero

Radioactive source	Mobilized activity (Bq)	Release fraction (%)	Off-site dose (rem)
HTO	6.2E+16	23	0.16
Xe	1.4E+16	100	4.69
Xe*	1.4E+16	100	0.24
Kr	8.8E+15	100	0.11
Total w/Xe	7.6E+16		4.85
Total w/Xe*	7.6E+16		0.40
Total/w/Kr	7.0E+16		0.27

Xe* = Xe without iodine and cesium activation products

In this case the tritium dose is only 0.16 rem, but the Xe would still produce an off-site dose over 4 rem if the iodine and cesium activation products were included in the release. If these isotopes were removed by the chamber vacuum system, the final dose would be 0.4 rem. For the modified design using Kr, we get an accident dose of 0.27 rem. In these last two cases with final dose below 1 rem, an evacuation plan would not be needed. A summary of the results of the Sombrero safety analysis is presented in the next paragraphs.

As we did with the other analyses, here we have also performed a parametric study of the atmospheric conditions and elevation of the release, obtaining the adequate DCFs from the expanded libraries described above. It has been found that in case of conservative weather conditions (Case 2), then the calculated doses would be about 10 times higher. However if we assumed an elevated release in typical weather conditions (Case 3) this would result in doses an order of magnitude lower than those calculated in the case of a ground level release.

Next we summarize the most relevant findings of our accident analysis for the Sombrero IFE power plant design.

We have studied a loss of flow accident with a simultaneous break in the Sombrero building wall, which allows the surrounding air to penetrate the confinement area. In the case of an air ingress event, graphite structures will suffer oxidation with air, resulting in mobilization of the carbon, including the tritium trapped in it, and the Li₂O granules from the blanket. The oxidation of graphite with air is a mayor issue that should be prevented introducing passive safety features, protective coatings, or alternate FW and/or blanket materials.

Assuming that the oxidation takes place, the calculated off-site dose results in 5.64 rem. Removing the iodine and cesium activation products from the Xe gas would result in a dose of 1.19 rem. If Kr is used as alternative gas for the reactor atmosphere this value would be reduced to 1.06 rem. If we assume that the iodine and cesium can be removed from the Xe gas, or that Kr is used instead, doses below 1 rem could be achieved with simple design modifications such as increasing the steel content in the confinement building (to 50% vol.) or adding aluminium (3% vol.) to the concrete. The higher thermal conductivity of the material would allow a softer temperature excursion of the building walls and more tritium could condense on the confinement inner surface. If oxidation could be prevented, then the off-site dose would be 4.85 rem if the non-xenon activation products were included in the release, and 0.4 rem if the iodine and cesium isotopes were removed by the chamber vacuum system. In the case were Kr is used instead of Xe, the final dose results to be 0.27 rem. The cases with total dose below 1 rem would meet the requirement given by the DOE Fusion Safety Standards in order to avoid public sheltering and evacuation.

The results of this analysis were presented at the 14th ANS Technology of Fusion Energy Meeting, (Park City, Utah, Oct. 2000), and have been submitted for publication to the journal Fusion Technology.

SAFTFAB.- SAFETY ANALYSIS RESULTS FOR A GENERIC TARGET FABRICATION FACILITY

Early IFE power plants will use deuterium-tritium (DT) fuel, and thus, every IFE power plant will require a target fabrication facility on-site. The target factory is a major source of tritium and activated target material subjected to potential accident release. The steady-state tritium inventory, and thus, the quantity of tritium that might be mobilized during an accident, is a function of the target fabrication and fill technologies. For indirect-drive target designs, radioactive, recycled target high-Z materials will also be present in the target fabrication facility. In order to reduce the tritium and high-Z material inventories in the facility, it is important to minimize the production time per target and thus the inventory of targets being handled at any one time.

Designing fusion power plants for safe operation and limited, acceptable accident consequences will be essential for fusion to be successful. Typical IFE power plant designs call for repetition rates of 5-10 Hz (~ 500,000 targets per day). Most target designs require ~ 0.8 TBq (~ 20 Ci) of tritium, thus, sustaining a daily throughput of 500,000 targets would translate into a tritium inventory on the order of 1 kg. However, the steady-state tritium inventory, and thus, the quantity of tritium that might be mobilized during a severe accident is a function of the target fabrication and fill technologies. Additionally, for indirect-drive target designs, radioactive, recycled high-Z target materials will also be present in the target fabrication facility.

In the present study, we estimate the steady-state tritium inventory for a generic plant producing various types of targets and using various production techniques. We postulate a severe accident in the plant, and use the MELCOR thermal-hydraulics code for aerosol transport calculations which are used to model tritium and high-Z materials releases. The results presented here are part of a deeper study that was presented at the 14th ANS Technology of Fusion Energy Meeting, (Park City, Utah, Oct. 2000), and have been submitted for publication to the journal Fusion Technology.

SAFTFAB.1.- Target design

The overall tritium inventory existing in the target fabrication facility at the moment of the accident is a strong function of the specific target design.

SAFTFAB.1.1.- Indirect Drive Targets

We will focus in the most recent heavy-ion driven, distributed-radiator design developed by the target engineers at Lawrence Livermore National Laboratory. The “full-size” target is driven by 5.9 MJ for a gain of 68, while the “close-coupled” target requires only 3.3 MJ and has a gain of 133. Even though these designs use a beryllium shell and ablator it is expected that IFE power plants will use plastic shells to enable diffusion fill of capsules. Whereas the tritium inventories in both types of capsule are around 2.4 mg, the volume of the close-coupled design is more than 2 times smaller than that of the full-size target (volumes are 1.6 cm³ for the full-size design and only 0.7 for the close-coupled target).

Indirect-drive targets require high-Z materials for the conversion of laser or ion energy into x-rays that ablate the outer shell of the capsule and cause the target implosion. Although the most recent baseline target designs call for a high-Z mixture of gold and gadolinium, neither of these materials is particularly attractive from the cost, fabrication or extraction point of view, so other candidates should be considered in future work.

Here we will consider a generic high-Z material for our reference indirect drive target for our safety analysis. Once the release fraction of such material under accident conditions is obtained, we will use those results to estimate the consequences of using any of the elements typically proposed in the latest target reference designs.

SAFTFAB.1.2.- Direct Drive Targets

The reference designs that we will assume for the direct-drive target is based in the Sombrero power plant study. This capsule consists of a plastic shell ablator with an inner solid DT fuel layer. The ablator would be vaporized by the energy deposition and would be blown away from the fuel surface, pushing against the fuel and causing the implosion. The tritium inventory of this target would be 2.4 mg. It would be shot at 6.7 Hz with a yield of 400 MJ for a production of 1000 MW of net electric power.

We can advance that in the case of direct-drive targets, the fill time are significantly longer due to the relatively thin-walled capsules, which will not support as great pressure gradients as in the case of indirect-drive designs.

SAFTFAB.2.- Tritium inventory estimation

In order to estimate tritium inventories in the target fabrication facility, we assume a daily throughput of 500,000 targets each of which yield 400 MJ. For the purpose of reducing the tritium and high-Z material inventories in the facility, it is important to minimize the production time per target and thus the inventory of targets being handled at any one time. This can be achieved by designing a compact production equipment and overall building area. Important safety features include segmenting the inventory into multiple parallel production lines, and including an expansion tank to limit releases.

In determining the tritium inventory for the target fabrication facility, we will assume that the facility is divided into multiple, parallel production lines. Each production line is capable of manufacturing a 3-hour supply of targets in each batch (62,500 targets/batch). In all cases, the target fill time is a key parameter in determining the overall inventory. For the indirect-drive cases, the relative timing of target fill and assembly is also of importance. A schematic of two parallel production lines being fed by the tritium reservoir is shown in Figure SAFTFAB.1.

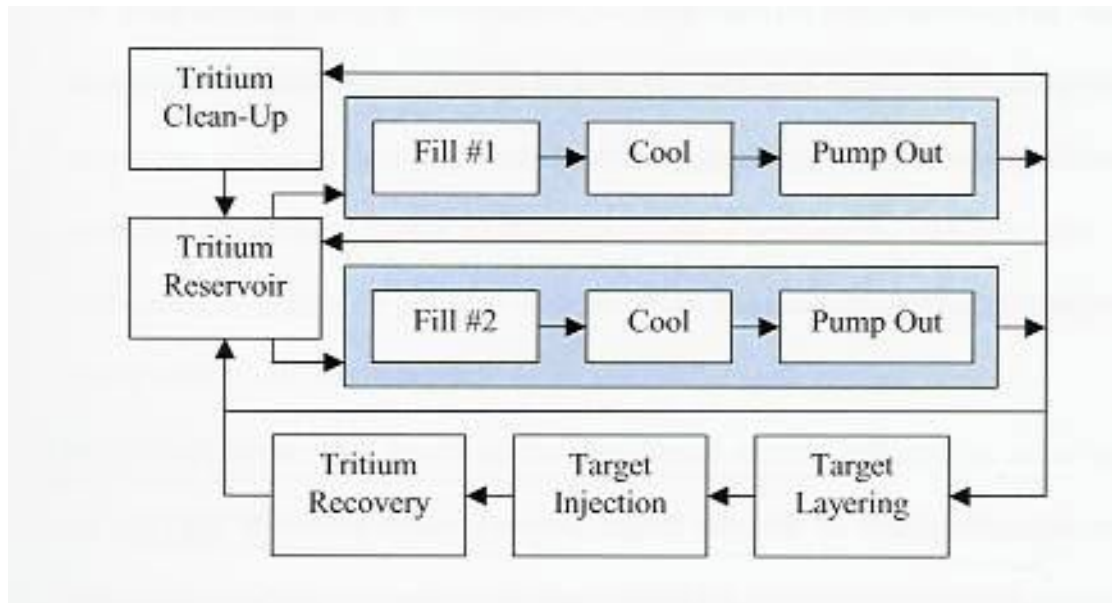


Figure SAFTFAB.1. Schematic of two parallel target production lines

Each line includes target fill, cool down, and pump out. At the end of each line, filled targets go to layering, while the pumped-out DT gas goes either to the tritium clean-up system or back to the reservoir. Following layering, targets are injected and unburned and bred tritium is recovered from the chamber and coolant. In reality, there may be many more production lines, and they will be staggered to ensure the staggered completion of targets.

The filling process of the target with DT gas at high-pressure is the pacing step in the production process for any of the target designs considered. The filling time will be a strong function of the temperature and of the peak pressures that the target is capable to support.

For indirect-drive targets, the duration of the filling process ranges from 24 hours if filled at a temperature of 300 K down to 11 hours for a temperature of 400 K. The peak pressures are 68 and 84 MPa, respectively. The remaining steps are expected to require about 6 hours.

Another key issue for indirect-drive targets is the ordering of target fill relative to target assembly. The simplest approach is warm assembly followed by diffusion fill of the capsule while it resides within a hohlraum (a small hole would allow DT gas to enter the interior of the hohlraum). With warm assembly, one must accommodate the entire hohlraum volume, and thus, peak tritium inventories within a canister are significantly higher. However, if capsules can be filled, cooled, and then assembled into hohlraums –“cold assembly”- then only the capsule volume must be accommodated in the fill canisters. For the full-size target, cold assembly leads to canisters that are 30 times smaller in size, while the close-coupled target requires 13 times less volume.

In the case of direct-drive targets, capsule fill times are significantly longer due to the relatively thin-walled capsules, which will not support as great a pressure gradient. For a fill temperature of 300 K, 580 hours would be required with a peak pressure of 128 MPa. At 400 K and a peak pressure of 161 MPa, the fill time is still 285 hours. Clearly, research and development into materials with higher diffusion rates or the ability to handle higher temperatures is needed.

In order to estimate tritium inventories for this preliminary safety assessment we have assumed a range of different cases, considering the different types of targets (full-size and close-coupled for indirect drive and the Sombrero type target for direct drive) and different filling technologies (different filling temperatures and cold/warm assembly for the indirect drive cases).

As expected, the worst results are those obtained when assuming maximum filling times and warm assembly followed by fill within the hohlraum in the indirect drive cases, whereas the best results have been obtained for the cases of minimum fill time and cold assembly in the cases of indirect drive. Tritium inventories have been estimated and the results are summarized in Table SAFTFAB.1.

Table SAFTFAB.1 Basic tritium parameters for a target fabrication facility

Case	Capsule fill time (h)	Canister volume (L)	Peak canister T inventory	# of canister	Total plant T inventory (kg)
Indirect-drive: Full-size or close-coupled target/400 K fill/Cold assembled	11	5.9	0.26	6	0.8
Indirect-drive: Full-size target/30 K fill/ Warm assembled	24	116	5.15	10	25.7
Indirect-drive: close-coupled target/300 K fill/Warm assembled	24	51	2.25	10	11.3
Direct drive: Plastic target/400 K fill	285	5.9	0.26	97	12.7
Direct drive: Plastic target/300 K fill	580	5.9	0.26	196	25.7

It must be noted that none of the tritium inventory results includes a quantity going through the tritium clean-up system or an allowance for additional targets in storage in case of a system failure. In the case of indirect-drive targets, the plant tritium inventory ranges from 0.8 to 11.3 kg for the close-coupled target and 0.8 to 25.7 kg of the full-size target. Clearly, these results show the tremendous benefits of fast diffusion fill times and the ability to perform cold assembly. For the indirect-drive, plastic targets, the tritium inventory varies from 12.7 to 25.7 kg and depends entirely upon the fill temperature, which determines the diffusion fill time.

SAFTFAB.3.- Radioactivity release and off-site doses

The MELCOR thermal-hydraulics code has been used to model the tritium and high-Z material transport and release. This version of the code has been modified for use in fusion applications by Idaho National Engineering and Environmental Laboratory (INNEL). Tritium is transported in the more radiotoxic HTO form and we use lead material as an example of the high-Z material in the case of indirect drive targets.

The MELCOR model used to simulate the progression of the accident consists of multiple volumes. It includes a main building with a fill room and a canister inside it. The fill room is connected to an expansion tank through a pipe equipped with a rupture disk. The expansion tank itself is equipped with a pressure relief valve (PRV) that opens to the main building. All volumes, except for the canister, are initially at a slight underpressure of ~ 500 Pa (2" water equivalent). This underpressure has little effect during an accident but it will help keep routine releases to low levels. A schematic of the model is shown in Figure SAFTFAB.2.

In order to perform accident analysis for the target fabrication facility we postulate an initiating event in a single canister –we assume a break with an area of 1 cm^2 . The high-pressure DT gas rapidly leaks from the canister into the fill room. In this simple analysis, each fill room has a volume of 12 m^3 , but this would have to be reduced for the direct-drive cases, which have a large number of canisters. Each fill room is equipped with a rupture disk that fails at an overpressure of 10 kPa. The disk area is 10 cm^2 , and each fill room is connected to an expansion tank by a pipe. We assume that the fill rooms serve to isolate the canisters; a failure of one canister will not affect the other canisters. Once the rupture disk fails, tritium and high-Z particulate flow into the expansion tank. The expansion tank is equipped with a PRV that opens at an overpressure of 10 kPa. While a rupture disk never closes once it fails, PRVs are able to return to a closed state once the pressure differential falls below 10 kPa. Gas released from the expansion tank flows into the larger confinement building and may be released to the environment via a 1 m^2 break in the building.

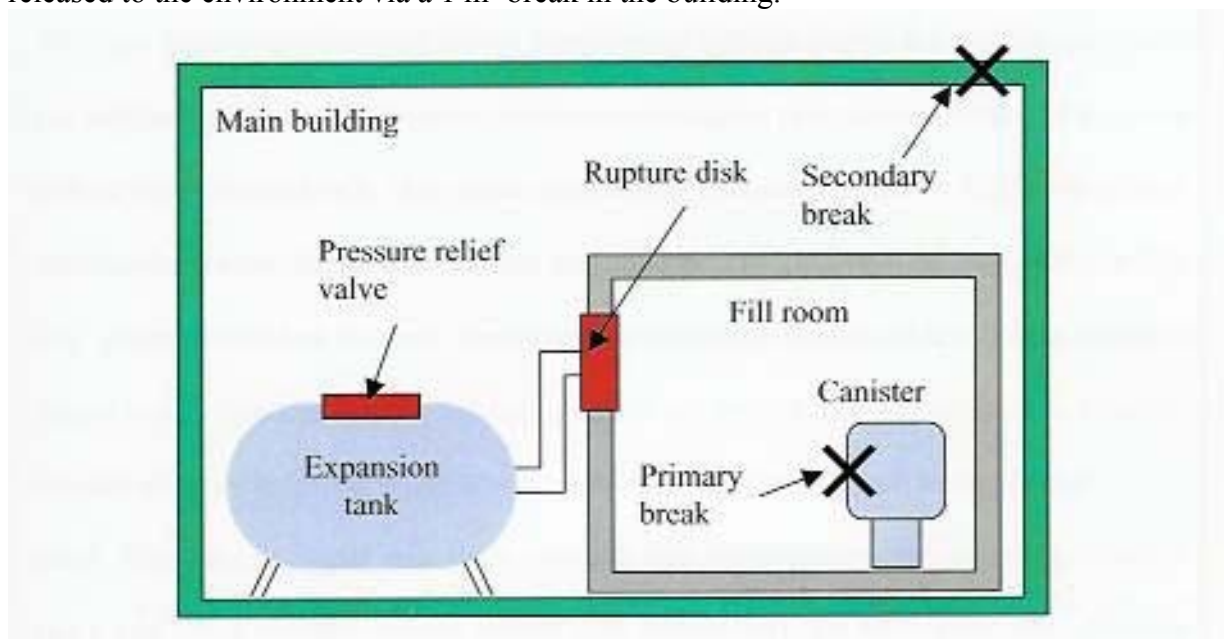


Figure SAFTFAB.2. Schematic of the MELCOR model used to simulate tritium and high-Z material transport and release during the accident

In order to estimate the tritium release fractions, we take no credit for filtration, and we conservatively assume a ground-level radioactivity release. Early doses are calculated assuming typical weather conditions as recommended by the U.S. DOE Fusion Safety Standards.

In order to perform aerosol physics calculations for the high-Z material, we assume a conservative particle size distribution (PSD) of $0.1\text{-}10 \mu$ diameter. Such small particles are apt

to transport great distances before settling. This PSD is conservative, because there is no clear mechanism for production of such fine particles.

A. Tritium results

For the tritium transport calculations we have assumed an expansion tank that is a 5-m-long and 3.5 m-radius cylinder with hemispherical ends. The volume of the tank is 372 m³. As would be expected, the volume of the tank has a great influence on the release fractions, which will decrease with increasing volumes of the tank and vice-versa.

Results show that the release fractions are the greatest for the largest canister volume at the highest temperature and pressure (full-size target design with warm assembly and fill at 300 K). This results in a tritium release fraction 3.2%, and a site boundary dose of 5.8 mSv (0.58 rem). This result would meet the 10 mSv (1 rem) requirement established by the U.S. DOE Fusion Safety Standards to avoid public sheltering and evacuation.

In the case of the direct-drive targets, the results are very optimistic. Due to the small volume of the capsules, the Sombrero-like-direct-drive design and the bare capsules from the indirect-drive design would not produce any tritium release.

B. High-Z materials results

The accidental release of high-Z target materials has been analysed using the same MELCOR model used for the tritium transport and release. The target material has been modelled as a fine (0.1-10 µm) particulate, assuming a material density of 10 g/cc. We have simulated an aerosol source that releases 100 kg/s during 0.1 s in the moment of the beginning of the accident (the real masses would be 16 kg in the “close-coupled case” and 37 kg in the “full-size” case, but the release fraction is constant). The results should be accurate for any element that would be transported as a particulate during the accident. For elements such as fluorine, for example, chemistry dictates that alternate chemical forms would be taken and the following results are invalid. For most elements, however, these results are indeed of interest.

Figure SAFTFAB.3 shows the results on the release fraction of the high-Z target material release for different volumes of the expansion tank. It can be observed that even in the worst case the release fraction is less than 1%. In order to be consistent with the tritium calculations here we assume that our expansion tank has a volume of 372 m³. This way the high-Z release fraction can be kept to less than 0.3%. Further, a more reasonable PSD of 1-100 µm would reduce the release by about 4 times. Additional increases in the PSD would further reduce the release percentage.

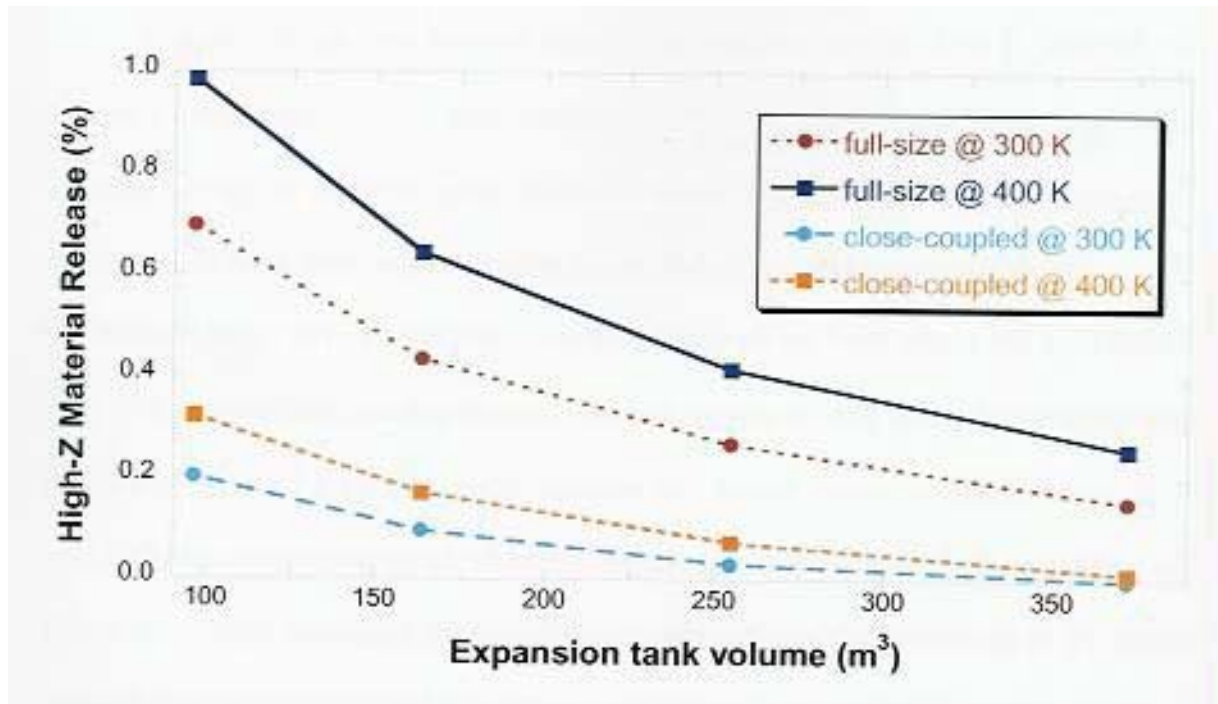


Figure SAFTFAB.3. High-Z material releases for different volumes of the expansion tank

Once that the release fraction is known, we have obtained the accident doses for the reference materials included in the latest target designs: gold and gadolinium. Using the activation values and the DCFs from previous work on target fabrication materials selection, we have estimated the early doses resulting from the release of 0.3% of the high-Z material present in the facility as a consequence of the accident. Results for both candidate materials show off-site doses below the 10 mSv (1 rem) limit. However neither of these materials is particularly attractive from the cost, fabrication or extraction point of view, so other candidates should be considered in the future research.

As a summary of the previous analysis we can say that in the area of total plant tritium inventory, three characteristics make a large difference in the final results. First, the target fill time is crucial in determining the tritium inventory longer fill times require a higher number of canisters to meet the needs of the power plant. Second, the ability to perform cold assembly (assemble targets that have already been filled) provides a large savings in the tritium inventory for the indirect-drive designs a factor of 30 for the full-size target and 13 for the close-coupled target. Third, targets with higher burn-up result in a target fabrication facility with a lower tritium inventory.

In the area of accident safety, the total plant tritium inventory does not matter as much as that which is vulnerable. If designs for target fabrication facilities can ensure that canisters/fill rooms can remain isolated from each other (an accident in one does not affect another), then this will go a long way towards meeting the accident safety goals. There will, of course, always be a trade-off between a reasonable number of canisters and the tritium inventory in each. The design of future target fabrication facilities should optimize the maximum number of canisters. Once this number is known, reduction of the vulnerable tritium inventory can only be accomplished via cold assembly and/or reductions in the target fill time.

The large reductions in the vulnerable tritium inventory that are offered by bold assembly (for 13 to 30 times less inventory for the two indirect-drive target designs), suggest that this technology should be supported and developed.

In order to select the most appropriate high-Z materials for indirect drive targets, one must consider not only the accident does, but also the environmental factors such as the Waste Disposal Radio (WDR) and the contact dose rate. Both the safety and environmental characteristics of the materials will be critical in order to determine the ideal candidate.

Radiological hazards and safety criteria

1 Radiological hazards of IFE

IFE has the potential for superior S&E characteristics relative to other energy options, which is one of the main reasons for developing inertial fusion power. Although the S&E characteristics of fusion energy have long been emphasized, these benefits are not automatically achieved, as noted the previous work. Tritium, neutrons, and neutron-activation products existing in fusion reactors present radiological hazards. In addition, non-nuclear risks such as chemical hazards must be considered.

Traditionally, three classes of radiological hazards have been identified. These include power plant accidents, routine and occupational exposures, and waste disposal. Each of these areas will affect the overall acceptability of a particular design.

The present research work focuses on IFE accident analysis, introducing state-of-the-art codes and methodologies for realistic safety assessment of IFE power plant designs, in an attempt to address the oversights of previous works. Under the accident analysis point of view, the most important goal consists on avoiding the need of off-site public evacuation even for worst-case accidents. To help meet this requirement the IFE safety work must focus on the following key areas:

1. understanding the behaviour of the largest sources of radioactive and hazardous materials in a IFE power plant.
2. understanding how energy sources could mobilize those materials under accident conditions.
3. developing integrated state-of-the-art computer codes and methods needed to calculate in a realistic way the release fractions of activated material during an accident and the resulting doses to the public.

Once radioactive release fractions and off-site doses have been estimated for a range of possible accident scenarios, results must be compared to a consistent safety criteria and modifications must be proposed an intelligent decisions made early in the inertial fusion design process.

IAEA safety standards

The International Atomic Energy Agency (IAEA) has developed an effort during the past several decades in order to harmonize the existing radiation protection and safety standards internationally. As a result of this effort the IAEA developed the International Basic Safety

Standards for Protection against Ionizing Radiation and for the Safety of Radiation Sources (IAEA 96). These standards are jointly sponsored by the Food and Agriculture Organization of the United Nations (FAO), the International Atomic Energy Agency (IAEA), the International Labour Organization (ILO), the Nuclear Energy Agency of the Organization for Economic Co-operation and Development (OECD/NEA), the Pan American Health Organization (PAHO) and the World Health Organization (WHO).

Purpose and scope of the IAEA safety standards

The purpose of these Standards is to establish basic requirements for protection against the risk associated with exposure to ionizing radiation and for the safety of radiation sources that may deliver such exposure. The Standards have been developed from widely accepted radiation protection and safety principles, such as those published in the Annals of the International Commission on Radiological protection (ICRP) and the IAEA Safety Series. They are intended to ensure safety of all types of radiation sources and, in doing so, to complement standards already developed for large and complex radiation sources, such as nuclear reactors and radioactive waste management facilities.

The IAEA Standards comprise basic requirements to be fulfilled in all activities involving radiation exposure. The requirements have the force that is derives from the statutory provisions of the Sponsoring Organizations. They do not entail any obligation for the different States to bring their legislation in conformity with them, they are aimed rather to server as a practical guide for public authorities and services, employers and workers, specialized radiation protection bodies, enterprises and safety and health committees. These Standards cover a broad range of practices and sources that give rise or could give rise to exposure of radiation, and many of the requirements have therefore been drafted in general terms.

The scope of the IAEA Standards in limited to the protection of human beings; it is considered that standards of protection that are adequate for this purpose will also ensure that no other species is threatened as a population. Moreover, the Standards apply only to ionizing radiation. They do not apply to non-ionizing radiation such as microwave, ultraviolet, visible light and infrared radiation. They do not apply either to he control of non-radiological aspects of health and safety. The Standards recognize that radiation is only one of many sources of risk in life, and that the risks associated with radiation should not only be weighed against its benefits but also viewed in perspective with other risks.

Basic principles of the IAEA safety standards

As mentioned in the previous section, the Standards have been developed from widely accepted radiation protection and safety principles, such as those published in the Annals of the ICRP and the IAEA Safety Series. The detail off these principles can be found in the publications of these bodies and it is not in the scope of the present work to list their entire formulation here. However, a brief summary of those principles is given next.

- a) A practice that entails exposure to radiation should only be adopted if it yields sufficient benefit to the exposed individuals or to society to outweigh the radiation detriment it could cause (i.e. the practice must be justified).
- b) Individual doses due to the combination of exposures from all relevant practices should not exceed specified dose limits.

- c) Radiation sources and installations should be provided with the best available protection and safety measures under the prevailing circumstances, so that the magnitudes and likelihood of exposures and the number of individuals exposed be as low as reasonably achievable, economic and social factors being taken into account, and the doses they deliver and the risk they entail be constrained (i.e. protection and safety should be optimized).
- d) Radiation exposure due to sources of radiation that are not part of a practice should be reduced by intervention when this is justified, and the intervention measures should be optimized.
- e) The legal person authorized to engage in a practice involving a source of radiation should bear the primary responsibility for protection and safety.
- f) A safety culture should be inculcated that governs the attitudes and behaviour in relation to protection and safety of all individuals and organizations dealing with sources of radiation.
- g) In-depth defensive measures should be incorporated into the design and operating procedures for radiation sources to compensate for potential failures in protection or safety measures.
- h) Finally, protection and safety should be ensured by sound management and good engineering, quality assurance, training and qualification of personnel, comprehensive safety measures and a sound attention to lessons learned from experience and research.

Dose limits and guidelines

The Schedule II in the International Basic Safety Standards for protection against Ionizing Radiation and for the Safety of Radiation Sources, establishes that the estimated average doses to the relevant critic groups of members of the public that are attributable to practices shall not exceed the following limits:

- a) an effective dose of 1 mSv in a year;
- b) in special circumstances, an effective dose of 5 mSv in a single year provided that the average dose over five consecutive years does not exceed 1 mSv per year;
- c) an equivalent dose to the lens of the eye of 15 mSv in a year; and
- d) an equivalent dose to the skin of 50 mSv in a year.

The dose limits set out in this part shall not apply to comforters of patients, i.e., to individuals knowingly exposed while voluntarily helping (other than in their employment or occupation) in the care, support and comfort of patients undergoing medical diagnosis or treatment, or to visitors of such patients. However, the dose of any such comforter or visitor of patients shall be constrained so that it is unlikely that his or her dose will exceed 5 mSv during the period of a patient's diagnostic examination or treatment. The dose to children visiting patients who have ingested radioactive materials should be similarly constrained to less than 1 mSv.

The section of the Standards named as Schedule IV, describes the dose levels at which intervention is expected to be undertaken under any circumstances. Table 3.3.1 gives action levels of dose for acute exposure by organ or tissue, whereas Table 3.3.2 gives action levels of dose rate for chronic exposure by organ or tissue.

Finally, the Schedule V in the Standards gives the guidelines for intervention levels and action levels in emergency exposure situations, which we will summarize next.

- a) Intervention levels are expressed in terms of affordable dose, i.e., a protective action is indicated if the dose that can be averted is greater than the corresponding intervention level.
- b) The values of avertable dose specified in the intervention levels refer to the average over suitably chosen samples of the population, not to the most exposed (i.e. critical groups of) individuals. However projected doses to critical groups of individuals should be kept within the dose levels specified in Schedule IV.
- c) General principles governing the selection of intervention levels for radiological emergencies have been recommended by the ICRP together with a broad range of values within which such levels can be expected to fall.
- d) The IAEA has developed values resulting from the generic application of these principles to the most common forms of protective action.
- e) Site specific intervention levels may be higher or in some cases lower than these generic optimized values owing to consideration of site specific or situation specific factor.
- f) With these factors taken into account, the values specified can then be taken as starting points for the judgments required for decisions to select intervention levels for emergency exposure situations.
- g) The generic optimized intervention level for sheltering is 10 mSv of avertable dose in a period of no more than 2 days.
- h) The generic optimized intervention value for temporary evacuation is 50 mSv of avertable dose in a period of no more than a week.

Once again it must be noted that the IAEA Standards have the purpose to lay down the basic principles and indicate the different aspects that should be covered by an effective radiation protection program. They are not intended to be applied as they stand in all the countries and regions, but should be interpreted to take account of local situations, technical resources, the scale of installations and other factors which will determine the potential for application.

Application of safety standards in this work

In the present work we perform a safety analysis for IFE power plant designs. Once the accident doses are obtained in each case, one needs compare these results to the appropriated set of the reference exposure values for safety evaluation. The IAEA has established an international regulation for nuclear power plants, which we have described in a previous section of this Chapter, allowing for each country to introduce slight modifications in accordance with federal, state, and local regulatory and permit requirements.

It is necessary analyze the accident doses resulting from the various accident scenarios considered in each IFE power plant design, and in order to be conservative, we have compared this result to the 10 mSv (1 rem) limit for no public evacuation from the U.S. DOE Fusion Safety Standards.

For this purpose we have calculated early doses, defined as the equivalent effective doses with 50 years commitment, resulting from the first 7 days of exposure during the plume passage. In addition to direct cloudshine and inhalation during plume passage, our doses also consider contributions from groundshine, and inhalation for resuspended materials. Although the Fusion Safety Standards recommend that doses should be calculated in average weather conditions, a parametric study considering varying weather conditions and elevation of the release is also included in this work.

As the ultimate goal of the work is to demonstrate the potential attractiveness of IFE from the S&E point of view, the safety features of the plants will be highlighted and modifications to the designs will be proposed when necessary in order to completely meet the established safety goals.

REFERENCES for the FUSION TECHNOLOGY SECTIONS

The major references for the content of the fusion technology sections of this report are:

- White Paper: Laser System and Target Chamber Design Needs for Inertial Fusion Energy Experiments in the National Ignition Facility
Grant Logan and Mike Tobin, March 30, 1995
- Meeting organized by G. Logan, W. Meier and collaborators at Lawrence Livermore National Laboratory in March 18-19, 1999 already published as IFE Chamber and Target Technology Meeting.
- Report UCRL-LR-142678 (May 2001) of Susana Reyes, Safety and Assessment for Inertial Confinement Fusion Energy Power Plants: Methodology and Application to the Analysis of the HYLIFE-II and SOMRERO Conceptual Designs.
- Fast ignition Laser Fusion Reactor KOYO-F: From T. Norimatsu (Institute of Laser Engineering, Osaka University IFE Forum), Presented at US-Japan workshop on Power Plant Studies and related Advanced Technologies with EU participation (2006)
- For ARIES reactor: Windows for IFE Power Plants, Farrokh Najmabadi and the ARIES Team UC San Diego, 16th ANS Topical Meeting on the Technology of Fusion Energy, September 14-16, 2004; and F. Najmabadi, A. R. Raffray, Aries-IFE Team: S. I. Abdel-Khalik, L. Bromberg, L. A. El-Guebaly, D. Goodin, D. Haynes, J. Latkowski, W. Meier, R. Moore, S. Neff, C. L. Olson, J. Perkins, D. Petti, R. Petzoldt, D. V. Rose, W. M. Sharp, P. Sharpe, M. S. Tillack, L. Waganer, D. R. Welch, M. Yoda, S. S. Yu, M. Zaghoul, Operational Windows for Dry-Wall and Wetted-Wall IFE Chambers, Fusion Science and Technology Vol. 46 Nov. 2004, Pages 401-416

APPENDIX 2 : The cryogenic target system for HIPER facility

This appendix has been prepared by D.Chatain and J.P. Périn,

DIRECTION DES SCIENCES DE LA MATIERE,
DEPARTEMENT DE RECHERCHE FONDAMENTALE SUR LA MATIERE
CONDENSEE, SERVICE DES BASSES TEMPERATURES

Original document reference number : CT 07-30

1	INTRODUCTION:	239
2	RECALL:	239
3	STATE OF ART	240
3.1	STATE OF DEVELOPMENT DONE FOR LMJ.....	240
3.1.1	<i>Cryocompressor</i>	240
3.1.2	<i>Cryogrip and transfer</i>	241
3.1.3	<i>Thermal regulation</i>	242
3.1.4	<i>Thermal shroud</i>	243
3.2	INFRASTRUCTURE CRYOSTATS	244
4	CONCEPTUAL DESIGN PROPOSED FOR HIPER SINGLE SHOT:	246
4.1	THE TARGET:.....	246
4.2	THE TARGET POSITIONER:	246
4.3	THE SHROUD REMOVER :	250
4.3.1	<i>The shroud grip</i>	252
4.3.2	<i>The propulsion device</i>	253
5	REFERENCES :	254

1 INTRODUCTION:

This report describes the cryogenic target system for HIPER facility proposed by the Low Temperature Laboratory of the CEA/Grenoble (France).

2 RECALL:

The HIPER facility consists in a 10 meters vacuum chamber at the centre of which a 2mm in diameter cryogenic target is irradiated by 40 laser beams (**ref 1**). The energy of the laser beams is 200kJ in 5ns. The energy of the PW beam line is 70kJ in 10ps. The awaited gain is 100.

The target is a hollow sphere filled with DT. It is a direct drive target. The dimensions are as follows:

- External radius of DT :1.044mm
- Internal radius of DT :0.833mm
- Vapour density :0.1mg/cm³ (that means a temperature of 16.3K)
- Solid DT volume :2.35mm³
- Solid DT mass :593 µg
- β heating power :116µW

3 STATE OF ART

3.1 State of development done for LMJ

From 1994 the Low Temperature Laboratory of CEA/Grenoble (SBT) is in charge of the conceptual design and prototypes realization of the cryogenic infrastructure of the Laser Megajoule project (LMJ).

3.1.1 Cryocompressor

The filling of the LMJ targets is carried out by permeation through the wall of the micro balloon. To have the desired quantity of matter, the pressure of the spheres must lie between 1000 and 1500 bars at the ambient temperature. To prevent that the targets do not break down under the effect of the pressure, the pressure difference between the internal and external walls must be lower than one bar. SBT tested an original idea to solve this problem. DT mixture is liquefied in a small volume in connection with the filling cell maintained at 300 K. Then this small volume is heated from 20 K to 300 K by controlling the temperature on the wall. This system is able to limit the rise in pressure (ΔP on the μ balloon wall) and it is possible today to ensure periods of filling which can vary from 4 to 48 hours what corresponds to slopes from 0,5 to 6 bars per minute. This cryocompressor was delivered to the research center of Valduc during the summer 2003 to be installed in a tritium cell. The construction of 2 compressors working out of tandem was committed at the end of 2005. This system will have to ensure the production of the targets for one period of at least 30 years. This system is intrinsically sure because it does not have any moving part with the difference of piston compressors. Moreover when the system is abandoned with itself (simulation of a loss of the control system) the increase in temperature with the natural losses of the system authorizes only one pressure of 400 bars. (ref 2)

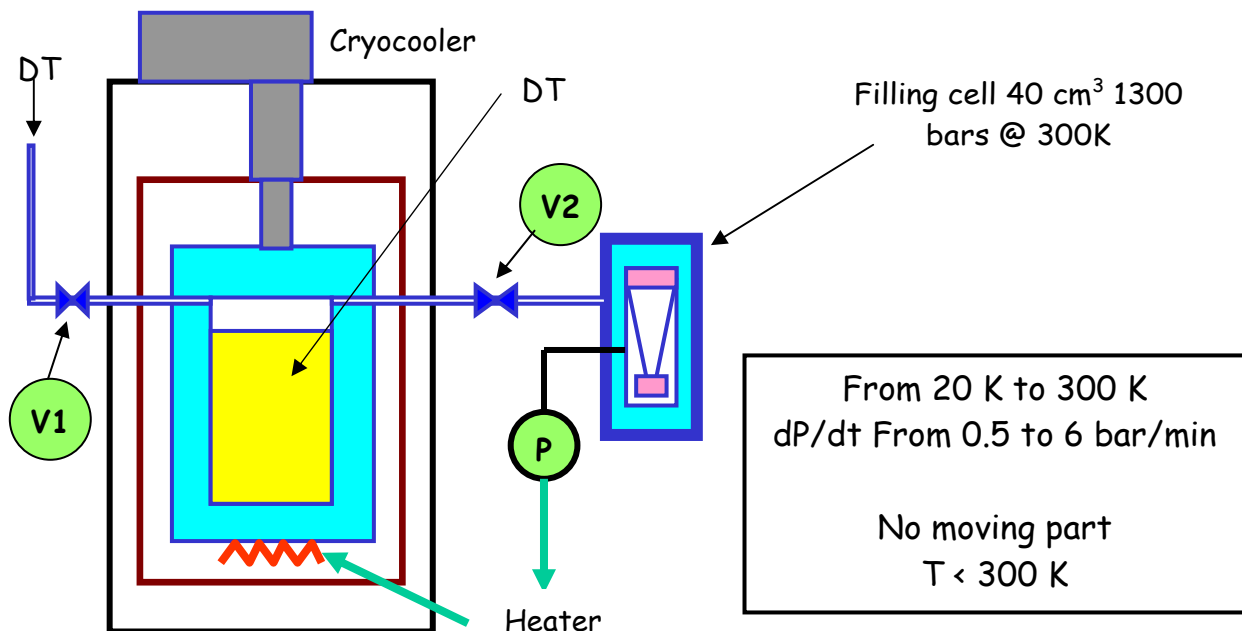


Figure 1. Principle of operation of the thermal cryocompressor

3.1.2 Cryogrip and transfer

Once the targets filled, they are cooled around 25 K and, in any case, cannot be heated with the risk to be destroyed. It was necessary to develop cryogenic grips able to handle the targets at temperatures close to 25 K. These grips must provide two important functions: the transfer of heat (power dissipated by T2 and radiation heat load) and the transfer of information. The coating of surfaces was studied in order to obtain thermal resistances of contact between the target and the grip lowest as possible. This point is extremely important, because this thermal resistance, being inversely proportional to the temperature, conditions on one hand the size of the cold source and on the other hand its limiting temperature. Indeed, if this thermal resistance is bad (3 K/W), to maintain the target to 19 K it will be necessary to have on the cold grip a lower temperature for the price of a cold source more powerful and thus bulkier. During transfers the temperature of the target must be known, it obliges the grip to ensure reliable electrical contacts and thus free from any trace of pollution what obliges to ensure the transfers under a very good vacuum by observing draconian procedures. Today procedures of manufacture of the targets are set up to guarantee this criterion of thermal resistance. SBT undertook a research program on this subject and today SBT is able to carry out thermal contacts of low resistance (1 K/W) at 17 K. The cryogenic grip is a key point of the cold chain. Its development required several years and will still require improvements. It is one of the most important technological bolts that it was necessary solve in priority (ref 3).

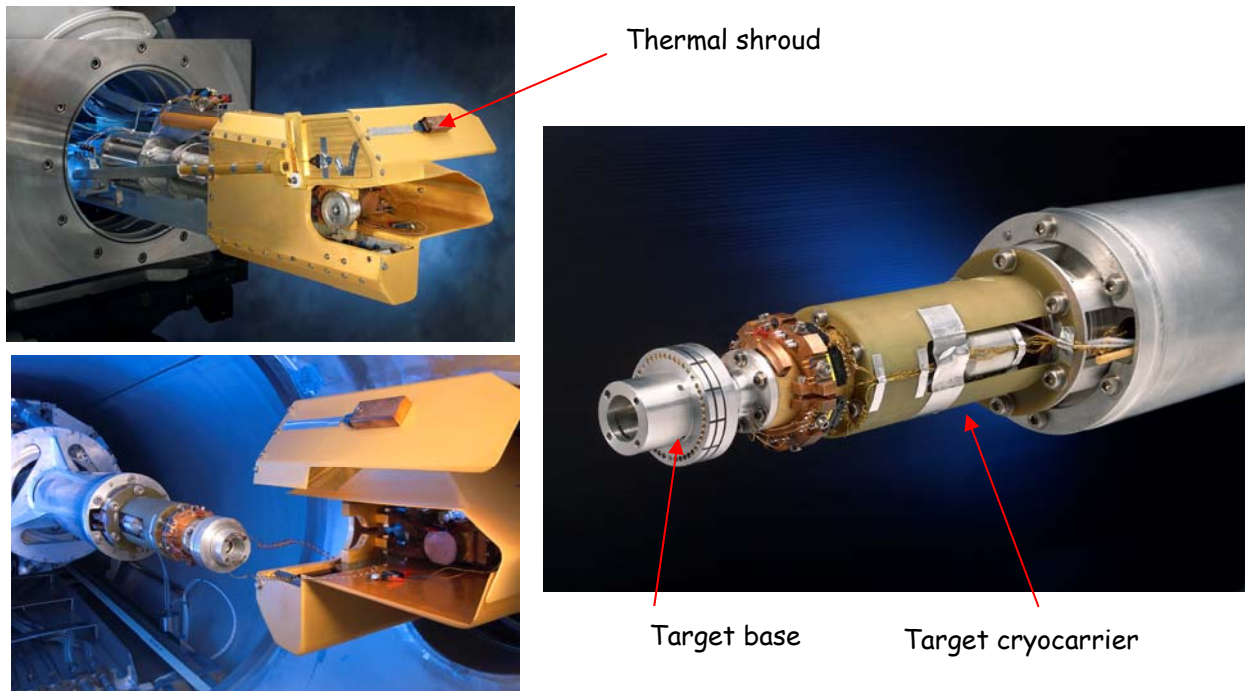


Figure 2. Photographs of the transfer of a base plate of target at 20K and connection on the cryogenic target door.

3.1.3 Thermal regulation

The thermodynamic way for the solidification of DT mixture can be followed only if we have of a thermal regulation able to carry out stabilities within 2 mK in the range 10-20 K and slopes of temperatures of 1 mK per minute

These objectives were achieved by developing the electronic ones based on synchronous detections and “multivariable” algorithms of regulation. These algorithms make it possible with several data input as well as possible to adjust the parameters of regulation. Moreover this technique allows, by simple tests in situ, to introduce into the software the true physical values of the variables. This software is not very sensitive to the environmental disturbances what is necessary for reliability in quasi industrial installations like the LMJ. This thermal regulation (0.2 mK at 20 K) and the cooling of the target with a speed of 1 mK per minute will ensure the physicists a powerful tool to reach the necessary geometrical characteristics of the ice layer (ref 4).

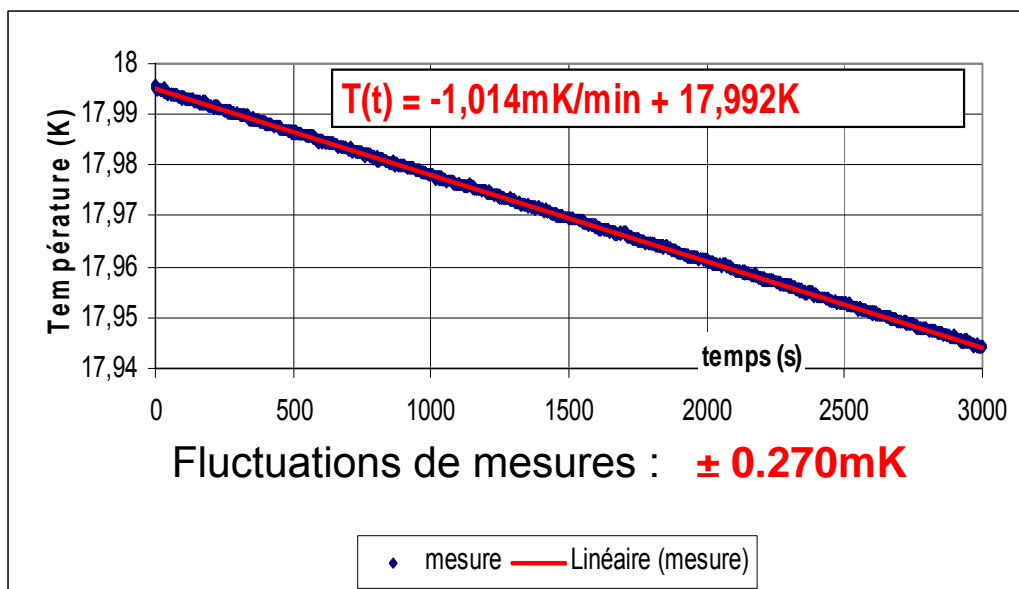


Figure 3: Recording of the target temperature during a 3000 seconds cooling obtained on model of laboratory.

3.1.4 Thermal shroud

The last important bolt to raise is the shrinking of the thermal shroud. During all handling, from its filling to the shooting, the target is protected from the surrounding thermal radiation by a cooled shroud which must be withdrawn very quickly before the shooting. When the target sees the vacuum chamber radiation at 300 K, its lifetime is only 180 ms (this time was obtained by a numerical calculation). The problems are complex; the shrinking of the screen should not generate on the target vibrations of an amplitude higher than 5 μm and the thermal field around the target should not vary more than 10 mK. Studies are led on the coupling of two cold sources and on the procedures of alignment of the two arms (target carrier and shroud carrier in the experimental chamber). A model of this unit will be brought into service at the beginning of 2007 (ref 5).

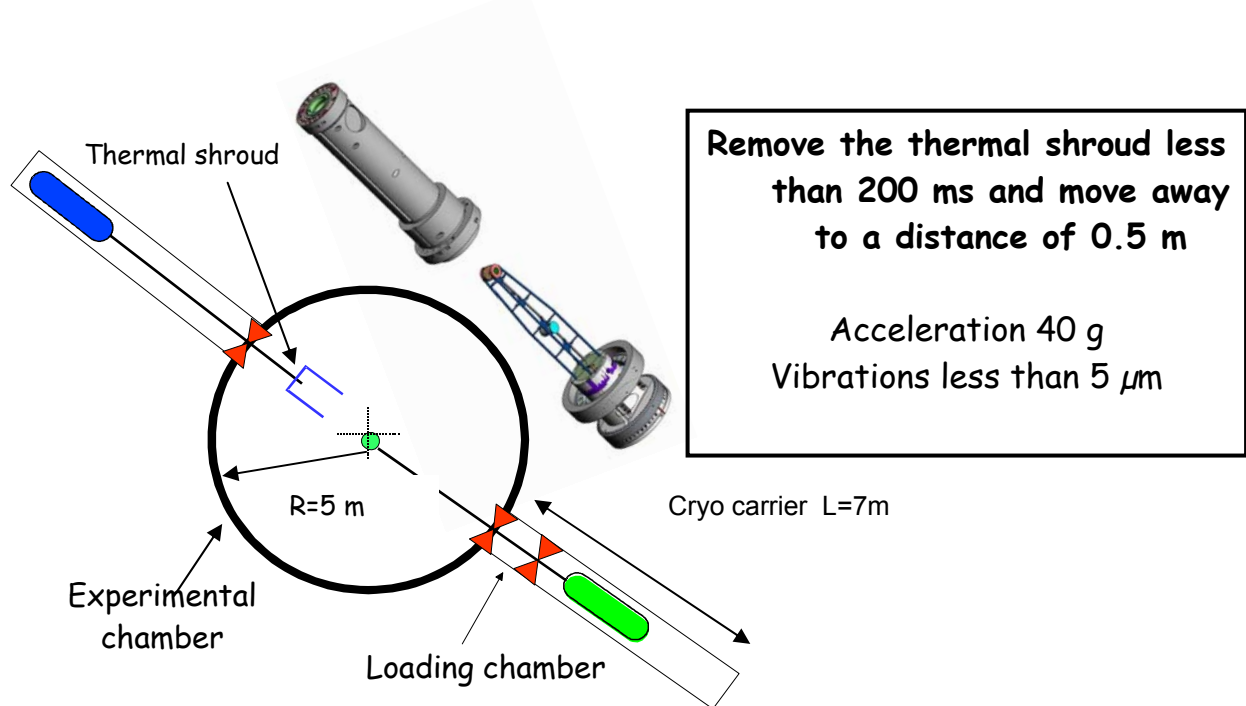


Figure 4. Principle of the withdrawal of thermal shroud.

3.2 Infrastructure cryostats

To answer the strong constraints of environment as well in the field of the robustness of the components as in the field of the biological shielding of the operators, we built a mock-up of the LMJ cryogenic infrastructure to validate the choices which answer the imposed criteria. This installation DEMOCRYTE (fig 5) which includes several cryostats (cryogenic target carrier, unit of transfer and shroud remover) was studied and built in 2001. It allowed to test in full-scale the first main components of the cryogenic target door. This evolutionary desired equipment will receive the entire systems specific to the transfer of the targets, with the conformation of the layer by will infra red, with the withdrawal of thermal shroud so that they are tested and validated. With this cryostat we tested the transfer of a target arriving from Valduc on the cryogenic target loading door. This transfer was done at 24 K then it was followed by a fine regulation at 18 K to simulate the solidification of the Deuterium-Tritium mixture with a temperature stability of +/- 2 mK.

DEMOCRYTE = {

- « Echelle1 »
- « UTCC »
- « PPET »

 Positioning, thermal regulation
 Target transfer
 Thermal shroud retractor

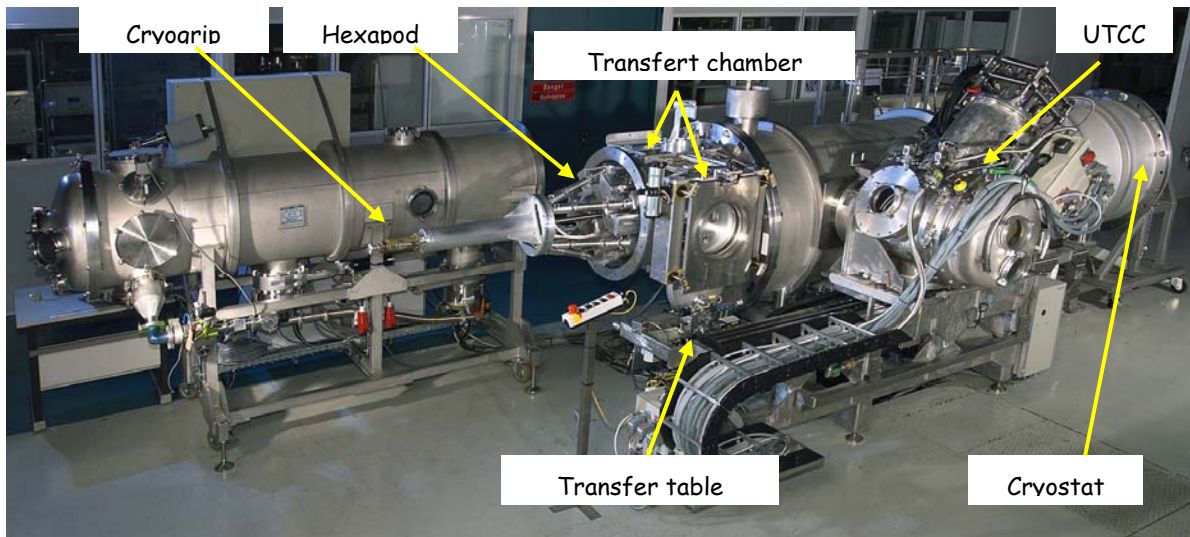


Figure 5: A view of the DEMOnstrator of CRYoTEchnologies for the LMJ.

The next step will be to test the shrinking of the thermal shroud in 2007. This work, done step by step, shows that it possible to validate the physical concepts and to check their technological feasibility. In this manner by moving back to the maximum the definition of total cryogenic architecture, the risks incurred by a premature choice are minimized. Indeed, in a project like the LMJ or any other great project of high technology, several subjects advance in parallel and are inter-connected. It is thus necessary to make choices a priori without sometimes having all information. However to be conservative is not always the best solution because that can lead to take too important safety margins and to direct research towards unrealistic or unrealizable solutions. To dissociate the problems, to find several solutions to them and then to confront all these results with the final objective were our philosophy to lead this project of great scale. The results obtained on the prototypes of the cryogenic installations of the LMJ made it possible to sit the credibility the relevance of the technical choices. Our work was recognized in 2004 and 2005 during meetings of co chair meeting which brings together the reponsibles and experts of the American (NIF) and French (LMJ) projects. This committee elected by the CEA and the DOE went to a conclusion about the cogency of the technical choices

suggested for the cryogenics of the targets and validate the programs suggested. This favourable report enabled SBT to engage the continuation of the realization of the prototypes of demonstration of feasibility (ref 6,7).

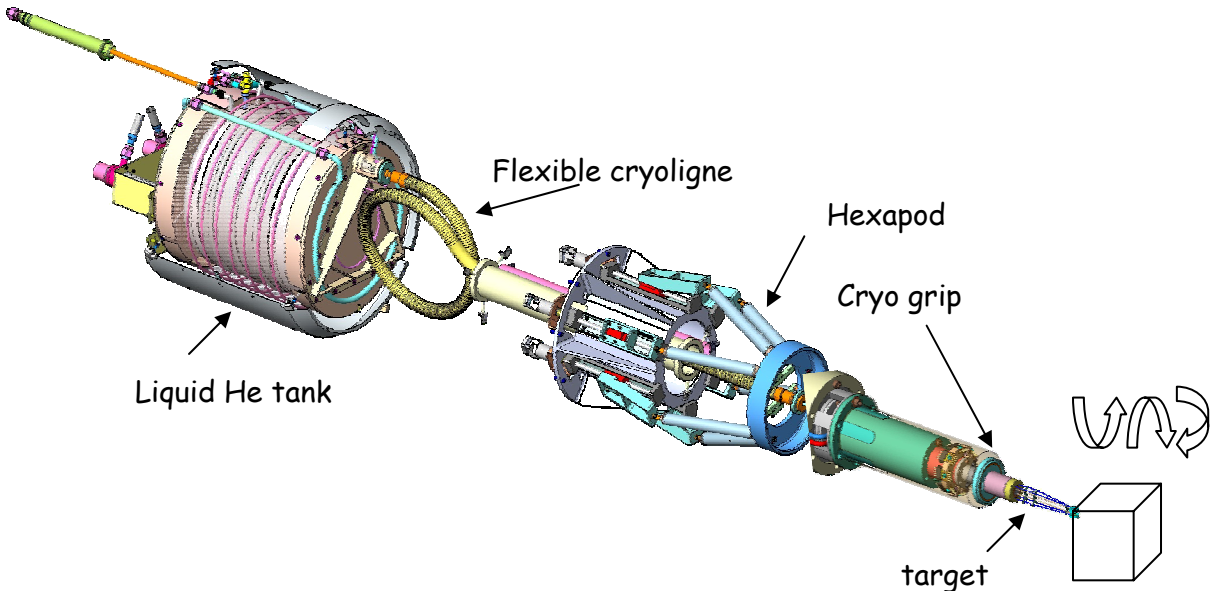


Figure 6: Burst sight of the coolant circuit of the targets and the positioner with 6 arms (hexapod).

4 CONCEPTUAL DESIGN PROPOSED FOR HIPER SINGLE SHOT:

4.1 The target:

In a first time, we propose to use targets filled with DT by a fill tube as those developed for the NIF facility (**fig 7**). This concept avoids using permeation cells and cold transfers. A thermal shroud surrounding the target will make it possible to cool down the target via Helium gas. The shroud will be equipped with sapphire windows for the target alignment.

The assembly of the target on the target positioner is performed to the hand at 300K. The indium seal allows to improve the heat transfer between the target base and the grip and makes it possible to create a tight junction during the pumping and filling steps. The different steps to follow with the target before the shot are:

- Assemble the target on the target positioner at 300K,
- Pump the target via the capillary,
- Cool down the target positioner grip (and the target base) at about 22K,
- Introduce DT in the capillary (DT is liquefied in the micro balloon),
- Cool down the target positioner grip to 16K (The DT freezes in the micro balloon),
- Let the β layering operate (the time constant is 1500 s (**ref 8**)),
- Extract slowly the shroud from the target base,
- Align the target with a good accuracy,
- Remove quickly the shroud (the membrane is torn) and shoot.

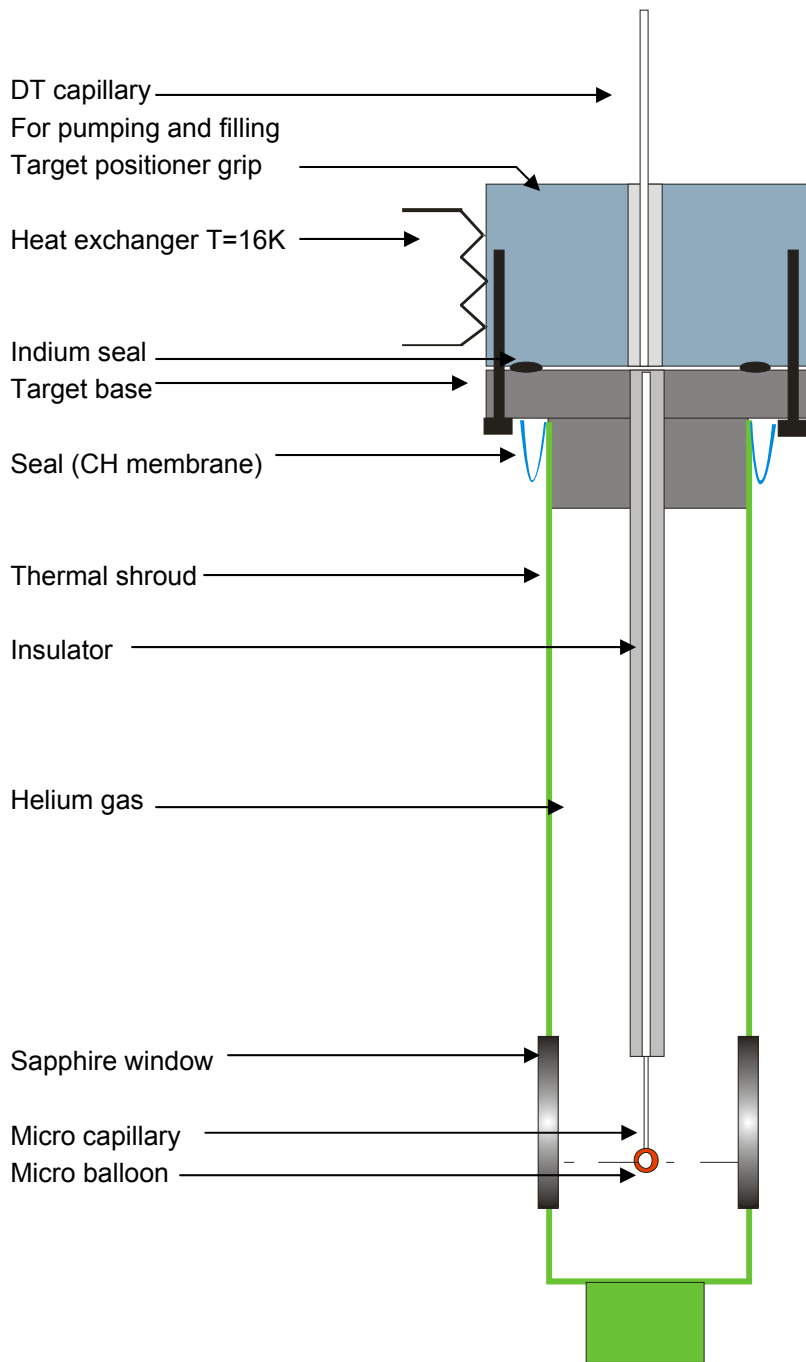


Figure 7: A schematic view of the direct drive target.

4.2 The target positioner:

For Hiper we advise to have a vertical target positioner located at the top of the vacuum chamber (on OMEGA it is at the bottom of the vacuum chamber). It can be similar to which was developed for the laser Megajoule facility (fig 9 & 10).

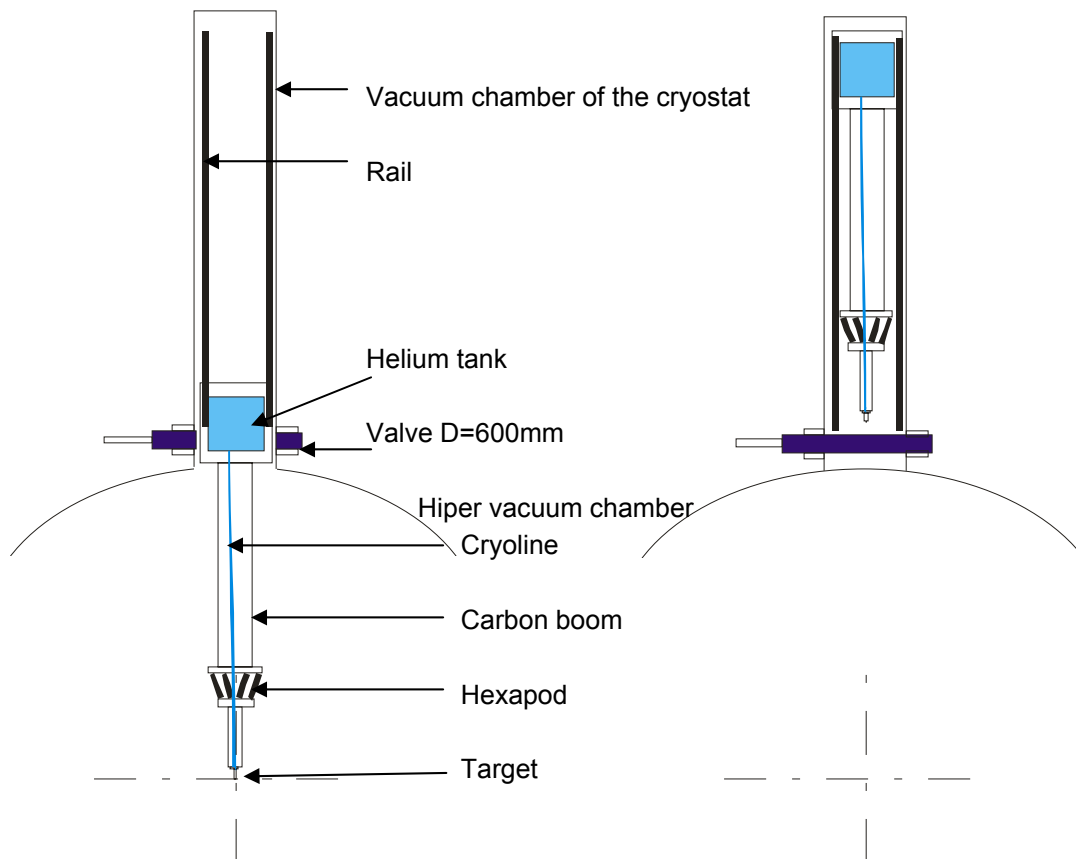


Figure 8: A schematic view of the target positioner.

It is equipped with

- A 100L helium tank which give 30 hours of self sufficiency,
- A hexapod which gives the target 6 degrees of freedom in a cube of 100mm with an accuracy of 50 μ m (today),
- A specific temperature regulation device which gives a stability of the target temperature at 1mK.

If necessary it could be envisaged to use a cold head to cool down the target. This would avoid the use of liquid Helium.

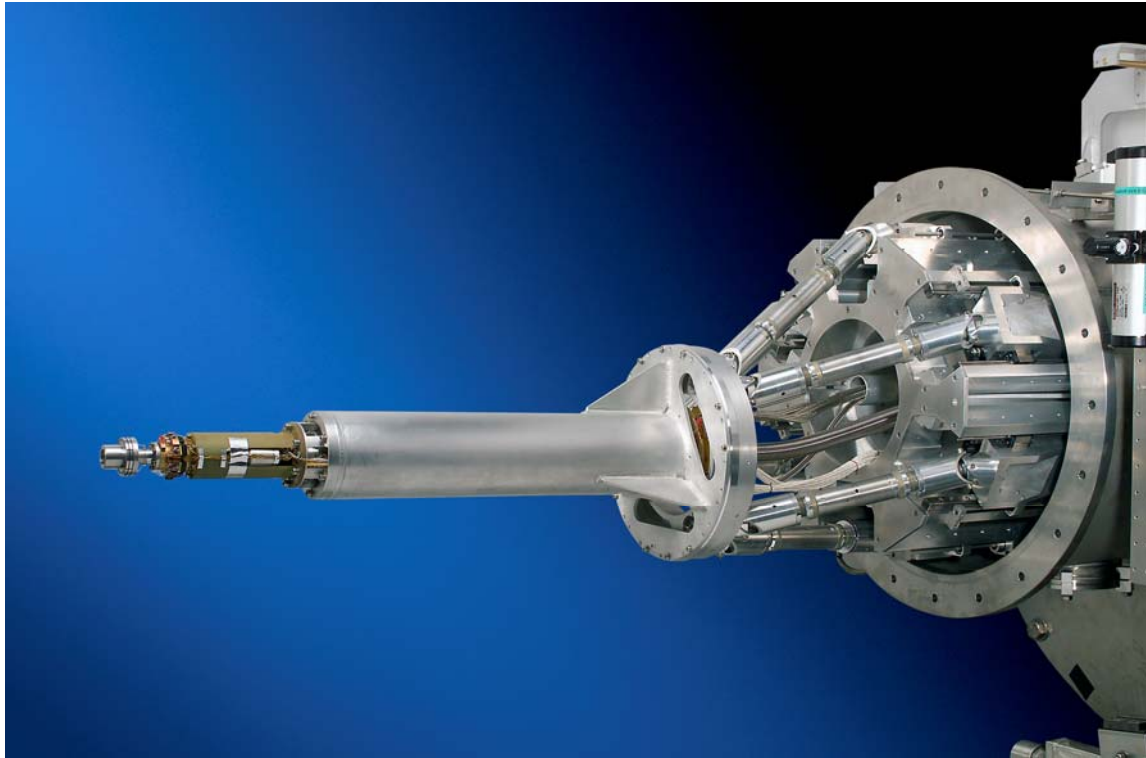


Figure 9: photography of the hexapod and the cryogenic grip developed for LMJ facility.

4.3 The shroud remover :

The shroud remover is situated at the opposite port of the cryogenic target positioner (**fig 10**). For HIPER it could be possible to develop the same as which was developed for the LMJ. It is placed on the moving part of a hexapod (**fig 11**) which will make it possible to align the shroud grip with the target grip before taking the shroud. Like for the target positioner, the target shroud remover grip will be cooled by helium gas taken in a helium tank inside the carbon boom of the target shroud remover.

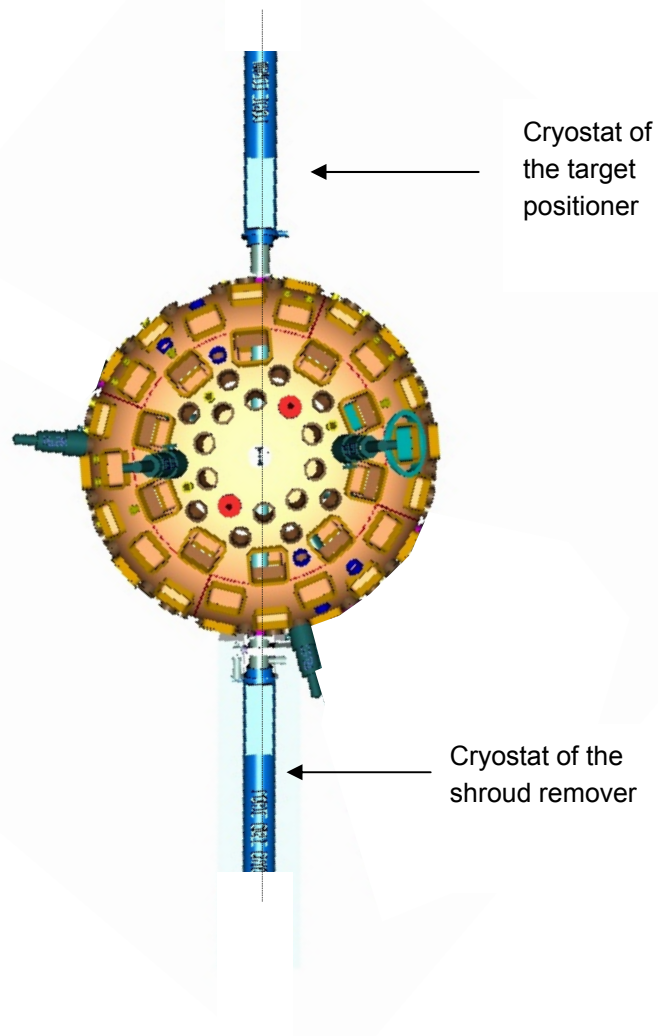


Figure 10: A view of the vacuum chamber and the two cryostats.

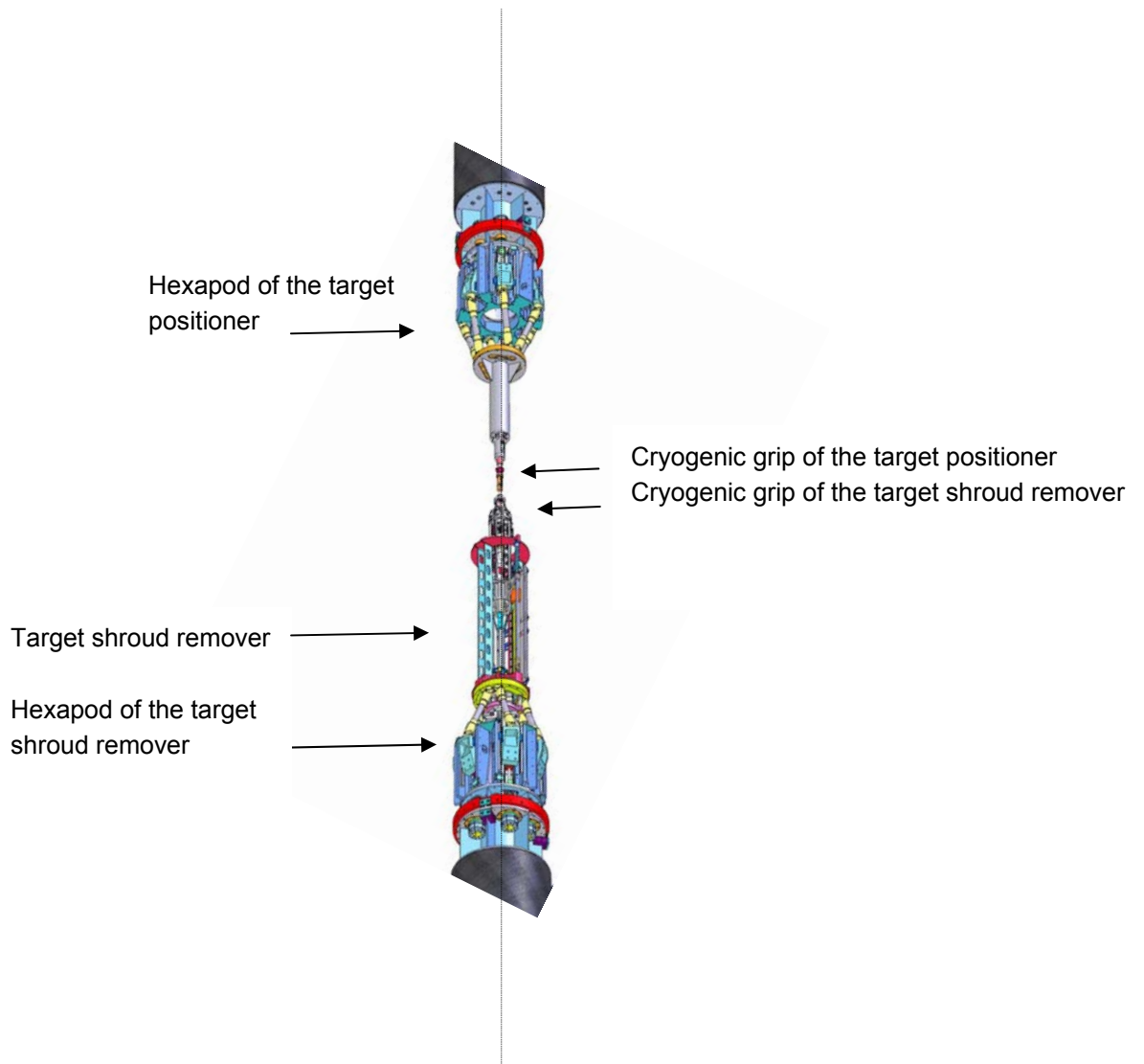


Figure 11: A view of the target shroud remover on the moving part of its hexapod.

4.3.1 The shroud grip

The shroud grip developed for the LMJ is equipped with a helium heat exchanger. A 1000N spring provides a good thermal contact between the shroud and the grip. Specific electrical contacts are used for the heaters and thermometers of the shroud. A specific device based on G10 rods gives five light degrees of freedom to the grip to absorb defects of misalignment. The mechanical connection of the shroud on the grip is based on a balls and groove device (fig 12).

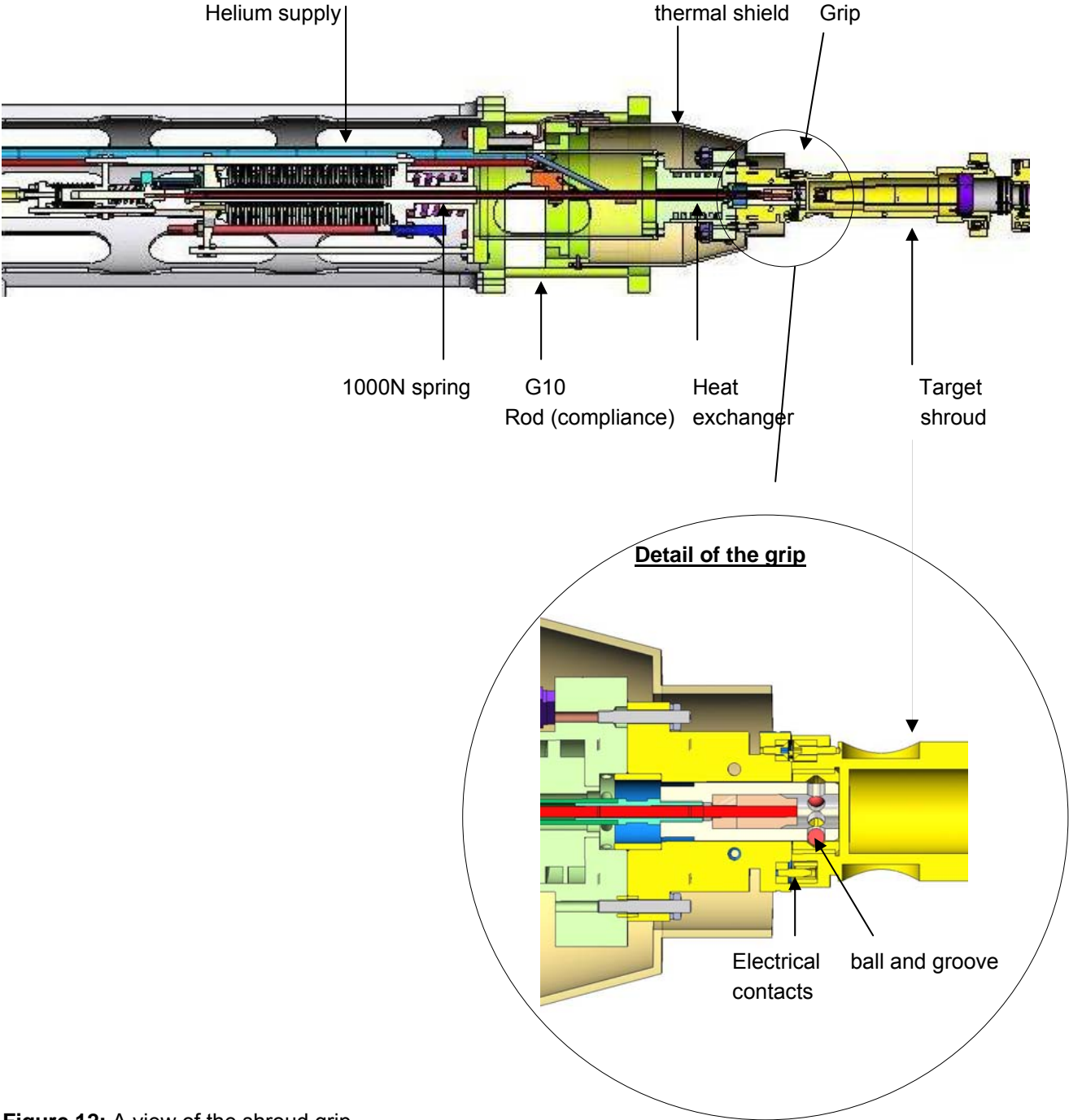


Figure 12: A view of the shroud grip

4.3.2 The propulsion device

The propulsion is based on a 2 springs device (**fig 13**). This device makes it possible to move back the shroud on a distance of 0.5m in 0.1s.

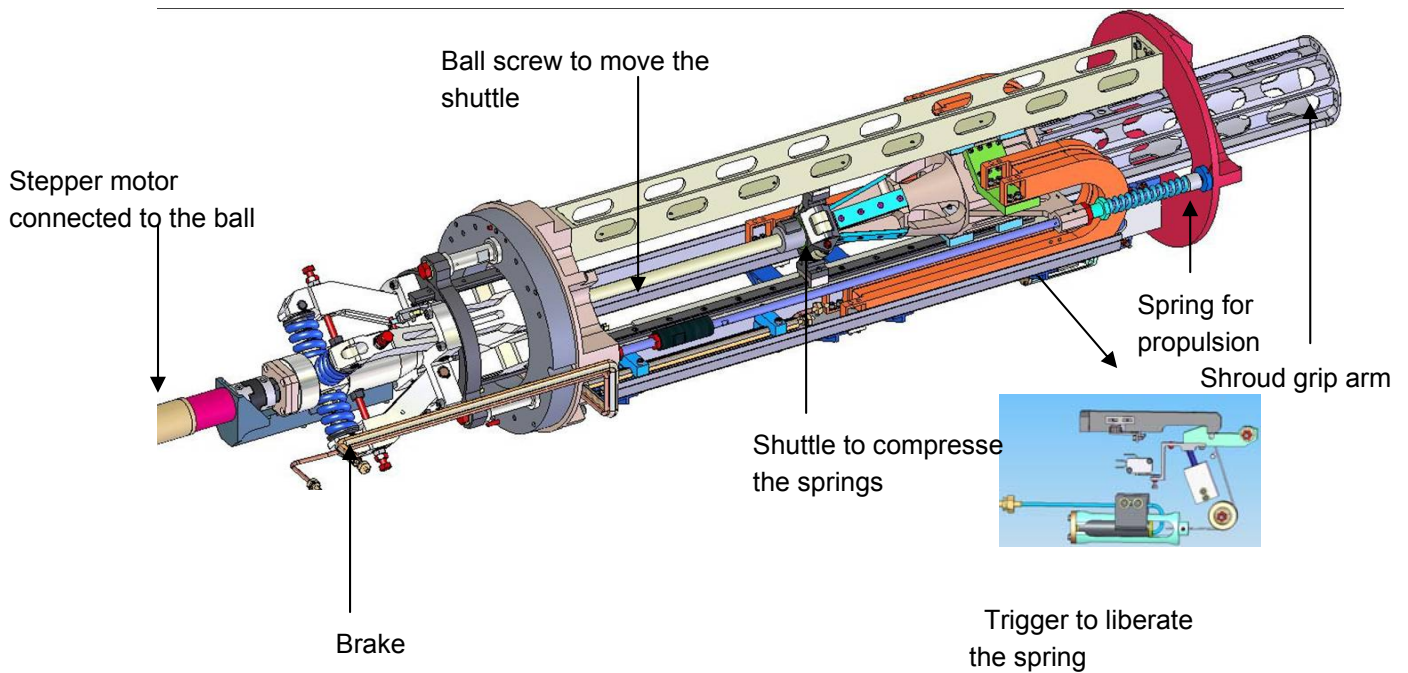


Figure 13: A view of the propulsion device.

It works in the following way:

- The shuttle is moved forward with the stepper motor to compress the spring,
- The shroud is caught by the grip,
- The shuttle is slowly moved back with the stepper motor to extract the shroud from the target base,
- When the shroud is disconnected, the trigger stops the carriage,
- The shuttle is completely removed back along with the stepper motor,
- The trigger is rocked to liberate the springs,
- The carriage is stopped by the brake.

5 REFERENCES :

1. <http://www.hiper-laser.org/docs/technical/HiPERoverview.pdf>
2. 6th International Symposium of Nuclear Fusion Technology (Fev. 2002, San Diego USA)
A 1500bar cryocompressor for the Megajoule Facility.
F; Viargues, D Chatain, JP Perin
3. 15th Target Fabrication Meeting (Juin. 2003, Portland USA).
First results on the prototype of LMJ Cryogenic Target Positioner.
G. Paquignon, D. Chatain, J.P. Périn, B. Cathala, D. Brisset, P. Bonnay, E. Bouleau, V. Lamaison.
4. 20th International Cryogenic engineering Conference (Mai 2004, Pekin)
The Laser Megajoule CryoTarget Thermal Regulation.
Lamaison V., Brisset D., Cathala B., Paquignon G., Bonnay P., Chatain D., Communal D., Périn J-P.
5. 17th Target Fabrication Meeting (Oct. 2006, San Diego, USA)
The Cryogenic Shroud Extractor Prototype for the Laser Megajoule Facility.
D. Chatain, V. Lamaison, P. Bonnay, E. Bouleau, J-P. Périn.
6. 17th Target Fabrication Meeting (Oct. 2006, San Diego, USA)
Laser Megajoule cryogenic target : a way from automatic transfer to laser conditions.
G. Paquignon, J. Manzagol, V. Lamaison, D. Brisset, D. Chatain, P. Bonnay, E. Bouleau, D. Communal, J-P. Périn.
7. 20th International Cryogenic engineering Conference (Août 2005, Keystone, USA)
Automatic transfer between two cryogenic robots for the Laser Megajoule Facility.
G. Paquignon, J. Manzagol, V. Lamaison, D. Brisset, D. Chatain, P. Bonnay, E. Bouleau, J-P. Périn.
8. J.Vac.Sci.Technol. May/Jun 1988. p.1885.
Beta energy driven uniform D-T ice layer in reactor size.
Martin and Simms
9. Cryogenic targets production using magnetic levitation
Note SBT/CT 00-03, 04/02/2000
D. Chatain.

Appendix 3 : 10kJ DPSSL Study

This appendix has been prepared by Jean-Christophe Chanteloup, Laboratoire Utilisation des Lasers Intenses (LULI), Palaiseau, France

Appendix 3 Contents

1.	INTRODUCTION.....	257
2.	GAIN MEDIUM.....	257
2.1.	INTRODUCTION.....	257
2.2.	TEMPERATURE.....	259
2.2.1.	<i>Spectroscopic properties.....</i>	259
2.2.2.	<i>Thermal properties.....</i>	260
2.2.3.	<i>Bandwidth.....</i>	261
2.2.4.	<i>Short pulse operation.....</i>	261
2.2.5.	<i>Cryo-cooled impact on DPSSL efficiency.....</i>	262
3.	PUMPING ARCHITECTURE.....	263
3.1.	TRANSVERSE DISTORTIONS MANAGEMENT	263
3.2.	EXTRACTION AND PUMPING LIGHT MULTIPLEXING.....	265
3.2.1.	<i>Spectral multiplexing.....</i>	265
3.2.2.	<i>Vectorial multiplexing.....</i>	265
3.2.3.	<i>Angular multiplexing.....</i>	265
3.2.4.	<i>Side pumping.....</i>	266
4.	COOLING TECHNIQUE.....	267
4.1.	EXTRACTION BEAM TRAVELLING THROUGH COOLANT	267
4.2.	GAIN MEDIUM BACK SIDE COOLING.....	267
5.	EXTRACTION ARCHITECTURE.....	268
5.1.	EXTRACTION FLUENCE.....	268
5.2.	SCALABILITY	268
6.	COST.....	269
6.1.	INTRODUCTION.....	269
6.2.	DRIVER COST.....	270
6.3.	MERCURY DATA.....	271
6.4.	LUCIA AND POLARIS DATA.....	272
6.5.	DATA COLLECTED FOR HIPER (CONFIDENTIAL).....	273
6.6.	HIPER 10 KJ BEAMLINE COST ESTIMATION.....	274
6.6.1.	<i>Diodes Budget.....</i>	274
6.6.2.	<i>Drivers/CC budget.....</i>	274
6.6.3.	<i>Gain medium Budget.....</i>	274
6.6.4.	<i>Other costs.....</i>	274
6.6.5.	<i>Conclusion.....</i>	274
7.	REFERENCES.....	275

1. INTRODUCTION

This document gives a tentative list of key aspects to be addressed in order to build a 10kJ class Diode Pump Solid State Laser (DPSSL) for HiPER. Chapter 6 is devoted to cost estimation for such a beam-line.

Currently, four known 100 Joules level DPSSL are being constructed throughout the world, Mercury (Livermore, USA), Polaris (Jena, Germany), Halna (Osaka, Japan) and Lucia (Palaiseau, France). A Chinese DPSSL is probably being studied by the Chinese Academy of Science.

2. GAIN MEDIUM

2.1. INTRODUCTION

Selecting the gain medium for a DPSSL beamline results from a compromise between numerous factors. A non exhaustive list is given in table 2.1:

Factor	Related issue
Diode pumping requirement	Budget
Availability	Project timeframe
Thermal properties	Rep. rate/cooling power
Upper state lifetime	Diode investment
Emission cross section	Parasitics management/laser damage

Table 2.1

The selected material absorption cross section spectral bandwidth will have a direct impact on diode cost. Figure 2.1-a shows a factor 5 in bandwidth for the 3 main candidates for 10 kJ class DPSSL gain medium: 15 nm (Yb:YAG), 12.5 nm (Nd:Glass) and 3.4 nm (Yb:SFAP). Constraints on corresponding diodes emission bandwidth are consequently affected.

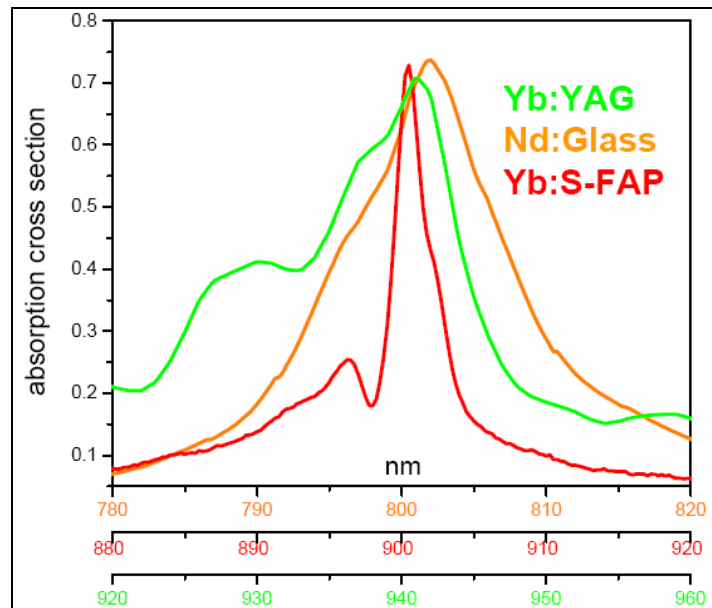


Figure 2.1-c: Normalized absorption cross section spectrum for 3 potential gain medium candidates for 10 kJ class DPSSL

Figure 2.1-b helps visualize the respective choices of the 4 DPSSL programs mentioned in introduction.

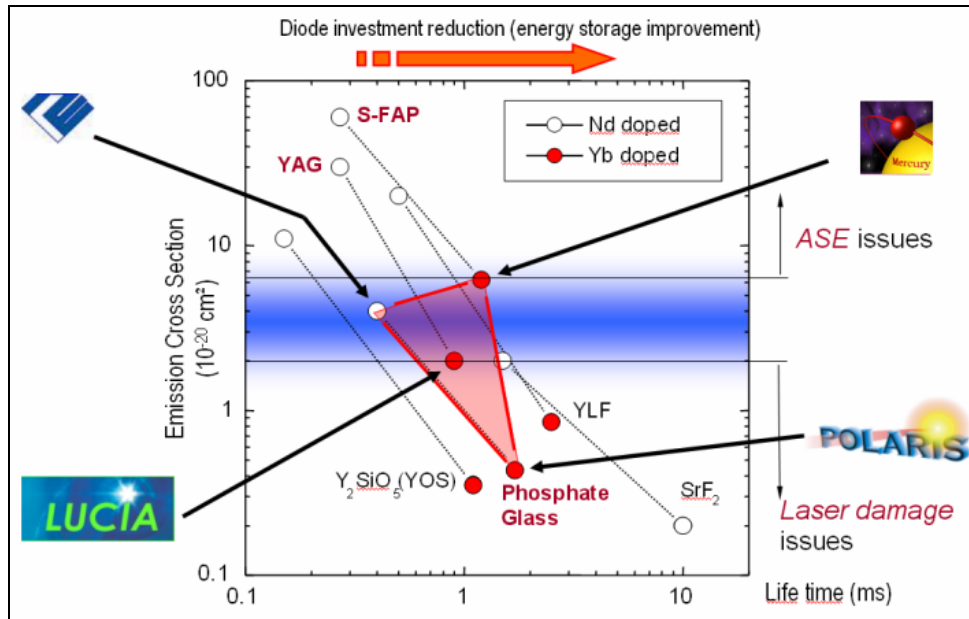


Figure 2.1-b: visualization in a log-log space of main DPSSL program laser media choice.

Thermal conductivity is a key factor to be carefully addressed together with the doping level. Indeed, a 10atm% doped Yb:YAG will, for instance, exhibit a 7 W/m.°C thermal conductivity to be compared with 13 W/m.°C for an undoped YAG (figure 2.1-c). Such degradation in thermal performances is related to the doping ion larger diameter than the Yttrium ion it is replacing, leading to the host matrix deformation.

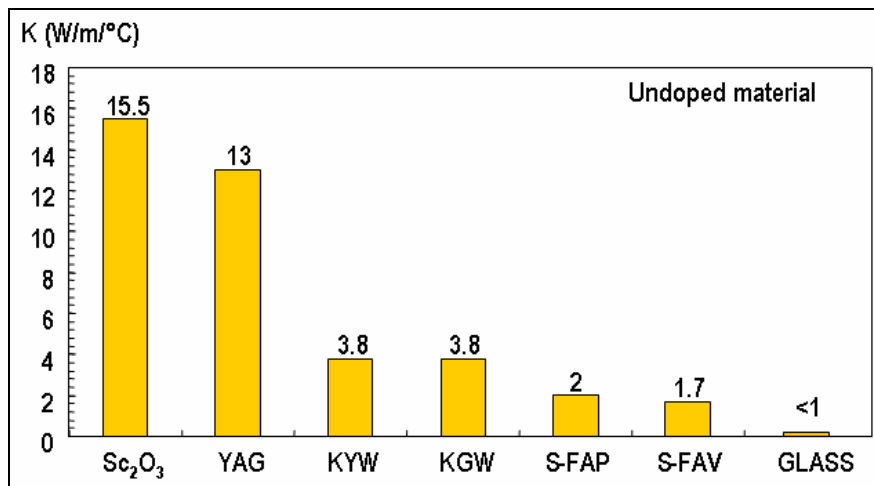


Figure 2.1-c: Thermal conductivity for several undoped host matrices

Nd³⁺:Glass strengths (well establish production capability, 4 level laser,...) are somehow balanced by a much shorter (5x) lifetime than Yb³⁺ and a limited thermal conductivity when compare to crystalline structure.

Yb³⁺:Crystals (S-FAP or YAG) are suffering from limited aperture (with respect to current availability) for kJ DPSSL size requirements.

Yb³⁺:Ceramics are probably a good candidate since such material scales like glass and its optical quality is comparable to glass whereas thermal properties are comparable to crystalline structures.

Nevertheless a 16 times increase in size would be required in order to match HiPER DPSSL requirements (~40x40 cm² versus 10x10 cm² today).

2.2. TEMPERATURE

2.2.1. Spectroscopic properties

Temperature operation will be a key choice for HiPER DPSSL beamline. Spectroscopic properties of laser materials are very dependant with temperature. The following graphs are all related to Yb:YAG.

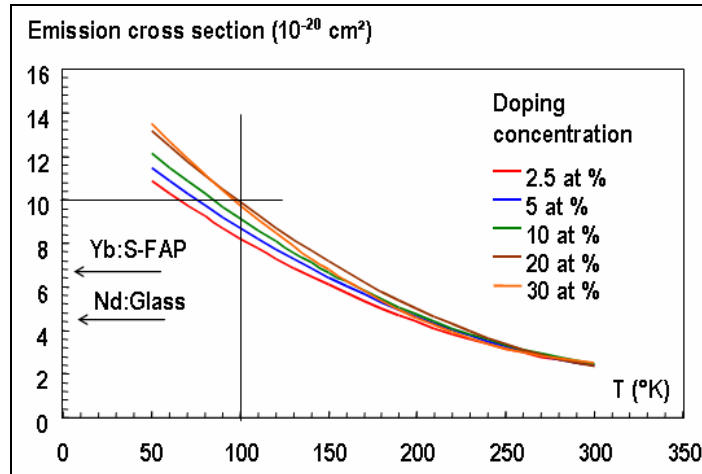


Figure 2.2-a : Yb:YAG (crystal) emission cross section variation vs temperature for several doping concentration [1].
The two left arrows are pointing towards the Yb:SFAP and Nd:Glass values.

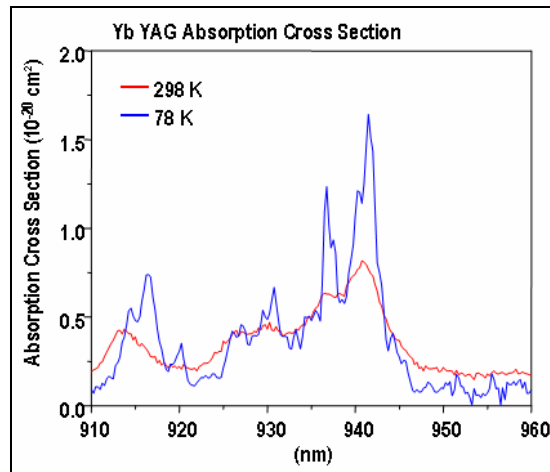


Figure 2.2-b : Yb:YAG (crystal) absorption cross section spectrum for two temperatures [2]

Impact on saturation fluence and intensity is given on figure 2.2-c. We can see that operating at low temperature allows to strongly relax the constraints on laser damage fluence. For instance, the Lucia laser is operating at room temperature and in order to extract 100 Joules in only 3 passes, an extraction fluence above 10 J/cm^2 is requested.

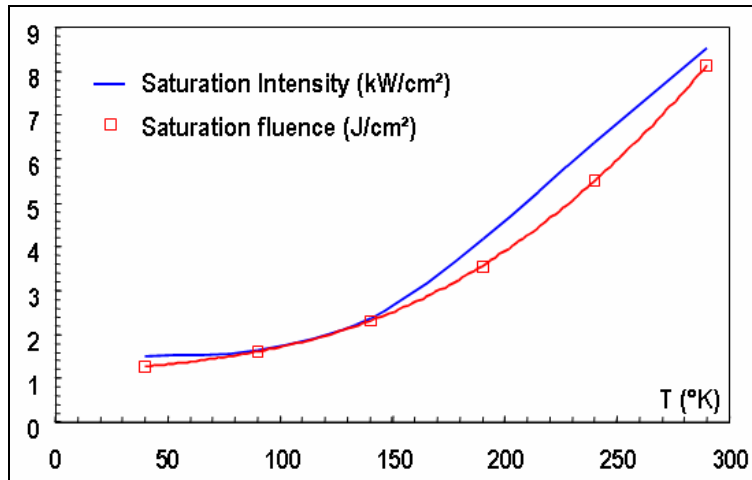


Figure 2.2-c : Saturation intensity and fluence variation with temperature

2.2.2. Thermal properties

Thermal conductivity can also be lowered dramatically when working at temperature around 100°K (see figure 2.2-d and notice that thermal conductivity unit is expressed in W/cm.K while comparing with figure 2.1-c)

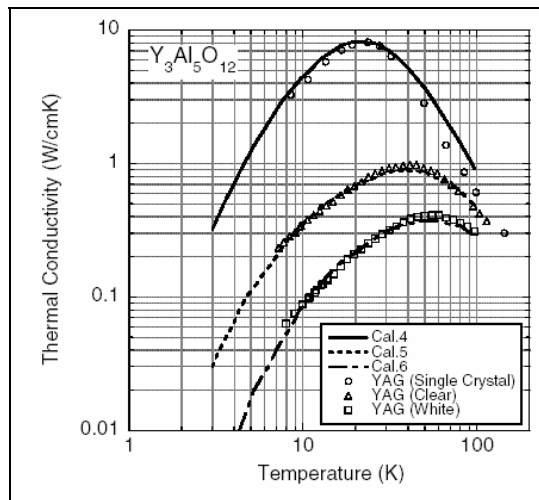


Figure 2.2-d : Thermal conductivity at low temperature for YAG [3]

The thermal shock parameter is also strongly dependent of temperature (fig. 2.2-e).

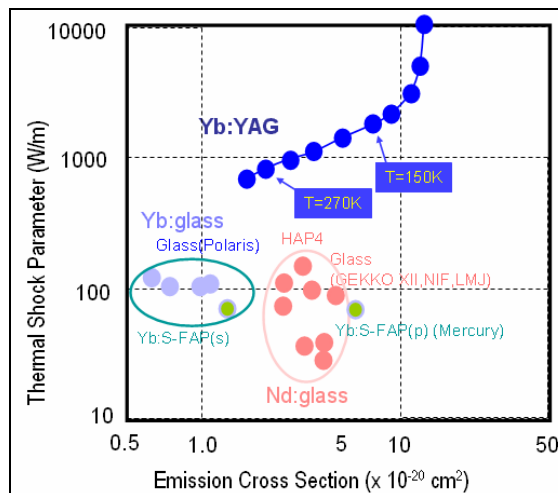


Figure 2.2-e : Thermal Shock Parameter dependence with temperature for High energy DPSSL key gain media [4]

2.2.3. Bandwidth

Going towards cryogenic temperature nevertheless presents a potential drawback in terms of pump source spectral requirements. 940 nm curve on figure 2.2-f exhibits indeed a strong narrowing of pump bandwidth with decreasing temperature.

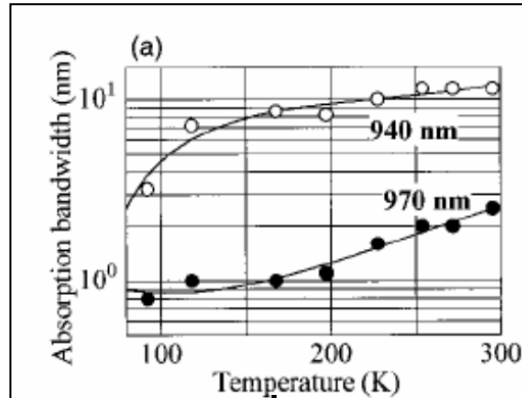


Figure 2.2-f : Spectral bandwidth variation with temperature for 940 nm and 970 nm absorption band of Yb:YAG [5].

This effect has to be related the so-called “thermal chirp” of laser diodes: in QCW regime, as a result of semiconductor heating, the diode wavelength drifts during pumping.

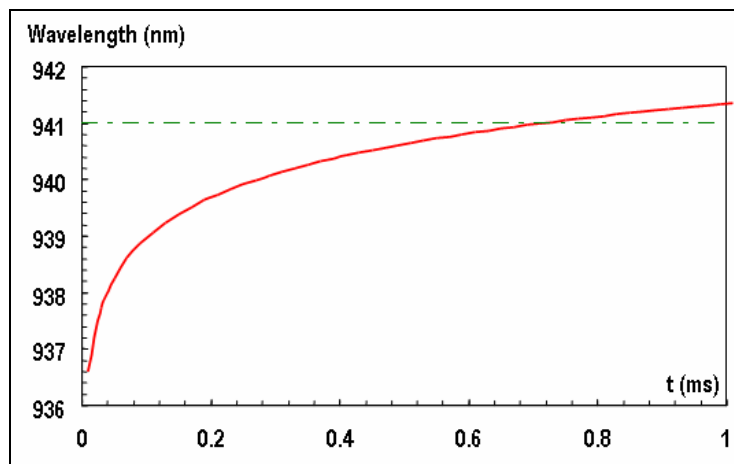


Figure 2.2-g : Peak wavelength thermal drift during a 1 ms pump pulse for laser diode driven by 120 Amperes.

2.2.4. Short pulse operation

Ultra-short pulse operation can be affected by cryogenics temperature operation. Figure 2.2-h shows for instance a drastic reduction in emission bandwidth around 100K.

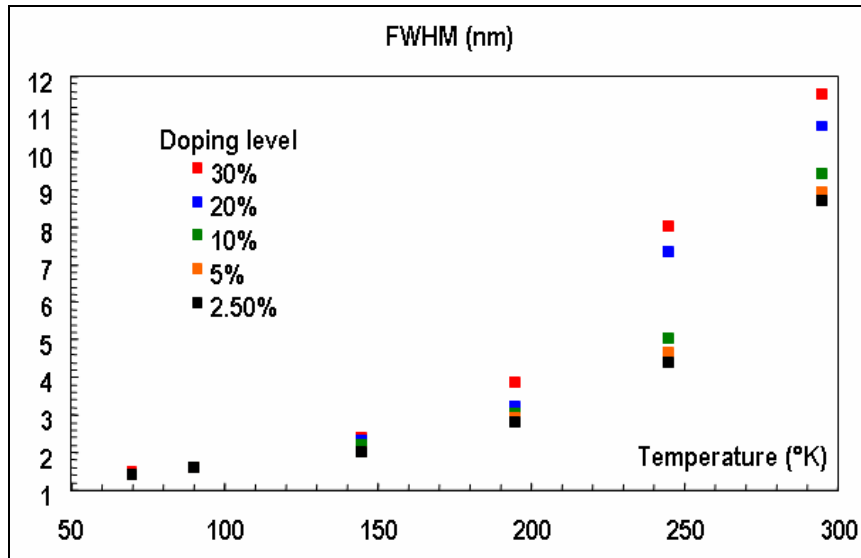


Figure 2.2-h :Yb:YAG Spectral bandwidth reduction with temperature for several doping level.

2.2.5. Cryo-cooled impact on DPSSL efficiency

Cryogenic cooling impact on global system power requirement can be analyzed using the laser system efficiency given by:

$$\text{System Efficiency} = \frac{\text{Average Laser Output Power}}{(\text{Diodes Electric Power}) + (\text{Power to Cool Diodes}) + (\text{Power to Cool Slabs})}$$

Figure 2.2-i shows power requirements curve for a 14.6kJ/1ω/10 Hz DPSSL. Laser diode (40KJ) electrical-to-optical (e-o) efficiency is taken at 50% and final optical-to-optical (o-o) efficiency is 36%.

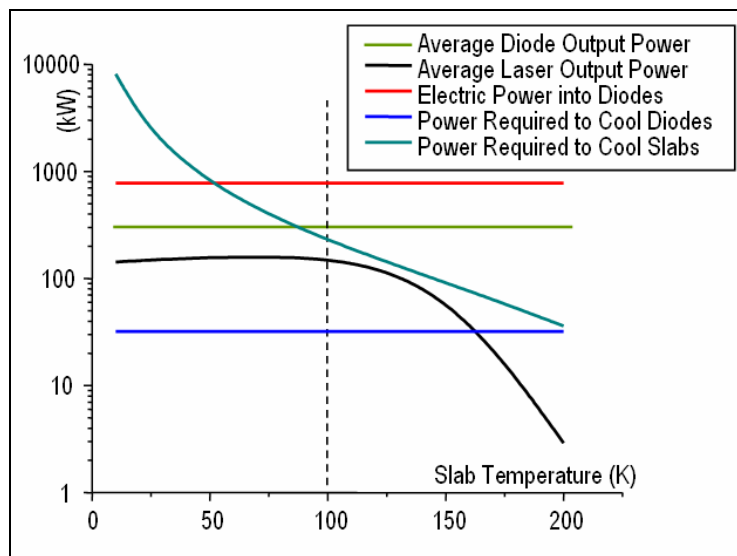


Figure 2.2-i: Power curves for a 14kJ output energy Yb:YAG laser [6].

Figure 2.2-j displays the system efficiency versus cooling temperature resulting to an optimum temperature around 100K.

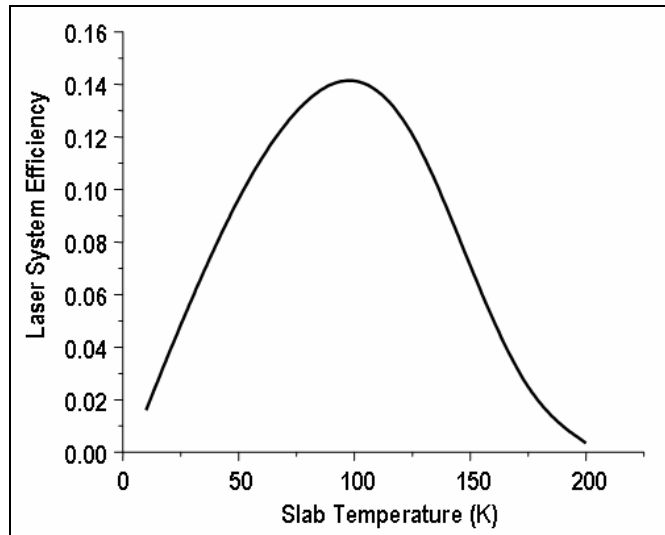


Figure 2.2-j: Laser system efficiency optimum is around 100K for Yb:YAG 10kJ class DPSSL [6]

It should be noticed that the power required to cool the edge claddings has been neglected here.

3. PUMPING ARCHITECTURE

3.1. TRANSVERSE DISTORTIONS MANAGEMENT

Allowing cooling, pumping and extraction axis to coincide allows better transverse distortions management.

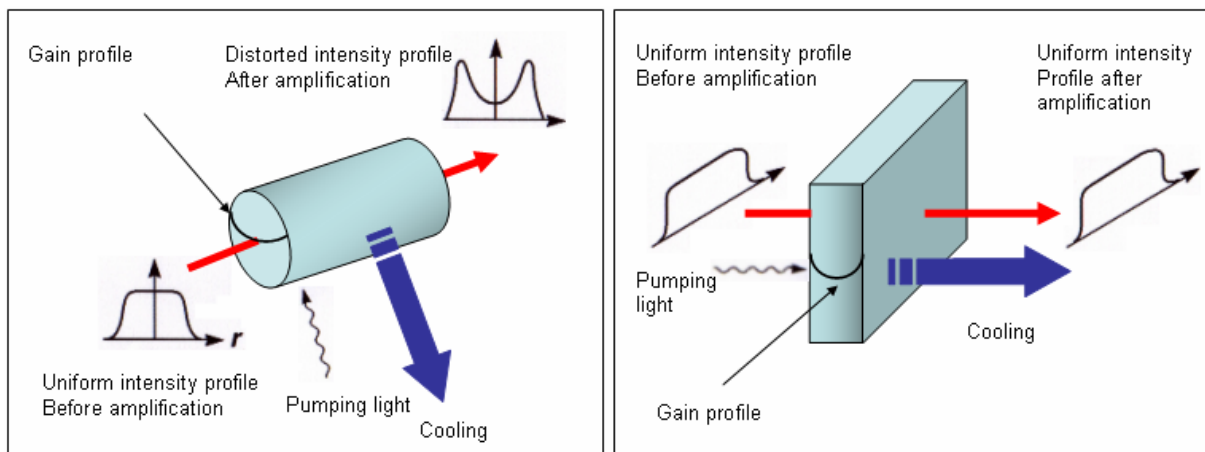


Figure 3.1-a: Two different distribution of cooling, pumping and extraction axis.

Among the 4 DPSSL programs currently under development, only Halna is relying on side pumping (figure 3.1-b). This choice is driven by the very specific zig-zag slab extraction architecture chosen for this project.

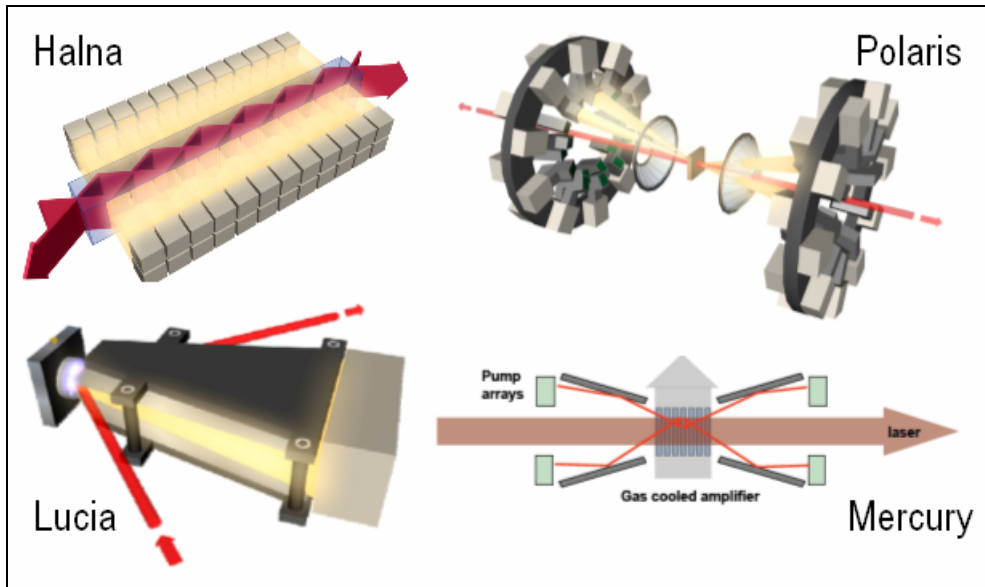


Figure 3.1-b: Pump and extraction axis for Halna, Polaris, Lucia and Mercury

Whereas Polaris and Mercury rely on counter-propagative pumps, Lucia is based on the so-called “active mirror” or “Thin Disk” concept (figure 3.1-c).

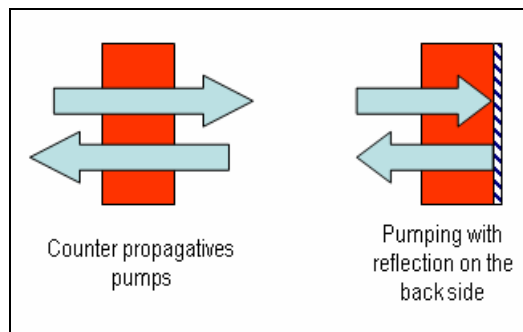


Figure 3.1-c: Polaris/Mercury counter-propagative scheme and lucia retro-reflection geometry (active mirror concept).

Japan (ILE, Osaka) is also proposing an IFE plant which DPSSL driver is based on the “thin disk concept” (figure 3-1-d).

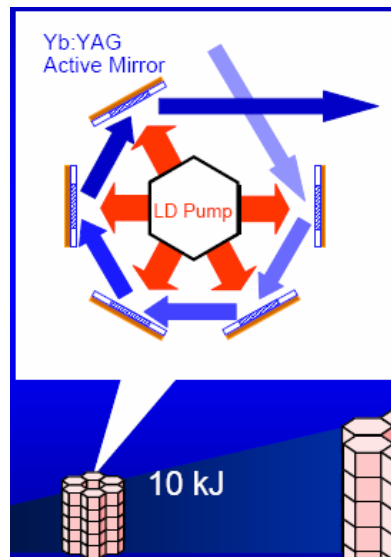


Figure 3.1-d: ILE concept for a 10 KJ class DPSSL [7].

3.2. EXTRACTION AND PUMPING LIGHT MULTIPLEXING

Several approaches can be envisioned for pumping and extraction light beam simultaneous management.

3.2.1. Spectral multiplexing

Spectral multiplexing has been proposed in the early stage of Mercury but technical challenges arose when looking at the feasibility of large spectral Beam Splitters (BS) having to satisfy:

- small spectral difference between pump and extraction light (~100 nm)
- extremely long lifetime (operation at 10 Hz)
- large optics

3.2.2. Vectorial multiplexing

Vectorial (or polarization) multiplexing might be possible since diode light is strongly polarized along the fast axis (better than 97% measured with DILAS stacks).

The following figure shows a proposal for a ~10kJ class amplifier module using spectral or polarization BS at 45°.

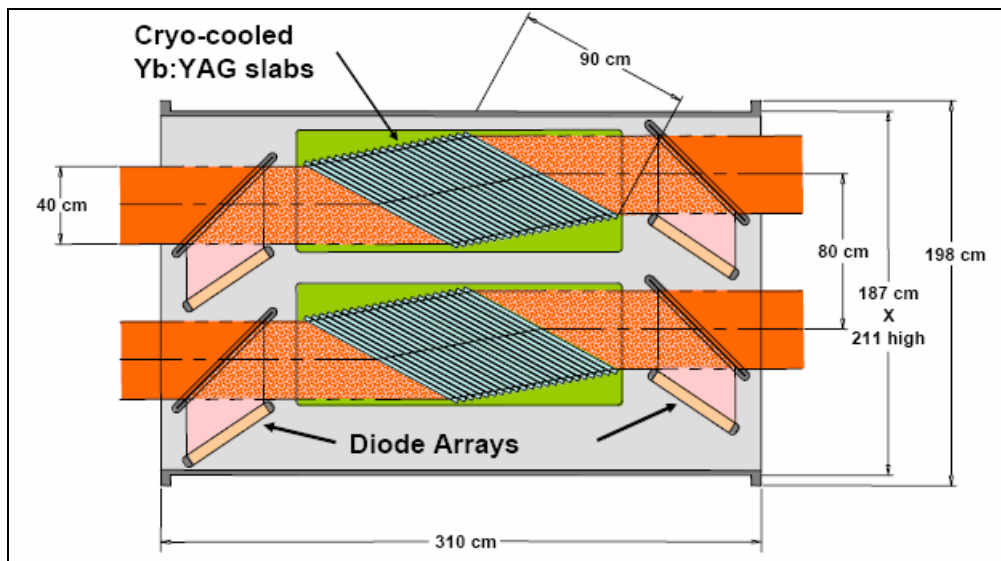


Figure 3.2-a: Spectral or vectorial multiplexing arrangement on a 10kJ-class DPSSL [6].

3.2.3. Angular multiplexing

At first sight, angular multiplexing seems uneasy to deal with, taking into account:

- large pumping beam size
- diode light divergence properties
- Compactness constraints (due to scalability requirements for instance).

In order to ensure lifetime (no AR degradation) and coupling efficiency, an obvious option for gain medium, is to rely on Brewster angled (61° for YAG) slabs with respect to extraction axis. In order to couple also pumping light into these slabs, several alternative planes of incidence can be used. This is especially true with Yb:YAG since its cross sections are polarization independent (not true for Yb:SFAP, see on fig. 2.2-e for instance). The figure 3.2-b describes a pumping scheme where the same plane of incidence is used, but for which the angle between extraction and pumping axis is equal to 2x Brewster angle.

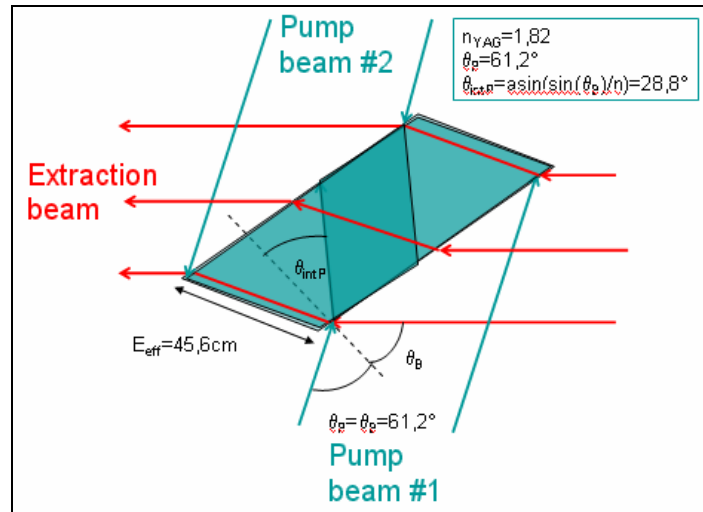


Figure 3.2-b: Pumping and extraction axis both at Brewster incidence in Yb:YAG. An inhomogeneous pumping density (darker area in the middle of the slab) would occur if pumping light is not transversally modulated in intensity.

As a result, the gain medium would suffer from very inhomogeneous pumping distribution. Figure 3.2-c shows the intensity distribution we would request from a diode array of width w .

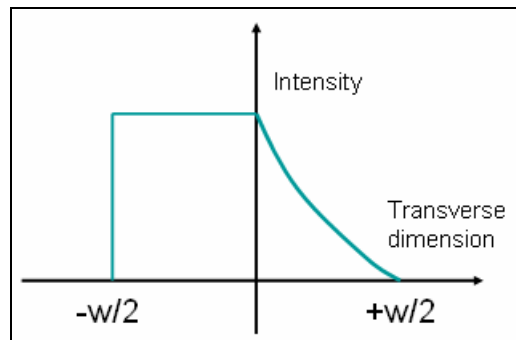


Figure 3.2-c: Possible transverse intensity distribution required in order to achieve uniform pumping in the architecture described on figure 3.2-b.

Taking into account the very composite nature of diode array will allow a great degree of flexibility in terms of pumping emission distribution. Indeed, diode arrays are made of stacks itself composed of bars made of emitters (the laser diodes).

The cost of a stack is the same whatever the driving current applied to it. Consequently, modulating the output power is not really cost effective. A better solution would be to adjust laterally the density of stacks so that the power density (W/cm^2) is transversally evolving like on figure 3.2-c. Of course the same goal could be achieved while relying on stacks having a number of bars decreasing from 25 to 5 (typical stack bars number).

3.2.4. Side pumping

Finally, in case compactness or cost (no microlensing affordable) imposes side pumping, one should not rule out the use of an edge cladding that is transparent to the pump while absorbing the extraction light (ASE). We could imagine confining the pump light through total internal reflection.

4. COOLING TECHNIQUE

As shown on figure 3.1-a, transverse distortions management makes preferable to rely on axial cooling with respect to extraction axis.

4.1. EXTRACTION BEAM TRAVELLING THROUGH COOLANT

The gain medium cooling technique will be strongly influenced by the extraction/pumping architecture. Gas cooling is suitable with extraction through a set of several Brewster angled slabs. As an example, Helium is used at room Temperature on Mercury and could be used at -77°K at several Atm pressures in a cryogenic scheme.

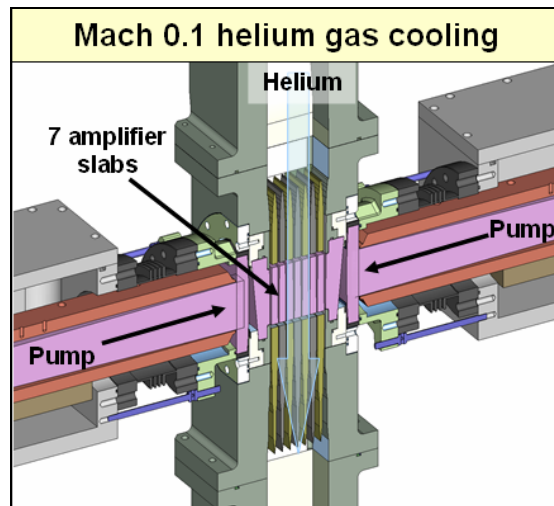


Figure 4.1: Mercury Helium cooled 7 wedged slabs head.

4.2. GAIN MEDIUM BACK SIDE COOLING

Thin disk based cooling offers the advantage of not letting the extraction beam travelling through the coolant but requires strong heat removal ability. Cooling techniques allowing extremely high heat exchange coefficient (W/m.K) have been developed by A.Giesen at the IFSW in Stuttgart (Germany). Values of 10^5 W/m.K are indeed achieved on a cm^2 scale for multi kW CW thin-disk lasers. Lucia (figure 4.2) amplifiers will also rely on such architecture (10cm^2 scale and 100 time smaller duty cycle).

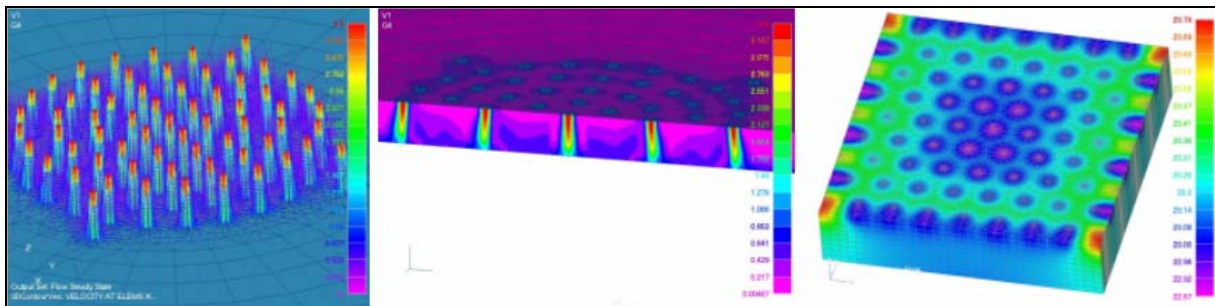


Figure 4.2: Left picture shows 1 mm diameter water jets hitting the back side of Lucia gain medium (Yb:YAG). Central picture is a vertical cut of water velocity distribution. Right picture is a 3D volumetric view of the $40 \times 40 \text{ mm}^2$ crystal temperature distribution.

5. EXTRACTION ARCHITECTURE

5.1. EXTRACTION FLUENCE

The level of saturation fluence, whereas it is dictated by gain medium choice (Polaris, Yb:Glass), doping level, or operation temperature (figure 2.2-a), will impact strongly on :

- extraction fluence (laser damage issue)
- number of passes (multiplexing complexity) required to get an efficient laser system.

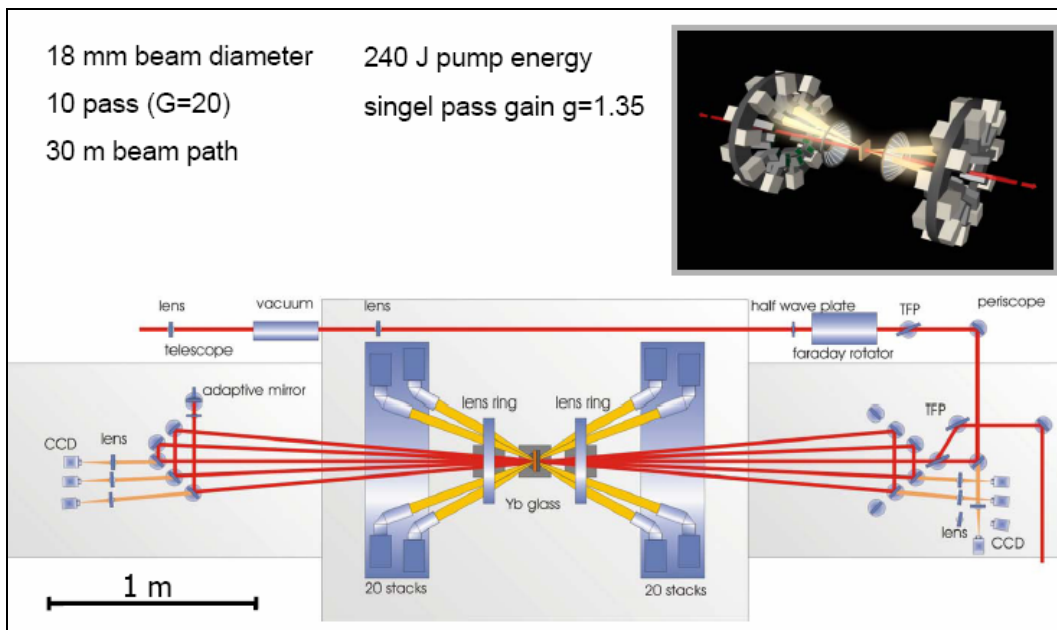


Figure 5.1: Polaris A4 (20 Joules) amplifier layout. Ten passes are requested.

5.2. SCALABILITY

State of the art DPSSL being developed currently are aiming at delivering 100J per pulse. None all of them are easily scalable. Reaching 10 kJ could either rely on kJ lines stacking (figure 5-2a) or on a single MOPA structure (figure 5-2b)

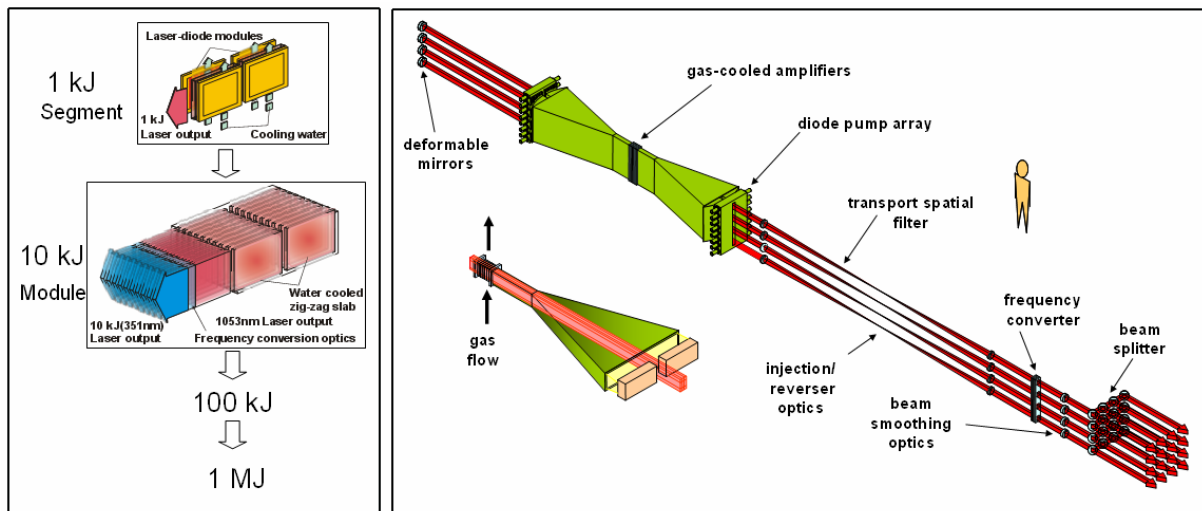


Figure 5.2-a :Halna (left and mercury (right) scaling approach

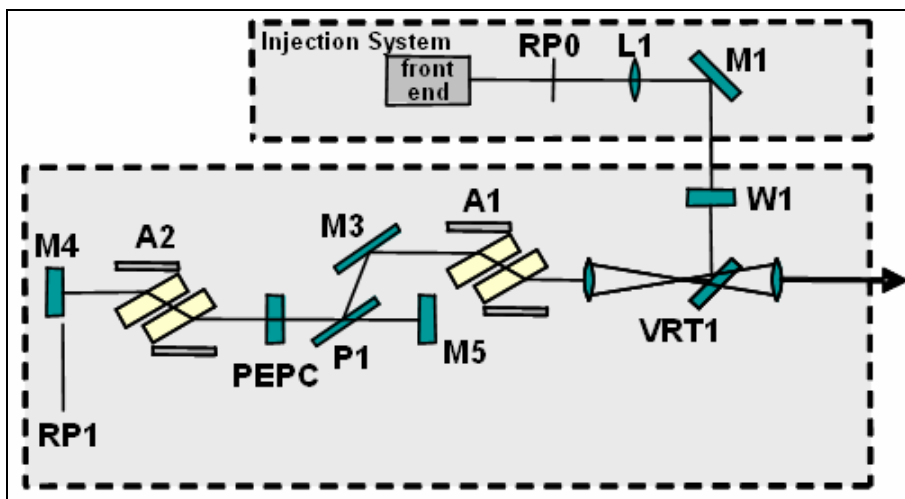


Figure 5.2-b :MOPA architecture. Injected pulse is amplified through A1, then trapped for 4 passes in the M4-M5 cavity to finally be dumped and encounter again A1 [6].

6. COST

6.1. INTRODUCTION

Table 6-1 is giving respective estimated costs for the 4 current kW average power DPSSL being developed. Large amplitudes (~10) in cost can be explained by several factors:

- The Mercury program has been running an expensive crystal growth effort for SFAP.
- The Mercury program has developed its own packaging for diodes stacks whereas the European projects rely on commercially available diode products.
- The Polaris program is facing costly compression grating requirements for short pulse operation.
- Personnel amount and program durations are easily fluctuating by a factor 2 depending of the program under consideration.

Name	Institution	Country	Spent	To be spent	Total w/salary	Total w/o salary
<i>Mercury</i>	LLNL	USA	47 M€	??	47 M€	31 M€
<i>Polaris</i>	Jena University	Germany	12 M€	5M€	17 M€	??
<i>Halna</i>	ILE	Japan	??	??	??	??
<i>Lucia</i>	LULI	France	2 M€	2M€	5.4 M€	4 M€

Table 6.1: 100J –class DPSSL program comparative costs.

Laser diode related technology is, from far, the driving cost for such program. Its cot breakdown is presented on figure 6.1; it includes:

- Laser diodes.
- Diode arrays mechanical mounts and cooling units.
- Drivers (electronic generators driving the diode stacks).
- Command-Control (Automate controlling simultaneously several hundreds of channels, one per stack).

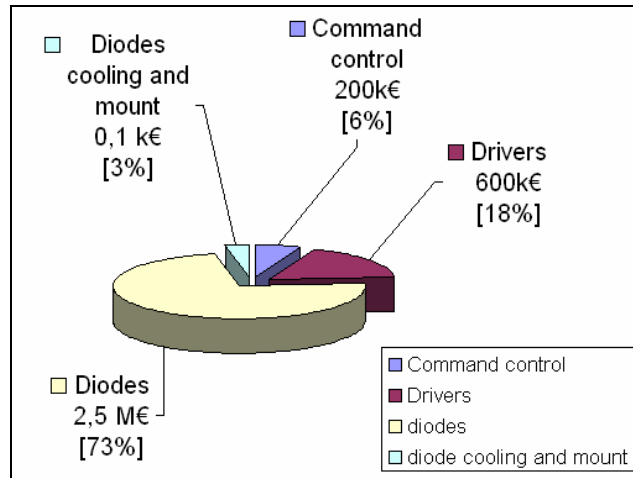


Figure 6-1 : Lucia program diode part cost breakdown.

Although such cost breakdown is not yet available for the 3 other programs besides Lucia, one should expect the same ratios since all these lasers are operated in a similar energy regime (100 to 150 J).

6.2. DRIVER COST

Using a cost distribution similar to fig 6.1 for a HiPER DPSSL beamline would lead to a 60 M€ budget (10kJ vs 100J with a 1.36€/w driver cost). But such simple extrapolation is not correct. It, indeed, must take into account several adjustment factors F_1 to F_5 listed below:

- The Lucia driver cost covers an estimated 30% of R&D work required to satisfy DILAS specs, i.e 1% duty cycle 150A/50V pulsed current together with a 100mA finely adjustable CW current for stack wavelength tuning.
 $F_1=70\%$
- The drivers used on Lucia are rather sophisticated and a lot of intelligence has been included in it in order to satisfy the “test-bed approach” requirements of Lucia. For instance a great degree of stack lifetime monitoring through V(I) curve has been implemented. Also rise, fall time, overshoot,... are simultaneously recorded for all 176 channels in a parallel way. Estimation for a basic driver without too many controls would lead to a device twice less expensive.
 $F_2=50\%$
- The stacks wall-plug (e-o) efficiency might increase as manufacturers make progress. For instance, over 3 years, Lucia DILAS stacks e-o efficiency increased from 50% to 56%. In North America, Defence industry is investing a lot of money to reach a 80% efficiency goal. But let's assume simply 10% more by the time HiPER starts.
 $F_3=80\%$
- The total amount of electrical power to be delivered by the drivers scales like the total energy of the beam line but the number of drivers scales with number of stacks. And the trend is to produce much powerful bars. Lucia bars are delivering 120 W, i.e. 3kW per stack of 25 bars. 150 Watts bars are now available. As will be pointed out later in this document new bars delivering 500 W should be available by the time HiPER starts. Driver voltage requirement would probably increase by a factor 3 (*triplet* bar concept), i.e. 150V instead of 50V for current stacks. When comparing with Lucia, $500/120=4$ times less drivers will be required to achieve the same pump intensity. Driver global cost could then decrease in the same proportion, leading to $F_4=25\%$.

But two aspects will contribute to moderate such decrease:

- cost of component will be a little bit more expensive (3 times larger capacitors for storage for instance)
- Four times more power will have to be carry towards the stacks. Transport cable losses issues will imply a very short distance between drivers and stacks. Consequently, drivers will have to be reduced in size at a cost.

Let's assume we have to adjust the gain from 4 to 3: $F_4=33\%$

- The diode market is not yet as mature as the electronic market on which is based the driver cost. A simple look at the diode market learning curves displayed in the following sections makes this obvious.

$F_5=90\%$

These 5 adjustment factors leads to a 92% reduction when compare with Lucia cost, i.e. 0.11€/w.

6.3. MERCURY DATA

Chart displayed on figure 6.3 (Nov. 2005) shows a classic learning curve where every doubling of quantity cuts the cost by 41%.

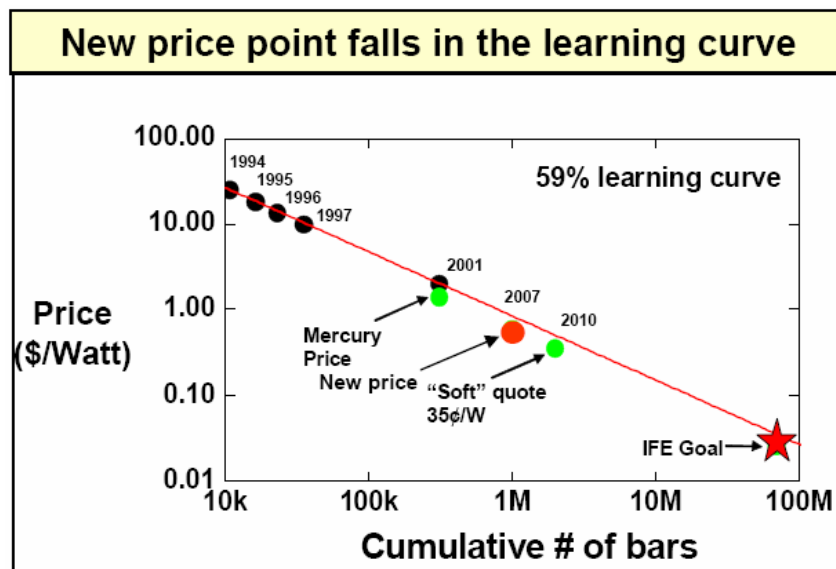


Figure 6.3 : LLNL estimation for diode bar cost evolution [8].

The relatively small cost taken into account here is probably for "bare" bars. Indeed, Mercury was, for a long time, only buying bars form Coherent and performing at LLNL the stack packaging. Costs greatly depend on:

- Packaging : up to 25 bars in stacks
- Collimation : a single microlens can cost 200 to 300€ including manpower (precise alignment and gluing cannot be automated)
- Operation mode: CW or QCW mode will request expensive microchannels or not.

According to R.Beach, this chart might have been computed by W.Krupke based on an estimated production of a 300.000 bars in 2001. As complementary information collected in Sept 2006, Hamamatsu is currently producing 90.000 bars/month.

6.4. LUCIA AND POLARIS DATA

Lucia and Polaris are somehow easier to compare (commercial 25 bars microlensed stacks).

Program	Bar quantity	€/watt	Manufacturer	Bars per stack	Microlensing
Polaris	7177	3.9	JOLD	25	Yes
Lucia	4400	4.8	DILAS	25	Yes

Table 6.4-a

It should be pointed out that Polaris diode delivery is part of a commercial agreement between the University of Jena and JOLD whereas Lucia diodes are bought through a tender won by DILAS.

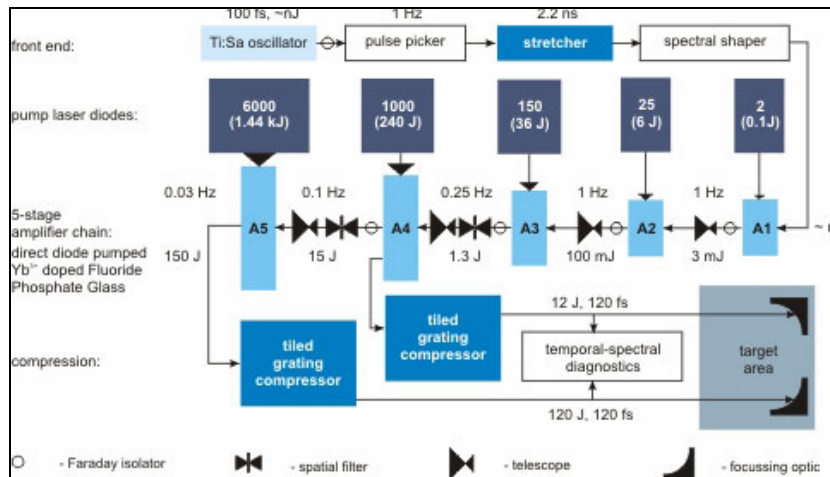


Figure 6.4-a : Polaris diode requirement.

Taking into account the different bar quantities requested for both European projects, a prospective two-points "learning curve" can be derived (figure 6.4-b).

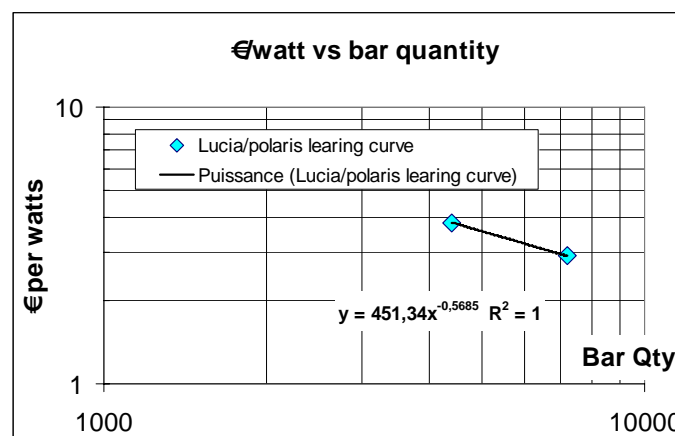


Figure 6.4-b : DILAS/JOLD « learning curve ».

Interestingly, both curves are somehow following the same trend as shown on the table below.

Learning curves	Mercury	Lucia/Polaris
Exponent	-0,7612	-0,5685
Learning %	59,00%	67,43%
Two fold energy results in the following % decrease in cost	41,00%	32,57%

Table 6.4-b

6.5. DATA COLLECTED FOR HiPER

In order to get a better picture for an HiPER beamline budget, contacts and visits have been established (2006) with the world key diode manufacturers. Compiled data are presented on figure 6-5.

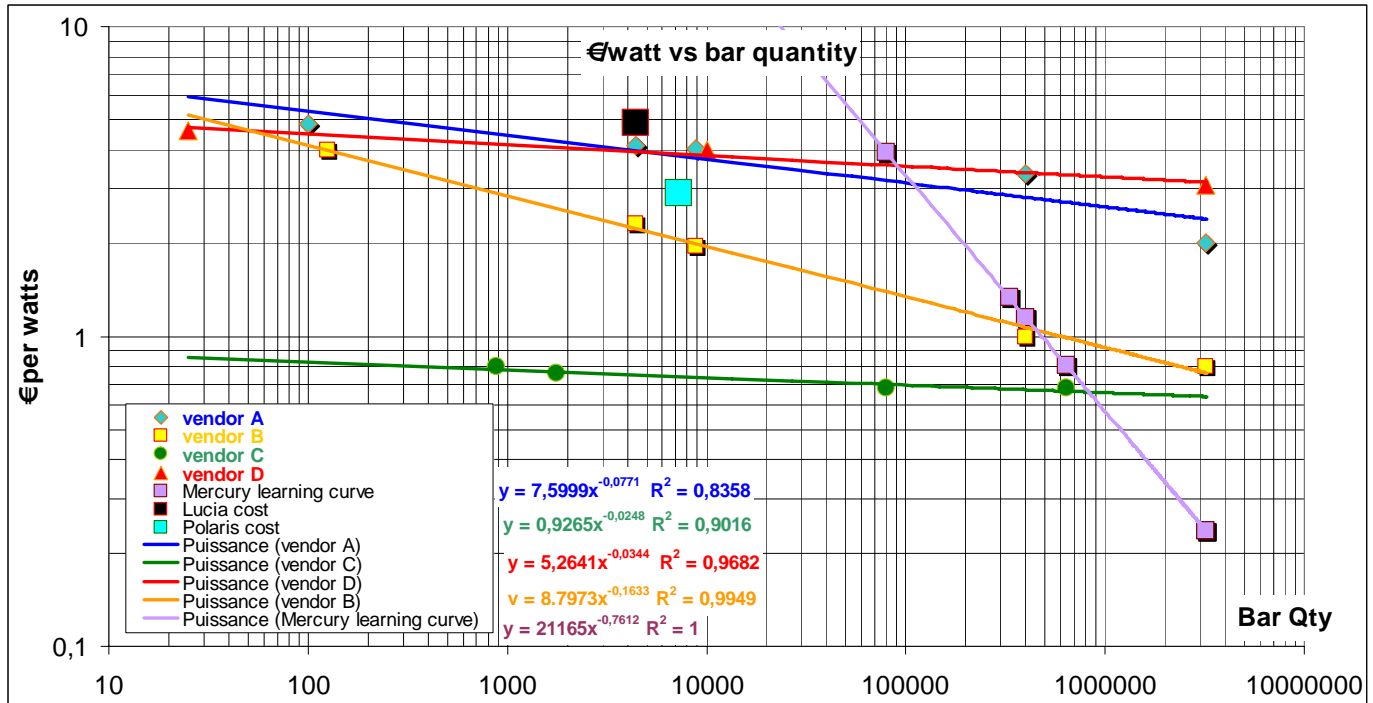


Figure 6.5 : Log-log graph showing €/w evolution with respect to diode bar quantity. All these numbers are related to packaged diodes (microlensed stacks) except for Mercury (purple curve).

The large single light blue square and the large single black square are related to actual Polaris (JOLD) and Lucia (DILAS) commercial investments. The purple line and squares are Mercury data taken from figure 6.3. Learning curves characteristics are summarized in the following table.

Learning curves	Mercury	Lucia/Polaris	Vendor B	Vendor A	Vendor D	Vendor C
Exponent	-0,761	-0,561	-0,163	-0,077	-0,034	-0,025
Learning %	59,00%	67,79%	89,30%	94,80%	97,64%	98,30%
Two fold energy results in the following % decrease in cost	41,00%	32,21%	10,70%	5,20%	2,36%	1,70%

Table 6.5

We observe:

- A similar trend for Lucia/Polaris and Mercury data (see previous § comment).
- A similar trend for vendors 1 and 2
- A relatively high and stagnant price evolution for vendor D which is probably not reflecting the real expectations.
- A very low stagnant price evolution for vendor C. It should be notice that this vendor is achieving such low price even with low quantities because these numbers are relying on 500 Watts per bar technology which is not yet mature. It makes sense to pretend that a 500W/bar stack will be essentially at the same price that a 100W/bar one, leading to a five time decrease in €/w. vendor A has actually presented a P(I) curve showing 400W per bars (QCW, 1% d.c.) at the same intensity (~150A) than conventional 100-120 Watts bars. BUT, such power was achieved with 3 times more voltage (in fact, these new "bars" are a triplet of bar directly structured at the

epitaxial level). This will have a big impact on global cable+driver losses and cost: A 25 bars stack made of 500W bars will be extremely bright (12.5kW over 2cm²) but will request to be driven by 150Volts x 150 Amperes...

6.6. HiPER 10 kJ BEAMLINE COST ESTIMATION

6.6.1. Diodes Budget

The following table summarized the estimated cost of a 10 kJ DPSSL beamline as of today, i.e. an average price of 60 to 80 M€.

10KJ beamline	Vendor C	Vendor B	Vendor A	Vendor D	mean
€/W for 40KJ diode	0,7005	1,0703	2,8502	3,3773	1,9996
cost for 40 kJ (M€)	28,02	42,81	114,01	135,09	79,982
€/W for 29KJ diode	0,7061	1,128	2,9217	3,4149	2,0427
cost for 29 kJ (M€)	20,477	32,711	84,729	99,032	59,237

Table 6.6

The first two lines are based on a ~25% efficient laser system (40kJ diode required, in an room T° Yb:YAG scheme for instance). A cryogenic Yb:YAG beamline should lead to a ~35% o-o efficiency: 29 kJ of diode would then be enough (last two lines).

Average global budget can then be estimated to be: **70M€**.

6.6.2. Drivers/CC budget

The 0.11€/w cost derived in section 6.2 implies a driver budget ranging from 3.3 M€ (35% o-o beamline) to 4.5 M€ (25% o-o beamline). On top of this number ~1 M€ would be required to satisfy for :

- Electronics studies (driver miniaturization)
- Command Control Hardware and conception (degree of parallelism in data collection from stack or cluster of stacks)

Average global budget is estimated to be: **4.9M€**

6.6.3. Gain medium Budget

Cost estimation for gain medium was not performed for this report, but for large quantities it seems not very probable that ceramics would be much more expensive than glass. The beamline described on Figure 5.2-b would require about 200.000 to 300.000 cm³ of lightly doped ceramic.

On the other hand, if crystal is selected as a gain material of choice, then a large technology step would be requested. And chances are dim that such step might be as cost effective as for what happened with KDP crystal growing for LMJ/NIF program.

6.6.4. Other costs

Other cost like mechanical support, optical element logistic tool,... would be similar to a classical flash-pump beamline of identical length. But depending of gain medium selected, total length might easily vary by a factor of 3. The potential compactness of a DPSSL beamline might consequently have an impact on cost.

6.6.5. Conclusion

Overall cost for an HiPER DPSSL beamline would probably be below **100 M€**.

7. REFERENCES

- [1] J. Dong et al., "Dependence of the Yb³⁺ emission cross section and lifetime on temperature and concentration in yttrium aluminium garnet" J. Opt. Soc. Am. B 20, 9 (2003) 1975-1979
- [2] T.Y. Fan , MIT Lincoln Laboratories, Lexington, MA, USA.
- [3] T. Numazawa, O Arai, Q Hu and T Noda "Thermal conductivity measurements for evaluation of crystal perfection at low temperatures » Meas. Sci. Technol. 12 (2001) 2089–2094 PII: S0957-0233(01)26694-6
- [4] J. KAWANAKA, "Conceptual Design of IFE Laser Reactor Driver Using Diode-Pumped Cryogenic Yb:YAG Ceramics ", 2006 HEC-DPSSL workshop, Lawrence Livermore National Laboratory, Livermore, California USA, May 17-19, 2006
- [5] T. Kasamatsu et al., "Temperature dependence and optimization of 970-nm diode-pumped Yb:YAG and Yb:LuAG lasers" Applied Optics 38, 24 (1999) 5149-5153
- [6] R. Beach, Lawrence Livermore National Laboratory, Livermore, California USA.
- [7] J. KAWANAKA, "A cryo-cooled ytterbium-doped laser materials for IFE", 2005 HEC-DPSSL Workshop, 11-12 June, 2005. F.Schiller Universität, Jena, Germany.
driver
- [8] R. Beach "Future Generation DPSSL systems", 11th High Average Power Laser Program Workshop, 3-4 March 2005 , Naval Research Laboratory Washington, DC, U.S.A.

APPENDIX 4: Proposal submitted to the European Commission

The formal submission to the European Commission to co-fund the “Preparatory Phase Project” is reproduced here (excluding financial annexes).

This submission falls under the “Construction of new infrastructures - preparatory phase”, FP7-INFRASTRUCTURES-2007-1 call, work programme topic:

INFRA-2007-2.2-01 preparatory phase for research infrastructure projects in the 2006 ESFRI roadmap

Proposal abstract

HiPER is a multi-national laser facility designed to allow Europe to take a leading position in the pursuit of Inertial Fusion Energy, whilst offering an internationally unique capability for science in extreme conditions. It will open up entirely new areas of research, providing access to physics regimes which cannot be explored on any other science facility. It has been formally endorsed by 7 European nations at the governmental or national funding agency level, 2 regional governments, over 20 scientific institutions and has direct involvement from industry.

Inertial Fusion Energy (IFE) lies at the heart of the design of HiPER. Fusion is the holy grail of energy sources – combining abundant fuel with no greenhouse gas emissions, minimal waste products, and a scale that can meet mankind’s long-term energy demands. Fusion combines hydrogen isotopes to create helium gas and a neutron which is captured to provide heat for a steam turbine. The IFE solution for fusion is a proven scientific concept. A laboratory demonstration of net energy production using lasers for IFE is now only 3 years away, marking the culmination of 40 years research. This will attract significant public and political attention, and so the HiPER project has been developed to provide a clear path forwards, based on a strong science mission.

The design has been produced over the past 2 years by scientists from 12 of the 15 nations now associated with HiPER. It has matured to a stage where formal negotiation of its construction is now required. This proposal combines all aspects relevant to a preparatory construction phase, as part of an integrated 68 M€, 3-year project.

The project already stretches beyond the EU, involving coordination with work in Japan, China, South Korea, Canada, Russia and the USA.

HiPER represents science with a strong societal goal. It is designed to secure the continued competitiveness of Europe into the next decades.

Table of Contents

(i) Summary Tables

(ii) Brief description of the new research infrastructure (or major upgrade)

1 Objectives and description of the activities foreseen

1.1 Objectives of the Preparatory Phase

1.2 Work plan

1.3 Deliverables, milestones and staff effort

1.4 Work packages to be supported by the EC

1.5 Work packages not directly supported by the EC

1.6 Focus on needs of users

1.7 Coordinating effect of Preparatory Phase

2 Implementation

2.1 Management Structure.

2.2 Relevant Parties.

2.3 Resources

3 Impact

3.1 Critical Questions

3.2 Attractiveness of ERA

3.3 Catalytic effect of EC contribution

(iii) Other issues

4 Ethical Issues

5 Consideration of gender aspects

(i) Summary Tables*Table 1a - List of **participants** in the proposal*

Participant no. *	Participant organisation name	Part. short name	Country
1	Science and Technology Facilities Council (Funding Agency)	STFC	UK
2	Commissariat à l'Énergie Atomique (Funding Agency)	CEA	France
3	Consiglio Nazionale delle Ricerche (Funding Agency)	CNR	Italy
4	Centre National de la Recherche Scientifique (Funding agency)	CNRS	France
5	Conseil Régional d'Aquitaine (Funding Agency)	CRA	France
6	Ente per le Nuove tecnologie, l'Energia e l'Ambiente (Funding Agency)	ENEA	Italy
7	Fundação para a Ciência e a Tecnologia (Funding Agency)	FCT	Portugal
8	General Secretariat for Research and Technology (Funding Agency)	GSRT	Greece
9	Ministry of Education, Youth and Sports (Funding Agency)	MSMT	Czech Republic
10	Universidad Politécnica de Madrid (Funding Agency as UPM are acting as a delegate of the Ministerio de Educacion Y Ciencia and also of the Comunidad Autonoma de Madrid)	UPM (MEC) (CAM)	Spain
11	Consorzio Nazionale Interuniversitario per le Scienze Fisiche della Materia	CNISM	Italy
12	Forschungsverbund Berlin e.V	FVB	Germany
13	General Atomics	GA	USA
14	Gesellschaft für Schwerionenforschung mbH	GSI	Germany
15	Institute of Applied Physics of Russian Academy of Science	IAP-RAS	Russia
16	Institute of Plasma Physics and Laser Microfusion	IPPLM	Poland
17	Instituto Superior Técnico, Universidade Técnica de Lisboa	IST	Portugal
18	P.N.Lebedev Physical Institute of Russian Academy of Sciences	LPI	Russia
19	Academy of Sciences of the Czech Republic	PALS	Czech Republic
20	Technological Educational Institute of Crete	TEI	Greece
21	Technische Universität Darmstadt	TUD	Germany
22	Technical University of Crete	TUC	Greece

*Table 1b - List of **other organisations** involved in the Preparatory Phase*

We note that the involvement of Japan, China, South Korea, Canada and the USA could be at the level of **project partners** in the subsequent construction phase. Preliminary discussions are already underway, which will be formalised as part of the plan presented in this proposal. Involvement of the institutions listed below has been designed to improve the prospects of such future internationalisation.

Organisation Name	Country	Description of the Organisation / Specific role or contribution to the preparatory phase
Korea Atomic Energy Research Institute (KAERI)	South Korea	<ul style="list-style-type: none"> • Involvement of the KAERI scientists on the technical development work, including their participation in experiments on European laser facilities. • Participation of HiPER scientists in KAERI facilities for
Shanghai Institute of Optics and Fine Mechanics (SIOM)	China	<ul style="list-style-type: none"> • Transfer of experience and knowledge in Laser optics. • Potential supplier of Laser components
Laboratory of Optical Physics, of Chinese Academy of Sciences	China	<ul style="list-style-type: none"> • Continuation of existing collaboration with European partners on laser-fusion physics. • Contribution to HiPER risk reduction programme through forthcoming fast ignition studies
Shanghai Jiaotong University	China	<ul style="list-style-type: none"> • Collaboration and input into HiPER risk reduction programme
Institute of Laser engineering, Osaka University	Japan	<ul style="list-style-type: none"> • Development of existing formal relationship to contribute to risk reduction programme
University of Alberta	Canada	<ul style="list-style-type: none"> • Collaboration and input into HiPER risk reduction programme
Department of Energy (DoE)	USA	<ul style="list-style-type: none"> • National US funding agency for fusion energy science • Collaboration and input into risk reduction programme • Exploration of internationalisation of HiPER
Lawrence Livermore National Laboratory (LLNL)	USA	<ul style="list-style-type: none"> • Transfer of critical technical knowledge through secondment of European personnel to and from LLNL

(ii) Brief description of the new research infrastructure

The High Power laser Energy Research facility, HiPER, is a multi-national initiative for Europe to take a leading role in the development of Inertial Fusion Energy (IFE), whilst offering an internationally unique capability in the science of extreme conditions. HiPER is designed to move from the imminent demonstration of fusion energy production in the laboratory (anticipated in 2010 in the USA) to an approach which opens up a credible route to fusion energy for commercial purposes. Whilst the energy mission addresses one of the highest societal priorities, the scientific requirement for HiPER is overwhelming. It meets the clear demand from the international science community to deliver a step-change in laser capabilities to open up entirely new research programmes in areas as diverse as laboratory astrophysics, extreme material science, turbulence, and fundamental atomic, nuclear and plasma physics (see section 1.6: user needs). The HiPER approach plays to the strengths of the European laser and plasma community, allowing us to take a true leadership position over the coming years.

IFE has been studied for many years as an attractive long-term energy solution, and as a means for creating the most extreme conditions achievable anywhere on Earth. The physics underlying inertial fusion is already proven. This is the approach adopted by Nature— inertial fusion powers the stars. Far more importantly, the process of net energy production from inertial fusion has already been demonstrated on Earth in an offshoot of the US defence mission in the 1980s. Demonstration of net energy production using a laser is now anticipated in 2010: just 3 years away. This world-altering event will require a clear response to the public – it is essential therefore that our scientific community clearly understands the future path to an energy programme following this event. The field is still in the Research and Development phase, requiring international cooperation over the next decade centred on a next generation laser facility. Europe is ideally placed to lead the world in this journey, but requires a focused programme to ensure timely progress.

Analysis during a 2-year design study involving 12 nations clearly indicated a prime technical solution that could provide the optimum balance of scientific excellence and long-term energy options, and so the HiPER project was initiated. The repetition rate of HiPER will be selected to provide the highest scientific output permitted by the next-generation of laser technology. No comparable laser system is underway anywhere in the world – HiPER will be a highly effective international attractor to Europe.

By opening up laser science into wholly new regimes, HiPER will attract scientists from many communities not traditionally associated with lasers. The anticipated size of the user community is thus many times that of the existing laser plasma groups, to be easily in excess of 1000 scientists.

The governance framework, uniting smaller scale laboratories from across Europe as part of the HiPER programme, will provide a highly effective training platform for new researchers. All aspects of the user support will follow from the excellent models already in practise in the laser community, allowing high impact science to arise from novice groups through to international laboratories.

There are currently no internationally owned academic user laser facilities in the world. HiPER will represent the first such infrastructure of its type. And because the scale of HiPER is significantly greater than existing lasers, an intermediate scale facility (PETAL, in the Région Aquitaine, France) has already been commissioned. This is a major commitment, providing an essential stepping stone, both in terms of the science and the technology for HiPER and the international user base.

This project has already attracted major funding commitments through identification of new resources and the redirection of many research programmes. 9 European national and 2 regional funding agencies are partners to this submission, along with 11 other European scientific institutions and 7 international collaborating institutions plus key industrial partners.

There are significant industrial opportunities for Europe as part of the HiPER project – in the design and build phase, the operational phase, and from the ensuing technical spin-out opportunities. Furthermore, the long-term industrial impact associated with laser fusion is huge in scope.

In summary, HiPER represents a unique opportunity for Europe to take a leading role in the area of extreme science and ensure it targets the key challenge facing mankind – long term clean energy

1. Objectives and description of the activities foreseen

1.1 Objectives of the Preparatory Phase:

This preparatory phase has been configured to allow a smooth transition to a pan-European construction phase. The Project is predominantly funded by national programmes which have been aligned as a result of the EC / ESFRI initiative. This involves: detailed research and development programmes; funded access to existing major laser facilities as part of a coordinated technical development programme; construction of the intermediate scale PETAL facility; direct involvement of European and international industry; and alignment with other international initiatives. Complementary, leveraging funding from the EC is required to ensure appropriate coordination and coherence of these activities.

EC involvement is also needed to develop the essential legal, governance and financial framework and crucially to address key strategic and risk reduction measures that would otherwise threaten the successful transition into a construction phase. The EC contribution is important if these large programmes from a wide range of international partners are to be coordinated successfully. The role of the EC funding will be to ensure the top-level objectives are met:

- Prepare the legal, financial and governance framework for HiPER construction, operation and decommissioning, to allow rapid transition at the end of the preparatory phase
- Ensure HiPER integrates fully effectively into the European and International science facility landscape, realising its potential to provide clear leadership in this field as the first truly international high energy laser facility
- Coordinate the international laser fusion community to ensure Europe takes a leading role through the construction of a facility optimised for long term energy and world-leading science missions. Importantly, this leverages the multi-billion Euro funding already invested by the US and French defence communities in relevant technologies.

Critical to the success of this next preparatory phase will be to convert the significant support already obtained from these nations into commitment for the construction phase. This will require a robust cost-benefit analysis, clarity in the through-life funding mechanisms and sources, an agreed framework for the accountabilities and responsibilities that follow from funding, an achievable procurement strategy, an agreed site, and a detailed understanding of how HiPER will impact the existing science and energy communities and facilities. The project also needs to ensure coordination between the fundamental building blocks of a laser fusion energy programme (the laser source; the target supply; the reactor design; and the inherent plasma physics) and management of key risks in these areas that could threaten construction.

The 3-year timing of the preparatory phase mirrors the expected timescale for demonstrating fusion energy production in the laboratory (anticipated between 2009 and 2012 on the National Ignition Facility, USA). The work breakdown structure maps these requirements against this timescale.

The prior design study selected a particular scientific solution with a scope set to allow multiple fusion options and a scale set to produce robust high gain. Following this study, a major technical work programme has been initiated using resources from laser institutions and their funding agencies. This covers the theoretical, modelling, experimental and facility development aspects of the work. EC funding is not sought for these activities, but concentrates on managing the coordination of the technical efforts and specific tasks which are not consistent with single agency funding. Examples of the latter are the transfer of technical capability from international partners and the defence industry into the civilian HiPER project, exploration of the potential scale and scope of the facility (balancing technological maturity with scientific requirements), and establishing a coherent theoretical framework for HiPER science across Europe.

The overriding task for the EC-funded elements of the preparatory phase study will be to ensure this broad base of work is effectively coordinated to address the principal risk factors affecting the formation of a Formal Agreement for the construction and operation of HiPER.

1.2 Work plan:*Table 2a - List of Preparatory Phase Work Packages foreseen under this proposal*

Work Pack. No	Title	Short description and specific objectives of the task	Lead Partner	Total budget (k€)	Expected National Co-funding (k€)	Requested EC funds (k€)
WP1	Management of the Preparatory phase project	Overall management of the Preparatory Phase Project. Coordinate the HiPER Project Plan and Cost Estimates for the detailed design, construction, and operation of HiPER.	STFC	4928	3877	1051
WP2	Financial, legal and governance frameworks	Establish and implement the legal, financial, and governance structures to support the Construction Phase. Establish funding frameworks through National agencies and the EIB. Set financial and governance guidelines and processes with WP1. Prepare the Formal Agreement for construction	STFC	6640	6000	640
WP3	Strategy for International industrial and academic and partnerships	Establish International partnerships, administrative structures, and cooperative agreements with on-going European programmes leading to full Partnerships for the construction of the facility. Establish and manage formal international partnership arrangements including foreign contributions and workshare. Evaluate and coordinate European and International industrial capability for the engineering and construction of HiPER.	STFC	2632	2000	632
WP4	Requirement analysis for Fusion and Science programmes	Generate robust point design and sensitivity analysis to provide the baseline specification of HiPER at high confidence. Perform appropriate level of benchmarking of codes and associated code framework such that the design can withstand intensive critical peer review. Generate Requirement Specifications	CNISM (Rome)	9983	7811	2172

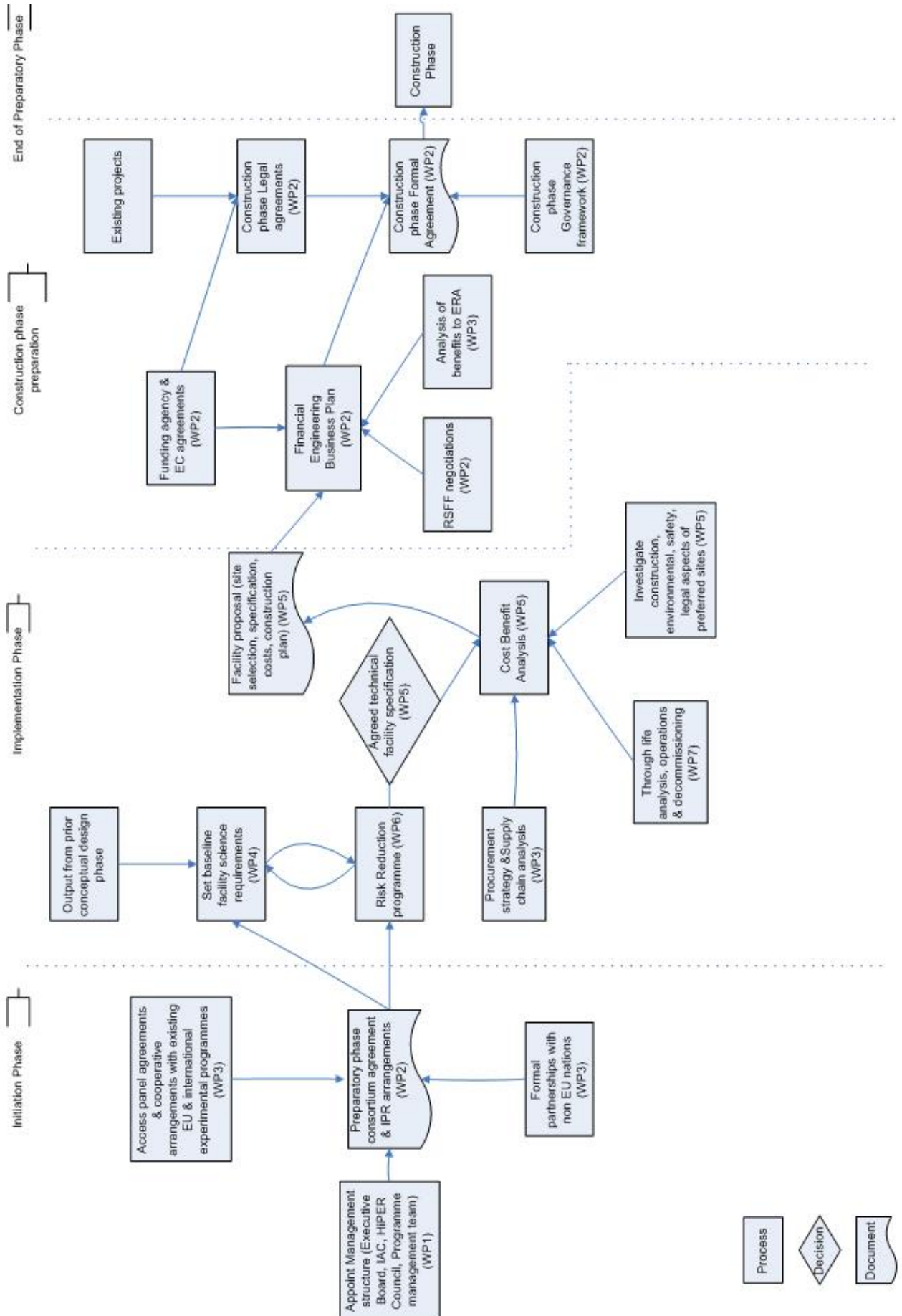
		for the targets, facilities, and diagnostics for HiPER experiments. Coordinate this work with allied efforts in the USA and Asia, as appropriate. Feed output into WP5 and WP6.				
WP5	Facility specification and costing	Provide costs for the baseline facility, including competing technology options for future down-selection. Plan an appropriate technology transfer strategy from existing facilities in Europe, USA and Asia. Evaluate options, component availability and capability to ensure future availability of critical items. Produce requirement specifications for facility buildings and associated infrastructure. Perform surveys and characterisation of proposed sites including support, infrastructure, location, logistics, and recruitment, to allow preferred site selection.	CEA	18227	13943	4284
WP6	Management of risk	Determine strategic path from existing infrastructures to HiPER. Manage the key risks to achieving the design intent for HiPER (that affect cost, location, user satisfaction and user breadth) to ensure it meets the needs of the scientific user community. Specify safety critical issues that could affect the environmental, health, safety and public body authorisation for construction.	UPM	26186	20088	6098
WP7	Through life planning and operational analysis and sustainability	Generate Overall System and Integration models; develop Life Cycle Cost, incorporating sustainable solutions; Performance and Risk Analysis techniques for the construction and operation of the facility.	CEA	141	0	141
Totals				68737	53719	15018

*Table 2b - List of **other Preparatory Phase Work Packages not directly supported by the EC***

As part of the prior 2-year design study we have developed an integrated work package model with a coordinated contribution from institutions, national and regional funding agencies, industry and the EC. As such, there are no separate work packages. Therefore table 2b is not applicable.

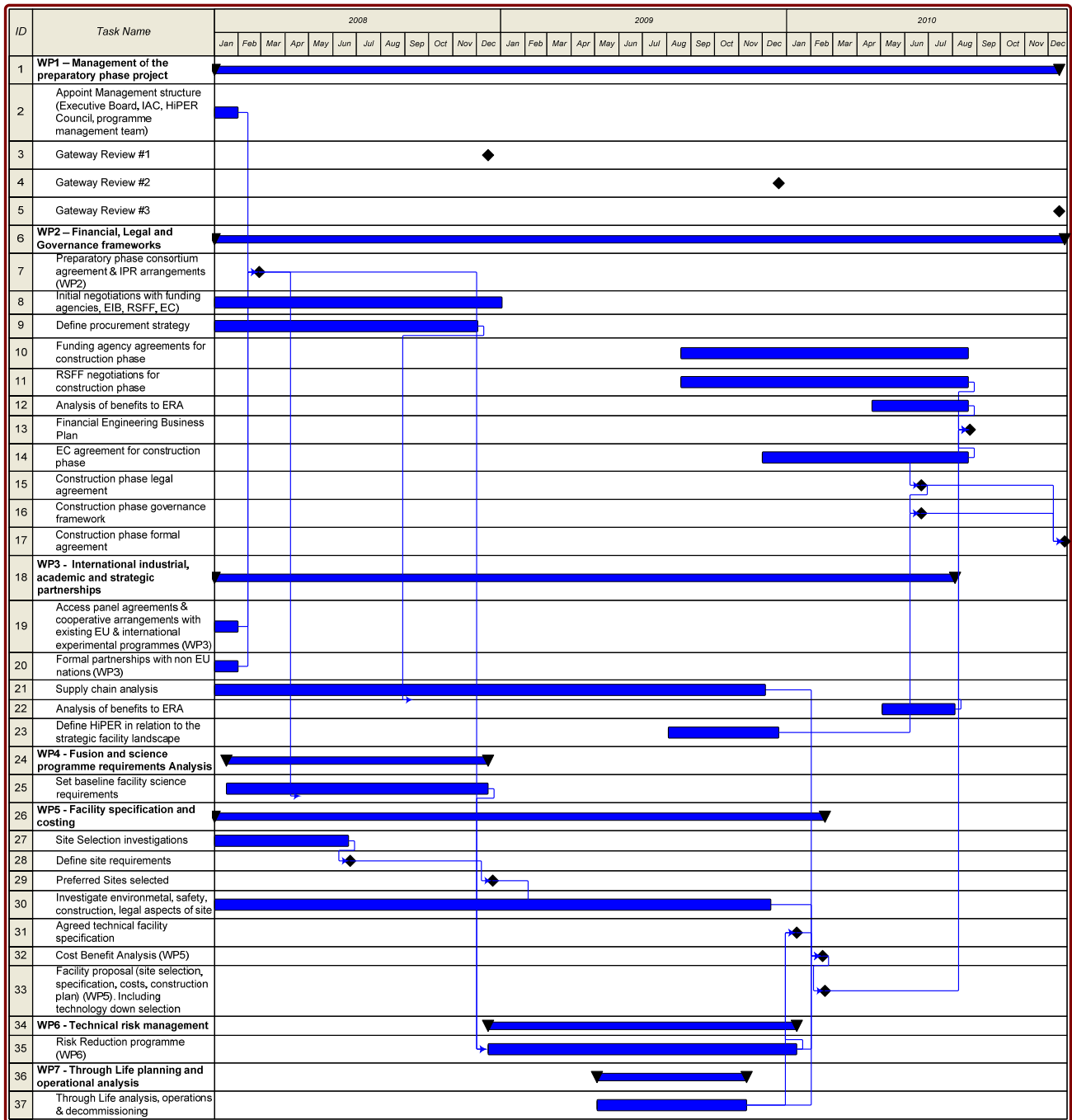
Network Diagram (next page)

This figure represents in a diagrammatic form the logical process and interdependencies of the project. Time does not strictly go from left to right, but the figure is split into three broad phases (initiation, implementation and construction phase preparation). This is intended to give the reader a graphical overview of how the various work package components link together. Gateway reviews are not shown for clarity and the components largely mirror the tasks shown in the Gantt chart that follows.



Gantt Chart

The Gantt chart below assumes a provisional start date of January 2008.



1.3 Deliverables, milestones and staff effort

Table 3a - *Deliverables List*

Del. no.	Deliverable name	WP no.	Nature	Dissemination level	Delivery date
1.1	Appoint Management structure (Executive Board, IAC, HiPER Council, programme management team)	WP1	R	PP	1
3.1	Access panel agreements and cooperative programmes with existing EU & international experimental programmes	WP3	R	PP	2
3.2	Formal partnership with non EU nations	WP3	R	PP	2
2.1	Preparatory phase consortium agreement & IPR arrangements	WP2	R	CO	2
4.1	Set baseline facility science requirements	WP4	R	PP	11
2.2	Define procurement strategy	WP2	R	PP	12
5.1	Preferred Sites selected	WP5	R	PP	12
1.2	Annual report to EC	WP1	R	PP	12
7.1	Through life analysis, operations and Decommissioning	WP7	R	PP	23
3.3	Supply chain analysis	WP3	R	PP	24
6.1	Risk Reduction status report	WP6	R	PP	24
5.2	Agreed technical facility specification	WP5	R	PP	24
5.3	Investigation on environmental, safety, construction, legal aspects of site	WP5	R	PP	24
1.3	Annual report to EC	WP1	R	PP	24
5.4	Cost Benefit Analysis	WP5	R	PP	26
5.5	Facility proposal (site selection, specification, costs, construction plan)	WP5	R	PP	26
2.3	Construction phase governance framework	WP2	R	PP	30
2.4	Construction phase Legal agreement	WP2	R	PP	30
2.5	Financial Engineering Business Plan (RSFF, EIB, Funding Agencies, EC) for construction phase	WP2	R	PP	32
3.4	Analysis of benefit to ERA	WP3	O	PP	32
1.4	Annual report to EC	WP1	R	PP	36
2.6	Construction phase Formal Agreement	WP2	R	CO	36

Table 3b - List of *milestones*

Milestone number	Milestone name	Work package(s) involved	Expected date Months	Means of verification
1	Preparatory phase consortium agreement and IPR arrangements	WP2	2	Document created and signed by relevant parties
2	Define Site Requirements	WP5	6	Report describing environmental, safety, stability aspects required for HiPER facility
3	Preferred Sites selected	WP5	12	Report produced of suitable sites (preferred and other option) selected to allow progression with legal, environmental safety aspects
4	Agreed technical facility specification and options	WP5	24	Technical facility specification and options document written and signed off by HiPER project team, and management teams
5	Cost-benefit analysis	WP5	26	Costed Facility proposal report written. To include all aspects to allow decision to be made on construction phase (environmental, utilities, costs, plan)
6	Technology down selection (coordination with other projects, industry and national programmes)	WP 5	26	Decision made regarding technical specification of facility. This selection report will form the specification section of the facility proposal document
7	Construction phase governance framework	WP2	30	Governance framework report agreed and ready to input into construction phase Formal Agreement
8	Construction phase legal agreement	WP2	30	Legal framework report agreed and ready to input into construction phase Formal Agreement
9	Construction Phase Safety Analysis	WP6	30	Full report into safety aspects of the facility – environmental impact, employee & operational safety regulations, maintenance. Costs will input into Facility proposal report at 26 months.
10	Construction phase financial business plan	WP2	32	Business plan created with input from EC, RSFF and funding agencies.

11	Construction phase Formal Agreement	WP2	36	Signature ready document created, allowing progression to the construction phase
12	Executive Board Meetings	WP1	3,9,15,21,27,33	Board meeting report including minutes and any decisions made
13	International Advisory Committee meetings.	WP1	6, 12, 18, 24, 30,	Committee meeting report including minutes, and recommendations for next stage
14	HiPER Council Meetings and Gateway reviews (technical, strategic and financial)	WP1	12, 24, 36	Council meeting report including minutes, recommendations and decisions made

Table 3c - Summary of staff effort

This table includes a summary of the staff effort funded by the EC. Bold indicates lead participant.

Participant no. / short name	WP1	WP2	WP3	WP4	WP5	WP6	WP7	Total person months
1 / STFC	94.5	42.75	18	36	123	68	6	388.25
2 / CEA	31.5	14.25	18	0	110	62	6	241.75
3 / CNR	0	0	0	0	0	51	0	51
4 / CNRS	0	0	0	36	34	23	0	93
5 / CRA	0	0	0	0	0	0	0	0
6 / ENEA	0	0	0	0	0	17	0	17
7 / FCT	0	0	0	0	0	0	0	0
8 / GSRT	0	0	0	0	0	0	0	0
9 / MSMT	0	0	0	0	0	0	0	0
10 / UPM	0	0	0	72	0	63	0	135
11 / CNISM	0	0	0	36	0	44	0	80
12 / FVB	0	0	0	0	0	20	0	20
13 / GA	0	0	0	0	0	36	0	36
14 / GSI	0	0	0	0	0	18	0	18
15 / IAP-RAS	0	0	0	0	21	0	0	21
16 / IPPLM	0	0	0	12	0	19	0	31
17 / IST	0	0	0	36	0	25	0	61
18 / LPI	0	0	0	24	0	27	0	51
19 / PALS	0	0	0	0	0	44	0	44
20 / TEI	0	0	0	0	0	36	0	36
21 / TUD	0	0	0	0	0	18	0	18
22 / TUC	0	0	0	0	0	17	0	17
Total	126	57	36	252	288	588	12	1359

1.4 Work packages to be supported by the EC:

Table 4.1 - Work package 1 description

Work package number	WP1	Start date or starting event:	Month 1				
Work package title	Management of the Preparatory Phase project						
Activity Type	MGT						
Participant number	1	2					
Person-months per participant:	94.5	31.5					

Objectives Overall Management and coordination of the preparatory phase project

Overall management and coordination of the preparatory phase project to ensure a successful outcome and thus smooth transition to a decision on the construction phase.

Coordination of all the partners, subcontractors and stakeholders.

Delivery of contractual commitments

Description of work

This management activity will be shared by two major partners (UK and France), making use of the existing support infrastructure at the Rutherford Appleton Laboratory (Didcot, UK) and at the Institut Lasers et Plasmas (Bordeaux, France).

Significant experience of managing this scale of project already exists in these two institutions, and independent advice specific to HiPER has already been obtained from major independent private companies with experience in preparing large-scale science projects.

Specific tasks [main participants in brackets]:

1. Establish the management structure and tools for managing the project, key internal management interfaces, reporting schedules and assignment of responsibilities. [STFC]
2. Ensure milestones, deliverables and costs are achieved according to the agreed schedule. [STFC, CEA]
3. Manage the preparatory phase contract(s), subcontractors and other external interfaces. [STFC, CEA]
4. Manage the governance of the preparatory phase (Council, Executive Board, International Advisory Board, and internal management meetings) [STFC, CEA]
5. Manage a web-based interface to coordinate the work of the partners and subcontractors, to disseminate information, to maintain communications with the EC and other stakeholders, to improve public awareness, and to manage media relations. [STFC]
6. Ensure the preparatory phase delivers a "signature ready" formal Agreement for the subsequent Construction Phase for consideration by the relevant parties. [STFC, CEA]

Deliverables

Appoint Management structure (Executive Board, IAC, HiPER Council, Programme management team): Month 1

Annual report to EC to review progress against plan, future work etc: Months 12, 24, 36

Table 4.2 - Work package 2 description

Work package number	WP2	Start date or starting event:				Month 1
Work package title	Financial, Legal and Governance frameworks					
Activity Type	SUPP					
Participant number	1	2				
Person-months per participant:	42.75	14.25				

Objectives

Establish institutional and funding agency commitments and future intentions for all stages of the HiPER project.

For the preparatory phase: Identify and exploit parallel funding opportunities and linkages, in-kind funding arrangements, contractual pre-agreement arrangements and other related financial instruments.

For the construction phase: Investigate and establish a funding framework and associated procurement strategy with National agencies and the EIB.

Establish the legal structures necessary for the Preparatory and Construction phases of HiPER.

Propose and agree an integrated governance framework and issue resolution procedures including management and IPR agreements.

Prepare formal Agreement documents for the preparatory and Construction phases.

Description of work

This work package lies at the very heart of the preparatory phase. It deliberately combines the financial, legal and governance aspects to ensure a fully integrated process that recognises the multiple trade-offs associated with a large-scale, multi-national project.

Specific tasks [main participants in brackets]:

1. FINANCIAL [STFC, CEA]

- a. Deliver the preparatory phase consortium agreement

This will require the resolution of any issues related to co-funding, IPR, use of existing facilities, and the roles and responsibilities of all partners.

- b. Establish a construction phase financial business plan that allows smooth transition from the Preparatory to Construction phases

This will involve consultation with trans-national, national and regional funding agencies, industrial partners, non-Governmental organisations (NGOs) and financial institutions such as the EIB.

- c. Integrate the procurement strategy (from WP3) into the financial model
- d. Establish financial boundary conditions for the “cost-benefit” analysis of options (WP5)

2. LEGAL [STFC, CEA]

- a. Provide legal input to the establishment of the preparatory phase consortium agreement (1a, above)
- b. Provide Memoranda of Understanding required for international (non-EU) participation in the Preparatory of Construction phases

This feeds into the Governance framework (3d, below)

- c. Establish an agreed legal framework for the Construction of HiPER, in the form of a “signature ready” formal Agreement between the relevant parties.

This will require analysis of national laws as part of the site selection process (3b, below), in concert with the relevant European and International laws, to provide a framework of legal statutes that enables HiPER to progress as a pan-European entity.

Existing arrangements indicate that this activity will be performed jointly with the ELI Preparatory Phase project, and will make use of the UK-coordinated EC working group on legal frameworks.

3. GOVERNANCE [STFC, CEA]

- a. Provide governance input to the establishment of the preparatory phase consortium agreement (1a, above)

Enacted by WP1, this activity establishes the framework for management of this phase, delineating the roles of the HiPER Council, Executive Board, International Advisory Board, internal management committees, key roles such as the Coordinator and Work Package Managers, and all relevant interfaces.

- b. Agree the preferred site for HiPER (using the detailed input from WP5)
- c. Establish an agreed methodology of interaction between HiPER and the existing and emergent European laser facilities, and with any trans-national organisations (such as the Laserlab-Europe integrated infrastructure initiative), and with all other external organisations (including local schools, universities, industry, etc).

This will ensure that HiPER is exploited to optimum effect, and makes best use of other science facilities and coordination instruments.

It will also define how researchers and other staff from the wider community can interact with the HiPER project and subsequently with the HiPER facility (including secondments, employment, re-integration following a tour-of-duty, salaries, terms of engagement, funding of external researchers costs, etc).

It will further define the mechanisms for promoting equal opportunities, encouraging minority group participation, and monitoring such aspects.

- d. Establish an agreed governance framework for non-EU involvement in HiPER

Due to the intense interest and likely participation in HiPER by significant laser nations outside the EU (in the preparatory, construction and operational phases), it will be essential to agree a common approach for external interactions. This will take input from the legal analysis (2b, above) and must take account of existing bilateral and multilateral agreements.

- e. Establish a through-life governance framework for HiPER, agreed by all Partners
- f. Due to the multi-disciplinary nature of HiPER, this will require an approach that merges the traditional laser governance model (national facilities with well defined internal and external users) and that used by the synchrotron community (wide-ranging access on widely varying timescales as part of multi-national arrangements).

Deliverables

Preparatory phase consortium agreement & IPR arrangements: Month 2

Define procurement strategy: Month 12

Construction phase governance agreement: Month 30

Construction phase legal agreement: Month 30

Financial Engineering Business Plan to include input from RSFF, EIB, EC, Funding Agencies:
Month 32

Construction phase Formal Agreement prepared for consideration by relevant parties: Month 36

Table 4.3 - Work package 3 description

Work package number	WP3	Start date or starting event:	Month 1
Work package title	Strategy for International, Industrial and Academic Partnerships		
Activity Type	SUPP		
Participant number	1	2	
Person-months per participant:	18	18	

Objectives

Establish formal international partnerships with major laser institutions and funding agencies to provide a through-life engagement strategy that ensures HiPER will be fully exploited by the international user community.

Establish trans-national European agreements to manage research access to existing facilities (for exploitation by WP5 and WP6), including joint technology development where appropriate.

Agree a common strategy for cooperation with on-going European coordination programmes, including the Laserlab-Europe Integrated Infrastructure Initiative (I3), and other instruments such as Marie-Curie (training networks) and ERANET (governmental programme coordination).

Investigate, coordinate, and establish European and International industrial capability for the engineering design and construction of the HiPER facility. Produce an agreed procurement strategy for the subsequent Construction phase.

Analyse the strategic benefits that HiPER offers to the European Research Area (ERA), and to society more generally

Explore non-European involvement in an "internationalised" HiPER

Description of work

The impact of HiPER in the existing laser community landscape will be very significant. As such, there is a considerable amount of work to be done in the strategic positioning of HiPER in relation to other facilities, access arrangements and coordination mechanisms. This Work Package will define an appropriate set of mechanisms to ensure the scientific impact and long-term societal benefits of HiPER are fully realised.

Specific tasks [main participants in brackets]:

1. Establish international agreements for non-EU involvement in HiPER [STFC]

It is noted that there are already bilateral and emerging multi-lateral international agreements with Japan, South Korea, China, Canada and the USA for coordinated, formal involvement in HiPER. This provides high confidence that full use can be made of the international community in ensuring a firm basis for the facility. This would involve the alignment of complementary programmes in Japan, USA and elsewhere as part of an internationally coherent roadmap for laser fusion and its associated science.

2. Establish trans-national European arrangements for access to existing facilities to undertake HiPER research and development [STFC, CEA]

It is noted that there are already formal agreements for the use of existing European facilities (CLF in the UK, LULI and PETAL in France, PALS in the Czech Republic). Dedicated time has been set aside on these facilities for HiPER research and development. Similarly, very significant research and development funds (totalling well in excess of 50 M€) has been identified as being targeted to HiPER by the Partners to this proposal.

The construction and operation of the PETAL facility in the Région Aquitaine (funded by the regional government) has been strategically aligned to become a central aspect of the HiPER project. A bilateral UK-France agreement has already been signed to ensure full coordination in the use of existing facilities, through PETAL, to HiPER.

3. Agree mechanisms of interaction with other European coordination and support activities (Laserlab-Europe, Marie-Curie, ERANET, other Preparatory Phase projects, and other R&D activities) [CEA]

Alignment with the Laserlab-Europe Integrated Infrastructure Initiative has been debated at their Participants Council, such that there is clear agreement on the positive impact of HiPER on the European laser community, and initial identification of the appropriate mechanisms to ensure close coordination.

Alignment with the Marie-Curie training network is underway, and discussions to form an ERANET in this field are already starting.

As such, the objective of this task will be to build from these positive starting points to deliver a through-life strategy for engagement and interaction.

4. Analyse the supply chain for strategically important materials, processes, services and components. [CEA, STFC]

This is a critically important task, as there are many components whose supply is not yet secured. Whilst there are many possible international options, this remains a key risk which must be addressed by the preparatory phase project. Technical input to this task will be provided by WP5.

5. Establish industrial and/or governmental agreements to protect the supply of any strategically important aspects required for the Construction and operational phases of HiPER [CEA, STFC]

Initial discussions with industry have indicated that they are fully receptive to the emerging options for HiPER. Coordination with other international projects (initially with Japan and China) has already commenced.

6. Prepare a procurement strategy based on these analyses and agreements [CEA, STFC]
7. Engage with relevant industries, Non-Governmental Organisations, governments, public opinion and related stakeholders to establish the appropriate balance of scientific and societal benefit work on HiPER [STFC, CEA]
8. Establish the impact of HiPER on the European Research Area, taking input from the site selection, science case, and societal benefit analyses [CEA, STFC]

Deliverables

Access panel agreements and cooperative programmes with existing EU and international experimental programmes: Month 2

Formal partnership with non EU nations: Month 2

Supply chain analysis to assess potential suppliers and foster industrial relationships: Month 24

Analysis of Benefit to ERA: Month 32

Table 4.4 - Work package 4 description

Work package number	WP4	Start date or starting event:					Month 1
Work package title	Requirements analysis for Fusion and Science Programmes						
Activity Type	RTD						
Participant number	1	4	10	11	16	17	18
Person-months per participant:	36	36	72	36	12	36	24

Objectives

Generate Requirement Specifications for the technical aspects of the facility.

Generate robust baseline design(s) for the laser-plasma interaction, with appropriate sensitivity analyses to define the technical specification of HiPER with high confidence. Perform appropriate level of benchmarking of codes and associated code framework such that the design can withstand intensive critical peer review.

Coordinate this work with allied efforts in the USA and Asia, as appropriate.

Feed output into WP5 and WP6 risk reduction and pre-construction engineering tasks

Description of work

The conceptual design for HiPER has been prepared during a 2-year Design Study involving over 50 senior scientists from many EU and non-EU nations. The technical basis for HiPER has been published in the peer-reviewed academic literature [see Dunne et al, Nature Physics 2, 2-5 (2006); Atzeni et al, Phys. Plasmas (2007), Atzeni et al, J. Phys. IV France 133, 429-432 (2006); Honrubia et al, Nucl. Fusion 46 L25-L28 (2006)]. This has already sparked significant international involvement, and interest from the scientific and popular media (including the BBC, The Economist, Science, Nature, etc).

This Work Package aims to consolidate this conceptual design work to provide robust specifications for the facility. This is an essential task, on which a significant amount of risk reduction and technology selection decisions will be based. The work is divided roughly equally between the major theoretical laboratories across Europe (France, Italy, Poland, Portugal, Russia, Spain, and the UK) to provide a balance between independent assessment and coordinated analysis. The baseline facility requirements will be formally declared in Month 11 to prioritise the cost-benefit and risk reduction activities. Following this point, full configuration control will be imposed to manage any future evolution of the requirements.

Full consultation with the international user community will be held as part of this activity, to ensure HiPER fully meets the demand from scientists for a next-generation capability, and will remain internationally competitive throughout its lifetime.

The work will be held up for critical peer review at a series of international workshops, dedicated review sessions, and through the accepted publication process. Furthermore, the Work Package will sponsor international benchmarking activities with the international community (particularly the USA and Japan). Put together, this will ensure that the technical foundations of HiPER can be viewed with full confidence by the parties prior to Agreement on the construction phase.

Specific tasks [main participants in brackets]:

1. Agree a governance framework for code development, comparison and detailed technical exchange between the Partners, and any relevant external bodies [CNRS, CNISM, UPM, IST, STFC]
2. Establish a baseline design (also known as a "point design") to allow a full technical

specification for HiPER, based on the preceding Design Study analyses. This should focus on the most demanding requirement (i.e. fast ignition fusion) [CNRS, CNISM, UPM, IST, LPI, IPPLM, STFC]

3. Establish the secondary requirements for the HiPER facility to ensure an optimal level of flexibility and capability to attract a broad user community [IST, IPPLM, CNRS, STFC]
4. Establish a “baseline model” approach for any subsequent revision to the point design. This will ensure full configuration control, and will provide a transparent mechanism for authorisation of any changes and the associated impact analysis. [CNRS, CNISM, UPM, IST, LPI, IPPLM, STFC]
5. Provide technical support to the risk-reduction activities (under WP5 and WP6) that flow from the point design specification [CNRS, UPM, IST, STFC]
6. Undertake user consultations to underpin the specification [CNRS, CNISM, UPM, IST, LPI, IPPLM, STFC]

Deliverables

Set baseline facility science requirements (Report of the output of theoretical modelling work to define facility specification) : Month 11

Table 4.5 - Work package 5 description

Work package number	WP5	Start date or starting event:				Month 1
Work package title	Facility Specification and Costing					
Activity Type	SUPP					
Participant number	1	2	4	15		
Person-months per participant:	123	110	34	21		

Objectives

Deliver a full facility proposal (site selection, specification, costs, construction plan, etc) for input to the construction phase business plan (WP2):

Provide cost-benefit analysis for the baseline facility, including competing technology options for future down-selection.

Plan an appropriate technology transfer strategy from existing programmes in Europe, USA and Asia.

Evaluate facility options, component availability and capability to ensure future supply of critical items (tying to strategic work in WP3).

Produce requirement specifications for facility buildings and associated infrastructure.

Select a preferred site for HiPER. Perform surveys and characterisation of proposed sites including support, infrastructure, transport, logistics, recruitment, planning requirements, economic impact, and all other related issues.

Description of work

HiPER is in the fortunate position that it can leverage information from very substantial prior investment (~ 10 B€) on allied laser facility projects. As such, the route to a costed, high confidence facility proposal is significantly eased.

Full advantage still needs to be taken, however, from emerging technologies that would be appropriate for a facility that enters service late next decade. For example, options for greatly enhancing the repetition rate, for remote handling of the samples, and for ultra-high intensity probe beams must be assessed as part of the technology down-selection process.

In addition, the unique nature of HiPER means that there are still aspects of the technology which need development. These will be predominantly funded by national or international programmes, and include the methods for handling very high energy short pulse beam lines (for the ignitor beam), and frequency conversion of the ignitor beam (to reduce the scientific risks). The first issue has much in common with the large area optical telescope community and the ELI project, and so a joint approach is being investigated. Use of the intermediate step facility, PETAL, will be critical for many of these issues.

Europe is in a very healthy position to complete this Work Package. The work will be predominantly performed by the French partners, with specific input from the UK, Germany, Czech Republic and Russia. Non-European involvement will be secured if required via sub-contracts, but is not anticipated to be large in scale.

Specific tasks [main participants in brackets]:

1. Confirm the baseline facility design, based on the requirements set out in WP4. [CEA, STFC

The conceptual design has already been completed. Confirmation activities and detailing of

this conceptual design are required to produce an acceptable margin or error on the cost.

2. Assess technology options and down-select [STFC, CEA, CNRS, IAP]

Enhanced capability could be achieved by adopting new technological solutions. A full assessment of the risks and benefits associated with these options will be produced.

The potential to transfer technology, know-how and capability from non-EU nations into the HiPER project will be explored.

3. Establish options for the supply of key components, processes, services and materials. Interact with WP3 to establish strategic supply routes as appropriate. [STFC, CEA, IAP]
4. Prepare a detailed cost breakdown model [CEA, STFC]

This has to be at a level of accuracy commensurate with financial planning requirements (from WP2)

5. Perform a cost-benefit analysis to establish the preferred solution, and associated options. [STFC, CEA, CNRS]

This must take into account the various technical options, the levels of scientific, technical and commercial risk, supply chain analyses, site-specific aspects, through-life issues (WP7), and industrial and international engagement options.

6. Prepare a construction plan. This will involve an industrial team, selected through a competitive bidding process, to determine the size, configuration, design parameters, and environmental needs of conventional facilities to house and operate the scientific equipment. Early involvement of this team will also provide realistic cost and duration for construction of conventional facilities and delivery/on-site storage/installation of scientific equipment. [CEA, STFC]
7. Select the preferred site, and fall-back option(s). This will follow a transparent process in which site selection criteria will be published, detailed submissions prepared by candidate hosts, and assessments performed by independent evaluators. These technical assessments will be fed to Work Package 2 (Governance) for consideration by the HiPER Council. [STFC, CEA]

Deliverables

Preferred sites selected following on from definition of site requirements: Month 12

Agreed technical facility specification following on from output of risk reduction programme: Month 24

Investigation on environmental, safety, construction, legal aspects of site: Month 24

Cost Benefit analysis: Month 26

Facility proposal (site selection, costs, specification, construction plan): Month 26

Table 4.6 - Work package 6 description

Work package number	WP6					Start date or starting event:					Month 12						
Work package title	Management of Risk																
Activity Type	RTD																
Participant number	1	2	3	4	6	10	11	12	13	14	16	17	18	19	20	21	22
Person-months per participant:	68	62	51	23	17	63	44	20	36	18	19	25	27	44	36	18	17

Objectives

Determine the strategic path from existing infrastructures to HiPER

Manage the key risks to achieving the design intent for HiPER (that affect cost, location, user satisfaction and user breadth) to ensure it meets the needs of the scientific user community.

Specify safety critical issues that could affect the environmental, health, safety and public body authorisation for construction.

Description of work

This work package pulls together the complex array of technical risks, user requirements, facility options, and interactions with ongoing work. It prioritises those issues which would threaten the achievement of a trans-national Agreement to construct.

The vast majority of the work performed under this task is the purview of national programmes. The role of the EC is twofold: to ensure full coordination of these large-scale national activities, and to address critical issues which would not normally be prioritised by national programmes.

This series of tasks involves most of the project Partners. Use will be made of the experiences of the Institut Lasers et Plasmas in organising and coordinating a broad array of distributed capabilities for a common purpose.

Specific tasks [main participants in brackets]:

1. Determine the strategic path from existing infrastructures to HiPER. This task will define the technical requirements for use of current laser facilities, moving onto the emerging PETAL facility, and finally onto HiPER. It will bring together the use of large scale laser facilities funded through national programmes (UK, France, Czech Republic) as well as coordinating the involvement of the smaller scale laboratories. WP3 will provide the strategic framework to allow such activities to be undertaken. [CNR, TEI, IST, IPPLM, CNISM, PALS]
2. Define high impact parameters for HiPER (that affect cost, location, user satisfaction and user breadth) to ensure it meets the needs of the scientific user community. Generate Requirement Specifications for HiPER experiments to allow adequate costing and risk analysis. [CNR, CEA, CNISM, PALS, UPM, TEI, TUC, GSI, ENEA]
3. Manage the key risks to achieving Fast Ignition and thus the successful operation of HiPER. Coordinate Fast Ignition and related science experiments across Europe (and with cognisance of work in USA and Asia) to confirm physics and design parameters for HiPER. [STFC, CNRS, CNISM, PALS, IPPLM, CNR, TEI, FVB]
4. Generate requirement specifications and assess capability for the targets and associated technical infrastructure for the initial experiments on the facility. Plan a technology transfer strategy for target capability from the USA to Europe. [UPM, STFC, CEA, GA, LPI, TUD]

5. Specify safety critical issues that could affect the environmental, health, safety and public body authorisation for construction. This may include target area configuration including shielding and radiation handling, and requirements for the initial experimental programme. Specify diagnostic instruments and the associated diagnostic data handling architecture, hardware, data structures, and software to ensure the needs of the broad user community will be fully met during the operational phase. [CNR, STFC, CEA]

Deliverables

Risk reduction programme status report. This will be a consolidation of all of the above work into a single coherent document that will allow a detailed cost benefit analysis to be performed (WP5):
Month 24

Table 4.7 - Work package 7 description

Work package number	WP7	Start date or starting event:	Month 16				
Work package title	Through Life Planning and Operational Analysis						
Activity Type	SUPP						
Participant number	1	2					
Person-months per participant:	6	6					

Objectives

Develop and adapt models for optimising the performance, operation, and management of the HiPER facility during construction, through operations and into decommissioning.

Develop or adapt system engineering tools to optimise total system capital and operation costs.

Develop or adapt logistics and resource management systems for optimising operations.

Description of work

A critical aspect of any major facility is to ensure it is fully optimised for its operational phase, and due account is taken of decommissioning needs. These need to be addressed up-front during the preparatory phase and must not be delayed to the construction or operational phases.

Optimisation of operations during the preparatory phase can significantly improve the through-life costs and the scientific impact of the facility.

Decommissioning analyses performed in the preparatory phase can ensure a transparent approach to site selection, planning approval, and future financial commitments

Specific tasks [main participants in brackets]:

1. Provide an optimised operational model. [CEA]

This will include the use of “Life Cycle”, “Risk”, and “Cost as an Independent Variable” models applied to designs produced by WP5

It will include the use of logistics and resource management systems for operations. Advantage will be taken of ongoing experience at large-scale infrastructures, and direct use will be made of systems models developed for Laser Megajoule.

2. Provide an optimised capital and engineering cost model. [CEA, STFC]
3. Provide an assessment of decommissioning costs and associated impact [CEA]

Deliverables

Through life analysis, operations and decommissioning: Month 23

1.5 Work packages not directly supported by the EC:

As part of the prior 2-year design study we have developed an integrated work package model with a coordinated contribution from institutions, national and regional funding agencies, industry and the EC. As such, there are no separate work packages. Therefore this is not applicable

1.6 Focus on needs of users:

The specification of HiPER has been derived from lengthy consultation with the international user community. There have been 10 plenary meetings within Europe dedicated to the HiPER design over the past 2 years, along with specific consultation meetings in Japan, China, USA and Canada, and more informal consultations with scientists in South Korea and members of the International Atomic Energy Agency's working groups.

Following from the initial proposal [Dunne et al, Nature Physics 2, 2-5 (2006)], a comprehensive CONCEPTUAL DESIGN REPORT (CDR) has been produced. This was produced to make certain that the full needs of the users, not just simply the baseline laser specification, have been analysed in detail. The full text of this report is available on the HiPER website (www.hiperlaser.org). Its scope covers:

- The role of IFE, its relationship with MFE, and the roadmap to fusion energy
- Fusion Science case, point designs, sensitivity analyses, and resultant facility specifications
- Fundamental science case, and specific requirements to ensure world-leading capability
- The roadmap from existing laser infrastructures, to PETAL, to HiPER
- The role of other laser facilities when HiPER is operational
- Baseline laser design, and likely industrial partners
- Laser development options for high-end capability
- Target delivery requirements for HiPER and a future reactor programme
- Fusion technology development requirements
- Building design, site and costing issues
- Industrial Engagement
- Operational, through-life analysis
- The role of other funding instruments (I3, Marie-Curie, ERANET, ...) in the HiPER project
- International project planning

The content of this CDR will not be reproduced here. The guiding principle over the past 2 years has been to ensure that the project delivers a world-leading capability for Europe which will attract international users and be fully competitive on the rapidly developing world stage throughout the life of the project.

A critical aspect of the through-life planning was to ensure the project encompasses a range of development options, including: high repetition rate laser beam lines; multiple target areas to ensure the needs of a diverse array of users can be catered for simultaneously with meeting the needs of the mainline fusion programme; productive coordination with the other laser facilities across Europe; and the potential to enhance the maximum laser power from HiPER via innovative beam amplification schemes. The latter is an important issue to address in the preparatory phase, as there is the potential to create an Exawatt beam line (10^{18} Watts) by using the high energy beams as a parametric pump. This would open up wholly new areas of science, as detailed in the CDR, but would represent a major configuration change option for the facility.

Key to the needs of the users is the provision of a flexible, responsive facility able to address a broad array of science programmes. The laser community has long experience of adapting its facilities for new users and new research areas. Lessons from facility operators and scientific users were pulled together in the conceptual design of HiPER to obtain a balance between the fusion energy mission and the wider science remit. The science programmes were selected for their compelling nature in terms of delivering an extreme science capability to Europe. The HiPER

facility specification was then developed to provide an internationally leading capability in these areas. The scope included:

- *Opacity and photoionization physics* - to address many outstanding fundamental atomic physics questions, along with their application to (for example) solar modelling.
- *Warm Dense Matter studies* – addressing the principal outstanding regime of material science in which there is no accepted theory (for which HiPER will offer exceptional probing and diagnostic capability).
- *Laboratory Astrophysics* – consistent with the fusion and high energy-density potential of HiPER, there is a wealth of astrophysical phenomena whose models could be tested in the laboratory, including supernovae evolution, proto-stellar jets, planetary nebulae, interacting binary systems, cosmic ray seeding and acceleration, and gamma-ray bursters.
- *Extreme Matter studies* – What are the fundamental properties of matter in extreme states? This includes studies in Gigagauss magnetic fields (otherwise only found in highly compact stellar objects, and in which the magnetic field dominates the electric field in determining sub-atomic motion), in Gigabar pressure regimes, in radiatively dominated systems, in burning plasmas, etc.
- *Turbulence* – how do compressible, nonlinear flows transition to turbulence and subsequently evolve? This is one of the few remaining fundamental uncertainties in classical physics.
- *Laser-plasma interaction physics* – including the question of how waves and matter interact under highly nonlinear conditions
- *Nuclear physics* under transient, excited state conditions – to study the effect of dense plasmas on nuclear cross sections, the behaviour of isomeric states via pump-probe studies of dressed states, and the creation of high density electron-positron pair plasmas and the evolution of the ensuing pair-fireball.
- *Production and interaction of relativistic particle beams* – for example, whether macroscopic amounts of relativistic matter can be created (then studied and utilised)
- *Fundamental physics at the strong field limit*

It is clear that HiPER will open up entirely new areas of research, providing access to physics regimes which cannot be explored on any other science facility.

Full details of the science case are provided in the Conceptual Design Report on the HiPER website (www.hiperlaser.org)

1.7 Coordinating effect of Preparatory Phase:

EC participation in the Preparatory Phase project is critically important to ensure an appropriate level of coordination between the multiple partners.

Pan-European Coordination: At present there are no international, multiple-partner laser facilities. This is in direct contrast to other comparable fields, such as synchrotrons (e.g. ESRF), neutron scattering (e.g. ILL), astronomy, etc. HiPER will change this, and so requires development of the governance and strategic instruments that bind together the broad user base and the facilities themselves. At present the European laser community is well served by the Integrated Infrastructure Initiative, Laserlab-Europe, but this does not address the particular issues associated with a specific infrastructure such as HiPER. The HiPER project plan has therefore been designed to make best use of existing instruments such as the Laserlab-Europe Integrated Infrastructure Initiative, whilst providing dedicated extensions to the legal, financial and governance framework where appropriate. A similar situation is faced in the material science field by the Extreme Light Infrastructure (ELI) preparatory phase proposal. As such, the HiPER, ELI and Laserlab-Europe

management boards have formally agreed to pool their expertise and development actions where appropriate to ensure a cost-effective, pan-European solution is found to this novel situation in laser science. Further details of this agreement can be found on the HiPER website.

Technical coordination: There is presently a significant effort in the underlying science and technology associated with the HiPER mission, funded by national and regional agencies across Europe and linked to related activities in Japan, USA, Canada, China and South Korea. The HiPER activity associated with the partners to this proposal amounts to greater than 50 M€, which will be coordinated for the first time upon launch of this Preparatory Phase project. The design study over the past 2 years has ensured that this effort is directed towards common, coherent goals wherever possible, but such action is inevitably limited in its scope by the varying pressures associated with each laboratory and funding agency. The role of the EC in the preparatory phase proposal will be to ensure the effort from these distributed laboratories is fully aligned to the agreed goals. This requires management action, support action and some specific technical action.

User coordination: An important requirement is to join together the laser facility partners with the expanded user base anticipated for HiPER. This will require detailed exploration of the requirements they will impose on the facility, the consequences of this on the prioritisation of the facility specifications, and growth of their awareness in the capabilities of HiPER via introduction to existing and emerging systems such as PETAL.

Regional coordination: HiPER's links to regional agencies will be explored in terms of site options, European structural funds, strategic infrastructure development, and co-funding.

International facility coordination: Integration of the HiPER project with allied efforts by our international partners will be a central theme of the preparatory phase. In particular, the EC funded effort will ensure that best use is made of European engagement with intermediate scale facilities in the USA (OMEGA-EP) and Japan (GEKKO/FIREX), existing international groups, and emerging large-scale laser systems (NIF in the USA and LMJ in France). These coordination efforts will lever access to multi-Billion Euro scale programmes. The scope will cover strategic issues (e.g. the role of HiPER in the context of these other facilities), future partner status of non-European nations; technical risk management; and governance issues (e.g. non-European access, and lessons to be learned from foreign facilities). The EC-funded role will be to develop the numerous bilateral agreements between nations relating to HiPER and high power laser science into a meaningful contribution to the successful achievement of the construction and operation of the facility.

Energy industry coordination: A key task in the project will be to develop the long-term energy mission of HiPER in collaboration with the international and regional power supply industry and relevant Government departments. Coordination activity in this area is necessary to allow the exploration of the future strategic fit of HiPER in the industry's long-term plans, as well as the potential for industrial co-funding. Alongside this, coordination with environmental groups and lobbyists will be explored as part of the communications tasks.

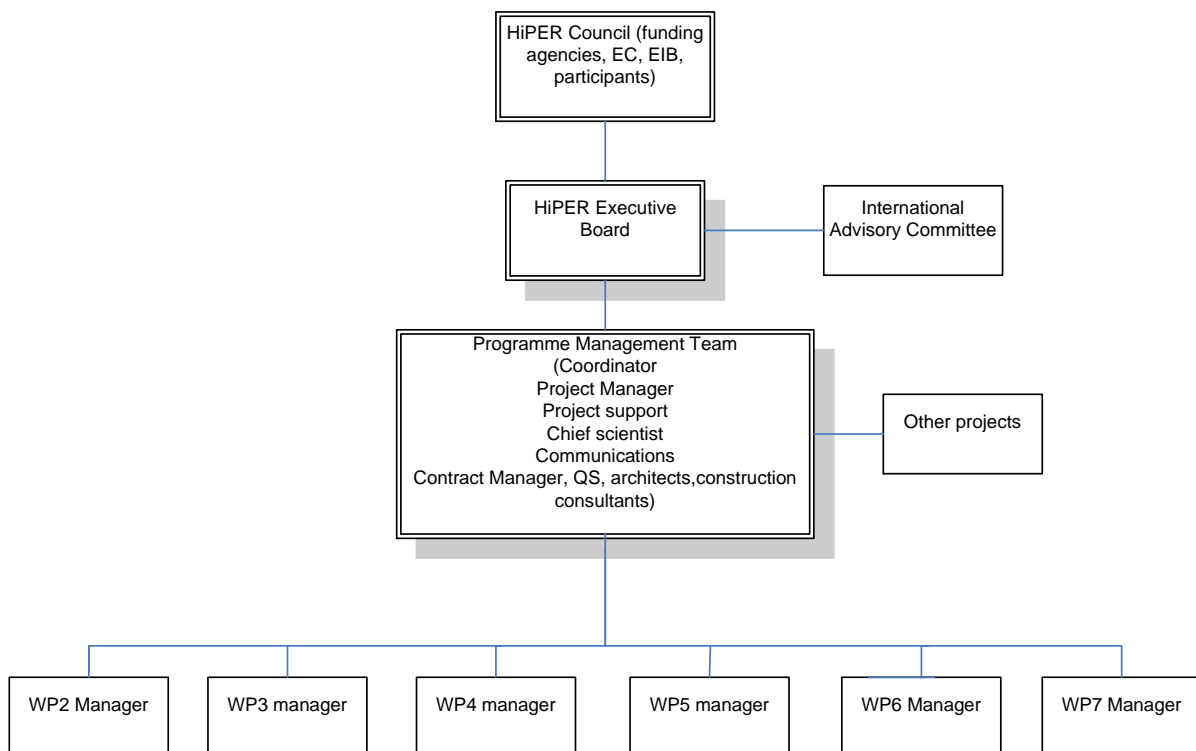
Supply-chain coordination: Finally, coordination between the project partners and the industrial supply chain will be developed in detail, to ensure the future delivery of high value and high risk components, and to produce a robust construction plan.

2 Implementation

2.1 Management Structure.

The management system that HiPER will use (shown in the Figure below) is essentially conventional in structure and follows best practise but is tailored to the particular needs of the HiPER project. It reflects in a more formal manner the informal structure that has been used over the last few years to develop the HiPER proposal, albeit with some important additions. Consequently, communication between most of elements involved is already well established and forms a solid base on which to build. The headquarters of the HiPER project will be established at RAL with a second management office established at the ILP in Bordeaux. Management meetings at appropriate levels (detailed below) will occur at regular intervals and these actually form part of the formal milestones of the project. HiPER has already had a significant catalytic effect within the European laser community and as such many synergies already exist amongst the partners which will be leveraged to enhance multi-lateral communication. Modern technology, such as personal and collective video conferencing will be used extensively to address, in part, the geographical issues that arise with such a multi-site project. The current policy of co-locating certain HiPER specific meetings at major international conferences will also continue.

The roles of the various organisational elements in the management structure are detailed below.



HiPER Council - A formal HiPER Council will be established which will be the ultimate decision making body for the project and consortium. Its rules of operation, procedures, mandate etc will be established through the *Consortium Agreement* in the very early stages of the HiPER project. The membership of the Council will reflect the various primary stakeholders that are part of the project and will include all of the participants of the *preparatory phase*, funding agencies, representatives of the user community, and representatives of the European Commission. The Council will also contain observer members such as those representing other international associated institutions and external independent advisors drawn from the legal and financial sectors etc and a representative of the European Investment Bank (EIB). The HiPER Council will meet on an annual basis to perform top level financial, strategic and technical Gateway Reviews of the project.

HiPER Executive Board - The strategic management of the project will be devolved by the HiPER Council to an steering body known as the HiPER Executive Board. The exact Terms of Reference for the HiPER Executive Board will also be established in the *Consortium Agreement* early in the project. This Board will act in an oversight manner ensuring that the project is progressing as per the timetable and scope defined in the contract established with the European Commission. It will also be the primary body responsible for holding to account the Project Coordinator (a formal EC role) and authorising any necessary significant action or changes to keep the project on plan. The HiPER Executive Board will meet formally every 6 months.

International Advisory Committee - An International Advisory Committee (IAC) will be established early in the project. The IAC will be a small committee of senior international figures drawn from the scientific, industrial, managerial and financial sectors which will meet on a 6 monthly basis to provide appropriate independent advice and guidance to the HiPER Executive Board as required.

HiPER Programme Management Team - A Project Management team will be established by the Executive Board for the day to day management of the project. It will be headed by the Preparatory Phase Coordinator who will act in a Programme Manager Role and will be supported by a significant management team. The Coordinator's primary role will be to nurture the environment in which the HiPER project operates, acting primarily as a team builder and advocate for HiPER mission and charged with catalysing a positive body of opinion amongst senior European governmental decision makers (ministers, funding agencies etc). The Coordinators primary responsibility during this *preparatory phase* will be as custodian of the political and scientific argument that will enable HiPER to proceed to the *construction phase*. He will have overall responsibility for delivering the project and for managing risk and change in an effective manner. The Coordinator will ensure that the HiPER mission is able to meet and successfully pass appropriate gateway reviews as may be required by national governments prior to major funding decisions. The Coordinator will also act as the primary conduit between the HiPER project and the EC, as well as the various European scientific funding agencies that currently or will have in the future an interest in HiPER. The Coordinator will also work with indirectly related stakeholders, such as some of the other *preparatory phase* projects, ITER and other International projects to ensure that the HiPER mission can be achieved in a cohesive and integrated manner. The Coordinator will formally report to the HiPER Executive Board

To form his programme management team the Coordinator will assign a work package manager for each of the work packages (except WP1), drawn from within the institutions that are involved in the particular work package. Each work package manager will be charged with the primary responsibility of co-ordinating the tasks and activities that are contained inside the work package and to act as the main reporting link between the work package and the programme management team.

To complete the programme management team and to assist in the delivery of the HiPER project, the Coordinator will also draw upon a significant management resource. For the internal management of the project, the Coordinator will delegate and rely on a full-time senior project manager (PM) recruited from the scientific sector, with appropriate experience of large scale project management in complex environments. The PM will act as a point of pivot between the various elements that form the *preparatory phase* project, balancing the internal demands and risks of the project whilst providing an appropriate response to ever changing external stimuli. Monitoring project progress through regular assessment, taking appropriate, balanced corrective action will be essential in this role. A Chief Scientist will also be appointed on a part-time basis to the project management team to provide key scientific and strategic advice as required. A full time project assistant and a full time contract manager will be appointed to look after the formal implementation and reporting aspects with respect to the European Commission contract and other stakeholders. A full time communications assistant will also be appointed to provide the necessary communications support for the Coordinator including the management of its internally and externally facing web sites

The project Coordinator will maintain and control a central pool of nationally funded contingency based on the value of un-awarded contracts, and will oversee the balanced allocation of funds to each partner. Release of contingency funds, changes to work package allocations or the introduction of new partners will require the written approval of the HiPER Executive Board, and authorisation by the EC as determined by the contract.

The project expects to pull in expertise in areas where this is required either through external consultants or through the use of “in house” expertise within the partner institutions.

2.2 Relevant Parties.

HiPER is an international project that benefits from the involvement, either formally or informally, of partners drawn from Europe, Asia and North America. Of the formal participants approximately half are engaged at the *funding agency* or ministerial level and almost all of the partners are providing significant levels of co-funding to advance the HiPER mission. The HiPER partnership strikes a healthy balance between the political engagement necessary to move key decisions forwards and academic engagement to principally address risk issues. Other European and International partners are involved due to their specific expertise in key areas. Great care has been taken during the 2-year design phase to select a balanced team capable of taking on the challenge of the preparatory phase project. Details of all related parties are presented below

European Commission - The European Commission is formally the contracting body for the HiPER Preparatory Phase Project. However, the preparatory phase process is very much one of building partnerships and thus the existing relationship between the HiPER consortium and the EC is much more one of parity and proactive engagement, rather than a traditional one of customer-supplier. In the preparation of the HiPER proposal this positive and active engagement from the Directorate General for Research Infrastructures, as a partner, has been very welcome and we fully expect this to continue during the preparatory phase. The EC brings considerable political and strategic advice which the HiPER mission will benefit greatly from. It also provides the basis for engagement with other European agencies, for example, the European Investment Bank (EIB) which will be vital for the financial engineering aspects of HiPER

United Kingdom – the project benefits from the formal involvement of the *Science and Technology Facilities Council* (STFC). This funding agency has the main responsibility within the UK for all strategic investments in major scientific infrastructures. It operates and develops a wide range of large scale infrastructures that include the world renowned *Rutherford Appleton Laboratory* (RAL), which includes the UK’s High Power Laser programme, the *Central Laser Facility* (CLF). Access to the CLF as part of the HiPER mission has been formally agreed by STFC. UK academia is also heavily involved in the HiPER project and this is also represented by the STFC involvement. The STFC has formally endorsed the project and has agreed to take the lead and co-ordinating role in the HiPER preparatory phase project. This level of engagement in the HiPER mission enables the STFC to credibly provide the strategic leadership that will be needed to advance the HiPER mission.

France – the engagement of France in the HiPER project is very substantial. Both of the major national funding agencies in France – the *Commissariat à l’Énergie Atomique* (CEA) and the *Centre National de la Recherche Scientifique* (CNRS) are formal participants of the project and are fully engaged at the highest levels of their respective organisations. Support for the HiPER mission in France has been formally secured at ministerial level. This level of political engagement of France in the HiPER mission has and will continue to be absolutely vital to its success.

The CEA has developed near Bordeaux (CEA-CESTA) over the last decade or so the *Ligne d’Intégration Laser* (LIL) and the multi-billion Euro *Laser MégaJoule* (LMJ) systems that are central pillars of its national strategy to advance the Inertial Confinement Fusion concept. It therefore brings to the HiPER project unrivalled expertise within Europe. The HiPER strategy relies very heavily on leveraging this expertise and the huge defence programme investment it represents into the civilian arena for the pursuit of fusion energy through the HiPER mission. The CEA’s technical and political involvement is substantial and they are formally prepared to make available to HiPER

people, information, technology, costs etc that will be crucial to developing HiPER. The CEA also provides an important portal to French industry that has developed most of the technology for LMJ.

Moreover, the local regional funding agency, the *Conseil Régional d'Aquitaine* (CRA) in conjunction with the French government, has recently invested more than 40 M€ in the PETAL enhancement to the LIL system to explore the fast ignition approach to Fusion Energy. CRA as a funding agency is also a formal partner in the HiPER project. Access to the PETAL system will be a key element of reducing risk within the HiPER project and crucially, in recognising the importance of the PETAL system to the HiPER mission, the CEA and CRA have agreed to the reconfiguration of PETAL system as per the needs of the HiPER project. An international panel of experts has thus recently been appointed to advise on the exact nature of this.

Furthermore, the CNRS and CEA support the operation and development of the *Laboratoire pour l'Utilisation des Lasers Intenses* (LULI) in Paris where some of the most advanced facilities in the world for experimental laser-plasma physics exist. Access to these facilities and the expertise contained therein will also be crucial for risk reduction in the HiPER mission. This access has now been formally agreed. Finally, both agencies support the *Centre Lasers Intenses et Applications* at the University of Bordeaux-I (CELIA) which hosts one of the worlds leading theoretical and computational plasma physics teams. This team has been placed at the disposal of the HiPER mission and will be important in developing target point designs for HiPER.

It has been agreed between these three agencies (CEA, CNRS, RA) that all HiPER related activity will be co-ordinated and managed by the *Institut Lasers et Plasmas (ILP)* in Bordeaux. ILP is the coordinating Institute in France for research in lasers and plasmas. It officially represents the associated laboratories working on these subjects from CNRS, CEA, University Bordeaux1 and Ecole Polytechnique.

Italy – The HiPER preparatory phase project benefits from the formal support of the Italian Science Ministry, the *Ministero dell' Università e della Ricerca* (MUR). This enables two of the primary national scientific funding agencies of Italy, the *Consiglio Nazionale delle Ricerche* (CNR) and the *Ente per le Nuove Tecnologie, l'Energia e l'Ambiente* (ENEA) to be formal participants of the HiPER project. In particular, CNR supports the *Intense Laser Irradiation Laboratory* (ILIL-CNR) which is focused on fundamental aspects of high-intensity laser interactions with matter. Studies of direct relevance to inertial fusion are also performed at ILIL within a Ministry of University project (MIUR-FIRB-BLISS), coordinated by ILIL. ENEA hosts a laser laboratory which has pioneered the field since the mid 60's. Finally, the project benefits from the formal participation of the Universities of Rome "La Sapienza", Milan-Bicocca and Pisa through the *Consorzio Interuniversitario per le Scienze Fisiche della Materia* (CNISM). It brings considerable academic expertise in theoretical and experimental laser-plasma and inertial fusion physics, including the advanced models and codes used for defining the HiPER parameters. These collaborating university groups are partly funded by national competitive programmes (MIUR-PRIN) on intense laser interaction and also participate in the above quoted FIRB-BLISS project

Spain – Spain's formal participation in the HiPER project at funding agency level has been agreed through the support of the *Ministerio de Educacion Y Ciencia* (MEC), as well as at regional funding agency level through the formal support of the *Direction General for Universities And Research, Comunidad Autonoma de Madrid* (CAM). This national and local ministerial level involvement is to be formally delegated to the *Universidad Politécnica de Madrid* (UPM) which will represent the Spanish interest in HiPER as well as bringing to the project crucial skills and capabilities. This includes some of the most advanced computational modelling of ICF and fast ignition physics at the *Grupo de Investigación en Fusión Inercial* (GIFI) which has formed the basis of the preliminary specification of HiPER. Furthermore, key target design and fabrication issues, materials studies and understanding the physics of technology for inertial fusion energy which are vital to the HiPER mission are enabled through the expertise at the *Instituto de Fusión Nuclear* (DENIM). The UPM is also an access portal to one of the world's most powerful supercomputers, MARENOSTRUM in Barcelona as well as MARGARIT supercomputer in Madrid. Access to both systems will be made available to the HiPER project through the UPM

Czech Republic – The *Ministry of Education, Youth and Sports* (MSMT), as a funding agency, are formal partners to the HiPER preparatory phase project. Execution of the Czech participation will be through the *Academy of Sciences of the Czech Republic* (CAS). The CAS operates and develops the *Prague Asterix Laser System* (PALS) and is one of the leading experimental facilities in Europe for laser plasma interactions. Access to this system will be made available for HiPER related work and a formal agreement covering this is now in place.

Greece – The participation of Greece in HiPER has been secured at funding agency level through the formal involvement as partners of the *General Secretariat for Research and Technology* (GSRT). Furthermore, the HiPER project benefits from the participation of the *Technological Educational Institute of Crete* (TEI) and the *Technical University of Crete* (TUC) who bring valuable expertise in experimental plasma physics and diagnostics.

Portugal – The Portuguese Science Ministry, the *Fundação para a Ciência e a Tecnologia* (FCT) has formally agreed to its involvement at a funding agency level as a partner to the HiPER project. Furthermore, the *Instituto Superior Técnico, Universidade Técnica de Lisboa* (IST) will be a formal partner in HiPER thereby securing the involvement of some of the world's foremost computational plasma scientists.

Poland – Poland will participate in the HiPER project through the formal involvement of the *Institute of Plasma Physics and Laser Micro-fusion* (IPPLM) in Warsaw. The institute has many years experience in laser plasma interactions and will concentrate on a variant of the fast ignition concept – *proton fast ignition*. Participation of the Polish Ministry of Science and Higher Education is currently being negotiated. Their future involvement could release additional national funds.

Germany – The involvement of Germany is through the participation of the *Gesellschaft für Schwerionenforschung mbH* (GSI) and the *Technische Universität Darmstadt* (TUD). GSI is a large organisation that is home to the PHELIX High Power Laser system. PHELIX is unique internationally in that it is coupled to a heavy ion accelerator and thus will offer major experimental opportunities both in fast ignition physics and other areas of Warm Dense Matter (WDM). This is complemented by the TUD who have significant expertise in WDM and target fabrication

Russia – Two institutes of the Russian Academy of Sciences are formal participants. These are the *Institute of Applied Physics* (IAP-RAS) in Nizhny Novgorod and the Quantum Radiophysics Division of the *P.N. Lebedev Physical Institute* (LPI) in Moscow. The involvement of these two partners brings access to the considerable resources of the RAS, and in particular advanced large aperture laser technology (IAP-RAS) and target design and fabrication (LPI)

United States of America – *General Atomics Inc.* (GA) is the world's leading organisation for the manufacture of ICF targets. Their role in developing and producing the specialist cone targets required for the fast ignition approach to ICF will be absolutely vital to the credibility of the HiPER mission. There is no other organisation worldwide that has the necessary skills or technology to make such targets to the specifications required in the timescale needed. This is reflected in many ways in the close working relationship that exists between GA and the CEA in France. The involvement of GA in the HiPER project brings key advantages as it will both enable HiPER to benefit from the many years of investment this expertise represents and will, through closer working, stimulate the growth of a European capability in this crucial area. It is expected that the US link will also see the secondment of EU personnel working on the HiPER project to the *Lawrence Livermore National Laboratory* (LLNL) as well as to GA to facilitate this technology transfer. Early engagement with the *US Department of Energy, Office of Fusion Energy Science* (DOE - OFES) has indicated a strong desire to align their science programme with HiPER as part of our long-term goal of a fully international roadmap.

Other international partnerships

Canada – Formal agreements are in place linking HiPER to the emerging fusion programme in the Alberta province of Canada. This is represented through the involvement of the *University of Alberta* (UofA) in the HiPER mission who are currently midway through a process of securing substantial funds for a Canadian Laser Fusion programme. Secondment of Canadian scientists to the HiPER partners in Europe is being planned as part of the early stages of this programme.

Korea – The *Korean Atomic Energy Research Institute* (KAERI) are supporting the HiPER mission and we fully expect a bi-lateral agreement between HiPER and KAERI once the HiPER project is launched. Collaborative access to their facilities and linking to their research programme has already been agreed. Korean Government funds to advance this collaboration are being sought.

China – Support for the HiPER project from China is strong. Formal agreements are planned once the project receives the go-ahead. A UK-China agreement has recently been signed which significantly aids this process and has already led to Chinese involvement in HiPER related science projects in the UK. As well as an obvious academic benefit, this will also open up alternative supply routes for key components, thereby reducing future risk. We have secured the formal engagement, at the highest levels, of the *Chinese Academy of Sciences* (CAS), *Shanghai Jiaotong University* (SJU), and the *Shanghai Institute of Optics and Fine Mechanics* (SIOM).

Japan – Academic collaborative links to Japan on laser fusion science are naturally very strong given the leading role that the *Institute of Laser Engineering* (ILE) at Osaka University has played in recent years. The ILE are very strong supporters of the HiPER mission and bi-lateral agreements are in place between the ILE and several of the European partners involved in HiPER. Continuation of this collaboration is already planned, which opens up access to the FIREX laser facility at the ILE for HiPER related work. The FIREX facility is a major laser infrastructure dedicated to the pursuit of the fast ignition approach to inertial fusion energy.

Industrial Links – Working with industrial partners will be a central issue during this preparatory phase to ensure costs are well known and supply routes are available for the construction of HiPER. Already, there has been a significant engagement with many potential industrial stakeholders in HiPER and this will continue during the preparatory phase. We attach as an annex a list of key industrial players with whom we have already engaged during the 2 year design phase.

Other Preparatory Phase Projects – There is much to be gained during the preparatory phase through working with the other projects. This applies equally to technical and scientific issues, as well as those related to strategic, governance, financial engineering and legal aspects. Furthermore, there is the potential for both risk and cost sharing in places. We propose to work with other projects and have already signed two Memoranda of Understanding (MoU) covering these issues with the Extreme Light Infrastructure (ELI) and the European Extremely Large Telescope (E-ELT). In a similar fashion we have signed an MoU with the Laserlab-Europe Integrated Infrastructure Initiative.

2.3 Resources

The HiPER system will cost of the order of 1 Billion € to develop and construct, and a similar sum to operate over its lifetime and to decommission. Clearly this is a significant sum of money and one of the key tasks for the preparatory phase will be determining the exact cost of the facility. Significant sums are set aside as part of the preparatory phase to cost the facility, both in its construction and its through life cost, to a level of uncertainty of 20%.

The financial engineering required to furnish this construction and operation cost is an issue of great importance and the HiPER project will, as part of the preparatory phase, develop a detailed strategy for how this will be achieved. Clearly, engagement with the key national agencies in developing this strategy will be a crucial step. HiPER benefits from the full participation of 9 national and 2 regional funding agencies distributed throughout Europe. It is therefore already very well placed to begin the development of the financial engineering strategy from early in the project lifetime. Anticipating the need to finance higher risk research and development projects under the Seventh Framework, the European Commission and the European Investment Bank (EIB) have jointly set up a risk sharing mechanism known as the Risk Sharing Finance Facility (RSFF). Access to this facility is expected to be a central pillar of the HiPER financial strategy and thus it will be essential to start discussions with the EIB from an early stage.

HiPER has attracted significant attention from non-European agencies as part of the 2-year design phase. This has already led to a number of bilateral agreements to share research and

development activities, facility designs, and scientific results associated with the fusion and basic science missions of HiPER. Cost sharing during this next 3-5 year phase, where a number of important scientific and technical questions will need to be resolved is already agreed. This will take the form of shared access to facilities, strategically aligned technology development, and pooling of scientific results. Advanced discussions are already underway with Japan and the USA in these terms, as these two countries possess the largest scale laser systems currently available. Associated negotiations with other nations with smaller programmes are also underway.

It will also be important to determine relatively early in the project a preferred location for HiPER as this is something that will directly affect the cost to national governments and thus the financial engineering options that may be available. It may for example, be possible to access EC Objective 1 or Objective 2 structural funds for locations in specific countries. This however will then need to be balanced by the additional infrastructural development that may be required in support of locating HiPER in a particular place. We will also explore the possibility of industrial sponsorship of HiPER, particularly from the large energy or oil companies who have a specific strategic interest in investing in high technology solutions to the long term security of energy supplies.

In regard of the preparatory phase almost all of the HiPER partner countries bring substantial co-funding to support the mission. The majority of this co-funding will be directed towards the risk reduction programme that will examine and reduce the technical risks that are associated with HiPER. This is summarised in the table below. It takes several forms, for example the re-direction of existing resources in support of the HiPER mission, the granting of access to major European facilities for HiPER specific research, or new money that will be provided by national governments in direct support of the HiPER programme.

Country	Total co-funding contribution (k€)
Czech Republic	4278 ⁽ⁱ⁾
France	19000
Germany	1136
Greece	3607
Italy	1326
Poland	450
Portugal	944
Spain	1859
UK	21119 ⁽ⁱⁱ⁾
European Commission	15018
TOTAL	68737

ⁱ Includes 3600k€ of new national funding subject to EC approval of the HiPER project

ⁱⁱ Includes an estimated 10000k€ of new national funding subject to EC approval of the HiPER project and completion of a *due process* in the UK.

As can be seen from the table, the prospect of European Commission investment in the HiPER preparatory phase has had a significant leveraging effect, especially so given the high degree of engagement of various national funding agencies.

It is also important to point out that due to the way we have structured the project, and in particular the involvement of the large European funding agencies, we are benefiting from major existing investments. For example, the results of the research and development activity associated with Laser Mégajoule (LMJ) and other large European laser infrastructures are directly available to us via personnel involvement and technology transfer. It is difficult to quantify the true financial benefit of this existing investment that we are effectively leveraging into the HiPER project, but these programmes have a scale of multiple billion Euros. Suffice to say that in all realistic terms it would be impossible for HiPER to proceed without it

3 Impact

3.1 Critical Questions

The laser community has never before developed a truly international, multi-partner facility. Significant work is therefore required to bring together the potential partners and to determine an appropriate structure under which they can reliably operate.

Many of the legal, governance and structural finance issues are common to any large-scale infrastructure. As such, the HiPER plan seeks to work cooperatively with other projects, existing facilities and EC offices to deliver the generic framework. Optimisation for HiPER is then planned for the final year of the project.

However, in addition to these “common” issues, there are a number of specific non-technical areas which will require unique solutions for HiPER. These include strategic work in defining the appropriate relationship between existing institutions, future local facility enhancements, and training and support requirements. The objective of the HiPER project is to secure a strong platform of locally-based laser laboratories to cultivate the rapidly expanding user community and to make best use of this distributed expertise to develop the key aspects of the new facility.

The relationship between HiPER and the magnetic fusion community (and the ITER project in particular) will need to be fully resolved. As currently envisaged HiPER is a generation behind ITER in terms of its technological maturity and thus sits firmly in the research and development phase under the FP7 Infrastructure remit. This is entirely compatible with the broad-based scientific mission of HiPER, with the scale of the facility set by its most demanding goal: achieving high gain fast ignition fusion. The scientific imperative is set by the demonstration of conventional ignition by the defence community, anticipated in ~2010.

The interaction of HiPER with the defence sector (in particular the laser programmes in France, UK, Russia and USA) is an important aspect to manage. Significant leveraging of the multi-Billion Euro investment by the defence sector is available to the EC project via appropriate partnerships, as is access to the industrial supply chain formed by that community. Such partnerships have been carefully developed in the preparation of this proposal, which has provided the EC and its Member States with a unique opportunity to take a leading position in the academic and commercial exploitation of laser fusion research. It is accepted by all parties that HiPER must remain a fully civilian, unclassified academic facility.

The step-change in scale from existing academic laser systems to HiPER means that considerable development is needed in the scientific underpinning, in the technology maturity, and in the approach of the community to its research programmes. A major step to tackling this has already been initiated in the construction of the PETAL facility in the Région Aquitaine. Preparation of the HiPER proposal has led to its formal joining together with PETAL under a common strategic plan. The agreed approach is to evolve from existing facilities, to PETAL, to HiPER, with all three tiers playing a major role during the operational phase of HiPER.

The work plan defined above has been derived from a detailed risk analysis, geared around the 3-year timescale on which a political decision on the future of IFE research must be made. It would be unacceptable following the demonstration of net energy production in ~2010 for the scientific community to be unable to answer the demanding questions of its national and European politicians. We must ensure that the research community can offer a credible, coherent plan for the development of this field. The next step must therefore be suitably defined to permit an informed decision on whether construction should proceed. The balance of technical, legal, governance, financial and strategic work in the project plan directly reflects the results of our 2-year risk analysis.

3.2 Attractiveness of ERA

HiPER represents a globally unique facility, which will lead the world in terms of its scientific output and its technological implementation. It will therefore provide a strong attractor for international scientists into the ERA, both to the facility itself and to the broad base of allied laboratories.

The scope of the HiPER project has been designed to make best use of European expertise and thus maximise the potential of the facility. The HiPER philosophy is to build upon local capabilities to create a “hub and spoke” European consortium of institutions centred on the major facility. The nature of laser science allows this distributed model to function very effectively. The role of smaller nations, convergence nations and neighbouring regions can therefore have a disproportionate impact to the benefit of both the project and the local region. The distributed model is also effective in developing the capability of the members of the ERA to play a greater role in international projects centred on facilities in the USA and (increasingly) in Asia. Thus, through a combination of national, regional and EC funded activity, this proposal seeks to pull together and enhance expertise in:

- High power, high energy laser beam line design and operation (principally involving UK, France, Germany and Czech Republic)
- Novel high power laser solutions (principally involving Russia, Portugal, UK, France and Germany)
- Target Fabrication technology (principally involving Spain, France, Russia, USA and UK)
- Diode pumped technology for high efficiency, high repetition rate sources (principally involving France and Germany)
- Plasma physics and applications (involving Italy, Spain, Portugal, France, UK, Russia Greece and Poland)
- Detector and diagnostic development techniques to ensure broad-based application and high quality, quantitative scientific delivery (principally involving Italy, Poland, Greece and France)
- Major facility construction and operation (principally France and UK)

Each of these areas has substantial “spin-out” potential – both for local programmes and for technological applications outside the scope of HiPER. International experience in this field has demonstrated that such knock-on impact can be truly significant.

Finally, HiPER positions Europe to take a leading role in the subsequent development of fusion power production, which is the only credible long-term option that meets the global demand for clean energy into the next century. The economic and industrial opportunities this represents cannot be overstated, nor can the security implications of energy self-sufficiency in the long term.

3.3 Catalytic effect of EC contribution

EC support in this preparatory phase is crucial. A broad consortium of institutions and funding agencies has been created as a result of the 2-year design study, but HiPER represents a major commitment and a step-change in laser science for Europe. Successful progress therefore requires a definite focus, rigorous deadlines, and the involvement of an independent agency whose funding is directed towards the most productive, balanced outcome for the community.

This proposal has been structured to ensure the work of the partner agencies is appropriately directed towards the common goal of realising a pan-European infrastructure, minimising the potential to focus on sub-critical national or institutional efforts.

The effect of the EC preparatory phase proposal has already had a dramatic effect *during the proposal generation phase*. The potential commitment of the EC to a pan-European laser fusion facility has so far resulted in:

- the re-direction of major existing programmes to be dedicated to the successful realisation of HiPER.
- the identification of wholly new resources to this project at the national and regional government level, along with the potential for significant additional resources if the EC approval is granted.
- tied together user access to the three highest energy European laser laboratories (CLF, LULI, PALS) for a coordinated scientific programme dedicated to HiPER over the next 3 years.
- attracted significant interest from outside the EU, resulting in coordinated programmes with the Japan, Canada, South Korea and China, along with partner status on this proposal from institutions in Russia and the USA
- all the major high power laser groups within Europe working coherently together to define a common plan for the coming years. This has never before happened. The details of this plan are contained in the Conceptual Design Report on the HiPER website.

Given this remarkable progress to date, the actual effects of the EC contribution are expected to be very significant in catalysing, coordinating, and leveraging work across the EU and in its international partners.

The EC funding is important to ensure a balanced approach to the development of this project. It will highlight the importance of tackling the political, financial and organisational issues prior to submission for construction funding, whilst providing a rigorous timetable against which these issues need to be resolved. This balanced approach is embedded in the project plan outlined above.

In a similar manner, the EC project will provide the mechanism for exploring other funding sources, including structural funds and risk-sharing (EIB) options, industrial partnerships, and formal agreements between the EC and other international agencies.

There is also a critical role for the EC in terms of risk reduction, wherein some limited funds for technical analyses will keep a strong focus on the realisation of the final infrastructure. Without such leveraging technical funds, the scope and direction of the work performed by each scientific group will inevitably gravitate towards more short-term, publication-focused research. The preparation of a facility of the scale of HiPER requires long-term research programmes encompassing sensitivity analyses and scaling studies. Such analyses are inevitably de-prioritised by access boards at the laser facilities in favour of isolated “quick-win” studies. On the technology side, a pan-European project such as HiPER requires integration effort and development of common systems to allow the national funding and the scientific community’s efforts to be consolidated into a joint infrastructure. The EC funding identified above is targeted to deliver this integrated approach.

4. Ethical Issues

As with any high technology science project, there is the potential for “dual-use” for defence/military purposes. There is no significant change from the status quo, in that research into the areas mentioned below is already underway across the world. Advice will be sought from the appropriate national and trans-national agencies to ensure there is no added risk related to “dual-use” that stems from the HiPER project.

HiPER will develop higher repetition rate laser sources (as will many other projects), which could conceivably be used by defence programmes for a variety of applications. However, this link is generic (not specific to the work done by HiPER), and indeed work in this area is being pursued by a number of commercial, private companies – for example in Germany and Japan.

HiPER will investigate the science of “hot dense matter”. This lies at the centre of fusion research. Aspects of laser driven fusion have been classified (although most of the field was declassified many years ago). The remaining security concerns relate mostly to the use of x-ray radiation drive – the approach adopted by the National Ignition Facility (USA) and Laser Mégajoule (France). This is because of the analogy to x-ray radiation drive in thermonuclear weapons. The approach adopted by HiPER is fundamentally different. It will use a purely optical system, avoiding entirely the radiation interaction issues associated with the weapons research. It is no coincidence that this is the laser fusion method being pursued in Japan, which strictly avoids any research into nuclear weapons.

Nevertheless, the sensitivities associated with weapons research are fully recognised, and so the HiPER project will maintain close communication with the relevant authorities to ensure that **no aspect of the research undertaken on HiPER will be classified**. This has been a guiding principle of the project and a central aspect of the consortium from its inception

ETHICAL ISSUES TABLE

	YES	PAGE
Informed Consent		
• Does the proposal involve children?		
• Does the proposal involve patients or persons not able to give consent?		
• Does the proposal involve adult healthy volunteers?		
• Does the proposal involve Human Genetic Material?		
• Does the proposal involve Human biological samples?		
• Does the proposal involve Human data collection?		
Research on Human embryo/foetus		
• Does the proposal involve Human Embryos?		
• Does the proposal involve Human Foetal Tissue / Cells?		
• Does the proposal involve Human Embryonic Stem Cells?		
Privacy		
• Does the proposal involve processing of genetic information or personal data (eg. health, sexual lifestyle, ethnicity, political opinion, religious or philosophical conviction)		
• Does the proposal involve tracking the location or observation of people?		
Research on Animals		
• Does the proposal involve research on animals?		
• Are those animals transgenic small laboratory animals?		
• Are those animals transgenic farm animals?		
• Are those animals cloning farm animals?		
• Are those animals non-human primates?		
Research Involving Developing Countries		
• Use of local resources (genetic, animal, plant etc)		
• Benefit to local community (capacity building ie access to healthcare, education etc)		
Dual Use		
• Research having potential military / terrorist application	yes	41
I CONFIRM THAT NONE OF THE ABOVE ISSUES APPLY TO MY PROPOSAL		

5. Consideration of gender aspects

The HiPER project will follow the principle of equal treatment between men and women and will make all its participants aware of current EU legislation. In addition, the project has identified specific areas to actively promote the gender equality especially in the field of Science and Technology.

Key areas where the project will ensure it has a positive impact on gender balance are: the recruitment level of young women in science and technology, their employment conditions and career progression opportunities for women. Specific issues that will be considered as part of the HiPER preparatory phase will include:

- Developing a policy on conditions of employment that introduce good work-life balances practices. This is a reflection of the fact that women during their careers may have extra family responsibilities that need to be balanced with their jobs.
- Actively encouraging women already employed by project partners to fill the required roles in the project, in particular at a senior level.
- Actively encouraging female graduate scientists to join the project. This will be achieved by engaging with existing professional women's networks and promoting the project within these networks. HiPER will encourage those academic partners that have access to existing careers offices to actively promote HiPER to the female student body.
- Seeking advice through its engagement with existing professional women's networks to ensure that best practices are followed to address some of the issues that women encounter in their careers.
- Creating a female network within the partners involved in the project to actively encourage the participation of young female scientists.
- Monitoring the number of female promotions, identifying those women that because of the impact of careers breaks may need to be on a fast track to achieve promotion at the same rate as male colleagues.
- Ensuring that senior management teams of the project have female representation and appointing a person at this level to monitor and advise on gender balance issues.
- Actively encouraging female representation at all Press and PR events, not only to highlight the role of women in the project, but also to encourage participation from other women outside the project

Finally, HiPER will monitor regularly the gender balance of all of its participants and will set a minimum target to ensure a fair equilibrium can be met. This target will be related to the natural gender balance of science, engineering and technology graduates in the European Union. Action will be taken if the ratio falls below this target.

Annex

List of Letters of Commitment and Support. Full details can be supplied upon request.

Partners :

Partner No.	Participant organisation name	Short name	Country	Signatory of Letter of Intent and position
1	Science and Technology Facilities Council (Funding Agency)	STFC	UK	Authorised by the top-level Executive Board for CCLRC. Note: On 1st April 2007, CCLRC changed its legal name to STFC
2	Commissariat à l'Énergie Atomique (Funding Agency)	CEA	France	Alain Bugat, Administrator General
3	Consiglio Nazionale delle Ricerche (Funding Agency)	CNR	Italy	Dr. Mario Ali Director General of Ministry of Universities and Research of Italy
4	Centre National de la Recherche Scientifique (Funding agency)	CNRS	France	Dany Vandromme, French Ministry of Research & Arnold Migus, Director General of CNRS
5	Conseil Régional d'Aquitaine (Funding Agency)	CRA	France	Alain Rousset, President
6	Ente per le Nuove tecnologie, l'Energia e l'Ambiente (Funding Agency)	ENEA	Italy	Sergio Martellucci, President of Scientific Committee of ENEA
7	Fundação para a Ciência e a Tecnologia (Funding Agency)	FCT	Portugal	Vice President
8	General Secretariat for Research and Technology (Funding Agency)	GSRT	Greece	General Secretariat for Research and Technology
9	Ministry of Education, Youth and Sports (Funding Agency)	MSMT	Czech Republic	Mgr. Dana Kuchtová
10	Universidad Politécnica de Madrid (Funding Agency as UPM are acting as a delegate of Spanish Ministry of Education and Science & Comunidad Autonoma de Madrid)	UPM (MEC) (CAM)	Spain	MEC: Carmen Andrade Director General for Technology Policy CAM: Alfonso Gonzalez, Subdirector General for Research UPM: Prof Dr Gonzalo Leon, Vice President
11	"Consorzio Nazionale Interuniversitario per le Scienze Fisiche della Materia"	CNISM	Italy	Giovanni Stefani, President of CNISM
12	Forschungsverbund Berlin e.V	FVB	Germany	Professor Dr. Wolfgang Sandner Director, Max Born Institute for Non Linear Optics
13	General Atomics	GA	USA	Joe Kilkenny, Vice President
14	Gesellschaft für Schwerionenforschung mbH	GSI	Germany	Prof. Dr. W. Henning, Managing Director Prof K Witte, Head of PHELIX Laser & science programme
15	Institute of Applied Physics of Russian Academy of Science	IAP-RAS	Russia	Dr. Sergei Andreev, Deputy Director
16	Institute of Plasma Physics and Laser Microfusion	IPPLM	Poland	Dr Zygmunt Skladanowski Director of IPPLM
17	Instituto Superior Técnico, Universidade Técnica de Lisboa	IST	Portugal	Professor Luis Silva

18	P.N.Lebedev Physical Institute of Russian Academy of Sciences	LPI	Russia	Sergey Gus'kov, Head Researcher
19	Academy of Sciences of the Czech Republic	PALS	Czech Republic	Dr Karel Jungwirth, Director of Institute of Physics
20	Technological Educational Institute of Crete	TEI of Crete	Greece	Prof Chara Athanasaki-Michailidou, President. Assoc Prof. Michael Tatarakis, Director dept of Electronics
21	Technische Universität Darmstadt	TUD	Germany	Prof Dr Markus Roth,
22	Technical University of Crete	TUC of Crete	Greece	Professor Joachim Grispolakis, Rector of the Institute

International Collaborating Organisations :

Organisation Name	Country	Signatory of letter of support
Korea Atomic Energy Research Institute (KAERI)	South Korea	Dr. Pil-Soo Hahn, Vice President of KAERI
Shanghai Institute of Optics and Fine Mechanics (SIOM)	China	Prof Ruxin Li, Vice Director
Laboratory of Optical Physics, of Chinese Academy of Sciences	China	Prof Zie Zhang, Director
Shanghai Jiaotong University	China	Prof Zie Zhang, President
Institute of Laser engineering, Osaka University	Japan	Kunioki Mima, Director, Professor of Institute of Laser Engineering of Osaka University
University of Alberta	Canada	Professor Allan Offenberger

Industrial Support :

Industrial partner	Previous expertise/ existing links	Potential supplier of:
AMTRON GmbH	LULI and Max Born Institute	Control and supply systems of high power laser diodes
Société Européenne de Systèmes Optiques (SESO)	Partnered with CEA on LMJ. Worked with LLNL. LULI, Osaka, RAL	High damage threshold optics, Direct off-axis manufacturing of mirrors, Serial production of large optics (lenses or plates);
DILAS	12 years experience in High Power Diode lasers	High Power Diode lasers – selecting, qualifying, testing
Hamamatsu Photonics KK	All major laser labs	Precision electronic and opto-electronic devices
Gooch and Housego PLC	Suppliers to NIF and LMJ	KDP and Quartz waveplates. General optics coated to withstand high laser fluences
CVI Technical Optics Ltd	All major laser labs	Fully customised complex optical components. Design and supply opto mechanical sub assemblies
Heraeus Noblelight Ltd	30 years experience in arc and flash lamp manufacture	Flash lamps
Kentech Instruments Ltd	All major laser labs	Pockel cell drivers. X-ray streak cameras, waveform generators for laser pulse shaping
Cleveland Crystals Inc	Supplier to NIF and LMF, LIL projects	KDP and KD*P crystals. Plasma electrode pockel cell crystals
Corning Inc	Involved in PHELIX, LMJ, LIL, NIF	Synthetic Fused Silica blankets
Glassman Europe Limited	All major laser labs	High voltage DC power supplies, HV dividers for accurate measurement
Saint-Gobain Ceramics	LMJ, LULI, GSI	Flash lamps
Plymouth Grating Laboratory	ILE, LLE	Gratings and Diffractive Optics
SAGEM - REOSC	LMJ	Refining the specification of optical components (mirrors, parabola, lenses)
HOYA	LMJ, NIF	Laser glass
Horiba Jobin Yvon	All major laser labs	Large aperture dielectric gratings
Tinsley	25 years experience and supplier to NIF, Omega, LMJ	Optical finishing processes
Thales	All major laser labs	Solid state lasers, power and nanosecond pump lasers
JENOPTIK Laser	IST, MPQ, Jena	Diode laser pump modules and pump optics. Optics for beam line configurations
OpTIC	Telescope Industry	Optronics technologies, capability in large optical surfaces and laser equipment